Characterization of a *C*–nucleophilic intermediate for the biocatalytic synthesis of β-hydroxy-amino acids

by

Anthony Ryan Meza

A dissertation submitted in partial fulfillment of
the requirements for the degree of

Doctor of Philosophy
(Biochemistry)

at the
UNIVERSITY OF WISCONSIN-MADISON
2023

Date of final oral examination: 07/20/2023

The dissertation is approved by the following members of the Final Oral Committee:

Andrew R. Buller, Assistant Professor, Chemistry
Brian Fox, Professor, Biochemistry
Philip Romero, Assistant Professor, Biochemistry
Jeffrey Martell, Assistant Professor, Chemistry

Dedication

A usual degree of certainty
Certainty that I would enjoy graduate school
Five years later and that certainty was validated

For what comes next
I am beyond excited for I trusted myself
With newfound knowledge and confidence
I will enjoy the next chapter, I am certain

I dedicate this thesis to my family for their constant support, motivation, and inspiration

Acknowledgements

The pursuit of a Ph.D. is commonly seen as an individual effort, and one day, a success. That is far from reality. A Ph.D. is a collective achievement and has its value increased by the dedication and commitment from friends, family, mentors, and colleagues. I am proud of my growth scientifically and for my understanding of what a Ph.D. represents. For those who made my journey a successful one, I thank you and want to provide specific examples how impactful your contributions were to my success.

I first need to define the two most important instances which I hold as defining moments in my scientific journey. The first is from what seems like over a half of a lifetime ago; a time when I was working with my dad and my older brother, Jordan. We were installing a tongue and groove roof on a cabin in Pinetop, Arizona. My dad would cut the boards and pass them to my brother and I to install. The boards came up the scaffolding a feverish pace and my dad would often be numerous boards ahead of us. As I watched my dad, I convinced myself that he had made a wrong cut and the board he passed had the wrong angle and wouldn't fit into place. After some bantering, we got to the place where this board would go, and to my disbelief, it went right into place. After cycling through my observations that led me to question the cut my dad had made, I was able to understand how my dad knew what angle to put on that cut. My curiosity for how things work and asking questions is a part of my personality and has led towards a career in science. It is sometimes challenging to identify as a scientist as a young graduate student. The second instance I would like to share is from my 2nd year of graduate school. I made an observation that the absorbance spectra of a protein I was working with changed after being left out. I began questioned what had happened and thought that the light in the room had affected the sample. After placing the sample in the sunlight, I was able to watch the protein change colors. This experience was gratifying and gave me munch needed confidence as I was still trying to

understand what it meant to be a scientist. Much like learning how my dad would cut boards, I yearned to understand more and continue to grow.

I want to thank the community of scientists that I have been able to work with and learn alongside. I want to acknowledge my advisor, Professor Andrew Buller. The amount of excitement that you exude for your trainees makes science so much more enjoyable. I am grateful that you enjoy science so much but will always prioritize this scientist. Science is hard and you understand this. Thank you for your patience, your guidance, and always reminding us that the data are the data. When I joined your lab, I was excited about the science I would learn and the projects I would contribute to. Early in some of our conversations, you had asked me what I would like to improve most on during graduate school. The answer was simple for me. Communication. I have grown so much as a scientist and am grateful for your high standards in the lab and high expectations for how we communicate science.

I packed up and ventured across the country for graduate school, I was full of excitement and against. I was welcomed by such a wonderful community in Madison. A major part of my choice to join IPiB was the energy that I felt when I visited Madison for recruitment. Once the semester started rolling, the fun never stopped. We worked hard and the classes we had together as a cohort were highlighted by seeing each other. Outside of class, we built friendships and discussed science, broadening of knowledge. I have too many people to thank for great memories who I've met during grad school. The scientific community is Madison was one of the most rewarding parts of graduate school. My time in Madison has been great and I must thank my partner, Brie, for contributing to my success and being such an influence on me over the last four years. Thank you for supporting my science, and more importantly, provided me a space where I could be myself and disconnect. Spending time with you has been one of my favorite parts of my time as a graduate student and I appreciate all your support.

As I had preluded, I can't recognize and thank my family and friends enough for their support. I had some great times with some of the people that are my friends for life the last few years before I left to graduate school. We always talked about when I was going to get out of there and I appreciate that I can roll back home, and we pick up right where we left off. Coming from a big family, I could easily spend the next seven pages detailing some of my favorite memories from growing up and over the last five years with my family. Michael, you set the example for the boys while we were growing up and did a great job. I was always excited about all your successes and loved your first car, a '66 Volkswagen Bug. I can still remember the first ride I took in it and can admit I was mad when you left home for college. Thank you for always welcoming me back to Arizona and asking if I needed anything. Patrick, you set the standard for finding what you enjoy in life and doing it. You also set the standard for work hard, play hard. I appreciate the time I got to live with you and look forward to our pool days in the future. Matthew, having lived together for four years during college, we really did get to see each other grow into our best. I remember when you were about to graduate and consider changing majors from accounting to science, I even invited you to come hang out in the lab. Funny enough, I had the same thoughts during graduate school… Nevertheless, it's exciting to see how great you've been in your career, and I appreciate how you would remind me that I there is light at the end of the tunnel (graduate school). You may have beat me to bachelors and the masters, but I got you on the doctorate. Jordan, I've got so many memories of us. From climbing trees to years of martial arts. I admire your work ethic and how calm your presence is. Your support has been unwavering, and you have always had my back. You exemplify the principles that our parents taught us. Sienna, none of my siblings were more excited than you for me to go to Wisconsin. I love that I grew out a mullet for your high school graduation and letting you straighten my hair was so much fun. Thank you for reminding me how challenging it is to understand what you want to do in life right out of high school and I know you'll be great. Jacob, you're a hard one to crack, always quiet, but you never miss when you speak up. Gaming with you is something I valued, and we need to

do more of it. You showed me so much in the last year and I have no doubt that you've well on your way. Mom and dad, you've done such a wonderful job raising us. Thank you for being persistent that we find something that we love doing and that we become the best at it. "If you love what you do, then it's easy to be your best". I appreciate your support and the work ethic you have instilled in us. I can't thank you enough.

Table of Contents

Chapter 1

Introduction

Chapter 1: Introduction

1. 1. Enzymes catalyze chemical reactions

All domains of life operate under a conserved set of processes that are dependent on the chemical energy liberated during metabolism. At the core of this process is the genetic code (DNA) which is the blueprint for all proteins and RNA that ultimately carry out most cellular processes.[1] Briefly, DNA is transcribed into mRNA which is then the template for protein synthesis by the ribosome. The product of mRNA translation is a polypeptide which folds into a protein based on the composition and arrangement of the amino acid residues that were originally encoding in the DNA sequence.[2] The amino acids that compose proteins are relatively similar and can be generally classified into four categories based on the properties on their side chains (Figure 1a). Even though proteins are composed of 20 homochiral amino acids with limited chemical diversity, they are endowed with diverse biological activities which arises from the tertiary three-dimensional structure that is adopted. Some of the primary functions of proteins in cells include providing structural support, sensing and transport of small molecules, and catalyzing chemical reactions in cellular metabolism.

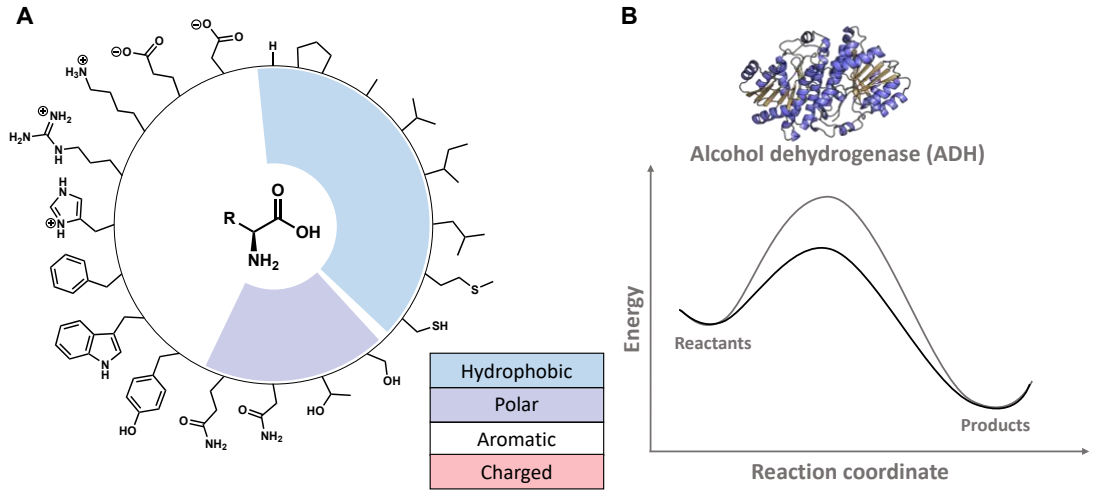

Figure 1. Enzymes are constructed from 20 amino acids. A) Classification of amino acid side chain properties into 4 categories hydrophobic (blue), polar (purple), aromatic (green), and charged (red). All amino acids have identical configuration at C_α (2*S*). **B)** Enzymes reduce the activation energy of chemical reactions. Reaction coordinate shown with the uncatalyzed reaction (grey) having a larger energy barrier than the enzyme catalyzed reaction (black).

The vast array of chemical transformations that are present in nature are predominately the result of enzymes, proteins that act as catalysts by accelerating chemical reactions (Figure 1b). Enzymes are central in metabolism where complex circuits of transformations occur through the consecutive action of enzymes, converting food into energy and key building blocks that can later be assembled into primary and secondary metabolites.[3,4] The unique three-dimensional arrangement of the chiral amino acid residues in enzymes endows them with high selectivity in the transformations they catalyze.[5] For example, lactase selectively targets D-lactose to liberate the sugar monomers of D-glucose and D-galactose over the many other sugar isomers (Figure 2).[6,7] Lactose can readily be hydrolyzed with strong acids and heat,[8] but biology achieves this transformation under physiological conditions through the molecular recognition and positioning of the highly hydrophilic substrate proximal to a catalytic glutamate residue. The glutamate residue adds into the anomeric carbon of the galactose monomer and release glucose followed by hydrolysis of the α-galactosyl intermediate, releasing galactose and completing the catalytic cycle. Other hydrolytic enzymes such as proteases, nucleases, and lipases follow similar mechanisms with covalently bound intermediates or use metal ions as a cofactor.[9–11]

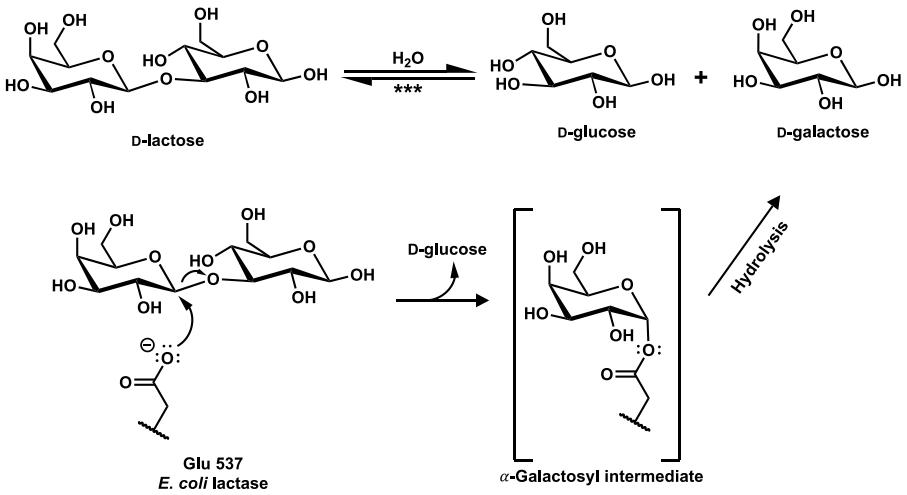

Figure 2. Enzymes utilize active site residues for substrate recognition and catalysis. The hydrolysis of D-lactose by lactase results in the release of saccharide monomers D-glucose and D-galactose. *** The reverse reaction is completed by beta-1,4-galactosyltransferase.[12]

The lack of chemical diversity in the 20 standard amino acids limits the chemical transformations that can be catalyzed without the use of cofactors or coenzymes (a non-protein organic molecule or metallic ion that is required by an enzyme).[13] It is estimated that around 50% of enzymes rely on cofactors for their activity and greater than 300 enzymes in humans rely on Mg^{2+}.[14] Cofactors have a variety of physiochemical properties and are broadly divided into two categories; organic and inorganic (minerals and metal complexes). Organic complexes include thiamin pyrophosphate, riboflavin, and heme which are essential nutrients and provide diverse chemical functionality as they interact with proteins through covalent and non-covalent interactions (Figure 3a). The evolution of proteins to bind and utilize cofactors for enzymatic activity has had a dramatic influence on the emergence of life and is discussed in a variety of scientific communities.[15–17] Nevertheless, cofactors provide chemical properties and functionality that is not genetically encoded in the standard amino acids.

A key feature of reactions catalyzed by enzymes is that the chiral environment of the protein can induce stereoselectivity during the chemical transformation. For example, the reduction of acetophenone by an NADH dependent ketoreductase can produce both enantiomers of the corresponding alcohol. However, the enzyme can bind the cofactor and substrate in a specific orientation to one another, thus reducing the activation energy for one isomer more than the other and resulting in a reduced product that is enantiomerically enriched (Figure 3b). NADH acts as a substrate in this reaction as it donates a hydride, forming NAD^+. Biology has evolved metabolic pathways that couple the regeneration of oxidants and reductants (NAD(H), NADP(H), FAD(H_2) as oxidation and reduction occurs in multiple metabolic cycles.[18] Chemist have leveraged these sets of enzymes and others for cofactor regeneration in biocatalytic transformations.[19]

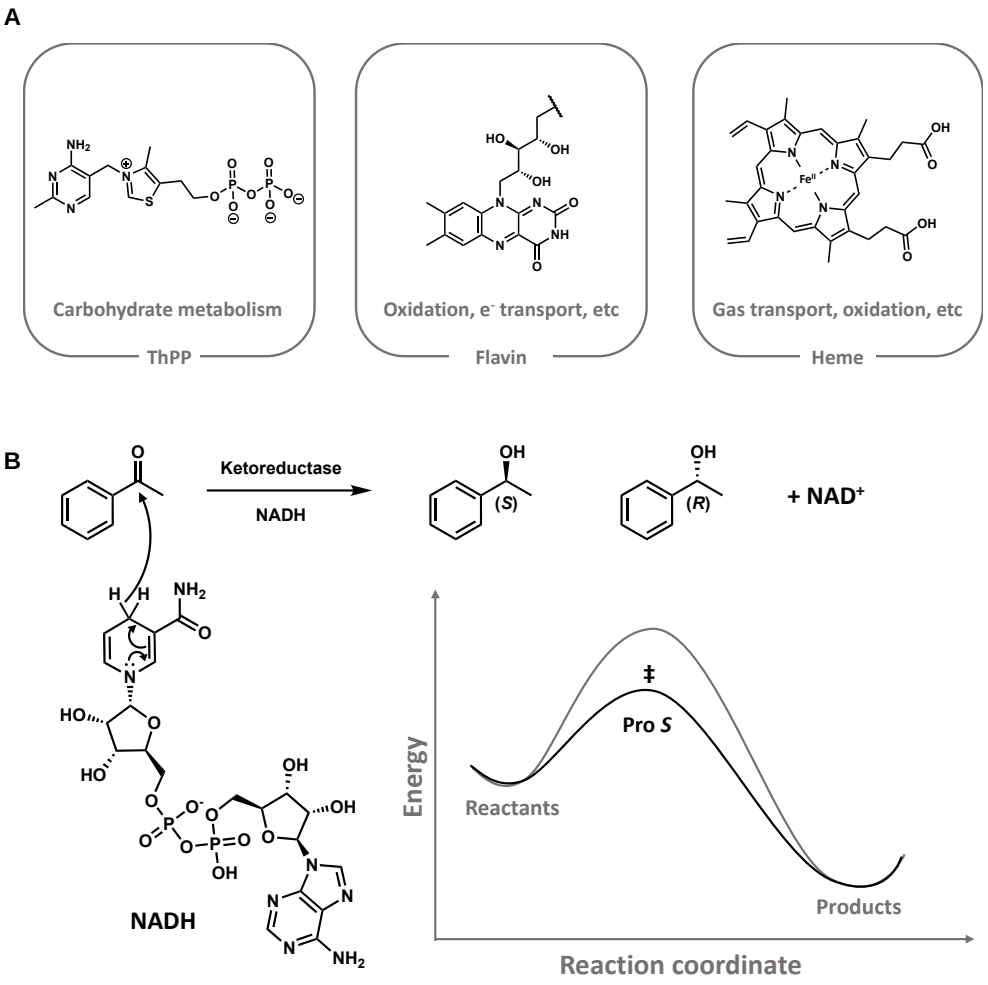

Figure 3. Enzymes commonly bind and use organic cofactors or coenzymes to achieve chemical transformations. A) Common organic cofactors. ThPP (thiamin pyrophosphate) and Flavin (riboflavin) are vitamin B_1 and B_2, respectively. Heme is biosynthesized by humans and is essential nutrient. **B)** The reduction of acetophenone by a ketoreductase produces the corresponding alcohols. The chiral environment of the enzyme active site influences the stereo outcome of the reaction by reducing the energy to one isomer more so than the other.

1. 2. Biocatalysts are valuable in chemical synthesis and consumer goods

The use of enzymes, extracts, or even entire organisms as biocatalysts has had substantial impacts on human history and well-being. Long before microbes were observed or described, they were being used in multiple fermentative processes including the production of ethanol in wine and beer. The cellular respiration of yeast spores in bread making resulted in leavening while a whole host of enzymes metabolized components of the grain, contributed to color, taste, and structure.[20] The discovery of penicillin in 1928 as a secondary metabolite of a

penicillium fungi provided a small molecule antimicrobial properties (Figure 4a).[21] However, isolation of the potential antibiotic from the native producer was challenging and the inherent stability of the β-lactam hindered its use as an antibiotic. A dedicated effort to mass produce penicillin in a stable form during World War II, successful through Pfizer's deep-tank fermentation, provided the desired small molecule in quantities that directly contributed to the success in World War II.[22] Modern fermentative processes use a variety of organisms in the production of natural products, foods, commodity chemicals, biofuels, as well as large scale preparations of enzymes (Figure 4b-c). Industrial enzymes have a variety of uses in consumer goods; glucose isomerase is used to produce high fructose corn syrup; proteases, amylases, and lipases are present in detergents to aid in the breakdown and removal of protein, starch, and lipid stains respectively; and there is a breadth of enzymes that are produced via fermentation and directly used as dietary supplements.[23]

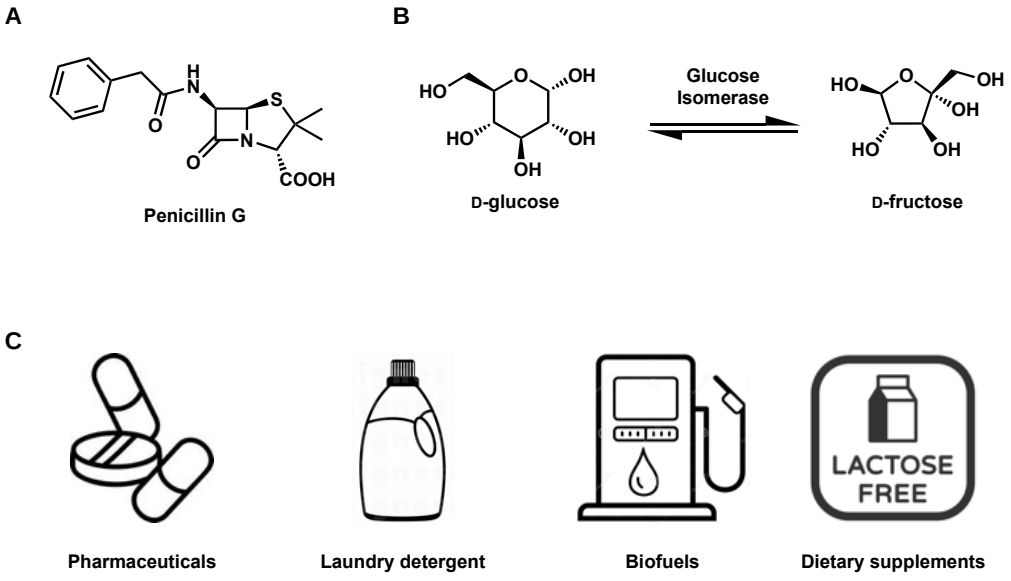

Figure 4. Modern biocatalysis is integrated into industrial chemical production. A) Penicillin G as an example for a natural product that is produced via fermentation of a natively producing organism.[24] **B)** Glucose isomerase produce fructose from glucose at a scale of 10^6 tons per year. **C)** Examples for where industrial enzymes are used.

Enzymes generally operate under mild conditions and are biodegradable, contributing to green chemistry initiatives.[25] While the ability to perform well-defined transformations with high degree of chemo-, regio-, and stereoselectivity makes them an attractive tool in synthesis.[26] Enzymes often lack the efficiency or properties required to be a productive biocatalyst outside their native context. Directed evolution and protein engineering enables scientists to alter the properties of enzymes to make them more suitable for a desired application.[27] The process of directed evolution begins with identifying an enzyme of interest and producing its parent gene sequence (Figure 5). A variety of mutagenesis techniques are applied to instill genetic diversity (library of genes). The library is then transformed into an expression strain and cultivated to produce the library of mutant enzymes. These enzymes are screened for a desired activity and high performers are chosen as new parent genes for subsequent rounds of evolution if necessary. Directed evolution of enzymes has had a tremendous impact on the development and application of biocatalysts.

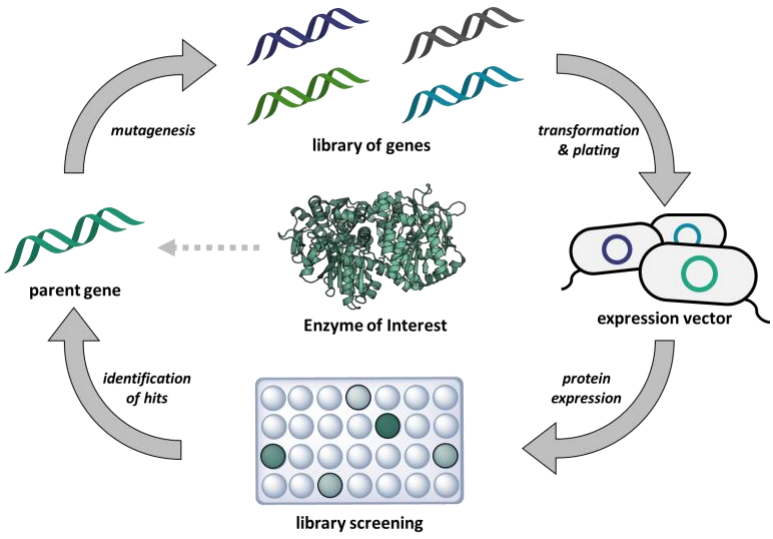

Figure 5. The directed evolution cycle. Figure generated by Peyton Higgins.

Enzymes have rapidly been incorporated into synthetic strategies to produce fine chemicals and complex pharmaceuticals. Notably, functional group interconversions using transaminases, imine reductases, and lipases have been successfully applied in the synthesis of numerous therapeutics.[28] More recently, multi-step enzymatic cascades have been begun to be implemented, streamlining syntheses, and reducing the isolation of intermediates (Figure 6). The synthesis of molnupiravir and islatravir highlight the molecular complexity that can be achieved with enzymes and protein engineering.[29,30]

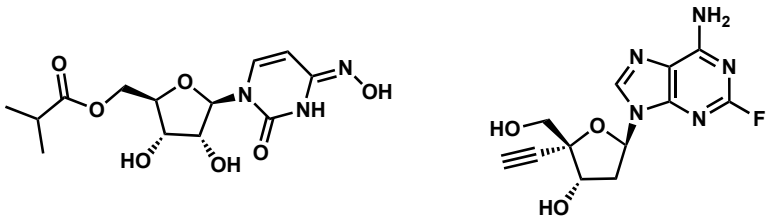

Molnupiravir **Islatravir**

Figure 6. Cascade biocatalytic synthesis of molnupiravir and islatravir. Molnnupiravir synthesis was mediated by 6 enyzmes: a commercially available lipase, an engineered kinase, an engineered uridine phosphorylase, and 3 accessory enzymes for ATP regeneration. Islatravir synthesis was mediated by 9 enzymes: 5 engineered enzymes in small assembly (oxidase, kinase, aldolase, phosphopentamutase, and a purine nucleoside phosphorylase. 4 auxillary enzymes were used to remove H_2O_2 and to transfer phosphate in the cascade.

1. 3. Nature evolved numerous routes for C–C bond formation

Nature has evolved numerous pathways to forge and break C–C bonds and many of these enzymes have been explored as biocatalysts. Preeminent in these transformations are aldol like reactions (Figure 7a). Aldol reactions consist of a donor nucleophile (typically an enolate or enamine) and electrophile (aldehyde or ketone). The primary challenge in biology is generating a nucleophilic species in aqueous conditions. To combat this challenge, Nature uses metal ions and covalent bonds to promote the formation of these vital nucleophiles. Metal ions are found in type II aldolases and stabilize the enolate enabling productive catalysis (Figure 7b). In type I

aldolases, the carbonyl is condensed onto a primary or secondary amine forming a covalent Schiff base intermediate within the protein scaffold. The Schiff base intermediate is electrophilic as an imine or iminium. Like type II aldolases, once the Schiff base is formed, an alpha proton to the imine can be deprotonated and tautomerize into an enamine (Figure 7b).

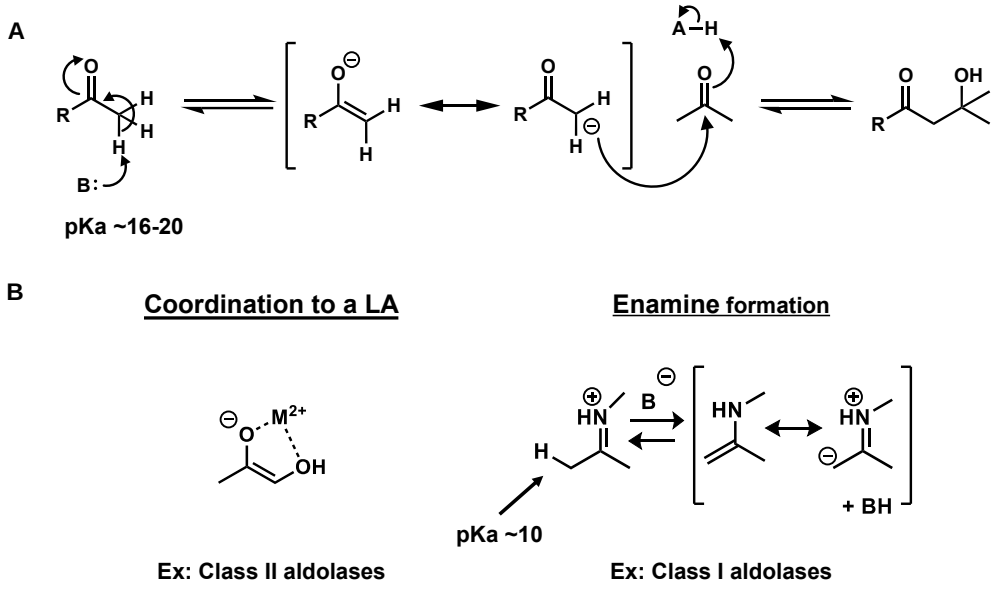

Figure 7. Aldol reactions form C–C bonds. A) Base catalyzed aldol reaction in organic synthesis. Deprotonation of C_α of a carbonyl containing substrate results in enolate formation and enables addition into an electrophile. **B)** Class II aldolases stabilize enolate species through coordination with divalent cations (LA = Lewis Acid). Formation of Schiff base intermediates in class I aldolases. Enamine formation is enabled through deportation of the Schiff base intermediate.

In both types of aldolases, nucleophile generation is achieved through stabilization of the conjugate base of the donor through coordination with a metal ion or through the formation of an enamine. In both cases, the nucleophile is generated via deprotonation of the carbon alpha to the carbonyl. Nucleophiles can also be generated from C–C bond cleavage in which one carbon partner acts as an electron acceptor and the other as an electron donor. A class of enzymes that exemplifies this behavior and has been used in industrial syntheses is the hydroxynitrile lyases (Figure 8a). These enzymes were identified in the catabolism of cyanohydrins and cleave the

carbon-nitrile bond through deprotonation the hydroxyl group, collapse of the oxyanion and elimination of a cyanide ion. HNLs have been successfully leveraged in C–C bond forming reactions in which a cyanide source can be added into a carbonyl electrophile.[31] The chiral cyanohydrin functional group serves as an advantageous synthon for subsequent diversification reactions with established synthetic methodologies for nitrile chemistry (Figure 8b).[32]

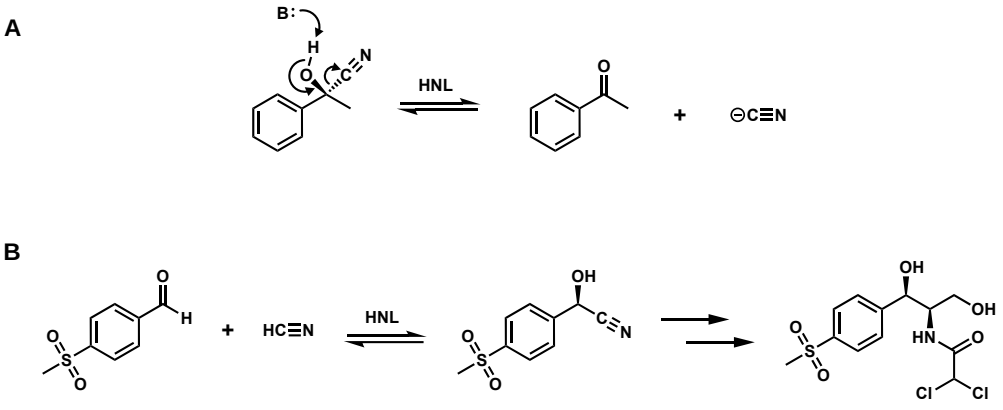

Figure 8. Hydroxynitrile lyases catalyze C–C bond formation between cyanide and ketones or aldehydes. A) Mechanism for HNL catabolism of cyanohydrins. **B)** Stereoselective chemo-enzymatic synthesis of thiamphenicol.

1. 4. PLP dependent enzymes catalyze C–C bond formation

PLP-dependent enzymes catalyze an array of transformations in amino acid metabolism and have been leveraged as synthases in the preparation of non-standard amino acids (nsAAs) (Figure 9a).[33–38] At the center of the diverse activity present in PLP-dependent enzymes is the ability for the cofactor to stabilize reactive intermediates. Binding of the amino acid substrates to the cofactor results in formation of the external aldimine, E(A_{ex}) (Figure 9b). Once bound to the PLP cofactor, the pKa of the C_α proton is dramatically decreased, enabling deprotonation and formation of an electron rich enzyme bound quinonoid, E(Q). Deprotonation of C_α is the first committed step in many PLP-dependent enzymes after amino acid binding. Numerous PLP-dependent enzymes can catalyze C–C bond formation. The key intermediates and respective enzymes-classes they belong to are highlighted in Figure 9c.

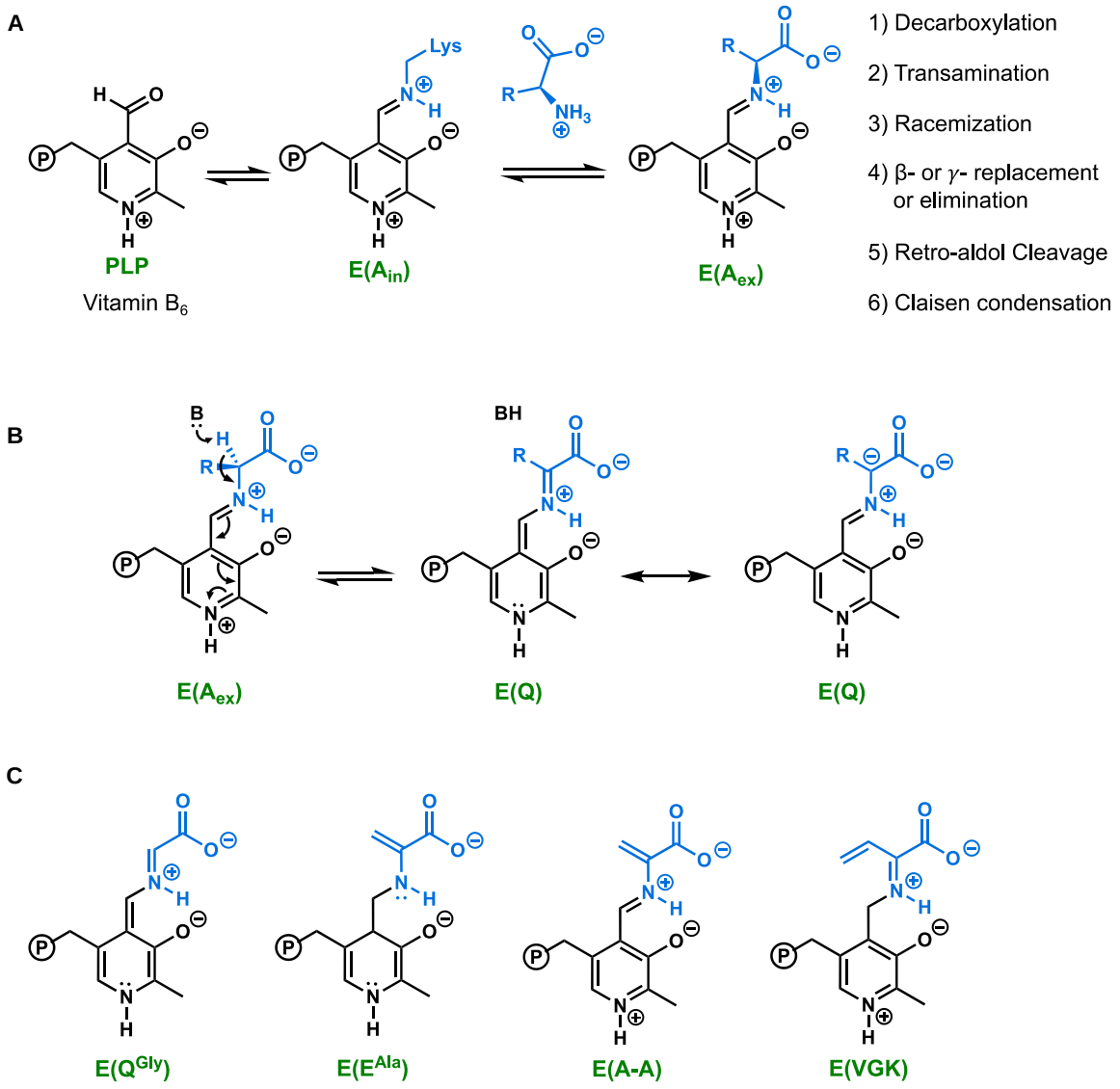

Figure 9. PLP-dependent intermediates in C–C bond forming reactions. A) PLP-dependent (Viatamine B_6) enzymes catalyze reactions in amino acid metabolism. **B)** C_α deportation results in the electron rich E(Q) intermediate. **C)** Highlighted intermediates in C–C bond formation. Nucleophilic intermediates: $E(Q^{Gly})$[36] and $E(E^{Ala})$.[37] Electrophilic intermediates E(A-A)[34] and E(VGK).[38]

PLP-dependent enzymes can generate nucleophilic intermediates through C–C bond cleavage. Threonine aldolases (TAs) and serine hydroxymethyl transferases (SHMTs) catalyze the retro-aldol cleavage of L-threonine (Thr) and L-serine (Ser), respectively, generating a glycyl quinonoid intermediate $E(Q^{Gly})$ (Figure 10a).[36] Natively, this highly basic intermediate is rapidly

protonated, forming glycine. By running these transformations in reverse with very high concentrations of glycine and aldehyde substrates, TAs and SHMTs have been leveraged for the synthesis of β-hydroxy amino acids. However, most native TAs catalyzed aldol reactions result in a mixtures of diastereomers at C_β.[39–42] It has been observed that diastereoselectivivity with these enzymes can be high, but products rapidly renter the active site and undergo retro-aldol cleavage which results in scrambling of the stereocenter at C_β.[43] Intensive directed evolution campaigns have yielded modest improvements in diastereomeric outcome of TA catalyzed reactions, but improvements generally don't translate to additional aldehyde substrates.[39] However, the intrinsic reversibility of TA catalyzed reactions has enabled successful dynamic kinetic resolution cascades where a downstream decarboxylases were selective for the respective isomers produces from TA reactions with glycine and benzaldehyde, leading to enantioenriched 1,2-amino alcohols.

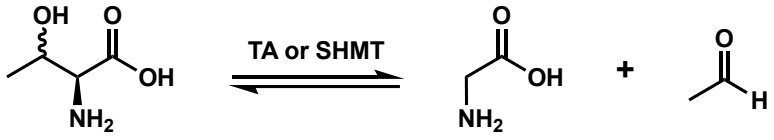

Figure 10. TAs and SHMTs reversibly breakdown Thr and Ser.

There is a set of PLP dependent enzymes, L-threonine transaldolases (LTTAs) that have begun to be described in the literature. In contrast to TAs, these enzymes natively synthesize β-hydroxy amino acids and are present in biosynthetic gene clusters that are producing secondary metabolites. LTTAs catalyze retro-aldol cleavage of Thr and a subsequent aldol-like addition into an aldehyde to form a new side chain, setting the stereochemistry of the C_β-OH group (Figure 11).[44] The first description of an LTTA came in 2001 where researchers identified the enzyme involved in the biosynthesis of fluorothreonine (F-LTTA).[45] In characterization of a biosynthetic gene cluster encoding a lipopeptidyl nucleoside, the next LTTA, LipK, was discovered. A gene that was related to a SHMT was found and hypothesized to be the source of the β-hydroxy amino

acid fragment in the natural product.[46] Two groups recently discovered an LTTA in the biosynthesis of obafluorin, a β-lactone Thr-aminoacyl tRNA synthetase inhibitor.[47–49] In the following chapters, our efforts in characterizing and applying ObiH to synthesize β-hydroxy amino acids is detailed.

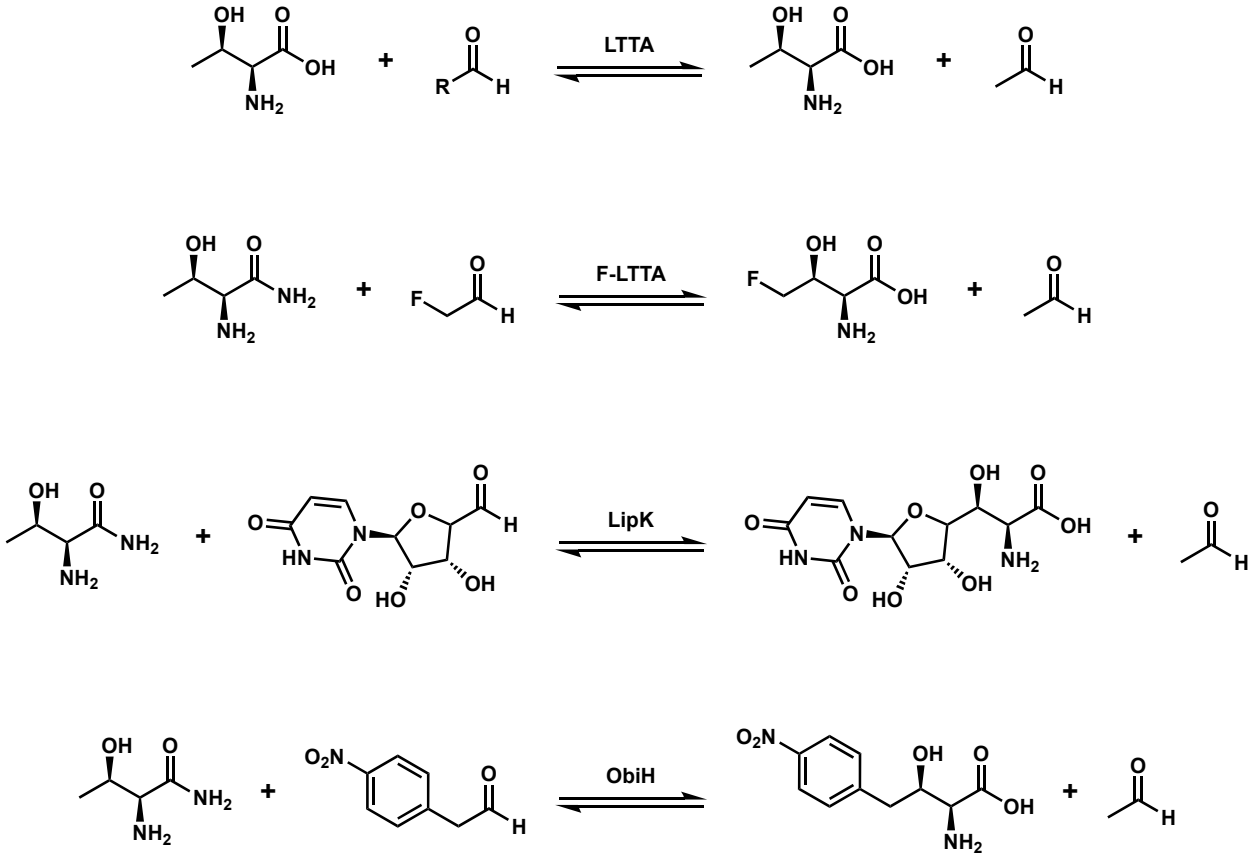

Figure 11: LTTA catalyzed reactions.

There have been a few additional LTTAs described in the literature, but biochemical characterization has been sparse, with these studies predominantly focusing on the natural product biosynthesis that they are a part of. The details that have been reported in the literature indicate that LTTAs form β-hydroxy amino acids with high stereo selectively. LTTAs could be a viable biocatalyst for the synthesis of β-hydroxy amino acids. An LTTA from Pseudomonas, PsLTTA was discovered through genome mining and applied as a biocatalyst in 2019. Xu et al. were successful in generating β-hydroxy amino acids with benzaldehyde analogs with good

diastereoselectivity (diastereomeric excess > 60%) However, only one reaction was completed at preparative scale and PsLTTA has 99% sequence identity to ObiH (discussed in chapters 2-4).

1. 5. Preface to remaining chapters

A fundamental challenge in C–C reactions with biocatalysis is identifying appropriate electrophiles and nucleophiles in aqueous conditions. The remaining chapters of this thesis describes our work in that characterization of the nucleophilic intermediate in ObiH, an LTTA, and that application of ObiH as a biocatalysts to synthesize β-hydroxy amino acid. In Chapter 2, we detail key mechanistic studies of ObiH and identify features of the nucleophilic intermediate, E(Q^{Gly}), that enable its unique reactivity. Chapter 3 highlights the synthetic utility of ObiH in a two-enzyme cascade. We successfully leverage styrene oxide isomerase to generate α-aryl aldehydes from styrene oxide analogs and capture these unstable intermediates in whole-cell biocatalysts. Finally, Chapter 4 discusses our efforts to synthesize tertiary-β-hydroxy amino acids by intercepting ketone substrates with ObiH. This work highlights the reactivity and selectivity of ObiH and demonstrates the synthetic utility of ObiH with the synthesis of numerous β-hydroxy amino acids.

Projects I have contributed to for this thesis work have resulted in publications as well as manuscripts in preparation:

1. Kumar P*, **Meza A***, Ellis JM, Carlson GA, Bingman CA, Buller AR. “L-ThreonineTransaldolase Activity Is Enabled by a Persistent Catalytic Intermediate” *ACS Chem. Biol*. 16, 86-95 *These authors contributed equally.
2. **Meza, A.;** Campbell, M. E.; Zmich, A.; Thein, S. A.; Grieger, A. M.; McGill, M. J.; Willoughby, P. H.; Buller, A. R. “Efficient chemoenzymatic synthesis of α-aryl aldehydes as intermediates in C–C bond forming biocatalytic cascades.” *ACS Catalysis*. 2022. 12, 17, 10700-10710

3. Bruffy, S. K.; **Meza, A.;** Doyon, T. J.; Huseth, K. G.; Buller, A.R. “Enzymatic aldol addition into un-activated ketones via a reactive carbon nucleophile” (*Manuscript in preparation*)

1. 5. References

(1) Crick, F. *Central Dogma of Molecular Biology*; 1970; Vol. 227.

(2) Anfinsen, C. B. *Principles That Govern the Folding of Protein Chains*; 1973; Vol. 181. http://science.sciencemag.org/.

(3) Noda-Garcia, L.; Liebermeister, W.; Tawfik, D. S. Annual Review of Biochemistry Metabolite-Enzyme Coevolution: From Single Enzymes to Metabolic Pathways and Networks. **2018**. https://doi.org/10.1146/annurev-biochem.

(4) Tibrewal, N.; Tang, Y. Biocatalysts for Natural Product Biosynthesis. *Annual Review of Chemical and Biomolecular Engineering*. Annual Reviews Inc. 2014, pp 347–366. https://doi.org/10.1146/annurev-chembioeng-060713-040008.

(5) Hedstrom, L. Enzyme Specificity and Selectivity. In *eLS*; Wiley, 2010. https://doi.org/10.1002/9780470015902.a0000716.pub2.

(6) Matthews, B. W. The Structure of E. Coli β-Galactosidase. *Comptes Rendus - Biologies*. Elsevier Masson SAS 2005, pp 549–556. https://doi.org/10.1016/j.crvi.2005.03.006.

(7) Yang, H.; Shi, L.; Zhuang, X.; Su, R.; Wan, D.; Song, F.; Li, J.; Liu, S. Identification of Structurally Closely Related Monosaccharide and Disaccharide Isomers by PMP Labeling in Conjunction with IM-MS/MS. *Sci Rep* **2016**, *6*. https://doi.org/10.1038/srep28079.

(8) Vujicic, I. F.; Lin, A. Y.; Nickerson, T. A. Changes During Acid Hydrolysis of Lactose. *J Dairy Sci* **1977**, *60* (1), 29–33. https://doi.org/10.3168/jds.S0022-0302(77)83824-1.

(9) López-Otín, C.; Bond, J. S. Proteases: Multifunctional Enzymes in Life and Disease. *Journal of Biological Chemistry*. American Society for Biochemistry and Molecular Biology Inc. November 7, 2008, pp 30433–30437. https://doi.org/10.1074/jbc.R800035200.

(10) Reis, P.; Holmberg, K.; Watzke, H.; Leser, M. E.; Miller, R. Lipases at Interfaces: A Review. *Advances in Colloid and Interface Science*. March 2009, pp 237–250. https://doi.org/10.1016/j.cis.2008.06.001.

(11) Yang, W. Nucleases: Diversity of Structure, Function and Mechanism. *Q Rev Biophys* **2011**, *44* (1), 1–93. https://doi.org/10.1017/S0033583510000181.

(12) Matthews, B. W. The Structure of E. Coli β-Galactosidase. *Comptes Rendus - Biologies*. Elsevier Masson SAS 2005, pp 549–556. https://doi.org/10.1016/j.crvi.2005.03.006.

(13) Fischer, J. D.; Holliday, G. L.; Rahman, S. A.; Thornton, J. M. The Structures and Physicochemical Properties of Organic Cofactors in Biocatalysis. *J Mol Biol* **2010**, *403* (5), 803–824. https://doi.org/10.1016/j.jmb.2010.09.018.

(14) Jahnen-Dechent, W.; Ketteler, M. Magnesium Basics. *CKJ: Clinical Kidney Journal*. February 2012. https://doi.org/10.1093/ndtplus/sfr163.

(15) Weiss, M. C.; Sousa, F. L.; Mrnjavac, N.; Neukirchen, S.; Roettger, M.; Nelson-Sathi, S.; Martin, W. F. The Physiology and Habitat of the Last Universal Common Ancestor. *Nat Microbiol* **2016**, *1* (9). https://doi.org/10.1038/nmicrobiol.2016.116.

(16) Kirschning, A. On the Evolution of Coenzyme Biosynthesis. *Natural Product Reports*. Royal Society of Chemistry 2022. https://doi.org/10.1039/d2np00037g.

(17) Krishnamurthy, R.; Hud, N. V. Introduction: Chemical Evolution and the Origins of Life. *Chemical Reviews*. American Chemical Society June 10, 2020, pp 4613–4615. https://doi.org/10.1021/acs.chemrev.0c00409.

(18) Xiao, W.; Wang, R. S.; Handy, D. E.; Loscalzo, J. NAD(H) and NADP(H) Redox Couples and Cellular Energy Metabolism. *Antioxidants and Redox Signaling*. Mary Ann Liebert Inc. January 20, 2018, pp 251–272. https://doi.org/10.1089/ars.2017.7216.

(19) Mordhorst, S.; Andexer, J. N. Round, Round We Go-Strategies for Enzymatic Cofactor Regeneration. *Natural Product Reports*. Royal Society of Chemistry October 1, 2020, pp 1316–1333. https://doi.org/10.1039/d0np00004c.

(20) Bock, J. E. Enzymes in Breadmaking. In *Improving and Tailoring Enzymes for Food Quality and Functionality*; Elsevier Inc., 2015; pp 181–198. https://doi.org/10.1016/B978-1-78242-285-3.00009-0.

(21) Fleming, A. *ON THE ANTIBACTERIAL ACTION OF CULTURES OF A PENICILLIUM, WITH SPECIAL REFERENCE TO THEIR USE IN THE ISOLATION OF B. INFLUENZ?1E*.

(22) *Development of Deep-Tank Fermentation Pfizer Inc*; 2008.

(23) Kirk, O.; Borchert, T. V.; Fuglsang, C. C. Industrial Enzyme Applications. *Current Opinion in Biotechnology*. Elsevier Ltd August 1, 2002, pp 345–351. https://doi.org/10.1016/S0958-1669(02)00328-2.

(24) Park, D.; Swayambhu, G.; Lyga, T.; Pfeifer, B. A. Complex Natural Product Production Methods and Options. *Synthetic and Systems Biotechnology*. KeAi Communications Co. March 1, 2021, pp 1–11. https://doi.org/10.1016/j.synbio.2020.12.001.

(25) Sharma, S.; Das, J.; Braje, W. M.; Dash, A. K.; Handa, S. A Glimpse into Green Chemistry Practices in the Pharmaceutical Industry. *ChemSusChem*. NLM (Medline) June 8, 2020, pp 2859–2875. https://doi.org/10.1002/cssc.202000317.

(26) Bell, E. L.; Finnigan, W.; France, S. P.; Green, A. P.; Hayes, M. A.; Hepworth, L. J.; Lovelock, S. L.; Niikura, H.; Osuna, S.; Romero, E.; Ryan, K. S.; Turner, N. J.; Flitsch, S. L. Biocatalysis. *Nature Reviews Methods Primers*. Springer Nature December 1, 2021. https://doi.org/10.1038/s43586-021-00044-z.

(27) Packer, M. S.; Liu, D. R. Methods for the Directed Evolution of Proteins. *Nature Reviews Genetics*. Nature Publishing Group July 19, 2015, pp 379–394. https://doi.org/10.1038/nrg3927.

(28) France, S. P.; Lewis, R. D.; Martinez, C. A. The Evolving Nature of Biocatalysis in Pharmaceutical Research and Development. *JACS Au*. American Chemical Society March 27, 2022. https://doi.org/10.1021/jacsau.2c00712.

(29) Mcintosh, J. A.; Benkovics, T.; Silverman, S. M.; Hu, M. A.; Kong, J.; Maligres, P. E.; Itoh, T.; Yang, H.; Verma, D.; Pan, W.; Ho, H.; Vroom, J.; Knight, A. M.; Hurtak, J. A.; Klapars, A.; Fryszkowska, A.; Morris, W. J.; Strotman, N. A.; Murphy, G. S.; Maloney, K. M.; Fier, P. S. Engineered Ribosyl-1-Kinase Enables Concise Synthesis of Molnupiravir, an Antiviral for COVID-19. **2021**. https://doi.org/10.1021/acscentsci.1c00608.

(30) Huffman, M. A.; Fryszkowska, A.; Alvizo, O.; Borra-Garske, M.; Campos, K. R.; Canada, K. A.; Devine, P. N.; Duan, D.; Forstater, J. H.; Grosser, S. T.; Halsey, H. M.; Hughes, G. J.; Jo, J.; Joyce, L. A.; Kolev, J. N.; Liang, J.; Maloney, K. M.; Mann, B. F.; Marshall, N. M.; McLaughlin, M.; Moore, J. C.; Murphy, G. S.; Nawrat, C. C.; Nazor, J.; Novick, S.; Patel, N. R.; Rodriguez-Granillo, A.; Robaire, S. A.; Sherer, E. C.; Truppo, M. D.; Whittaker, A. M.; Verma, D.; Xiao, L.; Xu, Y.; Yang, H. Design of an in Vitro Biocatalytic Cascade for the Manufacture of Islatravir. *Science (1979)* **2019**, *366* (6470), 1255–1259. https://doi.org/10.1126/science.aay8484.

(31) Dadashipour, M.; Asano, Y. Hydroxynitrile Lyases: Insights into Biochemistry, Discovery, and Engineering. *ACS Catalysis*. September 2, 2011, pp 1121–1149. https://doi.org/10.1021/cs200325q.

(32) Lu, W.; Chen, P.; Lin, G. New Stereoselective Synthesis of Thiamphenicol and Florfenicol from Enantiomerically Pure Cyanohydrin: A Chemo-Enzymatic Approach. *Tetrahedron* **2008**, *64* (33), 7822–7827. https://doi.org/10.1016/j.tet.2008.05.113.

(33) Du, Y.; Ryan, K. S. Natural Product Reports Pyridoxal Phosphate-Dependent Reactions in the Biosynthesis of Natural Products. *Nat. Prod. Rep.* **2018**. https://doi.org/10.1039/c8np00049b.

(34) Watkins-Dulaney, E.; Straathof, S.; Arnold, F. Tryptophan Synthase: Biocatalyst Extraordinaire. *ChemBioChem*. Wiley-VCH Verlag January 5, 2021, pp 5–16. https://doi.org/10.1002/cbic.202000379.

(35) Martínez-Montero, L.; Schrittwieser, J. H.; Kroutil, W. Regioselective Biocatalytic Transformations Employing Transaminases and Tyrosine Phenol Lyases. *Top Catal* **2019**, *62* (17–20), 1208–1217. https://doi.org/10.1007/s11244-018-1054-7.

(36) Fesko, K. Threonine Aldolases: Perspectives in Engineering and Screening the Enzymes with Enhanced Substrate and Stereo Specificities. *Applied Microbiology and Biotechnology*. 2016, pp 2579–2590. https://doi.org/10.1007/s00253-015-7218-5.

(37) Ellis, J. M.; Campbell, M. E.; Kumar, P.; Geunes, E. P.; Bingman, C. A.; Buller, A. R. Biocatalytic Synthesis of Non-Standard Amino Acids by a Decarboxylative Aldol Reaction. *Nat Catal* **2022**, *5* (2), 136–143. https://doi.org/10.1038/s41929-022-00743-0.

(38) Hai, Y.; Chen, M.; Huang, A.; Tang, Y. Biosynthesis of Mycotoxin Fusaric Acid and Application of a PLP-Dependent Enzyme for Chemoenzymatic Synthesis of Substituted l -Pipecolic Acids. *J Am Chem Soc* **2020**, *142* (46), 19668–19677. https://doi.org/10.1021/jacs.0c09352.

(39) Chen, Q.; Chen, X.; Feng, J.; Wu, Q.; Zhu, D.; Ma, Y. Improving and Inverting Cβ-Stereoselectivity of Threonine Aldolase via Substrate-Binding-Guided Mutagenesis and a Stepwise Visual Screening. *ACS Catal* **2019**, *9* (5), 4462–4469. https://doi.org/10.1021/acscatal.9b00859.

(40) Wang, L.; Xu, L.; Su, B.; Lin, W.; Xu, X.; Lin, J. Improving the Cβ Stereoselectivity of L-Threonine Aldolase for the Synthesis of l-Threo-4-Methylsulfonylphenylserine by Modulating the Substrate-Binding Pocket To Control the Orientation of the Substrate Entrance. *Chemistry - A European Journal* **2021**, *27* (37), 9654–9660. https://doi.org/10.1002/chem.202100752.

(41) Zha, R.; Lei, B.; Ma, J.; Zhang, Z.; Pan, Y.; Wang, B.; Qi, N. Improving the Cβ Stereoselectivity of L-Threonine Aldolase for the Preparation of L-Threo-3,4-Dihydroxyphenylserine, a Powerful Anti-Parkinson's Disease Drug. *Biochem Eng J* **2023**, *191*. https://doi.org/10.1016/j.bej.2022.108766.

(42) He, Y.; Li, S.; Wang, J.; Yang, X.; Zhu, J.; Zhang, Q.; Cui, L.; Tan, Z.; Yan, W.; Zhang, Y.; Tang, L.; Da, L. T.; Feng, Y. Discovery and Engineering of the L-Threonine Aldolase from Neptunomonas Marine for the Efficient Synthesis of β-Hydroxy-α-Amino Acids via C-C Formation. *ACS Catal* **2023**, *13* (11), 7210–7220. https://doi.org/10.1021/acscatal.3c00672.

(43) Kimura, T.; Vassilev, V. P.; Shen, G.-J.; Wong, C.-H. *Enzymatic Synthesis Of-Hydroxy-R-Amino Acids Based on Recombinant D-and L-Threonine Aldolases*; 1997. https://pubs.acs.org/sharingguidelines.

(44) Wang, S.; Deng, H. Peculiarities of Promiscuous L-Threonine Transaldolases for Enantioselective Synthesis of β-Hydroxy-α-Amino Acids. https://doi.org/10.1007/s00253-021-11288-w/Published.

(45) Murphy, C. D.; O'Hagan, D.; Schaffrath, C. Identification of a PLP-Dependent Threonine Transaldolase: A Novel Enzyme Involved in 4-Fluorothreonine Biosynthesis in Streptomyces Cattleya. *Angewandte Chemie - International Edition* **2001**, *40* (23), 4479–4481. https://doi.org/10.1002/1521-3773(20011203)40:23<4479::AID-ANIE4479>3.0.CO;2-1.

(46) Barnard-Britson, S.; Chi, X.; Nonaka, K.; P. Spork, A.; Tibrewal, N.; Goswami, A.; Pahari, P.; Ducho, C.; Rohr, J.; G. Van Lanen, S. C. *J Am Chem Soc* **2012**, *134* (45), 18514–18517. https://doi.org/10.1021/ja308185q.

(47) Schaffer, J. E.; Reck, M. R.; Prasad, N. K.; Wencewicz, T. A. β-Lactone Formation during Product Release from a Nonribosomal Peptide Synthetase. *Nat Chem Biol* **2017**, *13* (7), 737–744. https://doi.org/10.1038/nchembio.2374.

(48) Scott, T. A.; Heine, D.; Qin, Z.; Wilkinson, B. An L-Threonine Transaldolase Is Required for L-Threo-β-Hydroxy-α-Amino Acid Assembly during Obafluorin Biosynthesis. *Nat Commun* **2017**, *8* (May), 1–11. https://doi.org/10.1038/ncomms15935.

(49) Scott, T. A.; Batey, S. F. D.; Wiencek, P.; Chandra, G.; Alt, S.; Francklyn, C. S.; Wilkinson, B. Immunity-Guided Identification of Threonyl-TRNA Synthetase as the Molecular Target of Obafluorin, a β-Lactone Antibiotic. *ACS Chem Biol* **2019**, *14* (12), 2663–2671. https://doi.org/10.1021/acschembio.9b00590.

Chapter 2

Characterization of glycyl quinonoid intermediates

Content in this chapter is adapted from the following published work:

Kumar, P.;* **Meza, A.**;* Ellis, J. M.; Carlson, G. A.; Bingman, C. A.; Buller, A.R. “L-Threonine transaldolase activity is enabled by a persistent catalytic intermediate.” *ACS Chemical Biology*. 2021. 16, 86-95. *These authors contributed equally

This collaborative project was initiated by Dr. Prasanth Kumar. I was able to join the project and contribute mechanistic experiments while crystallographic studies were done in collaboration with Prof. Andrew Buller and Dr. Craig Bingman.

Chapter 2: Characterization of LTTA (ObiH)

2. 1. Introduction

L-Threonine transaldolases (LTTAs) and L-Threonine aldolases (LTAs) are mechanistically related pyridoxal-5′-phosphate (PLP) dependent enzymes. Enzymes from both classes catalyze retroaldol cleavage of L-Threonine (Thr) yielding an enzyme-bound glycyl quinonoid E(Q^{Gly}) intermediate, an electron rich, carbanion like species (Figure 1). LTAs catalyze protonation of the E(Q^{Gly}) intermediate, resulting in the thermodynamically favorable breakdown of Thr into glycine (Gly) and acetaldehyde. In contrast LTTAs that catalyze retroaldol cleavage of Thr and a subsequent aldol-like addition into an aldehyde to form a new side chain, setting the stereochemistry of the Cβ-OH group for a new amino acid (Figure 2a). The first LTTA to be discovered was the fluorothreonine transaldolase (FTA) from *Streptomyces cattleya*, which forms 4-fluoro-threonine from Thr and fluoroacetaldehyde.[1] Nucleoside antibiotics can also be formed through the action of LTTAs that transpose the side chain of Thr with the C5' aldehyde of a nucleoside.[2,3] Recently, two groups discovered in parallel that an LTTA, ObiH, reacts with *p*-nitrophenylacetaldehyde en route to obafluorin, a β-lactone aminoacyl tRNA synthetase inhibitor (Figure 2b).[4–6]

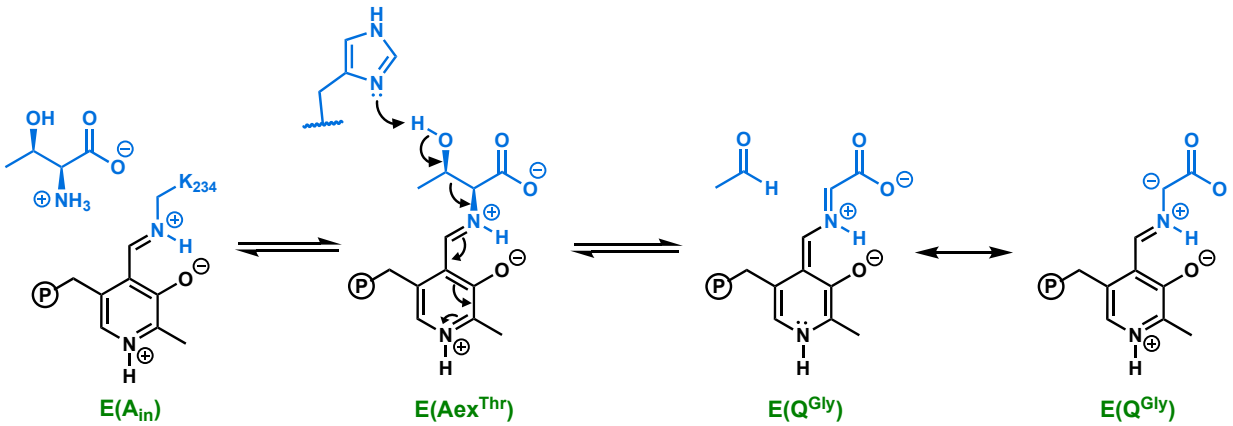

Figure 1: Generation of glycyl quinonoid E(Q^{Gly}) intermediate. Thr binds to PLP cofactor forming the external aldimine E(Aex^{Thr}). Deprotonation of the hydroxyl side chain by a conserved histidine (His) residue results in cleavage of the Cα-Cβ bond and formation of the the glycyl quinonoid intermediate, an electron rich, carbanion like intermediate.

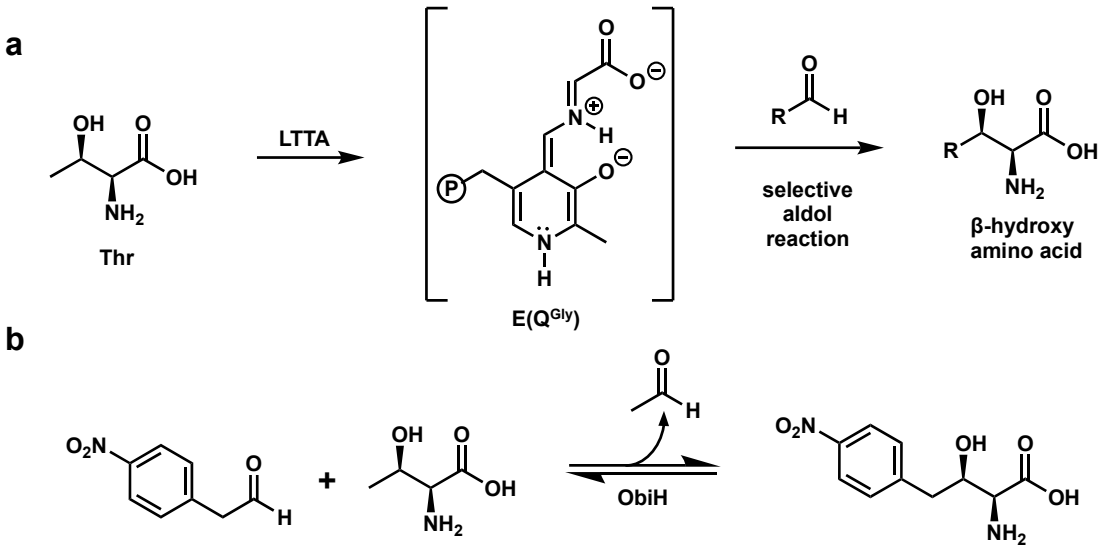

Figure 2: LTTA reactions. a) LTTAs break down Thr and catalyze stereoselective aldol addition into aldehydes, setting the stereochemistry at Cα and Cβ. **b)** Native ObiH reaction. β-hydroxy-*p*-nitro-homophenylalanine (right) is synthesized from p-nitrophenylacetaldehyde (left).

The mechanism of LTTA enzymes has not been studied in detail, and no structures are available. A mechanism has been proposed based on analogy to the homologous LTA and serine hydroxymethyltransferase (SHMT) enzymes, which perform related transformations.[7] This reaction begins with covalent capture of Thr as an external aldimine with PLP, E(Aex^{Thr}).[8] The enzyme orients the sidechain of Thr such that it is periplanar to the π-system of the cofactor, in accordance with Dunathan's stereoelectronic hypothesis.[9,10] Retroaldol cleavage is initiated by deprotonation of the hydroxyl side chain by a conserved histidine (His) residue that π-stacks with the cofactor, either directly or through a proton relay with water.[8] Cleavage of the Cα-Cβ bond releases acetaldehyde and the resultant Cα carbanion is stabilized through resonance as a highly basic glycyl quinonoid intermediate, E(Q^{Gly}).[8] The glycyl quinonoid is subsequently protonated to form the external aldimine of glycine, E(Aex^{Gly}), which is released to complete the catalytic cycle. The LTA reaction can be reversed to run in the synthetic direction in vitro by adding excess glycine and aldehyde. These enzymes have been shown to form diverse β-hydroxy amino acids, setting

two stereocenters in the process.[8,11,12] However, the reversibility of the reaction and its relatively modest selectivity leads to scrambling of the stereochemistry at the β-position, limiting synthetic utility.[13–16]

Alternatively, LTTAs cleanly form β-hydroxy amino acids in vivo using the same Thr starting material and PLP cofactor.[17] Although the molecular details have yet to be elucidated, it is believed that these enzymes function by intercepting a highly reactive E(Q^{Gly}) intermediate (Figure 3). Initial studies with the LTTAs demonstrate several promising features for synthetic applications. FTA and ObiH homologs have been shown to react with a variety of aliphatic and aromatic aldehydes.[18,19] In this chapter, I describe UV-vis spectroscopic analysis of ObiH, a model

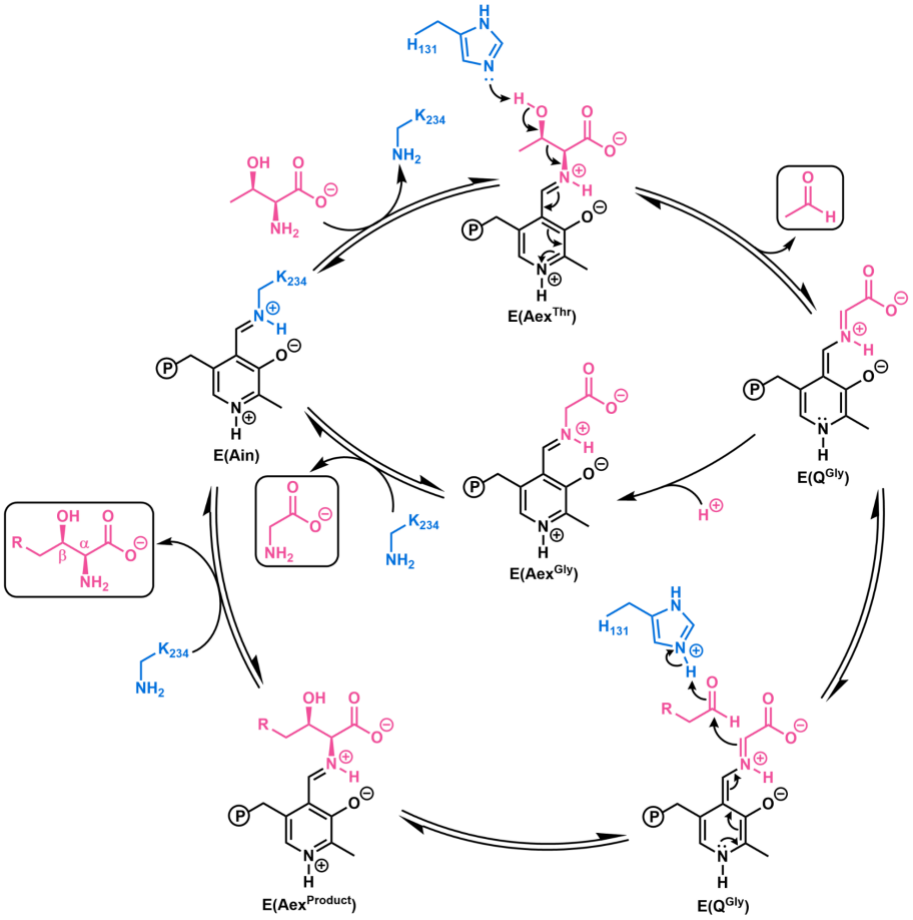

Figure 3: Catalytic mechanism of ObiH. The mechanism of ObiH catalysis with Thr and an aldehyde substrate (outer cycle) along with the disfavored shunt pathway (inner cycle). The PLP cofactor (black) is shown covalently bound either to the substrates/intermediates (pink) or to the relevant catalytic residues of the protein (blue). Figure generated by Prasanth Kumar.

LTTA, and detail key mechanistic findings of the unique reactivity of these enzymes. For completeness I include similar mechanistic and activity analysis of *Thermotoga maritima* threonine aldolase (*Tm*LTA), a previously-studied LTA.

2. 2. Results and Discussion

2. 2. 1. Spectroscopic analysis of PLP-Bound ObiH

Cloning and heterologous expression of *N*-His-ObiH in *E. coli* was completed by Prasanth Kumar, as was previously described.[20] Consistent with previous reports, the ObiH protein solution was pink in color whereas other PLP-dependent enzymes are yellow.[4,19,20] The UV-vis spectrum of ObiH at pH 8.5 shows a peak at 415 nm, characteristic of the covalently bound internal aldimine adduct E(Ain), as well as an additional peak at 515 nm, whose intensity varied between independent preparations of ObiH, that accounts for the pink color (Figure 4a). In early spectroscopy studies, it was noted that the absorbance spectra of purified ObiH varied as function of pH. At pH 7.0, the spectra of ObiH shows a peak at 340 nm in addition to the 415 and 515 nm peaks (Figure 4b). Interestingly, increasing the pH from 7.0 to 8.5 did not result in immediate transformation of the ObiH spectrum. Over the course of several minutes, this 340 nm band decreased and the 415 nm band increased, indicative of a slow isomerization between the

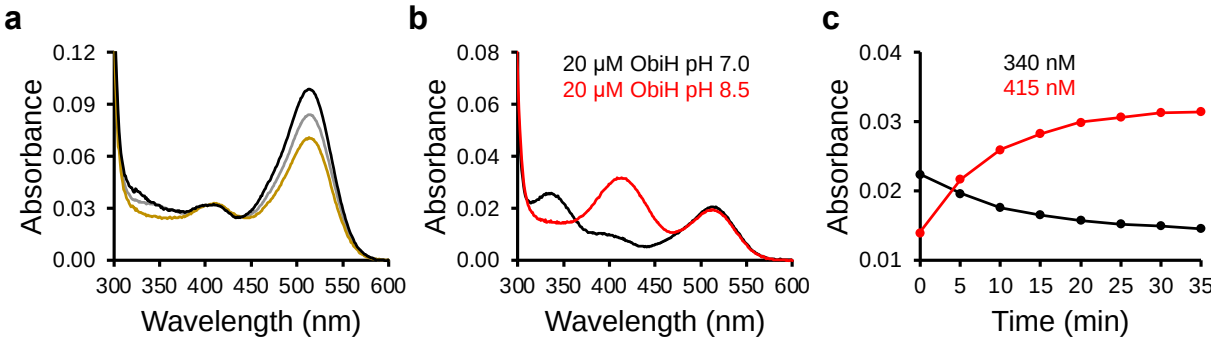

Figure 4. Spectroscopic analysis of PLP-bound ObiH. a) UV-vis spectra of as purified ObiH from three different preps following identical protocol. Variable amount of 515 nm species was observed between preps with 20 μM enzyme. **b)** UV-vis spectra of ObiH at pH 7.0 (black) and pH 8.5 (red). **c)** 340 μM ObiH in 100 mM KPi (pH 7.0) was diluted 17-fold into 100 mM KPi (pH 8.5). Spectra were gathered every 5 min. Signal at 415 nm (red) increases as signal at 340 nM

enolimine and ketoenamine forms of the cofactor, respectively (Figure 4c).[21] While proton transfers are typically fast, we hypothesized that this apparent tautomerization is coupled to a slower exchange process, such as a conformational or oligomeric change.

2. 2. 2. Photoexcitation of ObiH yields highly active catalyst

During our studies, it was observed that ObiH stock solutions slowly lost their pink color during the day. Intrigued by this unusual behavior, we placed a sample of purified ObiH in direct sunlight for 30 min, which transformed into a traditional yellow protein (Figure 5a). UV−vis analysis revealed complete abolishment of the 515 nm band and an increase at 415 nm. We also observed a decrease in the 515 nm species upon heating of ObiH at 37 °C (Figure 5b).

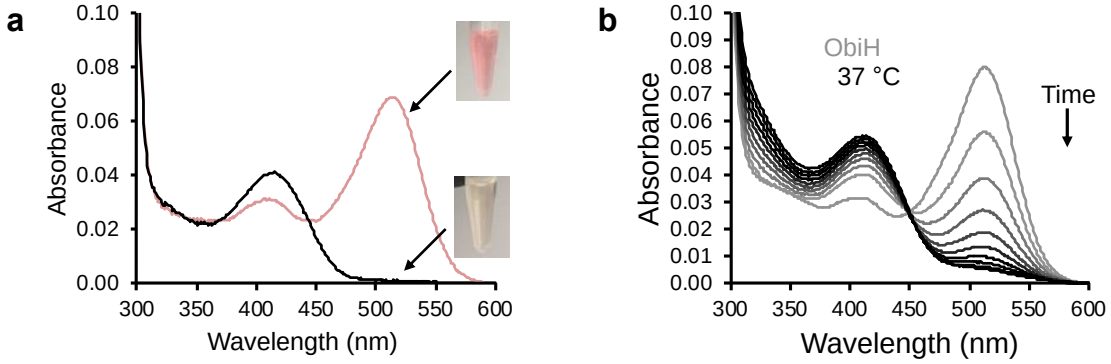

Figure 5. Effect of green light irradiation on ObiH catalytic states. a) Absorbance spectra of natively purified ObiH (pink) and phototreated ObiH (black). Phototreatment results in the complete loss of the 515 nm species and increase in the E(Ain) peak at 415 nm. Images of ObiH stock solutions before and after phototreatment. **c)** Incubation of as isolated ObiH at 37 ºC results in loss of 515 nm species. Traces gathered every 20 min over a 3 h time course.

To minimize the possibility of stochastic protein aggregation at higher temperature, we relied on phototreatment to produce homogeneous ObiH. To further increase reproducibility, purified ObiH was exposed to an 8 W, green LED for 10 min on ice, which led to the rapid and reproducible photoablation of the 515 nm peak and a temporary increase at 340 nm (Figure 6a). Consistent with previous experiments, the 340 nm band decreased and the 415 nm band increased. After isomerization of the 340 and 415 nm species, a small population of 515 nm species reformed. A second round of phototreatment removed the small amount of 515 nm

species leaving an ObiH spectra which only contained the 415 nm peak (Figure 6b). After storage at 4 °C overnight, phototreated ObiH samples equilibrated back to a mixture of states including the 515 nm species (Figure 6c).

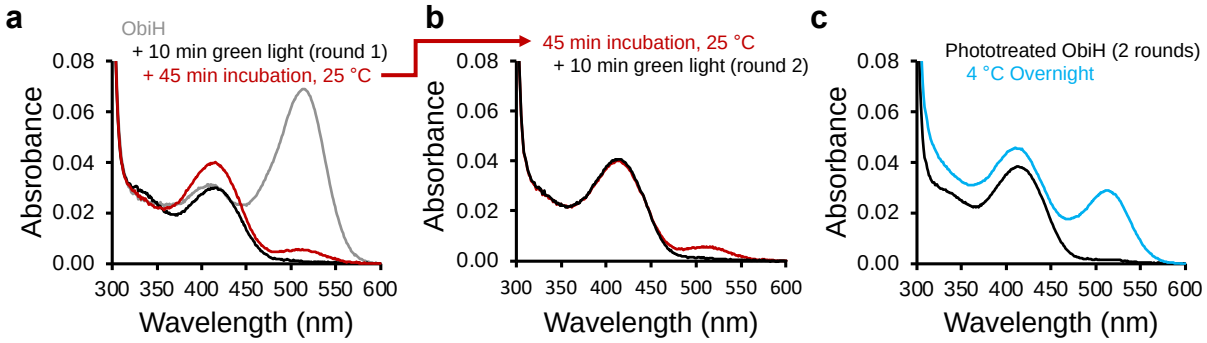

Figure 6. Phototreatment produces homogeneous ObiH. a) 1st round of phototreatment. 20 µM as-isolated ObiH (grey). Phototreatment with green light for 10 min results in complete ablation of 515 nm peak (black) and an increase at 340 nm. After 45 min (dark red), the 340 nm peak decreased as the 415 nm peak and the 515 nm increased. **b) 2nd round of phototreatment.** ObiH that had small peak at 515 nm (dark red) was photo-treated with green light for a second time to remove residual 515 nm species. Spectra 10 min after the second round of photo-treatment showed no residual 515 nm peak (black). **c)** Overnight incubation of phototreated ObiH resulted in the regeneration of the 515 nm species. Phototreated ObiH (black), and phototreated ObiH after overnight storage at 4 °C (blue).

To assess whether the phototreatment increases the concentration of active enzymes and not some other species, we measured the initial velocity of ObiH with isobutyraldehyde before and after phototreatment. Gratifyingly, we observed an approximate 2-fold increase in the rate of product formation with the phototreated enzyme (Figure 7). These data strongly suggest that heterologously expressed ObiH purifies as a mixture of chemically distinct states that can be photointerconverted and that the species absorbing at 515 nm is not catalytically active. Nevertheless, the phototreatment process afforded us the opportunity to cleanly assay the mechanistic properties of ObiH as a model LTTA.

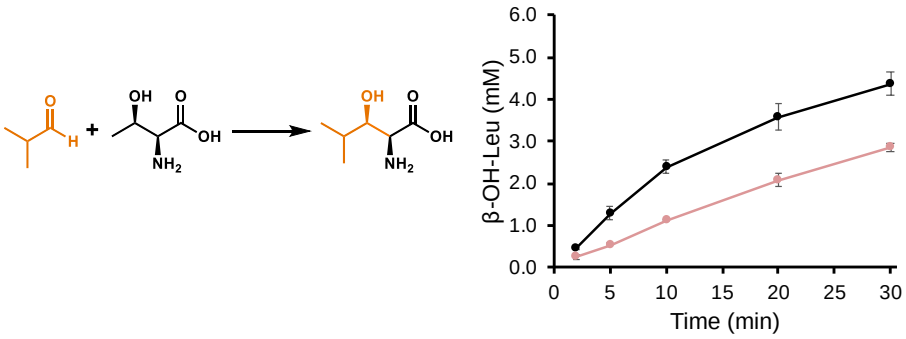

Figure 7. Activity analysis of phototreated ObiH. Comparison of product formation of (2*S*,3*R*)-β-hydroxyleucine between as isolated ObiH (pink) and phototreated ObiH (black). Corresponding reaction is shown on left. Phototreated ObiH had a 2-fold increase in initial turnover rate compared to as-isolated enzyme.

2. 2. 3. ObiH forms a kinetically shielded glycyl quinonoid

Previous steady-state kinetic analysis of ObiH established that the enzyme has a relatively high KM for Thr, 40 mM.[4] We began our detailed mechanistic study by adding 100 mM Thr to ObiH and monitored the reaction by UV−vis spectroscopy (Figure 8). The addition of Thr resulted

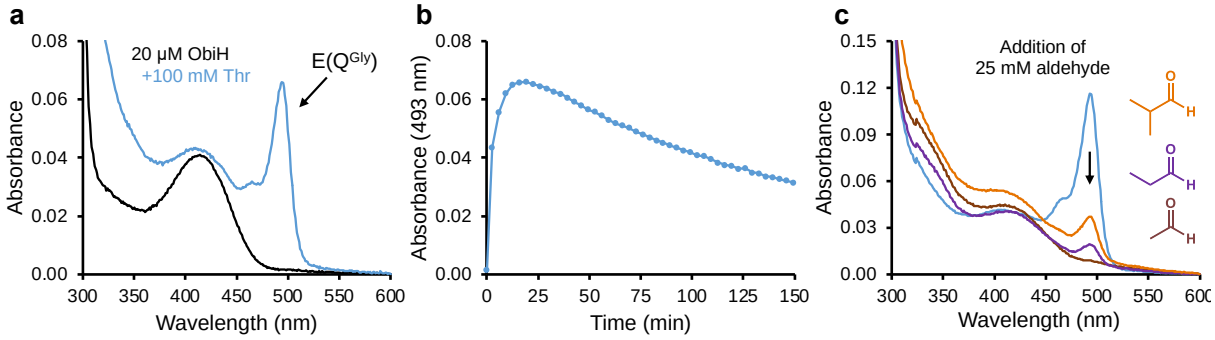

Figure 8. Spectroscopic characterization of ObiH catalytic intermediates. a) Absorbance spectra of phototreated ObiH (black) and after addition of Thr (blue). Addition of Thr results in large peak at 493 nm, E(Q^{Gly}). **b)** Plot of absorbance at 493 nm vs time after addition of Thr. 493 nm peak increases rapidly before reaching a maximum with subsequent decay over hours. **c)** On cycle reactivity of E(Q^{Gly}) with aliphatic aldehydes. A representative absorbance spectrum (average absorption spectra between 3 experiments) of ObiH after addition of Thr is shown in blue. Subsequent addition of acetaldehyde (brown), propanal (purple), or isobutyraldehyde (orange) results in substantial reduction of the 493 nm peak.

in an intense absorbance with λ_{max} = 493 nm, characteristic of a PLP quinonoid adduct (Figure 8a). We assign this species as E(Q^{Gly}), which is formed by retroaldol cleavage of a covalently bound PLP-Thr adduct, E(A_{ex}^{Thr}). We also performed this experiment with as-isolated enzymes (before phototreatment) and observed that the 515 nm peak was unchanged by reaction conditions. Further, as isolated enzymes formed a less intense E(Q^{Gly}) band, consistent with a lower population of the catalytically active enzyme (Figure 9).

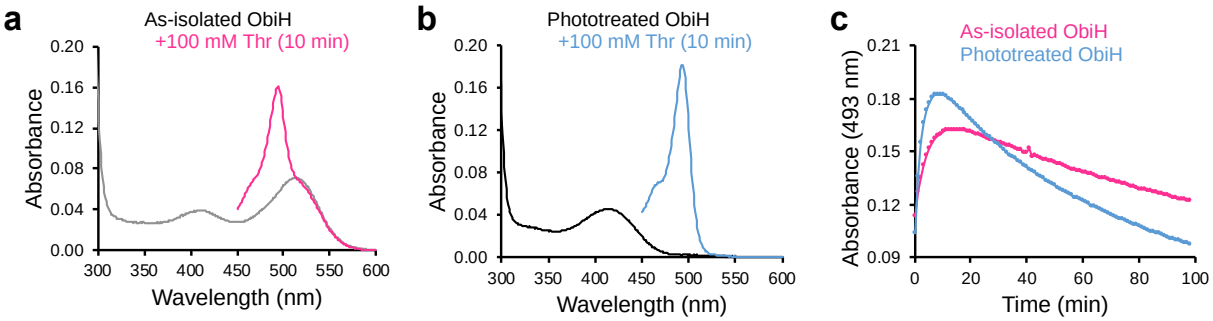

Figure 9. Photo-treatment of ObiH produces a larger population of E(Q^{Gly}). a) Spectra of as-isolated ObiH (grey). Spectra 10 min after the addition of 100 mM Thr (pink) **b)** Spectra of phototreated ObiH (black). Spectra 10 min after the addition of 100 mM Thr (blue). **c)** Absorbance at 493 nm over time for photo-treated (blue) and as isolated ObiH (pink). Addition of 100 mM Thr results in larger peak at 493 nm for phototreated (blue) than as isolated ObiH (pink). Spectra were gathered every minute from 450-600 nm.

The E(Q^{Gly}) absorbance band increased for several minutes before reaching a maximum and slowly decayed over the course of several hours (Figure 8b). To further probe the kinetics of the formation and breakdown of this species, we repeated the experiment with varied concentrations of Thr. Increasing the concentration of Thr above 100 mM resulted in a similarly intense E(Q^{Gly}) band, and lower concentrations of Thr significantly reduced the population of E(Q^{Gly}) (Figure 10).

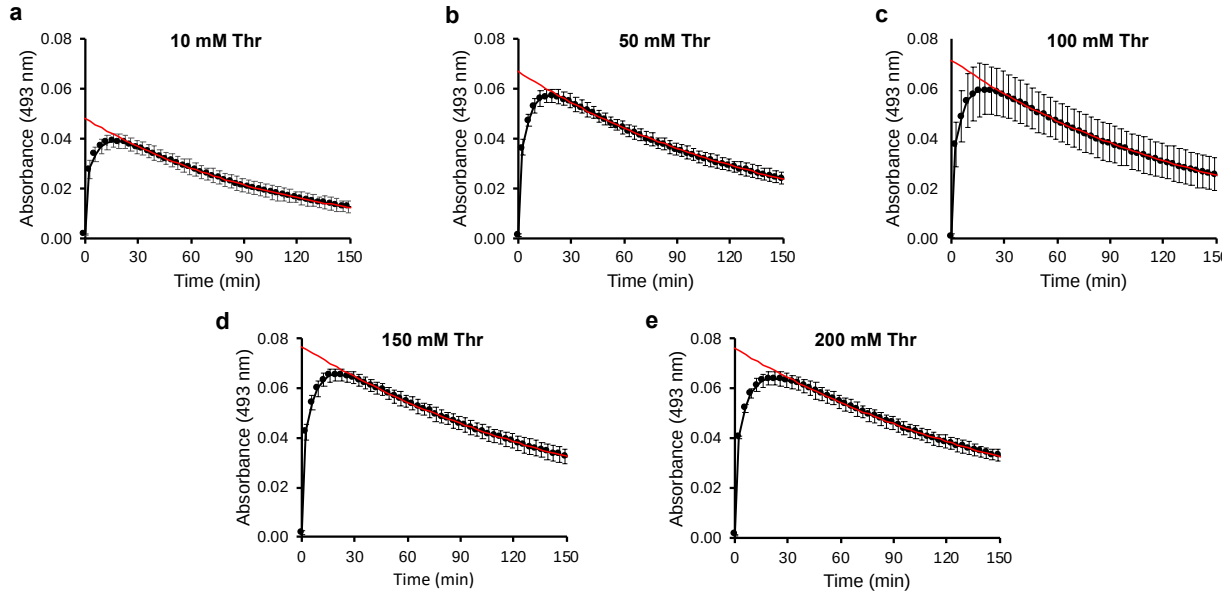

Figure 10. E(Q^{Gly}) population is dependent on concentration of Thr. Absorbance at 493 nm over time after the addition of 10 mM Thr **(a)**, 50 mM Thr **(b)**, 100 mM Thr **(c)**, 150 mM Thr **(d)**, and 200 mM Thr **(e)** to 20 μM ObiH. Experiments were performed in triplicate. 1st order decay was fit to the data from ~33-150 min.

We performed a global kinetic analysis of the time course for E(Q^{Gly}) formation and decay across a range of Thr concentrations using a three-state kinetic model with reversible Thr binding and retro aldol cleavage, followed by an irreversible decay event. However, this simple model decisively failed to fit the data. Hence, additional studies that can substantiate a more sophisticated model will be required to account for the slow formation of E(Q^{Gly}). Once formed, however, the reactivity of E(Q^{Gly}) cleanly fit to a single exponential with a half-life of 165 ± 20 min for concentrations ≥100 mM Thr (Figure 10). Given the time scale of this decay, many potential pathways may be responsible for the quenching of this species. We hypothesized that, in analogy to the distantly related LTA enzymes, E(Q^{Gly}) reacted through simple protonation to form the glycyl external aldimine, E(Aex^{Gly}).[8] Consistent with this hypothesis, kinetic analysis at lower pH showed a substantially faster quinonoid decay (Figure 11). In the absence of an electrophile substrate, ObiH formed a small, but measurable amount of Gly, corresponding to <50 turnovers in 16h. Glycine formation was completed by Prasanth Kumar.

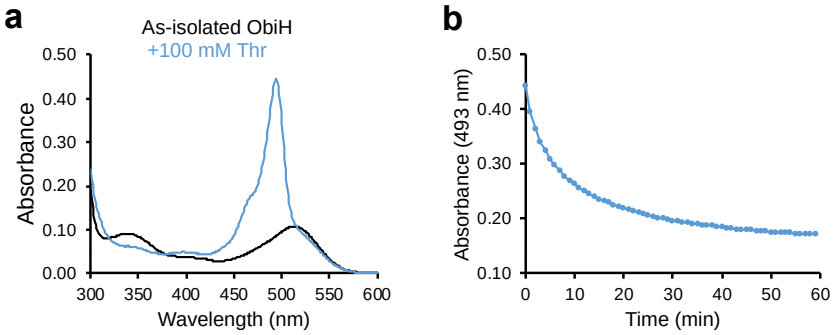

Figure 11. E(Q^{Gly}) decay at pH 7.0. a) ObiH was diluted to 20 µM into 100 mM Tris-HCl, pH 7.0 (black). Addition of 100 mM Thr resulted in a large peak at 493 nm (blue). **b)** absorbance at 493 nm over time reveals maximum quinonoid upon mixing and subsequent decay with over

To further confirm that Gly is formed through an ObiH mediated process, we added Thr to ObiH to form a large population of E(Q^{Gly}) and then reductively trapped the decay product as a secondary amine via the addition of $NaBH_4$. This reaction was monitored both spectrophotometrically and via UPLC-MS. Spectroscopic experiments showed depletion of the absorbing species in the range of 400−420 nm, indicating that the imines present E(A_{ex}^{Thr}), E(A_{ex}^{Gly}), or unreacted E(Ain) were rapidly reduced by $NaBH_4$ (Figure 12).

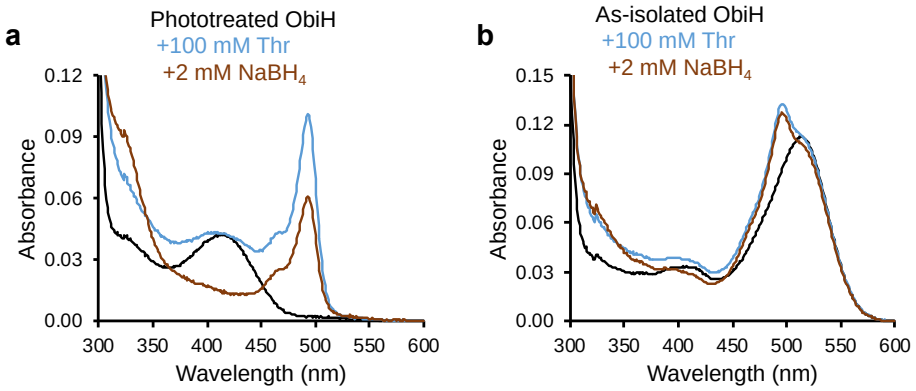

Figure 12. E(Q^{Gly}) and E(Q^{in}) are resistant to $NaBH_4$ reduction. Spectrum of phototreated ObiH (black). 100 mM Thr was added and E(Q^{Gly}) peak increased to a maximum at 10 min (blue). 2 mM $NaBH_4$ was then added and spectra were gathered every minute for 30 min. Spectra of reaction 25 min after the addition of $NaBH_4$ (brown) shows at increase at 340 nm and a decrease at 415 nm, as well as a large population of E(Q^{Gly}). **b)** Spectrum of 20 µM as-isolated ObiH (black). 100 mM Thr was added and E(Q^{Gly}) peak increased to a maximum at 10 min (blue). 2 mM $NaBH_4$ was then added to the reaction and spectra were gathered every minute for 30 min. Spectra of reaction 25 min after the addition of $NaBH_4$ (brown) shows the the 515 nm species was unchanged in the presence of $NaBH_4$.

A new absorbance band at 340 nm appeared, consistent with formation of a reduced, secondary amine adduct.[22] However, the E(Q^{Gly}) species (493 nm), which is electron-rich, was not immediately reduced by $NaBH_4$ and decayed at a similar rate to reactions containing only Thr. Notably, this experiment was performed with protein that had not undergone phototreatment and therefore retained the 515 nm absorbing species that can photoconvert to E(Ain). Whereas E(Q^{Gly}) was slowly depleted, presumably through an intermediate protonation step, the 515 nm band was completely resistant to reduction with $NaBH_4$. While the above data show that E(Q^{Gly}) is kinetically slow to react, they offer only indirect information on the thermodynamic stability of this intermediate. We therefore probed the effect of saturating Gly (1.0 M) on E(Ain) and observed no evidence of quinonoid formation, indicating that population of E(Q^{Gly}) is not enabled by thermodynamic stabilization in the enzyme active site (Figure 13). Instead, these data establish that E(Q^{Gly}) species is a kinetically trapped, high-energy intermediate.

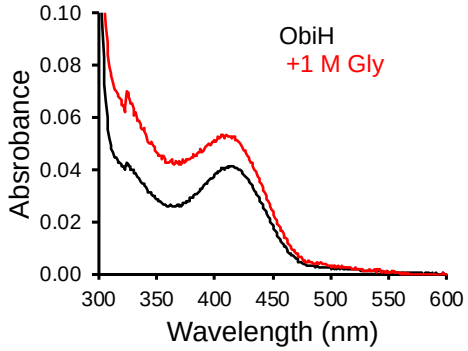

Figure 13. ObiH does not catalyze the retroaldol cleavage of Gly to form E(Q^{Gly}). Spectrum of 20 μM phototreated ObiH (black). 1 M Gly was added and spectra were acquired every 1 minute for 15 minutes. 10 min after addition of 1 M Gly (red) shows no evidence of a peak at 493 nm.

2. 2. 4. The ObiH Quinonoid Rapidly Reacts to Form

The native electrophile in the ObiH reaction is *p*-nitrophenylacetaldehyde, which is generated via a thiamine-dependent decarboxylation from the corresponding α-keto acid.[4,5] However, due to the inherent instability of arylacetaldehydes, we sought an alternative

electrophile for our mechanistic studies. Recent experiments using a biocatalytic cascade showed ObiH, as well as its downstream enzymes in obafluorin biosynthesis, can react with a range of aliphatic and benzylic aldehydes.[23] While the synthetic utility of ObiH with aromatic aldehydes has been recently reported,[24,25] we were drawn to the reaction with aliphatic aldehydes as mechanistic probes because they do not have confounding signals in their UV−vis spectra. We probed the on-path reactivity of ObiH via addition of reactive aldehyde to preformed E(Q^{Gly}). The addition of 25 mM acetaldehyde showed the rapid reaction of E(Q^{Gly}) within the mixing time of the experiment (<20 s) and the persistence of a small, steady population of quinonoid (Figure 14a, red). Because acetaldehyde reacts to reform the Thr starting material, a dynamic equilibrium is established. We repeated this experiment, titrating the active site with acetaldehyde and measuring the population of E(Q^{Gly}). These data fit cleanly to a single site binding isotherm, which indicates that acetaldehyde binds to E(Q^{Gly}) with a K_D of 430 ± 15 μM (Figure 14c).

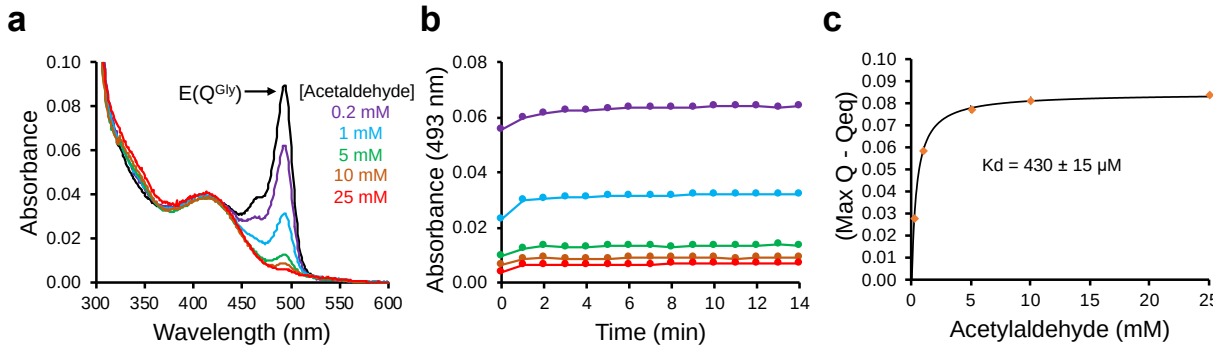

Figure 14. E(Q^{Gly}) rapidly reacts with acetaldehyde before reaching equilibrium. a) representative spectra (Spectra represents average of 5 experiments containing 20 μM ObiH + 100 mM Thr prior to the addition of acetaldehyde) of phototreated ObiH 5 minutes after the addition of Thr (black). Addition of 0.2 mM (purple), 1 mM (blue), 5 mM (green), 10 mM (brown), and 25 mM (red) acetaldehyde results in loss of the 493 peak. Spectra represent reaction 3 minutes after the addition of acetaldehyde. **b)** Absorbance over time at 493 nm after addition of + 0.2 mM (purple), 1 mM (blue), 5 mM (green), 10 mM (brown), and 25 mM (red) acetaldehyde. **c)** K_D of acetaldehyde for E(Q^{Gly}) was calculating by plotting the average maximum quinonoid minus the quinonoid population at equilibrium as a function of acetaldehyde concentration. K_D was calculated to be 430 ± 15 μM.

We next probed the reaction of E(Q^{Gly}) with different aliphatic aldehydes and measured the resulting steady-state quinonoid population. The addition of propanal resulted in a rapid loss of E(Q^{Gly}), but the steady-state population was higher than was observed in the acetaldehyde reaction (Figure 15). The addition of isobutyraldehyde differed from the previous two substrates

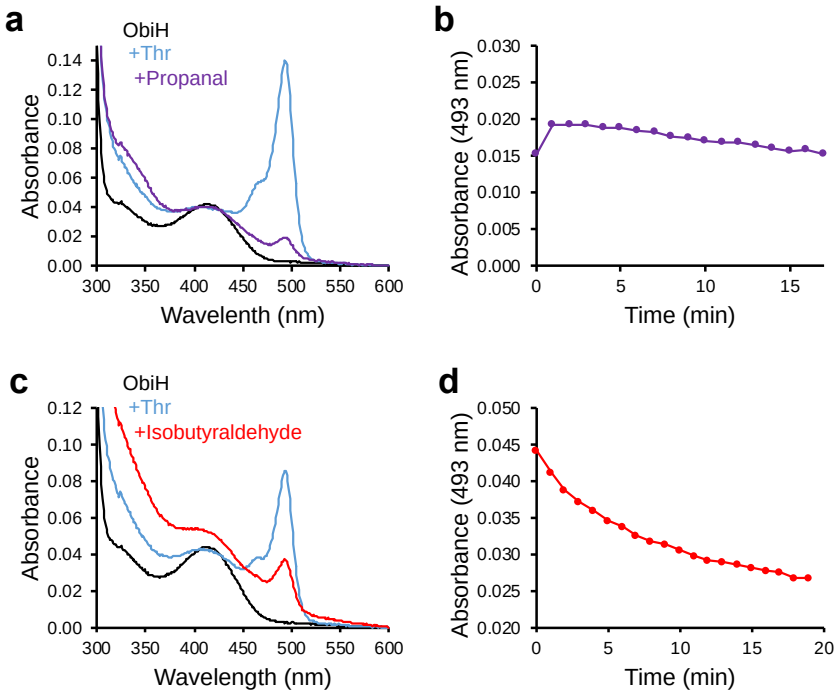

Figure 15. E(Q^{Gly}) reacts with aliphatic aldehydes. a) Spectra of phototreated ObiH (black). Spectra of ObiH + Thr 10 minutes after addition of Thr (blue). Addition of 25 mM propanal results in substantial reduction of E(Q^{Gly}) population (purple). Spectra represents reactions 3 minutes after the addition of aldehyde. **b)** Absorbance at 493 nm over time after the addition of propanal. **c)** Spectra of phototreated ObiH (black). Spectra of ObiH + Thr 10 minutes after addition of Thr (blue). Addition of 25 mM isobutyraldehyde results in reduction of E(Q^{Gly}) population (red). Spectra represents reactions 3 minutes after the addition of aldehyde. **d)** Absorbance at 493 nm over time after the addition of isobutyraldehyde.

and revealed that isobutyraldehyde reacts in at least two phases. Approximately half of the population of E(Q^{Gly}) is depleted in the mixing time of the experiment. The remaining fraction reacts more slowly, reaching the steady state over the course of 20 min. Subsequent data establish that this aldehyde does react through a productive catalytic cycle to form a β-hydroxy amino acid product (*vide infra*). Other effects that occur on slow time scales, such as protonation to form Gly, however, confound further interpretation of these data.

To characterize the full catalytic cycle in action, we monitored product formation over time using isobutyraldehyde. UPLC-MS analysis of reactions with isobutyraldehyde showed a single peak corresponding to β-hydroxy-Leu, indicative of a highly diastereoselective reaction. The reaction proceeded slowly and reached a 71% yield after 24 h. To confirm the identity of the product, we performed an overnight preparative scale reaction on the 5 mmol scale using 0.04 mol % catalyst. Purification of the β-hydroxy-Leu proved to be challenging. β-hydroxy-Leu and Thr had similar retention times by C18 flash chromatography, which necessitated multiple rounds of chromatography to isolate the pure product and resulted in isolation of 141 mg of β-hydroxy-leucine, corresponding to a 38% isolated yield. NMR analysis revealed a >98:2 diastereomeric ratio (dr) of syn/anti products. ObiH, like other fold type-I PLP dependent enzymes, is known to have exquisite selectivity for the 2*S* configuration.[26,27] Therefore, we assign this product as (2*S*,3*R*)-β-hydroxy-Leu, consistent with other studies of ObiH selectivity.[28] To probe the reactivity of this amino acid with ObiH, we added 25 mM β-hydroxy-Leu and observed a low population of E(Q^{Gly}) that formed slowly over the course of 30 min. These data demonstrate that the β-hydroxy-Leu product does not readily re-enter the catalytic cycle (Figure 16).

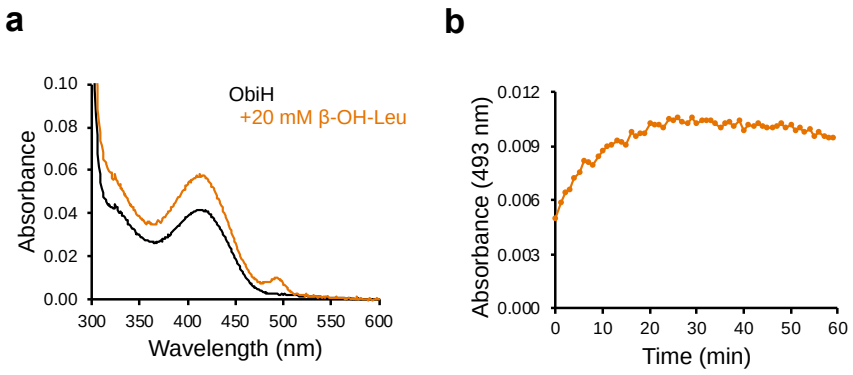

Figure 16. A small population of E(Q^{Gly}) is formed upon addition of β-OH-Leu. a) Spectra of phototreated ObiH (black). Addition of 20 mM β-OH-Leu (orange) produces a small population of E(Q^{Gly}) at 493 nm. **b)** Absorbance at 493 nm over time.

2. 2. 5. Analysis of LTA

This chapter has predominantly focused on the mechanistic characterization of ObiH as a model LTTA. In numerous sections, we referenced similar and contrasting proprieties of ObiH to LTA enzymes as reported in the literature.[8,11–16] Here I provide mechanistic and activity characterization of a well-studied LTA from *Themotoga maritima* (*Tm*LTA), a low specificity L-threonine/L-*allo*-threonine aldolase.[10] We began by adding 100 mM Thr and *allo*-Thr to *Tm*LTA and monitored the reactions by UV–vis spectroscopy. Both substrates produced a modest peak at 495 nm with *allo*-Thr producing a two-fold larger signal than Thr (Figure 17). As we monitored the reaction over time with Thr and *allo*-Thr, the signal corresponding to E(Q^{Gly}) converged in both reactions within 15 min. We repeated the reaction with Gly as substrate and noted a much large E(Q^{Gly}) population that was constant throughout the reaction, indicating that the E(Q^{Gly}) in *Tm*LTA is thermodynamically stable.

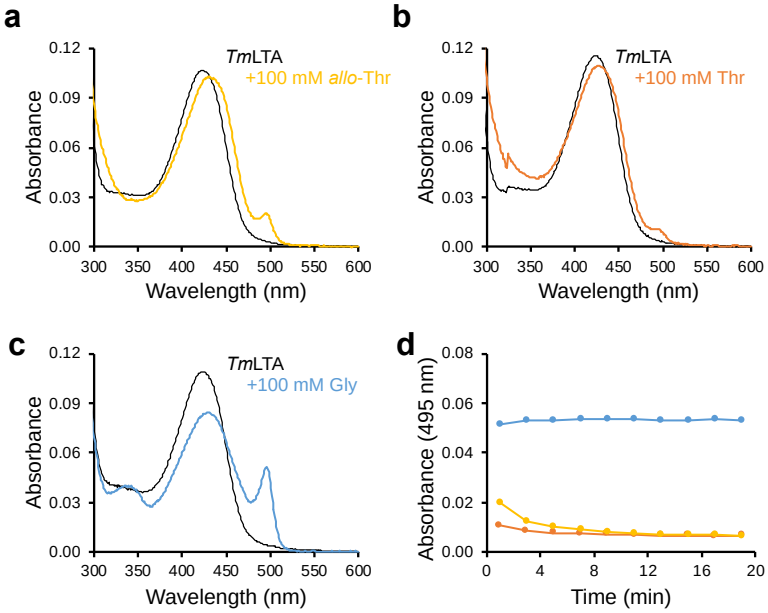

Figure 17: Spectroscopic characterization of *Tm*LTA catalytic intermediates. Absorbance spectra of *Tm*LTA prior to addition of substrate is shown in black. **a)** Absorbance spectra of *Tm*LTA with 100 mM *allo*-Thr (gold). **b)** Absorbance spectra of *Tm*LTA with 100 mM Thr (copper). **c)** Absorbance spectra of *Tm*LTA with 100 gly (blue). **d)** Plot of absorbance at 495 nm vs time after addition of *allo*-Thr (gold), Thr (copper) and Gly (blue).

2. 3. Conclusions

One of the most striking observations about ObiH, by us and others,[5,23] is the beautiful and uncommon pink color of the heterologously expressed protein. UV-vis analysis indicates the presence of an adduct that absorbs at 515 nm. The λ_{max} of this species is itself highly informative and suggests formation of an extended chromophore with the PLP-cofactor, such as a quinonoid. Indeed, the 515 nm band was originally hypothesized to arise from a small population of tightly bound glycyl quinonoid, E(Q^{Gly}).[5] However, addition of Thr yields a quinonoid with a distinct λ_{max} and the shoulder 515 nm remains, ruling out E(Q^{Gly}) as a co-purifiying species (Figure 9). Instead, we hypothesize this unusual spectral feature arises from a small population of a deprotonated Schiff base adduct, an internal quinonoid E(Qin) (Scheme 2). There are several lines of evidence that support this assignment. Through an as-yet-unknown process, light abolishes this species and increases the concentration of the E(Ain), establishing that the 515 nm species is a PLP adduct and not some trace contaminant (Figure 5). Such reactivity is uncommon, and doubtless will inspire further study, but is consistent with a previous report that light can alter the reactivity of PLP-dependent enzymes.[22] Here, we show the 515 nm species can interconvert to a catalytically active state through both photochemical and thermal means (Figure 5). However, the 515 nm band was inert to reduction with $NaBH_4$, indicating that it is electron rich (Figure 12). Lastly, the structure of ObiH was determined from pink crystals and despite the high, 1.66-Å resolution of the data, no trace of a sterically distinct chromophore was observed, consistent with an isosteric modification.

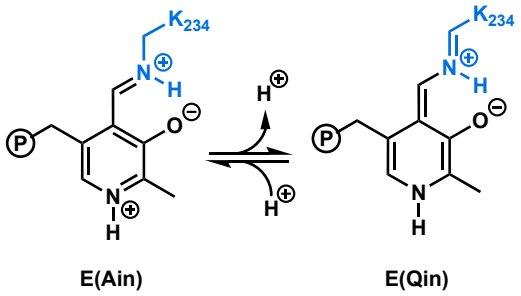

Scheme 2. Formation of protein-bound PLP quinonoid. Deprotonation of lysine at Cε of the internal aldimine, E(Ain) could promote the formation of the internal quinonoid, E(Q^{in}).

Each of the above lines of evidence support assignment of the 515 nm band as E(Qin), but none suggest why this species arises in the first place. Detailed pre-steady-state kinetic experiments conclusively established that the native function of ObiH involves formation of E(Q^{Gly}) (Figure 8). No trace of E(Q^{Gly}) is formed upon addition of Gly to solution indicating this intermediate is highly basic (Figure 13). However, the species persists for hours in the absence of an electrophile and is therefore kinetically shielded from protonation. We speculate these same features that underlie the catalytic reactivity of ObiH may also be responsible for stabilization of an E(Qin) state. While this is a parsimonious explanation, many details of E(Qin) formation remain unclear. What is the role of light and temperature in facilitating the apparent protonation of this species? Is this chemistry unique to ObiH, or common among LTTA enzymes? These and other questions leave fertile ground for future study.

Quinonoid intermediates are nearly ubiquitous among PLsP-dependent enzymes.[29] Some enzymes form thermodynamically stable quinonoids simply by binding substrates, products, or analogs thereof.[30–32] For example, addition of Gly to LTA enzymes results in formation of a thermodynamically stable quinonoid.[33] Other enzymes only transiently form quinonoids and rapid kinetic analysis is needed to observe them.[34] ObiH is exceptional, in that it forms a large population of thermodynamically *unstable* quinonoid. Were protonation and release of Gly to occur, this would be thermodynamically favored in vivo, precluding biosynthesis of new β-hydroxy

amino acids. Hence, there is a selective pressure to kinetically shield E(Q^{Gly}) from protonation. This intermediate rapidly reacts when an aldehyde substrate is added (Figure 8). This scenario also explains an otherwise perplexing observation made by previous studies of LTTA enzymes that Gly does not effectively enter the catalytic cycle: the E(Q^{Gly}) is thermodynamically unstable in LTTA active sites.

While the focus of the present work is on mechanism, experiments with the native *p*-nitrophenylacetaldehyde substrate were hindered by the instability of this compound in water. We therefore sought to probe the ObiH reaction with an α-branched isobutyraldehyde substrate that forms (2*S*,3*R*)-β-hydroxy-Leu. Synthesis of this desirable amino acid analog previously required multi-step methods, which are vastly simplified with this biocatalytic route.[35,36] Notably, initial velocity studies showed ObiH turns over isobutyraldehyde at a rate of 12 min^{-1} (Figure 7). Were the competing protonation pathway facile, formation of β-hydroxy-Leu would be severely limited. Hence, the long lifetime of the E(Q^{Gly}) intermediate enables reactivity with non-native aldehyde substrates.

We envision this mechanistic and structural information will spur future application of ObiH and other LTTA enzymes for preparative scale biocatalysis. Coupled enzyme reactions have shown ObiH can react with phenylacetaldehydes, as well as a handful of simpler aliphatic aldehydes.[23] Studies have also revealed that ObiH and its homologs can react with over a dozen aromatic aldehydes.[23,24] Unlike the LTAs, several of the resulting phenyl serine analogs can be formed with both high yield and excellent dr. Recently, the ObiH homolog, *Ps*LTTA (99% sequence identity) was engineered for improved yield and selectivity en route to (2*S*,3*R*)-*p*-methylsulfonylphenylserine.[24] A double mutant, N35S/C57N, was found that increased activity by 8-fold. The structure and MD simulations of ObiH reported here reveal that Asn35 is in the active site of the enzyme and that Cys57 is within a highly mobile loop. Although this variant has relatively low conversion with other substrates, the availability of structural data may facilitate

targeted engineering approaches to further improve the catalyst. This information, combined with the high expression titer of ObiH and its stability over months at -80 °C, make this enzyme highly attractive for future biocatalytic applications.

2. 4. Materials and Methods

General experimental procedures

Chemicals and reagents were purchased from commercial suppliers (Sigma-Aldrich, VWR, Chem-Impex International, Combi-blocks, Alfa Aesar, New England Biolabs, Zymo Research, Bio-Rad) and used without further purification unless otherwise noted. BL21 (DE3) *E. coli* cells were electroporated with a Bio-Rad MicroPulser electroporator at 2500 V. New Brunswick I26R, 120 V/60 Hz shaker incubators (Eppendorf) were used for cell growth. Optical density and UV-vis measurements were collected on a UV-2600 Shimadzu spectrophotometer (Shimadzu). UPLC-MS data were collected on an Acquity UHPLC with an Acquity QDa MS detector (Waters) using an ACQUITY UPLC CSH BEH C18 column (Waters) or an Intrada Amino Acid column (Imtakt). Preparative flash chromatographic separations were performed on an Isolera One Flash Purification system (Biotage). Proton NMR spectra were recorded on a Bruker AVANCE III-500 MHz spectrometer equipped with a DCH cryoprobe. Proton chemical shifts are reported in ppm (δ) relative to the solvent resonance (D_2O, δ 4.79 ppm). Data are reported as follows: chemical shift (multiplicity [singlet (s), doublet (d), doublet of doublets (dd), multiplet (m)], coupling constants [Hz], integration). All NMR spectra were recorded at ambient temperature (about 25 °C).

Cloning, expression, and purification of ObiH

A codon-optimized copy of the ObiH gene was purchased as a gBlock from Integrated DNA Technologies. This DNA fragment was inserted into a pET-28b(+) vector by the Gibson Assembly method.[37] BL21 (DE3) *E. coli* cells were subsequently transformed with the resulting cyclized DNA product via electroporation. After 45 min of recovery in Luria-Burtani (LB) media containing 0.4% glucose at 37 °C, cells were plated onto LB plates with 50 µg/mL kanamycin (Kan) and incubated overnight. Single colonies were used to inoculate 5 mL LB + 50 µg/mL Kan, which were grown overnight at 37 °C, 200 rpm. Expression cultures, typically 1 L of Terrific Broth (TB) + 50 µg/mL Kan (TB-Kan), were inoculated from these starter cultures and shaken (180 rpm) at 37 °C. After 3 hours (OD_{600} = ~0.6), the expression cultures were chilled on ice. After 30 min on ice, ObiH expression was induced with 0.5 mM IPTG, and the cultures were expressed for 16 hours at 20 °C with shaking at 180 rpm. Cells were then harvested by centrifugation at 4,300×*g* at 4 °C for 30 min. Cell pellets were pink in color and were frozen and stored at -20 °C until purification.

To purify ObiH, cell pellets were thawed on ice and then resuspended in lysis buffer (50 mM potassium phosphate buffer buffer (pH = 8.0), 500 mM NaCl, 1 mg/ml Hen Egg White Lysozyme (GoldBio), 0.2 mg/ml DNaseI (GoldBio), 1 mM $MgCl_2$, 1 X BugBuster Protein extraction reagent (Novagen), and 400 µM pyridoxal 5′-phosphate (PLP)). A volume of 4 mL of lysis buffer per gram of wet cell pellet was used. After 45 min of shaking at 37 °C, the resulting lysate was then spun down at 75,600×*g* to pellet cell debris. The pellet was colorless whereas the supernatant was pink in color. Ni/NTA beads (GoldBio) were added to the supernatant and incubated on ice for 45 min prior to purification by Ni-affinity chromatography with a gravity column. The column was washed with 5 column volumes of 20 mM imidazole, 500 mM NaCl, 10% glycerol, 50 mM potassium phosphate buffer (pH = 8.0). Washing with higher concentrations of imidazole resulted in slow protein elution. ObiH was eluted with 250 mM imidazole, 500 mM NaCl, 10% glycerol, 50 mM potassium phosphate buffer, pH 8.0. Elution of the desired protein product was monitored by the

disappearance of its bright red color (resulting from the release of ObiH) from the column. The protein product was dialyzed to < 1 µM imidazole in 100 mM Tris buffer, pH 8.5 containing 2 mM DTT, dripped into liquid nitrogen to flash freeze, and stored at -80 °C before use. The concentration of protein was determined by Bradford assay. Generally, this procedure yielded 200 – 250 mg per L culture.

Preparation of phototreated ObiH

ObiH stock solutions (150 – 400 µM) or diluted samples in quartz cuvettes were placed on ice directly under an 8 Watt, green LED bulb for 10 min. The protein solutions were subsequently kept on ice or in the UV-spectrophotometer for 45 min, followed by a second round of green light treatment for 10 minutes which ensured complete abolishment of the 515 nm band.

Kinetics and UV-Vis Spectroscopy

Data were collected between 600 and 250 nm on a UV-2600 Shimadzu spectrophotometer (Shimadzu) with a semi-micro quartz cuvette (Starna Cells) at 25 °C (unless stated otherwise). ObiH stock solutions were diluted to 20 µM in 100 mM Tris-HCl, pH 8.5 and phototreated.

For the Thr titration, a 500 mM Thr solution was prepared in 100 mM Tris-HCl, pH 8.5 to ensure consistent pH between titration experiments. Thr was added to the concentrations of 10, 50, 100, 150, and 200 mM. Time in seconds was recorded from addition of Thr to the time at which data collection at 493 nm occurred. Spectra from 600 – 250 nm were collected every 200 seconds for 2.5 h. All 5 concentrations were conducted at one time using an automated cell changer. A first order decay constant was fit to the data from 33 – 150 min. Decay constants for experiments with Thr > 100 mM were averaged to estimate the half-life of $E(Q^{Gly})$.

To monitor the aldol addition of aliphatic aldehyde to E(Q^{Gly}), 20 µM ObiH samples were prepared in 100 mM Tris-HCl, pH 8.5 and phototreated. 100 mM Thr was added and spectra were gathered while the E(Q^{Gly}) species reached a maximum (generally after ~10 min). Aliphatic aldehyde stocks were prepared as 500 mM solutions in DMSO. Aldehydes were added to final concentration of 25 mM, 5% DMSO. Spectra were recorded every 1 min from 600 – 250 nm.

To monitor equilibrium between acetaldehyde and E(Q^{Gly}), 20 µM ObiH samples were prepared in 100 mM Tris-HCL, pH 8.5 and phototreated. 100 mM Thr was added and spectra were gathered while the E(Q^{Gly}) species produced a strong signal. Acetaldehyde stock solutions were added 5 minutes after the addition of Thr and spectra were collected every minute for 15 minutes. 20X acetaldehyde solutions were prepared in DMSO to ensure each experiment contained 5% DMSO (500 mM, 200 mM, 100 mM, 20 mM, and 4 mM in DMSO).

To monitor product reentry, 20 µM ObiH samples were prepared in 100 mM Tris-HCl, pH 8.5 and phototreated. Purified β-OH-Leu stocks were prepared in water (100 mM). Products were added to a final concentration of 20 mM and spectra were gathered every 1 minute. A small background PLP contamination was noted for β-OH-Leu. To account for this absorbance from PLP, a spectrum of 20 mM β-OH-Leu in 100 mM Tris-HCl was gathered and subtracted from the plus enzyme spectrum.

To assess whether glycine can form E(Q^{Gly}), 2.0 M solution of glycine was prepared in 100 mM Tris-HCl, pH 8.5. 20 µM ObiH samples were prepared in 100 mM Tris-HCl, pH 8.5 and phototreated. Glycine was added to a final concentration of 1.0 M. Spectra from 600 – 250 nm were gathered every 1 minute.

$NaBH_4$ reduction experiments were conducted with phototreated and as-isolated ObiH. 20 µM samples of ObiH were prepared in 100 mM Tris-HCl, pH 8.5. 100 mM Thr was added and spectra were gathered while the E(Q^{Gly}) species reached a maximum. A fresh solution of 200 mM $NaBH_4$

was prepared in H_2O and added to the reaction mixture to a final concentration of 2 mM 10 minutes after the addition of Thr. Spectra were gathered from 600 – 250 nm every 1 minute. UV-vis experiments for E107Q and D204N variants were performed similar to that of the wild-type protein.

Initial velocity comparison between phototreated and as-purified ObiH

ObiH was thawed and centrifuged at 20,000×*g* for 20 min to pellet aggregated protein. The resulting supernatant was split into two separate tubes and kept on ice. One sample was wrapped in foil to preserve the 515 nm species while the other underwent phototreatment (10 min green light, 45 min on ice, 10 min green light). Reactions were prepared in 100 mM Tris-HCl, pH 8.5 with 100 mM Thr, 25 mM isobutryaldehyde, 20 µM ObiH, and 100 µM PLP in triplicate. Reaction mixtures were pre-incubated in a water bath at 37 °C prior to addition of enzyme. After addition of ObiH, 20 µL of reaction mixture was removed and quenched with 20 µL of acetonitrile at 2, 5, 10, 15, and 30 min. Quenched reactions were centrifuged at 20,000×*g* for 20 min to pellet aggregated protein. Supernatant was diluted 10-fold into a 1:1 H_2O:acetonitrile solution and analyzed via UPLC-MS for product quantification. Reaction mixtures progressed overnight and a reaction sample was taken at 24 hours for additional quantification.

Preparative scale synthesis of (2*S*,3*R*)-β-hydroxyleucine

ObiH was thawed and centrifuged at 20,000×*g* for 20 min to pellet aggregated protein. Protein stock concentration was obtained using the Bradford assay on a representative sample. Thr (1.19 g, 10 mmol), isobutyraldehyde (0.361 g, 5 mmol), 5 mL MeOH, and ~85 mL with 100 mM Tris-HCl, pH 8.5 buffer were added to a 100 mL round bottom flask. Pyridoxal-5'-phosphate was added to a final concentration of 100 µM, followed by ObiH to a final concentration of 20 µM (0.04 mol

% catalyst). The reaction mixture was incubated for 24 h at 37 °C. The reaction mixture was then heated to 70 °C for 30 minutes to denature ObiH. The reaction mixture was transferred to 50 mL conical vials and centrifuged at 4,300×*g* for 10 minutes to pellet aggregated protein. The supernatant was transferred to 500 mL round bottom flask and concentrated by rotary evaporation. For purification, ½ of the resulting reaction mixture was loaded onto a Biotage SNAP Ultra 12g C18 column and purified on a Biotage flash purification system using a water/methanol gradient. Fractions were analyzed by UPLC-MS to identify product containing fractions. Fractions containing pure product were set aside. Fractions containing both Thr and product were pooled, concentrated, and subjected to a second round of chromatography. All pure product containing fractions from both rounds of purification were then pooled, concentrated by rotary evaporation, and dried via lyophilization (141 mg, 38%). ^{1}H NMR (500 MHz, D_2O) δ 3.743 (s, 1H), 3.736 (dd, J = 3.8, 10.6 Hz, 1H), 1.78 (m, J = 6.74 Hz, 1H), 1.03 (d, J = 6.59, 1H), 0.98 (d, J = 6.78, 1H)

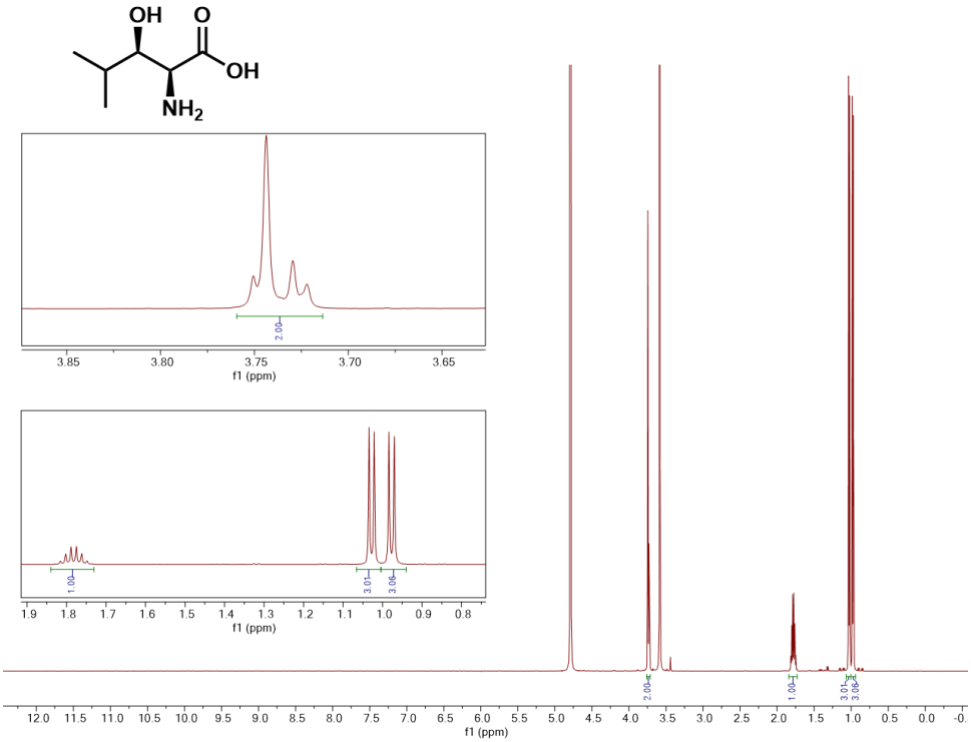

Figure 18: ^{1}H NMR spectra of (2*S*,3*R*)-β-hydroxyleucine

2.5 References

(1) Murphy, C. D.; O'Hagan, D.; Schaffrath, C. Identification of a PLP-Dependent Threonine Transaldolase: A Novel Enzyme Involved in 4-Fluorothreonine Biosynthesis in Streptomyces Cattleya. *Angewandte Chemie International Edition* **2001**, *40* (23), 4479–4481. https://doi.org/10.1002/1521-3773(20011203)40:23<4479::AID-ANIE4479>3.0.CO;2-1.

(2) Barnard-Britson, S.; Chi, X.; Nonaka, K.; P. Spork, A.; Tibrewal, N.; Goswami, A.; Pahari, P.; Ducho, C.; Rohr, J.; G. Van Lanen, S. Amalgamation of Nucleosides and Amino Acids in Antibiotic Biosynthesis: Discovery of an l-Threonine:Uridine-5′-Aldehyde Transaldolase. *J Am Chem Soc* **2012**, *134* (45), 18514–18517. https://doi.org/10.1021/ja308185q.

(3) Ushimaru, R.; Liu, H. Biosynthetic Origin of the Atypical Stereochemistry in the Thioheptose Core of Albomycin Nucleoside Antibiotics. *J Am Chem Soc* **2019**, *141* (6), 2211–2214. https://doi.org/10.1021/jacs.8b12565.

(4) Scott, T. A.; Heine, D.; Qin, Z.; Wilkinson, B. An L-Threonine Transaldolase Is Required for L-Threo-β-Hydroxy-α-Amino Acid Assembly during Obafluorin Biosynthesis. *Nat Commun* **2017**, *8* (May), 1–11. https://doi.org/10.1038/ncomms15935.

(5) Schaffer, J. E.; Reck, M. R.; Prasad, N. K.; Wencewicz, T. A. β-Lactone Formation during Product Release from a Nonribosomal Peptide Synthetase. *Nat Chem Biol* **2017**, *13* (7), 737–744. https://doi.org/10.1038/nchembio.2374.

(6) Scott, T. A.; Batey, S. F. D.; Wiencek, P.; Chandra, G.; Alt, S.; Francklyn, C. S.; Wilkinson, B. Immunity-Guided Identification of Threonyl-TRNA Synthetase as the Molecular Target of Obafluorin, a β-Lactone Antibiotic. *ACS Chem Biol* **2019**, *14* (12), 2663–2671. https://doi.org/10.1021/acschembio.9b00590.

(7) Contestabile, R.; Paiardini, A.; Pascarella, S.; Di Salvo, M. L.; D'Aguanno, S.; Bossa, F. L-Threonine Aldolase, Serine Hydroxymethyltransferase and Fungal Alanine Racemase: A Subgroup of Strictly Related Enzymes Specialized for Different Functions. *Eur J Biochem* **2001**, *268* (24), 6508–6525. https://doi.org/10.1046/j.0014-2956.2001.02606.x.

(8) Salvo, M. L.; Remesh, S. G.; Vivoli, M.; Ghatge, M. S.; Paiardini, A.; Aguanno, S. D.; Safo, M. K.; Contestabile, R.; Biochimiche, S.; Fanelli, A. R.; Universit, S. On the Catalytic Mechanism and Stereospecificity of Escherichia Coli L -Threonine Aldolase. *FEBS* **2014**, *281*, 129–145. https://doi.org/10.1111/febs.12581.

(9) Dunathan, H. C. Conformation and Reaction Specificity in Pyridoxal Phosphate Enzymes. *Proc Natl Acad Sci U S A* **1966**, *55* (4), 712–716. https://doi.org/10.1073/PNAS.55.4.712.

(10) Kielkopf, C. L.; Burley, S. K. X-Ray Structures of Threonine Aldolase Complexes: Structural Basis of Substrate Recognition. *Biochemistry* **2002**, *41* (39), 11711–11720. https://doi.org/10.1021/bi020393+.

(11) Steinreiber, J.; Schürmann, M.; Wolberg, M.; Van Assema, F.; Reisinger, C.; Fesko, K.; Mink, D.; Griengl, H. Overcoming Thermodynamic and Kinetic Limitations of Aldolase-Catalyzed Reactions by Applying Multienzymatic Dynamic Kinetic Asymmetric

Transformations. *Angewandte Chemie - International Edition* **2007**, *46* (10), 1624–1626. https://doi.org/10.1002/anie.200604142.

(12) Steinreiber, J.; Fesko, K.; Mayer, C.; Reisinger, C.; Schürmann, M.; Griengl, H. Synthesis of γ-Halogenated and Long-Chain β-Hydroxy-α-Amino Acids and 2-Amino-1,3-Diols Using Threonine Aldolases. *Tetrahedron* **2007**, *63* (34), 8088–8093. https://doi.org/10.1016/J.TET.2007.06.013.

(13) Fesko, K.; Strohmeier, G. A.; Breinbauer, R. Expanding the Threonine Aldolase Toolbox for the Asymmetric Synthesis of Tertiary α-Amino Acids. *Appl Microbiol Biotechnol* **2015**, *99* (22), 9651–9661. https://doi.org/10.1007/s00253-015-6803-y.

(14) Kimura, T.; P. Vassilev, V.; Shen, G.-J.; Wong, C.-H. Enzymatic Synthesis of β-Hydroxy-α-Amino Acids Based on Recombinant d- and l-Threonine Aldolases. *J Am Chem Soc* **1997**, *119* (49), 11734–11742. https://doi.org/10.1021/ja9720422.

(15) Fesko, K. Threonine Aldolases: Perspectives in Engineering and Screening the Enzymes with Enhanced Substrate and Stereo Specificities. *Applied Microbiology and Biotechnology*. 2016, pp 2579–2590. https://doi.org/10.1007/s00253-015-7218-5.

(16) Chen, Q.; Chen, X.; Feng, J.; Wu, Q.; Zhu, D.; Ma, Y. Improving and Inverting C $_{\beta}$ -Stereoselectivity of Threonine Aldolase via Substrate-Binding-Guided Mutagenesis and a Stepwise Visual Screening. *ACS Catal* **2019**, *9* (5), 4462–4469. https://doi.org/10.1021/acscatal.9b00859.

(17) Murphy, C. D.; O'Hagan, D.; Schaffrath, C. Identification of a PLP-Dependent Threonine Transaldolase: A Novel Enzyme Involved in 4-Fluorothreonine Biosynthesis in Streptomyces Cattleya. *Angewandte Chemie - International Edition* **2001**, *40* (23), 4479–4481. https://doi.org/10.1002/1521-3773(20011203)40:23<4479::AID-ANIE4479>3.0.CO;2-1.

(18) Wu, L.; Tong, M. H.; Raab, A.; Fang, Q.; Wang, S.; Kyeremeh, K.; Yu, Y.; Deng, H. An Unusual Metal-Bound 4-Fluorothreonine Transaldolase from Streptomyces Sp. MA37 Catalyses Promiscuous Transaldol Reactions. *Appl Microbiol Biotechnol* **2020**, *104* (9), 3885–3896. https://doi.org/10.1007/s00253-020-10497-z.

(19) Xu, L.; Wang, L. C.; Xu, X. Q.; Lin, J. Characteristics of L-Threonine Transaldolase for Asymmetric Synthesis of β-Hydroxy-α-Amino Acids. *Catal Sci Technol* **2019**, *9* (21), 5943–5952. https://doi.org/10.1039/c9cy01608b.

(20) Schaffer, J. E.; Reck, M. R.; Prasad, N. K.; Wencewicz, T. A. β-Lactone Formation during Product Release from a Nonribosomal Peptide Synthetase. *Nat Chem Biol* **2017**, *13* (7), 737–744. https://doi.org/10.1038/nchembio.2374.

(21) Heinert, D.; Martell, A. E. Pyridoxine and Pyridoxal Analogs. VII. Acid-Base Equilibria of Schiff Bases. *J Am Chem Soc* **1963**, *85* (2), 188–193. https://doi.org/10.1021/ja00885a018.

(22) Hill, M. P.; Carroll, E. C.; Vang, M. C.; Addington, T. A.; Toney, M. D.; Larsen, D. S. Light-Enhanced Catalysis by Pyridoxal Phosphate-Dependent Aspartate Aminotransferase. *J Am Chem Soc* **2010**, *132* (47), 16953–16961. https://doi.org/10.1021/ja107054x.

(23) Kreitler, D. F.; Gemmell, E. M.; Schaffer, J. E.; Wencewicz, T. A.; Gulick, A. M. The Structural Basis of N-Acyl-α-Amino-β-Lactone Formation Catalyzed by a Nonribosomal Peptide Synthetase. *Nat Commun* **2019**, *10* (1), 1–13. https://doi.org/10.1038/s41467-019-11383-7.

(24) Xu, L.; Wang, L. C.; Su, B. M.; Xu, X. Q.; Lin, J. Multi-Enzyme Cascade for Improving β-Hydroxy-α-Amino Acids Production by Engineering L-Threonine Transaldolase and Combining Acetaldehyde Elimination System. *Bioresour Technol* **2020**, *310*, 123439. https://doi.org/10.1016/j.biortech.2020.123439.

(25) Xu, L.; Wang, L. C.; Xu, X. Q.; Lin, J. Characteristics of L-Threonine Transaldolase for Asymmetric Synthesis of β-Hydroxy-α-Amino Acids. *Catal Sci Technol* **2019**, *9* (21), 5943–5952. https://doi.org/10.1039/c9cy01608b.

(26) Grishin, N. V.; Phillips, M. A.; Goldsmith, E. J. Modeling of the Spatial Structure of Eukaryotic Ornithine Decarboxylases. *Protein Science* **1995**, *4* (7), 1291–1304. https://doi.org/10.1002/pro.5560040705.

(27) Eliot, A. C.; Kirsch, J. F. Pyridoxal Phosphate Enzymes: Mechanistic, Structural, and Evolutionary Considerations. *Annu Rev Biochem* **2004**, *73* (1), 383–415. https://doi.org/10.1146/annurev.biochem.73.011303.074021.

(28) Schaffer, J. E.; Reck, M. R.; Prasad, N. K.; Wencewicz, T. A. β-Lactone Formation during Product Release from a Nonribosomal Peptide Synthetase. *Nat Chem Biol* **2017**, *13* (7), 737–744. https://doi.org/10.1038/nchembio.2374.

(29) Toney, M. D. Reaction Specificity in Pyridoxal Phosphate Enzymes. *Archives of Biochemistry and Biophysics*. 2005, pp 279–287. https://doi.org/10.1016/j.abb.2004.09.037.

(30) Buller, A. R.; Roye, P. Van; Cahn, J. K. B.; Scheele, R. A.; Herger, M.; Arnold, F. H. Directed Evolution Mimics Allosteric Activation by Stepwise Tuning of the Conformational Ensemble. *J Am Chem Soc* **2018**, *140*, 7256–7266. https://doi.org/10.1021/jacs.8b03490.

(31) Milić, D.; Demidkina, T. V.; Faleev, N. G.; Phillips, R. S.; Matković-Čalogović, D.; Antson, A. A. Crystallographic Snapshots of Tyrosine Phenol-Lyase Show That Substrate Strain Plays a Role in C-C Bond Cleavage. *J Am Chem Soc* **2011**, *133* (41), 16468–16476. https://doi.org/10.1021/ja203361g.

(32) Masuo, S.; Tsuda, Y.; Namai, T.; Minakawa, H.; Shigemoto, R.; Takaya, N. Enzymatic Cascade in *Pseudomonas* That Produces Pyrazine from A-Amino Acids. *ChemBioChem* **2020**, *21* (3), 353–359. https://doi.org/10.1002/cbic.201900448.

(33) di Salvo, M. L.; Remesh, S. G.; Vivoli, M.; Ghatge, M. S.; Paiardini, A.; D'Aguanno, S.; Safo, M. K.; Contestabile, R. On the Catalytic Mechanism and Stereospecificity of *Escherichia Coli* <scp>l</Scp> -Threonine Aldolase. *FEBS Journal* **2014**, *281* (1), 129–145. https://doi.org/10.1111/febs.12581.

(34) LANE, A. N.; KIRSCHNER, K. The Mechanism of Binding of L-Serine to Tryptophan Synthase from Escherichia Coli. *Eur J Biochem* **1983**, *129* (3), 561–570. https://doi.org/10.1111/j.1432-1033.1983.tb07086.x.

(35) J. Hale, K.; Manaviazar, S.; M. Delisser, V. A Practical New Asymmetric Synthesis of (2S,3S)- and (2R,3R)-3-Hydroxyleucine. *Tetrahedron* **1994**, *50* (30), 9181–9188. https://doi.org/10.1016/S0040-4020(01)85384-9.

(36) Makino, K.; Okamoto, N.; Hara, O.; Hamada, Y. Efficient Enantioselective Synthesis of (2R,3R)- and (2S,3S)-3-Hydroxyleucines and Their Diastereomers through Dynamic Kinetic Resolution. *Tetrahedron Asymmetry* **2001**, *12* (12), 1757–1762. https://doi.org/10.1016/S0957-4166(01)00306-8.

(37) Gibson, D. G. Enzymatic Assembly of Overlapping DNA Fragments; 2011; pp 349–361. https://doi.org/10.1016/B978-0-12-385120-8.00015-2.

Chapter 3

Chemoenzymatic synthesis and functionalization of α-aryl aldehydes in a C–C bond forming cascade

Content in this chapter is adapted from the following published work:

Meza, A.; Campbell, M. E.; Zmich, A.; Thein, S. A.; Grieger, A. M.; McGill, M. J.; Willoughby, P. H.; Buller, A. R. “Efficient chemoenzymatic synthesis of α-aryl aldehydes as intermediates in C–C bond forming biocatalytic cascades.” *ACS Catalysis*. 2022. 12, 17, 10700-10710

I thank Prof. Patrick Willoughby for initiating this project while being a visiting scientist in the Buller lab. It was a joy to train Pat in molecular cloning and biocatalysis while learning from his expertise in catalysis and synthetic chemistry. I thank Meghan Campbell for extensive help with small molecule characterization and leading the effort on the SOI-UstD cascade.

Chapter 3: Chemoenzymatic synthesis of α-aryl aldehydes in C–C bond forming cascade

3. 1. Introduction

Enzymatic cascades are highly sought for their potential to rapidly build molecular complexity and circumvent the need to isolate intermediates.[1,2] The opportunities enabled by multi-enzyme cascades are exemplified by the recent process-scale syntheses of islatravir and molnupiravir, in which enzymes from multiple species were engineered to produce high value target molecules.[3,4] While some enzymatic cascades have been leveraged for preparative-scale synthesis, the scope of currently accessible products is dwarfed in comparison to the vast molecular diversity achieved in Nature.[1] This natural diversity is accomplished by a constellation of enzymes that are often tuned to perform specific chemical transformations on single a substrate in a complex cellular environment.[1] In contrast, broadly useful synthetic methodologies are characterized by their ability to perform well-defined transformations on large numbers of substrates. To meet this synthetic ideal with enzymatic cascades, each enzyme in the cascade must have a complementary and broad substrate scope. There have been phenomenal advances in the development of such promiscuous biocatalytic cascades that perform sophisticated functional group interconversions, such as the conversion of racemic alcohols into chiral amines.[5,6] However, there are comparatively few biocatalytic cascades that catalyze a well-controlled C–C bond forming reaction on diverse substrates, in part due to the limited availability of water-stable reactive carbon precursors. Hence, biocatalytic strategies to produce reactive carbon electrophiles are poised to enable a plethora of enzymatic cascades capable of rapidly and efficiently constructing complex molecular scaffolds.

Aldehydes are preeminent substrates for C–C bond forming enzymes. A key characteristic of their reactivity (and of other carbonyl containing molecules), is their ability to tautomerize and form both electrophilic and nucleophilic carbon species. The exploitation of this dual reactivity is widespread in Nature and a key theme in central metabolism.[7] Correspondingly, multiple enzymes

that feature aldol chemistry have independently evolved to catalyze these valuable transformations. Their ability to catalyze enantioselective transformations with simple starting materials has motivated many engineering and synthetic studies. For example, aldolases have been leveraged to perform key C–C bond forming steps in biocatalytic systems that produce complex carbohydrates[8,9], functionalized α-ketoacids[10,11], and amino acid analogs.[12–15] Independent of the particular enzyme employed, aldol chemistry is fundamentally constrained by substrate availability. Although thousands of aromatic and aliphatic aldehydes are commercially available, the simple α-aryl aldehydes are notably scarce. This sparsity is likely due to the intrinsic instability of α-aryl aldehydes. Conjugation with the arene stabilizes the enol tautomer, promoting their nucleophilic reactivity and homo-coupling reactions that lead to rapid depletion of the reagent. Given the ubiquity of aldehydes in biocatalytic cascades, the development of a robust method to synthesize and capture α-aryl aldehydes in C–C bond forming reactions would provide access to valuable reagents for diverse biocatalytic transformations.

In Nature, α-aryl aldehydes are typically generated through the Ehrlich pathway (Figure 1a),[16] which is involved in aromatic amino acid catabolism and provides key intermediates in the metabolic synthesis of bioactive natural products (Figure 1b, 1c).[17] Wang and coworkers utilized enzymes from the Ehrlich pathway to produce an α-aryl aldehyde substrate for norcoclaurine synthase *en route* to benzylisoquinoline alkaloid analogs.[18] However, to access the α-aryl aldehyde synthon through the Ehrlich pathway, multiple enzymes must operate on a corresponding non-standard aromatic amino acids (nsAAs), hampering the viability of this method in a preparative synthetic context. A potentially competitive approach to generating α-aryl aldehydes involves redox-mediated transformations of carboxylic acids or primary alcohols.[19] Such enzymes are generally quite effective, but the requirement of accessory enzymes for cofactor regeneration and redox balance adds to the complexity of such an approach. The direct,

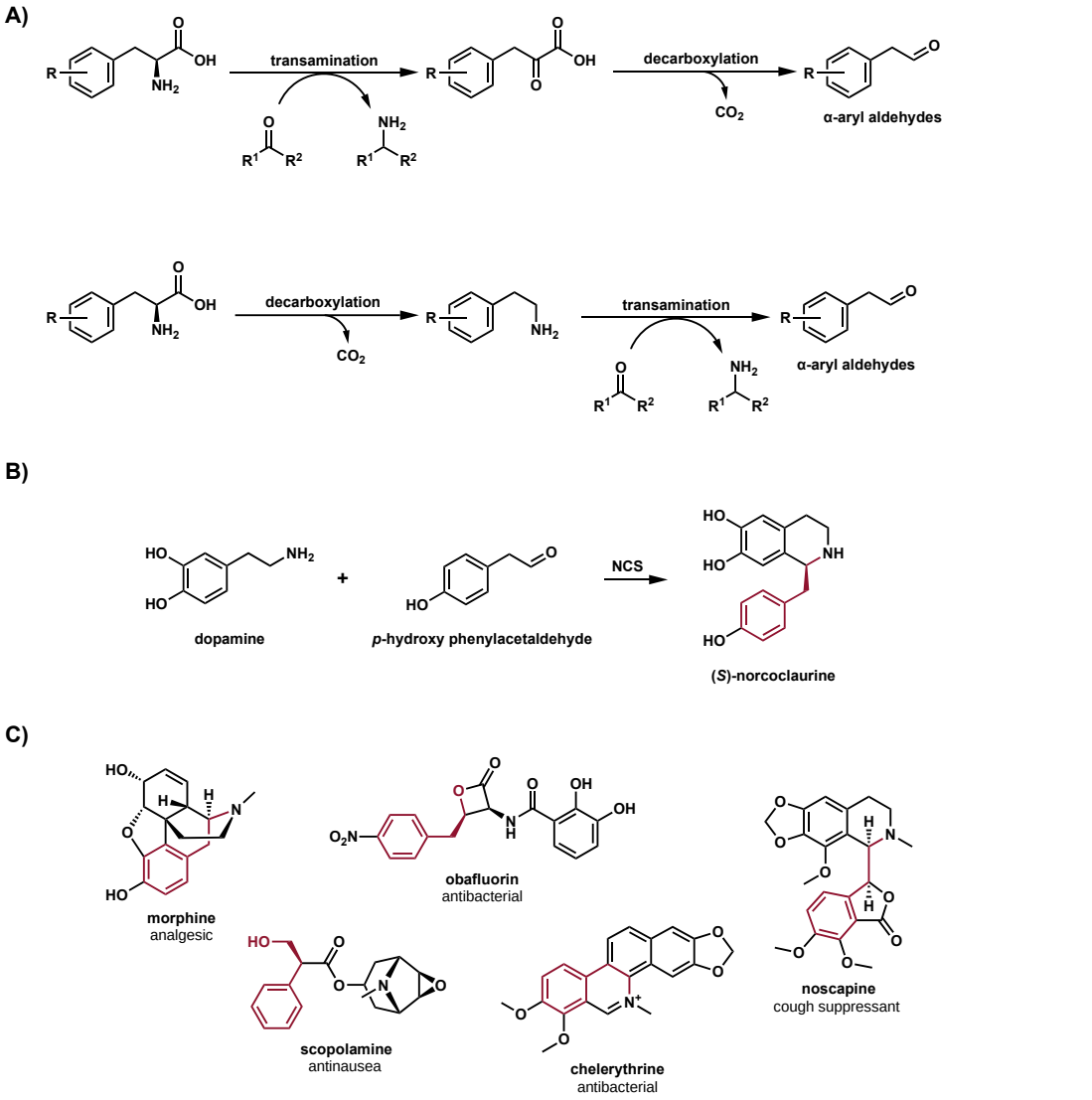

Figure 1. The Ehrlich Pathway produces α-aryl aldehydes and primary amines that are the substrates for norcoclaurine synthase (NCS). A) Decarboxylation and transamination of aromatic amino acids produce α-aryl aldehydes. **B)** (*S*)-Norcoclaurine is produced from dopamine and *p*-hydroxy phenylacetaldehyde and is a key intermediate en route to diverse benzylisoquinoline alkaloids. **C)** α-aryl aldehydes intermediates in biosynthesis. The carbons derived from α-aryl aldehydes are shown in dark red.

biocatalytic anti-Markovnikov oxidation of styrene was previously demonstrated by Hammer and coworkers.[20] While the transformation is compelling, the scope of the engineered P450 oxidase is limited at preparative scales. In comparison, purely synthetic approaches involve Wittig-like

reactions that require purification of the unstable α-aryl aldehydes prior to utilization in downstream reactions.[21]

We were drawn to recent reports from the Zhi Li lab who produced α-aryl aldehydes using a two-enzyme cascade from *Pseudomonas sp. VLB120*.[22–25] In this system, a flavin-dependent styrene monooxygenase (SMO) catalyzes epoxidation of styrene to produce styrene oxide. This molecule is the substrate for styrene oxide isomerase (SOI), an integral membrane enzyme. SOI catalyzes a redox neutral Meinwald rearrangement[26] to produce α-aryl aldehydes, which were shown to be amenable to a variety of functional group interconversions in cascade reactions with transaminases and dehydrogenases (Figure 2).[22,27–29] However, the SMO-SOI cascade has

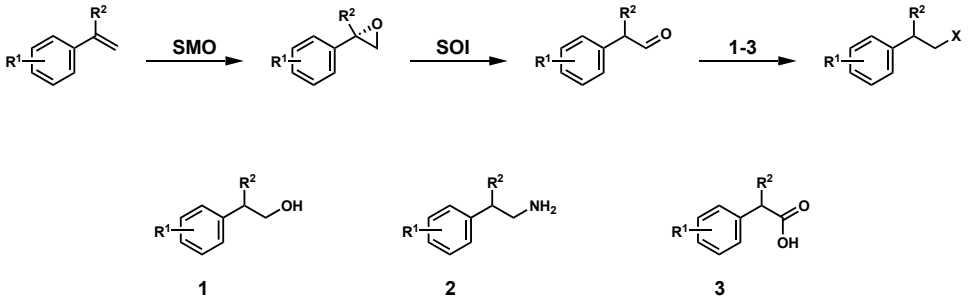

Figure 2. Previous biocatalytic cascades featuring SOI. Wu et al. produced α-aryl aldehyde from styrene analogs with styrene oxide monooxygenase (SMO) and styrene oxide isomerase (SOI). The α-aryl aldehydes were subsequently oxidized or reduced into alcohol, amine, or carboxylic acids with reductases (1), ω-transaminases (2) and dehydrogenases (3).[22,23]

limitations. Chiefly, efficient formation of the α-aryl aldehyde intermediate requires both enzymes to react with non-natural substrate analogs. The challenge of using two enzymes to generate the α-aryl aldehyde intermediate is compounded when considering the functional diversity of commercially available styrenes is relatively low (Figure 3a).

Here, we design and implement a chemoenzymatic route to access a wide array of α-aryl aldehydes for subsequent biocatalytic elaboration through C–C bond forming reactions (Figure 3b). To circumvent SMO, most aryl epoxides were made in a single step via the Corey-Chaykovsky reaction from the vast pool of inexpensive aryl aldehydes or through bromination of

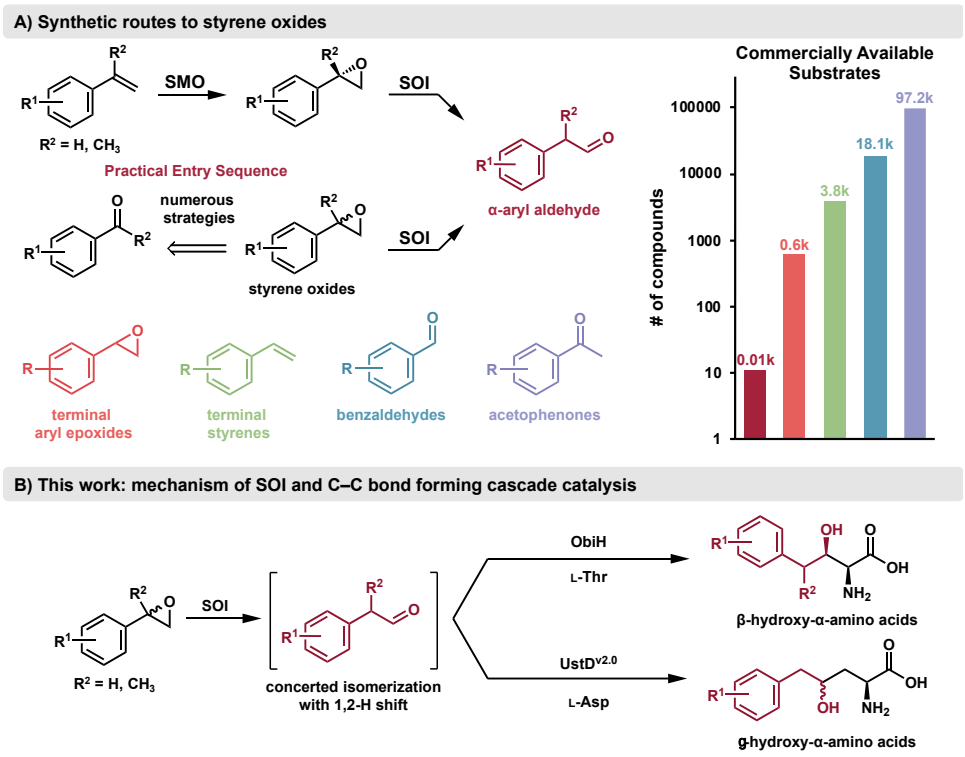

Figure 3. *α*-Aryl aldehydes motifs in biosynthesis and *in situ* generation for biocatalysis. A) Styrene oxide analogs are the ideal entry point for the generation of *α*-aryl aldehyde intermediates. Previous work utilizing styrene, styrene monooxygenase (SMO), and styrene oxide isomerase (SOI) successfully produced α-aryl aldehydes. Chemoenzymatic synthesis of styrene oxides from aryl carbonyl compound expands the potential substrate pool for SOI. **B)** This work: mechanism of SOI and C–C bond forming cascade catalysis to produce non-standard amino acids (nsAAs). α-Aryl aldehydes generated by SOI are intercepted by PLP-dependent, C–C bond forming enzymes yielding structurally diverse amino acids.

acetophenones and subsequent reductive epoxidation (Figure S1). These substrates were reacted with SOI in whole-cell fashion, and the resulting aldehydes were intercepted *in situ* by C–C bond forming enzymes. The L-threonine (Thr) transaldolase ObiH was shown to react with an exceptionally broad scope of SOI-generated aldehydes, yielding non-standard β-hydroxy amino acids with excellent d.r. and *ee*. We used isotopically labeled substrates to clarify the mechanism of SOI and show that SOI catalyzes a concerted isomerization with a stereospecific 1,2-hydride-shift. We further showcase the utility of SOI by combining it with an additional C–C bond forming enzyme, UstD. UstD is a pyridoxal phosphate (PLP)-dependent enzyme that catalyzes a formal decarboxylative aldol reaction of L-aspartate into diverse aldehydes, generating γ-hydroxy-α-

amino acids.[30,31] We show that UstD can intercept the α-aryl aldehydes intermediates to generated structurally diverse nsAAs. Together, these data demonstrate the use of SOI in tandem with C–C bond forming enzymes, adding a robust method for accessing metastable *C*-electrophiles in aqueous conditions.

3. 2. Results and Discussion

3. 2. 1. α-aryl aldehydes produced from SOI can be intercepted with ObiH

We began by testing the ability of purified ObiH to intercept phenylacetaldehyde produced by heterologously-expressed SOI and commercially-available styrene oxide (**2a**). Following the report from Wu et al., we expressed the membrane-integrated SOI enzyme as a *C*-6xHis construct in *E. coli* BL21(DE3).[22,23] Rather than purify the catalyst, which is a notoriously cumbersome process for membrane-integrated proteins, we tested the activity of the cascade in reactions with whole cells expressing SOI, purified ObiH and its substrate Thr (**1**), and styrene oxide (**2a**), to generate a stable amino acid product in a one-pot reaction (Figure 4a). Gratifyingly, we observed significant accumulation of β-hydroxyhomophenylalanine (**2b**) by UPLC- MS and confirmed that product formation requires the combination of SOI and ObiH (Figure S2). By changing the

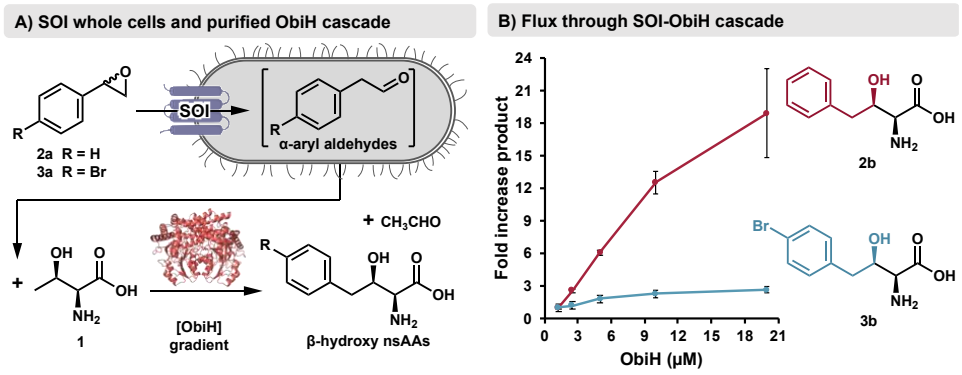

Figure 4. One-pot biocatalytic cascade with SOI and ObiH. **A)** BL21 (DE3) cells expressing SOI and purified ObiH generate a stable amino acid from 25 mM styrene oxide (**2a** or **3a**), 100 mM Thr (**1**), 100 mM Tris•HCl pH 8.5, 0.1% dry cell weight (dcw) and variable amounts of purified ObiH. **B)** Fold increase in total product observed from styrene oxide (**2a**) and *p*-bromostyrene oxide (**3a**) is shown as a function of ObiH concentration. Data indicate how the flux-limiting step shifts as a function of substrate.

concentration of ObiH, we were able to study the efficiency of the two-enzyme system (Figure 4b). Increasing the concentration of ObiH in these reactions resulted in a commensurate increase in product formation when reactions were run to incomplete conversion. These data indicate that, under these conditions, SOI rapidly converts styrene oxide into phenylacetaldehyde and ObiH catalyzes the flux-limiting step.

Based on our observation that ObiH limits flux through the cascade with styrene oxide, we hypothesized substrates that react more sluggishly with SOI would be less dependent on ObiH concentration. In particular, styrene oxide analogs substituted with electron withdrawing groups would destabilize the positive charge that is proposed to accumulate at the benzylic carbon during isomerization.[22] We repeated the ObiH titration with *p*-bromostyrene oxide (**3a**), which revealed a shallower dependence on ObiH concentration; a 16-fold increase in ObiH concentration only produced a ~2.5-fold increase in product formation (Figure 4b). Nevertheless, these data showed that α-aryl aldehydes generated via SOI in whole cell catalysis could be intercepted by ObiH.

3. 2. 2. Co-expression of SOI-ObiH yields a whole-cell biocatalyst

Operational simplicity is a critical element for the adoption of new synthetic methods. We therefore sought to develop a whole cell catalyst in which SOI and ObiH are co-expressed in *E. coli* BL21 (DE3) on separate expression vectors. Such approaches are well precedented and greatly simplify the work required by preparing both catalysts in parallel as a single unit (Figure 5a).[22] We used two common methods for preparing and deploying the whole cell catalysts. Cell pellets harvested from expression cultures were either extruded through a syringe and flash-frozen in liquid nitrogen or simply frozen and lyophilized. Activity comparison between the two methods showed that each produced highly active catalysts that can be stored for months while maintaining activity. Lyophilized cells were utilized during optimization and initial exploration of the substrate scope for accurate accounting of catalyst mass and reproducible handling. Frozen

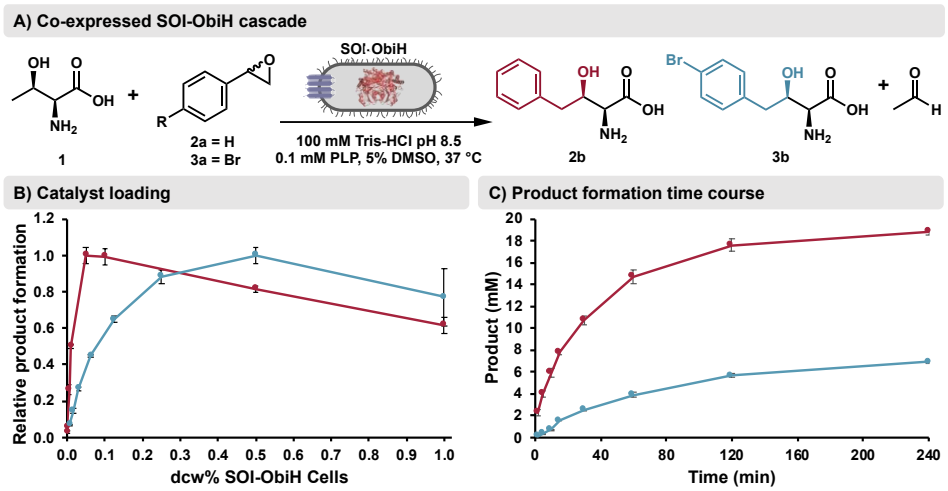

Figure 5. **Activity analysis of *E. coli* co-expressing SOI and ObiH. A)** Cascade catalysis with cells co-expressing SOI and ObiH efficiently produces β-hydroxy-α-amino acids from epoxides and Thr. **B)** Product formation of β-hydroxyhomophenylalanine (**2b,** dark red) and *p*-bromo-β-hydroxyhomophenylalanine (**3b,** blue) with SOI-ObiH cells in overnight reactions. Relative product formation is scaled to the maximum observed product for each compound. **C)** Product formation over time for **2b** (dark red) and **3b** (blue) with 0.1% dcw SOI-ObiH cells. Catalysts loaded experiments with substrate **2b** were completed by Prof. Patrick Willoughby.

wet cells were used for subsequent preparative-scale reactions as lyophilization requires additional time and specialized equipment that may not be accessible in all laboratory settings. Importantly, both preparations yielded catalysts that can easily be deployed in preparative scale reactions.

We next sought to understand the impact of catalyst loading on product formation (Figure 5b). The product concentration reached a maximum with 0.05% dry cell weight (dcw), with yields corresponding to ~80% of the theoretical titer with **2a** as the substrate. When we added more cells, instead of plateauing, we observed that reaction yields decreased. We considered whether endogenous reducing enzymes could consume the phenylacetaldehyde intermediate. A strain of *E. coli* in which multiple reducing enzymes were knocked out, *E. coli* K-12 MG1655 (DE3) RARE, was engineered by the Prather Lab and has been used in biocatalytic applications that feature aromatic aldehydes.[32] We hypothesized that use of this strain might ameliorate depletion of the aldehyde in whole-cell reactions. However, when we expressed the SOI-ObiH cascade in this

strain of *E. coli* we observed no change in product formation in comparison to the more commonly used BL21 DE3 strain, which was used for the rest of this study (Figure S3). While the complex cellular milieu prevents the determination of the specific pathway that is consuming the intermediate, aldehydes as well as the epoxide starting material are generally prone to reactions with cellular nucleophiles, which may be sequestering the substrate and intermediate at higher cell loadings. Cell loading experiments were repeated with **3a**. In these reactions, 10-fold higher cell loadings were required to achieve maximal product formation relative to styrene oxide (Figure 5b), which we attribute to the lower activity of SOI on the *p*-bromo substrate (Figure 4b).

To test the scalability of this two-enzyme cascade, we measured reaction progress and conducted preparative scale reactions. With **2a** at 25 mM and catalyst loading of 0.1% dcw, reaction yields reached 50% in ~30 minutes and slowly increased to 83% overnight (Figure 5c). While we were interested in tracking the abundance of phenylacetaldehyde during this process, such studies were precluded by its instability. Isolated yields for **2b** changed little as substrate loading, catalyst preparation, and catalyst loading were varied; with yields between 52-69% (Figure 7). Inspired by this success, reactions with **2a** were scaled to 10 mmol, from which 1.21 g of **2b** was isolated, corresponding to a 62% yield (Figure 6). Reactions with 25 mM **3a**, which reacts slower than **2a**, reached a 37% yield overnight on analytic scale. Initial preparative-scale reaction conditions with **3a** produced **3b** with just 12% isolated yield. Increasing the catalyst loading 10-fold to 1.0% wcw (wet cell weight) resulted in an increase in **3b** to 32%. We observed a large fraction of insoluble **3a** remained after these overnight reactions. Therefore, substrate loading was reduced 10-fold to 2.5 mM **3a** while maintaining 100 mM Thr, which increased the isolated yield to 51% at 0.1% wcw. We attempted reactions with 2.5 mM **3a** and 1.0% wcw, but isolation of the relatively dilute product was stymied by the large amount of cellular material and unreacted Thr.

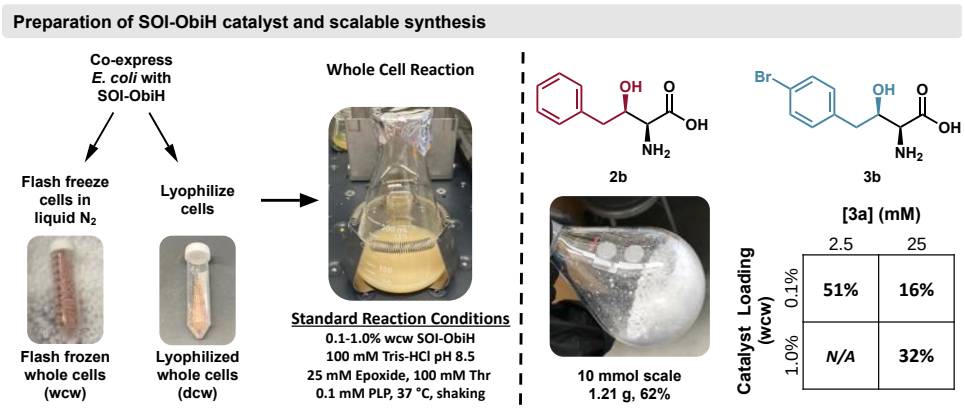

Figure 6. SOI-ObiH preparative synthesis. Preparation of catalyst as either frozen wet cell or dry cells. Gram-scale synthesis and isolation of **2b** at 10 mmol scale. Synthesis of **3b**, which has low aqueous solubility, was improved by either increasing catalyst loading or decreasing substrate concentration. Prepartive synthesis and isolation of **3b** with 25 mM **3a** and 0.1% wcw catalysts was completed by Anna Zmich.

Previous studies by us and others have shown that ObiH has excellent stereoselectivity.[14,33,34] The *S*-isomer at the 2- position (C_α) is formed due to the complete facial selectivity of the ObiH quinonoid nucleophile. ObiH forms the 3-(*R*)-isomer with high, >20:1 selectivity under initial velocity conditions for most substrates tested, which matches the absolute configuration of obafluorin, the natural product produced in the biosynthetic pathway encoding ObiH.[33] NMR analysis and derivatization with the chiral shift reagent L-FDAA (Marfey's Reagent)[35] followed by UPLC-MS analysis both showed that **2b** and **3b** are formed as single diastereomer, which we assign as (2*S*, 3*R*). Notably, this high stereochemical purity is maintained even as reactions proceed to high yield, which stands in contrast to the well-studied Thr aldolases[36] and the reaction of ObiH with aryl aldehydes.[14]

3. 2. 3. SOI-ObiH forms a promiscuous biocatalytic cascade

We next sought to explore the substrate scope of the SOI-ObiH cascade. Commercial epoxide substrates were used when available, but the majority of substrates assayed were synthesized through the Corey-Chaykovsky reaction. This one-step C–C bond forming reaction readily converts aldehydes and ketones into terminal epoxides using sulfonium iodide and NaH

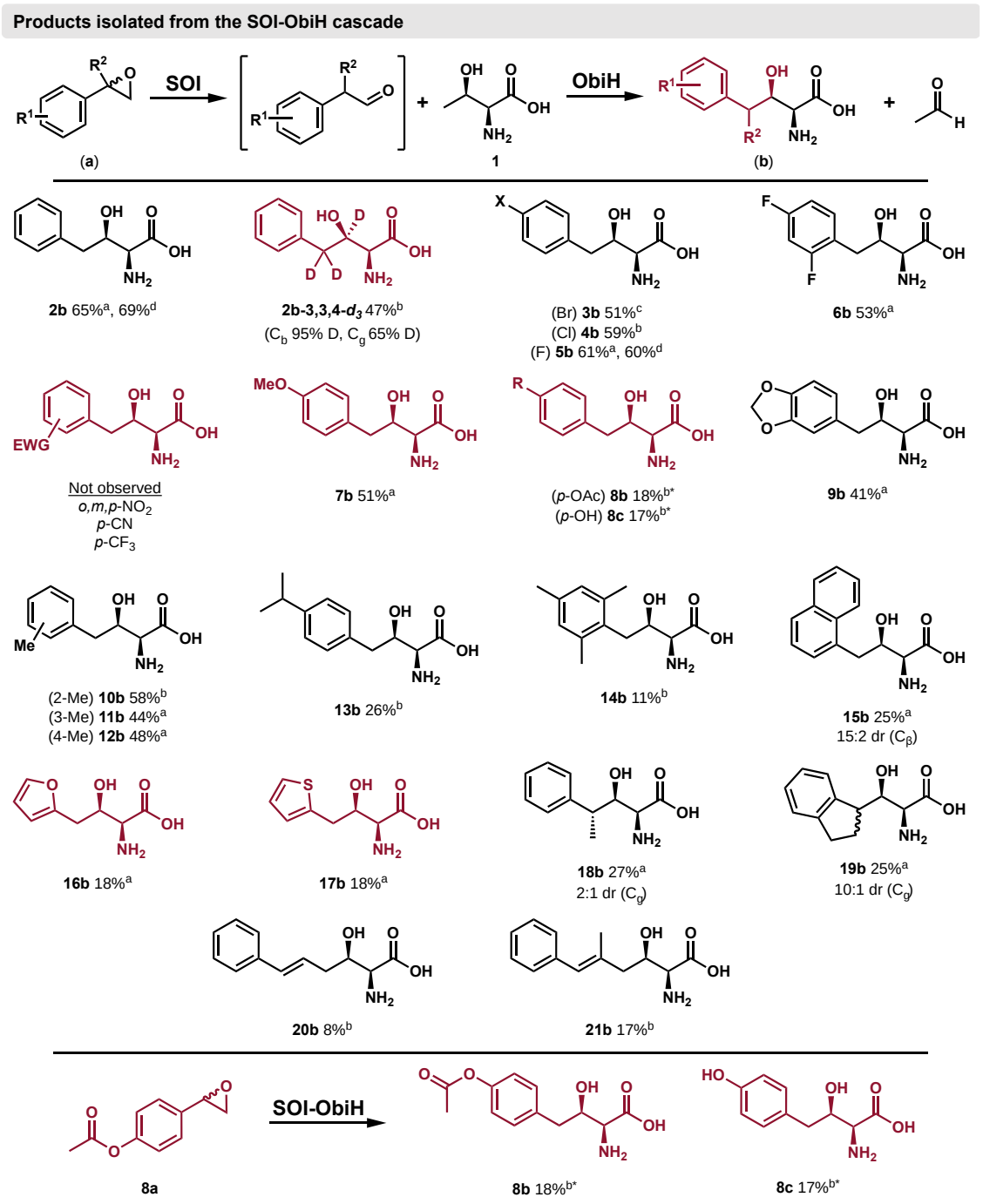

Figure 7. Preparative scale reactions with SOI-ObiH whole cells. Reactions were conducted with 1 mmol epoxide unless otherwise stated. General reaction conditions used 25 mM epoxide, 100 mM L-Thr, 100 uM PLP, 100 mM Tris•HCl pH 8.5, 5% EtOH, and variable concentrations of SOI-ObiH whole cells: 0.1% wcw[a], 1.0% wcw[b], or 0.1% dcw[d]; **3b**[c] (1 mmol epoxide, 2.5 mM, 0.1% wcw), **2b**[d] and **5b**[d] (2.5 mmol epoxide, 25 mM, 0.1% dcw). Products **8b** and **8c** were isolated from a single reaction with **8a**. Product purity was assessed via ^{1}H NMR. All products were derivatized with Marfey's reagent to determine dr indicating that all products were isolated with dr >19:1 and ee >99:1 with clean 2*R*, 3*S* stereochemistry unless otherwise noted. We estimate reactions at 1.0% wcw to have 5 µM ObiH present. Compounds synthesized or assayed by Prof. Patrick Willoughby are highlighted in dark red.

(Figure S1). These starting materials provide one of the most structurally diverse entry points for the synthesis of α-aryl acetaldehyde analogs (Figure 3a). Furthermore, the multi-enzymatic transformation was tolerant of contaminants present in crude mixtures of epoxide substrates, allowing us to utilize epoxides that are otherwise sensitive to chromatographic purification with silica gel. With this approach, we were able to generate and intercept diverse α-aryl aldehydes with ObiH and demonstrate the preparative-scale utility of this cascade (Figure 4).

We assayed the efficiency of the SOI-ObiH cascade with a series of styrene oxides. We began with an isotopically labeled styrene oxide in which the oxirane is fully substituted with deuterium (**2a-2,3,3-*d*$_3$**) which gave an amino acid product (**2b-3,4,4-*d*$_3$**) with deuterium at C_β and C_γ in 48% yield with 1.0% wcw, indicating the intramolecular transfer of a hydride during isomerization. We discuss the mechanistic implications associated with deuterated styrene oxides below and transitioned to epoxides with substitutions on the arene ring. Under standard reaction conditions, *p*-bromostyrene oxide (**3a**) and *p*-chlorostyrene oxide (**4a**) produced modest isolated yields of 16% and 36% respectively with equivalent catalyst loading (0.1% wcw). Increasing catalyst loading to 1.0% wcw with 25 mM **4a** enabled product isolation in 59% yield. In contrast, *p*-fluorostyrene oxide (**5a**) was isolated in 61% yield at 0.1% wcw catalyst loading. Additional halogen substitutions were tolerated as the product from a reaction with 2,4-difluorostyrene oxide (**6a**) resulted in an isolated yield of 53%. When considering other functional groups, we were excited about the possibility of entering the cascade with *p*-nitrostyrene oxide substrate, which would generate the native substrate for ObiH (4-nitrophenylacetaldehyde). However, we were unable to detect amino acid product from this substrate. Given that 4-nitrophenylacetaldehyde is the native substrate of ObiH, we attribute the lack of activity in the cascade to SOI and hypothesize that the electron withdrawing properties of this substrate destabilizes the partial positive charge build up on the benzyl carbon during isomerization. Other styrene oxide analogs functionalized with electron withdrawing groups also failed to generate product through the cascade (*o*-NO2, *m*-

NO2, *p*-CN, and *p*-CF3). In contrast, styrene oxides functionalized with electron rich substituents showed high activity in the SOI-ObiH cascade. *p*-Methoxy styene oxide (**7a**) reacted in the cascade with a yield of 51% at 1.0% wcw. We were interested accessing β-hydroxyhomotyrosine (**8c**) from the SOI-ObiH cascade as it is an important motif in pharmaceutically relevant natural products.[35–37] The corresponding *p*-hydroxy stryene oxide proved difficult to access, but we successfully transformed the acetylated epoxide (**8a**) into **8b** and **8c** with isolated yields of 18% and 17% from a single reaction. The benzodioxole containing epoxide derived from piperonal (**9a**) into an amino acid product with a 41% yield at 1.0% wcw. We then transitioned to styrene oxides substituted with aliphatic functional groups (**10a-12a**). Styrene oxides substituted with methyl groups at various positions on the phenyl ring all produced β-hydroxy-α-amino acid products, with 37-48% yield at 0.1% wcw catalyst loading. Standard reaction conditions with **10a** gave **10b** in 37% yield. We increased the catalyst loading to 1.0% wcw, which afford **10b** in 58% yield. *p*-Isopropyl styrene oxide (**13a**) reacted less efficiently in the SOI-ObiH cascade, resulting in an isolated yield of 26% at 1.0% wcw. The isomeric 2,4,6-trimethylstryene oxide (**14a**) was successfully transformed through the cascade, albeit with a low yield of 11%. The reactivity of the trimethyl substrate suggested that other bulky substrates might also react in the SOI-ObiH cascade. Naphthyl-2-aldehyde was previously observed to react with ObiH.[14] Here, we observed that the naphthyl-1-epoxide **15a** reacted in the cascade to produce the corresponding amino acid **15b** with a 25% yield. To assess whether SOI could convert epoxide functionalized aromatic heterocycles into the corresponding α-aryl aldehyde, we synthesized oxiranyl pyridine substrates from 2-, 3-, and 4-pyridine carboxaldehydes. However, no product was observed from the SOI-ObiH cascade. We speculated the electron-deficient nature of the pyridine heterocycle prohibited the Meinwald-like rearrangement, which correlates well to the inactivity on electron deficient styrene oxides. We therefore screened reactions with the electron rich furan and thiophene-containing epoxides. Both epoxides were successfully transformed into the corresponding amino acids **16b** and **17b** with an 18% yield.

Di-substitution at the α-position in the epoxide starting material presents a distinct challenge for SOI. Activity with α-methyl styrene oxide (**18a**) had been reported previously by Wu et al. We observed that racemic **18a** reacted in the SOI-ObiH cascade to give γ-methyl-β-hydroxyhomophenylalanine (**18b**) in 27% yield as a 2:1 mixture of diastereomers at C_γ which were readily resolved via UPLC-MS (Figure 8a). ^{1}H-NMR analysis indicated the major isomer has an *anti*-relationship between the hydroxy and methyl groups at C3 and C4, respectively, implying a 4*R* configuration for the major isomer. We synthesized the epoxide from 1-indanone (**19a**) which reacted in the cascade to give the bicyclic amino acid product (**19b**) in 25% yield and 10:1 d.r. Additional α-branched styrene oxide analogs including 1-tetralone and α-methyl styrene oxide analogs were also tested and appeared to form stable amino acids products as determined by UPLC-MS analysis and ^{1}H-NMR data from preparative scale reactions. However, low yields and convoluted structural data precluded isolation and full characterization (Table S1).

The promiscuous nature of SOI encouraged us to probe epoxides that were not α-aryl epoxides. We observed the cinnamaldehyde-derived epoxide reacted to generate β-hydroxy nsAA **20b**, albeit with low yield. Substitution with an additional methyl group increased the reactivity of the substrate, producing **21b** in 17% yield. We assayed other seemingly suitable non-aryl epoxides but failed to detect SOI activity with any epoxides that are not adjacent to an extended pi system (Table S1). Nevertheless, these are the first data demonstrating the SOI can catalyze a reaction with non-aryl epoxides. The overall scope presented here demonstrates the compatibility of SOI and ObiH to efficiently synthesize a variety of complex β-hydroxy nsAAs.

3. 2. 4. SOI catalyzes a concerted and stereospecific isomerization

We rationalized that diastereomeric enrichment observed in **18b** was a result of either SOI or ObiH exerting a stereopreference for one of the α-methyl-styrene oxide enantiomers or the disubstituted aldehyde intermediates, respectively. The intermediate produced by SOI in this reaction, 2-phenylpropanal (**22**), is commercially available and was subjected to reactions with

purified ObiH. Analysis via UPLC-MS revealed that ObiH forms the two diastereomers of **18b** in nearly equal populations, indicating ObiH exerts negligible stereoselectivity with this substrate (Figure 8b). We next subjected ***rac*-18a** to the SOI-ObiH cascade and quenched the reaction at early time points, which revealed a 70:30 mixture of diastereomers, which is consistent with the known stereochemical preference of SOI (Figure 8c).[22] To study the stereochemical outcome of the hydride transfer, we next prepared both enantiomers of α-methyl styrene oxide (**(*S*)-18a** and

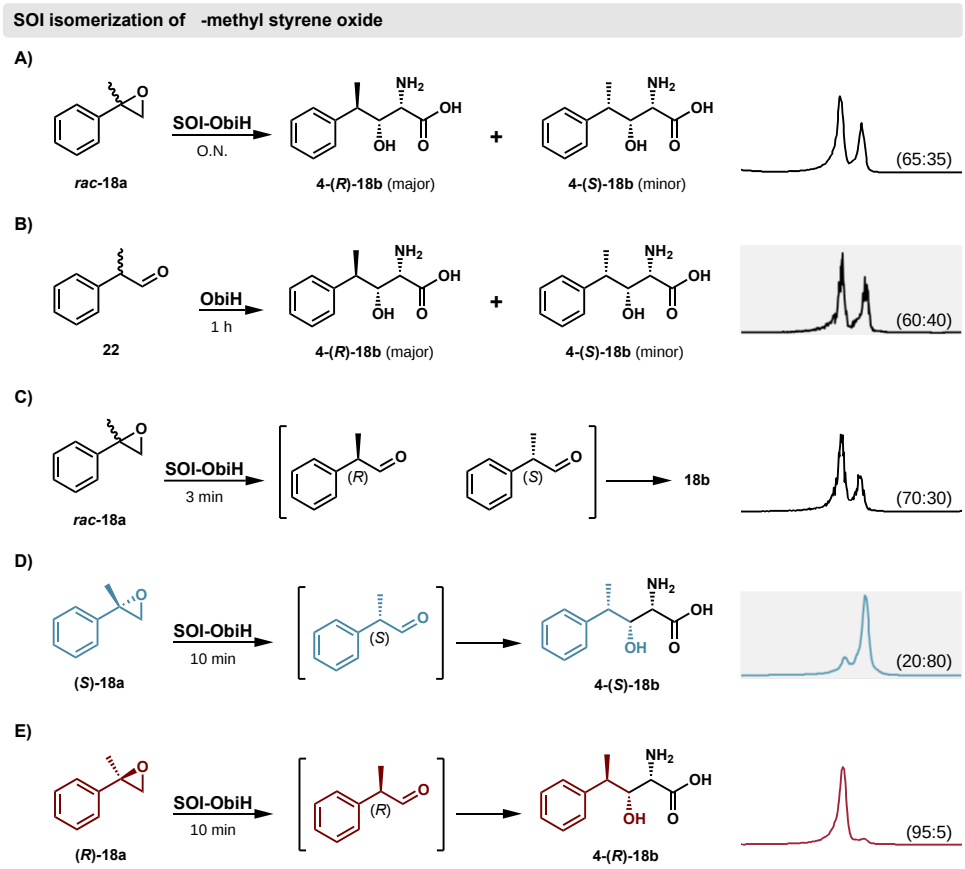

Figure 8. Stereochemical analysis of the SOI reaction. A) Reactions were run with 25 mM **18a** and 0.1% wcw SOI-ObiH catalyst. Products were analyzed via UPLC-MS, which resolves the diastereomers formed at the 4-position of **18b**. Isolated material from preparative scale reactions contains two diastereomers at C-4 with product ratios of 65:35. 1H-NMR analysis indicates that the 4*R* configuration is the major product. **B)** Reactions with 20 μM purified ObiH and 20 mM 2-phenylpropanal (**22**) were quenched after 1 h and yield **18b** with a 60:40 mixture of diastereomers. **C)** Reactions with 25 mM ***rac*-18a** and 0.1% wcw SOI-ObiH catalyst were quenched after 3 min and yield **18b** with a 70:30 mixture of diastereomers. **D)** Reactions with 25 mM **(*S*)-18a** and 0.1% wcw SOI-ObiH catalyst were quenched after 10 min and yield **18b** with a 20:80 mixture of diastereomers. **E)** Same as D), except **(*R*)-18a** is used and yields a 95:5 ratio of diastereomers.

(*R*)-18a) and subjected them to the SOI-ObiH cascade. A change in the Cahn-Ingold-Prelog priorities during the transformation of **18a** implies that inversion of configuration maintains the *S/R* designation in the product. Analysis via UPLC-MS clearly showed that each substrate generated a distinct stereoisomer when reactions were analyzed at early timepoints, **4-(*S*)-18b** (20:80) (Figure 8d) and **4-(*R*)-18b** (95:5) (Figure 8e), precluding a carbocation intermediate. Previously, Wu et al. noted that the SOI reaction is enantiorententive for substrates with substituents at the benzyl carbon (C-2) and has a slight preference for **(*R*)-18a** from kinetic resolution studies with ***rac*-18a**.[22] It was hypothesized SOI forms a carbocation intermediate after C–O cleavage and that the active site environment directs a stereospecific hydride shift to produces a single enantiomer of α-methyl-phenylacetaldehyde.[22,25,28] However, reactions with ***rac*-18a** produced both enantiomers of the corresponding aldehyde. If the mechanism were to proceed through a sp^2-hybridized, carbocation intermediate, a stereospecfic hydride shift would only produce a single enantiomer of the chiral aldehyde. *Instead, these data indicate that SOI catalyzes isomerization with inversion of configuration, which is indicative of a concerted Meinwald rearrangement.*

Cascade reactions with **(*S*)-18a** and **(*R*)-18a** were also allowed to progress past the initial velocity regime and we observed that the diastereomeric ratio decreased overnight to 53:47 and 65:35 for **(*S*)-18a** and **(*R*)-18a**, respectively (Figure S4). We hypothesized that decrease in d.r. was a result of accumulation and enolization of 2-phenylpropanal prior to being intercepted by ObiH. To probe enolization of α-aryl aldehydes under these conditions, the SOI-ObiH cascade was performed in D_2O with **2a** as a substrate. The amino acid product isolated from this reaction showed 85% deuterium incorporation at C_γ (Figure S5), providing strong evidence that the phenylacetaldehyde intermediate readily undergoes enolization under these reaction conditions.

We were intrigued by the concerted mechanism of SOI, which we sought to further substantiate through deuterium labelling experiments. As previously noted, reactions with **2a-2,3,3-*d*$_3$** gave an amino acid product (**2b-3,4,4-*d*$_3$**) with deuterium at C_β and C_γ, consistent with isomerization via a hydride shift (Figure 9a). However, it was unclear which of the two terminal hydrogen atoms were being transferred from C-3 to C-2 during isomerization. To this end, we synthesized stereo-enriched *cis* and *trans* β-monodeutero styrene oxides (**(±)-*cis*-2a-3-*d*$_1$** and **(±)-*trans*-2a-3-*d*$_1$**) (Figure 9b). Each substrate was reacted with the SOI-ObiH cascade and the location of deuterium atoms in the final α-amino acid product was determined by ^{1}H-NMR after product isolation. In the case with the deuterium *cis* to the phenyl ring (**(±)-*cis*-2a-3-*d*$_1$**), the amino

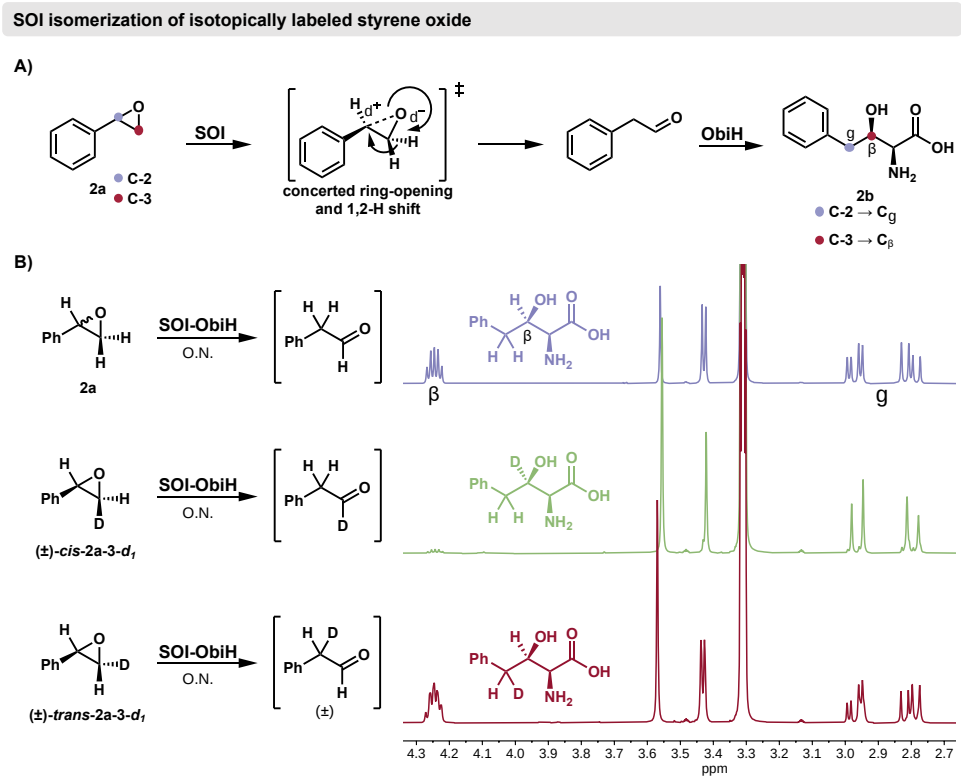

Figure 9. SOI catalyzes a concerted, stereoselective hydride transfer. A) Proposed mechanism for SOI catalyzed isomerization involving concerted ring-opening concomitant with a 1,2-H shift. **B)** Reactions with 25 mM **2a** and 0.1% wcw SOI-ObiH catalyst were allowed to proceed overnight followed by isolation of the products. ^{1}H-NMR spectra for isolated β-hydroxyhomophenylalanine and isotopologs. The presence of ^{2}H is inferred by diagnostic changes in the splitting and loss of a signal relative to the fully protic product (purple). Residual proton at C_β with **(±)-*cis*-2a-3-*d*$_1$** is due to incomplete deuteration of the starting material (green), see SI for details. Reaction with **(±)-*trans*-2a-3-*d*$_1$** results in ^{2}H-transfer followed by exchange with the protic solvent, which increases the proton integration (red).

acid product contained deuterium only at C_β, indicative of migration of the *trans* hydrogen (Figure 9b). Concurrently, work from the Zhi Li lab also demonstrated that SOI is stereospecific for the trans migration by observing transfer of a trans-methyl group over the cis-hydrogen.[25] Consistent with this observation, reactions with the **(±)-*trans*-2a-3-*d*$_1$** showed no deuterium at C_β and 25% deuterium at C_γ. The theoretical maximum labelling at C_γ would be 50%, indicating efficient transfer by SOI followed by hydrogen exchange due to enolization in protic solvent. Together, these experiments clarify the mechanism of SOI, which catalyzes a concerted isomerization with stereospecific 1,2-hydride-shift**.**

3. 2. 5. α-aryl acetaldehydes can be intercepted by an additional C–C bond forming enzyme.

We were originally attracted to ObiH because its native substrate is an α-aryl aldehyde.[33,34] To further establish the synthetic utility of these reactive intermediates, we sought to couple SOI with a different C–C bond forming enzyme. UstD is a PLP-dependent enzyme originally identified in the biosynthesis of Ustiloxin that catalyzes a stereoselective, decarboxylative aldol addition into diverse aldehydes to generate γ-hydroxy amino acids.[31] We recently engineered UstD for increased activity, which yielded a variant containing seven mutations from wild-type, named UstD$^{v2.0}$, that can react with a variety of aldehydes.[30] To test whether the α-aryl aldehydes generated by SOI can be intercepted by UstD$^{v2.0}$, we co-expressed each enzyme in *E. coli* BL21 (DE3). We observed evidence of product formation via UPLC-MS from styrene oxide (**2a**). We conducted an analytical substrate scope for the SOI-UstD cascade which showed that UstD was also capable of intercepting numerous aldehyde intermediates produced by SOI (Supplemental figure 6), albeit with low apparent activity.

To increase yields for preparative reactions with **2a**, cell loading was raised from 0.03-3% wcw but were still low-yielding (<30% yield) and the excess cell mass stymied product isolation. Given our experiences with the SOI-ObiH cascade, we hypothesized that UstD was flux-limiting

for the reaction. Therefore, we tested reactions with just 0.1% wcw SOI-only cells and high concentrations, 2.5–5 μM, of purified UstD$^{v2.0}$, which would reduce the introduction of cell mass that impedes purification. Use of this reaction format significantly increased yield of **24** to 74%, which was subsequently shown via Marfey's analysis to be a 5:2 mixture of diastereomers (Figure 10). This modest diastereoselectivity at C_γ is in contrast with previous studies, which showed that UstD forms the *4S* isomer with high selectivity with aryl aldehydes.[30] The stereocenter at the 2 position is set in a separate step in the proposed mechanism, and generally occurs with pristine *S*-selectivity with fold-type I PLP-dependent enzymes. A deuterated analogue of **24** was synthesized by performing the cascade reaction in D_2O. The product (**24-2,5,5-*d*$_3$**) was isolated with a 44% yield and a 2:1 mixture of diastereomers. We observed deuterium incorporation at C_δ (75%) and C_α (90%). This labeling is consistent with the proposed mechanism of UstD by Ye, which proceeds through a proton exchange at C_α.[31] Reactions with *p*-fluoro styrene oxide (**5a**) were also successful, and **25** was isolated in 53% yield and 7:2 d.r. We also noticed significant accumulation of a white precipitate in this reaction. We isolated this material and assigned the structure as a trimer of the α-aryl aldehyde formed by SOI (**26**). The formation of such species highlights the challenge of intercepting α-aryl aldehydes more broadly, as non-catalytic reaction pathways can be a significant hurdle. We tested reactions with the epoxide derived from cinnamaldehyde (**20a**) and although we observed evidence of product formation by analytical Marfey's derivatizations and NMR, the yield was too low for complete characterization. The yield and diastereoselectivity could plausibly be improved by directed evolution of UstD. For such studies, observation of a small amount of initial activity is often the largest uncertainty to developing a robust reaction. Together, these experiments demonstrate that the α-aryl aldehyde can be generated in situ by SOI under whole cell conditions and be intercepted with a C–C bond forming enzyme that does not natively react with this class of substrate, thereby rapidly building molecular complexity.

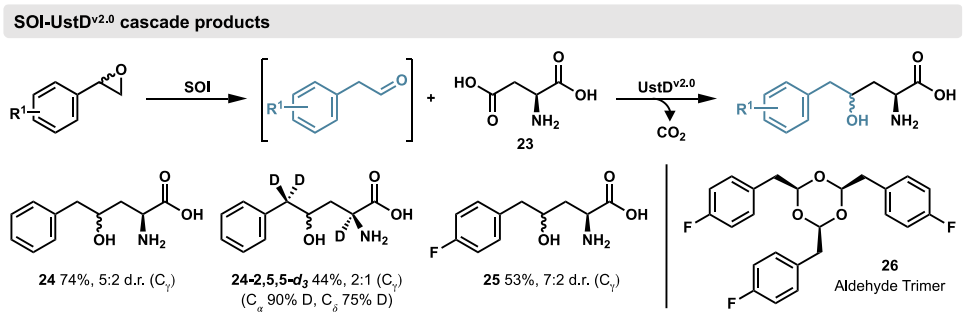

Figure 10. Synthesis of γ-hydroxy amino acids through a cascade reaction with SOI and UstD$^{v2.0}$. Reactions were conducted with 1 mmol epoxide. General reaction conditions used 25 mM epoxide, 50 mM L-Asp (**23**), 100 µM PLP, 100 mM KPi pH 7.0, 100 mM NaCl, 5% EtOH, 2.5-5 µM UstD$^{v2.0}$, and SOI whole cells at 0.1% wcw. Product purity and d.r. was assessed via ^{1}H NMR and derivatization with Marfey's reagent. The aldehyde trimer **26** was isolated as a side product from a reaction of **5a** under the standard reaction conditions. Compounds in this section were prepared by Meghan Campbell and Matthew McGill.

3. 3. Conclusions

Here we demonstrated a chemoenzymatic approach to generating diverse α-aryl aldehydes, which are versatile synthons for the synthesis of structurally diverse molecules. We show that the SOI-ObiH cascade is highly promiscuous and can generate a large panel of functionally rich, β-hydroxy-α-amino acids, which are highly sought molecules due to their prevalence in bioactive compounds. ObiH can deliver these nsAAs in both good yield and exceptional diastereoselectivity, which has been a challenge with the related Thr aldolase enzymes and traditional synthetic methodologies. Prompted by the utility of these α-aryl aldehydes, we sought to rectify conflicting mechanistic information about the Meinwald rearrangement catalyzed by SOI. A series of labelling studies indicate that SOI catalyzes a stereospecific, concerted 1,2-hydride shift without the intermediacy of a benzylic carbocation. While α-aryl aldehydes have often been avoided in past studies due to their intrinsic instability, this work establishes robust chemoenzymatic methodology to access these intermediates and provides a foundation for their elaboration in C–C bond forming cascades.

3. 4. Materials and Methods

General experimental procedures

Commercially available chemicals and reagents were purchased from Sigma-Aldrich, VWR, Chem-Impex International, Combi-blocks, Alfa Aesar, New England Biolabs, Zymo Research, Bio-Rad and used without further purification unless otherwise noted. Pyridoxal 5'-phosphate (i.e., PLP) was purchased as the hydrate from Sigma-Aldrich. BL21 (DE3) *E. coli* cells were electroporated with a Bio-Rad MicroPulser electroporator at 2500 V. New Brunswick I26R, 120 V/60 Hz shaker incubators (Eppendorf) were used for cell growth. Optical density was measured with an Amersham Biosciences Ultraspec 10 cell density meter. UPLC-MS data were collected on an Acquity UHPLC with an Acquity QDa MS detector (Waters) using an ACQUITY UPLC CSH BEH C18 column (Waters) or an Intrada Amino Acid column (Imtakt). High resolution mass spectrometry data were collected with a Q Extractive Plus Orbitrap instrument (NIH 1S10OD020022-1) with samples ionized by electrospray ionization (ESI) or an Agilent 6230 TOF LC/MS accurate-mass time-of-flight instrument (NSF CHE-1429616) with samples ionized by electrospray ionization (ESI). Preparative flash chromatographic separations were performed on a Biotage Isolera One or Teledyne Rf 200 flash chromatography system. NMR spectra were recorded on a Bruker AVANCE III-500 MHz spectrometer equipped with a DCH cryoprobe or a Variant Mercury Vx 300 NMR. ^{1}H NMR chemical shifts are reported in ppm (δ) relative to the solvent resonance for D_2O (δ 4.79 ppm), DMSO-d_6 (δ 2.50 ppm), and CD_3OD (δ 3.31 ppm). ^{1}H NMR spectra acquired in $CDCl_3$ were referenced to TMS (δ 0.00 ppm). ^{13}C NMR spectra were acquired with ^{1}H decoupling. ^{13}C NMR chemical shifts are reported in ppm (δ) relative to the solvent resonance for $CDCl_3$ (δ 77.16 ppm), DMSO-d_6 (δ 39.52 ppm), and CD_3OD (δ 49.00 ppm). All ^{19}F NMR and ^{13}C NMR acquired in D_2O without an internal standard were referenced to the absolute frequency of 0.00 ppm in the corresponding, internally referenced ^{1}H NMR spectrum (i.e., "Absolute Reference" or "Absolute Referencing").[37] Data are reported as follows: chemical

shift (multiplicity [singlet (s), doublet (d), doublet of doublets (dd), multiplet (m)], coupling constants [Hz], integration). All NMR spectra were recorded at ambient temperature.

Cloning Optimization and Expression

SOI cloning and expression

A codon-optimized copy of the *Pseudomonas sp.* VLB120 *StyC* (SOI) gene was purchased as a gBlock from Integrated DNA Technologies. This DNA fragment was inserted into a pET22b vector by the Gibson Assembly method.[38] BL21 (DE3) *E. coli* cells were subsequently transformed with the cyclized DNA product via electroporation. After 45 min of recovery in Terrific Broth (TB) media at 37 °C, cells were plated onto LB plates with 100 µg/mL ampicillin (Amp) and incubated overnight. Following initial cloning into the pET22b vector, the gene encoding SOI was transferred to a pBAD vector (p15A origin, Kanamycin resistant).

Single colonies were used to inoculate 10 mL TB + 50 µg/mL Kan (TB-Kan), which were grown overnight at 37 °C, 200 rpm. Expression cultures, typically 1 L of TB-Kan, were inoculated with starter cultures (1% inoculum) and shaken (200 rpm) at 37 °C. After ~3 hours (OD_{600} = ~0.6), the expression cultures were chilled on ice. After 30 min on ice, expression of the protein was induced with 0.2% w/v arabinose. The cultures were expressed for 16-24 hours at 20 °C with shaking at 200 rpm. Cells were then harvested by centrifugation at 4,300×*g* at 4 °C for 10 min. Cell pellets were either freeze dried via lyophilization or extruded from a syringe and flash frozen in liquid nitrogen as small pellets to give flash frozen “wet” cells.

SOI/ObiH Expression

N-His ObiH was cloned into pET22b for origin and antibiotic resistance compatibility. *E. coli* (BL21 DE3) were transformed with the two plasmids encoding SOI and ObiH and plated on LB-agar containing Amp and Kan. Single colonies were used to inoculate 10 mL TB + 100 µg/mL Amp + 50 µg/mL Kan (TB-Amp-Kan), which were grown overnight at 37 °C, 200 rpm. Expression

cultures, typically 1 L of TB-Amp-Kan, were inoculated with starter cultures (1% inoculum) and shaken (200 rpm) at 37 °C. After ~3 hours (OD_{600} = ~0.6), the expression cultures were chilled on ice for 30 min. Expression of the two proteins was induced with 0.2% w/v arabinose (SOI) and 1.0 mM IPTG (ObiH). The cultures were expressed for 16-24 hours at 20 °C with shaking at 200 rpm. Cells were then harvested by centrifugation at 4,300×*g* at 4 °C for 10 min. Cell pellets were either freeze dried via lyophilization or transferred to a syringe and flash frozen into liquid nitrogen as wet *E. coli*.

SOI/UstD$^{v2.0}$ Expression

E. coli were transformed with the two plasmids encoding SOI and UstD$^{v2.0}$ and plated on LB-agar containing Amp and Kan. Single colonies were used to inoculate 5 mL TB + 100 µg/mL Amp + 50 µg/mL Kan (TB-Amp-Kan), which were grown overnight at 37 °C, 200 rpm. Expression cultures, typically 1 L of TB-Amp-Kan, were inoculated with starter cultures (1% inoculum) and shaken (200 rpm) at 37 °C. After ~3 hours (OD_{600} = ~0.6), the expression cultures were chilled on ice. After 30 min on ice, expression of the two proteins was induced with 0.2% w/v arabinose (SOI) and 1.0 mM IPTG (UstD$^{v2.0}$). The cultures were expressed for 16-24 hours at 20 °C with shaking at 180 rpm. Cells were then harvested by centrifugation at 4,300×*g* at 4 °C for 15 min. Cell pellets were frozen by extruding through a syringe into liquid nitrogen. Frozen cells were transferred to 50 mL falcon tubes and stored at -80 °C until further use.

UstD$^{v2.0}$ Expression

UstD$^{v2.0}$ was expressed according to the previously reported literature.[30]

Procedure for Analytical Scale Reactions (i.e., total reaction volume < 1 mL)

Coexpressed SOI/ObiH analytic whole cell reaction conditions

Lyophilized cells harboring ObiH and SOI were resuspended in 100 mM Tris-HCl pH 8.5 at 2X the desired concentration for analytical reactions. The 2X cell solution was added to reactions with final concentration of 25 mM epoxide (delivered via a 500 mM stock dissolved in DMSO, 5% DMSO in reaction), 100 mM L-Thr, 0.1 mM PLP, and 100 mM Tris-HCl pH 8.5 unless otherwise stated. Epoxide stocks were prepared at 500 mM in DMSO. Analytical reactions were incubated in glass vials at 37 °C and quenched with equal volume of acetonitrile. Quenched reactions were centrifuged at 15,000-20,000×*g* for 10 min to pellet cell debris. Supernatant was removed and analyzed via UPLC-MS for product quantification.

SOI whole cell reactions with purified ObiH

Lyophilized whole cells only expressing SOI were resuspended in 100 mM Tris-HCl pH 8.5 at 2X (2 mg/mL) the desired concentration. The 2X cell solution was added to reactions with 20 µM ObiH unless stated otherwise and reagent concentrations of 25 mM epoxide (delivered via a 500 mM stock dissolved in DMSO, 5% DMSO in reaction), 100 mM L-Thr, 0.1 mM PLP, and 100 mM Tris-HCl pH 8.5. Reactions were incubated in glass vials at 37 °C and quenched with equal volume of acetonitrile. Quenched reactions were centrifuged at 15,000-20,000×*g* for 10 min to pellet cell debris. Supernatant was removed and analyzed via UPLC-MS for product quantification.

Reactions with purified ObiH

Reactions with purified ObiH were conducted with the following concentrations. 20 µM ObiH and reagent concentrations of 20 mM 2-phenylacetaldehyde (delivered via a 500 mM stock dissolved in DMSO, 5% DMSO in reaction), 100 mM L-Thr, 0.1 mM PLP, and 100 mM Tris-HCl pH 8.5. Reactions were incubated in glass vials at 37 °C and quenched with equal volume of acetonitrile.

Quenched reactions were centrifuged at 15,000-20,000×*g* for 10 min to pellet cell debris. Supernatant was removed and analyzed via UPLC-MS for product quantification.

Co-expressed SOI/UstD$^{v2.0}$ cell loading

Frozen wet cells harboring UstD$^{v2.0}$ and SOI were resuspended in buffer (100 mM KPi pH 7.0 with 100 mM NaCl) at 2X the desired concentration for analytical reactions. The 2X cell solution (final cell concentrations 0.03125, 0.063, 0.125, 0.25, 0.5, 1, 2, 3 w/v%) was added to reactions with final concentration of 25 mM styrene oxide, 5% DMSO, 50 mM l-Asp, 0.05 mM PLP, and 100 mM KPi pH 7.0, 100 mM NaCl. Epoxide stocks were prepared at 500 mM in DMSO. Analytical reactions were incubated in microcentrifuge tubes at 37 °C and quenched with equal volume of acetonitrile. Quenched reactions were centrifuged at 15,000-20,000×*g* for 10 min to pellet cell debris. Supernatant was removed and analyzed via UPLC-MS for product quantification.

SOI cell loading comparing BL21 and RARE strains with purified UstD$^{v2.0}$

Frozen wet cells (either BL21 or RARE strain) harboring SOI were resuspended in buffer (100 mM KPi pH 7.0 with 100 mM NaCl) at 2X the desired concentration for analytical reactions. The 2X cell solution (final cell concentrations 0.1, 0.5, 1 w/v%) was added to reactions with final concentration of 25 mM styrene oxide, 5% DMSO, 50 mM l-Asp, 0.25 mM PLP (10x UstD$^{v2.0}$ concentration), 0.025 mM UstD$^{v2.0}$, and 100 mM KPi pH 7.0, 100 mM NaCl. Epoxide stocks were prepared at 500 mM in DMSO. Analytical reactions were incubated in microcentrifuge tubes at 37 °C and quenched with equal volume of acetonitrile. Quenched reactions were centrifuged at 15,000-20,000×*g* for 10 min to pellet cell debris. Supernatant was removed and analyzed via UPLC-MS for product quantification.

General Procedures

General Procedure A: Preparative Scale Whole Cell SOI/ObiH Reactions

Epoxide (typically 1.0-2.5 mmol), indicated co-solvent (5% of total reaction volume), buffer (40 mL per mmol of epoxide, 100 mM Tris-HCl pH 8.5), l-Thr (4.0-10 mmol, 4 equiv, final reaction concentration 100 mM), and PLP [delivered from a previously prepared 20 mM aqueous stock solution (200 μL of solution per 1.0 mmol of epoxide) for a final reaction concentration of 0.1 mM] were added to an Erlenmeyer flask. Whole cells (SOI-ObiH, 0.1 or 1% m/v%) were massed and added directly to reaction flasks. Reactions were incubated overnight at 37 °C, 200 RPM. To lyse the cells, the reaction mixture was diluted with an equal volume of MeCN, transferred to centrifuge tubes or bottles, frozen at -20 or -80 °C, and thawed at 50–75 °C for 30 minutes. The resulting mixture was centrifuged at ca. 4,000-10,000x*g* at ambient temperature for 10 min to pellet cell debris. The clarified supernatant was passaged over filter paper, and the filtrate was concentrated by rotary evaporation. The resulting material was loaded onto a reversed-phase column (C18) and purified by automated flash purification with a water/methanol gradient. Fractions were analyzed by LC-MS to identify product containing fractions. Fractions containing pure product were pooled, concentrated by rotary evaporation, and dried via lyophilization.

General Procedure B: Marfey's Derivatization Reactions

All Amino acid products were derivatized with l-FDAA to determine diastereomeric purity in accordance with the procedure by Marfey.[35] Derivatization reactions were completed with crude reactions mixtures or isolated product. For crude reaction mixtures, samples were quenched with 1 volume of MeCN and clarified through centrifugation. The resulting supernatants were diluted 10 fold with 1:1 MeCN:H_2O. For isolated product, a small amount of isolated product (~1-2 mg) was dissolved in 1 mL of 1:1 MeCN:H_2O. In a microcentrifuge tube, 30 μL of reaction or product sample (final amine concentration < 1 mM) was added to a solution of 150 μL of 15 mM $NaHCO_3$

(7.5 mM final concentration) followed by addition of 120 µL 10 mM L-FDAA dissolved in MeCN (4 mM final concentration) to bring the total reaction volume to 300 µL. Each reaction was placed in a dark 37 °C incubator for 12-16 h, then quenched with 300 µL of MeCN:60 mM HCl (30 mM post-quench) before analyzing by Waters Acquity UPLC-PDA-MS using a BEH C18 column (Waters).

General Procedure C: Synthesis of Epoxides Starting Materials from Aldehydes

Sodium hydride (26.8 mmol, 2.0 equiv, 60% in mineral oil) was added to an oven-dried round bottom flask, washed with hexanes (3 x 10 mL), and resuspended with THF (16 mL) and DMSO (14 mL). Trimethylsulfonium iodide (26.8 mmol, 2.0 equiv) was added at rt with stirring under inert atmosphere. After 30 min, the resulting mixture was cooled to 0 ºC, the carbonyl substrate (13.4 mmol, 1.0 equiv) was added as a solution in THF (5 mL), and the reaction was allowed to gradually warm to room temperature. After 12–24 h, the reaction was quenched by addition of 5–20 g of ice, diluted with ethyl acetate (50 mL). The resulting mixture was sequentially washed with water and brine, dried ($MgSO_4$), filtered, and concentrated to provide the crude epoxide with varying amounts of DMSO and ethyl acetate contamination. Due to the instability of styrene oxides on silica, the crude material was used without further purification.

General Procedure D: Synthesis of Epoxides Starting Materials from Ketones from α-Bromo Ketones

Sodium borohydride (12 mmol, 1.5 equiv) was added to a mixture of α-bromo ketone (8 mmol, 1.00 equiv) in methanol (20 mL) at 0 ºC with stirring. After 1 h, the reaction mixture was concentrated by rotary evaporation, diluted in ethyl acetate (50 mL), sequentially washed with ammonium chloride and brine, dried ($MgSO_4$), filtered and concentrated. ^{1}H NMR analysis indicated the crude reaction contained a mixture of halohydrin and epoxide. The crude mixture was diluted with THF (20 mL) and 1M NaOH (20 mL) and set to a vigorous stir. After 2 h, the mixture was diluted in ethyl acetate (50 mL), sequentially washed with water and brine, dried

($MgSO_4$), filtered and concentrated to give the crude epoxide, which was sufficiently pure (i.e., often >95%) for subsequent biocatalytic transformations.

3. 5. Supplemental Figures and Tables

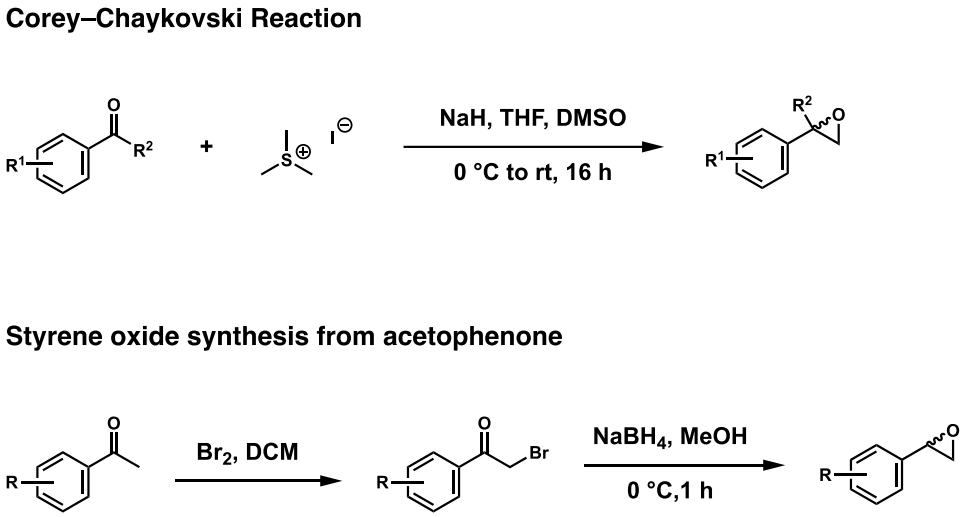

Figure S1. Synthesis of α-aryl aldehydes. Aryl aldehydes and acetophenones are readily converted into aryl epoxides.

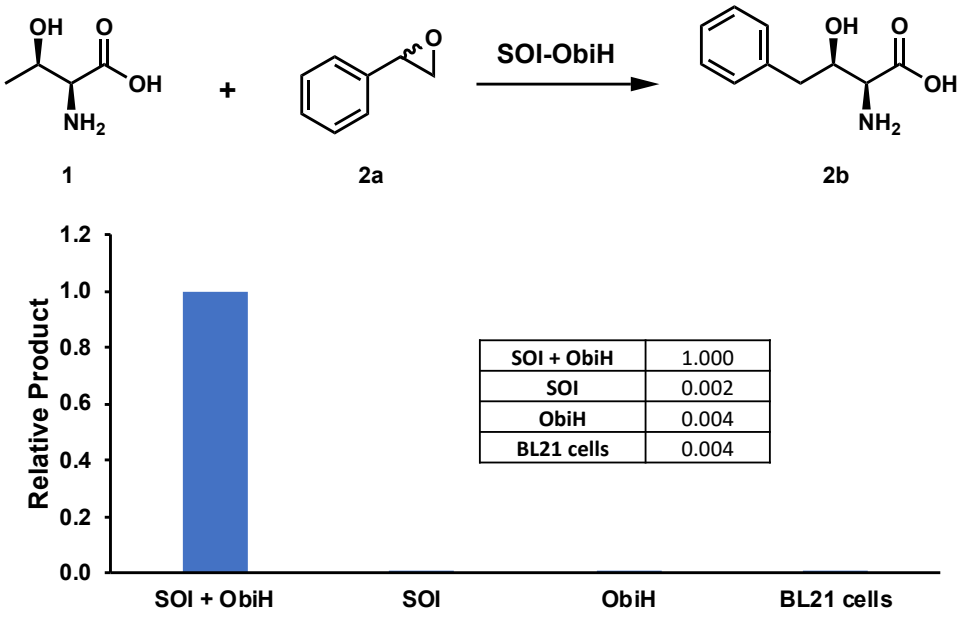

Figure S2. Reaction controls with BL21 cells expressing SOI and purified ObiH. SOI cells were pelleted after overnight expression and resuspending in 1/3 volume in 100 mM Tris-HCl pH 8.5 to produce a 3X cell stock for reactions. Reaction conditions: 25 mM styrene oxide (**2a**), 100 mM Thr (**1**), 0.1 mM PLP, 5% DMSO, in 100 mM Tris-HCl pH 8.5. Reactions were quenched with equal volume MeCN and analyzed via UPLC-MS for product formation. Product formation requires the combination of SOI and ObiH. Reactions containing all reagents on only SOI or only ObiH resulted in no product formation. The relative integration is equal to reactions containing BL21 cells containing no plasmid (i.e. *E. coli* cells that do no have SOI nor ObiH).

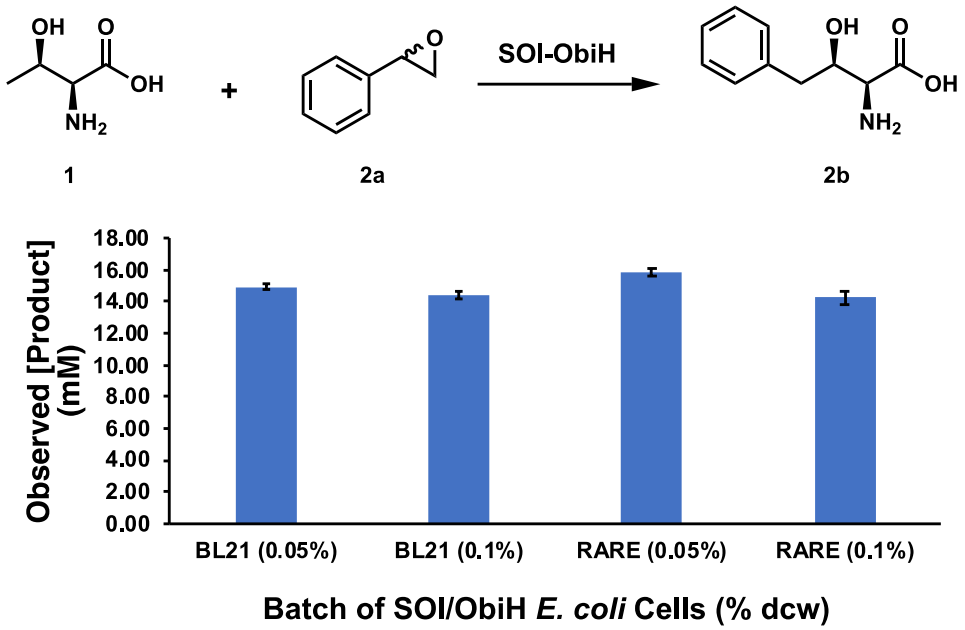

Figure S3. Comparison of SOI-ObiH cascade activity when expressed in *E. coli* BL21 (DE3) and *E. coli* K-12 MG1655 RARE (DE3). Analytical reactions with either BL21 or RARE cells at 0.05% and 0.1% dcw with standard reaction conditions in overnight reactions: 25 mM styrene oxide (**2a**), 100 mM Thr (**1**), 0.1 mM PLP, 5% DMSO, in 100 mM Tris-HCl pH 8.5. Reactions were quenched with equal volume MeCN and analyzed via UPLC-MS for product formation. Cell type comparison was completed by Prof. Patrick Willoughby.

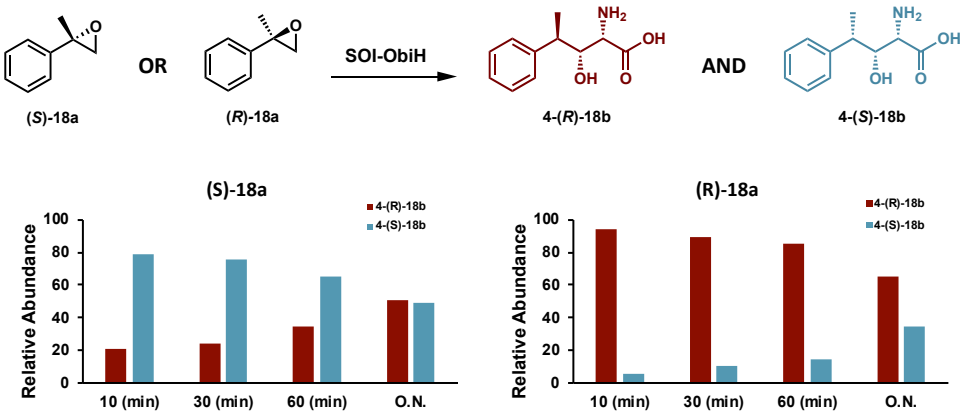

Figure S4. Reactions with (*S*)-α-methyl styrene oxide and (*R*)-α-methyl styrene oxide. Reactions were analyzed via UPLC-MS to determine product ratios for γ-methyl-β-hydroxyhomophenylalanine (**18b**). Reactions with both **(*S*)-18a** and (***R*)-18a** were conducted with 25 mM epoxide, 100 mM Thr, 0.1 mM PLP, 0.1% wcw, and 5% DMSO in 100 mM Tris-HCl pH 8.5. Reaction samples were removed and quenched at 10 min, 30 min, 60 min, and after overnight incubation at 37 °C with equal volume MeCN.

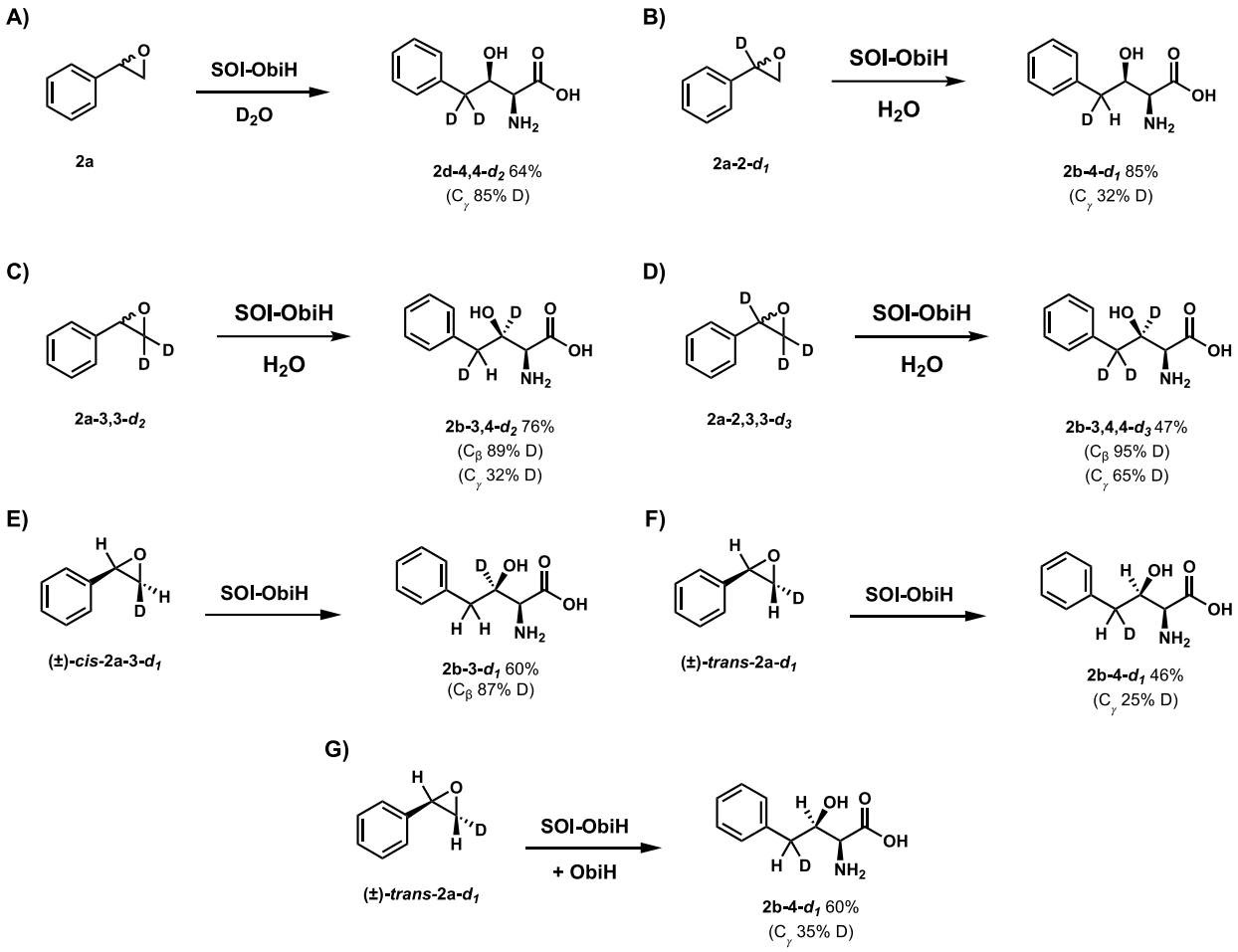

Figure S5. Preparative scale reactions for deuterated β-hydroxyhomophenylalanine (**2b**). Detailed descriptions for reactions conditions are included in small molecule preparation and characterization section.

Table 1: Epoxide substrates that failed to produce amino acid product in the SOI-ObiH cascade.

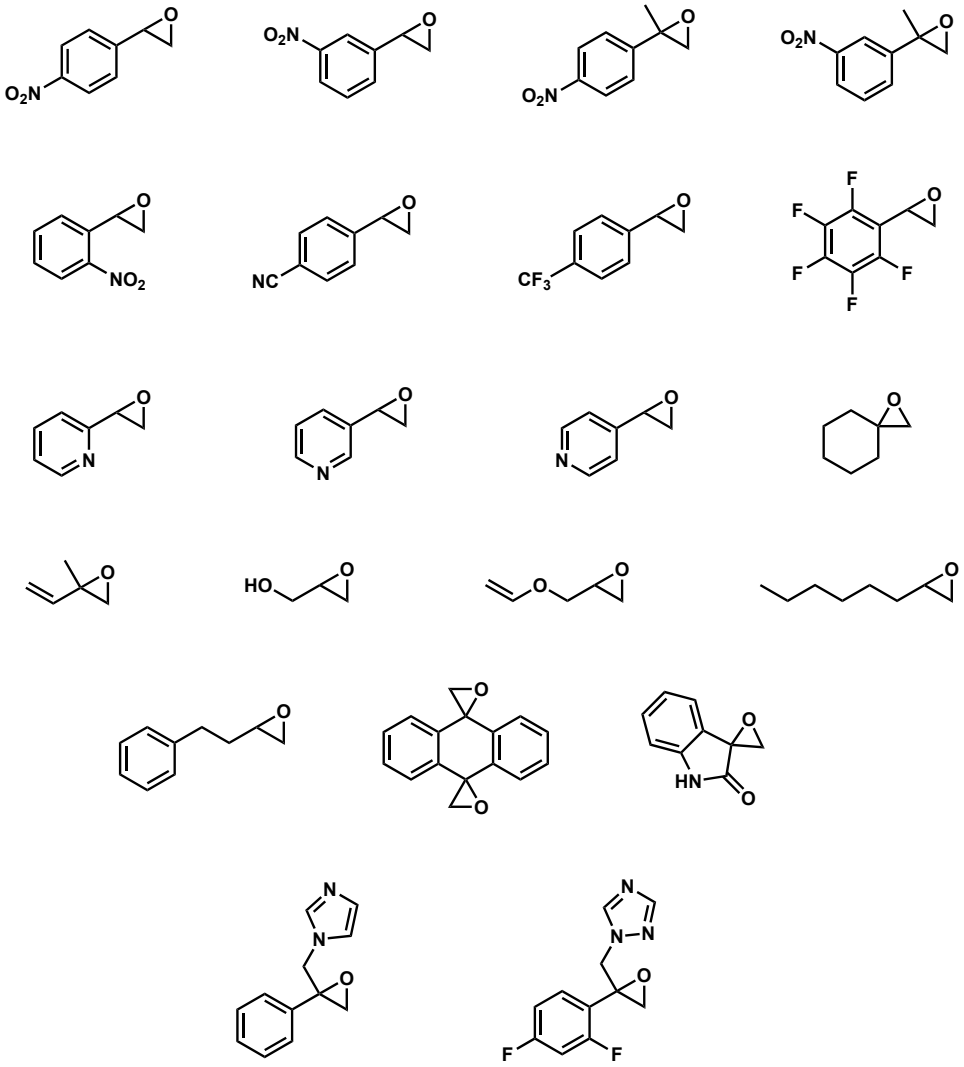

Table 2: Compounds produced through the SOI-ObiH cascade that were not fully characterized. Analytical techniques validating product formation; UPLC-MS (a), HRMS (b), Marfey's derivatization (c), ^{1}H NMR (d). Data for Marfey's derivatization is included below.

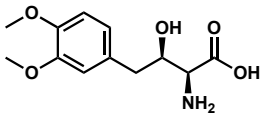

S1 (a, b, c, d)

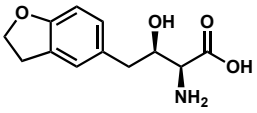

S2 (a, b, c)

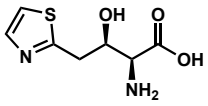

S3 (a, b)

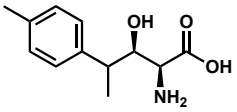

S4 (a, c)

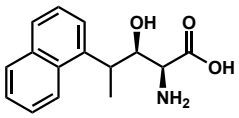

S5 (a, b)

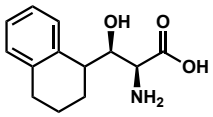

S6 (a, b, c)

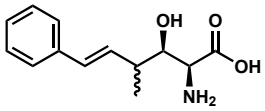

S7 (a, b, c)

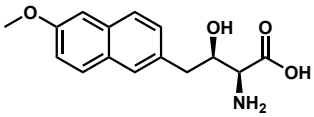

S8 (a, c, d)

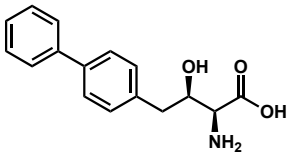

S9 (a, c, d)

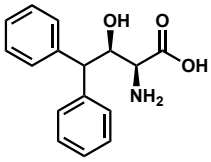

S10 (a, b, c)

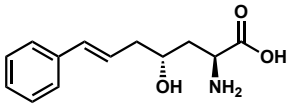

S11 (a, b, c, d)

Details on the Preparation and Characterization of All New Compounds and Select Known Compounds

Compounds Discussed in Figure 7:

(2*S*,3*R*)-2-Amino-3-hydroxy-4-phenylbutanoic Acid (2b)

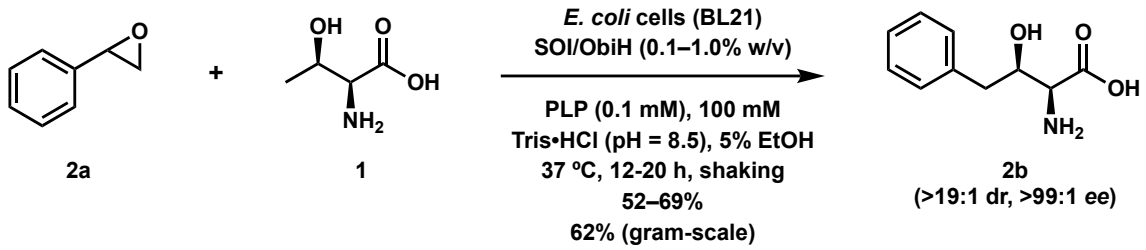

2a 1 2b

(>19:1 dr, >99:1 *ee*)

[1.0–2.5 mmol scale] Amino acid **2b** was prepared following General Procedure A with commercially available styrene oxide (**2a**, 118 mg, 0.98 mmol), L-Thr (**1**, 480 mg, 4.0 mmol), PLP (200 µL via 20 mM solution in water, 0.004 mmol), flash frozen SOI/ObiH *E. coli* BL21 wet whole cells (0.040 g, 0.1% w/v) in Tris•HCl buffer solution (37.6 mL, 100 mM, pH = 8.5), and 2 mL EtOH. Purification by automated gradient flash chromatography (C18, MeOH:H_2O 1:99 to 1:0 over 30 column volumes) and subsequent lyophilization gave 133 mg of product as a white solid with 34 mg tris base contamination as determined by ^{1}H NMR, yielding 99 mg of **2b** (0.51 mmol, 52%). Increasing the wet whole cell loading to 1.0% w/v (i.e., 400 mg) in an otherwise identical procedure with styrene oxide (**2a**, 120 mg, 1.0 mmol) provided 135 mg of product as a white solid with 8 mg tris base contamination as determined by ^{1}H NMR, yielding 127 mg of **2b** (0.65 mmol, 65%). Replacing the wet whole cells with lyophilized whole cells (i.e., 100 mg, 0.1% w/v) with styrene oxide (**2a**, 300 mg, 2.5 mmol) provided 376 mg of product as a white solid with 37 mg tris base contamination as determined by ^{1}H NMR, yielding 339 mg of **2b** (1.74 mmol, 69%).

[Gram-Scale] Amino acid **2b** was prepared following General Procedure A with styrene oxide (**2a**, 1.20 g, 10.0 mmol), L-Thr (**1**, 4.78 g, 40.1 mmol), PLP (2.0 mL via 20 mM solution in water, 0.04 mmol), flash frozen SOI/ObiH *E. coli* BL21 wet whole cells (0.401 g, 0.1% w/v) in Tris•HCl buffer solution (376 mL, 100 mM, pH = 8.5), and 20 mL EtOH. Purification by automated gradient flash chromatography (C18, MeOH:H_2O 1:99 to 1:0 over 40 column volumes) and subsequent lyophilization gave 1.28 g of product as a white solid with 70 mg tris base contamination as determined by ^{1}H NMR, yielding 1.21 of **2b** (6.2 mmol, 62%).

[Using KPi buffer] Amino acid **2b** was prepared following General Procedure A with styrene oxide (**2a**, 116 mg, 0.97 mmol), L-Thr (**1**, 480 mg, 4.0 mmol), PLP (200 µL via 20 mM solution in water, 0.04 mmol, 0.1 mM final reaction conc.), flash frozen SOI/ObiH *E. coli* BL21 wet whole cells (403 mg, 1.0% w/v) in KPi buffer solution (38 mL, 100 mM, pH = 8.0), and 2 mL EtOH. Purification by automated gradient flash chromatography (C18, MeOH:H_2O 1:99 to 1:0 over 30 column volumes) and subsequent lyophilization gave **2b** as a white solid (72 mg, 0.37 mmol, 38%).

Marfey's analysis (cf. General Procedure B) was used to confirm the stereochemical purity (i.e., >19:1 dr and >99% *ee*), and the relative configuration was assigned based previously observed ObiH stereoselectivities.[13,14] Comparing the ^{1}H and ^{13}C NMR chemical shifts to the previously reported[39] *erythro* epimer showed differences at all nuclei, and the greatest difference in ^{1}H shifts was observed [Dd 0.54 ppm for 3.68 (reported here) vs 4.22 ppm (reported *erythro* epimer)].

^{1}H NMR (500 MHz, CD_3OD): δ 7.33 – 7.25 (m, 4H), 7.25 – 7.16 (m, 1H), 4.25 (ddd, *J* = 9.0, 4.6 4.6 Hz, 1H), 3.43 (d, *J* = 4.4 Hz, 1H), 2.97 (dd, *J* = 13.9, 4.7 Hz, 1H), and 2.81 (dd, *J* = 13.9, 9.0 Hz, 1H).

^{1}H NMR (500 MHz, D_2O): δ 7.46 – 7.41 (m, 2H), 7.39 – 7.33 (m, 3H), 4.33 (ddd, *J* = 9.3, 4.5 4.5 Hz, 1H), 3.68 (d, *J* = 4.8 Hz, 1H), 3.06 (dd, *J* = 14.1, 4.4 Hz, 1H), and 2.85 (dd, *J* = 14.1, 9.7 Hz, 1H).

^{13}C{^{1}H} NMR (126 MHz, D_2O, referenced to CH_3OH internal standard at δ 49.50): δ 173.4, 138.1, 130.0, 129.4, 127.5, 71.5, 59.6, and 40.4.

HRMS (ESI$^-$): Calcd for $C_{10}H_{13}NO_3^-$ [M – H]$^-$ requires 194.0823; found 194.0823.

2-Phenyloxirane-2,3,3-d_3 (2a-2,3,3-d_3)

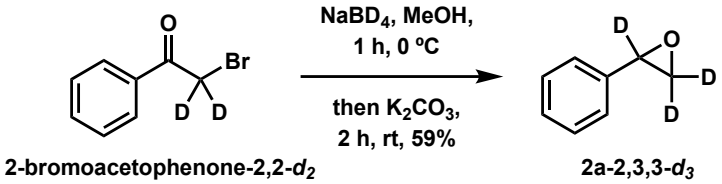

2-bromoacetophenone-2,2-d_2 **2a-2,3,3-d_3**

2-Phenyloxirane-2,3,3-d_3 (**2a-3,3-d_2**) was prepared from 2-bromoacetophenone-2,2-d_2. 2-Bromoacetophenone-2,2-d_2 using a slightly modified protocol previously reported by Kass.[40] Namely, deuterium incorporation of 2-bromoacetophenone was enhanced by increasing the amounts of reactants and extending the reaction time from 3 hours to 24 hours. Specifically, *t*-BuOK (2.0 g, 18 mmol) was added portionwise to a mixture of 2-bromoacetophenone (2.0 g, 10 mmol) and $CDCl_3$ (12 mL) at 0 ºC with stirring (CAUTION: A vigorous exotherm forms upon addition of potassium *tert*-butoxide. The caustic reagent must be added slowly.). After 1 h, D_2O (7.5 mL) was added dropwise and additional *t*-BuOK (1.3 g, 12 mmol) is added portionwise and the mixture is allowed to stir overnight, warming to room temperature. After 24 h, the mixture was transferred to a separatory funnel and diluted in $CDCl_3$ (20 mL). The organic phase was dried ($MgSO_4$), filtered, and concentrated to give 2-bromoacetophenone-2,2-d_2 (1.3 g, 64% crude) with ~85% deuterium incorporation at C2.

Sodium borodeuteride (280 mg, 6.7 mmol) was added portionwise to a mixture of 2-bromoacetophenone-2,2-d_2 (1.34 g, 6.66 mmol) in MeOH (15 mL) at 0 ºC with stirring. After 1 h, potassium carbonate (1.0 g, 7.2 mmol) was added, and the mixture was allowed to stir at room temperature. After 2 h, the mixture was concentrated by rotary evaporation, and the residue was suspended in ethyl acetate (50 mL) and water (50 mL). The aqueous phase was separated, and the organic phase was washed with brine, dried ($MgSO_4$), filtered, and concentrated. Purification by gradient flash chromatography (SiO_2, hexanes:ethyl acetate 1:0 to 19:1) using silica gel that was pre-rinsed with 1% Et_3N in hexanes gave epoxide **2a-2,3,3-d_3** (485 mg, 3.94 mmol, 59%). ^1H

NMR analysis of the crude product mixture suggested the presence of **2a-2,3,3-*d*$_3$** (i.e., >95% deuterium incorporation) due to ablation of the aliphatic resonances (i.e., d ~3.8, 3.1, 2.8 ppm) in the typical spectrum of styrene oxide.

^{1}H NMR (300 MHz, $CDCl_3$): δ 7.48 – 7.22 (m, 5H), 3.87 (s, <0.01H), 3.14 (s, 0.02H), 2.80 (s, 0.02H).

HRMS (ESI^+): Ions were observed corresponding with ***d*$_3$** only (i.e., Calcd for $C_8H_6D_3O^+$ $[M + H]^+$ requires 124.0836; found 124.0828).

HRMS (ESI^+): Calcd for $C_8H_6D_3O^+$ $[M + H]^+$ requires 124.0836; found 124.0828

(2*S*,3*R*)-2-Amino-3-hydroxy-4-phenylbutanoic-3,4,4-*d*$_3$ Acid (2b-3,4,4-*d*$_3$)

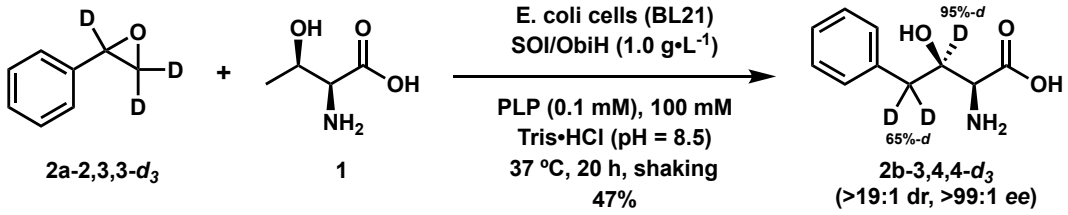

Amino acid **2b-3,4,4-*d*$_3$** was prepared following General Procedure A with 2-phenyloxirane-2,3,3-*d*$_3$ (**2a-2,3,3-*d*$_3$**, 132 mg, 1.07 mmol), L-Thr (**1**, 480 mg, 4.0 mmol), PLP (200 µL via 20 mM solution in water, 0.004 mmol, 0.1 mM final reaction conc.), wet SOI/ObiH *E. coli* BL21 whole cells (411 mg, 1% w/v%) in Tris•HCl buffer solution (38 mL, 100 mM, pH = 8.5. Purification by automated linear gradient flash chromatography (C18, MeOH:H_2O 1:99 to 1:0 over 25 column volumes) gave **2b-3,4,4-*d*$_3$** as a white solid (99 mg, 0.50 mmol, 47%). The relative configuration of the product and the stereochemical purity (i.e., dr and *ee*) was identical to that of unlabeled **2b**. Retention of deuterium was evaluated by ^{1}H NMR analysis, which showed the product was 95% at C_b and 65% at C_g.

^{1}H NMR (500 MHz, CD_3OD): δ 7.33 – 7.25 (m, 4H), 7.24 –7.18 (m, 1H), 4.25 (ddd, *J* = 9.0, 4.6 4.6 Hz, 0.05H), 3.44 (ap s, 1H), 2.99 – 2.93 (m, 0.34H), 2.84 – 2.76 (m, 0.36H).

HRMS (ESI^+): Ions were observed corresponding with ***d*$_3$** (i.e., Calcd for $C_{10}H_{11}D_3NO_3^+$ $[M + H]^+$ requires 199.1156; found 199.1155), ***d*$_2$** (i.e., Calcd for $C_{10}H_{12}D_2NO_3^+$ $[M + H]^+$

requires 198.1094; found 198.1095), and ***d*₁** (i.e., Calcd for $C_{10}H_{13}D_1NO_3^+$ $[M + H]^+$ requires 197.1031; found 197.1033).

(2*S*,3*R*)-2-Amino-3-hydroxy-4-(4-bromophenyl)butanoic Acid (3b)

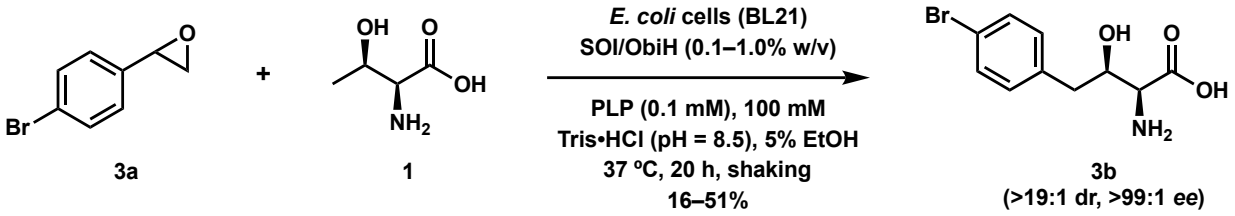

Amino acid **3b** was prepared following General Procedure A with commercially available 2-(4-bromophenyl)oxirane (**3a**, 199 mg, 1.0 mmol), L-Thr (**1**, 480 mg, 4.0 mmol), PLP (200 µL via 20 mM solution in water, 0.004 mmol), flash frozen SOI/ObiH *E. coli* BL21 wet whole cells (40 mg, 0.1% w/v%) in Tris•HCl buffer solution (37.6 mL, 100 mM, pH = 8.5), and 2 mL EtOH. Purification by automated gradient flash chromatography (C18, MeOH:H_2O 1:99 to 1:0 over 30 column volumes) and subsequent lyophilization gave 56 mg of product as a white solid with 4 mg tris base and 9 mg of L-Thr contamination as determined by ^{1}H NMR, yielding 43 mg of **3b** (0.16 mmol, 16%). Increasing the wet whole cell loading to 1.0% w/v (i.e., 400 mg) in an otherwise identical procedure with 2-(4-bromophenyl)oxirane (**3a**, 200 mg, 1.0 mmol) provided 93 mg of product as a white solid with 4 mg tris base contamination as determined by ^{1}H NMR, yielding 89 mg of **3b** (0.32 mmol, 32%).

[~2.5 mM epoxide concentration experiment] Amino acid **3b** was prepared following General Procedure A with commercially available 2-(4-bromophenyl)oxirane (**3a**, 220 mg, 1.1 mmol, 2.8 mM final conc.), L-Thr (**1**, 4784 mg, 40.0 mmol), PLP (2 mL via 20 mM solution in water, 0.004 mmol), flash frozen SOI/ObiH *E. coli* BL21 wet whole cells (397 mg, 1.0% w/v%) in Tris•HCl buffer solution (377 mL, 100 mM, pH = 8.5) and 20 mL EtOH. Purification by automated gradient flash chromatography (C18, MeOH:H_2O 1:99 to 1:0 over 30 column volumes) subsequent lyophilization

gave 158 mg of product as a white solid with 4 mg tris base contamination as determined by ^{1}H NMR, yielding 154 mg of **3b** (0.56 mmol, 51%). Marfey's analysis (cf. General Procedure B) was used to confirm the stereochemical purity (i.e., >19:1 dr and >99% *ee*), and the relative configuration was assigned based on that of **2b**.

^{1}H NMR (500 MHz, CD_3OD): δ 7.43 (d, *J* = 8.4 Hz, 2H), 7.22 (d, *J* = 8.4 Hz, 2H), 4.11 (ddd, *J* = 9.0, 4.4, 4.4 Hz, 1H), 3.35 (d, *J* = 4.7 Hz, 1H), 2.93 (dd, *J* = 13.9, 4.2 Hz, 1H), 2.73 (dd, *J* = 13.9, 9.2 Hz, 1H).

^{13}C{^{1}H} NMR (126 MHz, CD_3OD): δ 175.4, 139.3, 132.6, 132.3, 121.1, 73.1, 60.7, 41.1.

HRMS (ESI$^-$): Calcd for $C_{10}H_{11}BrNO_3^-$ [M – H]$^-$ requires 271.9931; found 271.9928.

(2*S*,3*R*)-2-Amino-3-hydroxy-4-(4-chlorophenyl)butanoic Acid (4b)

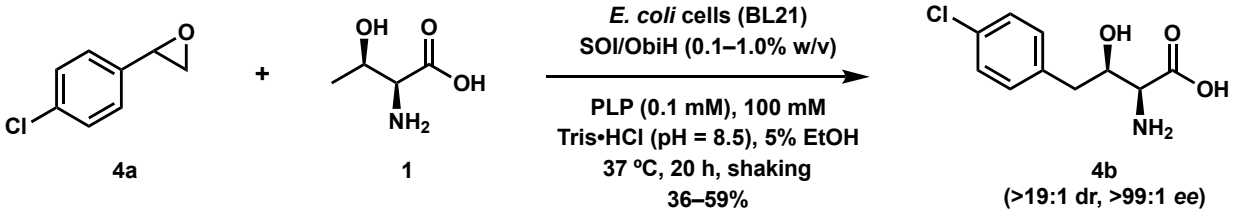

Amino acid **4b** was prepared following General Procedure A with commercially available 2-(4-chlorophenyl)oxirane (**4a**, 155 mg, 1.0 mmol), L-Thr (**1**, 480 mg, 4.0 mmol), PLP (200 µL via 20 mM solution in water, 0.004 mmol), flash frozen SOI/ObiH *E. coli* BL21 wet whole cells (37 mg, 0.93% w/v%) in Tris•HCl buffer solution (37.6 mL, 100 mM, pH = 8.5), and 2 mL EtOH. Purification by automated gradient flash chromatography (C18, MeOH:H_2O 1:99 to 1:0 over 30 column volumes) and subsequent lyophilization gave 89 mg of product as a white solid with 6 mg tris base contamination as determined by ^{1}H NMR, yielding 83 mg of **4b** (0.36 mmol, 36%).

Increasing the wet whole cell loading to 1.0% w/v (i.e., 400 mg) in an otherwise identical procedure with 2-(4-chlorophenyl)oxirane (**4a**, 160 mg, 1.0 mmol) provided 148 mg of product as a white solid with 7 mg tris base contamination as determined by ^{1}H NMR, yielding 141 mg of **4b** (0.61 mmol, 59%). Marfey's analysis (cf. General Procedure B) was used to confirm the stereochemical

purity (i.e., >19:1 dr and >99% *ee*), and the relative configuration was assigned based on that of **2b**.

^{1}H NMR (500 MHz, CD_3OD): δ 7.31 – 7.26 (m, 4H), 4.18 (ddd, *J* = 9.0, 4.4, 4.4 Hz, 1H), 3.41 (d, *J* = 4.6 Hz, 1H), 2.96 (dd, *J* = 13.9, 4.2 Hz, 1H), 2.78 (dd, *J* = 13.9, 9.2 Hz, 1H).

^{13}C{^{1}H} NMR (126 MHz, CD_3OD): δ 173.7, 138.5, 133.3, 132.2, 129.4, 72.3, 60.4, 41.2.

HRMS (ESI^-): Calcd for $C_{10}H_{11}ClNO_3^-$ $[M - H]^-$ requires 228.0433; found 228.0436.

(2*S*,3*R*)-2-Amino-3-hydroxy-4-(4-fluorophenyl)butanoic Acid (5b)

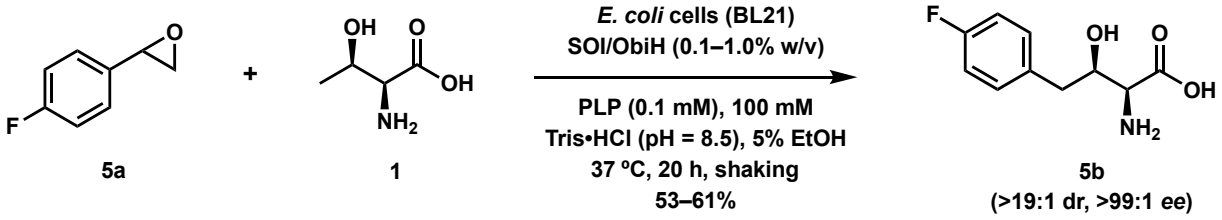

Amino acid **5b** was prepared following General Procedure A with commercially available 2-(4-fluorophenyl)oxirane (**5a**, 148 mg, 1.07 mmol), L-Thr (**1**, 480 mg, 4.0 mmol), PLP (200 µL via 20 mM solution in water, 0.004 mmol), flash frozen SOI/ObiH *E. coli* BL21 wet whole cells (44 mg, 0.11% w/v%), and Tris•HCl buffer solution (37.6 mL, 100 mM, pH = 8.5), and 2 mL EtOH. Purification by automated gradient flash chromatography (C18, MeOH:H_2O 1:99 to 1:0 over 30 column volumes) and subsequent lyophilization gave 170 mg of product as a white solid with 32 mg tris base contamination as determined by ^{1}H NMR, yielding 138 mg of **5b** (0.65 mmol, 61%).

Increasing the wet whole cell loading to 1.0% w/v (i.e., 400 mg) in an otherwise identical procedure with 2-(4-fluorophenyl)oxirane (**5a**, 140 mg, 1.0 mmol) provided 146 mg of product as a white solid with 20 mg tris base contamination as determined by ^{1}H NMR, yielding 126 mg of **5b** (0.59 mmol, 58%). Replacing the wet whole cells with lyophilized whole cells (i.e., 100 mg, 0.1% w/v) with 2-(4-fluorophenyl)oxirane (**5a**, 300 mg, 2.5 mmol) provided 440 mg of product as a white solid with 87 mg tris base and 30 mg L-Thr contamination as determined by ^{1}H NMR, yielding 323

mg of **5b** (1.51 mmol, 60%). Marfey's analysis (cf. General Procedure B) was used to confirm the stereochemical purity (i.e., >19:1 dr and >99% *ee*), and the relative configuration was assigned based on that of **2b**.

^{1}H NMR (500 MHz, CD_3OD): δ 7.34 – 7.25 (m, 2H), 7.05 – 6.95 (m, 2H), 4.16 (ddd, *J* = 9.0, 4.4, 4.4 Hz, 1H), 3.39 (d, *J* = 4.6 Hz, 1H), 2.95 (dd, *J* = 14.0, 4.3 Hz, 1H), 2.77 (dd, *J* = 13.9, 9.2 Hz, 1H).

^{13}C{^{1}H} NMR (126 MHz, CD_3OD): δ 174.3, 163.1 (d, *J* = 242.6 Hz), 135.7 (d, *J* = 3.2 Hz), 132.2 (d, *J* = 7.9 Hz), 115.9 (d, *J* = 21.4 Hz), 72.7, 60.4, 41.0.

^{19}F{^{13}C} NMR (377 MHz, CD_3OD): δ -120.09.

HRMS (ESI^-): Calcd for $C_{10}H_{11}FNO_3^-$ $[M - H]^-$ requires 212.0728; found 212.0730.

(2*S*,3*R*)-2-Amino-4-(2,4-difluorophenyl)-3-hydroxybutanoic Acid (6b)

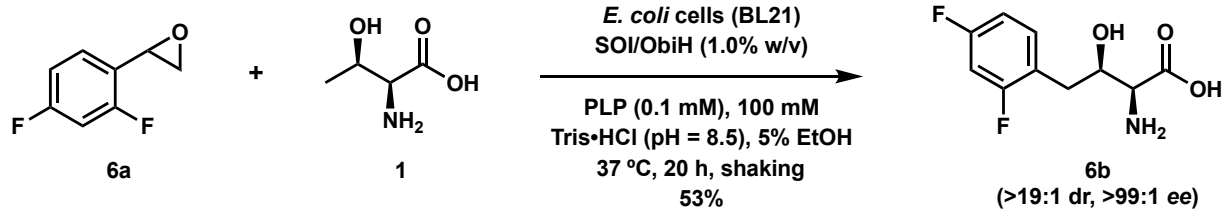

Amino acid **6b** was prepared following General Procedure A with 2-(2,4-difluorophenyl)oxirane (**6a**, 177 mg, 1.13 mmol), L-Thr (**1**, 480 mg, 4.0 mmol), PLP (200 µL via 20 mM solution in water, 0.004 mmol), flash frozen SOI/ObiH *E. coli* BL21 wet whole cells (448 mg, 1.1% w/v%) in Tris•HCl buffer solution (38 mL, 100 mM, pH = 8.5), and 2 mL EtOH. Purification by automated gradient flash chromatography (C18, MeOH:H_2O 1:99 to 1:0 over 30 column volumes) and subsequent lyophilization gave 141 mg of product as a white solid with 2 mg tris base contamination as determined by ^{1}H NMR, yielding 139 mg of **6b** (0.60 mmol, 53%). Marfey's analysis (cf. General Procedure B) was used to confirm the stereochemical purity (i.e., >19:1 dr and >99% *ee*), and the relative configuration was assigned based on that of **2b**.

^{1}H NMR (500 MHz, CD_3OD): δ 7.37 (br q, *J* = 8 Hz, 1H), 6.95 – 6.87 (m, 2H), 4.24 (ddd, *J* = 9.1, 4.5, 4.5 Hz, 1H), 3.46 (d, *J* = 4.5 Hz, 1H), 3.05 (dd, *J* = 14.1, 4.4 Hz, 1H), 2.80 (dd, *J* = 14.1, 9.4 Hz, 1H).

^{13}C NMR (126 MHz, CD_3OD): δ 172.7, 163.4 (dd, *J* = 246.5, 12.8 Hz), 162.8 (dd, *J* = 246.6, 11.8 Hz), 134.0 (dd, *J* = 9.5, 6.3 Hz), 122.4 (dd, *J* = 15.9, 3.9 Hz), 112.0 (dd, *J* = 21.2, 3.7 Hz), 104.3 (dd, *J* = 26, 26 Hz), 70.8, 60.3, 34.7.

^{19}F{^{13}C} NMR (377 MHz, CD_3OD): δ -115.60 (d, *J* = 6.8 Hz), -115.95 (d, *J* = 6.8 Hz).

HRMS (ESI^-): Calcd for $C_{10}H_{10}F_2NO_3^-$ $[M - H]^-$ requires 230.0634; found 230.0635.

(2*S*,3*R*)-2-Amino-3-hydroxy-4-(4-methoxyphenyl)butanoic Acid (7b)

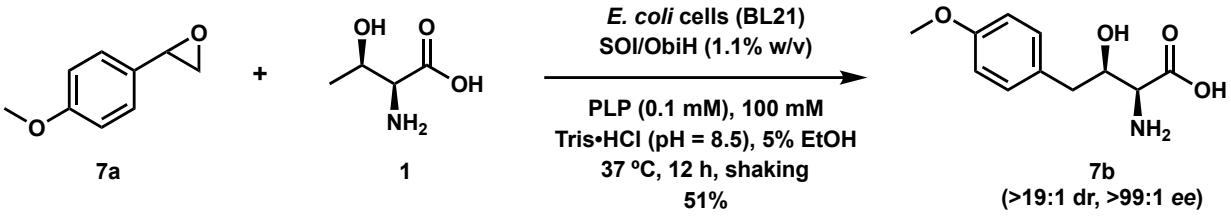

7a **1** **7b**
(>19:1 dr, >99:1 *ee*)

Amino acid **7b** was prepared following General Procedure A with 2-(4-methoxyphenyl)oxirane (**7a**, 203 mg, 80% purity, 1.08 mmol), L-Thr (**1**, 480 mg, 4.0 mmol), PLP (200 µL via 20 mM solution in water, 0.004 mmol), flash frozen SOI/ObiH *E. coli* BL21 wet whole cells (450 mg, 1.1% w/v%) in Tris•HCl buffer solution (38 mL, 100 mM, pH = 8.5), and 2 mL EtOH. Purification by automated gradient flash chromatography (C18, MeOH:H_2O 1:99 for 15 column volumes, 3:7 for 10 column volumes, and 1:0 over column volumes) and subsequent lyophilization gave 126 mg of product as a white solid with 2 mg tris base contamination as determined by ^{1}H NMR, yielding 124 mg of **7b** (0.55 mmol, 51%). Marfey's analysis (cf. General Procedure B) was used to confirm the stereochemical purity (i.e., >19:1 dr and >99% *ee*), and the relative configuration was assigned based on that of **2b**.

^{1}H NMR (500 MHz, D_2O): δ 7.31 (d, *J* = 8.6 Hz, 2H), 7.03 (d, *J* = 8.6 Hz, 2H), 4.30 (ddd, *J* = 9.4, 4.5, 4.5 Hz, 1H), 3.86 (s, 3H), 3.69 (d, *J* = 4.7 Hz, 1H), 3.00 (dd, *J* = 14.2, 4.5 Hz, 1H), 2.81 (dd, *J* = 14.2, 9.5 Hz, 1H).

^{13}C{^{1}H} NMR (126 MHz, D_2O): δ 173.1, 157.7, 130.6, 130.1, 114.3, 71.1, 59.0, 55.5, 38.9.

HRMS (ESI^+): Calcd for $C_{11}H_{16}NO_4^+$ $[M + H]^+$ requires 226.1074; found 226.1074.

(2*S*,3*R*)-4-(4-Acetoxyphenyl)-2-amino-3-hydroxybutanoic Acid (8b) and (2*S*,3*R*)-2-Amino-3-hydroxy-4-(4-hydroxyphenyl)butanoic Acid (8c)

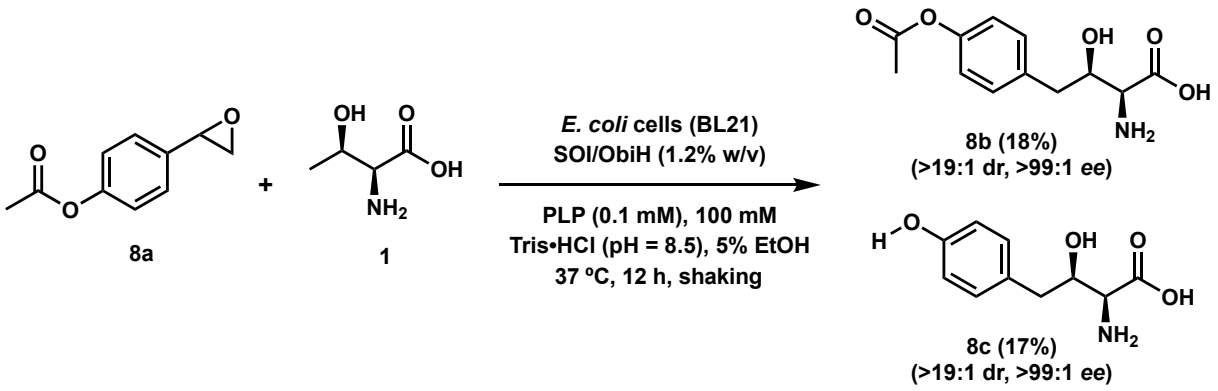

Amino acids **8b** and **8c** were prepared following General Procedure A with 4-(oxiran-2-yl)phenyl acetate (**8a**, 208 mg, 1.17 mmol), L-Thr (**1**, 480 mg, 4.0 mmol), PLP (200 µL via 20 mM solution in water, 0.004 mmol), flash frozen SOI/ObiH *E. coli* BL21 wet whole cells (480 mg, 1.2% w/v%) in Tris•HCl buffer solution (38 mL, 100 mM, pH = 8.5), and 2 mL EtOH. Purification by automated gradient flash chromatography (C18, MeOH:H_2O 0:1 to 1:0 over 30 column volumes) allowed for resolution of products **8b** (appeared at MeOH:H_2O 3:7) and **8c** (appeared at MeOH:H_2O 0:1). Lyophilization of the purified samples gave 55 mg of product **8b** as a white solid with 2 mg tris base contamination as determined by ^{1}H NMR, yielding 53 mg of **8b** (0.21 mmol, 18%). The lyophilized sample containing **8c** (60 mg, white solid) was contaminated with 8 mg tris base and 10 mg of tris base *N*-acetamide as determined by ^{1}H NMR, yielding 42 mg of **8c** (0.20 mmol, 17%). Marfey's analysis (cf. General Procedure B) was used to confirm the stereochemical purity of both **8b** and **8c** (i.e., >19:1 dr and >99% *ee* for each), and the relative configuration for each was assigned based on that of **2b**.

Spectral Data for 8b:

^{1}H NMR (500 MHz, CD_3OD): δ 7.32 (d, *J* = 8.5 Hz, 2H), 7.03 (d, *J* = 8.5 Hz, 2H), 4.23 (ddd, *J* = 9.0, 4.5, 4.5 Hz, 1H), 3.46 (d, *J* = 4.7 Hz, 1H), 3.00 (dd, *J* = 13.9, 4.3 Hz, 1H), 2.81 (dd, *J* = 13.9, 9.2 Hz, 1H), 2.26 (s, 3H).

$^{13}C\{^{1}H\}$ NMR (126 MHz, CD_3OD): δ 172.9, 171.4, 151.0, 137.2, 131.6, 122.6, 72.0, 60.2, 41.4, 20.9.

HRMS (ESI^+): Calcd for $C_{12}H_{16}NO_5^+$ $[M + H]^+$ requires 254.1023; found 254.1021.

Spectral Data for 8c:

^{1}H NMR (500 MHz, CD_3OD): δ 7.10 (d, *J* = 8.5 Hz, 2H), 6.72 (d, *J* = 8.4 Hz, 2H), 4.21 (ddd, *J* = 9.0, 4.7, 4.7 Hz, 1H), 3.42 (d, *J* = 4.1 Hz, 1H), 2.85 (dd, *J* = 14.0, 5.1 Hz, 1H), 2.73 (dd, *J* = 14.0, 8.6 Hz, 1H).

$^{13}C\{^{1}H\}$ NMR (126 MHz, CD_3OD): δ 173.2, 157.1, 131.5, 130.1, 116.2, 72.4, 59.9, 41.1.

HRMS (ESI^+): Calcd for $C_{10}H_{14}NO_4^+$ $[M + H]^+$ requires 212.0917; found 212.0917.

(2*S*,3*R*)-2-Amino-4-(benzo[*d*][1,3]dioxol-5-yl)-3-hydroxybutanoic Acid (9b)

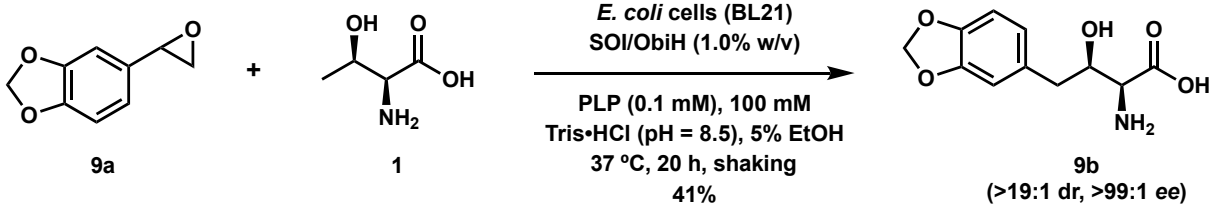

9a **1** **9b** **(>19:1 dr, >99:1 *ee*)**

Amino acid **9b** was prepared following General Procedure A with 5-(oxiran-2-yl)benzo[*d*][1,3]dioxole (**9a**, 161 mg, 1.02 mmol), L-Thr (**1**, 475 mg, 4.0 mmol), PLP (200 µL via 20 mM solution in water, 0.004 mmol), flash frozen SOI/ObiH *E. coli* BL21 wet whole cells (398 mg, 1.0% w/v%) in Tris•HCl buffer solution (37.2 mL, 100 mM, pH = 8.5), and 2 mL EtOH. Purification by automated gradient flash chromatography (C18, MeOH:H_2O 1:99 to 1:0 over 30 column volumes) and subsequent lyophilization gave 102 mg of product as a white solid with 3 mg tris base contamination as determined by ^{1}H NMR, yielding 99 mg of **9b** (0.41 mmol, 41%). Marfey's analysis (cf. General Procedure B) was used to confirm the stereochemical purity (i.e., >19:1 dr and >99% *ee*), and the relative configuration was assigned based on that of **2b**.

^{1}H NMR (500 MHz, CD_3OD): δ 6.81 (s, 1H), 6.74 (br s, 2H), 5.90 (s, 2H), 4.20 (ddd, *J* = 9.0, 4.6, 4.6 Hz, 1H), 3.42 (d, *J* = 4.3 Hz, 1H), 2.88 (dd, *J* = 14.0, 4.9 Hz, 1H), 2.73 (dd, *J* = 14.0, 8.7 Hz, 1H).

$^{13}C\{^{1}H\}$ NMR (126 MHz, CD_3OD): δ 172.9, 149.1, 147.7, 133.1, 123.6, 110.8, 109.1, 102.1, 72.2, 59.9, 41.6.

HRMS (ESI^-): Calcd for $C_{11}H_{12}NO_5^-$ $[M - H]^-$ requires 238.0721; found 238.0725.

(2*S*,3*R*)-2-Amino-3-hydroxy-4-(*o*-tolyl)butanoic Acid (10b)

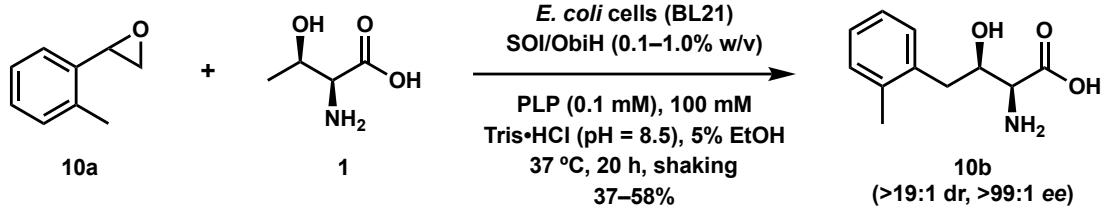

10a **1** **10b** **(>19:1 dr, >99:1 *ee*)**

Amino acid **10b** was prepared following General Procedure A with 2-(*o*-tolyl)oxirane (**10a**, 219 mg, 67% purity, 1.1 mmol), L-Thr (**1**, 480 mg, 4 mmol), PLP (200 µL via 20 mM solution in water, 0.004 mmol) flash frozen SOI/ObiH *E. coli* BL21 wet whole cells (40 mg, 0.1% w/v%) in Tris•HCl buffer solution (38 mL, 100 mM, pH = 8.5), and 2 mL EtOH. Purification by automated gradient flash chromatography (C18, MeOH:H_2O 1:99 to 1:0 over 30 column volumes) and subsequent lyophilization gave 89 mg of product as a white solid with 3 mg tris base contamination as determined by ^{1}H NMR, yielding 86 mg of **10b** (0.41 mmol, 37%). Increasing the wet whole cell loading to 1.0% w/v (i.e., 400 mg) in an otherwise identical procedure with 2-(*o*-tolyl)oxirane (**10a**, 194 mg, 67% purity, 0.97 mmol) provided 123 mg of product as a white solid with 6 mg tris base contamination as determined by ^{1}H NMR, yielding 117 mg of **10b** (0.56 mmol, 58%) of **10b**. Marfey's analysis (cf. General Procedure B) was used to confirm the stereochemical purity (i.e., >19:1 dr and >99% *ee*), and the relative configuration was assigned based on that of **2b**.

^{1}H NMR (500 MHz, CD_3OD): δ 7.25 – 7.18 (m, 1H), 7.16 – 7.07 (m, 3H), 4.23 (ddd, *J* = 9.1, 4.4, 4.4 Hz, 1H), 3.47 (d, *J* = 4.5 Hz, 1H), 3.02 (dd, *J* = 14.0, 4.3 Hz, 1H), 2.82 (dd, *J* = 14.0, 9.3 Hz, 1H), and 2.35 (s, 3H).

$^{13}C\{^{1}H\}$ NMR (126 MHz, CD_3OD): δ 173.5, 138.0, 137.8, 131.3, 131.3, 127.6, 126.9, 71.4, 60.5, 39.3, 19.8.

HRMS (ESI^-): Calcd for $C_{11}H_{14}NO_3^-$ $[M - H]^-$ requires 208.0979; found 208.0980.

(2*S*,3*R*)-2-Amino-3-hydroxy-4-(*m*-tolyl)butanoic Acid (11b)

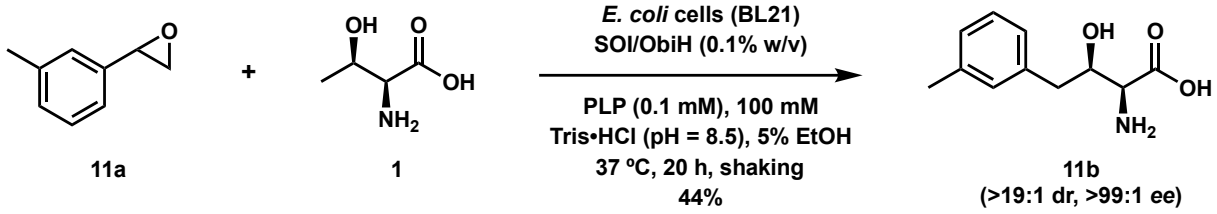

11a **1** **11b** **(>19:1 dr, >99:1 *ee*)**

Amino acid **11b** was prepared following General Procedure A with 2-(*m*-tolyl)oxirane (**11a**, 221 mg, 65% purity, 1.1 mmol), L-Thr (**1**, 480 mg, 4 mmol), PLP (200 µL via 20 mM solution in water, 0.004 mmol), flash frozen SOI/ObiH *E. coli* BL21 wet whole cells (40 mg, 0.1% w/v%) in Tris•HCl buffer solution (38 mL, 100 mM, pH = 8.5), and 2 mL EtOH. Purification by automated gradient flash chromatography (C18, MeOH:H_2O 1:99 to 1:0 over 30 column volumes) and subsequent lyophilization gave 104 mg of product as a white solid with 3 mg tris base contamination as determined by ^{1}H NMR, yielding 101 mg of **11b** (0.48 mmol, 44%). Marfey's analysis (cf. General Procedure B) was used to confirm the stereochemical purity (i.e., >19:1 dr and >99% *ee*), and the relative configuration was assigned based on that of **2b**.

^{1}H NMR (500 MHz, CD_3OD): δ 7.17 (t, *J* = 7.5 Hz, 1H), 7.12 (s, 1H), 7.07 (d, *J* = 7.6 Hz, 1H), 7.02 (d, *J* = 7.5 Hz, 1H), 4.25 – 4.20 (m, 1H), 3.44 – 3.39 (m, 1H), 2.93 (dd, *J* = 13.9, 4.8 Hz, 1H), 2.77 (dd, *J* = 13.8, 8.8 Hz, 1H), 2.31 (s, 3H).

^{13}C{^{1}H} NMR (126 MHz, CD_3OD): δ 173.8, 139.4, 139.1, 131.3, 129.3, 128.1, 127.6, 72.5, 60.2, 41.9, 21.4.

HRMS (ESI^-): Calcd for $C_{11}H_{14}NO_3^-$ $[M - H]^-$ requires 208.0979; found 208.0980.

(2*S*,3*R*)-2-Amino-3-hydroxy-4-(*p*-tolyl)butanoic Acid (12b)

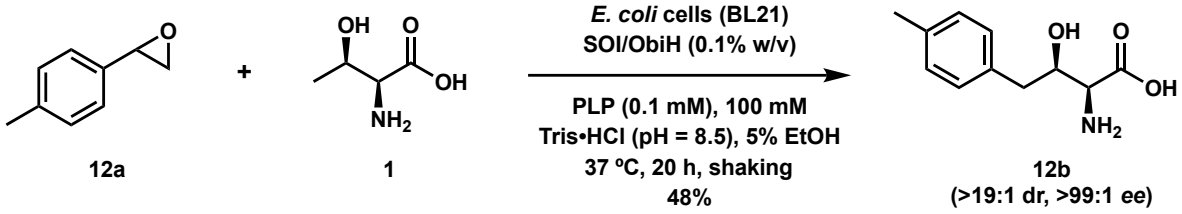

12a **1** **12b** **(>19:1 dr, >99:1 *ee*)**

Amino acid **12b** was prepared following General Procedure A with 2-(*p*-tolyl)oxirane (**12a**, 173 mg, 86% purity, 1.1 mmol), L-Thr (**1**, 480 mg, 4 mmol), PLP (200 µL via 20 mM solution in water, 0.004 mmol), flash frozen SOI/ObiH *E. coli* BL21 wet whole cells (40 mg, 0.1% w/v%) in Tris•HCl buffer solution (38 mL, 100 mM, pH = 8.5), and 2 mL EtOH. Purification by automated gradient flash chromatography (C18, MeOH:H_2O 1:99 to 1:0 over 30 column volumes) and subsequent lyophilization gave 114 mg of product as a white solid with 3 mg tris base contamination as determined by ^{1}H NMR, yielding 111 mg of **12b** (0.53 mmol, 48%). Marfey's analysis (cf. General Procedure B) was used to confirm the stereochemical purity (i.e., >19:1 dr and >99% *ee*), and the relative configuration was assigned based on that of **2b**.

^{1}H NMR (500 MHz, CD_3OD): δ 7.17 (d, *J* = 8.0 Hz, 2H), 7.10 (d, *J* = 7.8 Hz, 2H), 4.23 (ddd, *J* = 9.0, 4.6, 4.6 Hz, 1H), 3.41 (d, *J* = 4.2 Hz, 1H), 2.91 (dd, *J* = 13.9, 4.9 Hz, 1H), 2.76 (dd, *J* = 13.9, 8.8 Hz, 1H), and 2.29 (s, 3H).

^{13}C{^{1}H} NMR (126 MHz, CD_3OD): δ 173.7, 137.0, 136.4, 130.5, 130.1, 72.5, 60.1, 41.5, 21.1.

HRMS (ESI$^-$): Calcd for $C_{11}H_{14}NO_3^-$ [M – H]$^-$ requires 208.0979; found 208.0981.

(2*S*,3*R*)-2-Amino-3-hydroxy-4-(*p*-isopropylphenyl)butanoic Acid (13b)

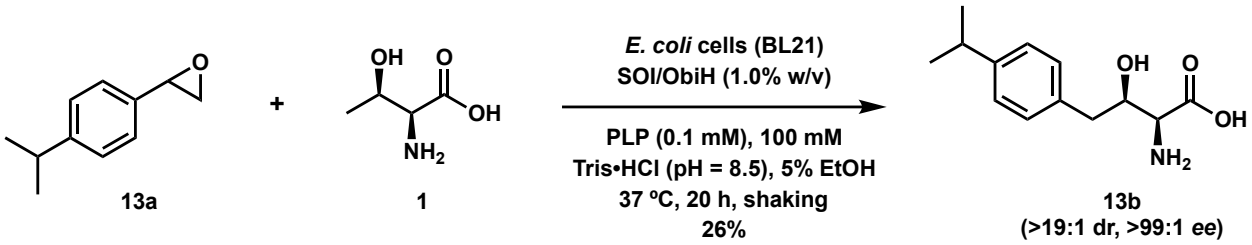

13a + **1** → **13b** (**>19:1 dr, >99:1 *ee***)

Amino acid **13b** was prepared following General Procedure A with 2-(4-isopropylphenyl)oxirane (**13a**, 287 mg, 59% purity, 1.0 mmol), L-Thr (**1**, 480 mg, 4 mmol), PLP (200 µL via 20 mM solution in water, 0.004 mmol), flash frozen SOI/ObiH *E. coli* BL21 wet whole cells (400 mg, 1.0% w/v%) in Tris•HCl buffer solution (38 mL, 100 mM, pH = 8.5), and 2 mL EtOH. Purification by automated gradient flash chromatography (C18, MeOH:H_2O 1:99 to 1:0 over 30 column volumes) and subsequent lyophilization gave **13b** as a white solid (63 mg, 0.26 mmol, 26%). Marfey's analysis (cf. General Procedure B) was used to confirm the stereochemical purity (i.e., >19:1 dr and >99% *ee*), and the relative configuration was assigned based on that of **2b**.

^{1}H NMR 500 MHz, CD_3OD): δ 7.20 (d, *J* = 8.2 Hz, 2H), 7.16 (d, *J* = 8.2 Hz, 2H), 4.25 – 4.15 (m, 1H), 3.38 (d, *J* = 4.1 Hz, 1H), 2.92 (dd, *J* = 13.9, 4.9 Hz, 1H), 2.86 (h, *J* = 7.0 Hz, 1H), 2.76 (dd, *J* = 13.9, 8.7 Hz, 1H), 1.22 (d, *J* = 6.9 Hz, 6H).

^{13}C{^{1}H} NMR (126 MHz, CD_3OD): δ 148.2, 137.0, 130.5, 127.4, 73.0, 60.2, 41.4, 35.1, 24.49, 24.48.

HRMS (ESI^-): Calcd for $C_{13}H_{18}NO_3^-$ $[M - H]^-$ requires 236.1292; found 236.1293.

(2*S*,3*R*)-2-Amino-3-hydroxy-4-mesitylbutanoic Acid (14b)

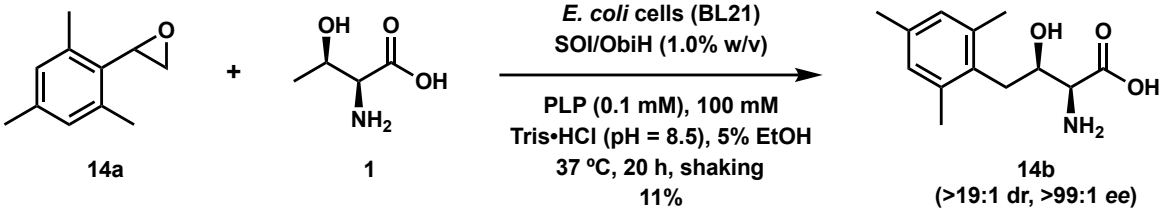

14a + **1** → **14b** (**>19:1 dr, >99:1 *ee***)

Amino acid **14b** was prepared following General Procedure A with 2-mesityloxirane (**14a**, 163 mg, 92% purity, 0.93 mmol), L-Thr (**1**, 480 mg, 4 mmol), PLP (200 µL via 20 mM solution in water, 0.004 mmol), flash frozen SOI/ObiH *E. coli* BL21 wet whole cells (402 mg, 1.0% w/v%) in Tris•HCl buffer solution (38 mL, 100 mM, pH = 8.5), and 2 mL EtOH. Purification by automated gradient flash chromatography (C18, MeOH:H_2O 1:99 to 1:0 over 30 column volumes) and subsequent lyophilization gave **14b** as a white solid (24 mg, 0.10 mmol, 11%). Marfey's analysis (cf. General Procedure B) was used to confirm the stereochemical purity (i.e., >19:1 dr and >99% *ee*), and the relative configuration was assigned based on that of **2b**.

^{1}H NMR (500 MHz, CD_3OD): δ 6.79 (s, 2H), 4.14 – 4.03 (m, 1H), 3.41 (d, *J* = 5.0 Hz, 1H), 2.94 (dd, *J* = 14.2, 3.3 Hz, 1H), 2.88 (dd, *J* = 14.1, 9.9 Hz, 1H), 2.31 (s, 6H), 2.20 (s, 3H).

^{1}H NMR (500 MHz, D_2O): δ 7.00 (s, 2H), 4.12 (dd, *J* = 6.3, 6.3 Hz, 1H), 3.60 (d, *J* = 5.4 Hz, 1H), 2.96 (d, *J* = 6.7 Hz, 2H), 2.32 (s, 6H), 2.27 (s, 3H).

^{13}C{^{1}H} NMR (126 MHz, D_2O): δ 175.7, 137.9, 136.7, 132.1, 128.9, 71.5, 60.3, 33.2, 19.8, 19.6.

HRMS (ESI^-): Calcd for $C_{13}H_{18}NO_3^-$ $[M - H]^-$ requires 236.1292; found 236.1295.

(2*S*,3*R*)-2-Amino-3-hydroxy-4-(naphthalen-1-yl)butanoic Acid (15b)

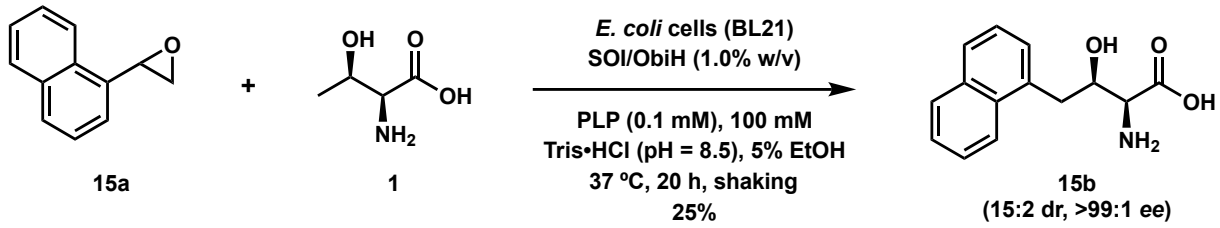

15a **1** **15b** **(15:2 dr, >99:1 *ee*)**

Amino acid **15b** was prepared following General Procedure A with 2-(naphthalen-1-yl)oxirane (**15a**, 186 g, 1.1 mmol), L-Thr (**1**, 480 mg, 4.0 mmol), PLP (200 µL via 20 mM solution in water, 0.004 mmol), flash frozen SOI/ObiH *E. coli* BL21 wet whole cells (431 mg, 1.1% w/v%) in Tris•HCl buffer solution (38 mL, 100 mM, pH = 8.5), and 2 mL EtOH. Purification by automated gradient flash chromatography (C18, MeOH:H_2O 1:99 to 1:0 over 30 column volumes) and subsequent lyophilization gave **15b** as a white solid (63 mg, 0.28 mmol, 25%). Marfey's analysis (cf. General Procedure B) was used to confirm the enantiomeric purity (i.e., >99% *ee*). The diastereomeric purity was evaluated using ^{1}H, COSY, and HSQC NMR, and the dr was found to be 15:2. The relative configuration of the major diastereomer was assigned based on that of **2b**.

^{1}H NMR (500 MHz, CD_3OD, major diastereomer (*): minor diastereomer (^) = 15:2) δ 8.16 (*, dd, *J* = 8.5 Hz, 1H), 7.86 (*, d, *J* = 7.4 Hz, 1H), 7.83 – 7.79 (^, m, 0.47H), 7.76 (*, d, *J* = 7.8 Hz, 1H), 7.55 – 7.38 (*^, m, 5H), 4.38 (*^, ddd, *J* = 9.2, 5.1, 4.1 Hz, 1.10H), 3.63 (*, dd, *J* = 14.2, 4.1 Hz, 1H), 3.57 (*, d, *J* = 5.0 Hz, 1H), 3.50 (^, d, *J* = 4.4 Hz, 0.13H), 3.17 (*^, dd, *J* = 14.2, 9.2 Hz, 1.13H), 2.99 (^, dd, *J* = 13.9, 8.9 Hz, 0.13H).

^{13}C{^{1}H} NMR (126 MHz, CD_3OD, major diastereomer (*): minor diastereomer (^)) δ 173.2*, 137.0^, 135.6*, 135.5*, 135.1^, 133.9^, 133.6*, 129.7*, 129.1^, 128.96^, 128.95*, 128.58^, 128.57^, 128.4*, 127.1*, 127.0^ 126.6*, 126.44^, 126.42*, 125.1*, 72.1^, 71.4*, 60.6*, 60.2^, 42.1^, 39.3*.

HRMS (ESI^-): Calcd for $C_{14}H_{13}NO_3^-$ $[M - H]^-$ requires 244.0979; found 244.0981.

2-(Oxiran-2-yl)furan (16a)

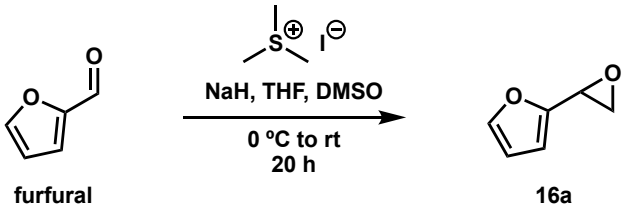

Epoxide **16a** was prepared following General Procedure C using furfural (1.7 mL, 21 mmol, dissolved in 8.0 mL of THF), trimethylsulfonium iodide (8.5 g, 42 mmol), NaH (1.7 g, 43 mmol, 60% w/w in mineral oil, pre-rinsed with hexanes), mixed in DMSO (20 ml), and THF (20 ml). The crude material (1.9 g) contained DMSO but was otherwise sufficiently pure for subsequent biocatalyic transformations.

^{1}H NMR (300 MHz, $CDCl_3$): δ 7.40–7.37 (m, 1H), 6.46 (br d, *J* = 3.3 Hz, 1H), 6.37 (dd, *J* = 1.9, 3.3 Hz, 1H), 3.89 (dd, *J* = 2.8, 4.2 Hz, 1H), 3.28 (dd, *J* = 2.6, 5.2 Hz, 1H), 3.16 (dd, *J* = 4.3, 5.3 Hz, 1H). DMSO-h_6 observed at δ 2.61 (25% w/w contamination).

^{13}C{^{1}H} NMR (75 MHz, $CDCl_3$): δ 150.3, 143.0, 110.8, 110.1, 48.0, 46.5. DMSO-h_6 observed at δ 41.1.

HRMS (ESI$^+$): Calcd for $C_6H_7O_2^+$ $[M + H]^+$ requires 111.0441; found 111.0442.

(2*S*,3*R*)-2-amino-4-(furan-2-yl)-3-hydroxybutanoic Acid (16b)

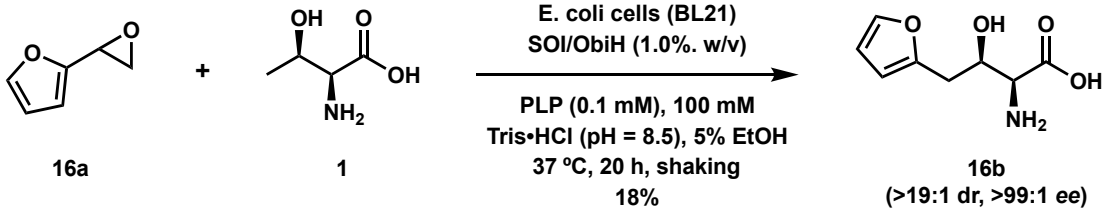

Amino acid **16b** was prepared following General Procedure A with 2-(oxiran-2-yl)furan (**16a**, 197 mg, 75% purity, 1.3 mmol,), L-Thr (**1**, 480 mg, 4.0 mmol), PLP (200 µL via 20 mM solution in water, 0.004 mmol), flash frozen SOI/ObiH *E. coli* BL21 wet whole cells (384 mg, 1.0% w/v%) in Tris•HCl buffer solution (38 mL, 100 mM, pH = 8.5), and 2 mL EtOH. Purification by automated

flash chromatography (loaded onto C18 with H_2O, eluted at 100% H_2O for 15 column volumes then 100% MeOH for 15 column volumes to clean the column) gave 58 mg of product as a pale-yellow solid with 15 mg tris base contamination as determined by ^{1}H NMR, yielding 43 mg of **16b** (0.23 mmol, 18%). Marfey's analysis (cf. General Procedure B) was used to confirm the stereochemical purity (i.e., >19:1 dr and >99% *ee*), and the relative configuration was assigned based on that of **2b**. The product did not strongly retain on C18 and required a second round of purification by automated flash chromatography to achieve appropriate NMR characterization. Specifically, ~30 mg of isolated material was dissolved in water and subjected to a second round of purification by automated flash chromatography. Fractions from the center of the elution peak were gathered for lyophilization yielding 11.1 mg of pure **16b**.

^{1}H NMR (500 MHz, CD_3OD): δ 7.44 – 7.36 (m, 1H), 6.33 (dd, *J* = 3.2, 1.9 Hz, 1H), 6.20 (dd, *J* = 3.2, 0.9 Hz, 1H), 4.37 (ddd, *J* = 8.1, 5.8, 4.2 Hz, 1H), 3.46 (d, *J* = 4.2 Hz, 1H), 3.02 (dd, *J* = 15.3, 5.8 Hz, 1H), 2.91 (dd, *J* = 15.2, 8.1 Hz, 1H).

^{13}C{^{1}H} NMR (126 MHz, CD_3OD): δ 172.7, 153.2, 142.9, 111.3, 108.2, 69.8, 59.8, 34.5.

HRMS (ESI^+): Calcd for $C_8H_{12}NO_4^+$ $[M + H]^+$ requires 186.0761; found 186.0741.

(2*S*,3*R*)-2-Amino-3-hydroxy-4-(thiophen-2-yl)butanoic Acid (17b)

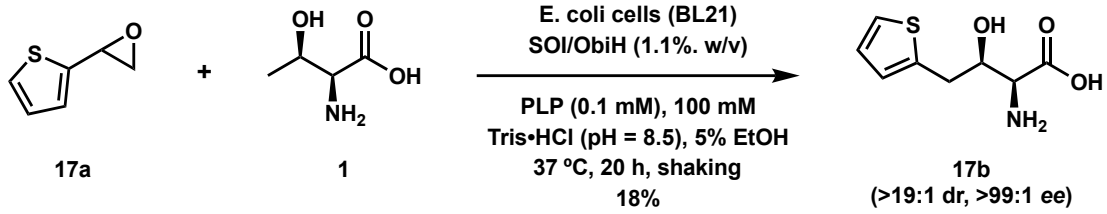

17a **1** **17b**
(>19:1 dr, >99:1 *ee*)

Amino acid **17b** was prepared following General Procedure A with 2-(thiophen-2-yl)oxirane (**17a**, 190 mg, 70% purity, 1.1 mmol,), L-Thr (**1**, 480 mg, 4.0 mmol), PLP (200 µL via 20 mM solution in water, 0.004 mmol), flash frozen SOI/ObiH *E. coli* BL21 wet whole cells (457 mg, 1.1% w/v%) in Tris•HCl buffer solution (38 mL, 100 mM, pH = 8.5), and 2 mL EtOH. Purification by automated linear gradient flash chromatography and subsequent lyophilization gave 67 mg of product as a white solid with 26 mg tris base contamination as determined by ^{1}H NMR, yielding 41 mg of **17b** (0.2 mmol, 18%). Marfey's analysis (cf. General Procedure B) was used to confirm the stereochemical purity (i.e., >19:1 dr and >99% *ee*), and the relative configuration was assigned based on that of **2b**. The product did not strongly retain on C18 and required a second round of purification by automated flash chromatography to achieve appropriate NMR characterization. Specifically, ~30 mg of isolated material was dissolved in water and subjected to a second round of purification by automated flash chromatography. Fractions from the center of the elution peak were gathered for lyophilization yielding 11.3 mg of pure **17b**.

^{1}H NMR (500 MHz, CD_3OD): δ 7.26 – 7.21 (m, 1H), 6.97 – 6.89 (m, 2H), 4.24 (ddd, *J* = 8.5, 4.6, 4.6 Hz, 1H), 3.47 (d, *J* = 4.6 Hz, 1H), 3.22 (dd, *J* = 15.0, 4.7 Hz, 1H), 3.06 (dd, *J* = 14.9, 8.6 Hz, 1H).

^{13}C{^{1}H} NMR (126 MHz, CD_3OD) δ 172.7, 141.1, 127.8, 127.3, 125.2, 71.8, 59.8, 36.1.

HRMS (ESI^{+}): Calcd for $C_8H_{12}NO_3S^{+}$ $[M + H]^{+}$ requires 202.0532; found 202.0520.

(2*S*,3*R*,4*R*)-2-Amino-3-hydroxy-4-phenylpentanoic Acid (18b-major) and (2*S*,3*R*,4*S*)-2-Amino-3-hydroxy-4-phenylpentanoic Acid (18b-minor)

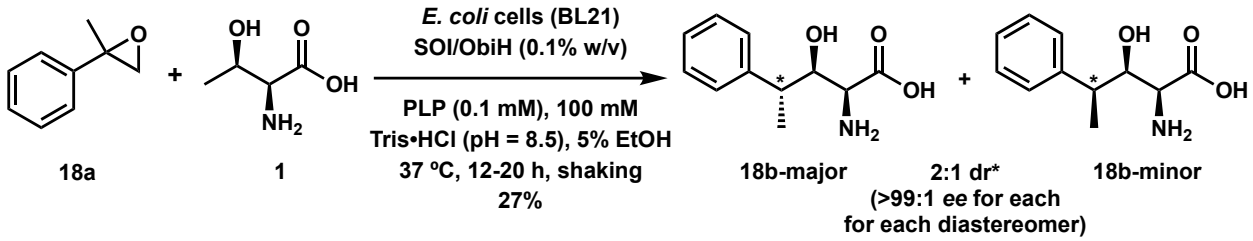

Amino acid **18b** was prepared following General Procedure A with 2-methyl-2-phenyloxirane (**18a**, 138 mg, 1.0 mmol), L-Thr (**1**, 474 mg, 1.0 mmol), PLP (200 µL via 20 mM solution in water, 0.004 mmol), flash frozen SOI/ObiH *E. coli* BL21 wet whole cells (40 mg, 0.1% w/v%) in Tris•HCl buffer solution (37.6 mL, 100 mM, pH = 8.5), and 2 mL EtOH. Purification by automated linear gradient flash chromatography and subsequent lyophilization gave 64 mg of product as a white solid with 7 mg tris base contamination as determined by ^{1}H NMR, yielding 57 mg of **18b** (0.27 mmol, 27%). Marfey's analysis (cf. General Procedure B) was used to evaluate the stereochemical purity of **18b** which indicated the presence of two diastereomers that were enantiomerically pure, but poor separation precluded accurate quantification of the dr. The mixture of **18b** diastereomers was resolved with baseline resolution using UPLC-MS with a C18 column, which indicated that the two diastereomers were formed with a dr 2:1 (65:35). ^{1}H-NMR further supported the presence of a 2:1 mixture of diastereomers. Please see the main text for a discussion on the assignment of relative configuration at C4 in **18b-major** and **18b-minor**.

^{1}H NMR (500 MHz, CD_3OD, major diastereomer (*): minor diastereomer (^) = 2:1) δ 7.37 – 7.27 (*^, m, 8H), 7.25 – 7.14 (*^, m, 3H), 4.29 (^, dd, *J* = 9.2, 2.5 Hz, 0.6H), 4.26 (*, dd, *J* = 8.1, 3.4 Hz, 1H), 3.63 (*, d, *J* = 3.3 Hz, 1H), 3.23 (^, d, *J* = 2.5 Hz, 0.6H), 2.96 (*, ap p, *J* = 7.2 Hz, 1H), 2.92 – 2.84 (^, m, 0.6H), 1.38 (^, d, *J* = 6.8 Hz, 2.4H), 1.31 (*, d, *J* = 7.2 Hz, 3H).

^{13}C NMR (126 MHz, CD_3OD major diastereomer (*): minor diastereomer (^) = 2:1) δ 173.32 (*), 173.29 (^), 145.2 (^), 144.9 (*), 129.9 (^, 2xC), 129.5 (*, 2xC), 129.3 (*, 2xC), 128.9 (^, 2xC), 127.8 (^), 127.5 (*), 75.1 (^), 74.7 (*), 57.93 (*), 57.91 (^), 44.6

(^), 44.3 (*), 19.3 (*), 18.8 (^). One resonance of one diastereomer was not observed/resolved.

HRMS (ESI$^-$): Calcd for $C_{11}H_{15}NO_3^-$ [M – H]$^-$ requires 208.0979; found 208.0981.

2,3-Dihydrospiro[indene-1,2'-oxirane] (19a)

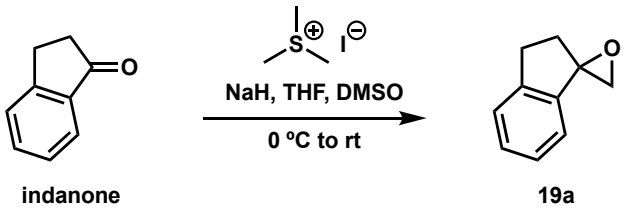

indanone 19a

Epoxide **19a** was prepared following General Procedure C from indanone (1.762 g, 13.3 mmol) in THF (5 mL), trimethylsulfonium iodide (5.5 g, 26.8 mmol), NaH (1.1 g, 26.8 mmol, 60% w/w in mineral oil), DMSO (14 ml), and THF (15 ml). The crude material (1.903 g, 13.0 mmol, 91% pure) contained ethyl acetate but was otherwise sufficiently pure for subsequent experiments.

^{1}H NMR (500 MHz, $CDCl_3$): δ 7.31 – 7.19 (m, 3H), 7.03 (d, *J* = 7.8 Hz, 1H), 3.26 (d, *J* = 4.9 Hz, 1H), 3.24 (d, *J* = 4.9 Hz, 1H), 3.20 – 3.11a (m, 1H), 3.00 (ddd, *J* = 15.5, 9.0, 6.2 Hz, 1H), 2.42 (ddd, *J* = 13.8, 9.0, 4.5 Hz, 1H), 2.30 (ddd, *J* = 14.3, 9.5, 6.2 Hz, 1H). Ethyl acetate was observed at δ 4.12 (q, *J* = 7.1 Hz, 0.35H), 2.04 (s, 0.56H), 1.25 (t, *J* = 7.1 Hz, 0.58H) (9% w/w contamination).

^{13}C{^{1}H} NMR (126 MHz, $CDCl_3$): δ 145.2, 140.2, 129.1, 127.0, 125.1, 121.5, 66.1, 55.6, 30.7, 29.1. Ethyl acetate was observed at δ 60.5, 21.2, 14.3.

HRMS (ESI$^+$): Calcd for $C_{10}H_{11}O^+$ [M + H]$^+$ requires 147.0804; found 147.0804.

(2*S*,3*R*)-2-Amino-3-(2,3-dihydro-1*H*-inden-1-yl)-3-hydroxypropanoic Acid (19b)

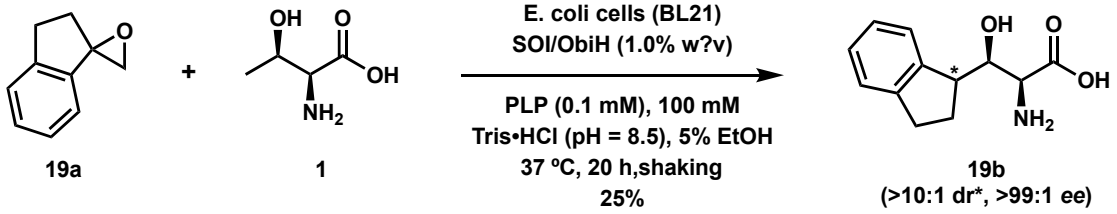

19a 1 19b
(>10:1 dr*, >99:1 *ee*)

Amino acid **19b** was prepared following General Procedure A with 2,3-Dihydrospiro[indene-1,2'-oxirane] (**19a**, 145 mg, 91% purity, 0.90 mmol), L-Thr (**1**, 480 mg, 4.0 mmol), PLP (200 µL via 20 mM solution in water, 0.004 mmol), flash frozen SOI/ObiH *E. coli* BL21 wet whole cells (404 mg, 1.0% wcw) in Tris•HCl buffer solution (38 mL, 100 mM, pH = 8.5), and 2 mL EtOH. Purification by automated gradient flash chromatography (C18, MeOH:H_2O 1:99 to 1:0 over 30 column volumes) and subsequent lyophilization gave **19b** as a white powder (50 mg, 0.23 mmol, 25%). Marfey's analysis (cf. General Procedure B) was used to confirm the stereochemical purity (i.e., 10:1 dr and >99% *ee*), and the relative configuration at C2 and C3 was assigned based on that of **2b**. Despite being formed with a high degree of stereopurity, we are not able to assign the configuration at the indan stereocenter.

^{1}H NMR (500 MHz, CD_3OD): δ 7.31 – 7.18 (m, 2H), 7.19 – 7.07 (m, 2H), 4.26 (dd, *J* = 6.1, 4.9 Hz, 1H), 3.60 (d, *J* = 6.1 Hz, 1H), 3.48 (ddd, *J* = 8.1, 5.3, 5.3 Hz, 1H), 3.02 (ddd, *J* = 17.8, 7.7, 7.7 Hz, 1H), 2.85 (ddd, *J* = 15.4, 7.7, 7.7 Hz, 1H), 2.32 – 2.14 (m, 2H).

^{13}C{^{1}H} NMR (126 MHz, CD_3OD): δ 173.0, 146.3, 144.5, 128.1, 127.3, 125.7, 125.2, 72.0, 59.5, 49.6, 32.1, 26.9.

HRMS (ESI^-): Calcd for $C_{12}H_{14}NO_3^-$ $[M - H]^-$ requires 220.0979; found 220.0980

(2*S*,3*R*,*E*)-2-Amino-3-hydroxy-6-phenylhex-5-enoic Acid (20b)

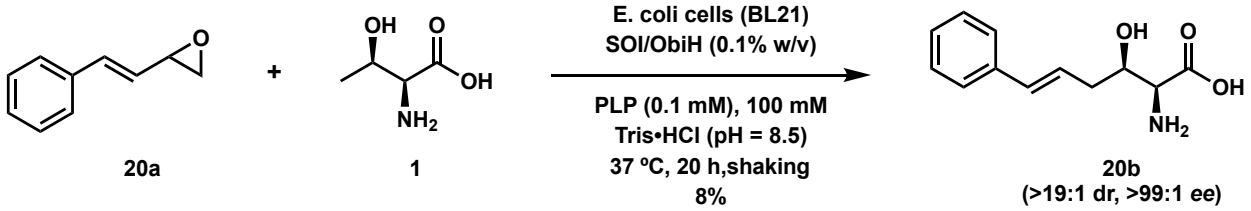

20a + **1** → **20b** (>19:1 dr, >99:1 *ee*)

Amino acid **20b** was prepared following General Procedure A with (*E*)-2-styryloxirane (**20a**, 148.8 mg, 1.0 mmol), L-Thr (**1**, 491 mg, 4.1 mmol), PLP (200 µL via 20 mM solution in water, 0.004 mmol), flash frozen SOI/ObiH *E. coli* BL21 whole cells (40 mg, 1.0% w/v%) in Tris•HCl buffer solution (37.6 mL, 100 mM, pH = 8.5) and 2 mL EtOH. Purification by automated gradient flash chromatography (C18, MeOH:H_2O 1:99 to 1:0 over 30 column volumes) and subsequent lyophilization gave 21 mg of product as a white solid with 3-4 mg tris base contamination as determined by ^{1}H NMR, yielding 17 mg of **20b** (0.08 mmol, 8%). Marfey's analysis (cf. General Procedure B) was used to confirm the stereochemical purity (i.e., >19:1 dr and >99% *ee*), and the relative configuration was assigned based on that of **2b**.

^{1}H NMR (500 MHz, CD_3OD): δ 7.40 – 7.36 (m, 2H), 7.30 – 7.25 (m, 2H), 7.20 – 7.15 (m, 1H), 6.53 (d, *J* = 15.9 Hz, 1H), 6.33 (dt, *J* = 15.9, 7.1 Hz, 1H), 4.10 (ddd, *J* = 11.0, 5.8, 5.8 Hz, 1H), 3.43 (d, *J* = 4.5 Hz, 1H), 2.56 (dddd, *J* = 14.3, 7.4, 5.5, 1.4 Hz, 1H), 2.47 (dddd, *J* = 14.4, 8.1, 6.7, 1.5 Hz, 1H).

^{13}C{^{1}H} NMR (126 MHz, CD_3OD): δ 174.6, 138.9, 134.1, 129.5, 128.2, 127.2, 127.1, 71.6, 60.3, 39.2.

HRMS (ESI$^-$): Calcd for $C_{12}H_{14}NO_3^-$ $[M - H]^-$ requires 220.0979; found 220.0978

(2*S*,3*R*,*E*)-2-Amino-3-hydroxy-5-methyl-6-phenylhex-5-enoic Acid (21b)

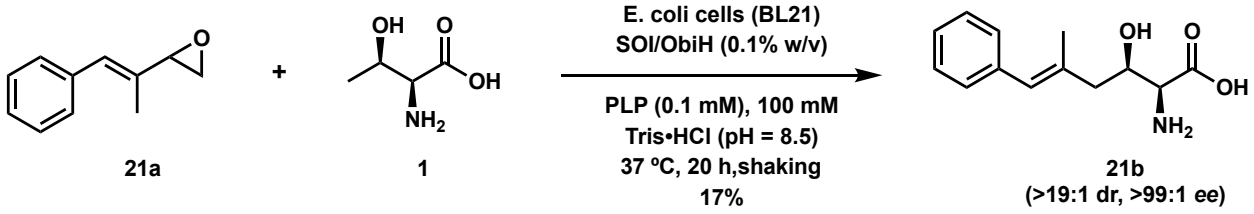

21a **1** **21b**
(>19:1 dr, >99:1 *ee*)

Amino acid **21b** was prepared following General Procedure A with (*E*)-2-(1-phenylprop-1-en-2-yl)oxirane (**21a**, 159 mg, 93% purity, 0.93 mmol), L-Thr (**1**, 488 mg, 4.1 mmol), PLP (200 µL via 20 mM solution in water, 0.004 mmol), flash frozen SOI/ObiH *E. coli* BL21 wet whole cells (40 mg, 0.1% w/v%) in Tris•HCl buffer solution (37.6 mL, 100 mM, pH = 8.5), 2 mL EtOH. Purification by automated gradient flash chromatography (C18, MeOH:H_2O 1:99 to 1:0 over 30 column volumes) and subsequent lyophilization gave **21b** as a white solid (39 mg, 0.16 mmol, 17%). Marfey's analysis (cf. General Procedure B) was used to confirm the stereochemical purity (i.e., >19:1 dr and >99% *ee*), and the relative configuration was assigned based on that of **2b**.

^{1}H NMR (500 MHz, CD_3OD): δ 7.33 – 7.28 (m, 2H), 7.27 – 7.24 (m, 2H), 7.20 – 7.15 (m, 1H), 6.42 (s, 1H), 4.33 (ddd, *J* = 9.0, 5.1, 4.0 Hz, 1H), 3.48 (d, *J* = 4.1 Hz, 1H), 2.54 (dd, *J* = 13.4, 4.9 Hz, 1H), 2.40 (dd, *J* = 13.7, 8.8 Hz, 1H), 1.93 (d, *J* = 1.4 Hz, 3H).

^{13}C{^{1}H} NMR (126 MHz, CD_3OD): δ 173.3, 139.5, 136.1, 130.0, 129.4, 129.0, 127.2, 69.4, 60.2, 46.8, 18.1.

HRMS (ESI^-): Calcd for $C_{13}H_{16}NO_3^-$ $[M - H]^-$ requires 234.1136; found 234.1136

Compounds Discussed in Figure 8

(*R*)-2-Methyl-2-phenyloxirane [(*R*)16a] and (*S*)-2-Methyl-2-phenyloxirane [(*S*)-18a]

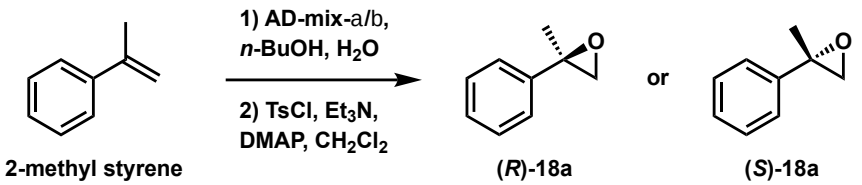

Syntheses by Prof. Patrick Willoughby. Enantioenriched samples of 2-methyl-2-phenyloxirane (i.e., **(*R*)-18a** and **(*S*)-18a**) were obtained from 2-methylstyrene by Sharpless asymmetric dihydroxylation followed by mono-sulfonylation and cyclization to the epoxide. Use of AD-mix-b provided the (*R*) enantiomer and use of AD-mix-a provided the (*S*) enantiomer. The following is a general procedure for the overall transformation, and the spectral data for each enantiomer matched those previously reported for the (*R*)[41] and (*S*)[42] enantiomer. Commercially available AD-mix (2.4 g) was added to a mixture of *n*-BuOH (6 mL) and water (8 mL) with stirring at room temperature. After 5 minutes, the mixture was cooled to 0 ºC, and 2-methylstyrene (200 mg, 1.70 mmol) was added. After 3 h, sodium sulfite (2.5 g) was added, the ice bath was removed, and the mixture was extracted with EtOAc (3x). The organic extracts were combined, washed with satd. aq. NaCl, dried (Na_2SO_4), and concentrated. The crude diol (~150 mg) was added to a solution of 4-dimethylaminopyridine (17 mg, 0.14 mmol) and Et_3N (1.5 mL, 11 mmol) in CH_2Cl_2 (10 mL) at 0 ºC with stirring. *p*-Toluenesulfonyl chloride (313 mg, 1.7 mmol) was added and the reaction mixture was heated at 35 ºC. After 24 h, the mixture was diluted in dichloromethane, washed with water, dried ($MgSO_4$), filtered, and concentrated. The crude material (~80 mg) was sufficiently pure for subsequent enzyme-catalyzed transformations.

Analytical reactions with enantioenriched samples (i.e., (*R*)-18a and (*S*)-18a)

Flash frozen SOI-ObiH wet whole cells were resuspended in 100 mM Tris-HCl pH 8.5 at 20 mg/mL (2X). The 2X cell solution (10 mg/mL final conc.) was added to reactions with final concentration of 25 mM epoxide (delivered via a 500 mM stock dissolved in DMSO, 5% DMSO in reaction), 100 mM L-Thr, 0.1 mM PLP, and 100 mM Tris-HCl pH 8.5 unless otherwise stated. Analytical reactions were incubated in microcentrifuge tubes at 37 °C, 800 rpm. Reaction samples were removed at 10 min, 30 min, and 60 min and quenched with equal volume MeCN. Reactions samples were also taken after overnight incubation. Quenched reactions were centrifuged at 15,000-20,000×*g* for 10 min to pellet cell debris. Supernatant was removed and analyzed via UPLC-MS for product quantification. Extracted ion chromatograms for each experiment are provided below.

Extracted ion chromatograms (EICs) of SOI-ObiH reactions described in Figure 8

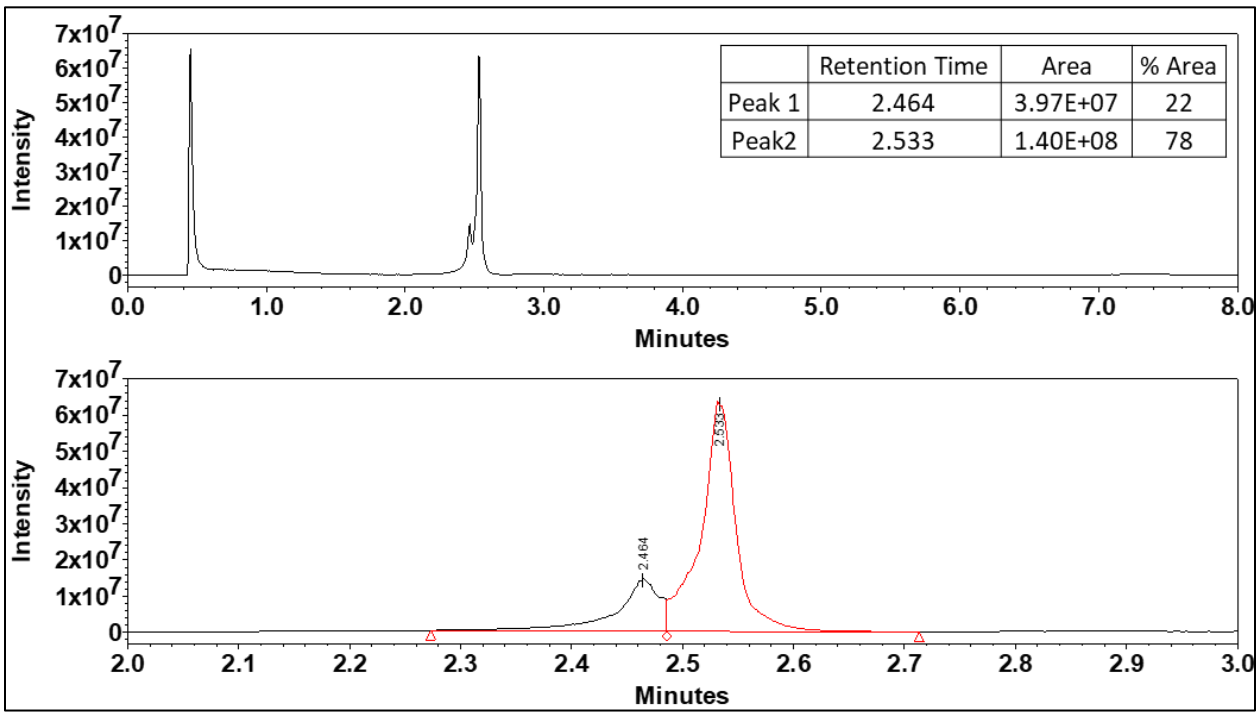

Figure S6. EICs of reactions with **(*S*)-18a** after 10 minutes

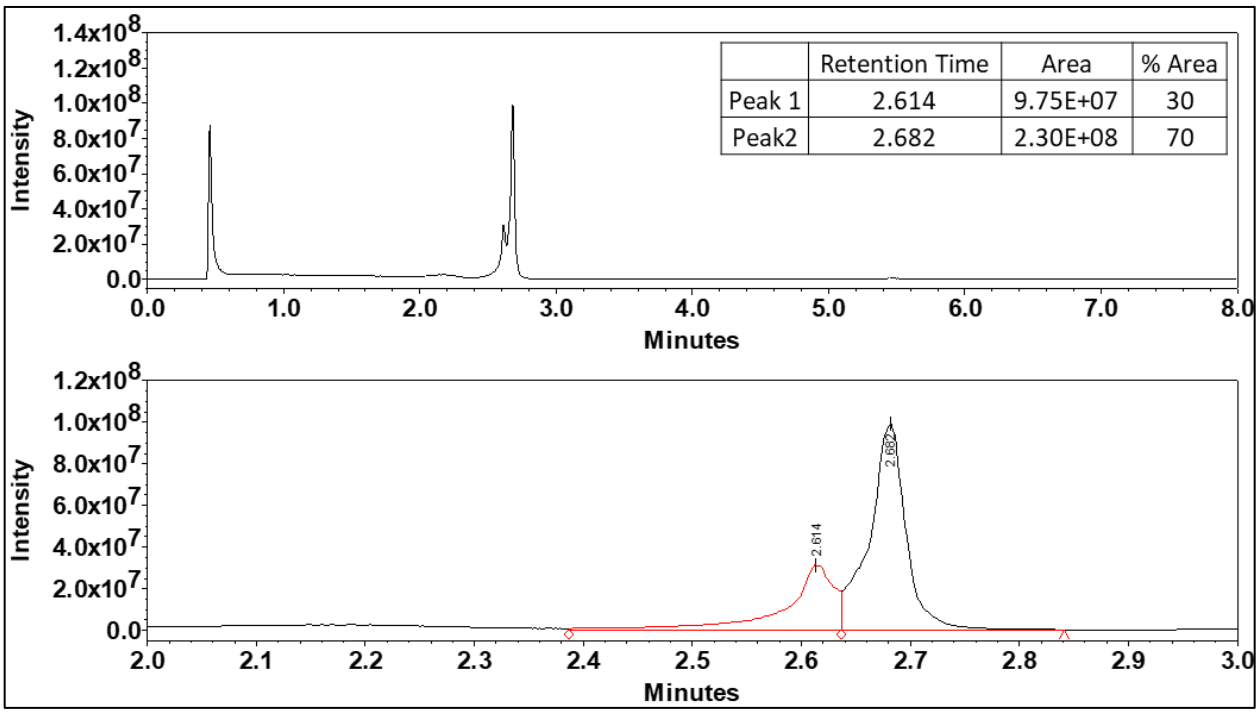

Figure S7. EICs of reactions with **(*S*)-18a** after 30 minutes.

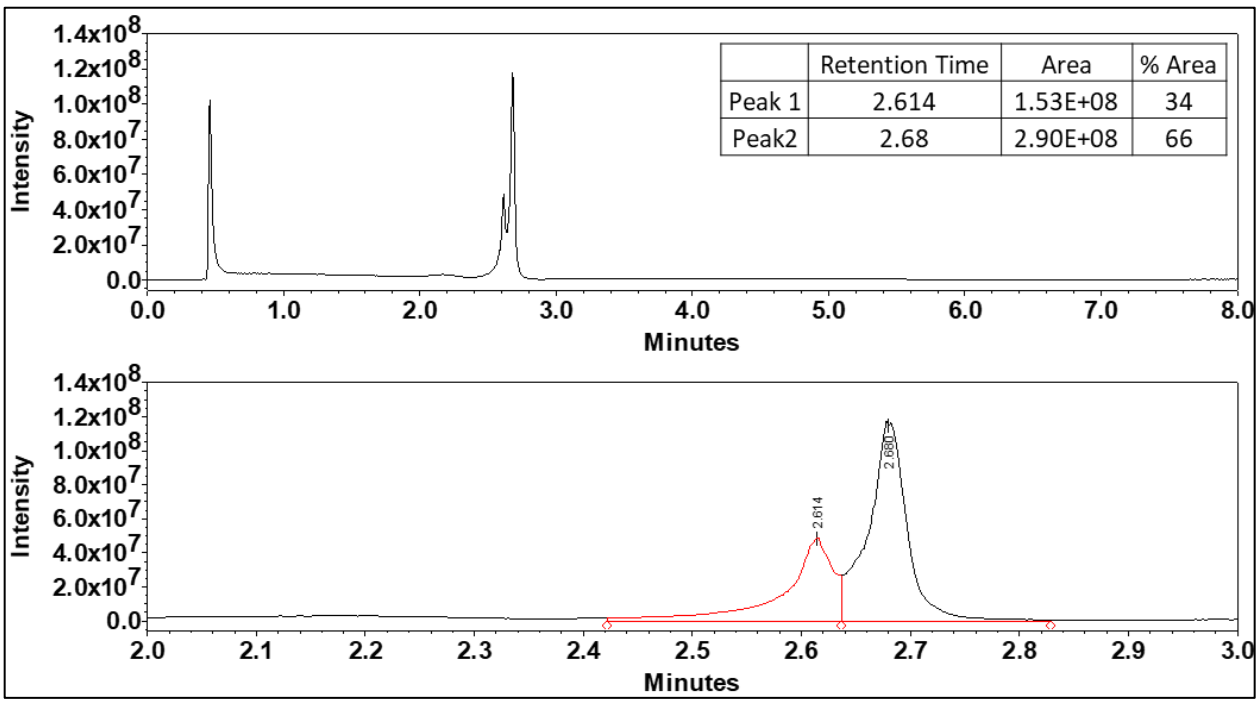

Figure S8. EICs of reactions with **(*S*)-18a** after 60 minutes.

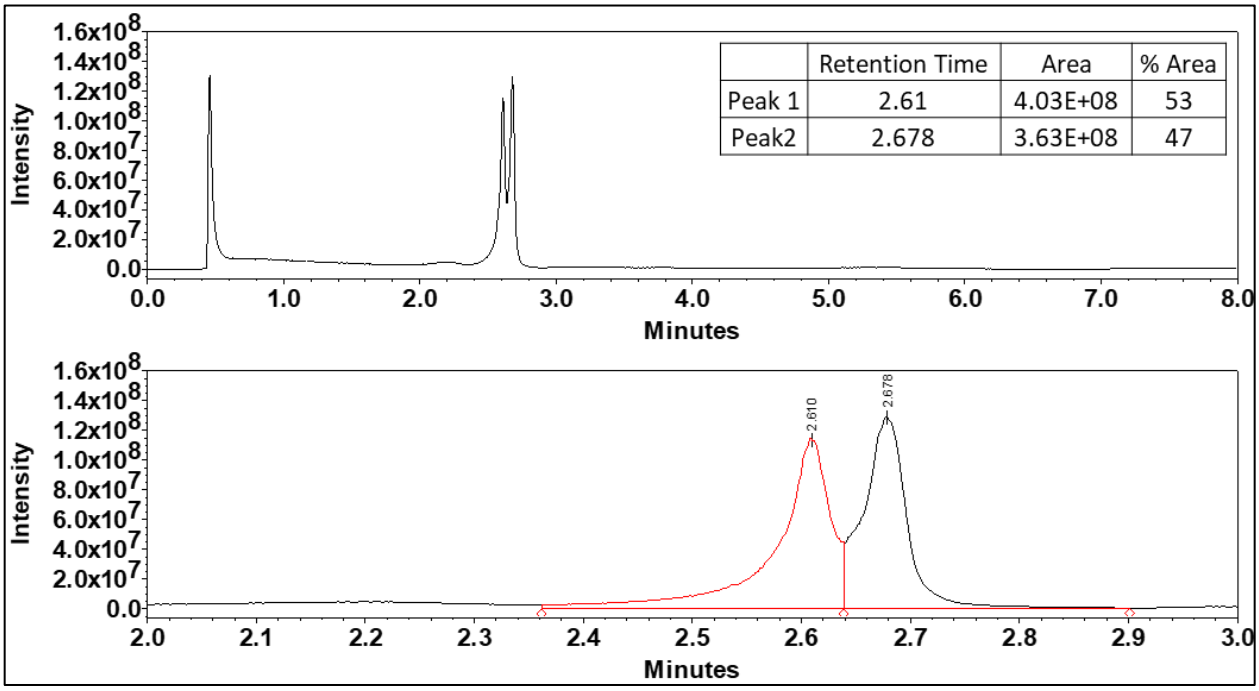

	Retention Time	Area	% Area
Peak 1	2.61	4.03E+08	53
Peak2	2.678	3.63E+08	47

Figure S9. EICs of reactions with **(*S*)-18a** after overnight (O.N.) incubation.

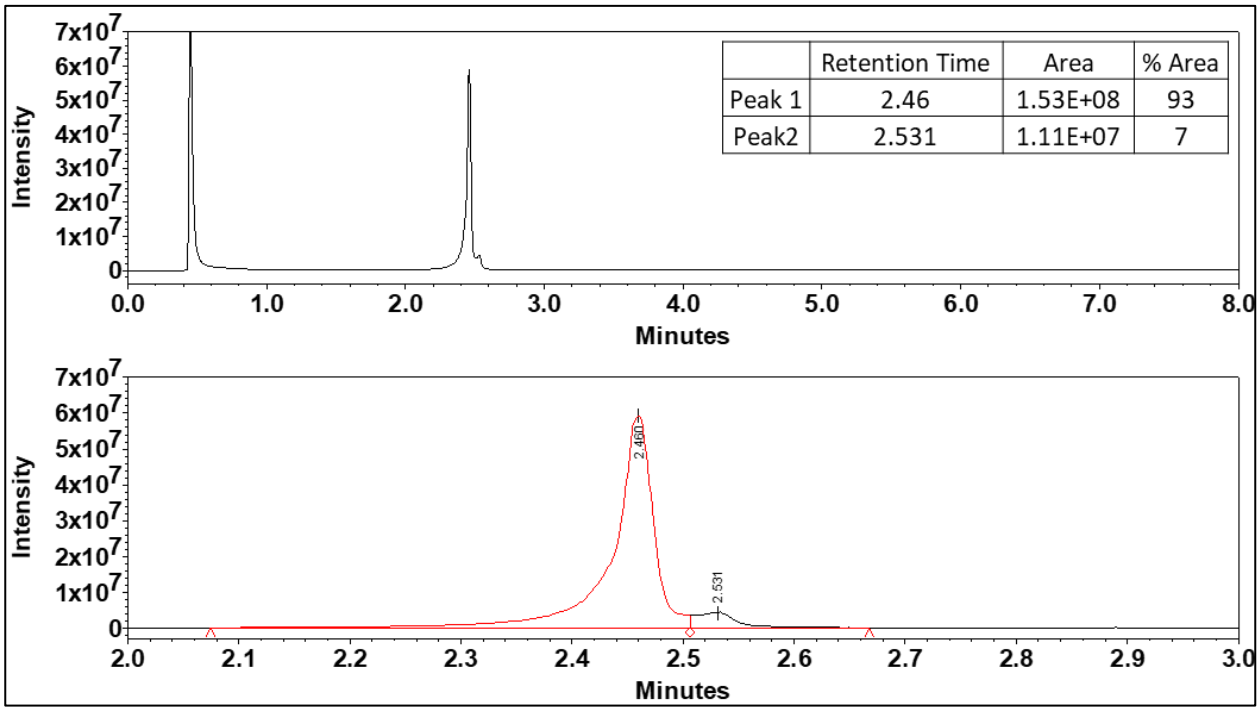

	Retention Time	Area	% Area
Peak 1	2.46	1.53E+08	93
Peak2	2.531	1.11E+07	7

Figure S10. EICs of reactions with **(*R*)-18a** after 10 minutes.

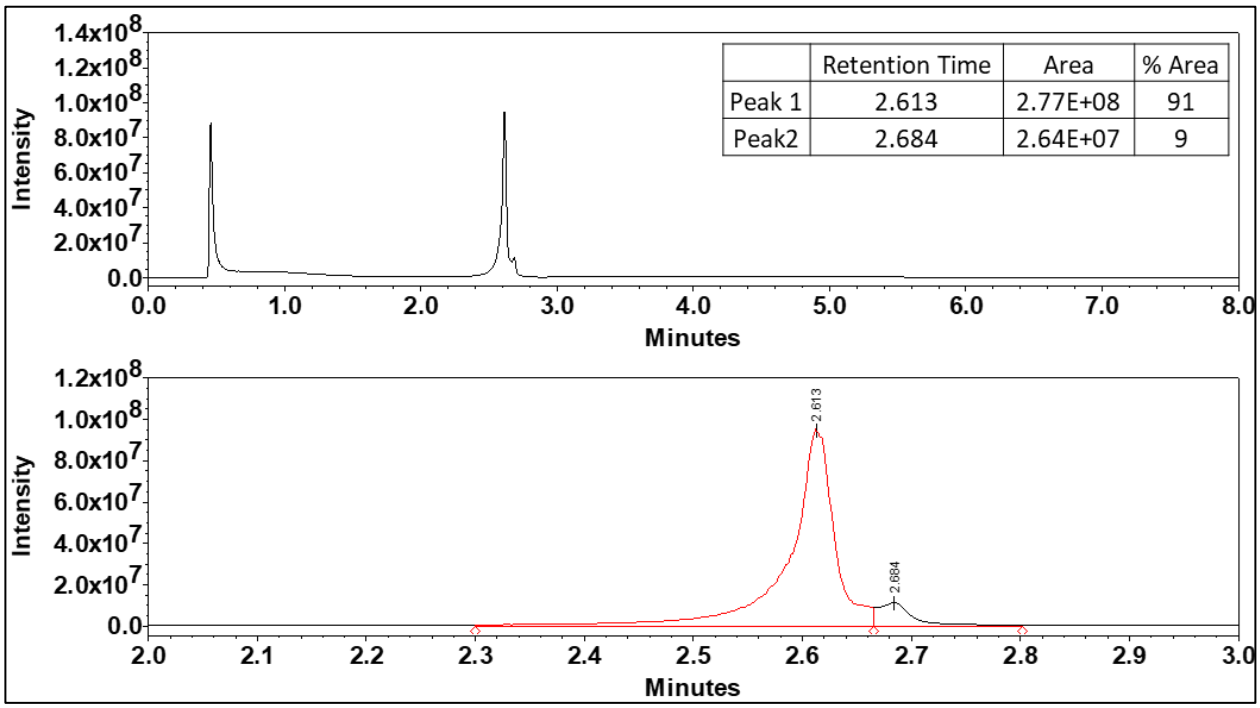

Figure S11. EICs of reactions with **(*R*)-18a** after 30 minutes.

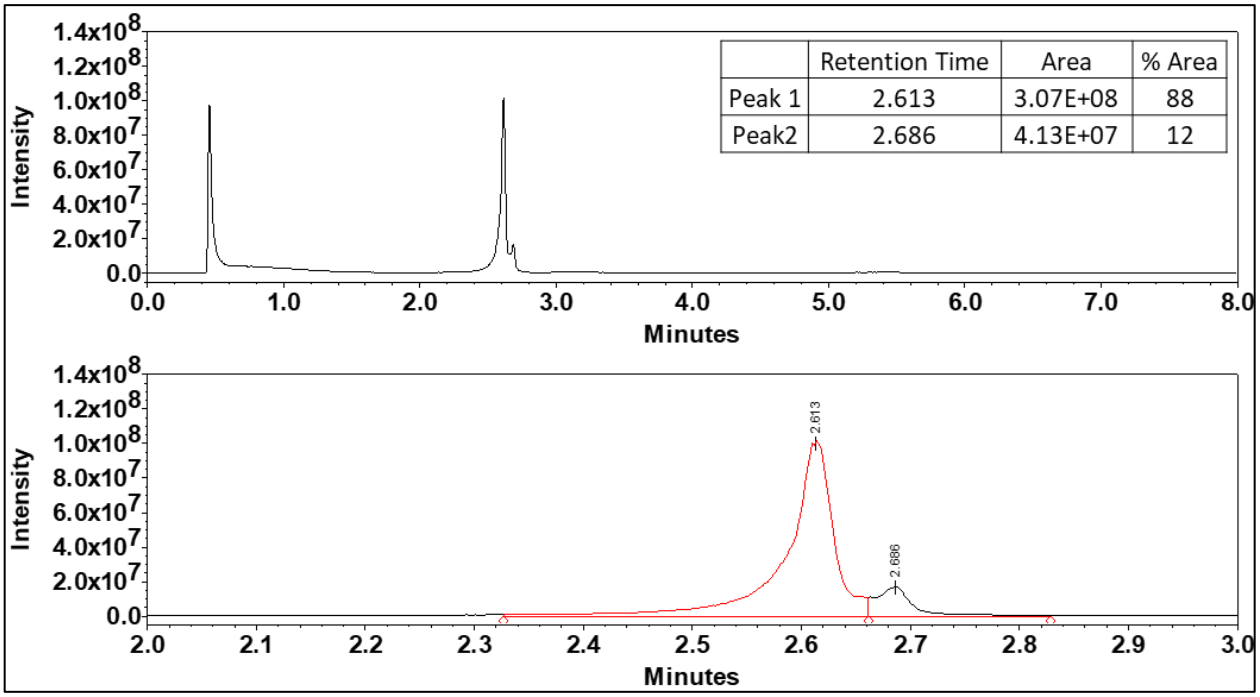

Figure S12. EICs of reactions with **(*R*)-18a** after 60 minutes.

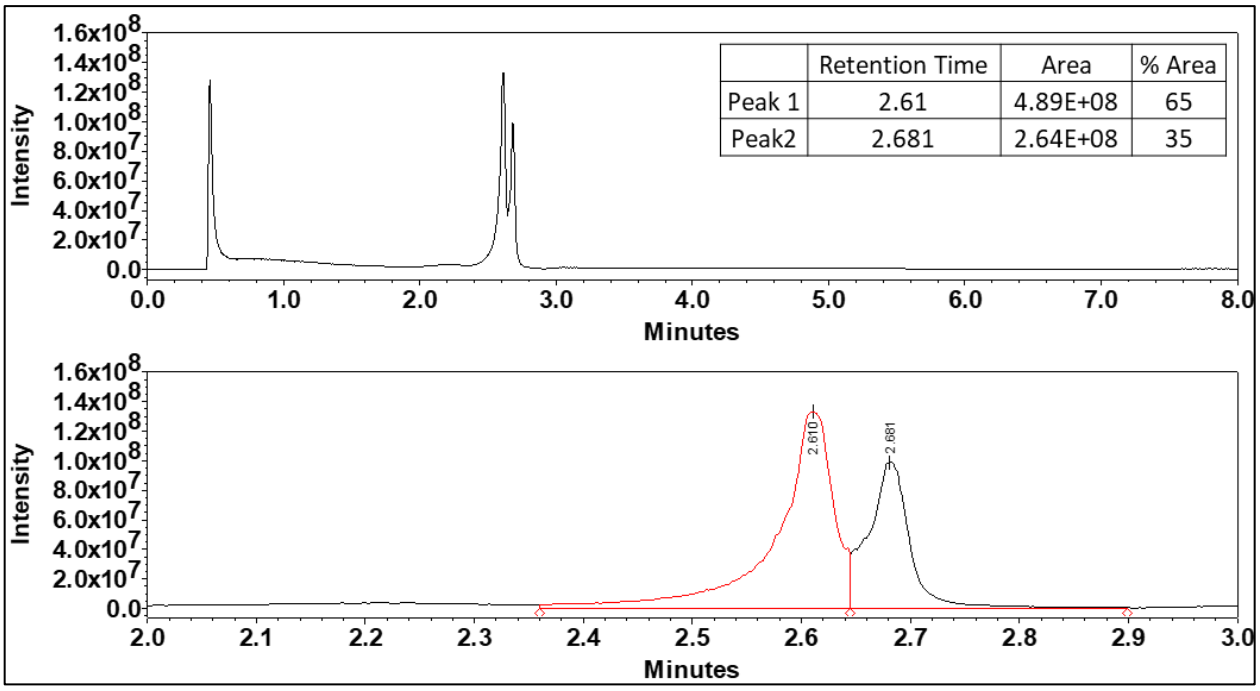

Figure S13. EICs of reactions with **(*R*)-18a** after overnight (O.N.) incubation.

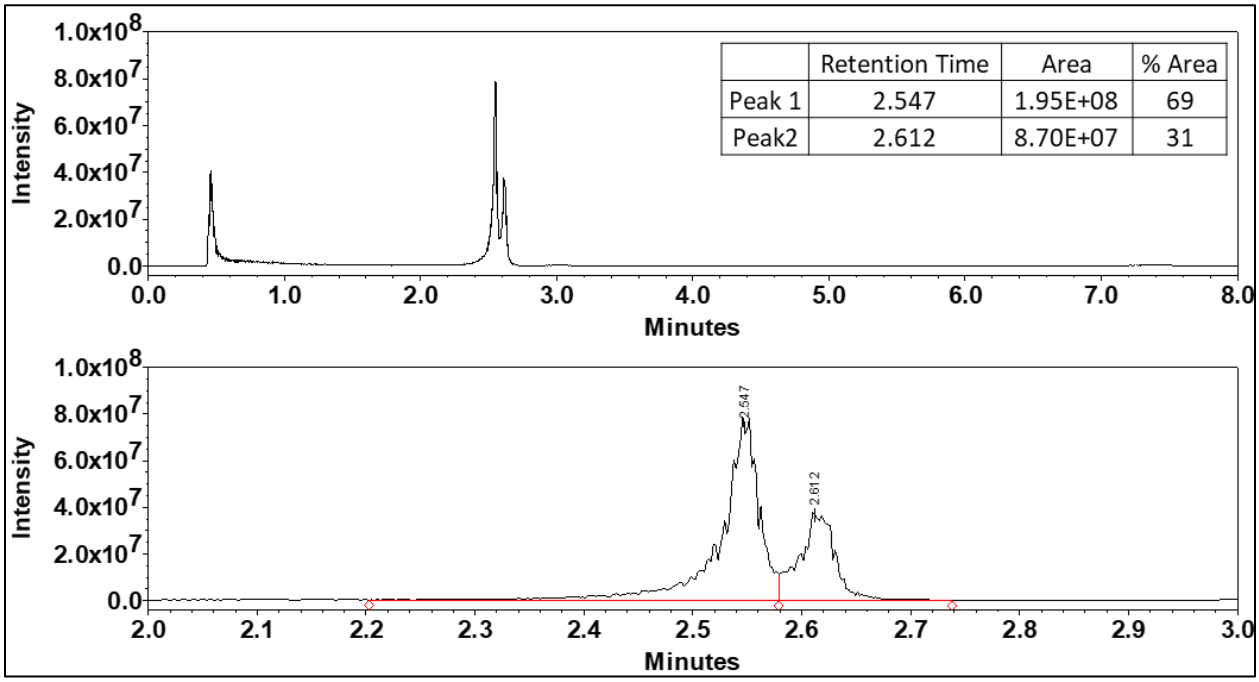

Figure S14. EICs of reactions with ***rac*-18a** after 3 minutes.

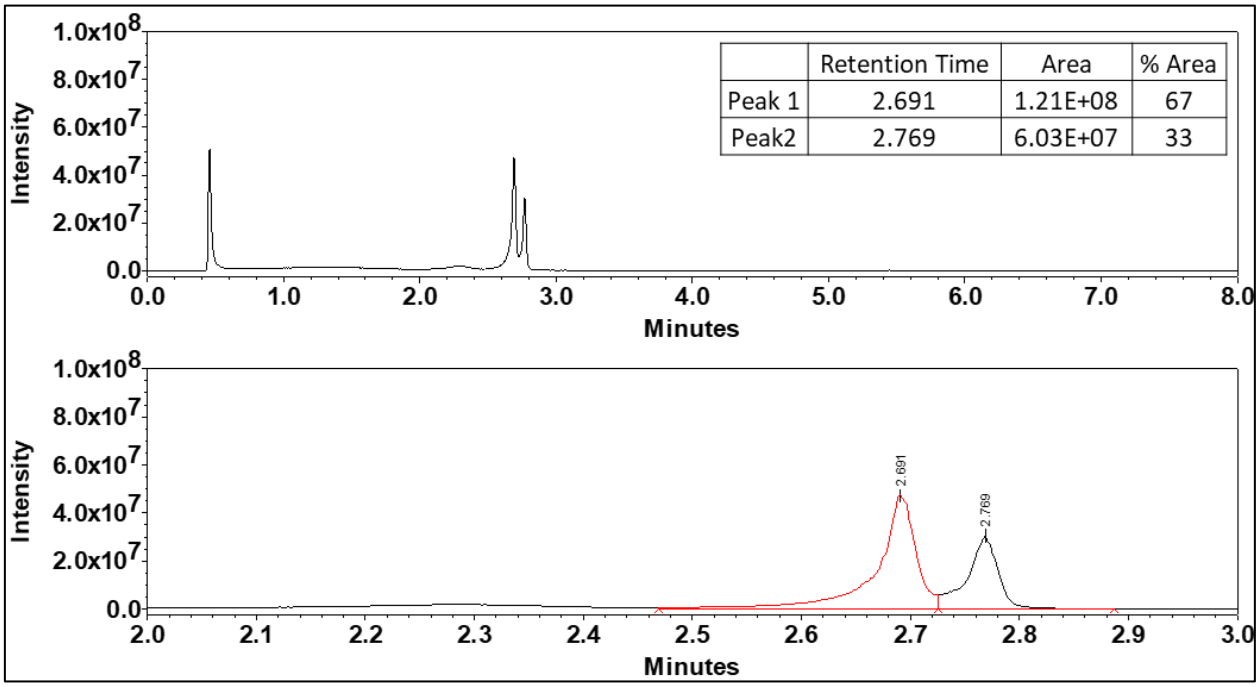

Figure S15. EICs of isolated product from SOI-ObiH preparative reactions with ***rac*-18a**.

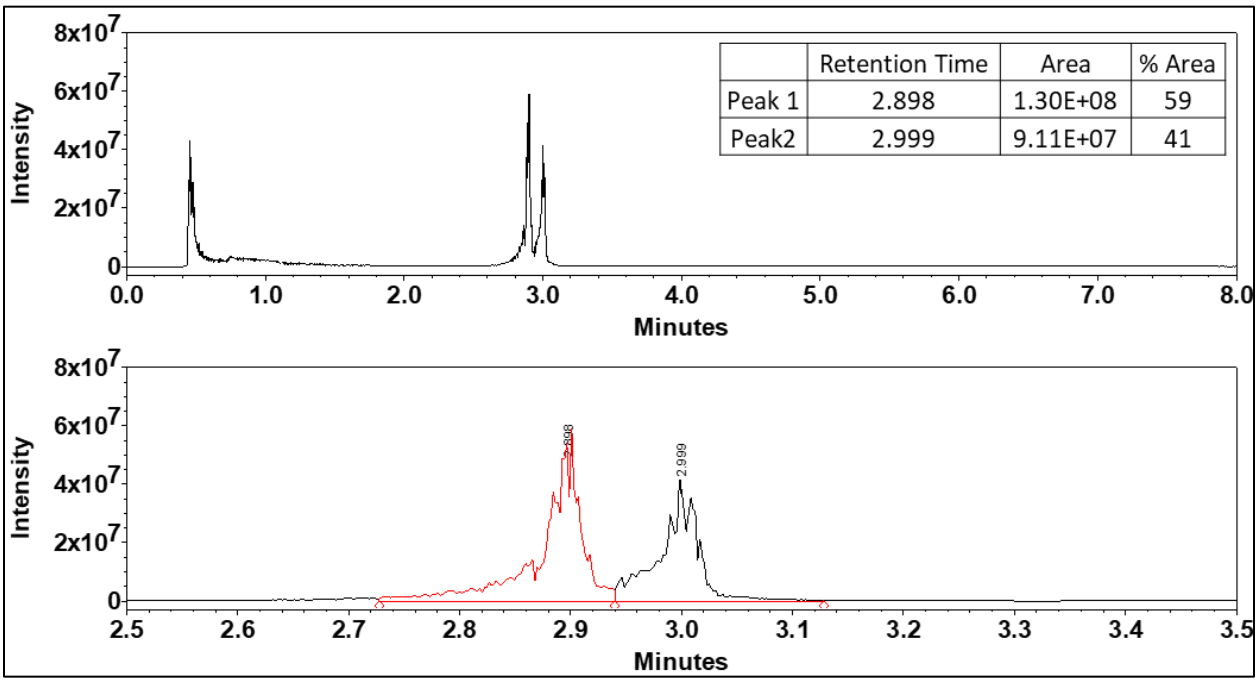

Figure S16. EICs or reactions with 2-phenyl propanal (**22**) and purified ObiH.

Compounds Discussed in Figure 9

2-Phenyloxirane-2-*d* (2a-2-d_1)

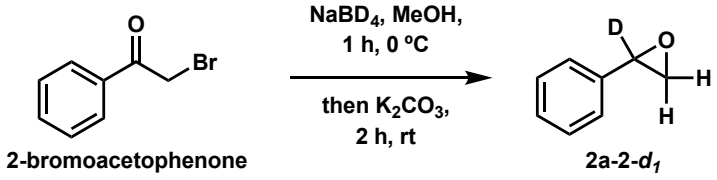

2-Phenyloxirane-2-*d* (**2a-2-d_1**) was prepared using a previously described protocol.[Error! Bookmark not defined.] Synthesis by Prof. Patrick Willoughby.

(2*S*,3*R*)-2-Amino-3-hydroxy-4-phenylbutanoic-4-*d* Acid (2b-4-d_1)

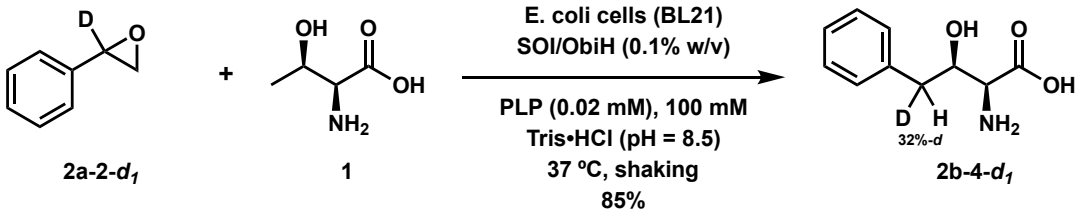

Amino acid **2b-4-*d*$_1$** was prepared following General Procedure A with 2-phenyloxirane-2-d (**2a-2-*d*$_1$**, 40 mg, 0.33 mmol, final conc. 3.4 mM), L-Thr (**1**, 1.14 g, 9.6 mmol), PLP (100 µL via 20 mM solution in water, 0.002 mmol, 0.02 mM final reaction conc.), dry SOI/ObiH *E. coli* BL21 dry whole cells (102 mg, 0.1% w/v%) in Tris•HCl buffer solution (93 mL, 100 mM, pH = 8.5), 5 mL EtOH. Purification by automated gradient flash chromatography (C18, MeOH:H_2O 1:99 to 1:0 over 30 column volumes) and subsequent lyophilization gave 61 mg of product as a white solid with 6 mg tris base contamination as determined by ^{1}H NMR, yielding 55 mg of **2b-4-*d*$_1$** (0.28 mmol, 85%). The relative configuration of the product and the stereochemical purity (i.e., dr and %*ee*) was identical to that of unlabeled **2b**. Retention of deuterium was evaluated by ^{1}H NMR analysis, which showed the product was 32% at C_g.

^{1}H NMR (400 MHz, CD_3OD): δ 7.35 – 7.12 (m, 5H), 4.33 – 4.18 (m, 1H), 3.44 (d, *J* = 4.4 Hz, 1H), 3.01 – 2.91 (m, 0.57H), 2.79 (d, *J* = 8.9 Hz, 0.79H).

HRMS (ESI^-): Ions were observed corresponding with ***d*$_1$** (i.e., Calcd for $C_{10}H_{11}DNO_3^-$ [M – H]$^-$ requires 195.0885; found 195.0886) and ***d*$_0$** (i.e., Calcd for $C_{10}H_{12}NO_3^-$ [M – H]$^-$ requires 194.0823; found 194.0824).

2-Phenyloxirane-3,3-*d*$_2$ (2a-3,3-*d*$_2$)

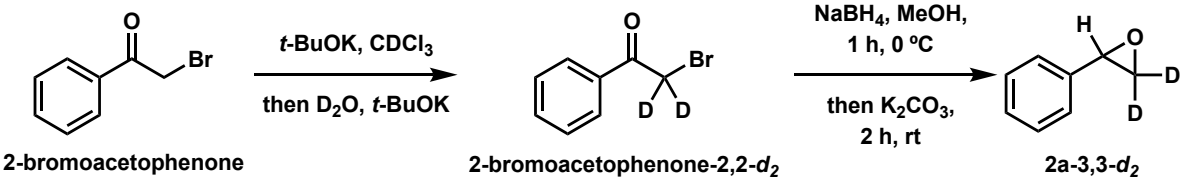

Synthesis by Prof. Patrick Willoughby. 2-Phenyloxirane-3,3-d_2 (**2a-3,3-*d*$_2$**) was prepared from 2-bromoacetophenone using a slightly modified protocol previously reported by Kass.[Error! Bookmark not defined.] Namely, deuterium incorporation of 2-bromoacetophenone was enhanced by increasing the amounts of reactants and extending the reaction time from 3 hours to 24 hours. The specific procedure for the synthesis of 2-bromoacetophenone-2,2-d_2 is described below. The conversion

of 2-bromoacetophenone-2,2-d_2 into 2-phenyloxirane-3,3-d_2 (**2a-3,3-d_2**) by sequential reduction and cyclization followed the same procedure as that of Kass.[Error! Bookmark not defined.] *t*-BuOK (2.0 g, 18 mmol) was added portionwise to a mixture of 2-bromoacetophenone (2.0 g, 10 mmol) and $CDCl_3$ (12 mL) at 0 ºC with stirring (CAUTION: A vigorous exotherm forms upon addition of potassium *tert*-butoxide. The caustic reagent must be added slowly.). After 1 h, D_2O (7.5 mL) was added dropwise and additional *t*-BuOK (1.3 g, 12 mmol) is added portionwise and the mixture is allowed to stir overnight, warming to room temperature. After 24 h, the mixture was transferred to a separatory funnel and diluted in $CDCl_3$ (20 mL). The organic phase was dried ($MgSO_4$), filtered, and concentrated to give 2-bromoacetophenone-2,2-d_2 (1.3 g, 64% crude) with ~85% deuterium incorporation at C2.

(2*S*,3*R*)-2-Amino-3-hydroxy-4-phenylbutanoic-3,4-d_2 Acid (2b-3,4-d_2)

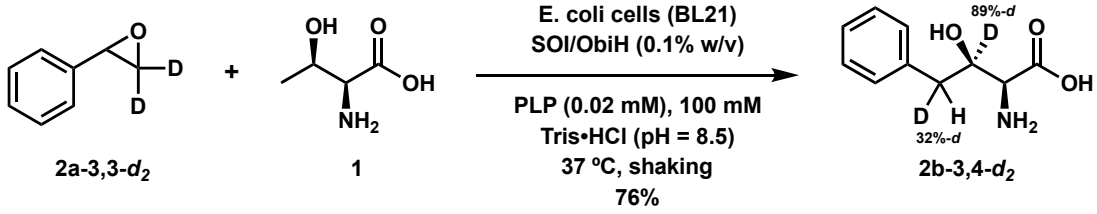

Amino acid **2b-3,4-d_2** was prepared following General Procedure A with 2-phenyloxirane-3,3-d_2 (**2a-3,3-d_2**, 95 mg, 0.78 mmol, final conc. 8.0 mM), L-Thr (**1**, 1.17 g, 9.8 mmol), PLP (100 µL via 20 mM solution in water, 0.002 mmol, 0.02 mM final reaction conc.), and dry SOI/ObiH *E. coli* BL21 whole cells (99.5 mg, 0.1% w/v%) in Tris•HCl buffer solution (93 mL, 100 mM, pH = 8.5). Purification by automated linear gradient flash chromatography (C18, MeOH:H_2O 1:99 to 1:0) gave **2b-3,4-d_2** as a white solid (117 mg, 0.59 mmol, 76%).The relative configuration of the product and the stereochemical purity (i.e., dr and %*ee*) was identical to that of unlabeled **2b**. Retention of deuterium was evaluated by ^{1}H NMR analysis, which showed the product was 89% at C_b and 32% at C_g.

^{1}H NMR (400 MHz, CD_3OD): δ 7.41 – 7.07 (m, 5H), 4.29 – 4.23 (m, 0.11H), 3.44 (s, 1H), 3.00 – 2.93 (m, 0.64H), 2.84 – 2.77 (m, 0.73H).

HRMS (ESI^-): Ions were observed corresponding with ***d_2*** (i.e., Calcd for $C_{10}H_{10}D_2NO_3^-$ $[M - H]^-$ requires 196.0948; found 196.0949), ***d_1*** (i.e., Calcd for $C_{10}H_{11}DNO_3^-$ $[M - H]^-$ requires 195.0885; found 195.0886), and ***d_0*** (i.e., Calcd for $C_{10}H_{12}NO_3^-$ $[M - H]^-$ requires 194.0823; found 194.0824).

(2*S*,3*R*)-2-Amino-3-hydroxy-4-phenylbutanoic-4,4-d_2 Acid (2b-4,4-d_2)

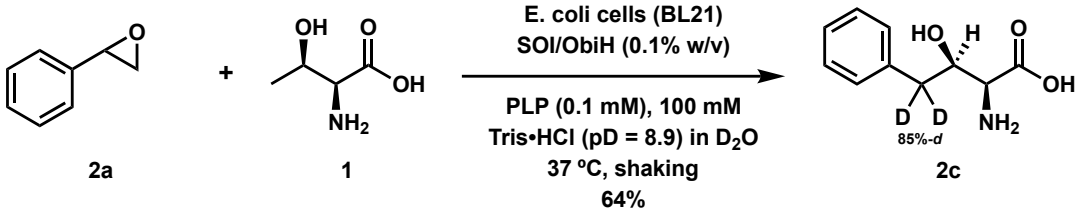

2a **1** **2c**

Amino acid **2c** was prepared with reagent concentrations presented in General Procedure A, but with the removal of H_2O and replacement with D_2O. L-Thr (**1**, 119 mg, 1 mmol), PLP (50 µL via 20 mM solution in water, 0.001 mmol), and Tris•HCl buffer solution (7.5 mL, 100 mM, pH = 8.5) were combined in a 20 mL scintillation vial and frozen at -80°C. The frozen solution was then lyophilized to remove H_2O. The resulting powder was hydrated with 7.5 mL of D_2O and combined with styrene oxide (**2a**, 30 mg, 0.25 mmol), dry SOI/ObiH *E. coli* BL21 whole cells (9.7 mg, 0.1% w/v%), and 0.5 mL CD_3OD. Purification by automated gradient flash chromatography (C18, MeOH:H_2O 1:99 to 1:0 over 30 column volumes) and subsequent lyophilization gave 35 mg of product as a white solid with 4 mg tris base contamination as determined by ^{1}H NMR, yielding 31 mg of **2b-4,4-d_2** (0.16 mmol, 64%). The relative configuration of the product and the stereochemical purity (i.e., dr and %*ee*) was identical to that of unlabeled **2a**. Retention of deuterium was evaluated by ^{1}H NMR analysis, which showed the product was 85% at C_b.

^{1}H NMR (400 MHz, CD_3OD): δ 7.33 – 7.17 (m, 5H), 4.23 (d, *J* = 4.4 Hz, 1H), 3.42 (d, *J* = 4.4 Hz, 1H), 2.95 (d, *J* = 4.5 Hz, 0.13H), 2.78 (d, *J* = 9.0 Hz, 0.13H).

HRMS (ESI^-): Ions were observed corresponding with ***d_2*** (i.e., Calcd for $C_{10}H_{10}D_2NO_3^-$ $[M - H]^-$ requires 196.0948; found 196.0949), ***d_1*** (i.e., Calcd for $C_{10}H_{11}DNO_3^-$ $[M - H]^-$ requires 195.0885; found 195.0886), and ***d_0*** (i.e., Calcd for $C_{10}H_{12}NO_3^-$ $[M - H]^-$ requires 194.0823; found 194.0824).

Racemic *cis*-2-Phenyloxirane-3-*d* [(+/-)-*cis*-2a-3-d_1]

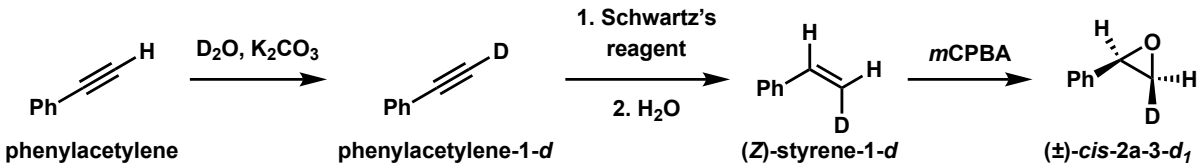

Synthesis by Prof. Patrick Willoughby. Epoxidation of (*Z*)-styrene-1-*d* with mCPBA gave *cis*-2-phenyloxirane-3-*d* [**(±)-*cis*-2a-3-d_1**].

Due to the volatility of styrene and styrene oxide, the isotopically labeled molecules described below were not isolated, and pentane-containing solutions of each were carried forward in subsequent transformations with additional purification.

(*Z*)-Styrene-1-*d* was prepared by a previously described method[43] from phenylacetylene-1-*d*. Specifically, Schwartz's reagent (i.e., zirconocene hydrochloride, 2.75 g, 10.7 mmol) was added portionwise to a solution of phenylacetylene-1-*d* (1.00 g, 9.70 mmol, available from phenylacetylene)[44] in dichloromethane (28 mL) at 0 ºC, in the dark, and with stirring. After two hours, water (1.4 mL, 78 mmol) was added, and the mixture was allowed to continue stirring in the dark. After two hours, the mixture was diluted with dichloromethane (50 mL), the aqueous phase removed using a separatory funnel, the organic phase was dried ($MgSO_4$), and filtered. The filtrate was concentrated under reduced pressure with an ambient temperature water bath until the liquid volume was ca. 3-10 mL, and the resulting mixture was diluted in pentane (50 mL). A plug of silica gel was sequentially washed with 1% Et_3N in hexanes followed by pentane, and the product mixture filtered through the silica gel pad with pentane eluent. The filtrate was concentrated under reduced pressure with an ambient temperature water bath to give a crude product mixture with varying amounts of pentane impurities (0.7–1.0 g obtained crude, depending on the amount of residual solvent). Consistent with the previous literature, ^{1}H NMR analysis of

the crude product mixture suggested the presence of (*Z*)-styrene-1-*d* (i.e., ~95% deuterium incorporation) via ablation of the doublet at d ~5.75 ppm included in the typical spectrum of styrene.

(*Z*)-Styrene-1-*d* was converted into *cis*-2-phenyloxirane-3-*d* [**(±)-*cis*-2a-3-d_1**] by mCPBA epoxidation. Specifically, the crude mixture obtained using the above procedure was diluted in dichloromethane (20 mL) and treated with mCPBA (2.0 g, 12 mmol) at room temperature and with stirring. The reaction was monitored by GC/MS to ensure complete consumption of styrene. In instances where incomplete conversion was observed, additional mCPBA (2.0 g, 12 mmol) was added. After stirring overnight, the mixture was diluted in dichloromethane (50 mL), washed with 1M $NaHCO_3$ (3x), dried ($MgSO_4$), filtered, and concentrated under reduced pressure using a room temperature water bath to a final volume of ~5 mL. The resulting mixture was purified by flash chromatography (SiO_2 pre-treated with 99:1 hexanes:Et_3N, 1:1 hexanes:diethyl ether eluent). Fractions containing the desired epoxide were pooled and concentrated under reduced pressure using a room temperature bath to a final volume of ~2 mL. ^{1}H NMR analysis was used to estimate the concentration of epoxide (14% purity by mass), and the sample was otherwise sufficiently pure for subsequent biocatalyic transformations. Consistent with the previous literature,[45] ^{1}H NMR analysis of the crude mixture suggested the presence of **(±)-*cis*-2a-3-d_1** (i.e., ~84% deuterium incorporation) via ablation of the doublet at d ~2.8 ppm in an otherwise typical spectrum of styrene oxide.

(2*S*,3*R*)-2-Amino-3-hydroxy-4-phenylbutanoic-3-*d* Acid (2b-3-d_1)

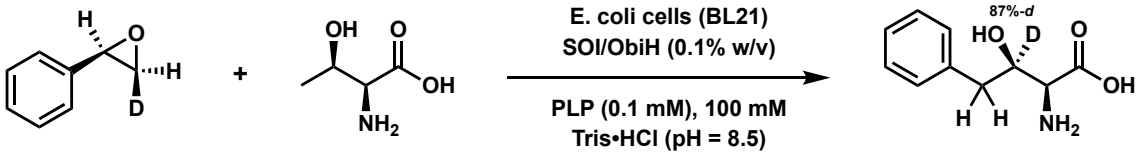

(±)-*cis*-2a-3-d_1 1 2b-3-d_1

Amino acid **2b-3-d_1** was prepared following General Procedure A with racemic *cis*-2-phenyloxirane-3-*d* [**(±)-*cis*-2a-3-d_1**, 27 mg, 14% purity, 0.03 mmol], L-Thr (**1**, 119 mg, 1.0 mmol), PLP (50 µL via 20 mM solution in water, 0.001 mmol, 0.1 mM final reaction conc.), and dry SOI/ObiH *E. coli* BL21 whole cells (10 mg, 0.1% w/v%) in Tris•HCl buffer solution (9.5 mL, 100 mM, pH = 8.5), 500 µL EtOH. Purification by automated gradient flash chromatography (C18, MeOH:H_2O 1:99 to 1:0 over 30 column volumes) and subsequent lyophilization gave 11 mg of product as a white solid with 2 mg tris base contamination as determined by ^{1}H NMR, yielding 9 mg of **2b-3-d_1** (0.05 mmol, 60%). The relative configuration of the product and the stereochemical purity (i.e., dr and %*ee*) was identical to that of unlabeled **2b**. Retention of deuterium was evaluated by ^{1}H NMR analysis, which showed the product was 87% at C_b.

^{1}H NMR (400 MHz, CD_3OD): δ 7.36 – 7.13 (m, 5H), 4.24 (ddd, *J* = 9.1, 4.7, 4.7 Hz, 0.13H), 3.42 (s, 1H), 2.96 (d, *J* = 13.9 Hz, 1H), 2.80 (d, *J* = 13.8 Hz, 1H).

HRMS (ESI^-): Ions were observed corresponding with ***d*$_1$** (i.e., Calcd for $C_{10}H_{11}DNO_3^-$ [M – H]$^-$ requires 195.0885; found 195.0886) and ***d*$_0$** (i.e., Calcd for $C_{10}H_{12}NO_3^-$ [M – H]$^-$ requires 194.0823; found 194.0824).

Racemic *trans*-2-Phenyloxirane-3-*d* [(+/-)-*trans*-2a-3-d_1]

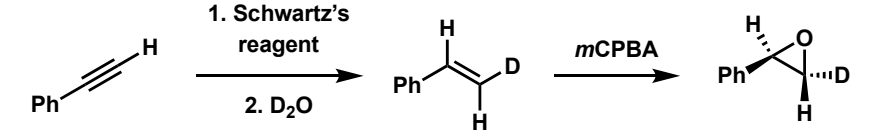

phenylacetylene (*E*)-styrene-1-*d* (±)-*trans*-2a-3-d_1

Synthesis by Prof. Patrick Willoughby. Epoxidation of (*E*)-styrene-1-*d* with mCPBA gave *trans*-2-phenyloxirane-3-*d* [**(±)-*trans*-2a-3-d_1**]. *Due to the volatility of styrene and styrene oxide, the isotopically labeled molecules described below were not isolated, and pentane-containing solutions of each were carried forward in subsequent transformations with additional purification.*

(*E*)-Styrene-1-*d* was prepared by revising the procedure for the synthesis of (*Z*)-styrene-1-*d* (cf. above) to use phenylacetylene (i.e., in place phenylacetylene-1-*d*) and D_2O in place of H_2O. Specifically, Schwartz's reagent (i.e., zirconocene hydrochloride, 1.87 g, 7.25 mmol) was added portionwise to a solution of phenylacetylene (0.73 mL, 6.6 mmol) in dichloromethane (19 mL) at 0 ºC, in the dark, and with stirring. After two hours, D_2O (0.94 mL, 52 mmol) was added, and the mixture was allowed to continue stirring in the dark, and with stirring. After two hours, the mixture was diluted with dichloromethane (50 mL), the aqueous phase removed using a separatory funnel, the organic phase was dried ($MgSO_4$), and filtered. The filtrate was concentrated under reduced pressure with an ambient temperature water bath until the liquid volume was ca. 3-10 mL, and the resulting mixture was diluted in pentane (50 mL). A plug of silica gel was sequentially washed with 1% Et_3N in hexanes followed by pentane, and the product mixture filtered through the silica gel pad with pentane eluent. The filtrate was concentrated under reduced pressure with an ambient temperature water bath to a volume of ~5 mL. Consistent with the previous literature,[46] ^{1}H NMR analysis of the pentane-rich mixture suggested the presence of (*E*)-styrene-1-*d* (i.e., >80% deuterium incorporation) via ablation of the doublet at d ~5.2 ppm in an otherwise typical spectrum of styrene.

(*E*)-Styrene-1-*d* was converted into *trans*-2-phenyloxirane-3-*d* by mCPBA epoxidation. Specifically, the pentane-rich solution obtained using the above procedure was diluted in dichloromethane (22 mL) and treated with mCPBA (2.0 g, 12 mmol) at room temperature and with stirring. The reaction was monitored by GC/MS to ensure complete consumption of styrene. In instances where incomplete conversion was observed, additional mCPBA (2.0 g, 12 mmol) was

added. After stirring overnight, the mixture was diluted in dichloromethane (50 mL), washed with 1M $NaHCO_3$ (3x), dried ($MgSO_4$), filtered, and concentrated under reduced pressure using a room temperature water bath to a final volume of ~5 mL. The resulting mixture was purified by flash chromatography (SiO_2 pre-treated with 99:1 hexanes:Et_3N, 1:1 hexanes:diethyl ether eluent). Fractions containing the desired epoxide were pooled and concentrated under reduced pressure using a room temperature bath to a final volume of ~2 mL. ^{1}H NMR analysis was used to estimate the concentration of epoxide (55% purity by mass), and the sample was otherwise sufficiently pure for subsequent biocatalyic transformations. Consistent with the previous literature,[47] ^{1}H NMR analysis of the pentane-rich mixture suggested the presence of **(±)-*trans*-2a-3-*d*$_1$** (i.e., >80% deuterium incorporation) via ablation of the doublet at d ~3.1 ppm in an otherwise typical spectrum of styrene oxide.

(2*S*,3*R*)-2-Amino-3-hydroxy-4-phenylbutanoic-4-*d* Acid (2b-4-*d*$_1$)

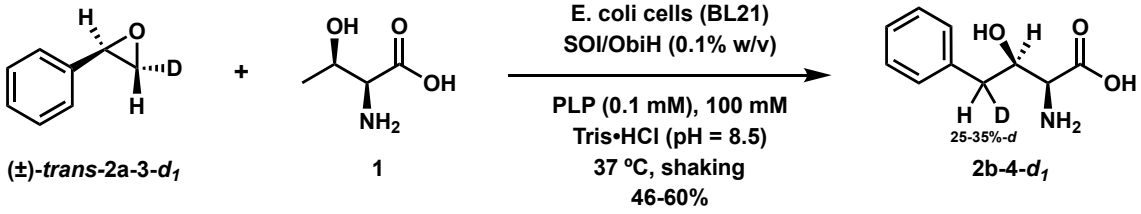

(±)-*trans*-2a-3-*d*$_1$ | 1 | 2b-4-*d*$_1$

Amino acid **2b-4-*d*$_1$** was prepared following General Procedure A with racemic *trans*-2-phenyloxirane-3-*d* [**(±)-*trans*-2a-3-*d*$_1$**, 29 mg, 55% purity, 0.13 mmol], L-Thr (**1**, 119 mg, 1.0 mmol), PLP (50 µL via 20 mM solution in water, 0.001 mmol, 0.1 mM final reaction conc.), and dry SOI/ObiH *E. coli* BL21 whole cells (10 mg, 0.1% w/v%) in Tris•HCl buffer solution (9.5 mL, 100 mM, pH = 8.5), and 500 µL EtOH. Purification by automated gradient flash chromatography (C18, MeOH:H_2O 1:99 to 1:0 over 30 column volumes) and subsequent lyophilization gave 13 mg of product as a white solid with 2 mg tris base contamination as determined by ^{1}H NMR, yielding 11 mg of **2b-4-*d*$_1$** (0.06 mmol, 46%). The relative configuration of the product and the

stereochemical purity (i.e., dr and %*ee*) was identical to that of unlabeled **2b**. Retention of deuterium was evaluated by ^{1}H NMR analysis, which showed the product was 25% at C_g.

[with additional purified ObiH] Amino acid **2b-4-*d*$_1$** was prepared following General Procedure A with racemic *trans*-2-phenyloxirane-3-*d* [**(±)-*trans*-2a-3-*d*$_1$**, 32 mg, 55% purity, 0.15 mmol], L-Thr (**1**, 117 mg, 1.0 mmol), PLP (50 µL via 20 mM solution in water, 0.001 mmol, 0.1 mM final reaction conc.), and dry SOI/ObiH *E. coli* BL21 whole cells (10 mg, 0.1% w/v%) in Tris•HCl buffer solution (3.5 mL, 100 mM, pH = 8.5), 100 µM ObiH (5.9 mL, 170 µM ObiH in 100 mM Tris•HCl, pH = 8.5), and 500 µL EtOH. Purification by automated gradient flash chromatography (C18, MeOH:H_2O 1:99 to 1:0 over 30 column volumes) and subsequent lyophilization gave **2b-4-*d*$_1$** as a white solid (17 mg, 0.09 mmol, 60%). The relative configuration of the product and the stereochemical purity (i.e., dr and %*ee*) was identical to that of unlabeled **2b**. Retention of deuterium was evaluated by ^{1}H NMR analysis, which showed the product was 35% at C_g.

^{1}H NMR (400 MHz, CD_3OD): δ 7.34 – 7.28 (m, 4H), 7.26-7.19 (m, 1H), 4.27 (ddd, *J* = 8.9, 4.4, 1.3 Hz, 1H), 3.46 (dd, *J* = 4.4, 1.2 Hz, 1H), 3.03 – 2.94 (m, 0.64–0.73H), 2.83 (dd, *J* = 13.6, 9.0 Hz, 0.66–0.77H).

HRMS (ESI^-): Ions were observed corresponding with ***d*$_1$** (i.e., Calcd for $C_{10}H_{11}DNO_3^-$ [M – H]$^-$ requires 195.0885; found 195.0886) and ***d*$_0$** (i.e., Calcd for $C_{10}H_{12}NO_3^-$ [M – H]$^-$ requires 194.0823; found 194.0824).

Compounds Discussed in Figure 10

(2*S*,4*R*)-2-Amino-4-hydroxy-5-phenylpentanoic Acid and (2*S*,4*S*)-2-Amino-4-hydroxy-5-phenylpentanoic Acid (24)

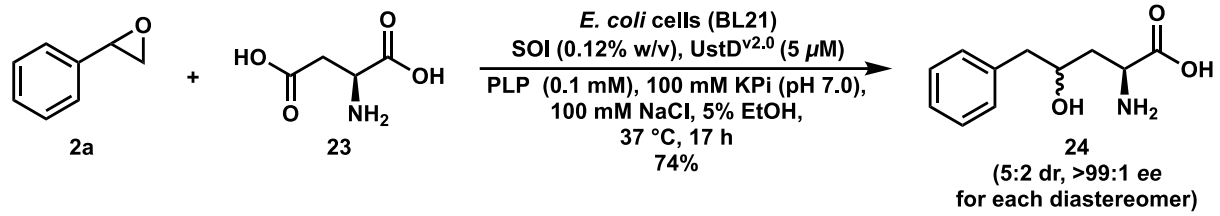

Styrene oxide (**2a**, 114 µL, 1.0 mmol, 25 mM final reaction concentration), EtOH (5% of total reaction volume), buffer solution KPi buffer solution (36.21 mL, 100 mM, pH 7.0, 100 mM NaCl), L-Asp (**23**, 230 mg, 1.3 mmol), PLP (200 µL via 20 mM solution in water, 0.004 mmol, 0.1 mM final reaction conc.), UstD$^{v2.0}$ (5,000 Max TON, 5 µM) were mixed in an Erlenmeyer flask. SOI was added via flash frozen *E. coli* BL21 wet whole cells (46.0 mg, 0.12% w/v%), and the mixture was incubated at 37 ºC. After 17 hours, the reaction mixture was frozen at -80 °C, thawed, then heated at 75 °C for 30 minutes. To lyse the cells, a half volume of MeCN (20 mL) was added to the reaction. The resulting mixture was passaged over filter paper, and the filtrate was concentrated by rotary evaporation. Purification by automated gradient flash chromatography (C18, MeOH:H_2O 1:99 to 1:0 over 30 column volumes) and subsequent lyophilization gave **24** as a white powder (156.0 mg, 0.74 mmol, 74%). Marfey's analysis (cf. General Procedure B) was used to evaluate the diastereomeric ratio (i.e., dr = 5:2 at Cg) and enantiomeric excess (i.e., >99% *ee* for each diastereomer).

^{1}H NMR (500 MHz, D_2O, major diastereomer (*): minor diastereomer (^) = 5:2) δ 7.45 – 7.38 (*^,m, 3H), 7.36 – 7.30 (*^, m, 4H), 4.14 (*,dddd, *J* = 9.6, 8.2, 4.9, 3.3 Hz, 1H), 4.10 – 4.03 (^, m, 0.48H), 3.78 (^,dd, *J* = 6.5, 5.4 Hz, 0.38H), 3.68 (*, dd, *J* = 8.4, 5.4 Hz, 1H), 2.92 (*^, ddd, *J* = 13.7, 5.1 Hz, 1.45 H), 2.79 (*^, ddd, *J* = 13.5, 8.0 Hz, 1.51H), 2.11 (*, ddd, *J* = 14.6, 5.4, 3.3 Hz, 1H), 1.97 (^, dd, *J* = 7.0, 5.4 Hz, 0.78H), 1.82 – 1.74 (*, m, 1H).

^{13}C{^{1}H} NMR (126 MHz, D_2O, major * minor^) δ 177.7*, 177.5^, 138.4, 129.7*, 129.6^, 128.7, 126.7, 71.5*, 69.9^, 54.5*, 53.3^, 43.3^, 43.2*, 38.5*, 37.7^.

HRMS (ESI$^-$): Calcd for $C_{11}H_{14}NO_3^-$ $[M - H]^-$ requires 208.0979; found 208.0978.

(2*S*,4*R*)-2-Amino-4-hydroxy-5-phenylpentanoic-2,5,5-d_3 Acid (22-2,5,5-d_3) and (2*S*,4*S*)-2-Amino-4-hydroxy-5-phenylpentanoic-2,5,5-d_3 Acid (22-2,5,5-d_3)

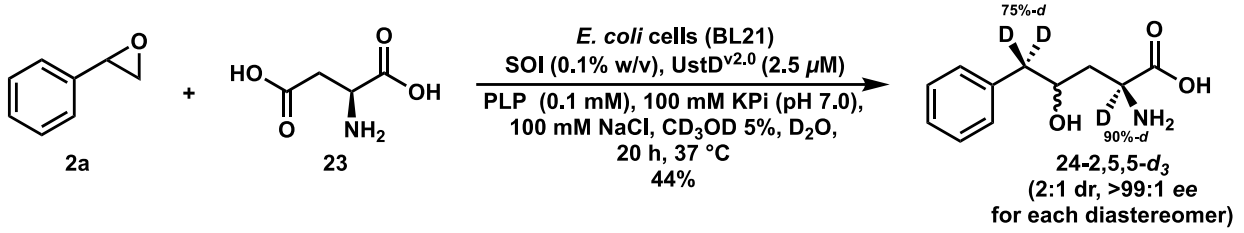

KPi buffer solution (9.3 mL, 100 mM, pH 7.0, 100 mM NaCl), L-Asp (**21**, 86.6 mg, 0.50 mmol), and PLP (50 µL via 20 mM solution in water, 0.001 mmol), were added to a 20 mL scintillation vial, frozen at -80 °C, and lyophilized (48 hours) to remove H_2O. Separately, additional buffer (30 mL, 100 mM, pH 7.0, 100 mM NaCl), was frozen in 20 mL scintillation vial and lyophilized (48 hours) to remove H_2O. The residue of the lyophilized sample containing buffer, L-Asp, and PLP was reconstituted in D_2O (9.3 mL) and transferred to a 20 mL scintillation vial. The residue of the lyophilized sample containing only buffer was reconstituted in D_2O (30 mL). UstD$^{v2.0}$ was thawed and centrifuged at 16,000 x g for 3 min. To remove H_2O, the protein was transferred to a Slide-A-Lyzer® and the buffer exchanged using 14 mL of the D_2O-reconstituted buffer at 4 ºC for 1 h. Following buffer exchange, UstD$^{v2.0}$ (10,000 Max TON, 2.5 µM final reaction concentration), a solution styrene oxide (**2a**, 28.5 µL, 0.25 mmol, 25 mM final reaction concentration) in CD_3OD (0.5 mL) were added to the D_2O-reconstituted mixture of buffer, L-Asp, and PLP. SOI was added to the mixture via lyophilized *E. coli* BL21 whole cells (10 mg, 0.1% w/v%), and the mixture was incubated at 37 ºC. After 20 hours, the reaction mixture was frozen at -80 °C, thawed, then heated at 75 °C for 30 minutes. To lyse the cells, a half volume of MeCN (20 mL) was added to the reaction. The resulting mixture was passaged over filter paper, and the filtrate was concentrated by rotary evaporation. Purification by automated gradient flash chromatography (C18, MeOH:H_2O 1:99 to 1:0 over 30 column volumes) and subsequent lyophilization gave **22-d_3** as a white powder (22.1 mg, 0.10 mmol, 44%). Marfey's analysis (cf. General Procedure B) was used to evaluate

the diastereomeric ratio (i.e., dr = 2:1 at Cg) and enantiomeric excess (i.e., >99% *ee* for each diastereomer). Retention of deuterium was evaluated by ^{1}H NMR analysis, which showed the product was 90% at C_α and 75% at C_δ.

^{1}H NMR (500 MHz, D_2O, major diastereomer (*): minor diastereomer (^) = 2:1) δ 7.45 – 7.38 (*^, m, 3H), 7.36 – 7.31 (*^, m, 4.54 H), 4.15 (*,dd, *J* = 9.9, 3.1 Hz, 1H), 4.06 (^, dd, *J* = 9.0, 3.9 Hz, 0.51H), 3.88 (^, dd, *J* = 8.9, 3.1 Hz, 0.17H), 3.73 (*, t, *J* = 6.0 Hz, 0.07H), 2.91 (*, ddt, *J* = 14.3, 9.2, 4.6 Hz, 0.23H), 2.86 – 2.75 (*^, m, 0.53H), 2.65 (^,dd, *J* = 17.2, 8.2 Hz, 0.26H), 2.15 (*, dd, *J* = 14.9, 3.0 Hz, 1H), 2.08 – 1.95 (^, m, 1H), 1.81 (*, dd, *J* = 14.8, 9.9 Hz, 1H).

HRMS (ESI$^-$): Calcd for $C_{11}H_{11}D_3NO_3^-$ [M-*d*$_3$ – H]$^-$ and $C_{11}H_{12}D_2NO_3^-$ [M-*d*$_2$ – H]$^-$ requires 211.1167 and 210.1105, respectively; found, 211.1166 and 210.1106, respectively.

(2*S*,4*R*)-2-Amino-5-(4-fluorophenyl)-4-hydroxypentanoic Acid and (2*S*,4*S*)-2-Amino-5-(4-fluorophenyl)-4-hydroxypentanoic Acid (25)

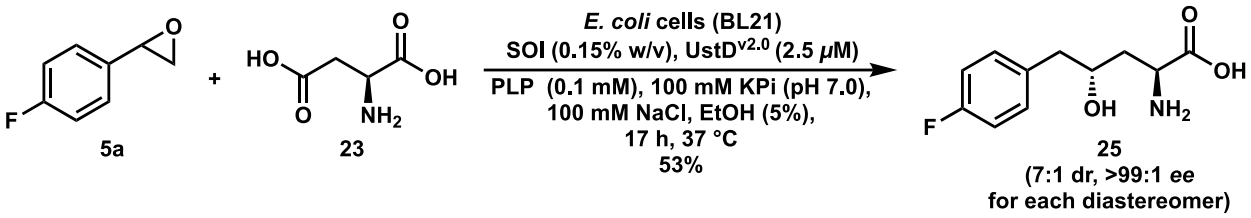

4-Fluorostyrene oxide (**5a**, 118.4 µL, 1.0 mmol, 25 mM final reaction concentration), EtOH (5% of total reaction volume), KPi buffer solution (36.9 mL, 100 mM, pH 7.0, 100 mM NaCl), L-Asp (**21**, 348.2 mg, 2.0 mmol), PLP (200 µL via 20 mM solution in water, 0.004 mmol, 0.1 mM final reaction conc.), UstD$^{v2.0}$ (10,000 Max TON, 2.5 µM) were mixed in an Erlenmeyer flask. SOI was added via flash frozen *E. coli* BL21 wet whole cells (60.0 mg, 0.15% w/v%), and the mixture was incubated at 37 ºC. After 17 hours, the reaction mixture was frozen at -80 °C, thawed, then heated at 75 °C for 30 minutes. To lyse the cells, a half volume of MeCN (20 mL) was added to the reaction. The resulting mixture was passaged over filter paper, and the filtrate was concentrated by rotary evaporation. Purification by automated gradient flash chromatography (C18, MeOH:H_2O 1:99 to 1:0 over 30 column volumes) and subsequent lyophilization to give **23** as a white powder

(120.8 mg, 0.53 mmol, 53%). Marfey's analysis (cf. General Procedure B) was used to evaluate the diastereomeric ratio (i.e., dr = 7:2 at Cg) and enantiomeric excess (i.e., >99% *ee* for each diastereomer).

^{1}H NMR (500 MHz, D_2O, major diastereomer (*): minor diastereomer (^) = 7:2) δ 7.34-7.27 (*^, m, 2.54H), 7.12 (*^, t, J = 8.9 Hz, 2.46H), 4.16 – 4.09 (*, m, 1H), 4.07-3.99 (^ , m, 0.29H), 3.84 (^, dd, J = 7.1, 4.5 Hz, 0.26H), 3.74 (*,dd, *J* = 8.7, 5.1 Hz, 1H), 2.94-2.85 (*^, m, 1.27H), 2.80-2.71 (*^, m, 1.30H), 2.14 (*, ddd, J = 14.8, 5.3, 3.1 Hz, 1H), 2.07 – 1.93 (^, m, 0.57H), 1.79 (*, ddd, J = 14.8, 9.8, 8.6 Hz, 1H).

^{13}C{^{1}H} NMR (126 MHz, D_2O, major diastereomer (*): minor diastereomer (^) = 7:2) δ 176.6*, 176.3^, 161.5 (*^, d, J = 241.4 Hz), 134.0 (*^, d, J = 3.1 Hz), 131.13 (*, d, J = 8.0 Hz), 131.11 (^, d, J = 8.1 Hz), 115.2 (*^, d, J = 21.3 Hz), 71.5*, 69.9^, 54.4*, 53.2^, 42.4*, 42.4^, 37.8*, 36.9^.

^{19}F{^{13}C} NMR (377 MHz, D_2O, major * minor^) δ -117.52^, -117.55*.

HRMS (ESI^-): Calcd for $C_{11}H_{13}FNO_3^-$ $[M - H]^-$ requires 226.0885; found 226.0885.

(2*s*,4*s*,6*s*)-2,4,6-Tris(4-fluorobenzyl)-1,3,5-trioxane (26)

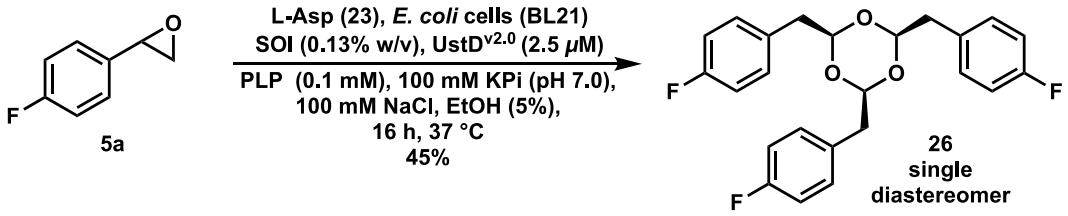

In addition to providing diastereomers of amino acid **25**, the previous procedure allowed for isolation of aldehyde trimer **26**. For clarity the procedure is also provided below with the focus on isolation of trimer **26**. 4-Fluorostyrene oxide (**5a**, 118.4 µL, 1.0 mmol, 25 mM final reaction concentration), EtOH (5% of total reaction volume), KPi buffer solution (37.4 mL, 100 mM, pH 7.0, 100 mM NaCl), L-Asp (**23**, 347.5 mg, 2.0 mmol), PLP (200 µL via 20 mM solution in water, 0.004 mmol, 0.1 mM final reaction conc.), $UstD^{v2.0}$ (10,000 Max TON, 2.5 µM) were mixed in an Erlenmeyer flask. SOI was added via flash frozen *E. coli* BL21 wet whole cells (52.6 mg, 0.13% w/v%), and the mixture was incubated at 37 ºC. After 16 hours, the reaction mixture was frozen at -80 °C, thawed, then heated at 75 °C for 30 minutes. To lyse the cells, a half volume of MeCN

(20 mL) was added to the reaction. The resulting mixture was passaged over filter paper, and the filtrate was concentrated by rotary evaporation. Purification by automated gradient flash chromatography (C18, MeOH:H_2O 1:99 to 1:0 over 30 column volumes) and subsequent lyophilization gave **26** as a white powder (63.2 mg, 0.15 mmol, 45%).

^{1}H NMR (500 MHz, D_2O): δ 7.46 – 7.40 (m, 6H), 7.21 – 7.15 (m, 6H), 4.81 (t, *J* = 6.0 Hz, 3H), 3.75 (d, *J* = 5.8 Hz, 6H).

^{13}C{^{1}H} NMR (126 MHz, D_2O): δ 162.3 (d, *J* = 243.2 Hz), 136.5 (d, *J* = 3.0 Hz), 128.3 (d, *J* = 8.3 Hz), 115.4 (d, *J* = 21.5 Hz), 73.4, 66.1.

^{19}F{^{13}C} NMR (377 MHz, D_2O): δ -115.23.

HRMS (ESI$^+$): Calcd for $C_{24}H_{21}F_3O_3$ $[M + NH_4]^+$ requires 432.1781; found 432.1774.

Derivatization with Marfey's Reagent

All products were derivatized with Marfey's Reagent as described in general procedure B

(2*S*,3*R*)-2-Amino-3-hydroxy-4-phenylbutanoic Acid (2b)

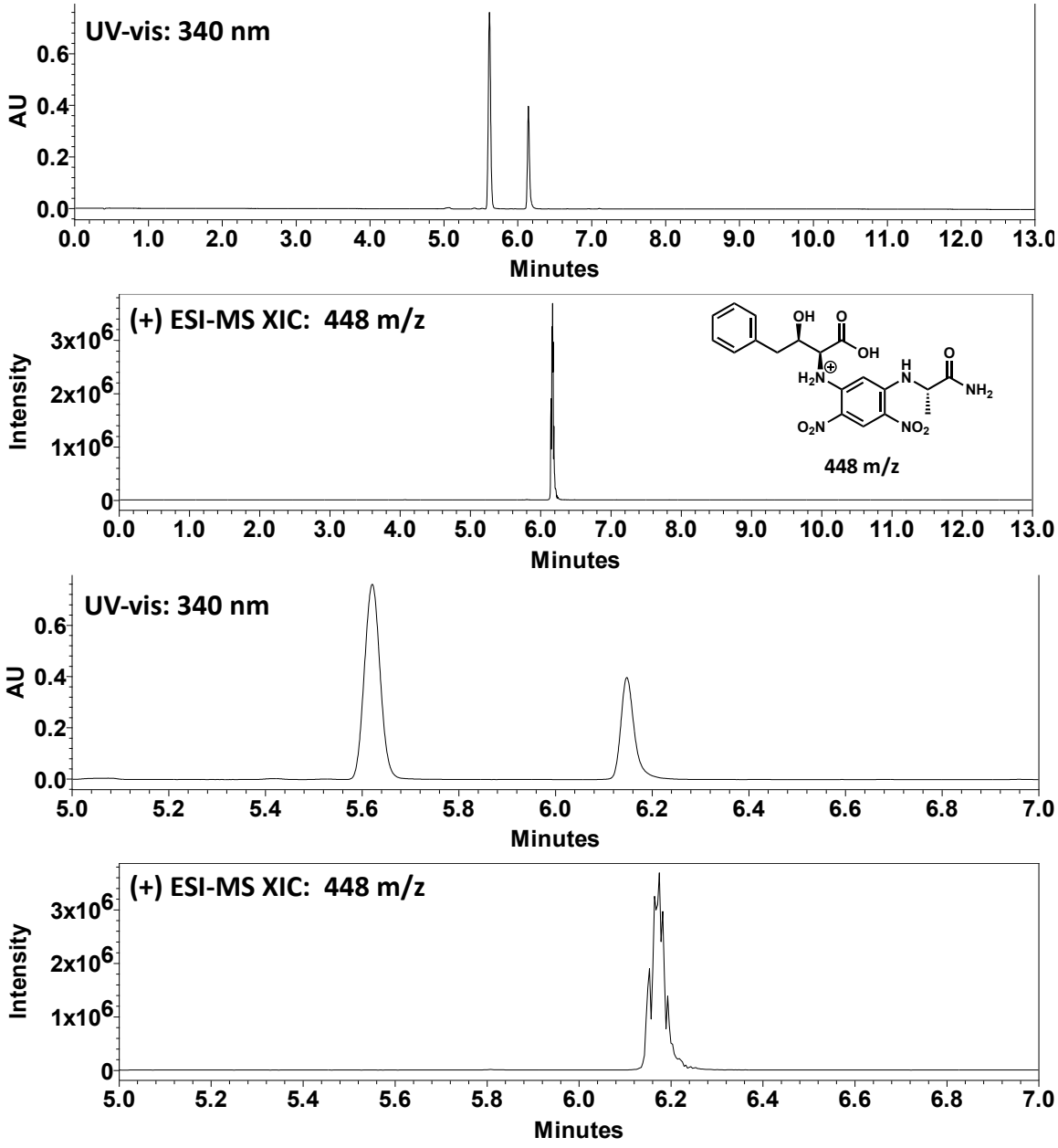

(2*S*,3*R*)-2-Amino-3-hydroxy-4-(4-bromophenyl)butanoic Acid (3b)

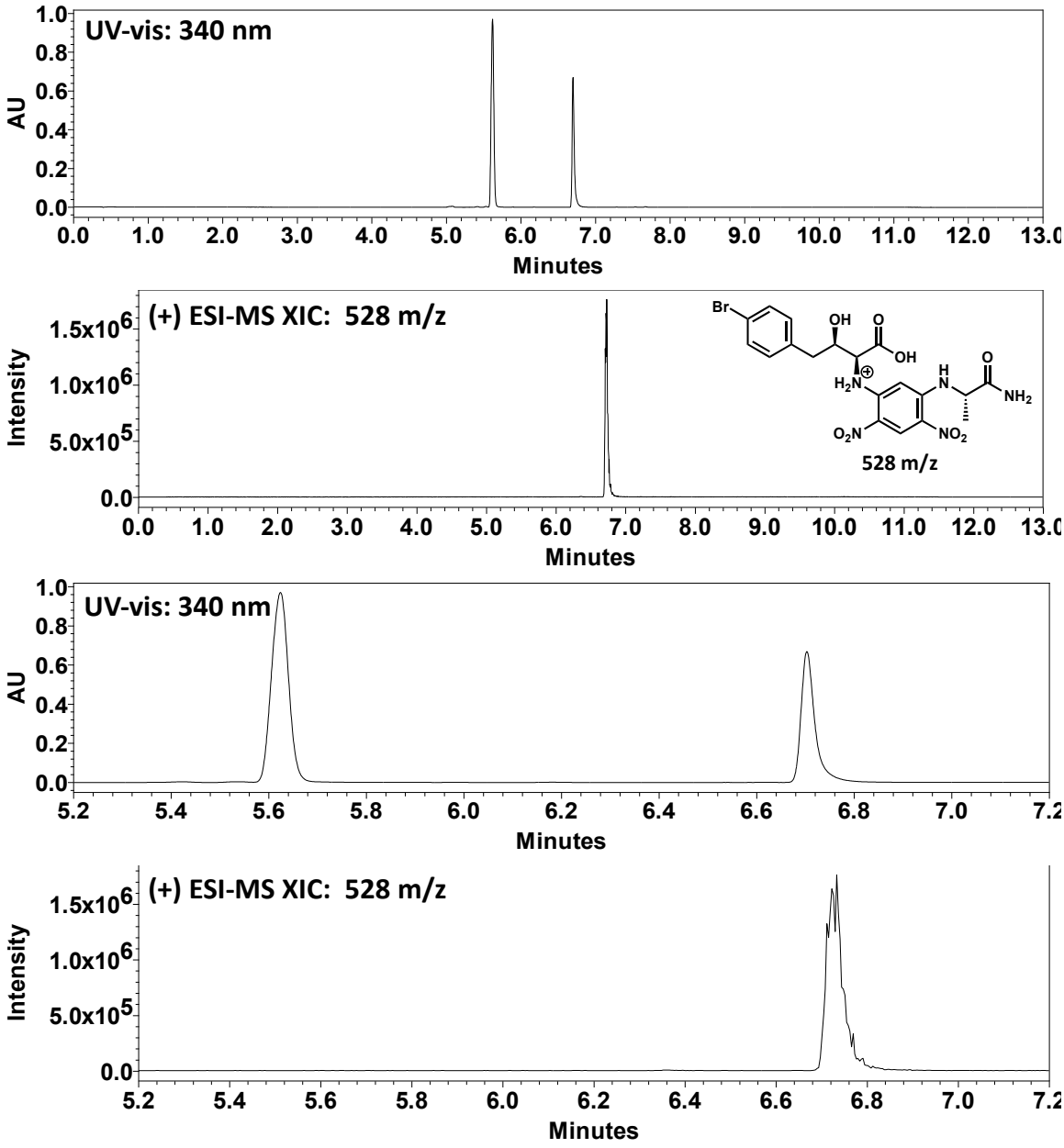

(2*S*,3*R*)-2-Amino-3-hydroxy-4-(4-chlorophenyl)butanoic Acid (4b)

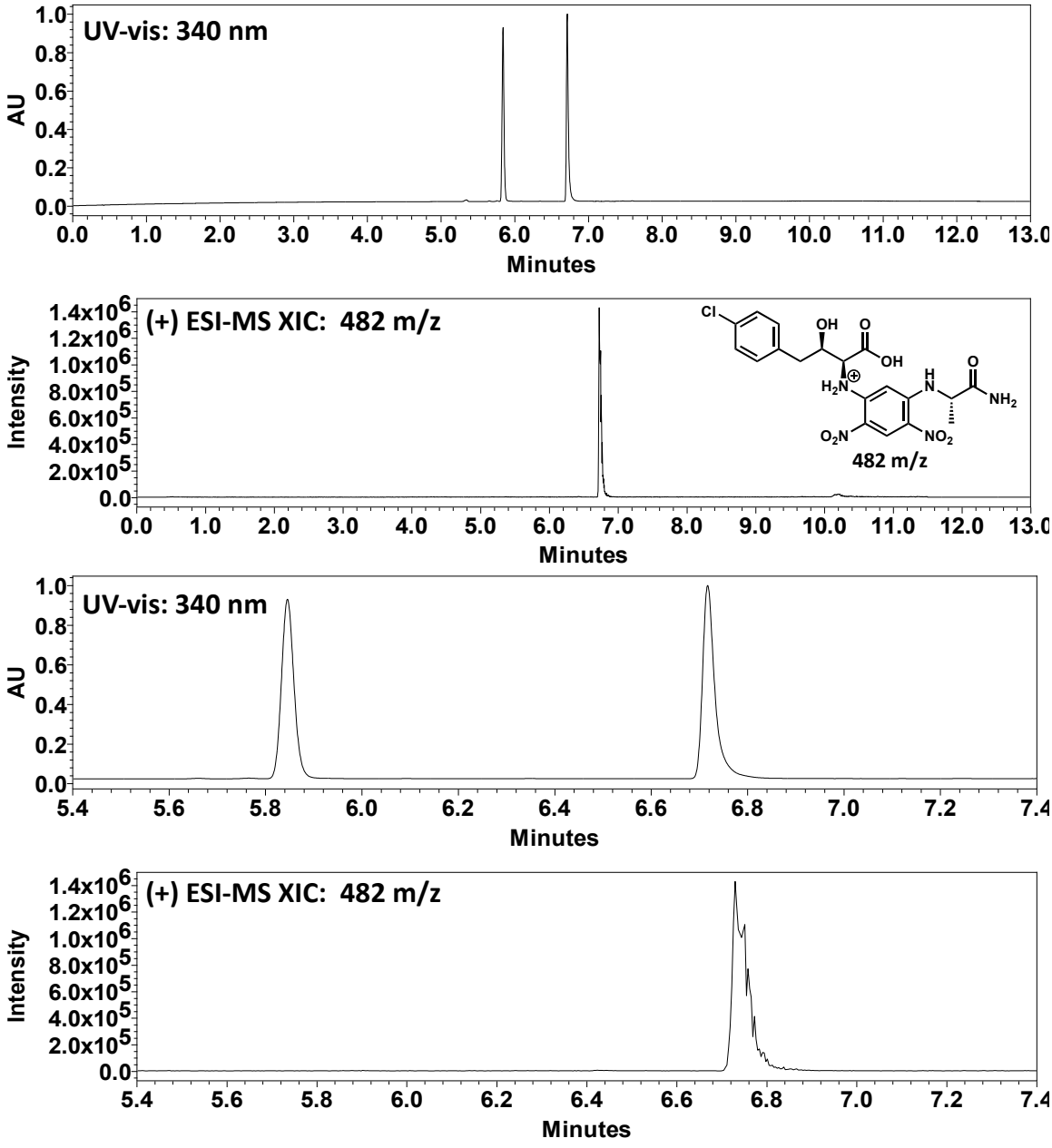

(2*S*,3*R*)-2-Amino-3-hydroxy-4-(4-fluorophenyl)butanoic Acid (5b)

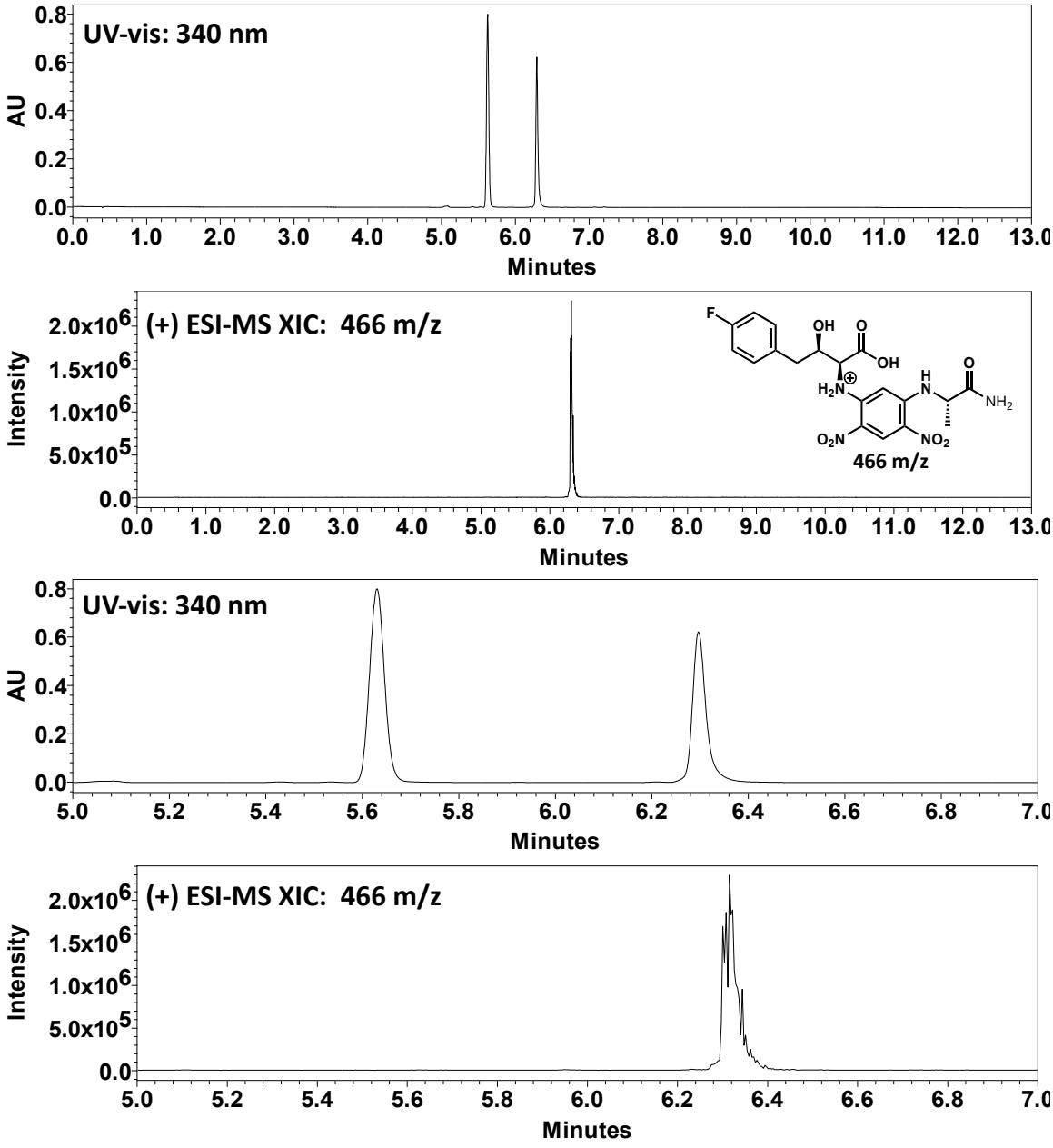

(2*S*,3*R*)-2-Amino-4-(2,4-difluorophenyl)-3-hydroxybutanoic Acid (6b)

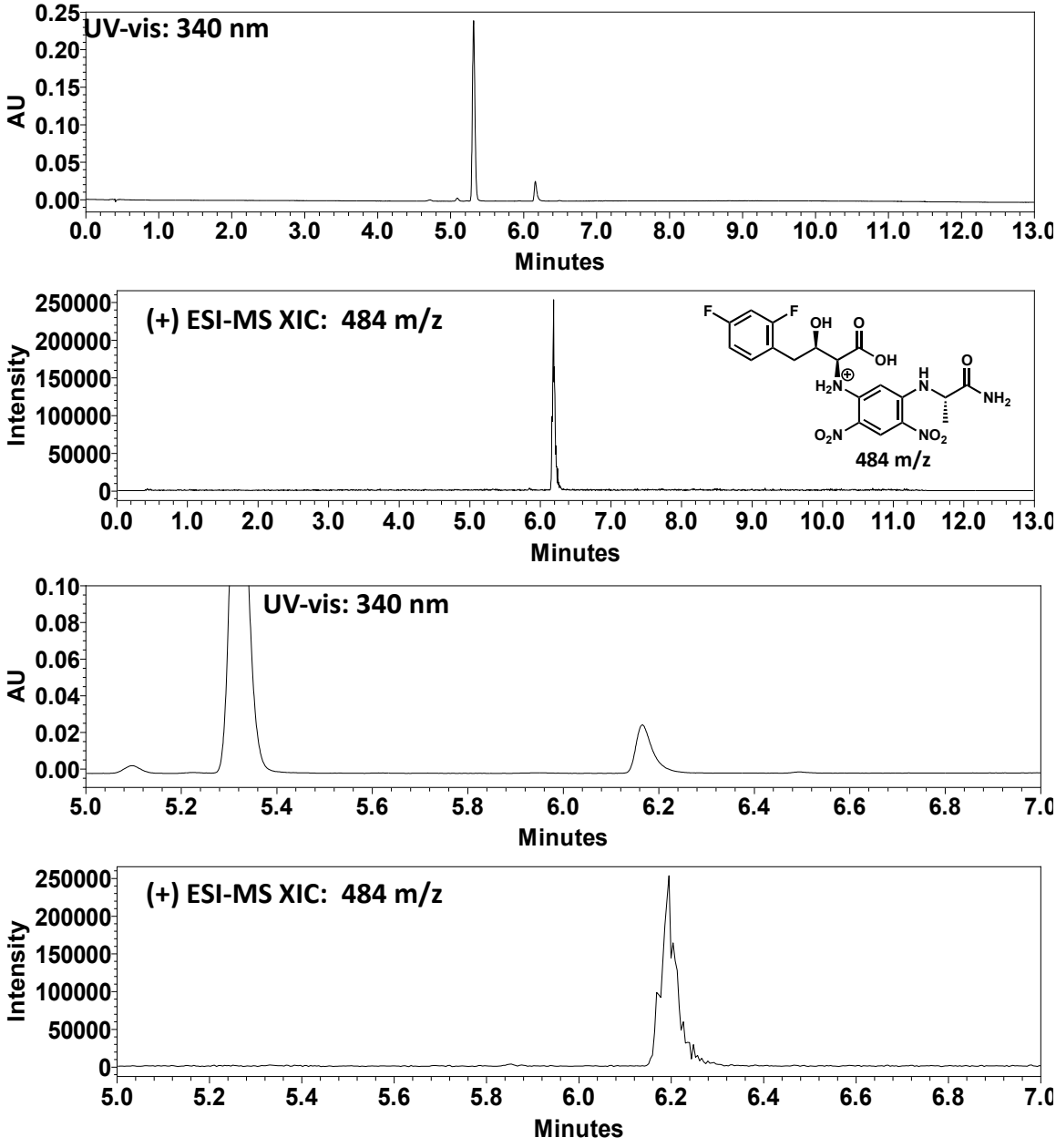

(2*S*,3*R*)-2-Amino-4-(benzo[*d*][1,3]dioxol-5-yl)-3-hydroxybutanoic Acid (7b)

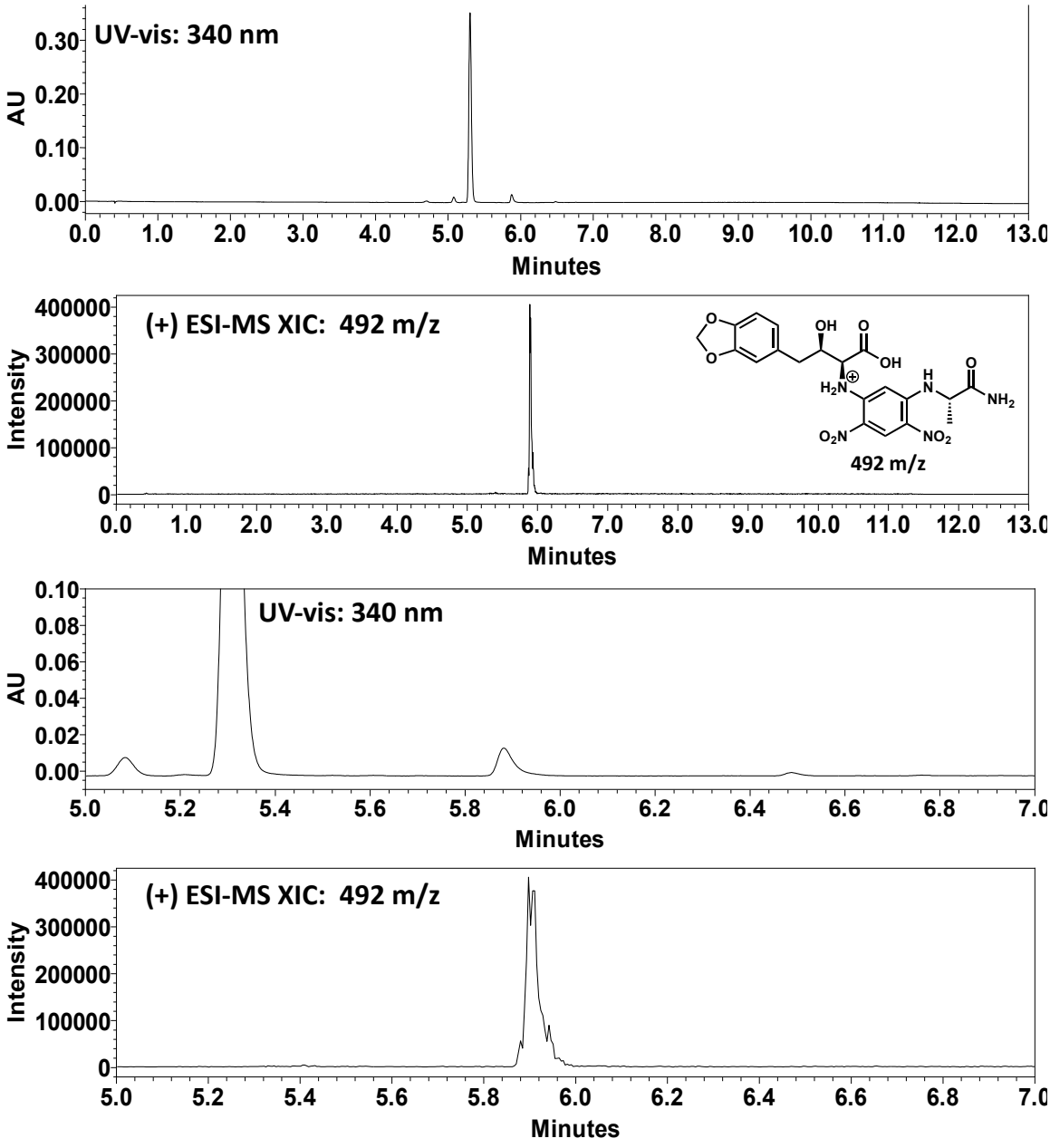

(2*S*,3*R*)-4-(4-Acetoxyphenyl)-2-amino-3-hydroxybutanoic Acid (8b)

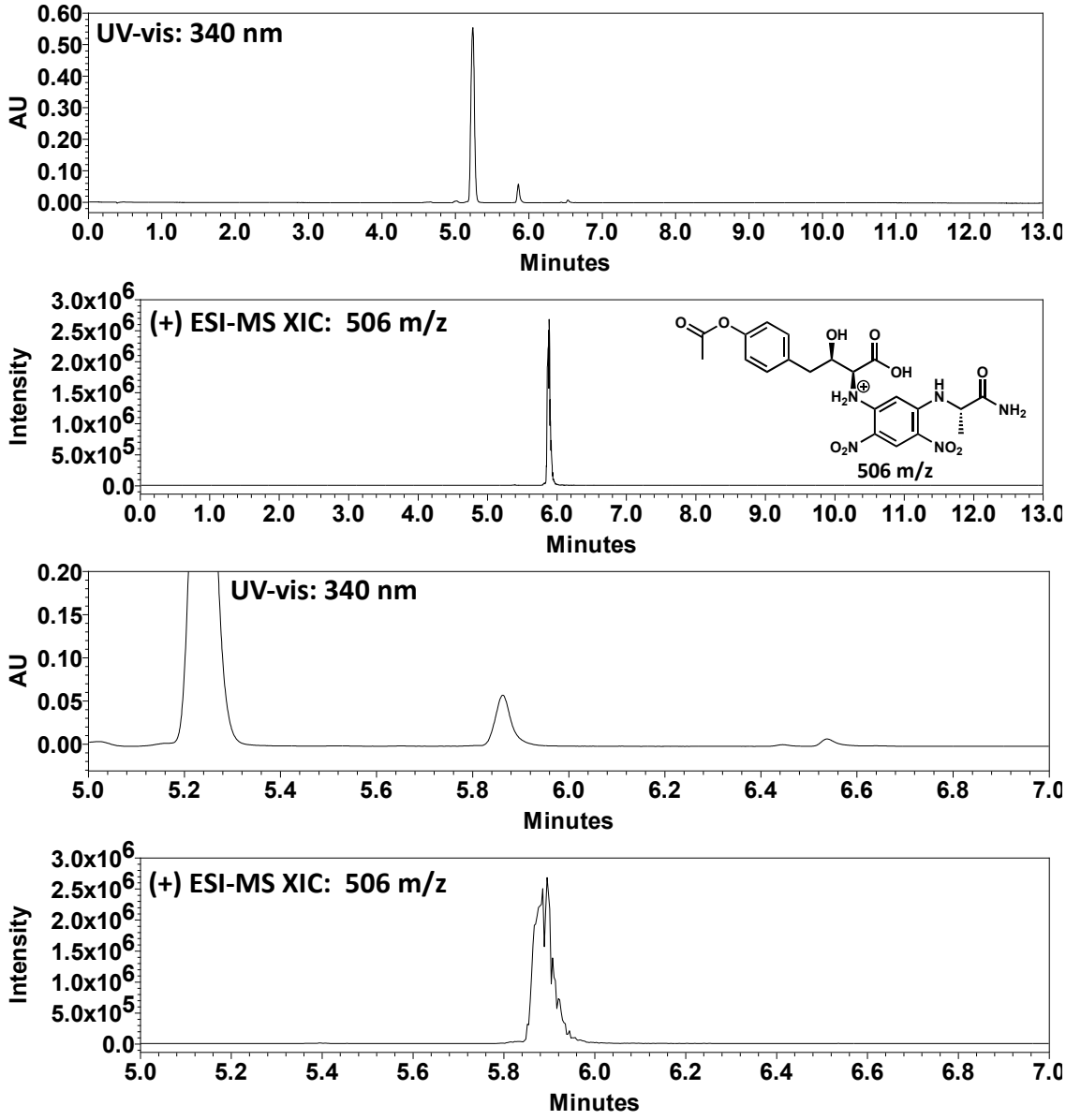

(2*S*,3*R*)-2-Amino-3-hydroxy-4-(4-hydroxyphenyl)butanoic Acid (8c)

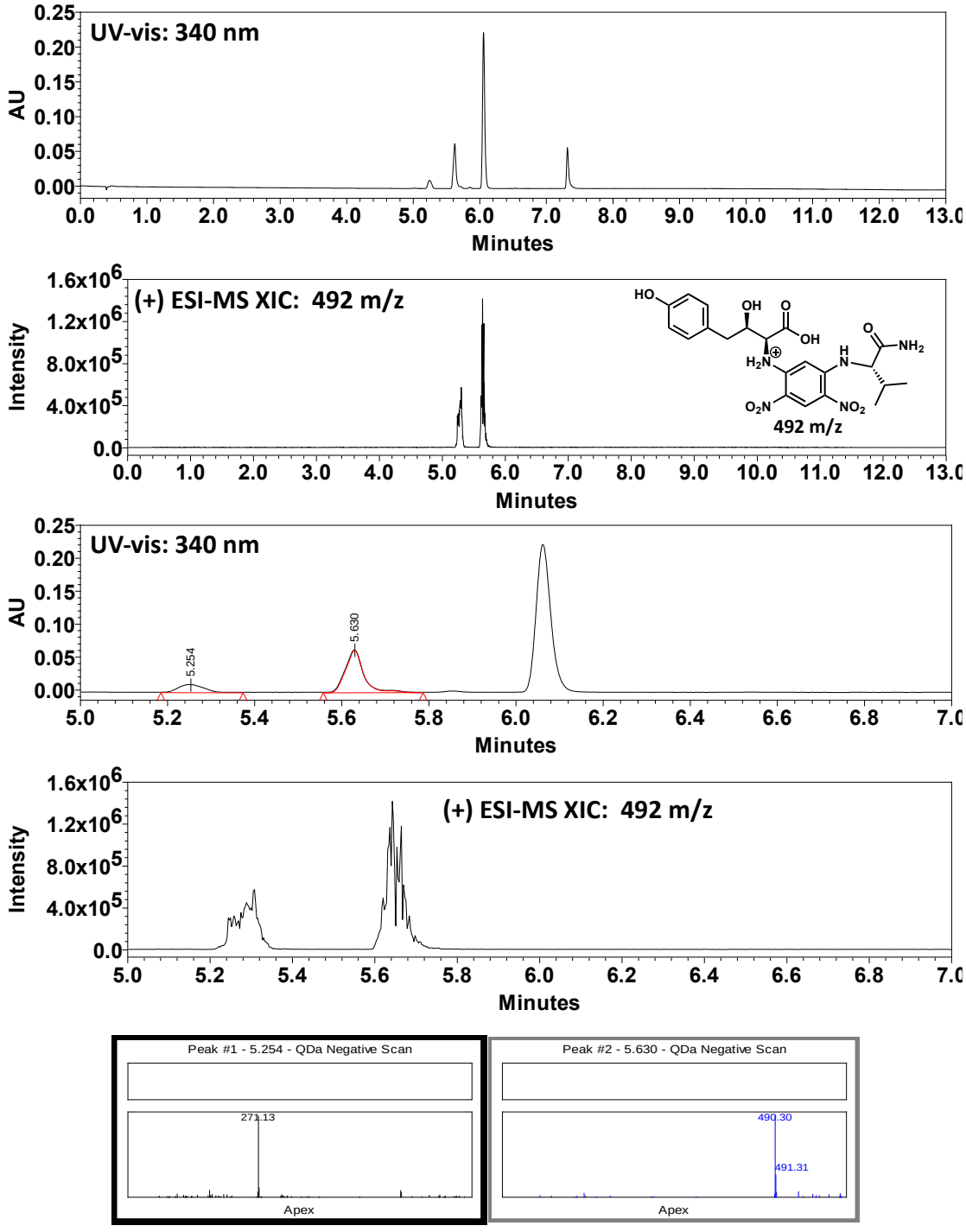

Product **8c** derivatized with L-FDAA did not resolve from unreacted Marfey's reagent via UPLC. L-FDVA (Valine Marfey's reagent) was used instead. (+) ESI-MS EIC: 492 m/z showed two peaks. Peak one (rt = 5.254) fragmentation indicated that this peak was a contaminant present in the reaction did not correspond to the derivatized product (Peak 2, rt = 5.630)

(2*S*,3*R*)-2-Amino-3-hydroxy-4-(4-methoxyphenyl)butanoic Acid (9b)

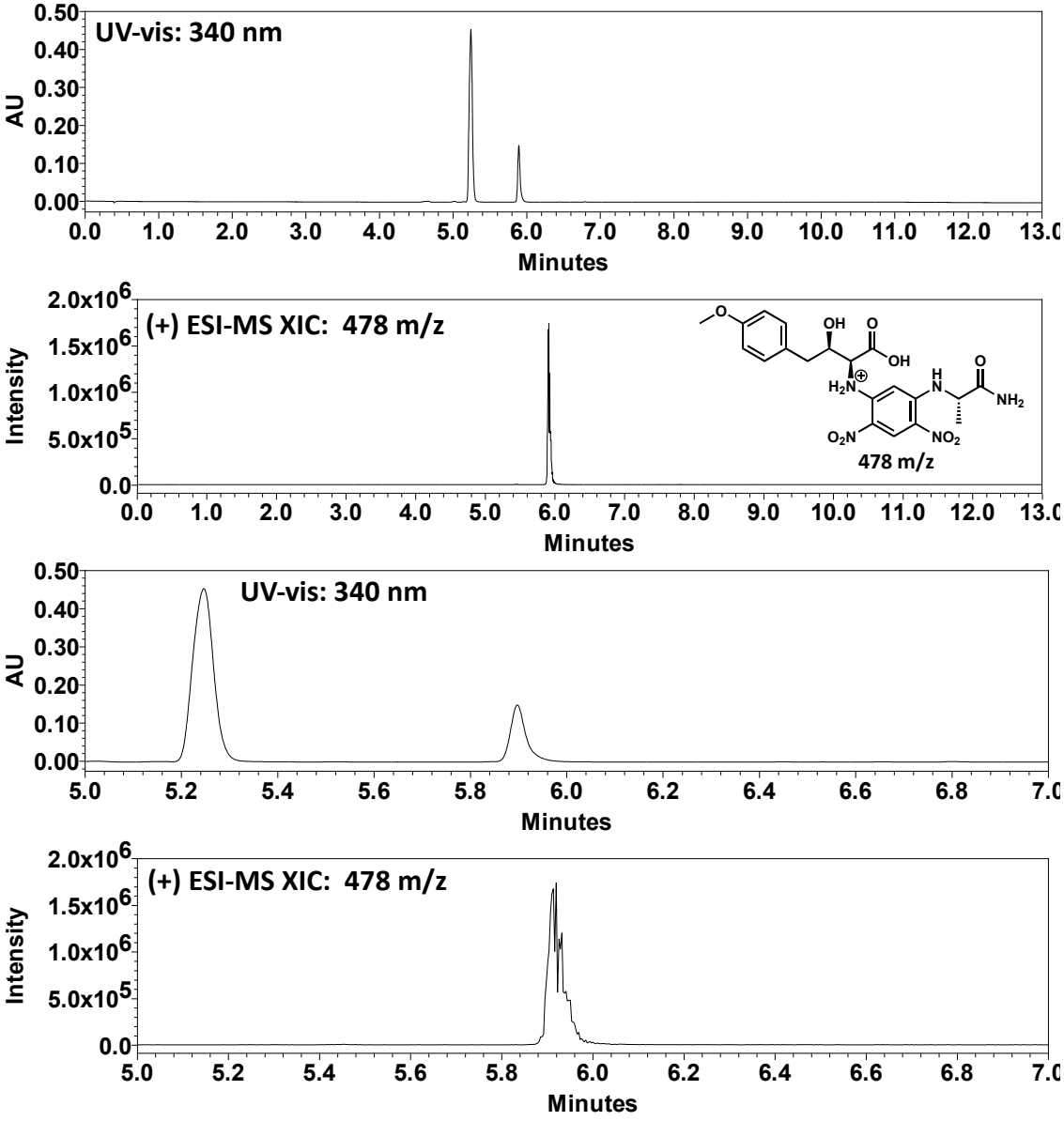

(2*S*,3*R*)-2-Amino-3-hydroxy-4-(*o*-tolyl)butanoic Acid (10b)

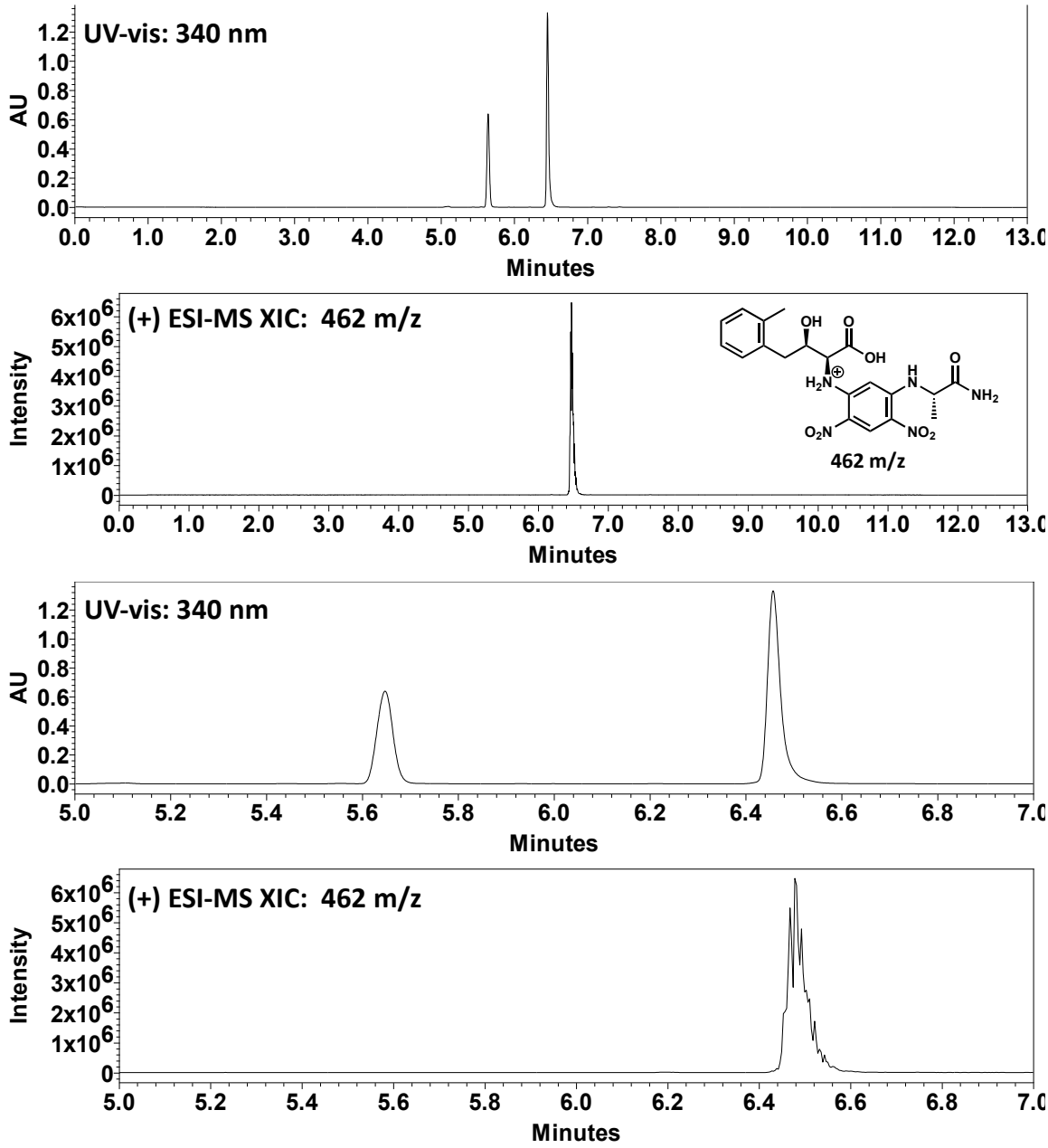

(2*S*,3*R*)-2-Amino-3-hydroxy-4-(*m*-tolyl)butanoic Acid (11b)

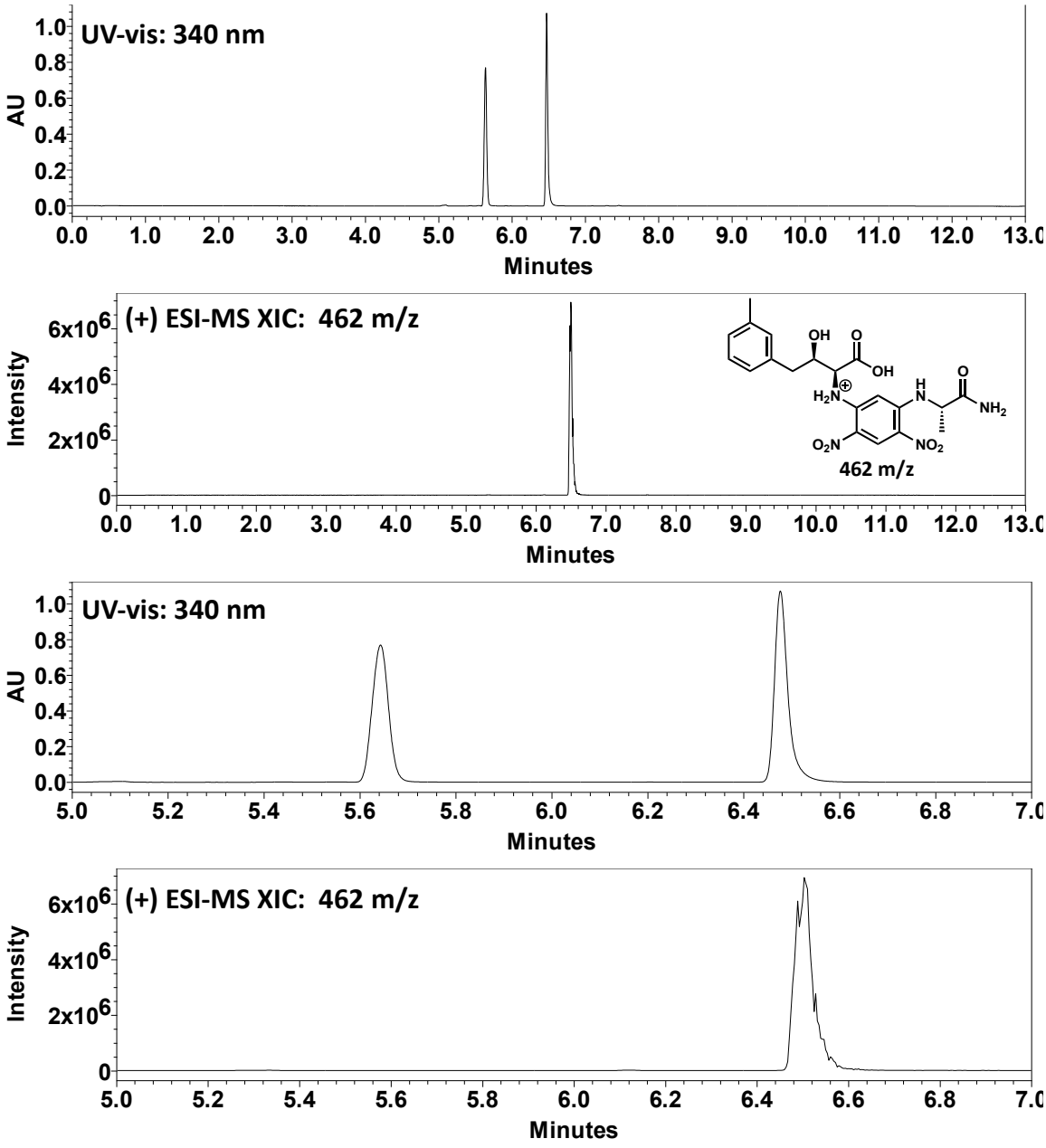

(2*S*,3*R*)-2-Amino-3-hydroxy-4-(*p*-tolyl)butanoic Acid (12b)

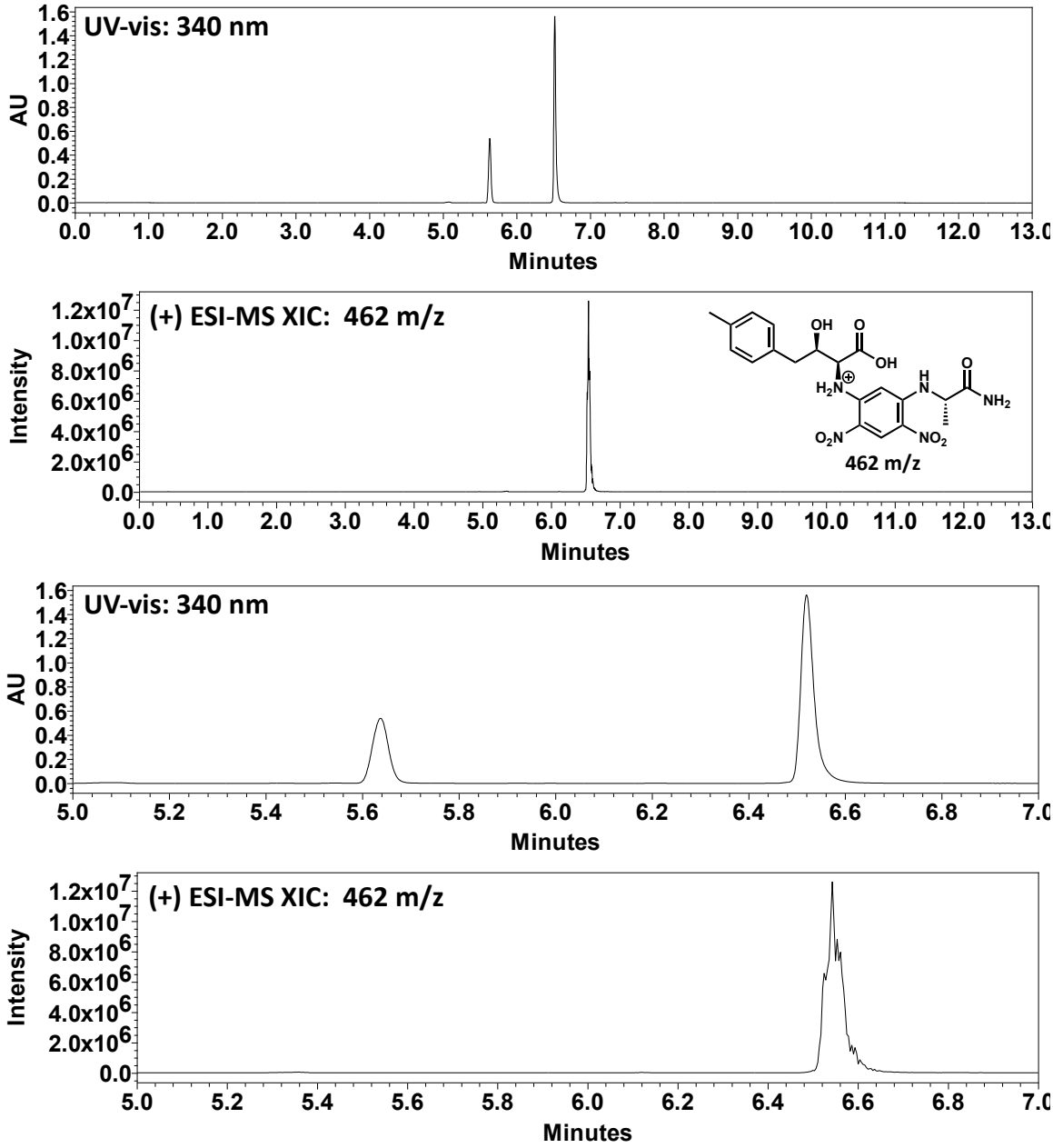

(2*S*,3*R*)-2-Amino-3-hydroxy-4-(*p*-isopropylphenyl)butanoic Acid (13b)

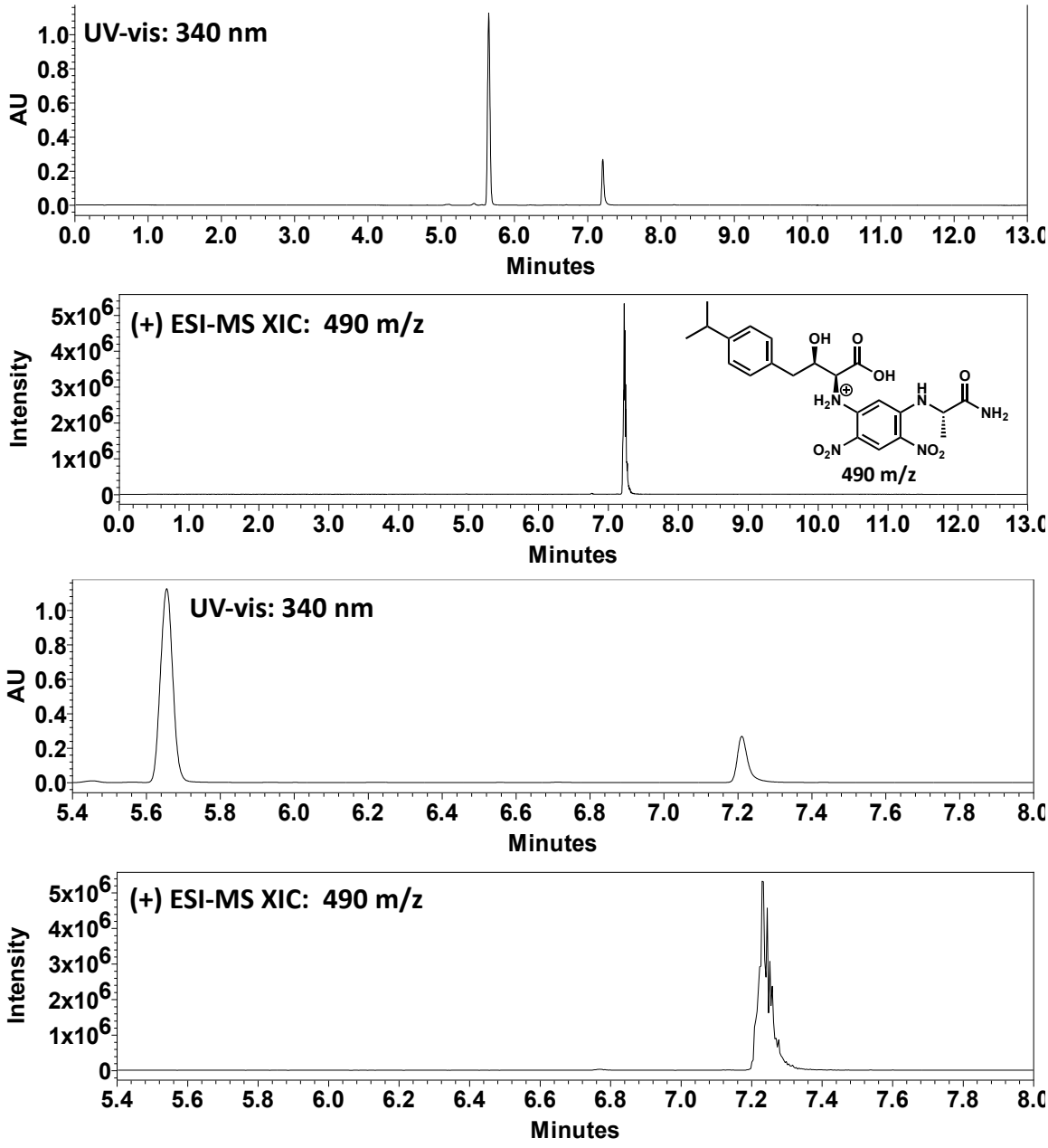

(2*S*,3*R*)-2-Amino-3-hydroxy-4-mesitylbutanoic Acid (14b)

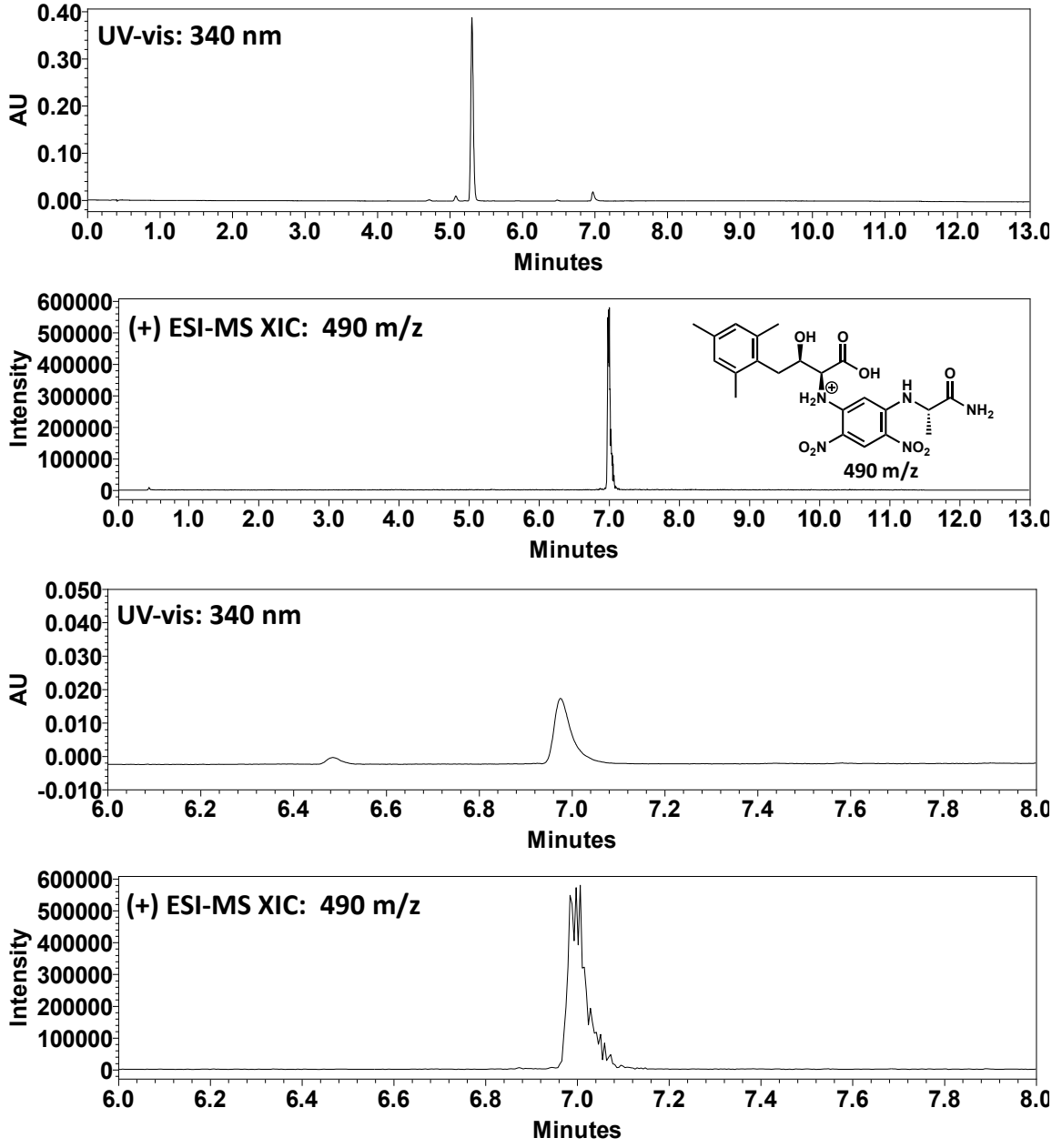

(2*S*,3*R*)-2-Amino-3-hydroxy-4-(naphthalen-1-yl)butanoic Acid (15b)

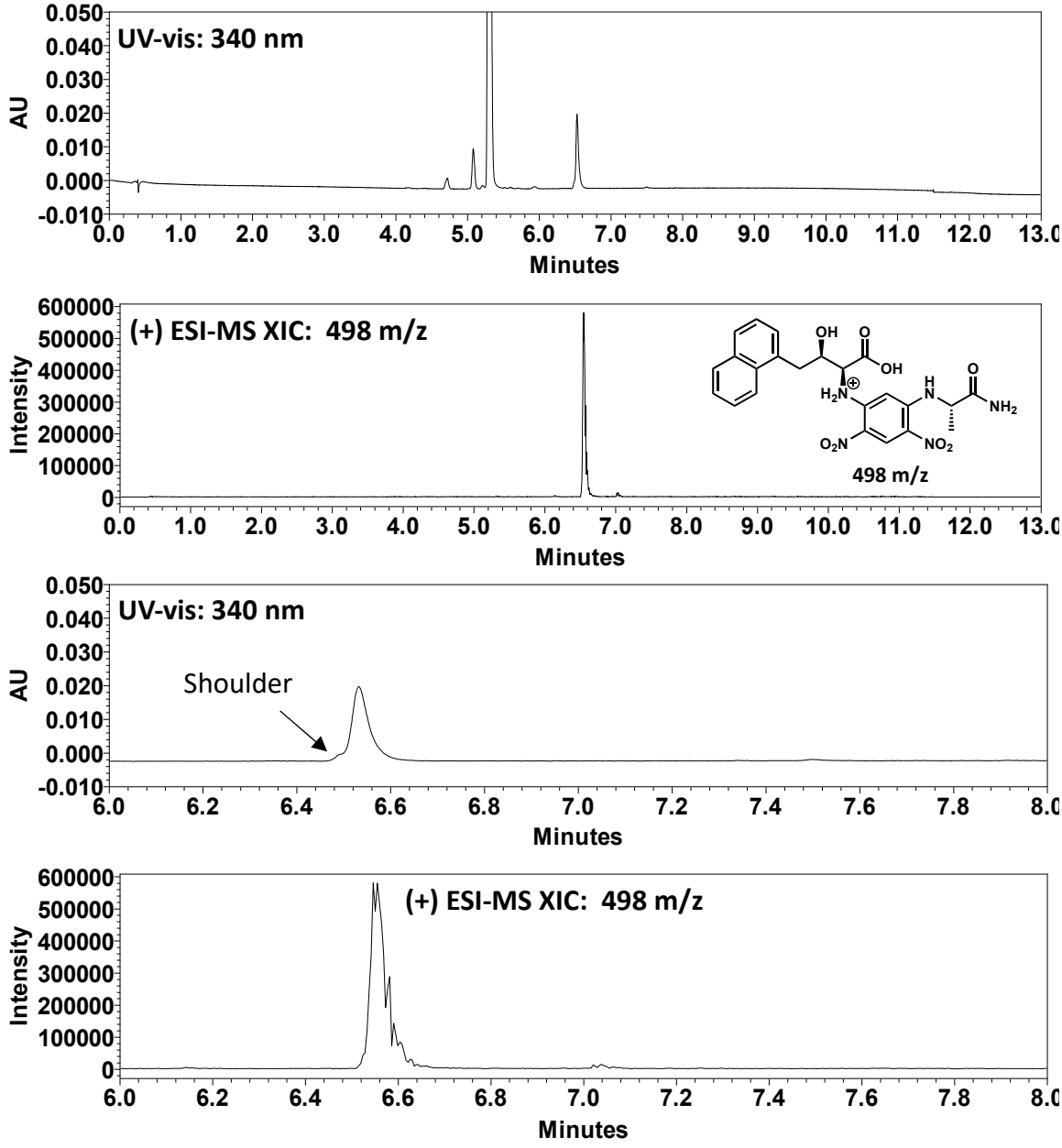

(2*S*,3*R*)-2-amino-4-(furan-2-yl)-3-hydroxybutanoic Acid (16b)

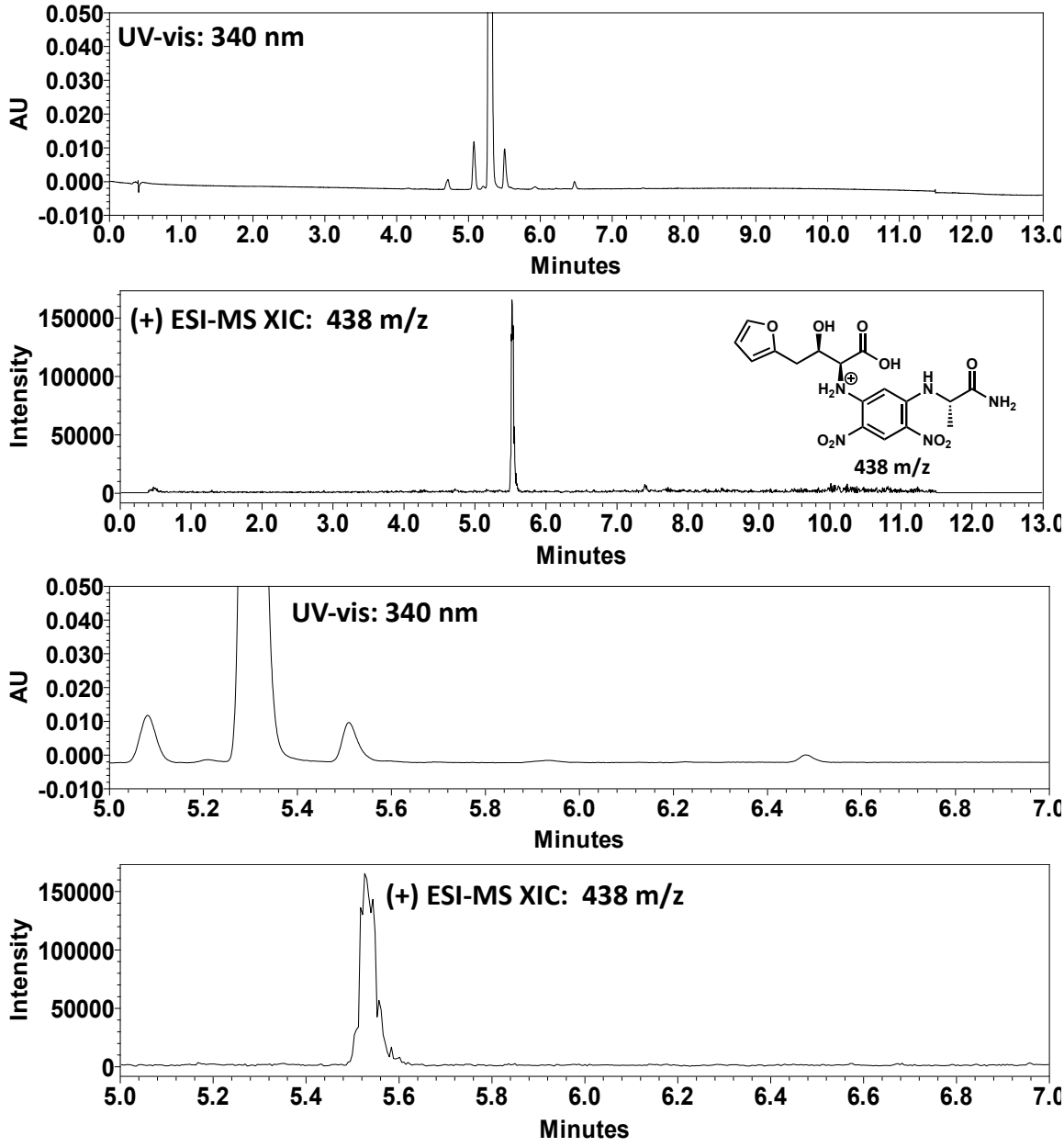

(2*S*,3*R*)-2-Amino-3-hydroxy-4-(thiophen-2-yl)butanoic Acid (17b)

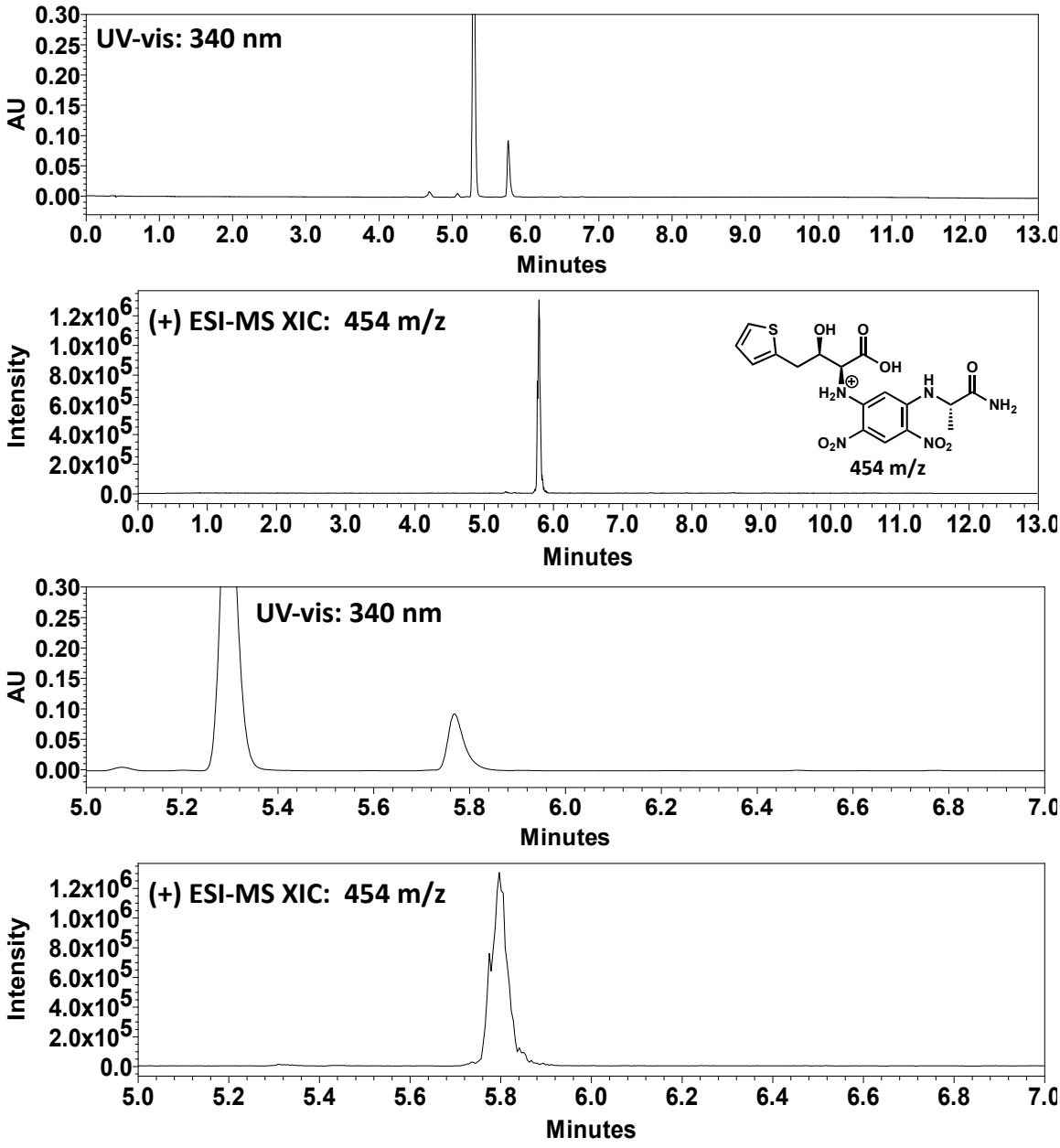

(2*S*,3*R*)-2-Amino-3-hydroxy-4-phenylpentanoic Acid (18b)

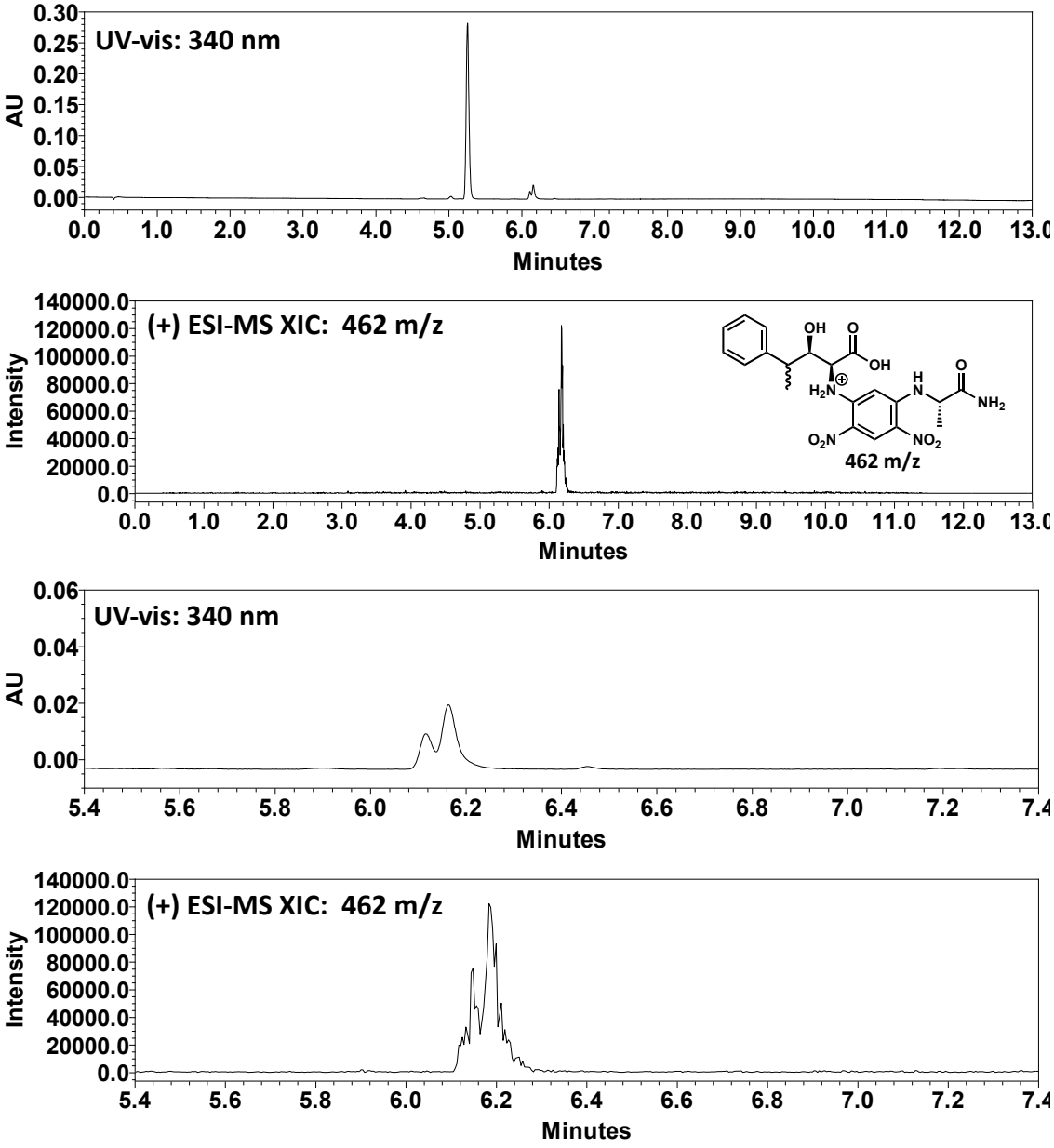

(2*S*,3*R*)-2-Amino-3-(2,3-dihydro-1*H*-inden-1-yl)-3-hydroxypropanoic Acid (19b)

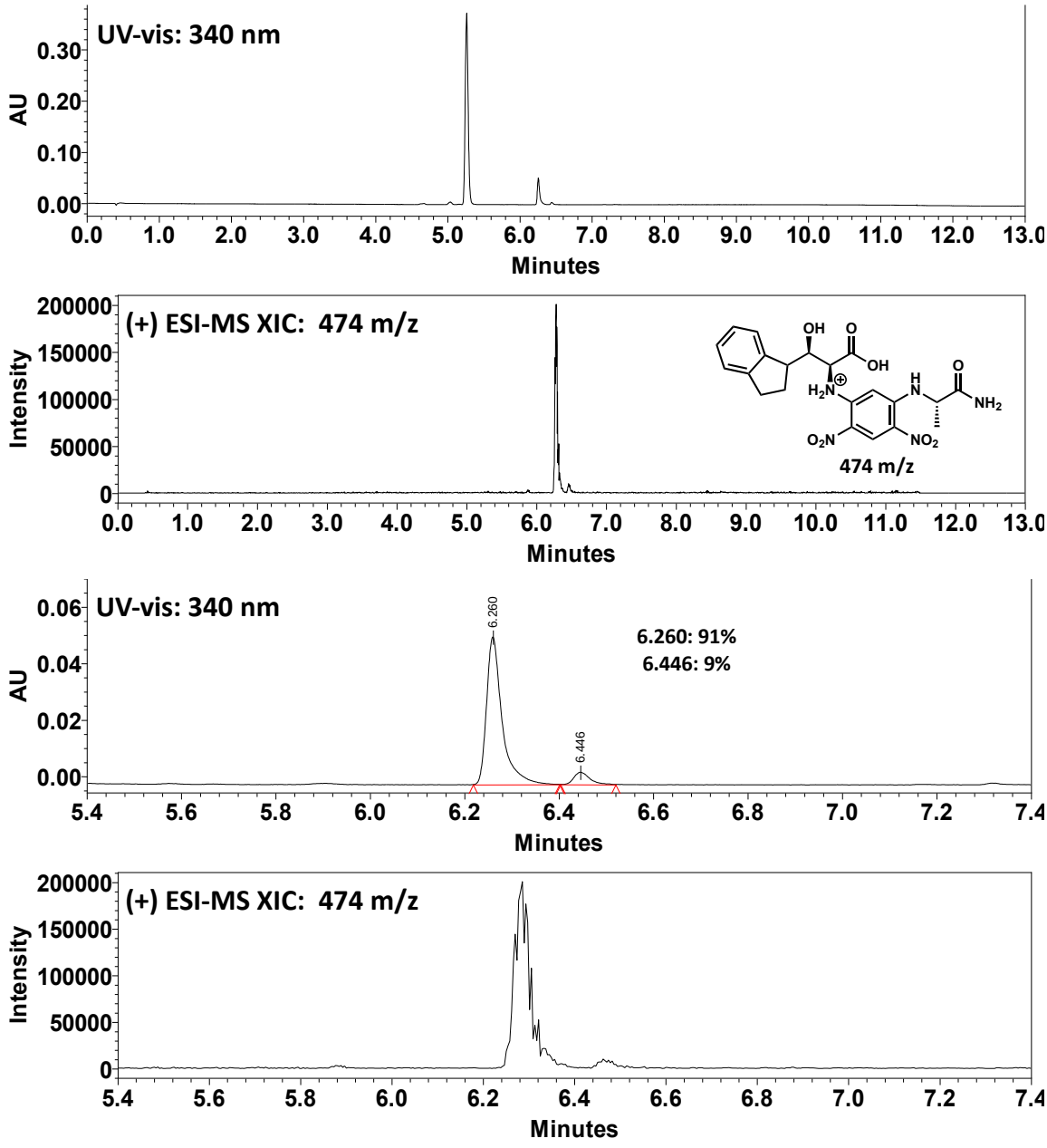

(2*S*,3*R*,*E*)-2-Amino-3-hydroxy-6-phenylhex-5-enoic Acid (20b)

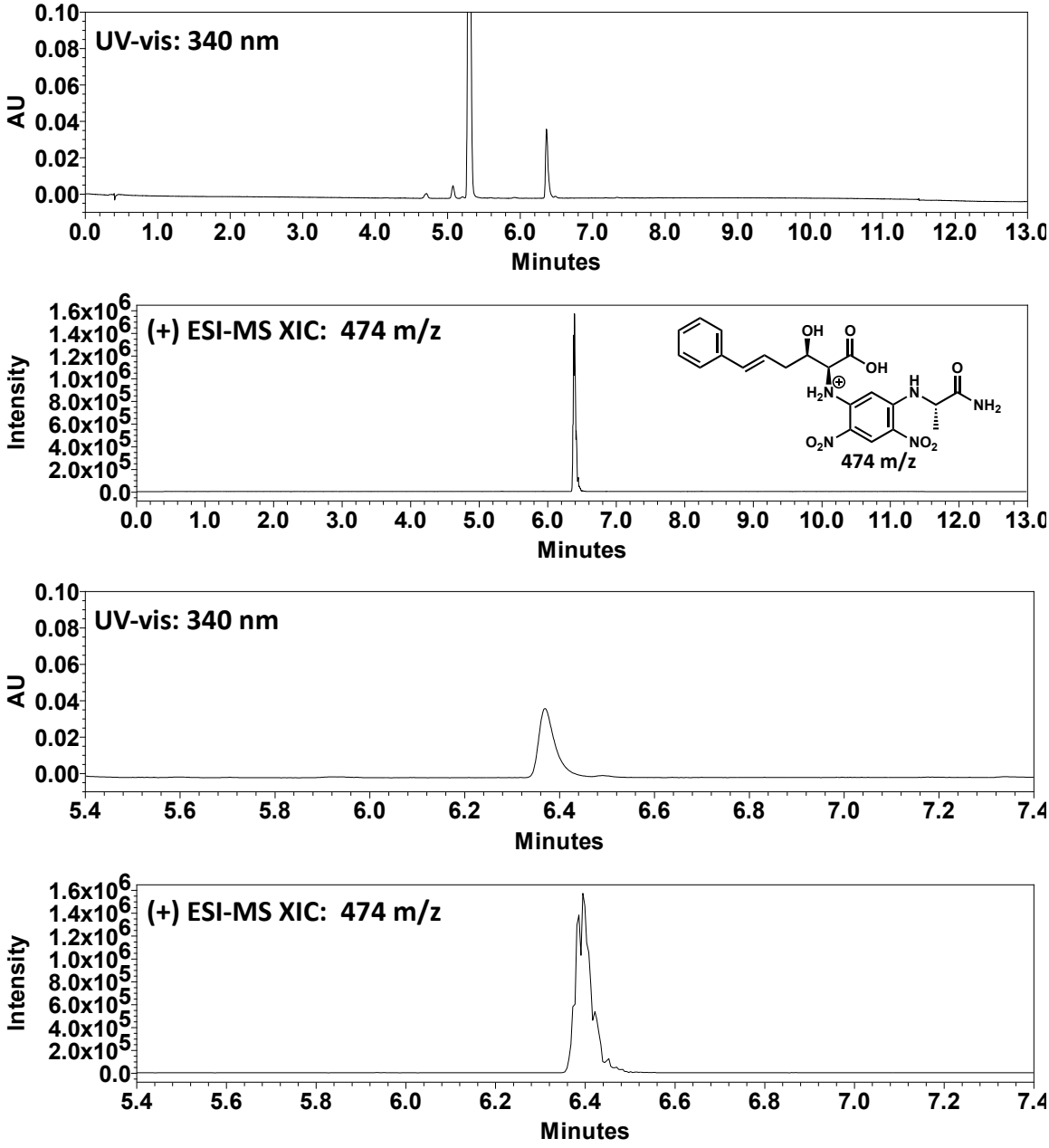

(2*S*,3*R*,*E*)-2-Amino-3-hydroxy-5-methyl-6-phenylhex-5-enoic Acid (21b)

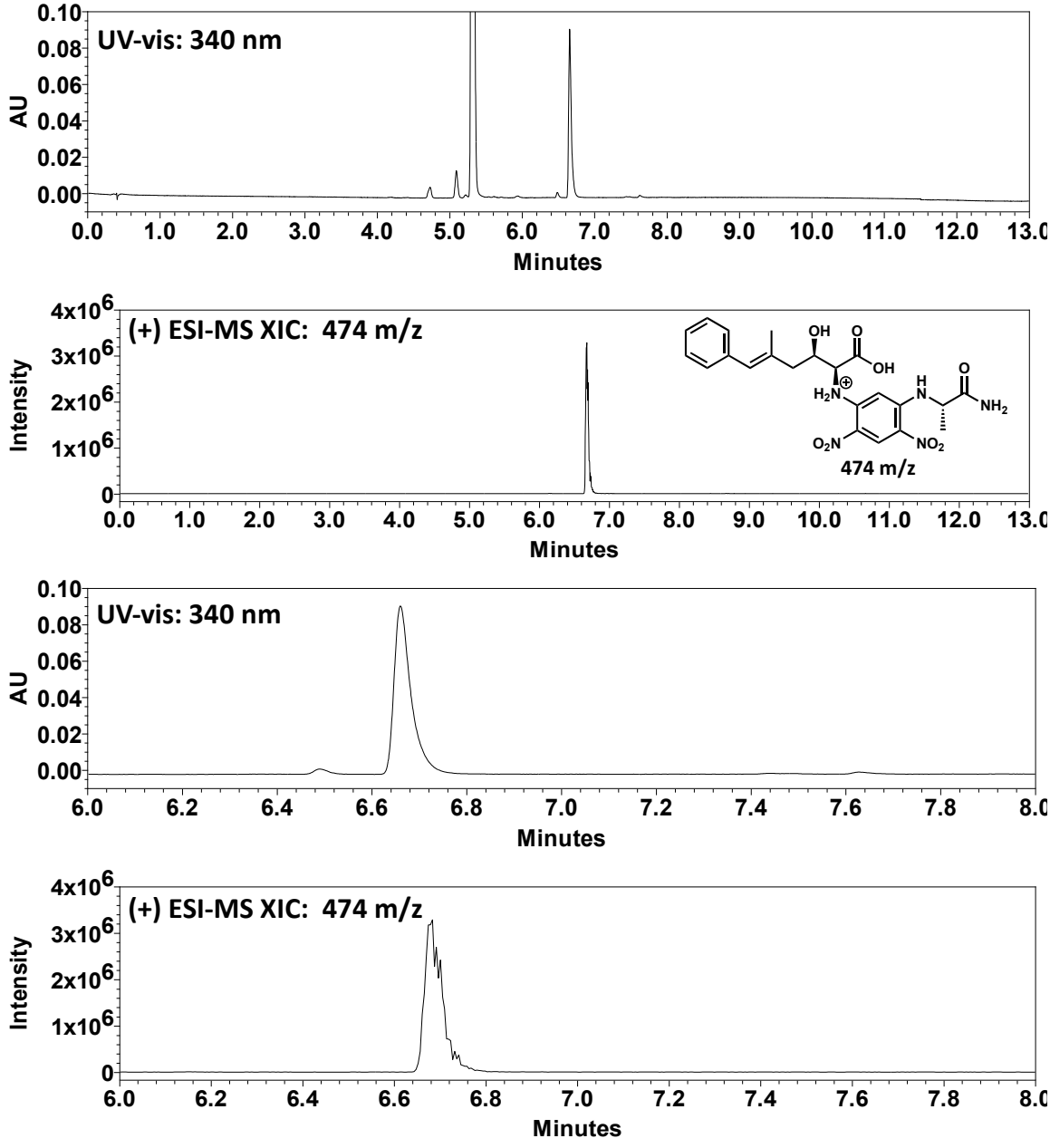

(2*S*,4*R*)-2-Amino-4-hydroxy-5-phenylpentanoic Acid (24)

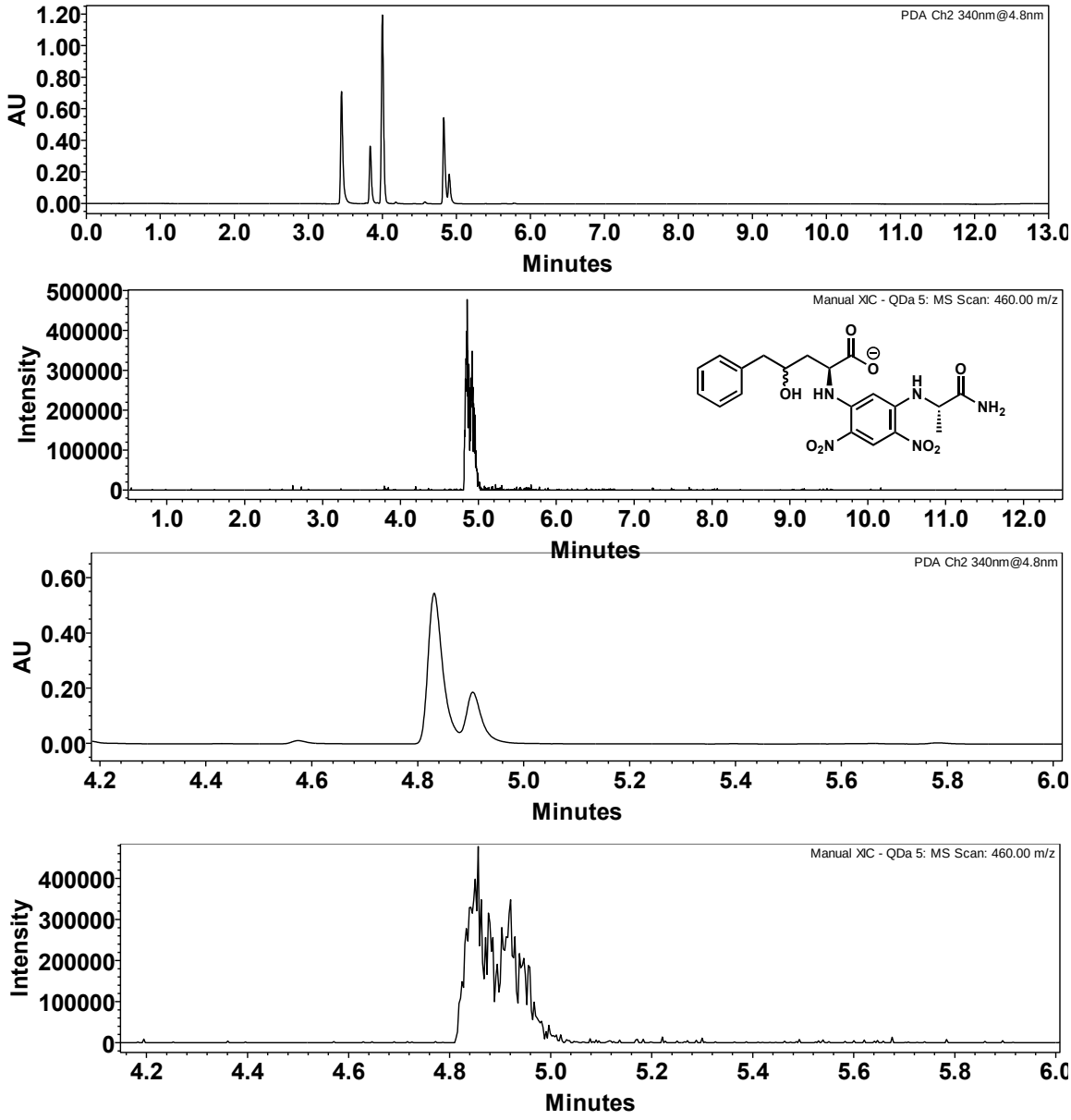

(2*S*,4*R*)-2-amino-5-(4-fluorophenyl)-4-hydroxypentanoic acid (25)

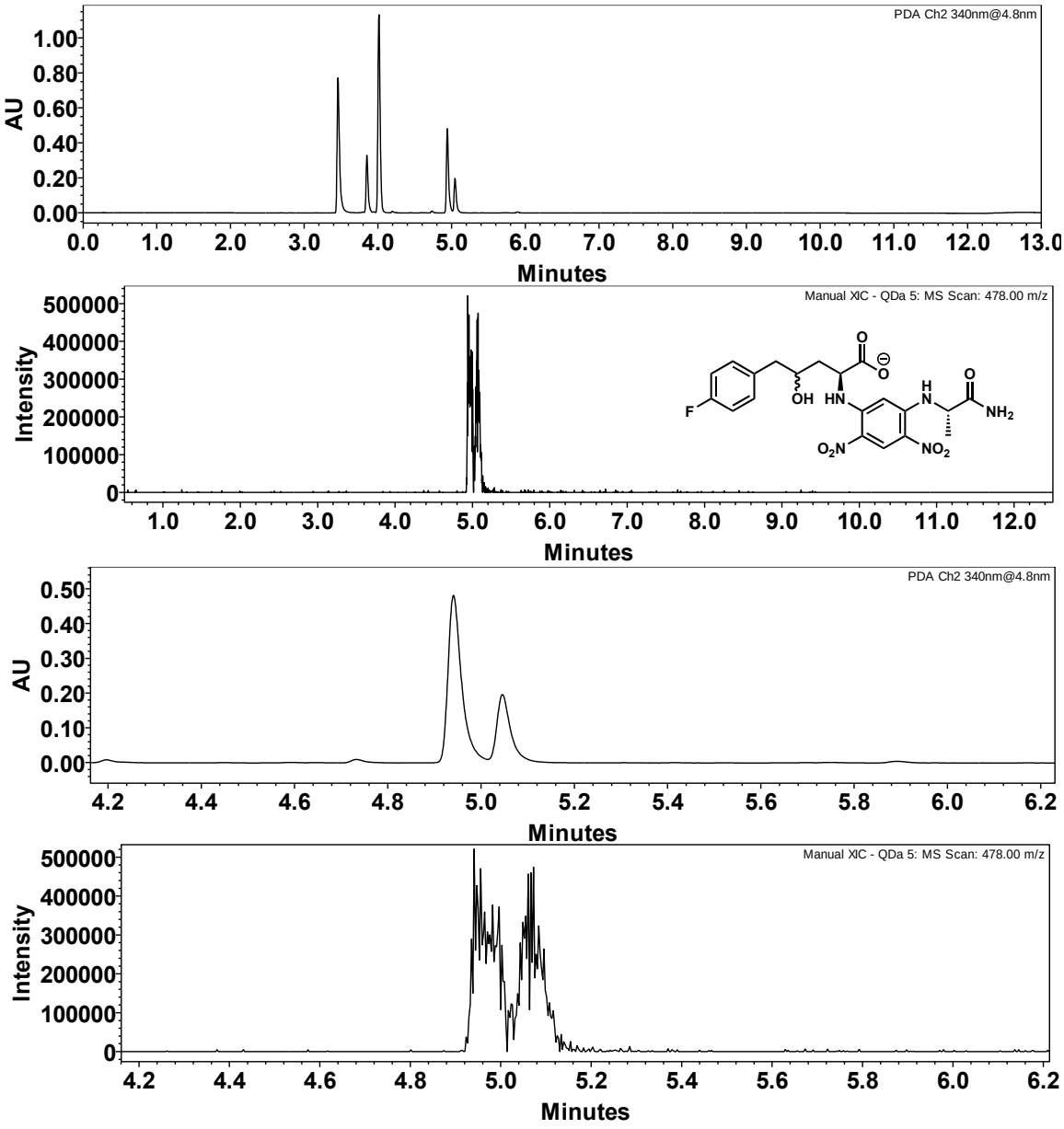

(2*S*,3*R*)-2-Amino-3-hydroxy-4-(3,4-dimethoxyphenyl)butanoic Acid (S1)

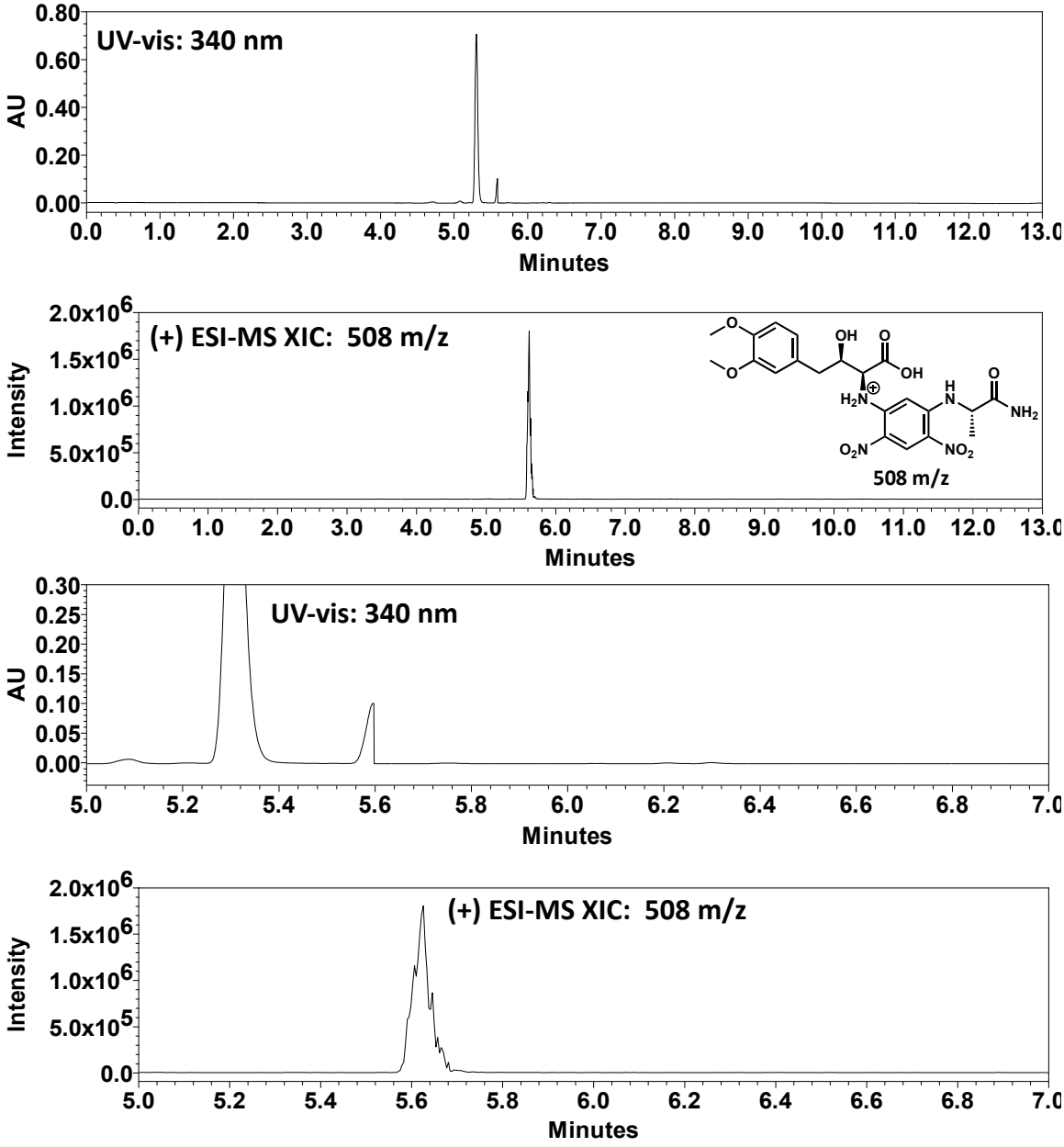

(2*S*,3*R*)-2-Amino-4-(2,3-dihydrobenzofuran-5-yl)-3-hydroxybutanoic Acid (S2)

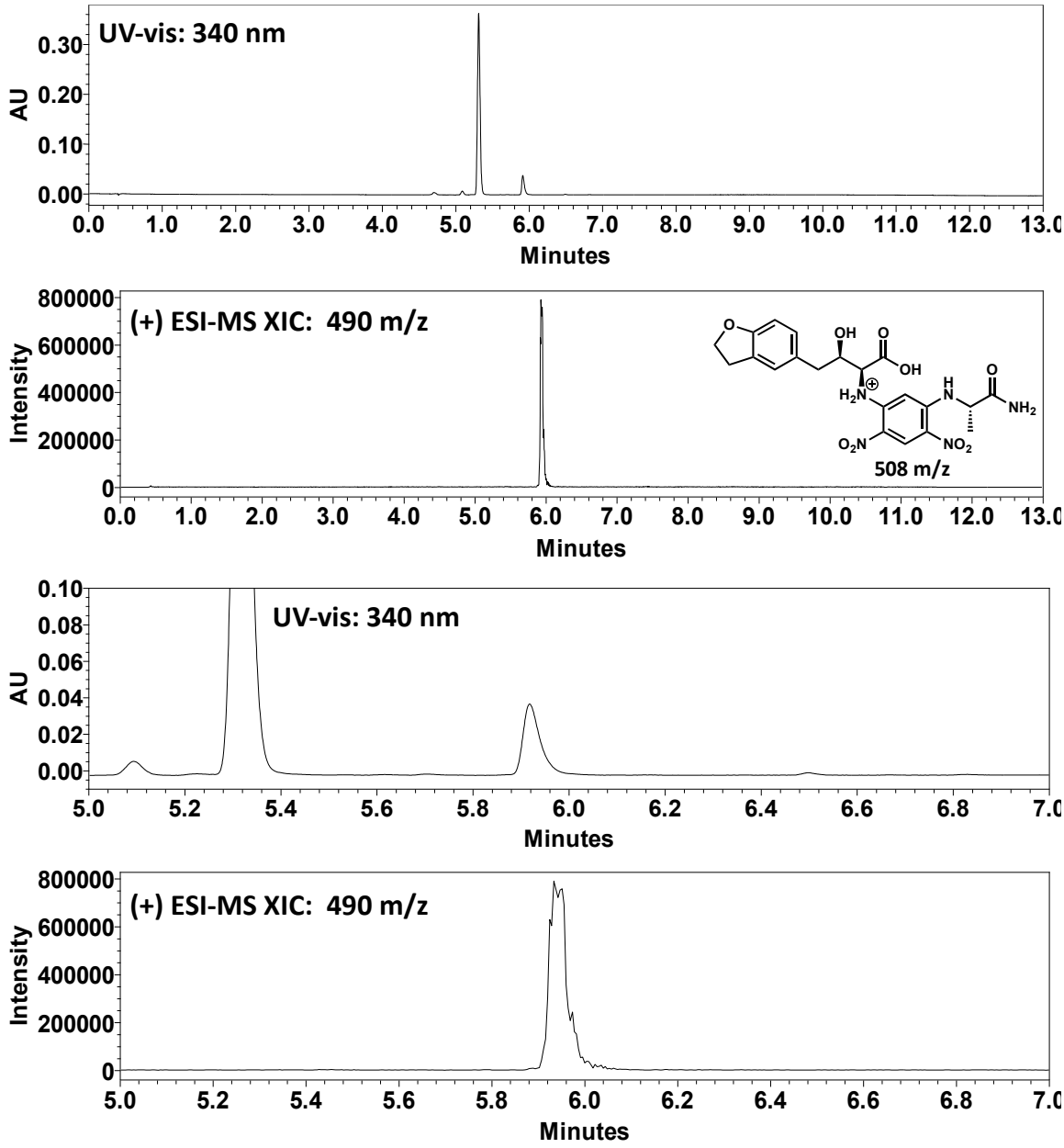

(2*S*,3*R*)-2-Amino-3-hydroxy-4-(*p*-tolyl)pentanoic Acid (S4)

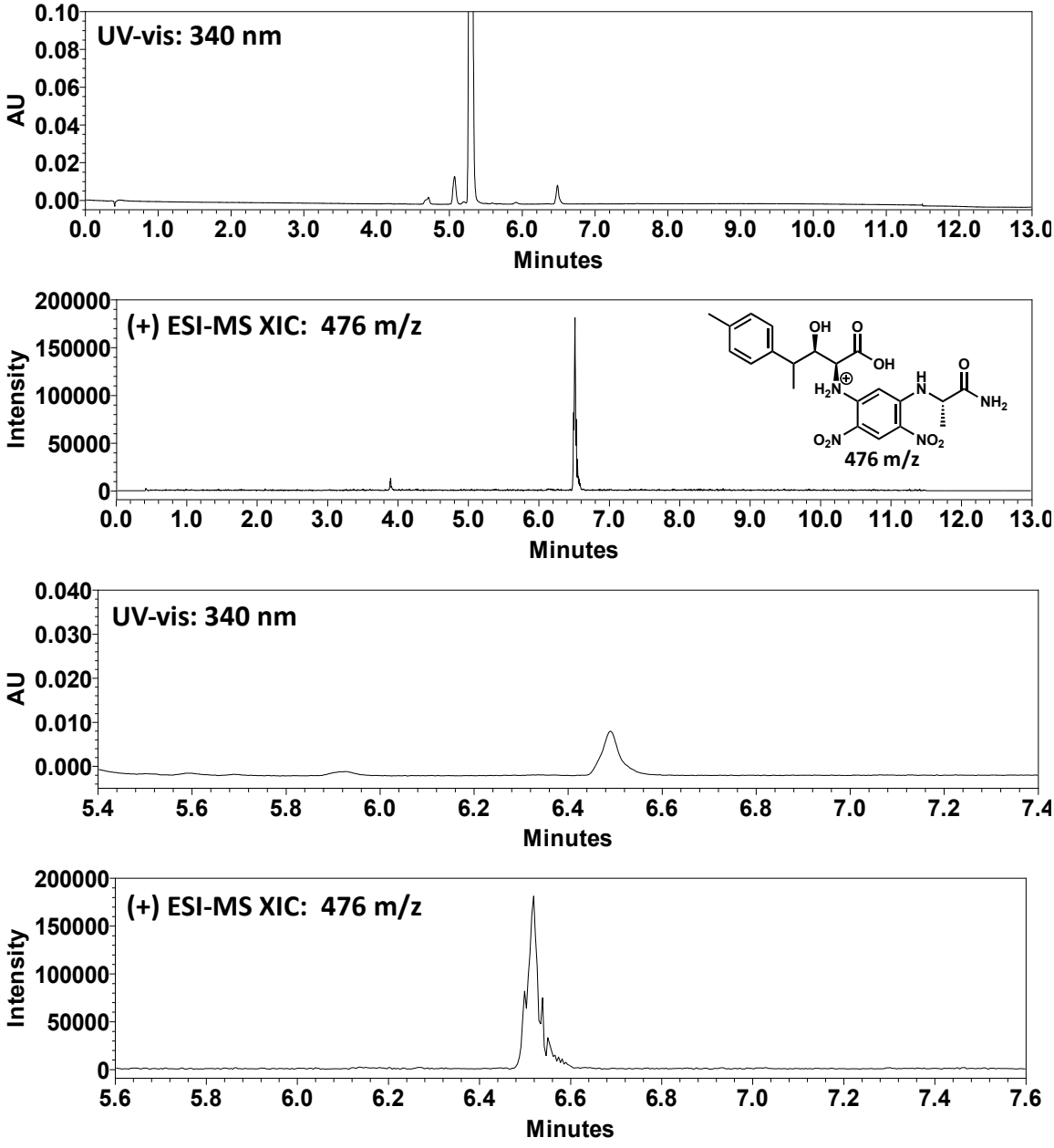

(2*S*,3*R*)-2-Amino-3-hydroxy-3-(1,2,3,4-tetrahydronaphthalen-1-yl)propanoic Acid (S6)

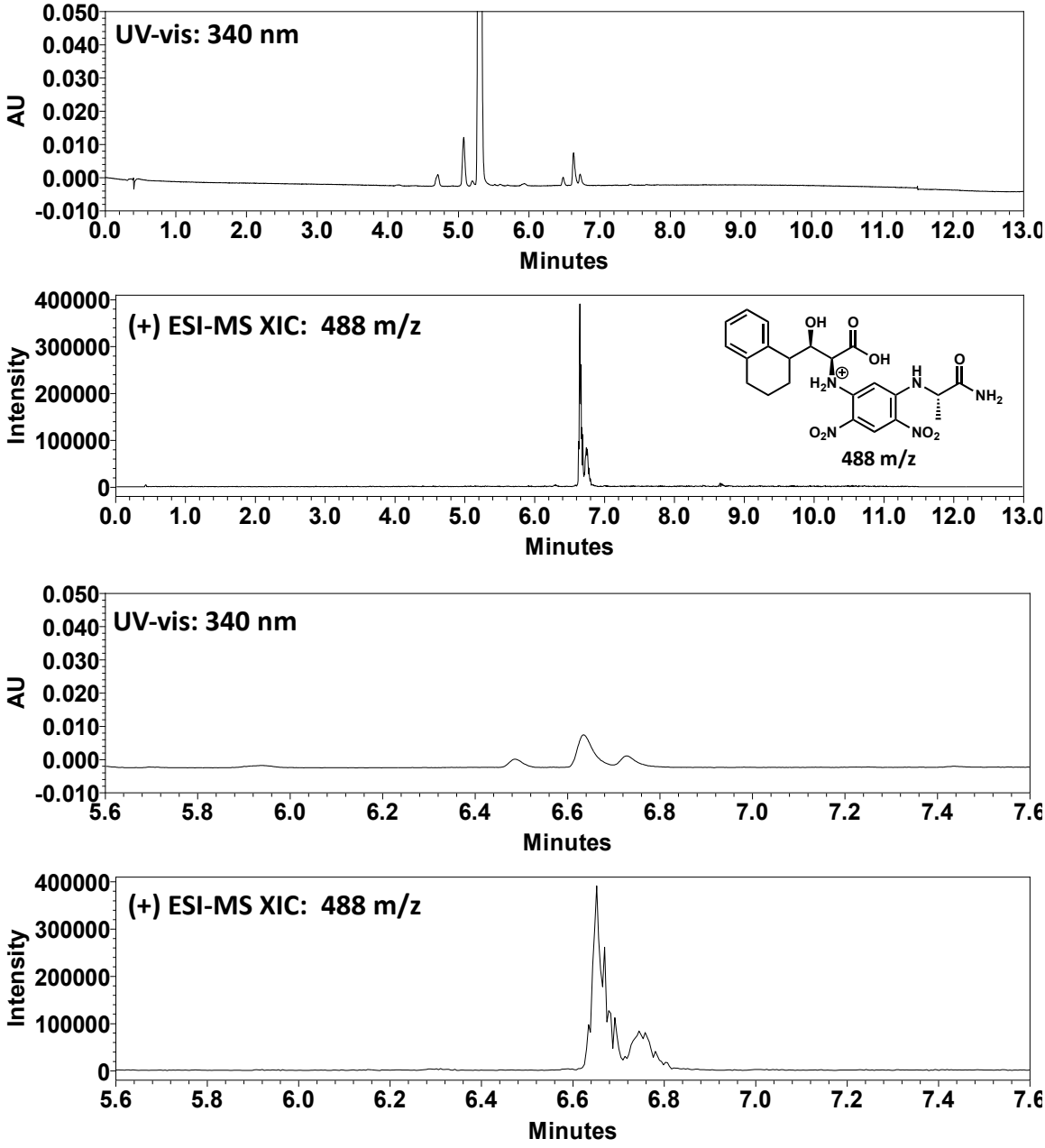

(2*S*,3*R*,*E*)-2-Amino-3-hydroxy-4-methyl-6-phenylhex-5-enoic Acid (S7)

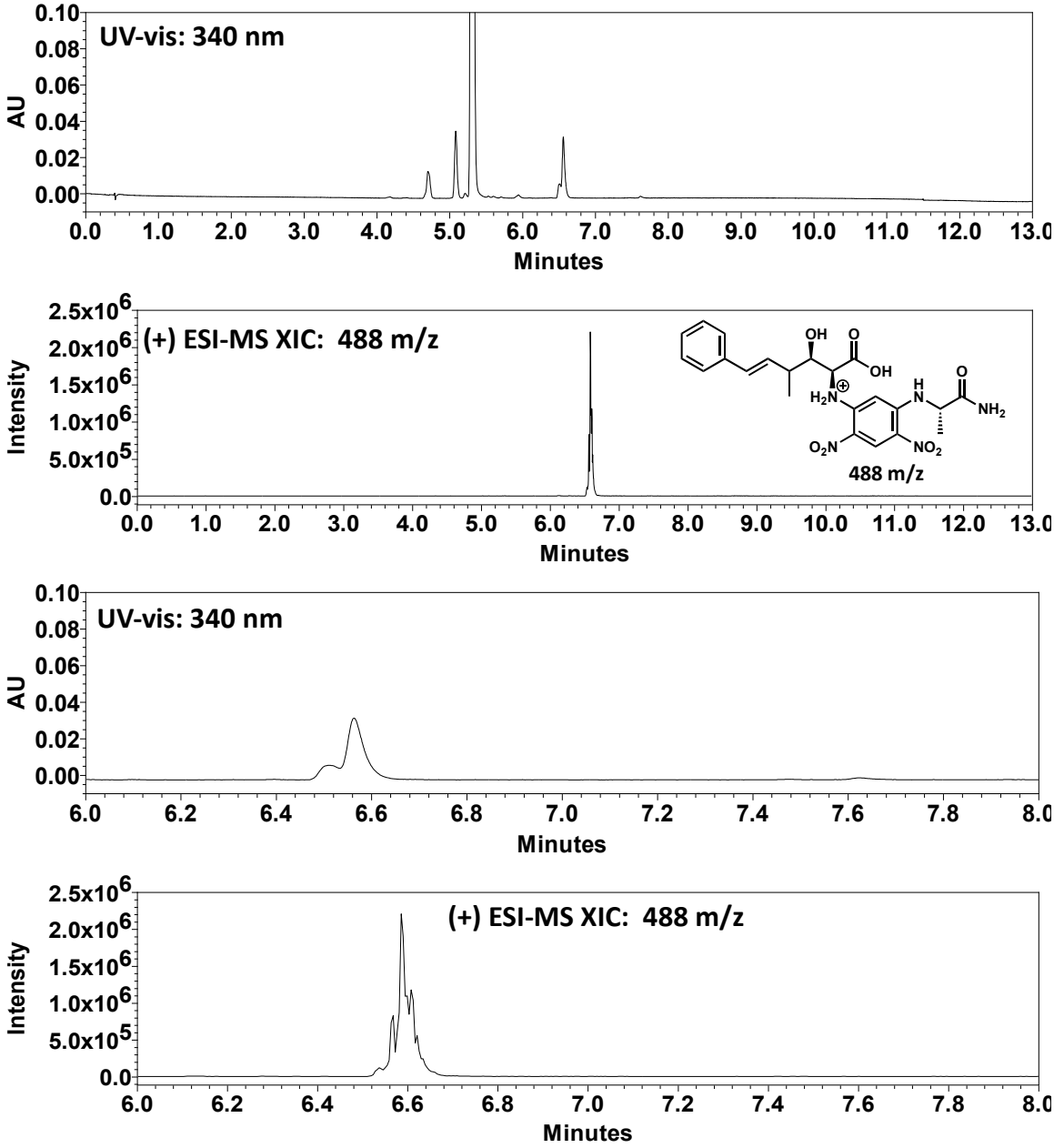

(2*S*,3*R*)-2-Amino-3-hydroxy-4-(6-methoxynaphthalen-2-yl)butanoic Acid (S8)

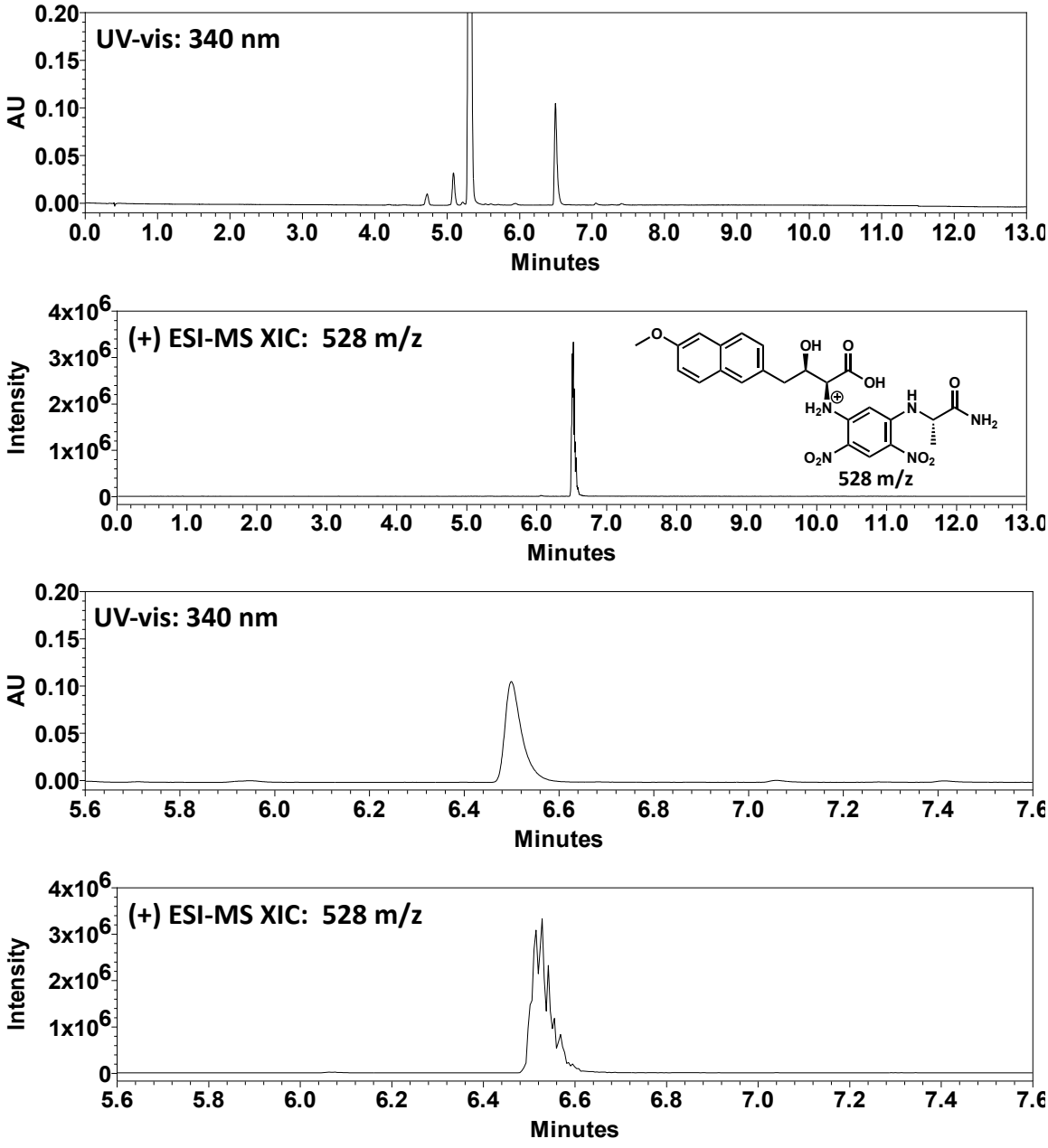

(2*S*,3*R*)-4-([1,1'-Biphenyl]-4-yl)-2-amino-3-hydroxybutanoic Acid (S9)

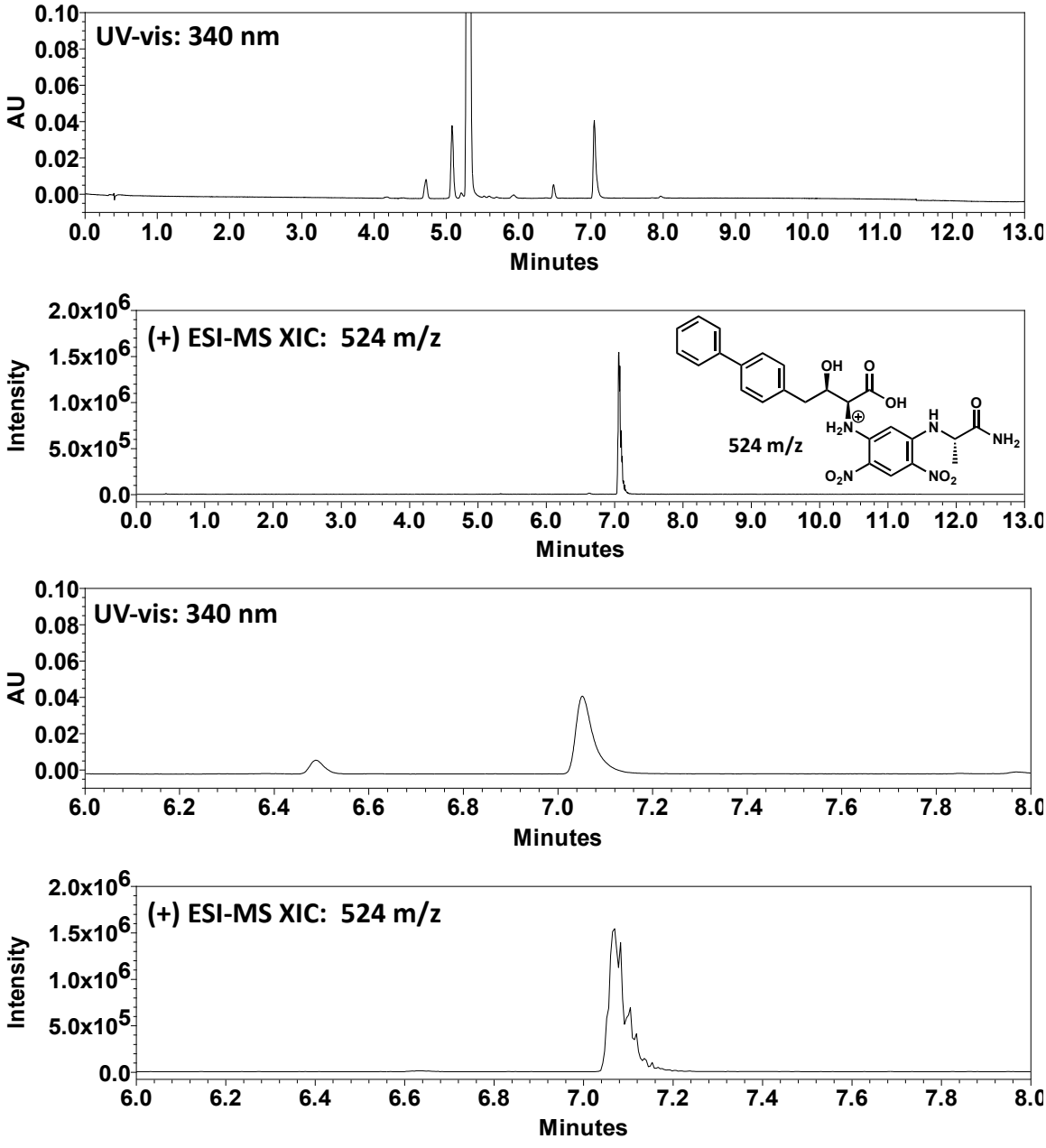

(2*S*,3*R*)-2-Amino-3-hydroxy-4,4-diphenylbutanoic Acid (S10)

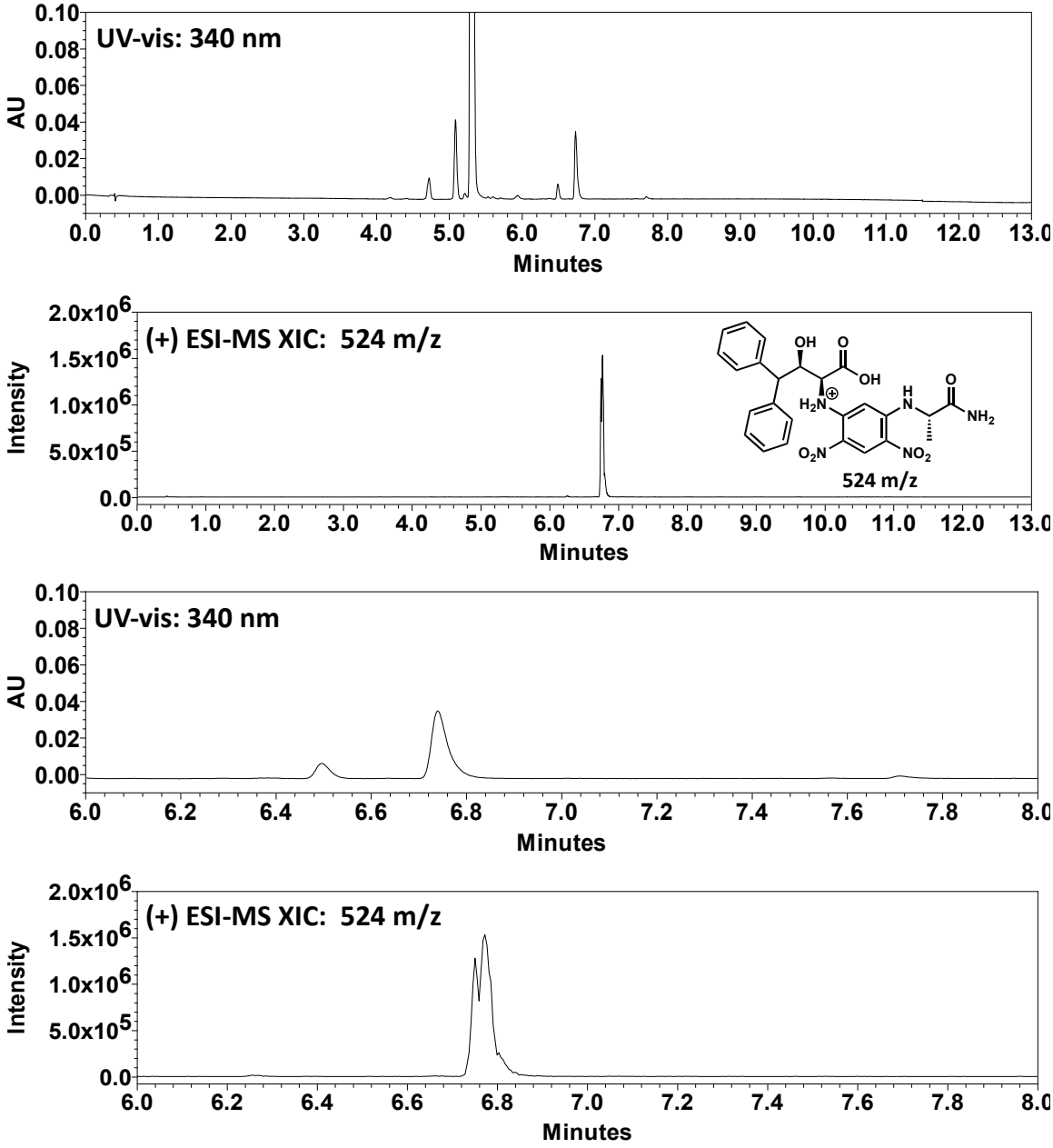

(2*S*,4*R*)-2-Amino-5-(4-fluorophenyl)-4-hydroxypentanoic Acid (S11)

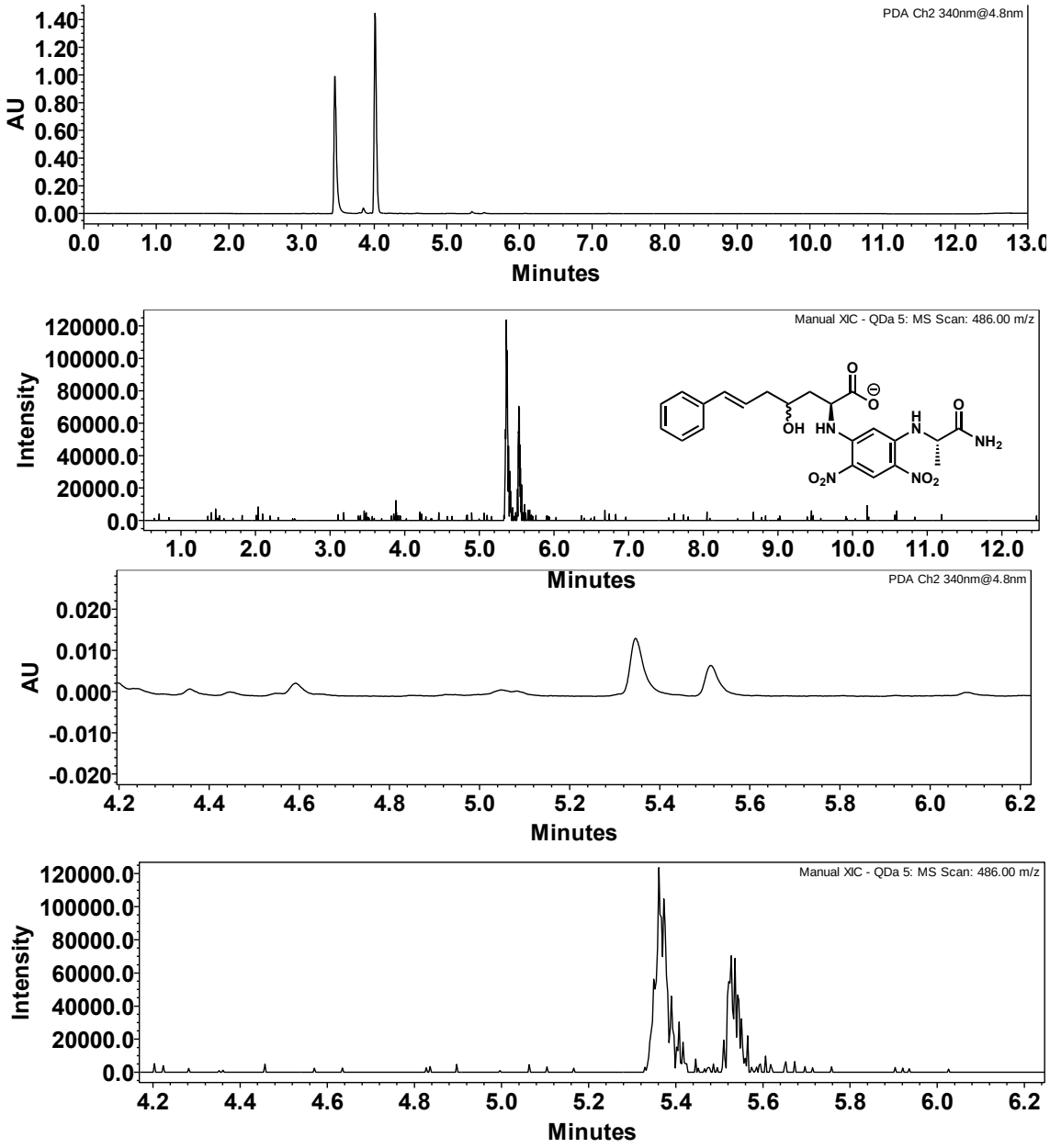

NMR Spectra

(2*S*,3*R*)-2-Amino-3-hydroxy-4-phenylbutanoic Acid (2b)

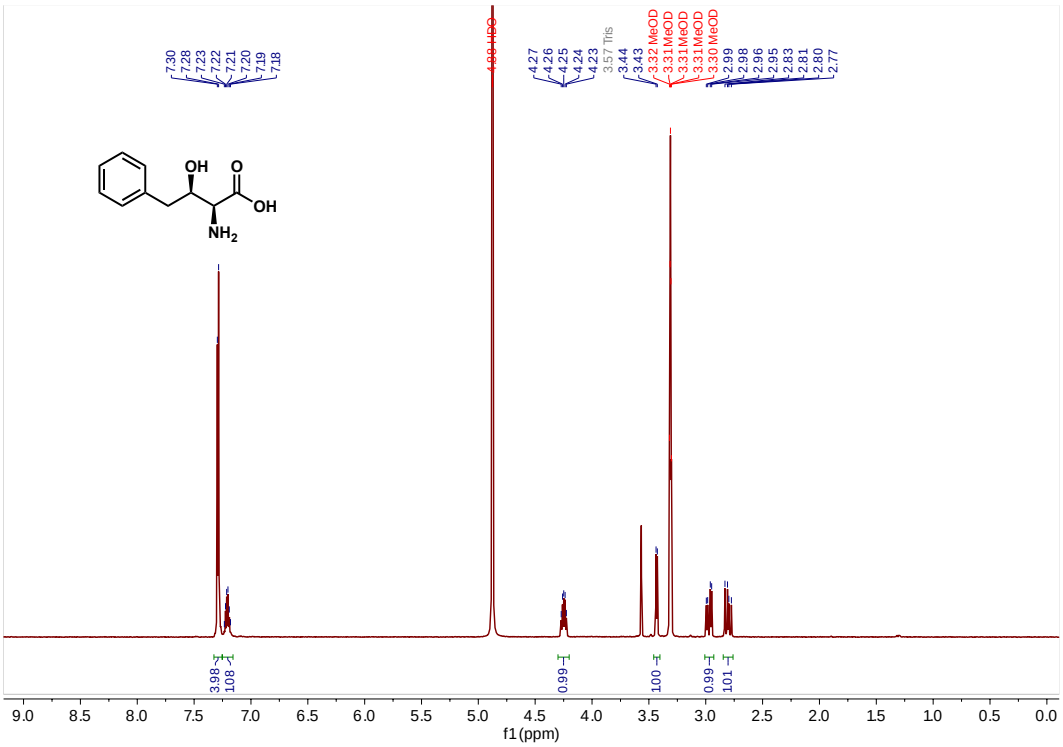

^{1}H NMR spectrum in CD_3OD at 500 MHz

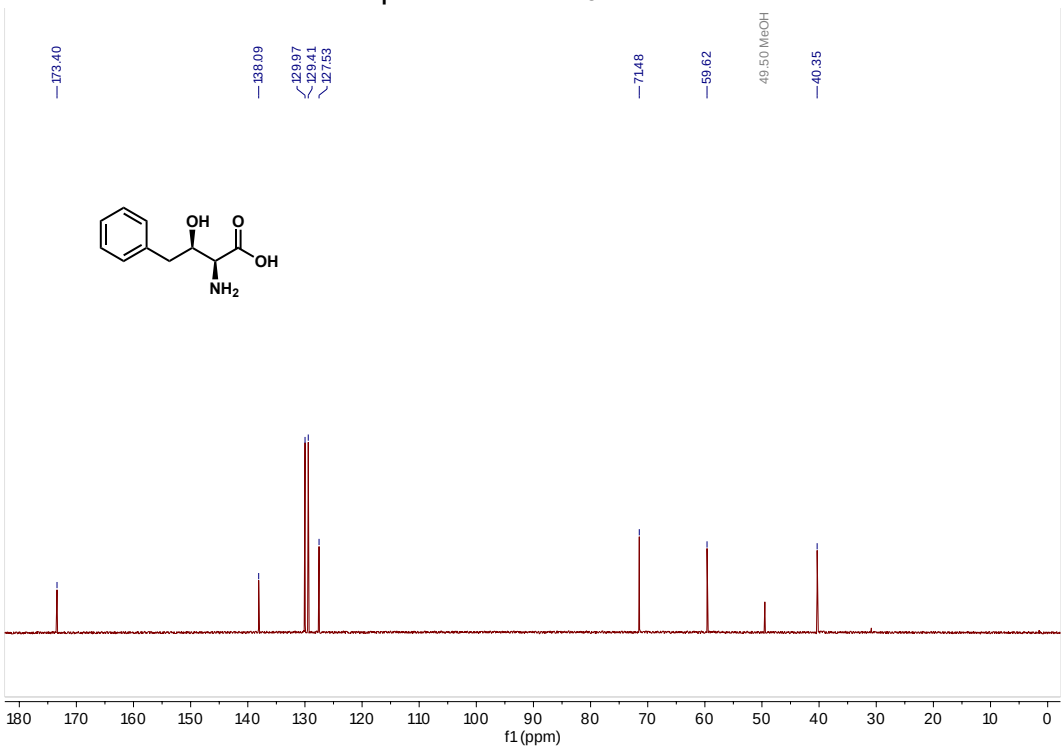

^{13}C NMR spectrum in D_2O at 126 MHz

2-Phenyloxirane-2,3,3-d_3 (2a-2,3,3-d_3)

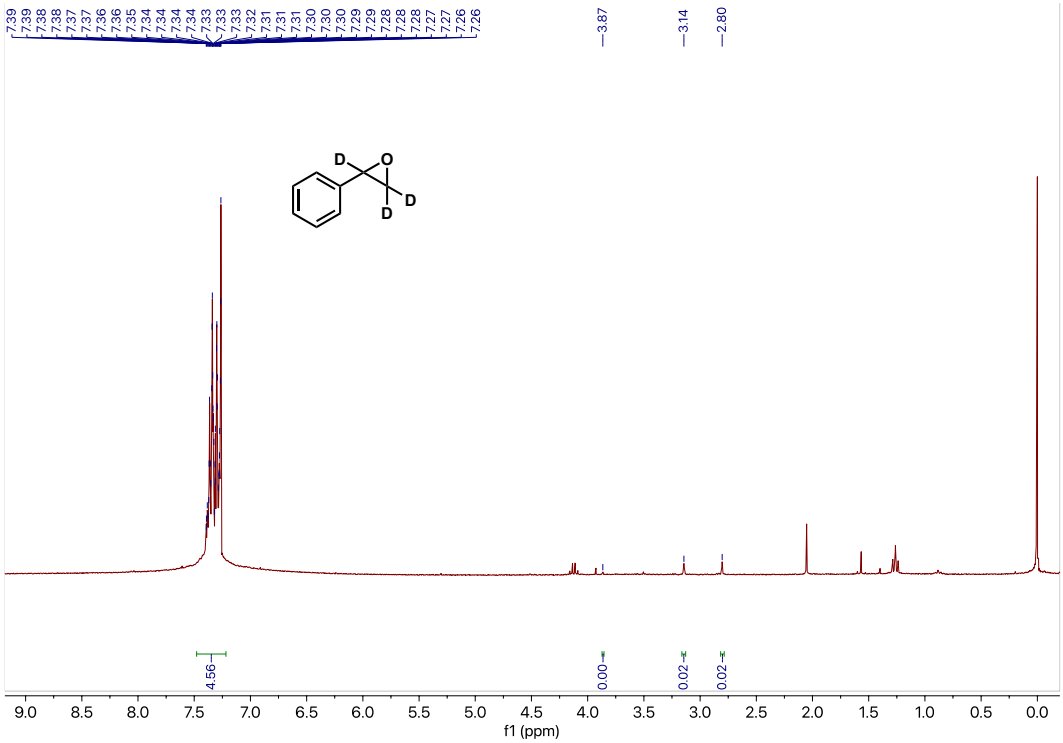

^{1}H NMR spectrum in $CDCl_3$ at 300 MHz

(2*S*,3*R*)-2-Amino-3-hydroxy-4-phenylbutanoic-3,4,4-d_3 Acid (2b-3,4,4-d_3)

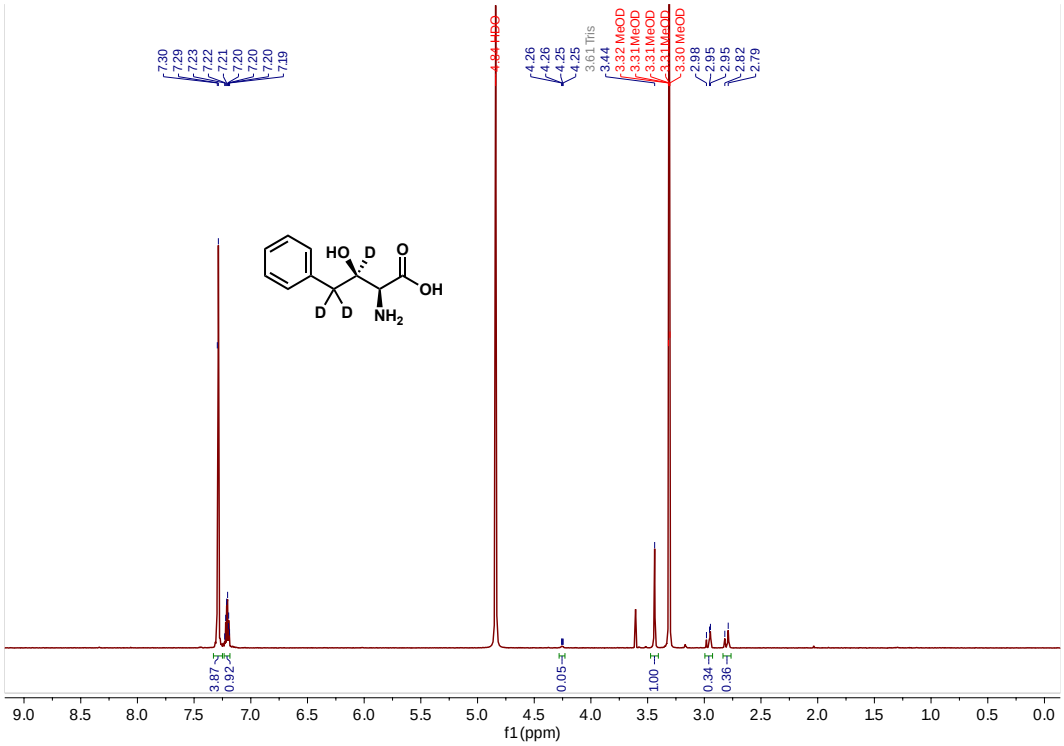

^{1}H NMR spectrum in CD_3OD at 500 MHz

(2*S*,3*R*)-2-Amino-3-hydroxy-4-(4-bromophenyl)butanoic Acid (3b)

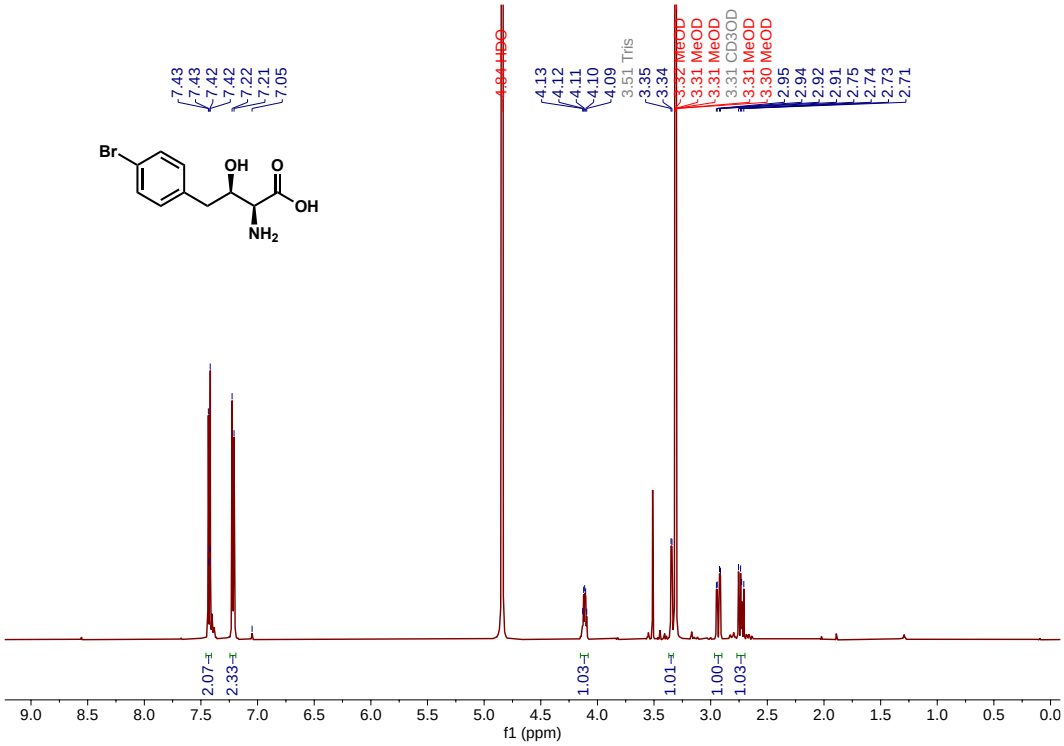

^{1}H NMR spectrum in CD_3OD at 500 MHz

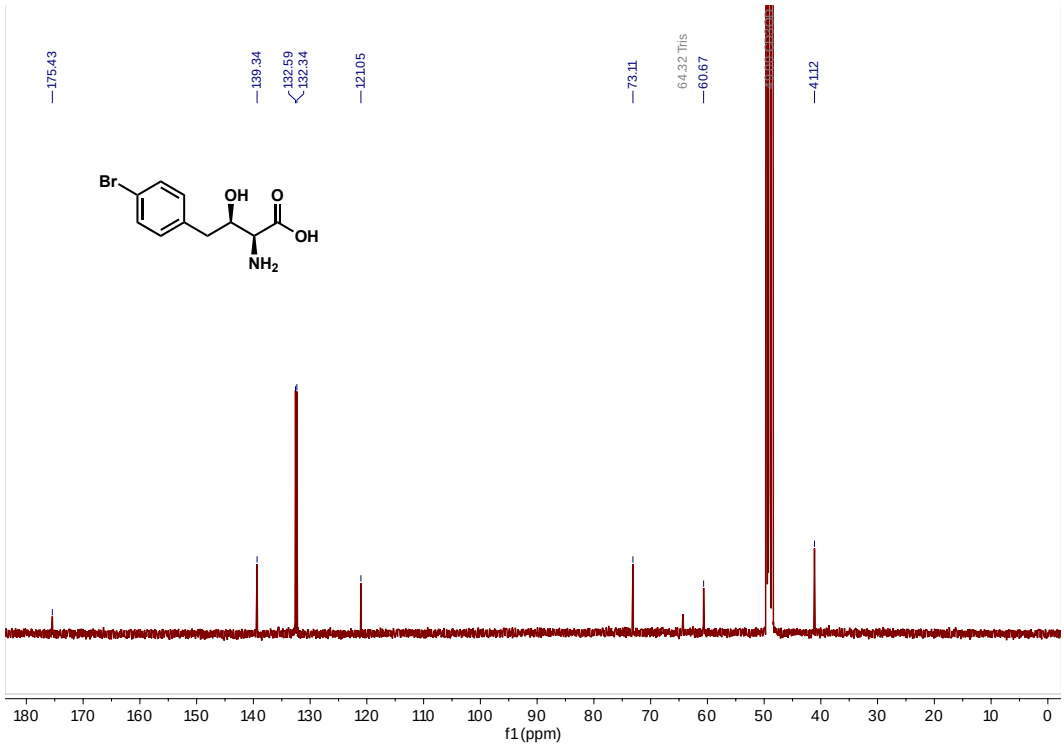

^{13}C NMR spectrum in CD_3OD at 126 MHz

(2*S*,3*R*)-2-Amino-3-hydroxy-4-(4-chlorophenyl)butanoic Acid (4b)

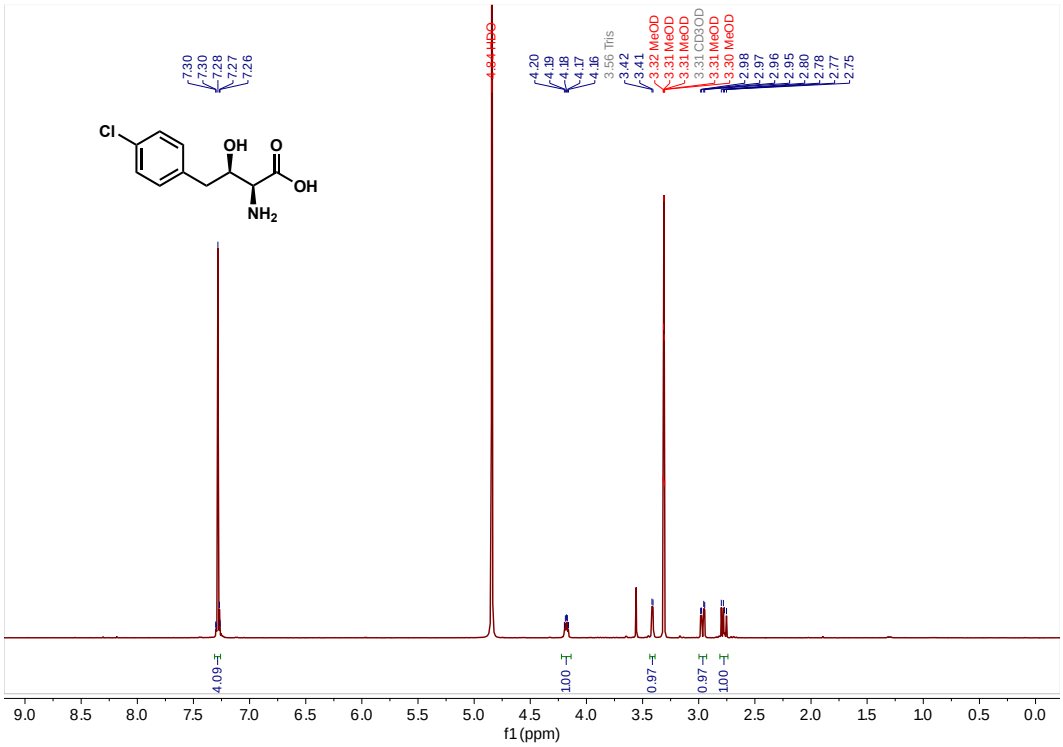

^{1}H NMR spectrum in CD_3OD at 500 MHz

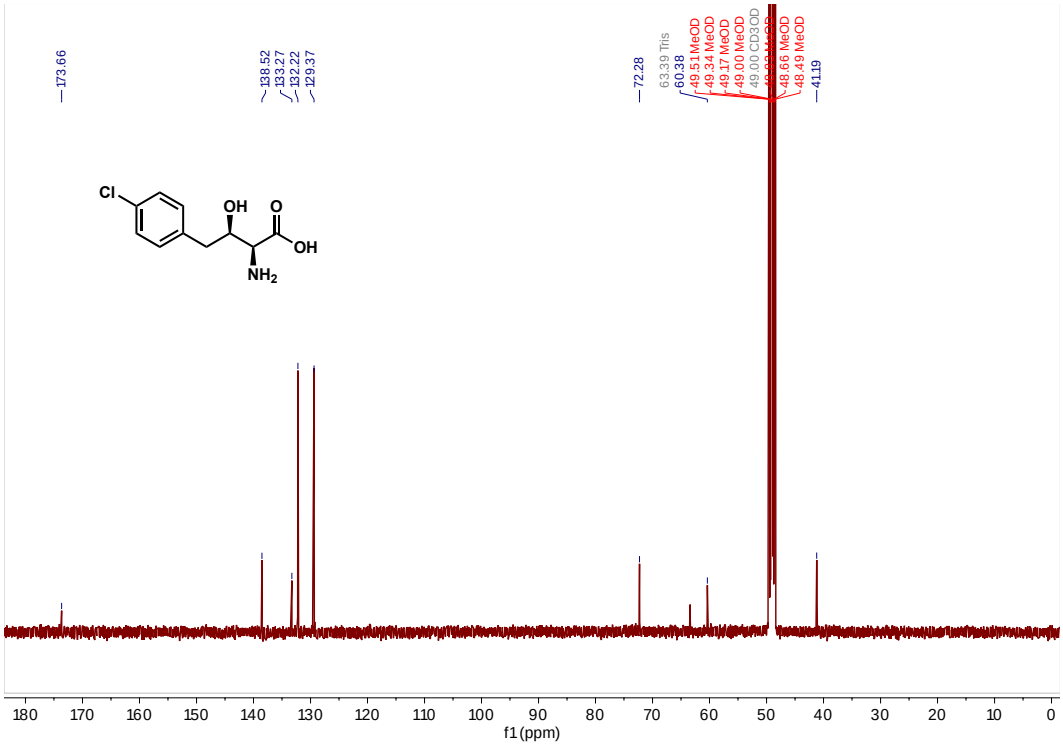

^{13}C NMR spectrum in CD_3OD at 126 MHz

(2*S*,3*R*)-2-Amino-3-hydroxy-4-(4-fluorophenyl)butanoic Acid (5b)

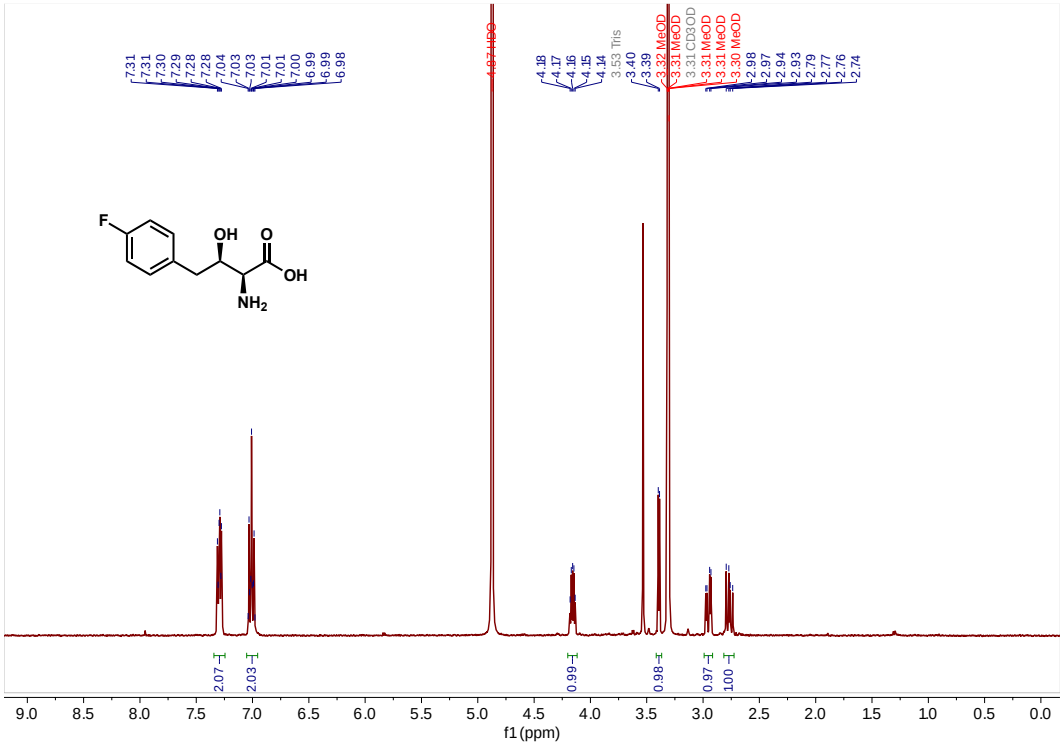

^{1}H NMR spectrum in CD_3OD at 500 MHz

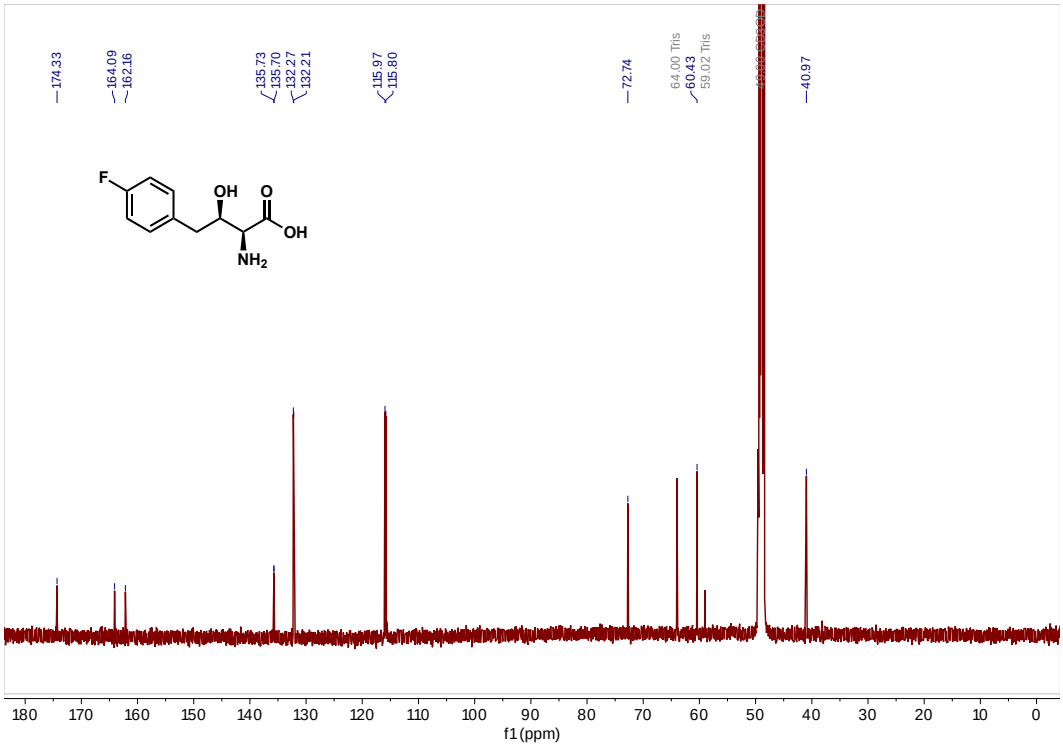

^{13}C NMR spectrum in CD_3OD at 126 MHz

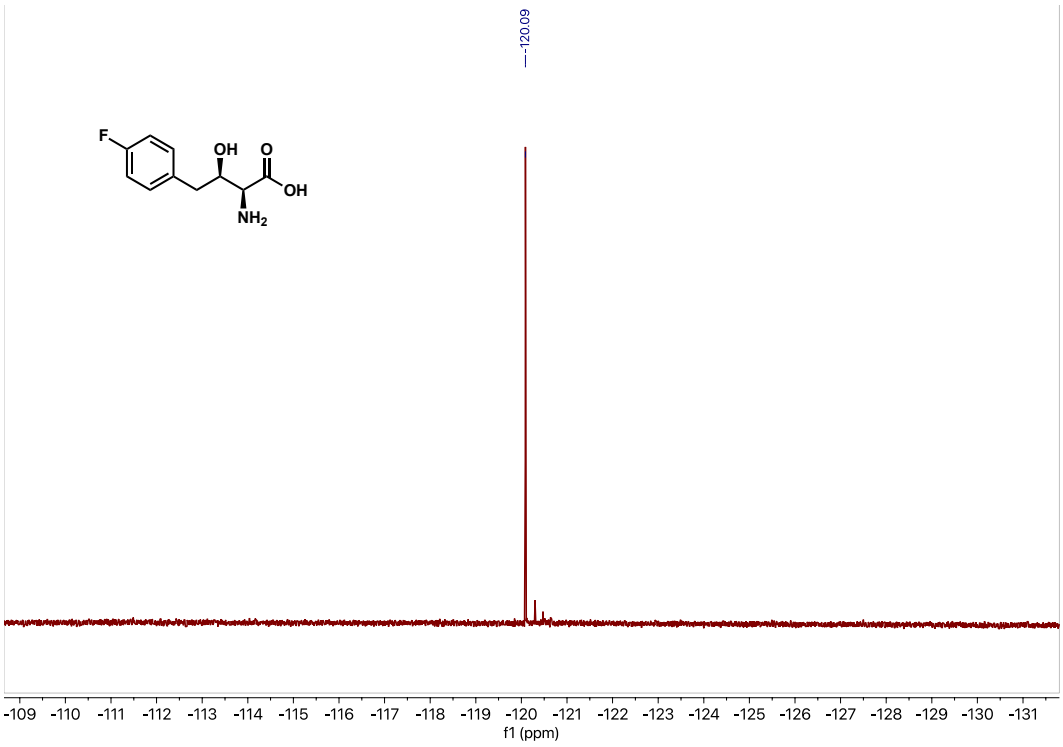

^{19}F NMR spectrum in CD_3OD at 377 MHz

(2*S*,3*R*)-2-Amino-4-(2,4-difluorophenyl)-3-hydroxybutanoic Acid (6b)

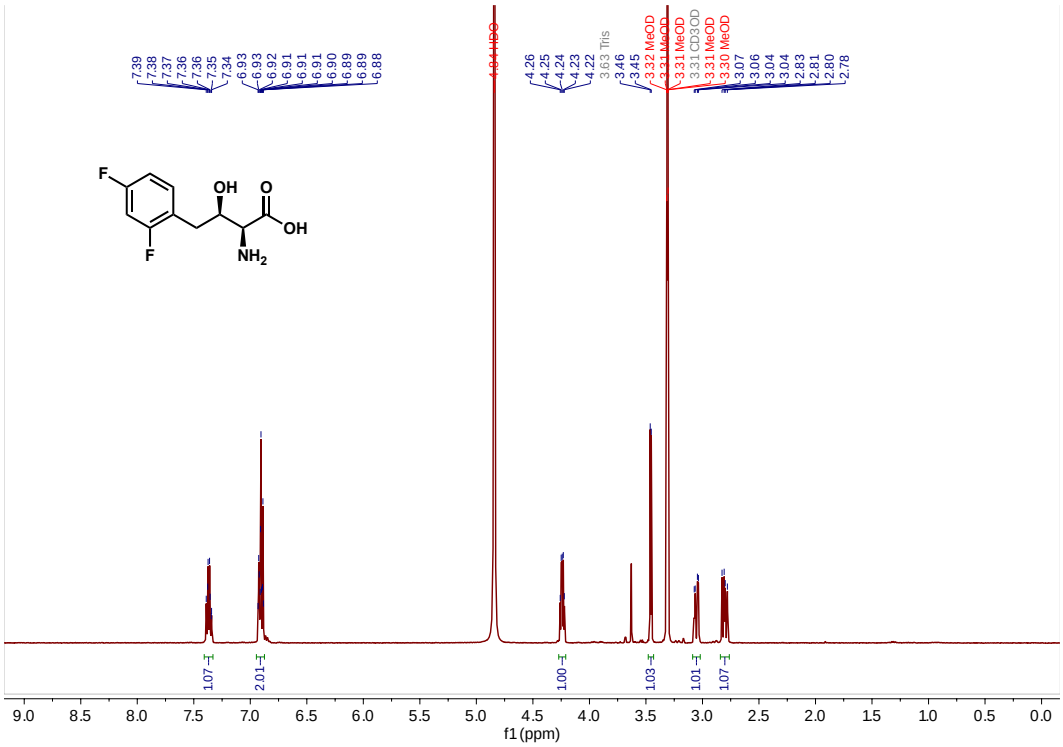

^{1}H NMR spectrum in CD_3OD at 500 MHz

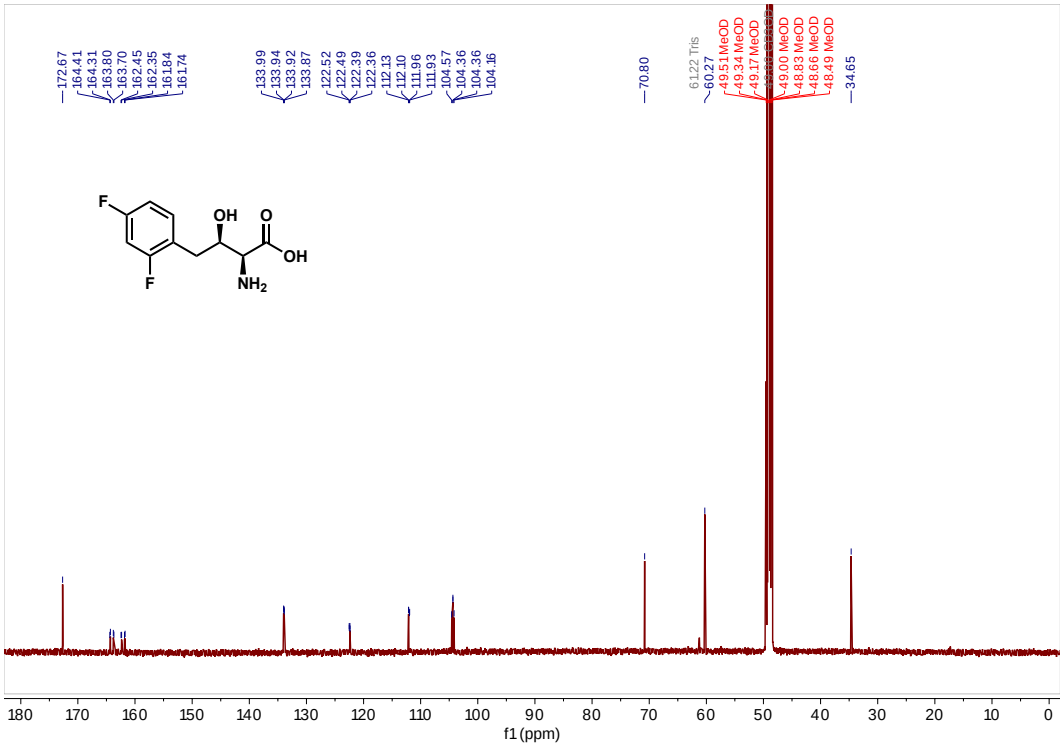

^{13}C NMR spectrum in CD_3OD at 126 MHz

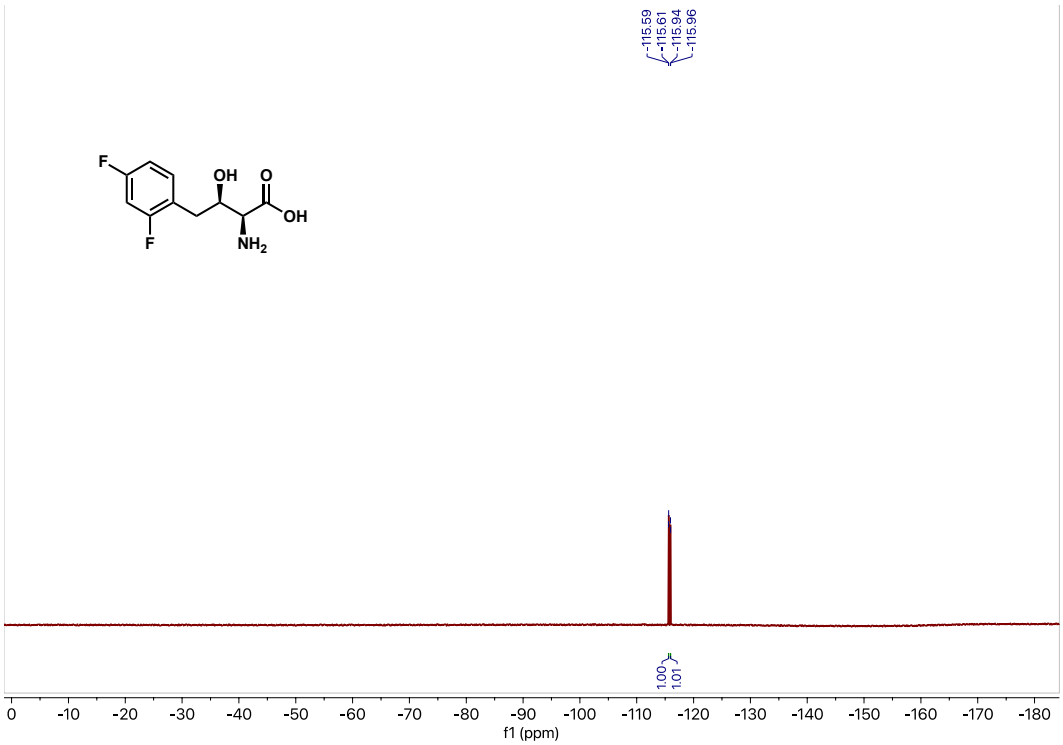

^{19}F NMR spectrum in CD_3OD at 377 MHz

(2*S*,3*R*)-2-Amino-3-hydroxy-4-(4-methoxyphenyl)butanoic Acid (7b)

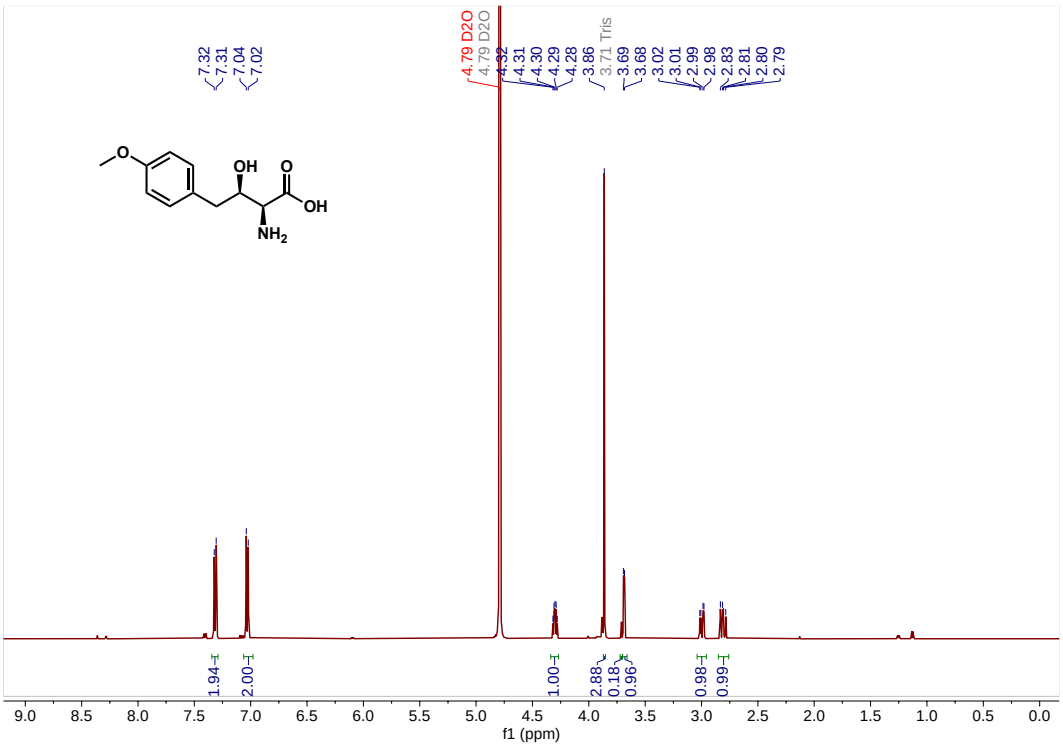

^{1}H NMR spectrum in D_2O at 500 MHz

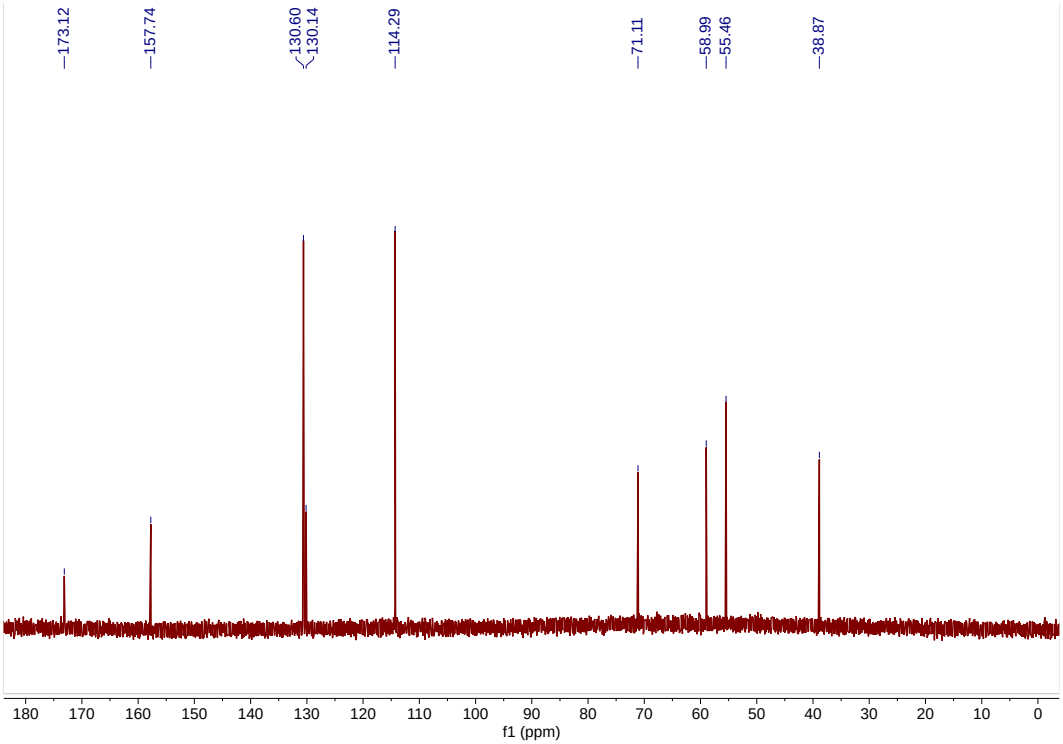

^{13}C NMR spectrum in D_2O at 126 MHz

(2*S*,3*R*)-4-(4-Acetoxyphenyl)-2-amino-3-hydroxybutanoic Acid (8b)

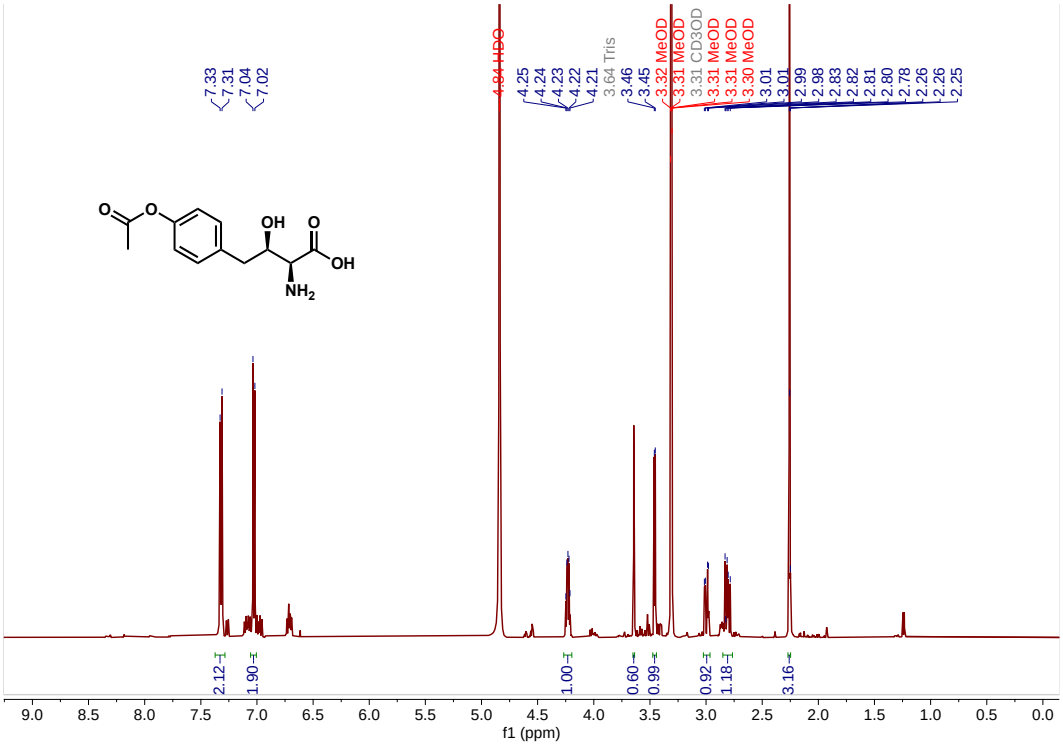

^{1}H NMR spectrum in CD_3OD at 500 MHz

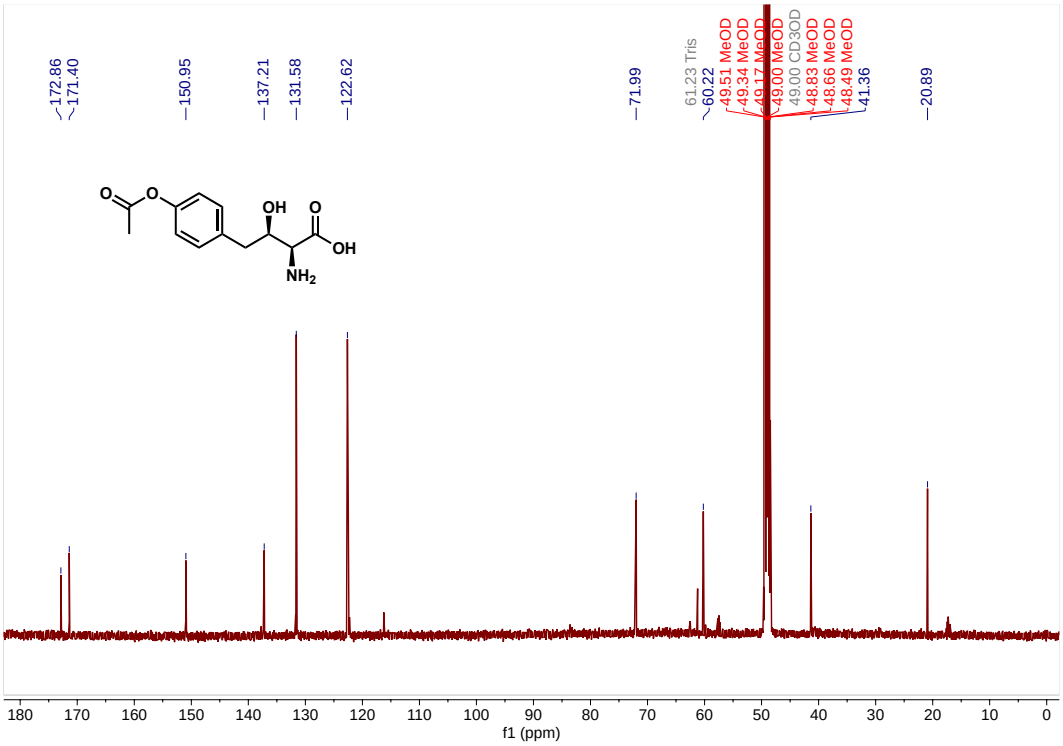

^{13}C NMR spectrum in CD_3OD at 126 MHz

(2*S*,3*R*)-2-Amino-3-hydroxy-4-(4-hydroxyphenyl)butanoic Acid (8c)

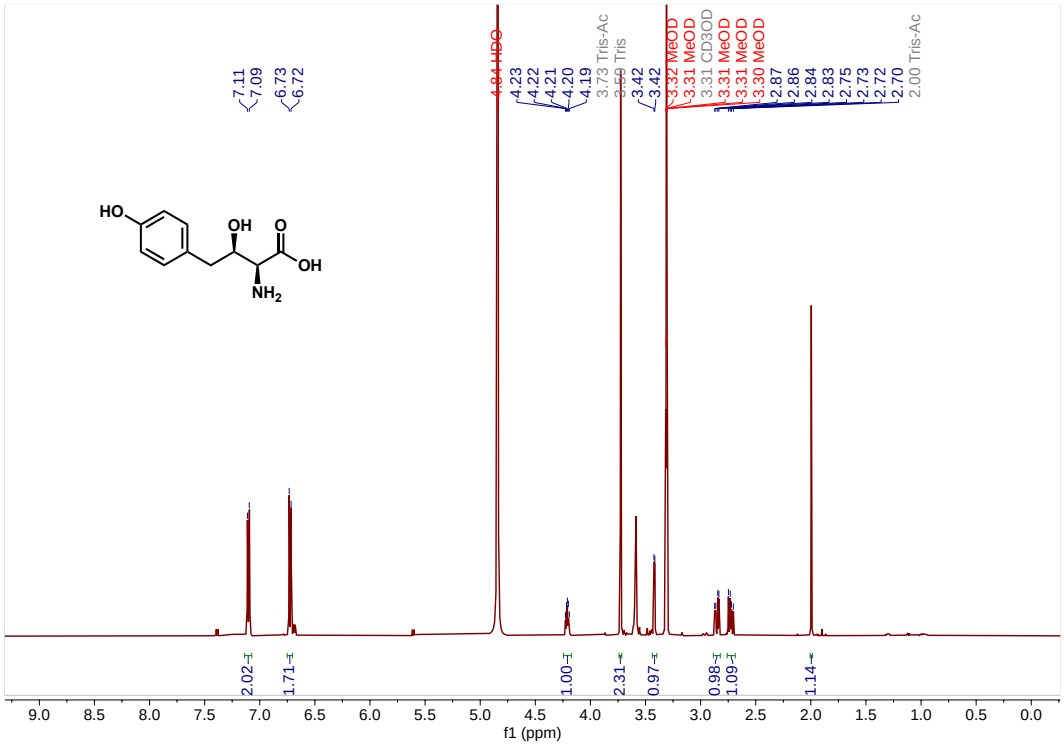

^{1}H NMR spectrum in CD_3OD at 500 MHz

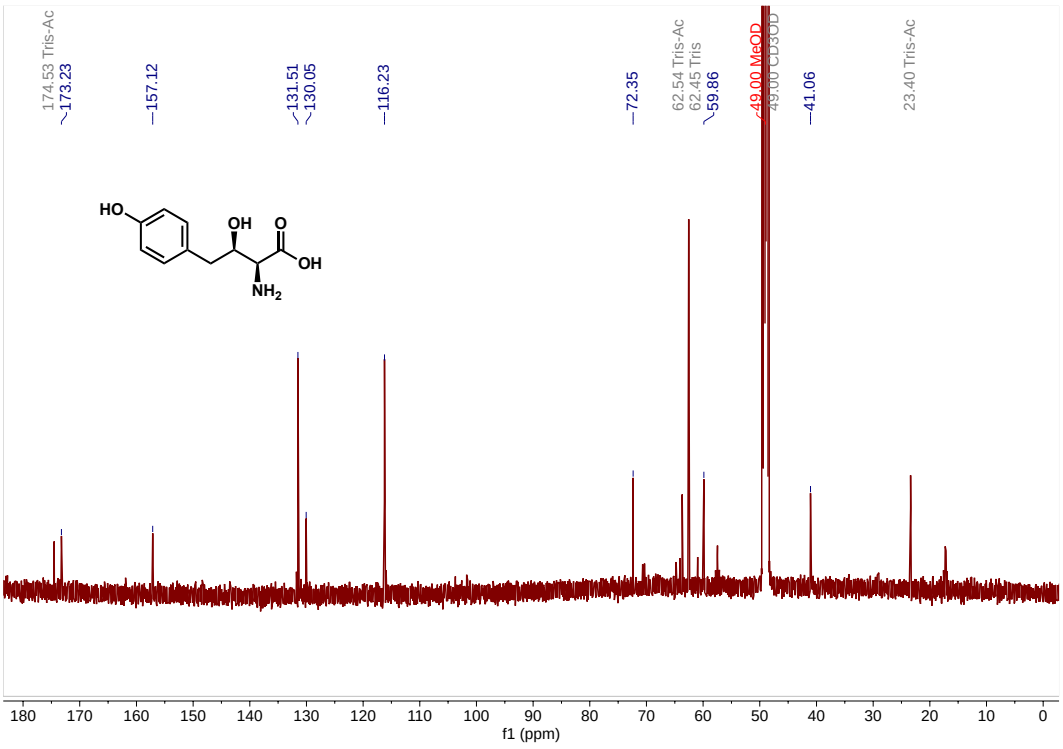

^{13}C NMR spectrum in CD_3OD at 126 MHz

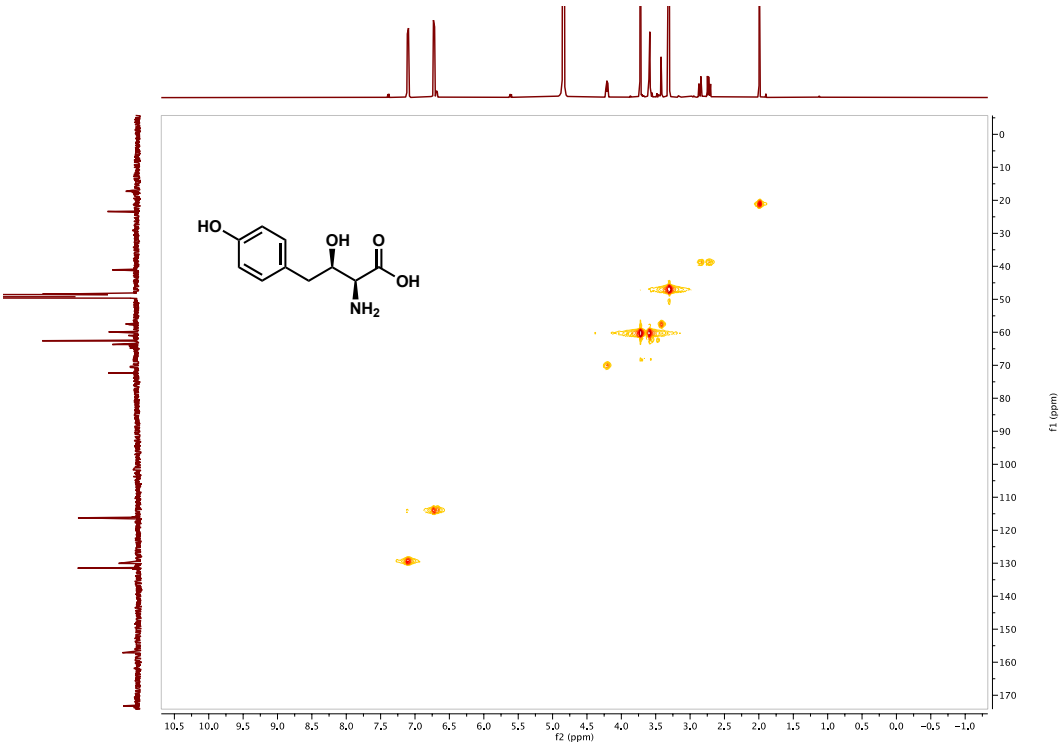

HSQC Spectrum in CD_3OD at 500 MHz and 126 MHz

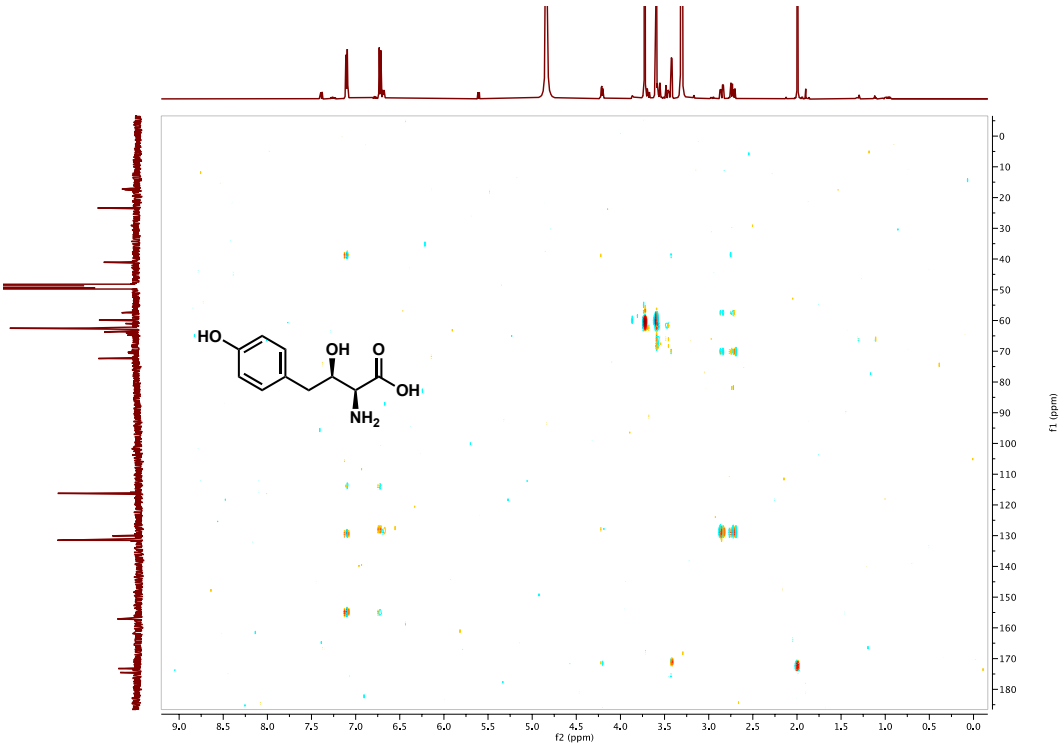

HSQC Spectrum in CD_3OD at 500 MHz and 126 MHz

(2*S*,3*R*)-2-Amino-4-(benzo[*d*][1,3]dioxol-5-yl)-3-hydroxybutanoic Acid (9b)

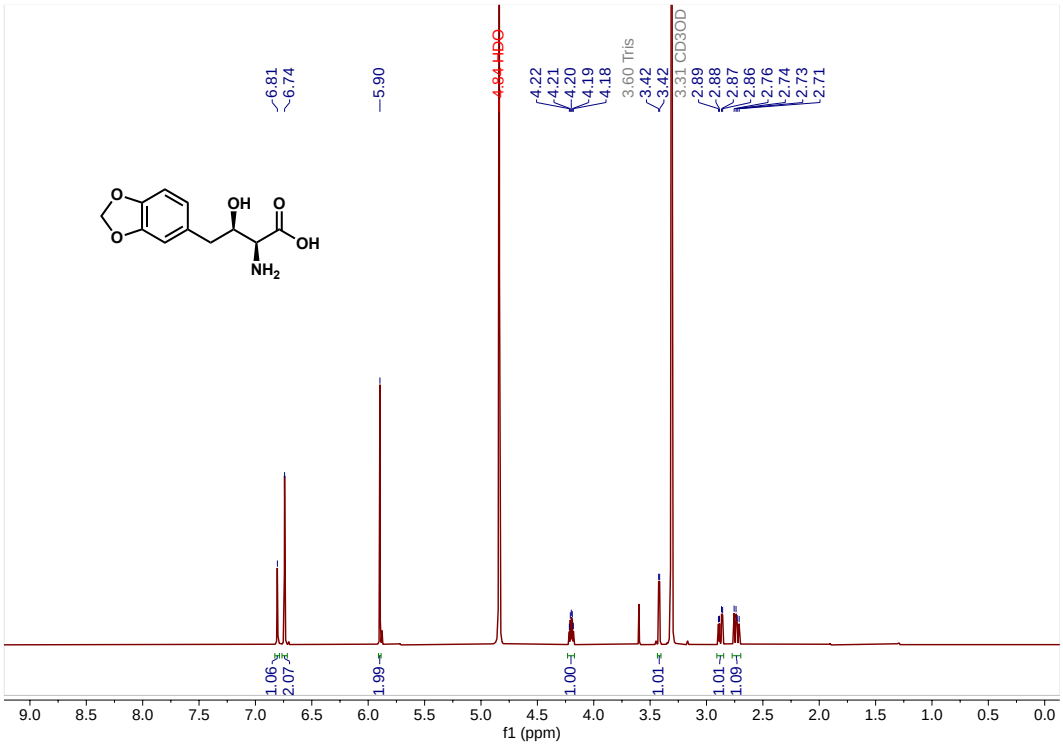

^{1}H NMR spectrum in CD_3OD at 500 MHz

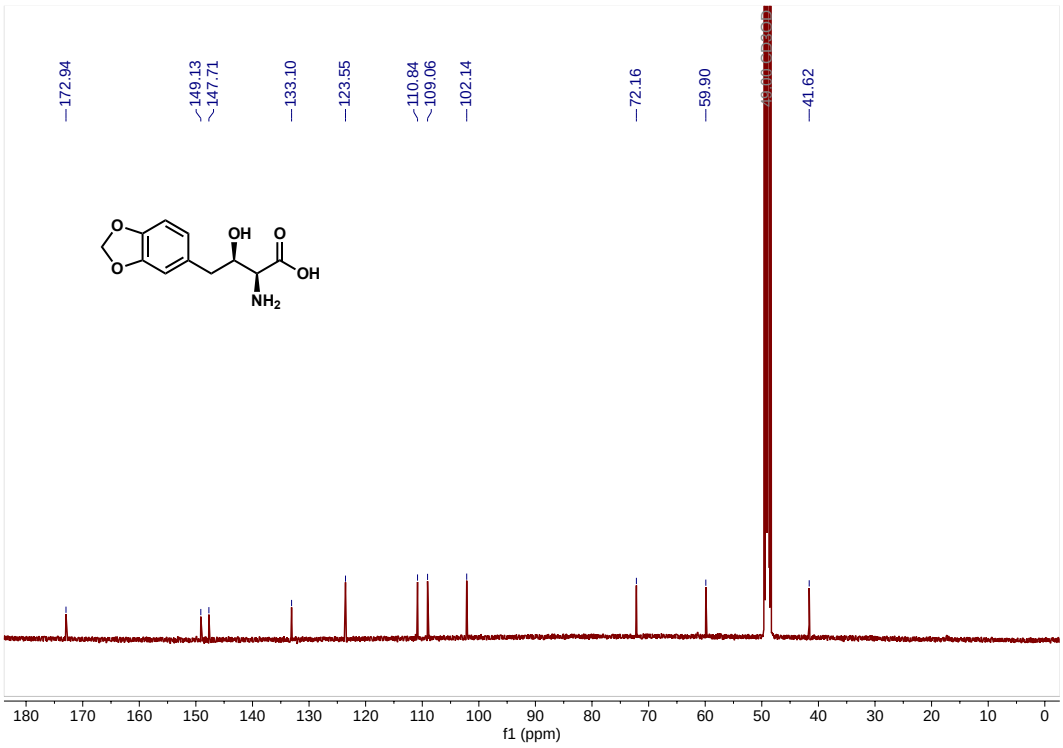

^{13}C NMR spectrum in CD_3OD at 126 MHz

(2*S*,3*R*)-2-Amino-3-hydroxy-4-(*o*-tolyl)butanoic Acid (10b)

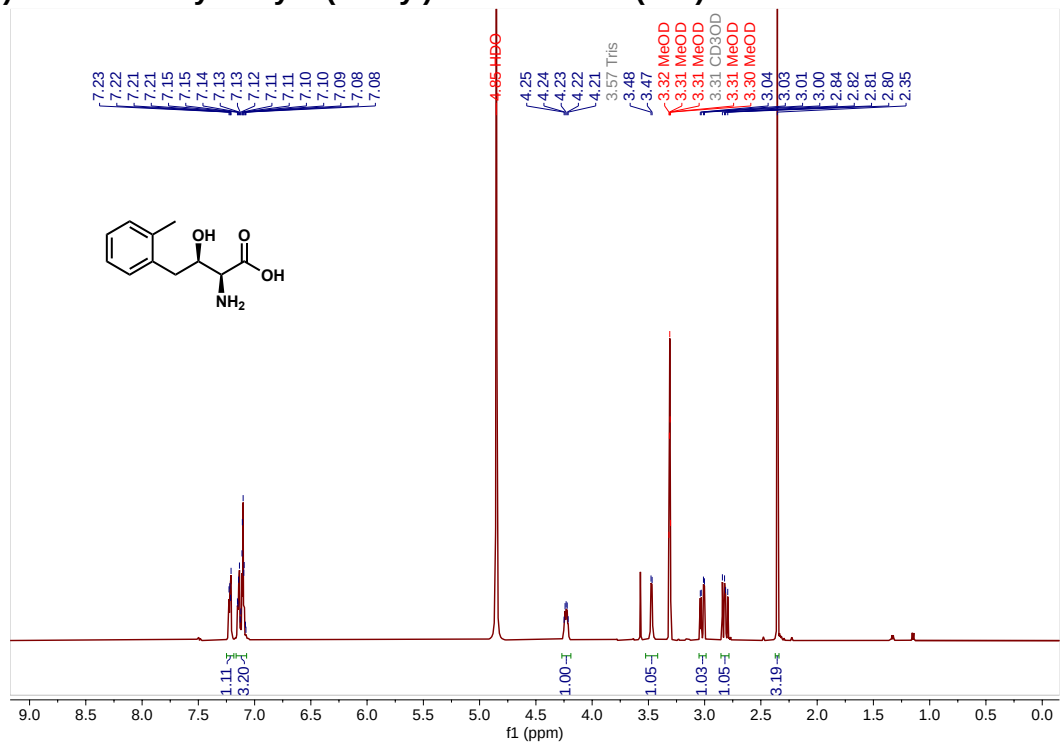

^{1}H NMR spectrum in CD_3OD at 500 MHz

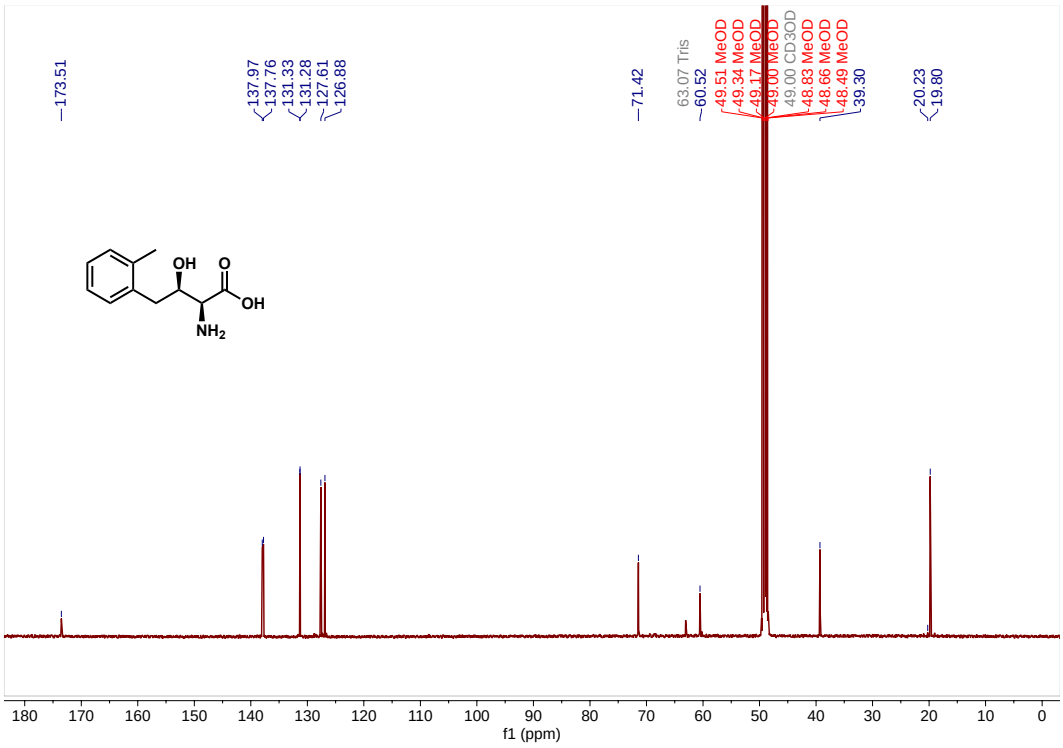

^{13}C NMR spectrum in CD_3OD at 126 MHz

(2*S*,3*R*)-2-Amino-3-hydroxy-4-(*m*-tolyl)butanoic Acid (11b)

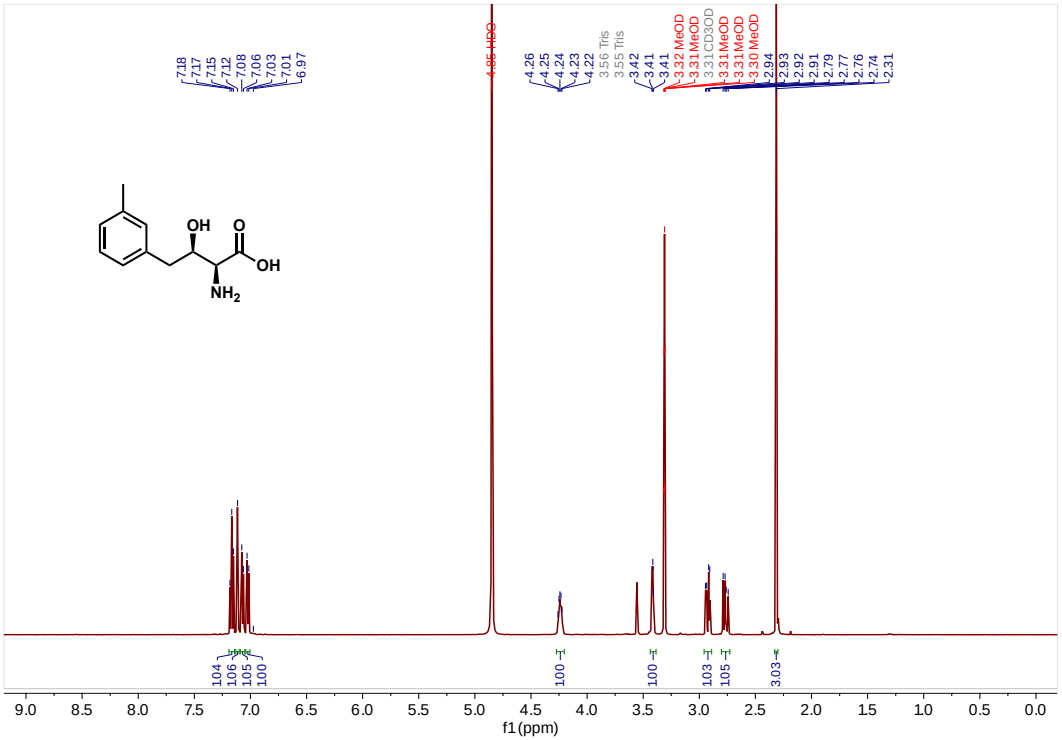

^{1}H NMR spectrum in CD_3OD at 500 MHz

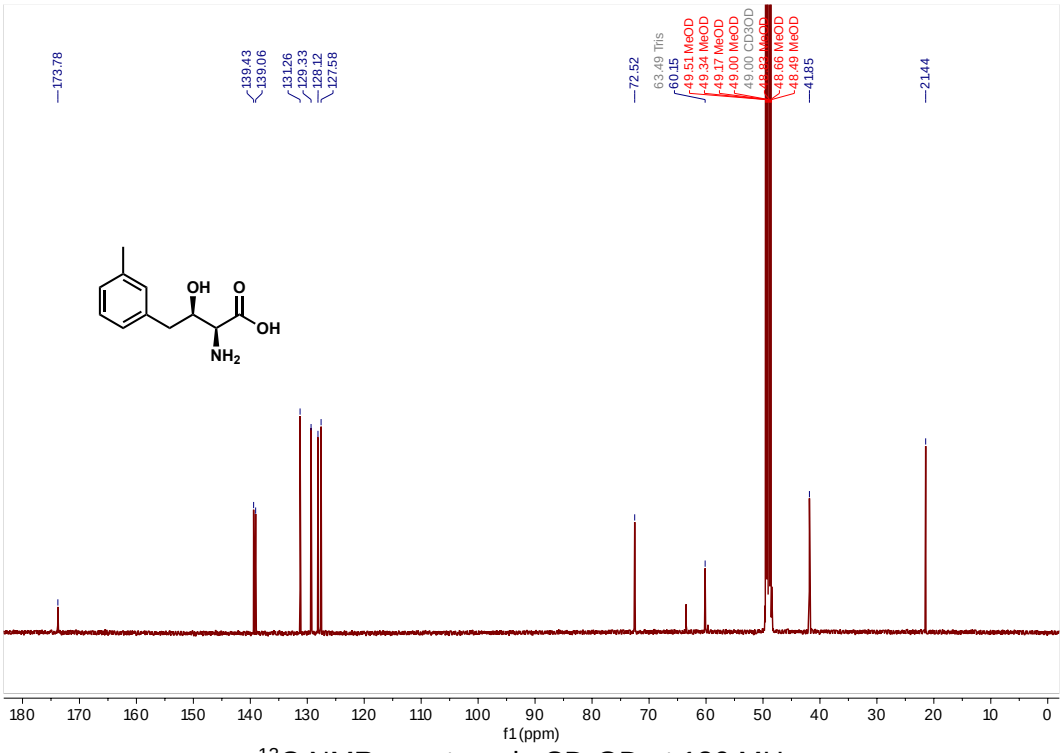

^{13}C NMR spectrum in CD_3OD at 126 MHz

(2*S*,3*R*)-2-Amino-3-hydroxy-4-(*p*-tolyl)butanoic Acid (12b)

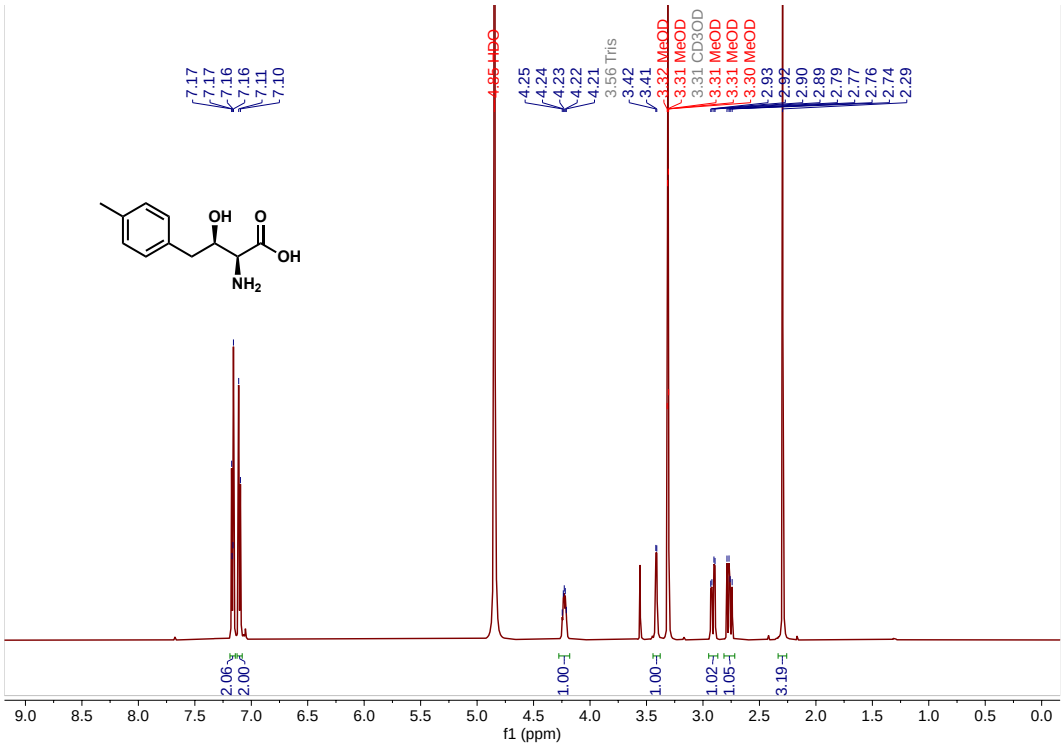

^{1}H NMR spectrum in CD_3OD at 500 MHz

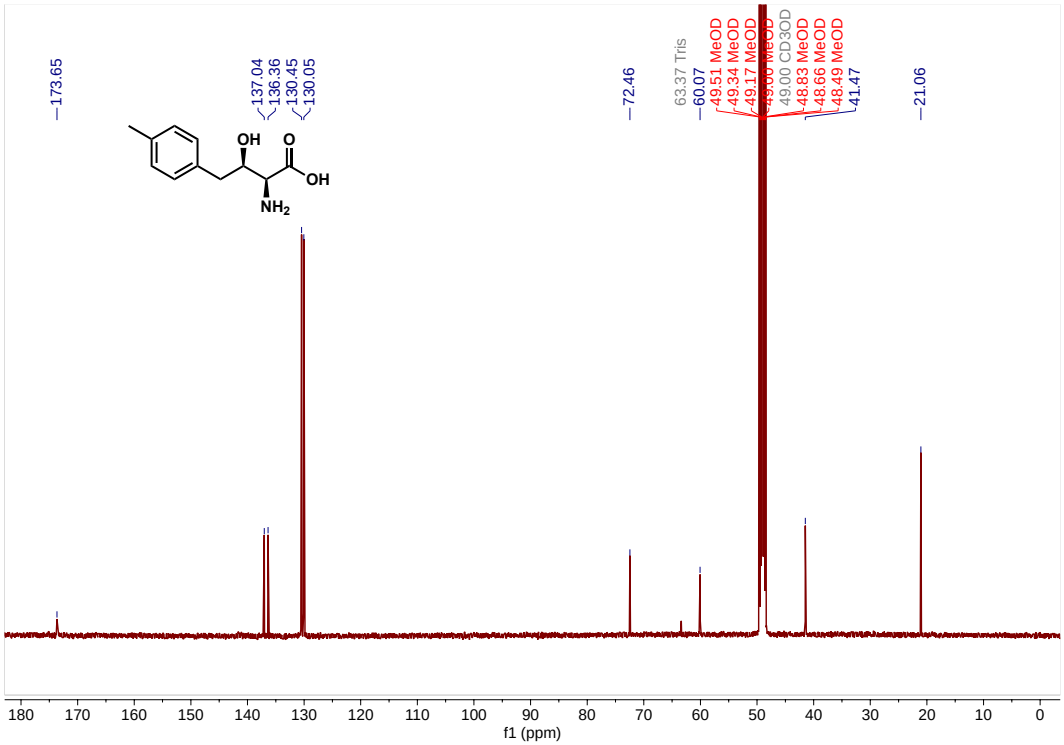

^{13}C NMR spectrum in CD_3OD at 126 MHz

(2*S*,3*R*)-2-Amino-3-hydroxy-4-(*p*-isopropylphenyl)butanoic Acid (13b)

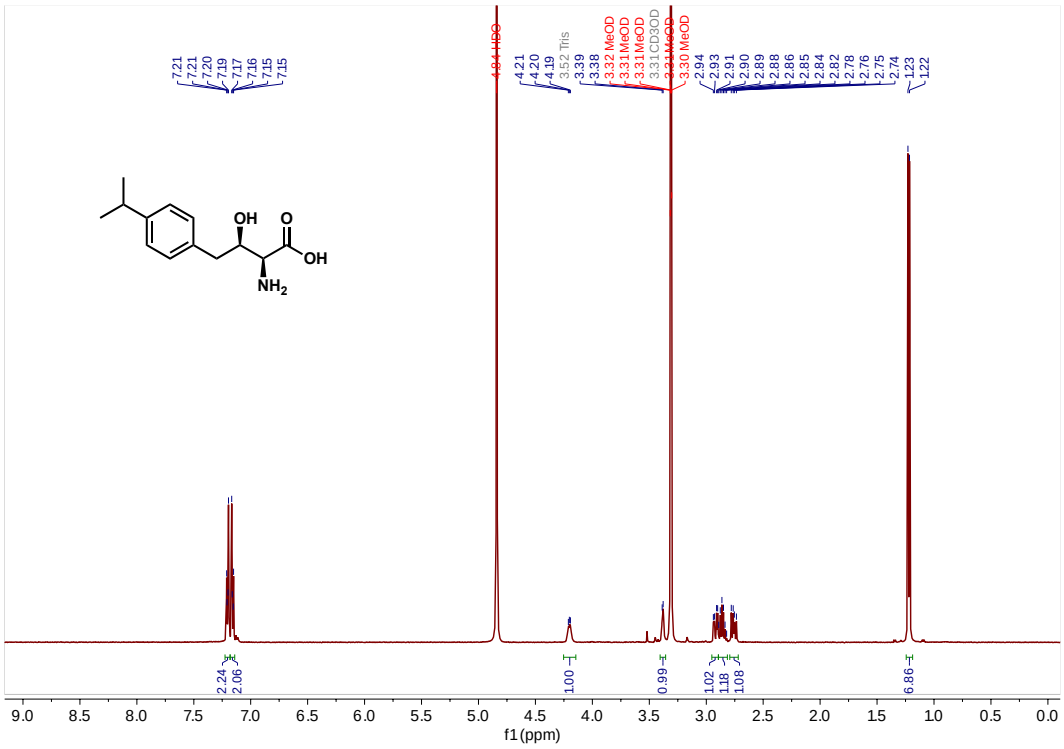

^{1}H NMR spectrum in CD_3OD at 500 MHz

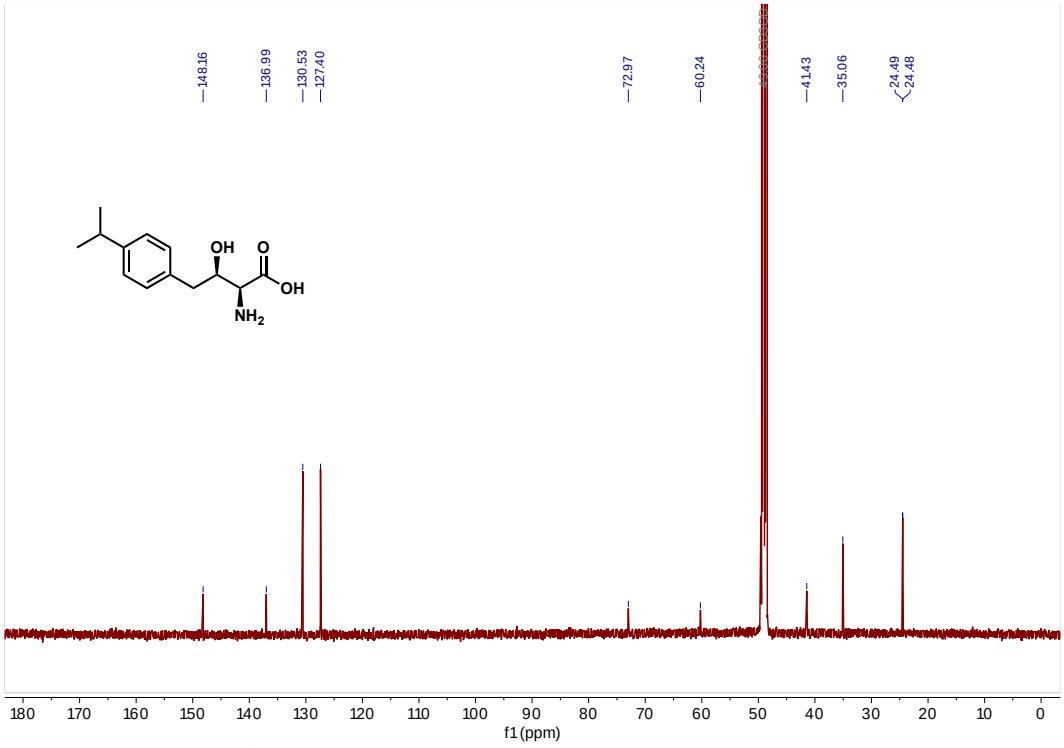

^{13}C NMR spectrum in CD_3OD at 126 MHz

(2*S*,3*R*)-2-Amino-3-hydroxy-4-mesitylbutanoic Acid (14b)

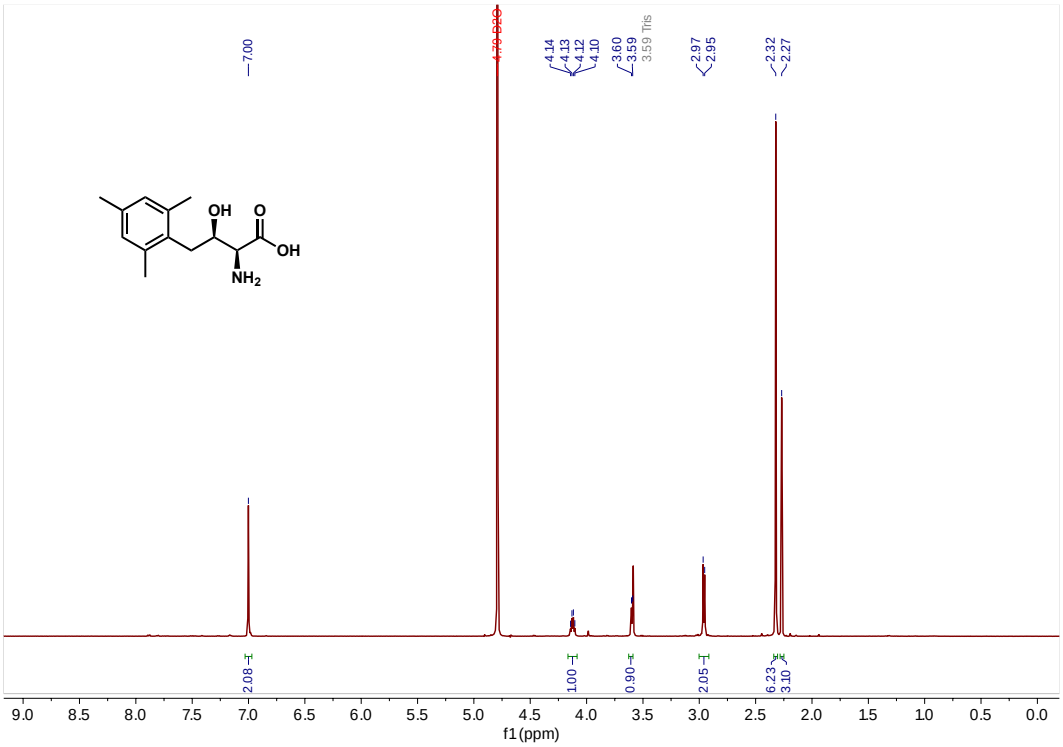

^{1}H NMR spectrum in D_2O at 500 MHz

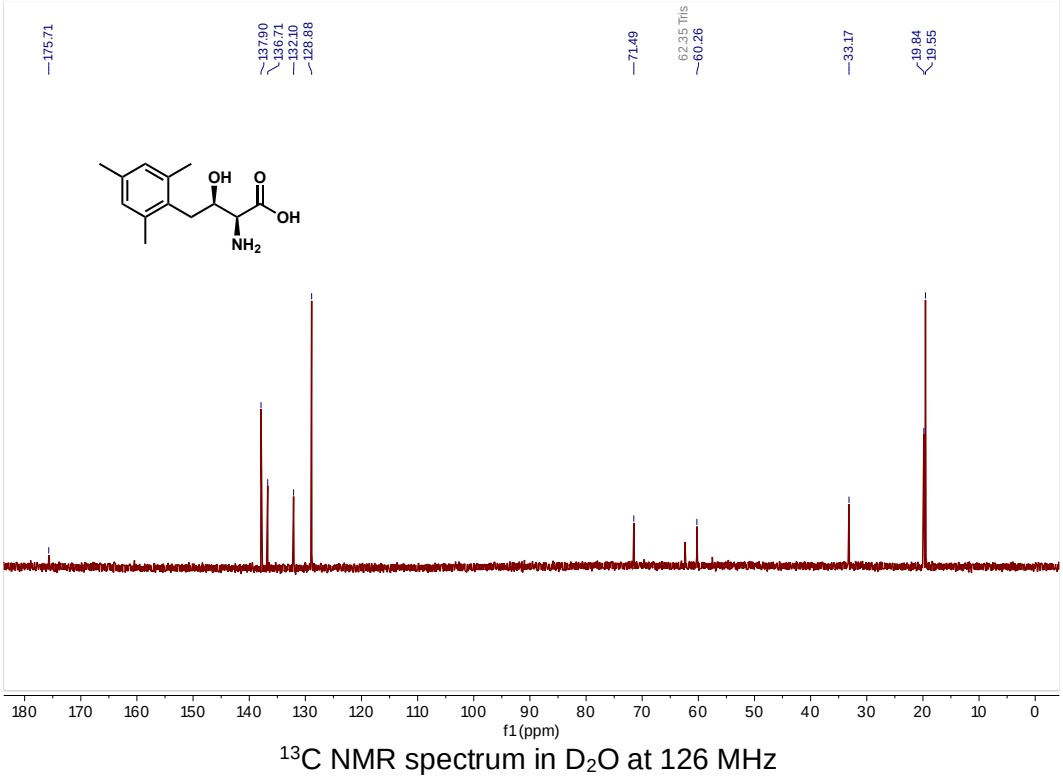

^{13}C NMR spectrum in D_2O at 126 MHz

(2*S*,3*R*)-2-Amino-3-hydroxy-4-(naphthalen-1-yl)butanoic Acid (15b)

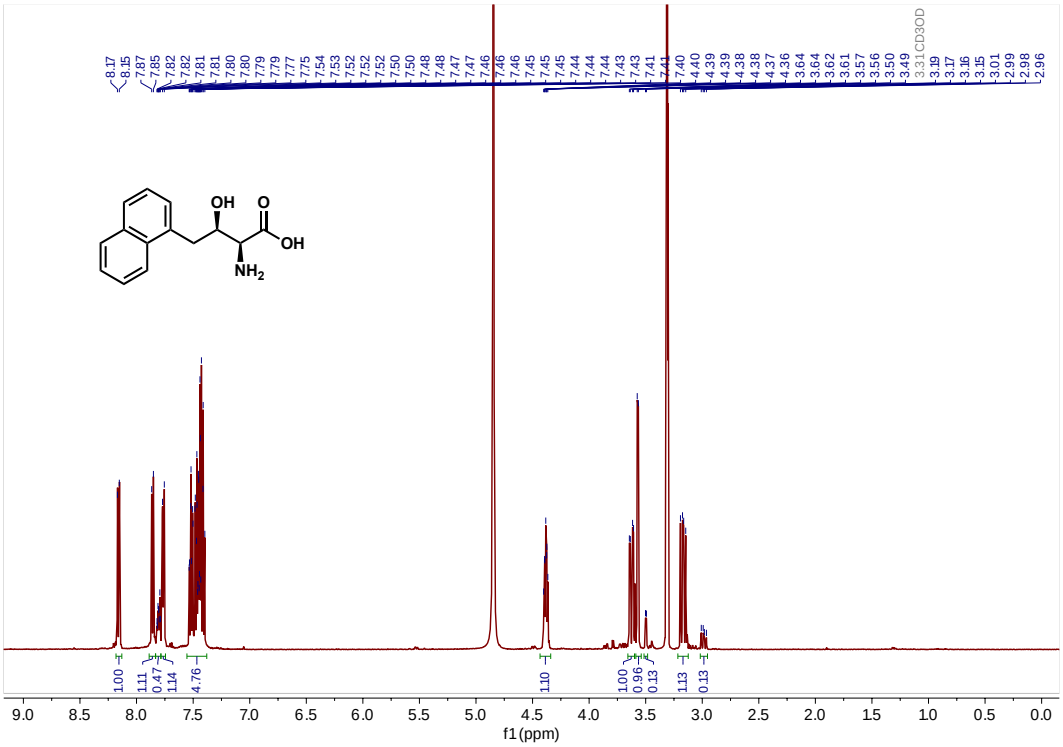

^{1}H NMR spectrum in CD_3OD at 500 MHz

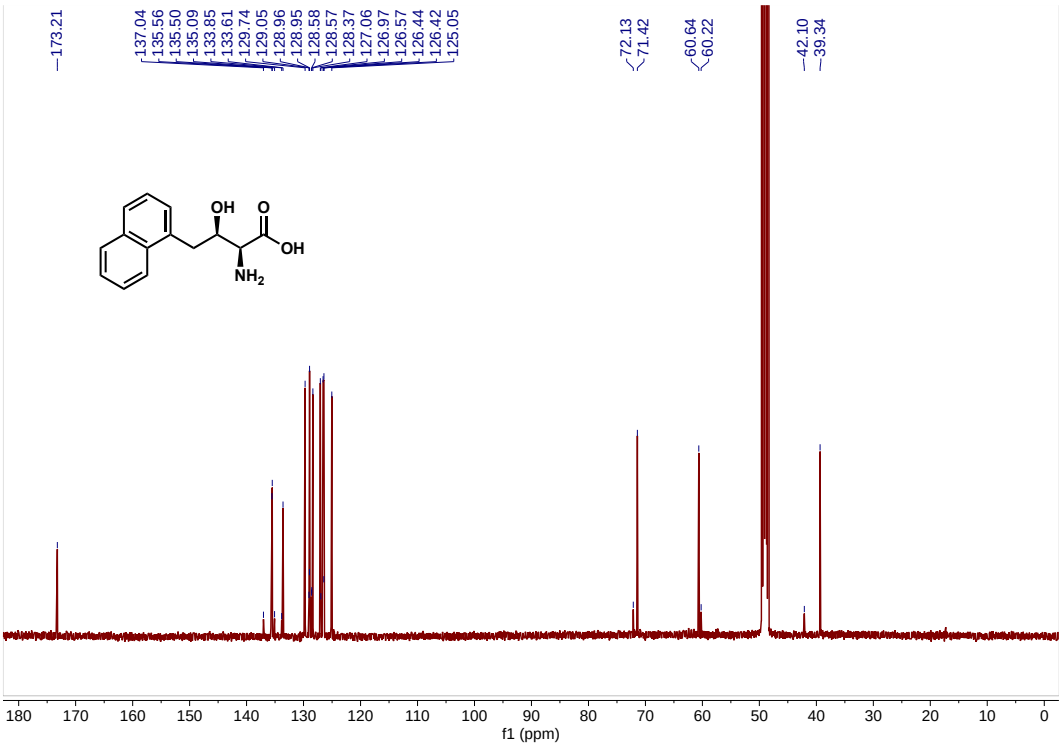

^{13}C NMR spectrum in CD_3OD at 126 MHz

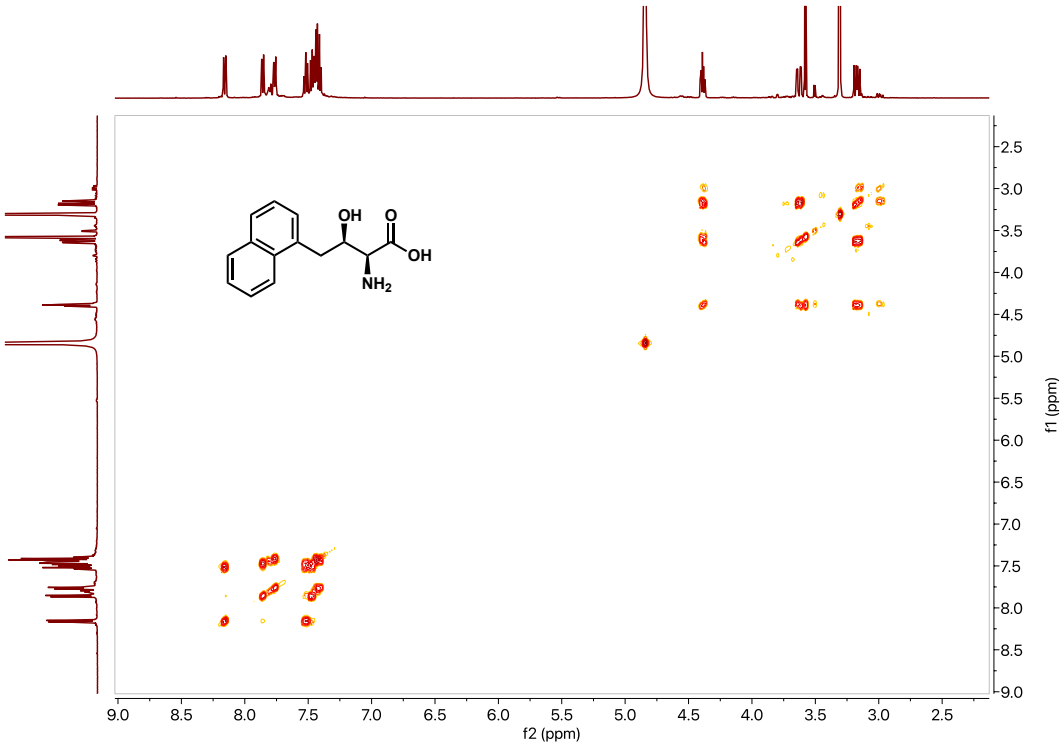

COSY Spectrum in CD_3OD at 500 MHz

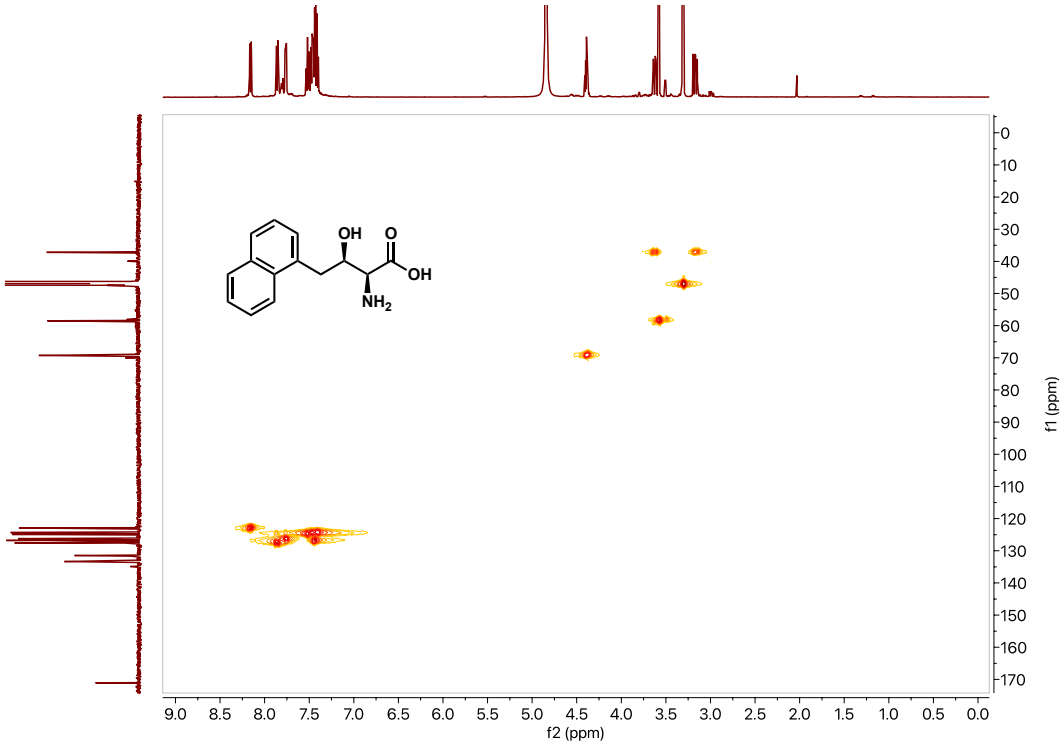

HSQC Spectrum in CD_3OD at 500 MHz and 126 MHz

2-(Oxiran-2-yl)furan (16a)

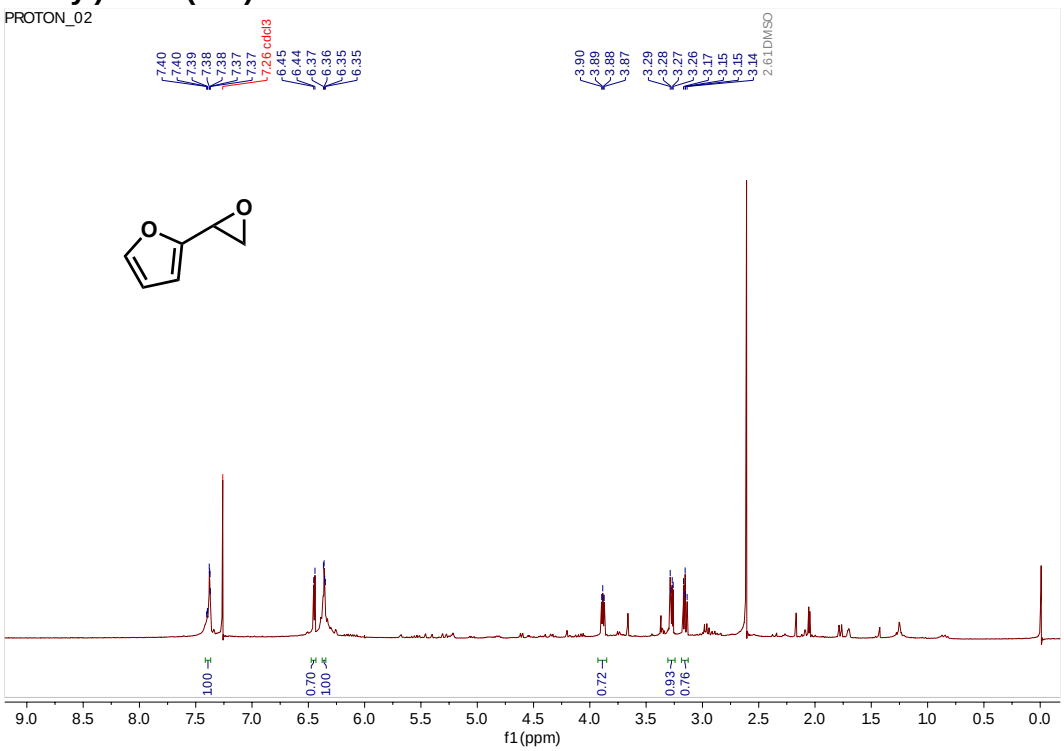

^{1}H NMR spectrum in $CDCl_3$ at 300 MHz

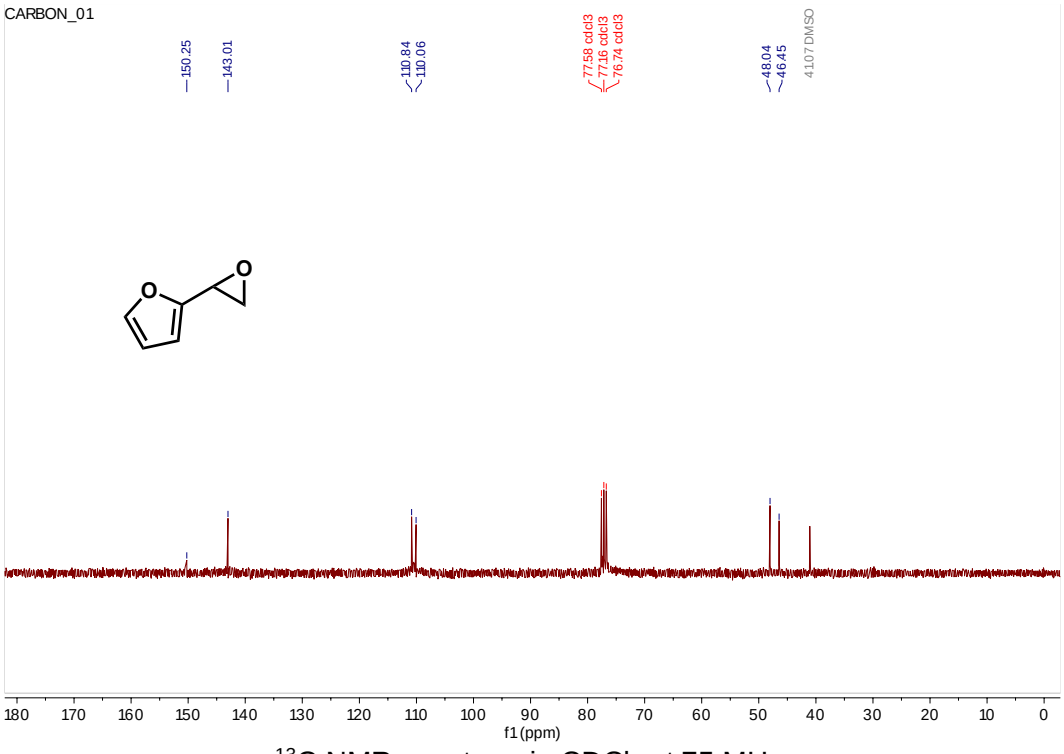

^{13}C NMR spectrum in $CDCl_3$ at 75 MHz

(2*S*,3*R*)-2-amino-4-(furan-2-yl)-3-hydroxybutanoic Acid (16b)

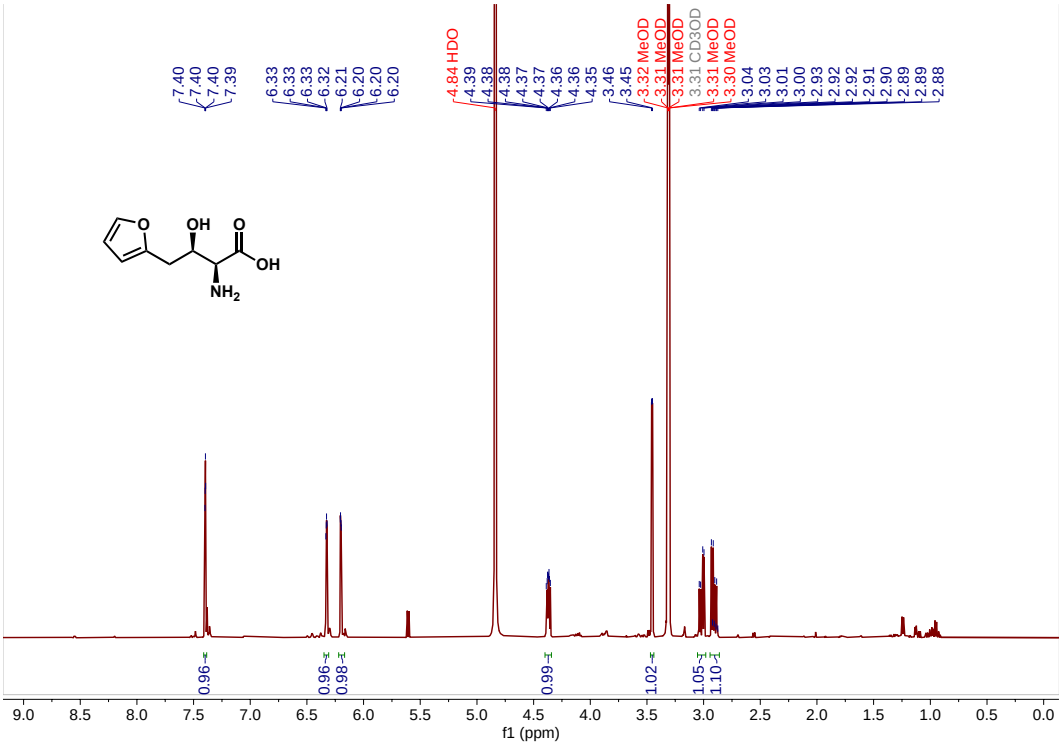

^{1}H NMR spectrum in CD_3OD at 500 MHz

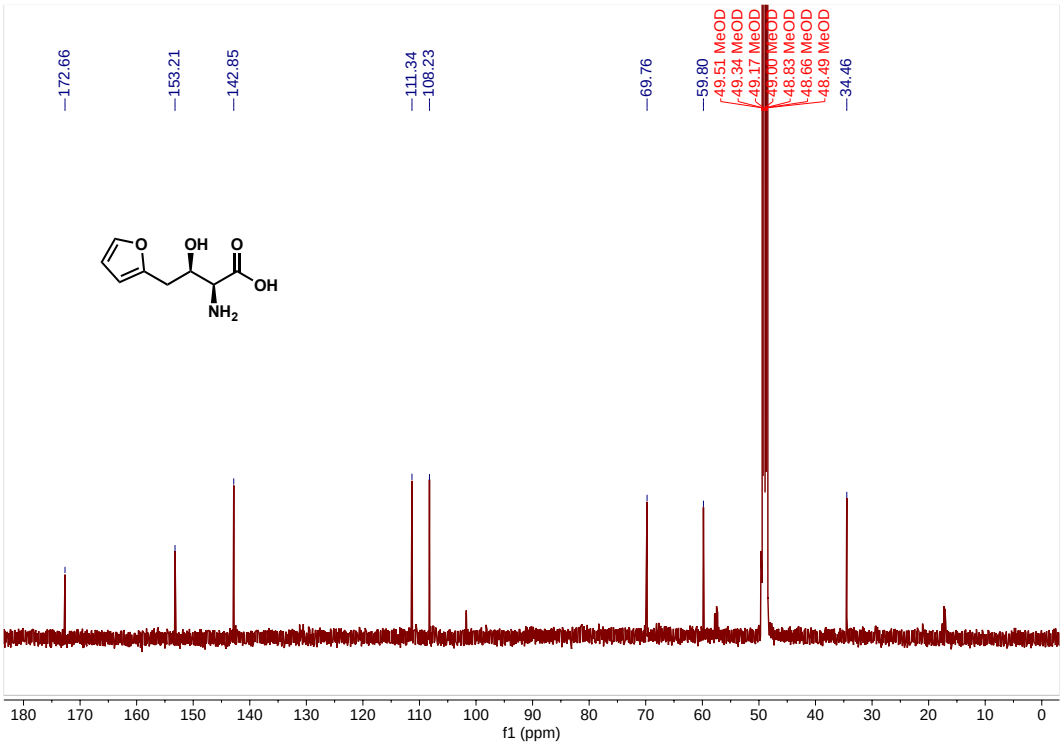

^{13}C NMR spectrum in CD_3OD at 126 MHz

(2*S*,3*R*)-2-Amino-3-hydroxy-4-(thiophen-2-yl)butanoic Acid (17b)

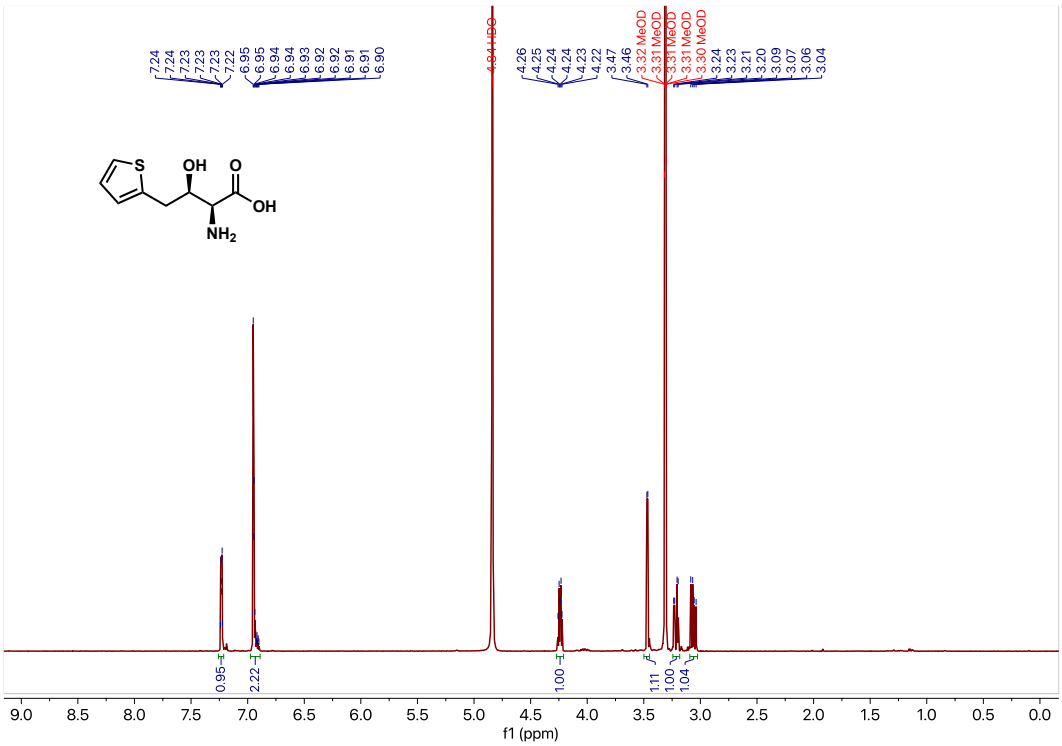

^{1}H NMR spectrum in CD_3OD at 500 MHz

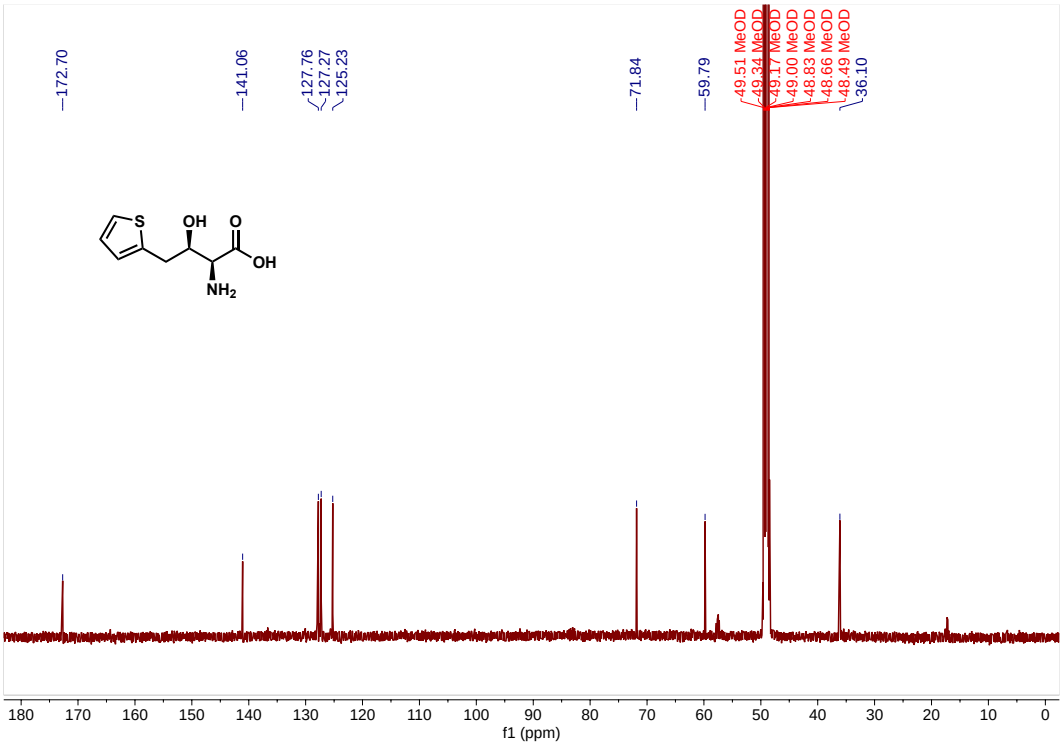

^{13}C NMR spectrum in CD_3OD at 126 MHz

(2*S*,3*R*,*4R*)-2-Amino-3-hydroxy-4-phenylpentanoic Acid (18b-major) and (2*S*,3*R*,*4S*)-2-Amino-3-hydroxy-4-phenylpentanoic Acid (18b-minor)

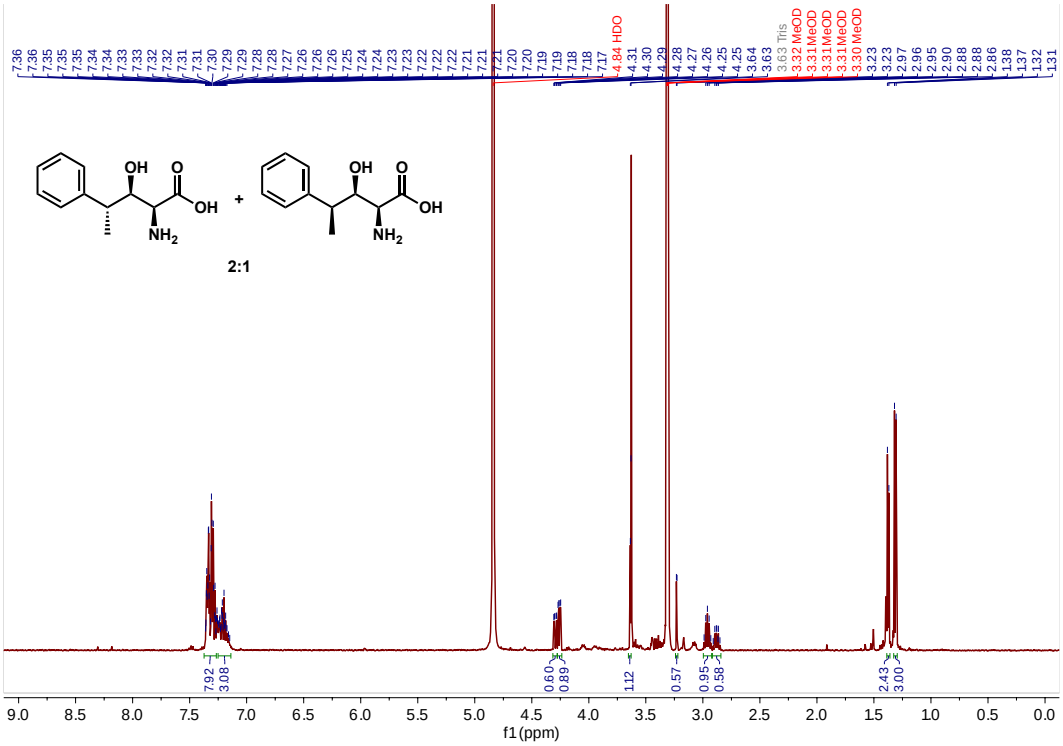

^{1}H NMR spectrum in CD_3OD at 500 MHz

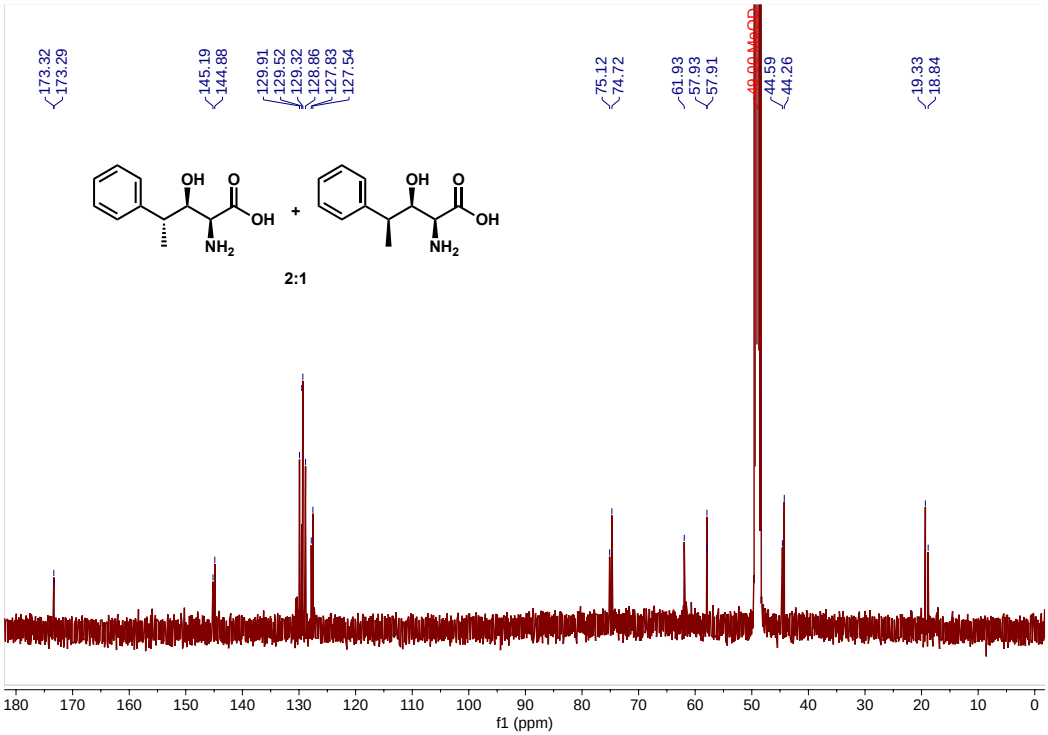

^{13}C NMR spectrum in CD_3OD at 126 MHz

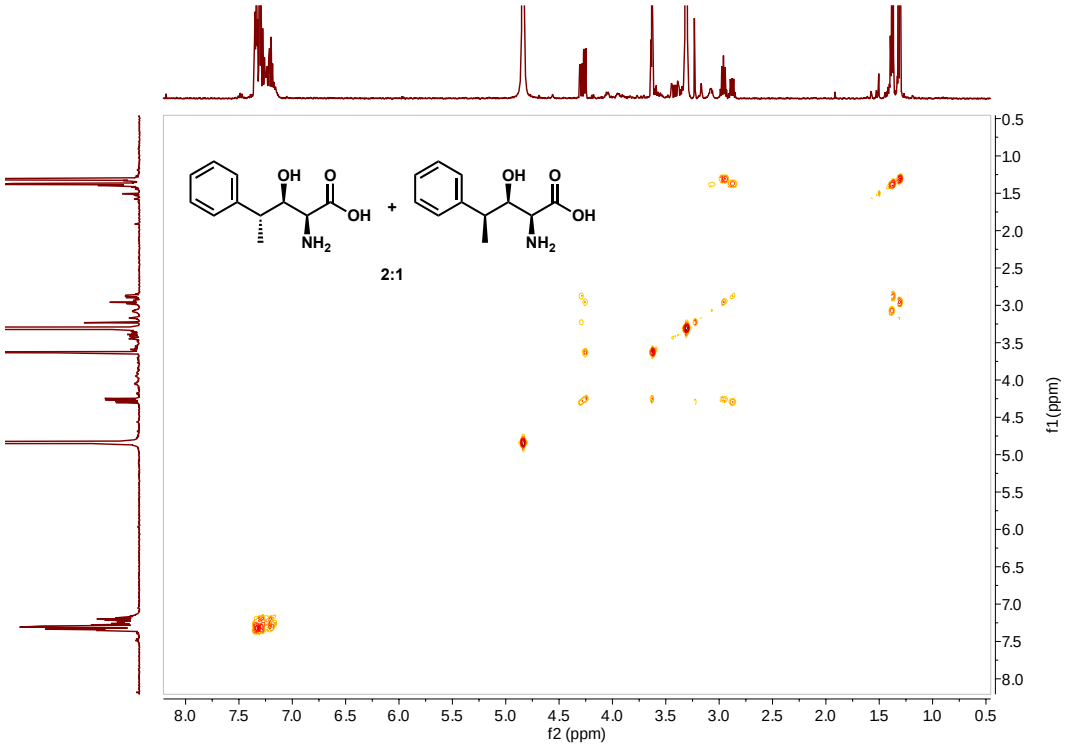

COSY Spectrum in CD_3OD at 500 MHz

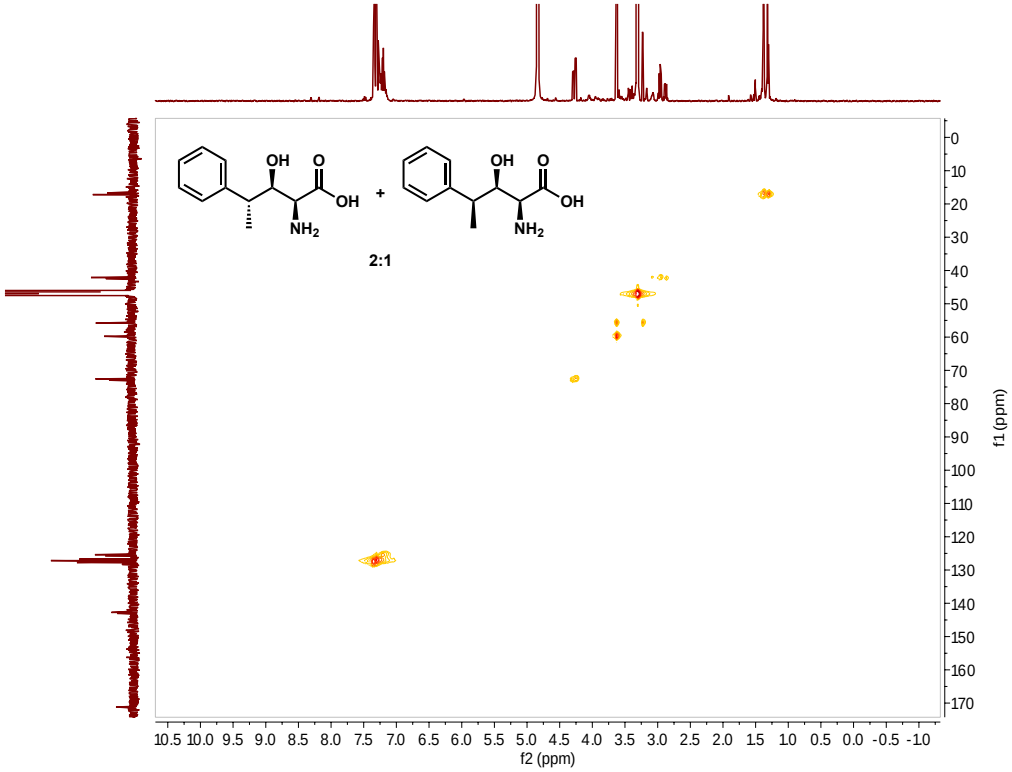

HSQC Spectrum in CD_3OD at 500 MHz and 126 MHz

2,3-Dihydrospiro[indene-1,2'-oxirane] (19a)

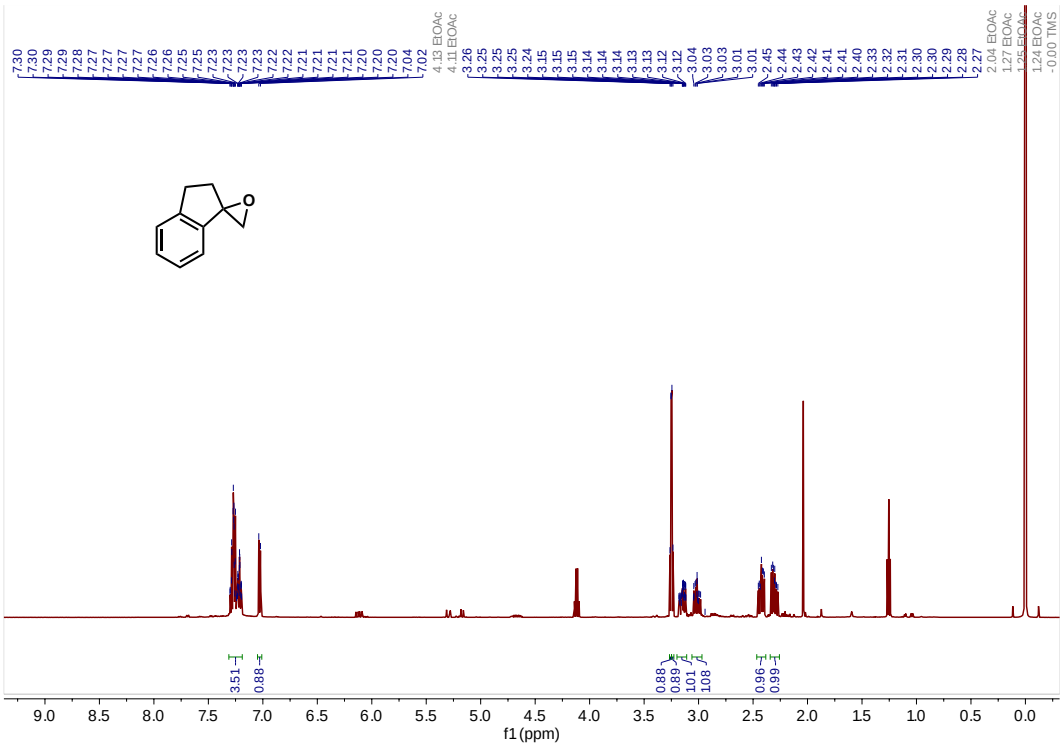

^{1}H NMR spectrum in $CDCl_3$ at 500 MHz

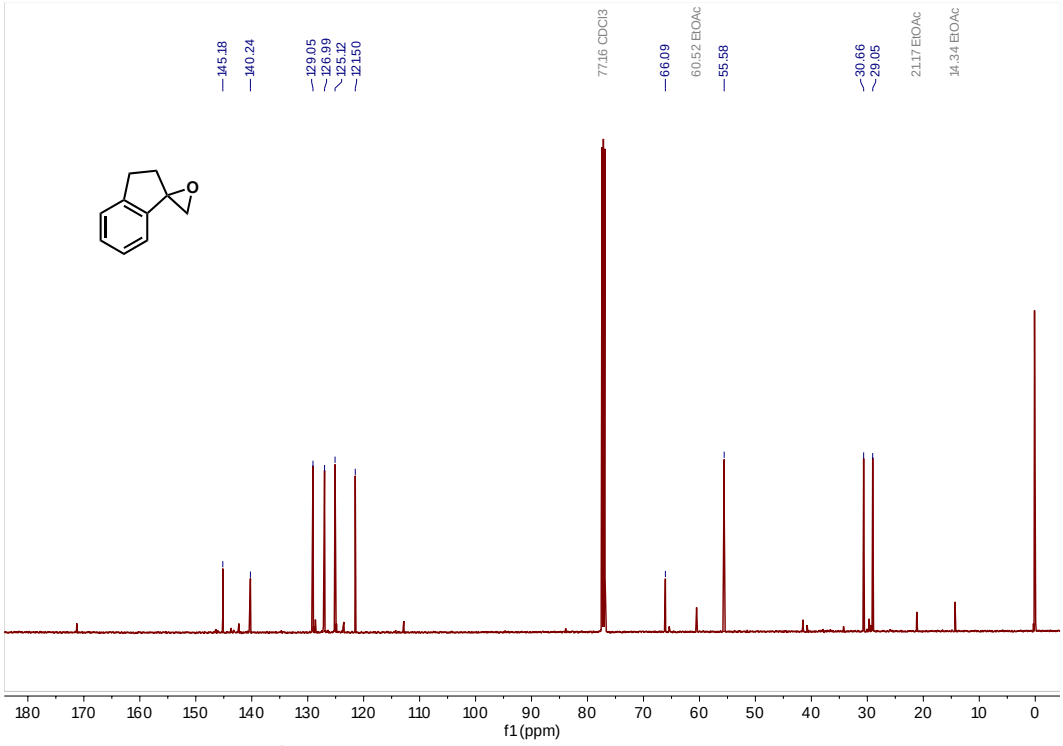

^{13}C NMR spectrum in $CDCl_3$ at 126 MHz

(2*S*,3*R*)-2-Amino-3-(2,3-dihydro-1*H*-inden-1-yl)-3-hydroxypropanoic Acid (19b)

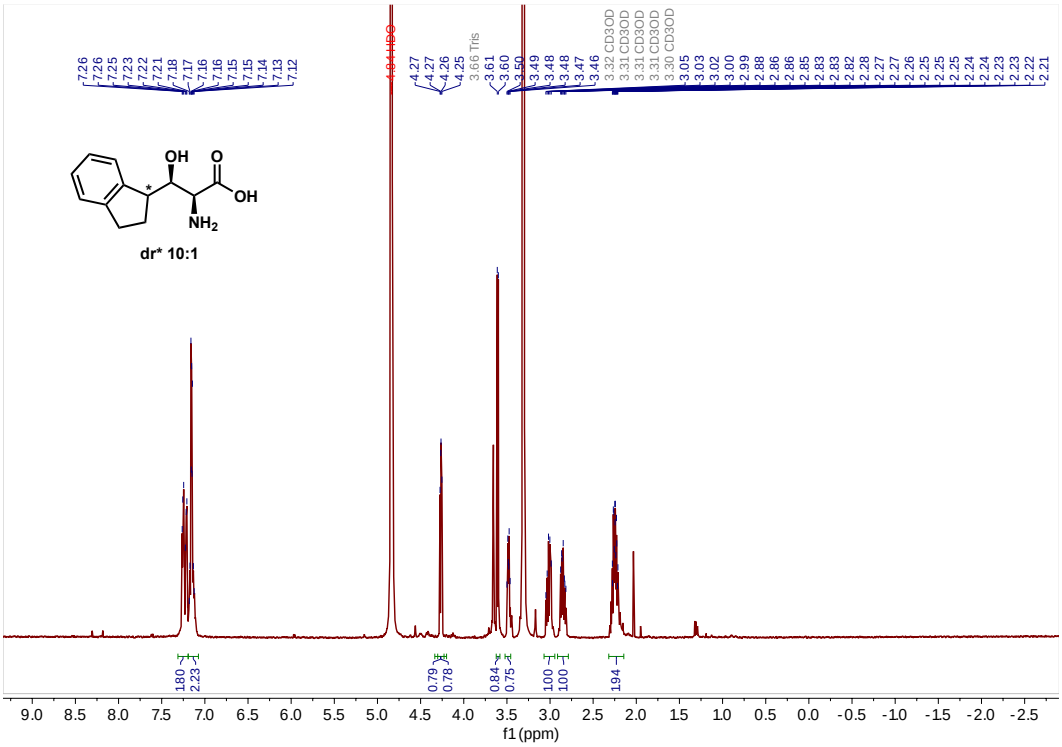

^{1}H NMR spectrum in CD_3OD at 500 MHz

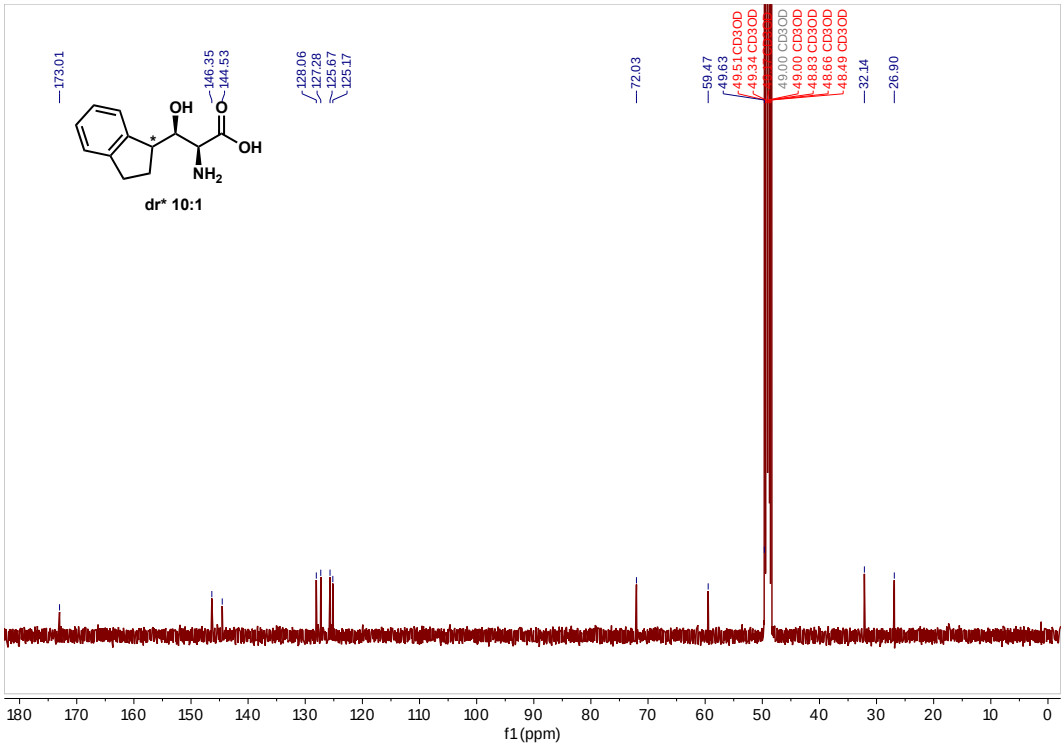

^{13}C NMR spectrum in CD_3OD at 126 MHz

(2*S*,3*R*,*E*)-2-Amino-3-hydroxy-6-phenylhex-5-enoic Acid (20b)

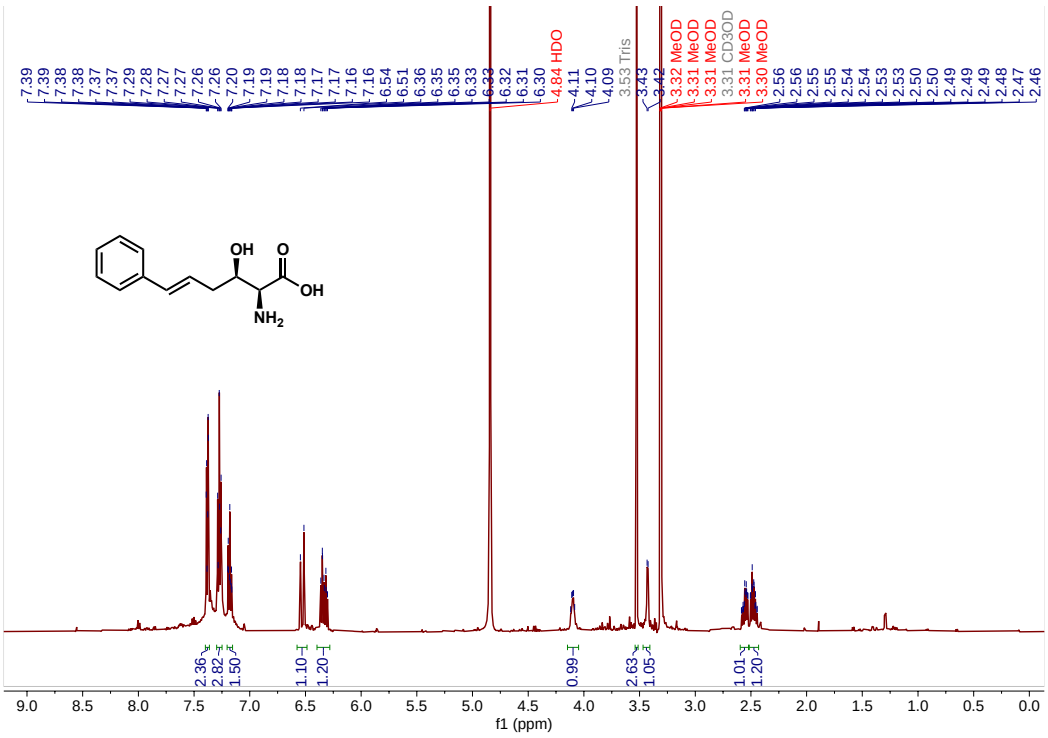

^{1}H NMR spectrum in CD_3OD at 500 MHz

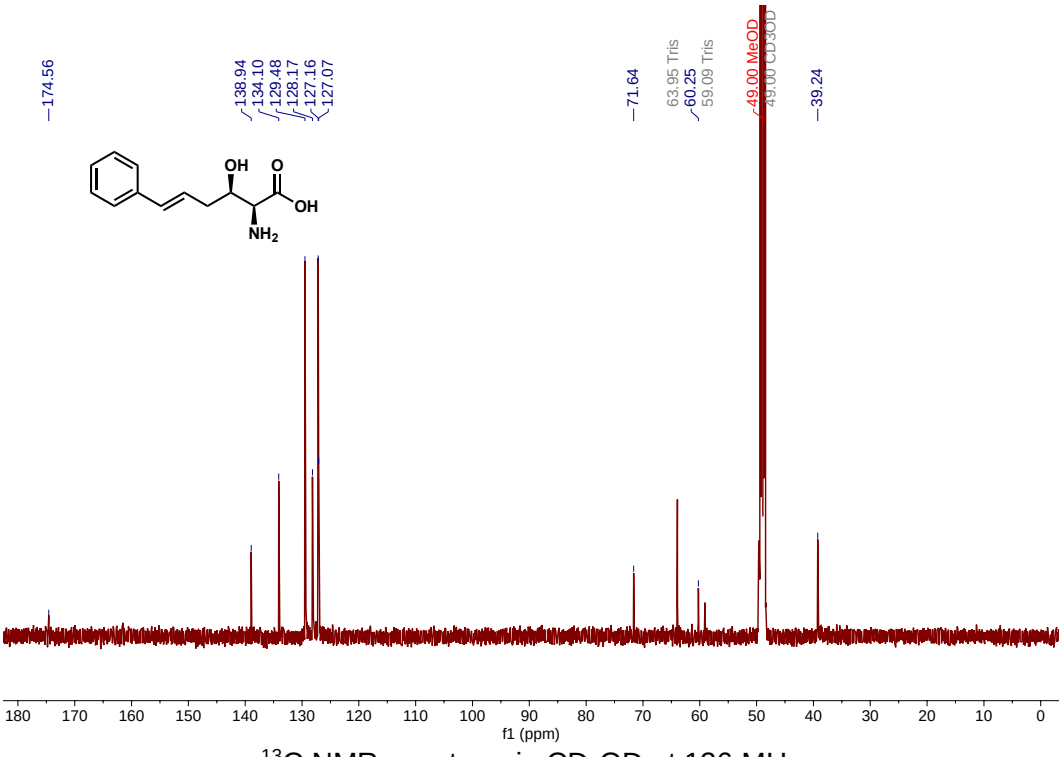

^{13}C NMR spectrum in CD_3OD at 126 MHz

(2*S*,3*R*,*E*)-2-Amino-3-hydroxy-5-methyl-6-phenylhex-5-enoic Acid (21b)

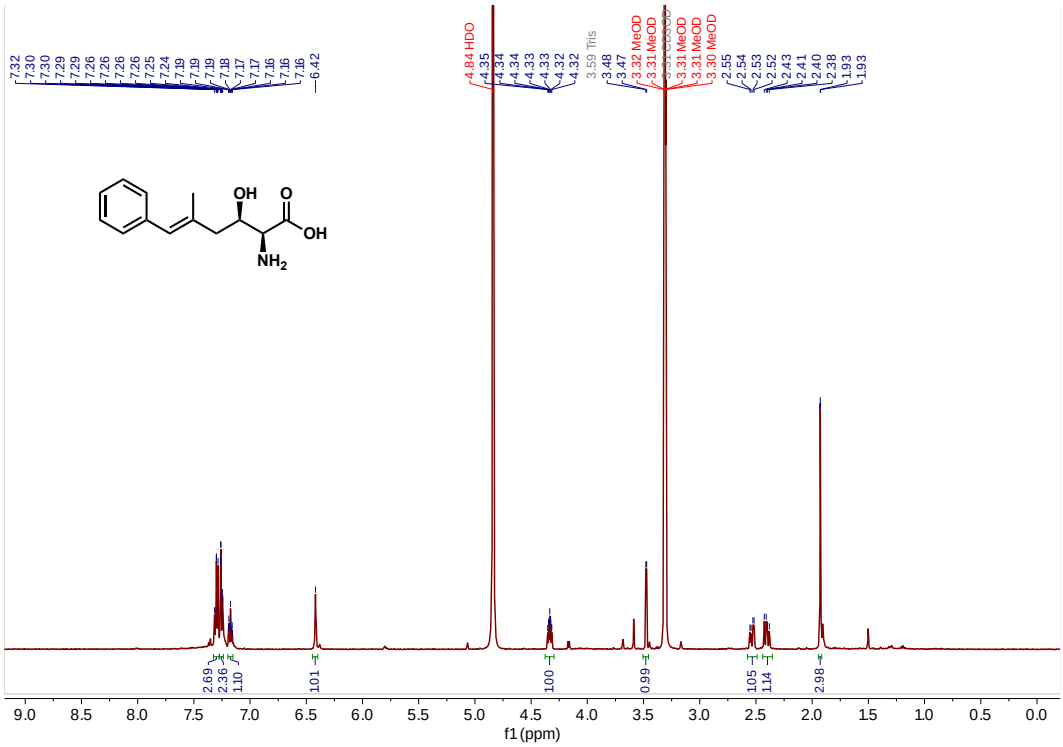

^{1}H NMR spectrum in CD_3OD at 500 MHz

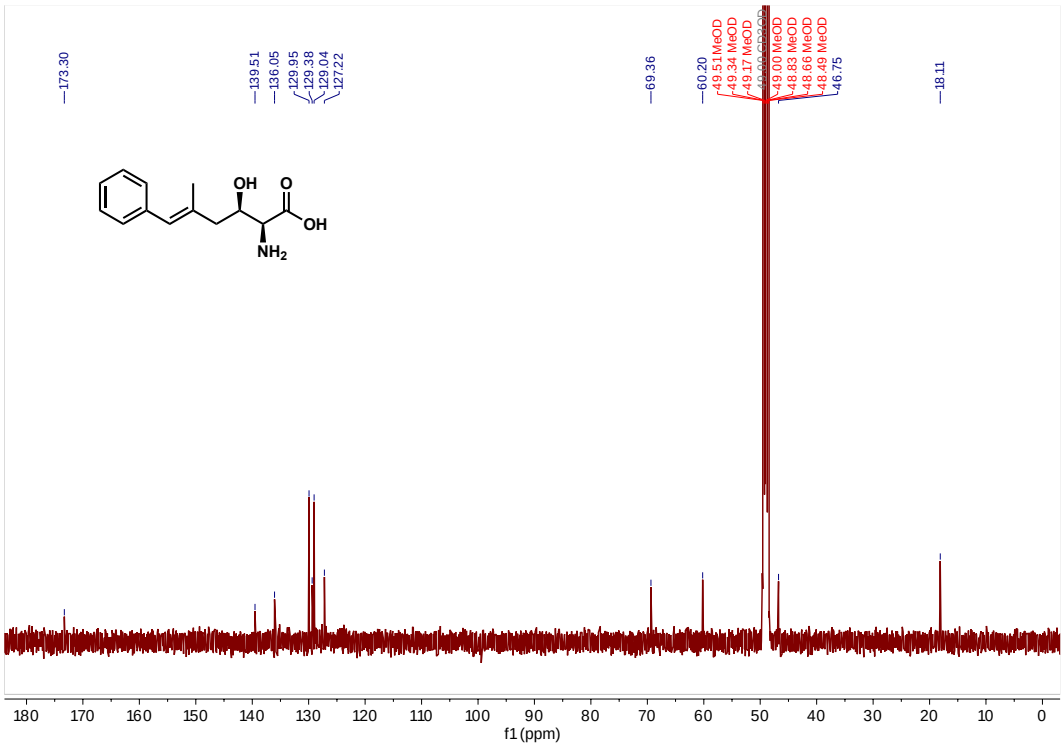

^{13}C NMR spectrum in CD_3OD at 126 MHz

(2*S*,3*R*)-2-Amino-3-hydroxy-4-phenylbutanoic-4-*d* Acid (2b-4-d_1)

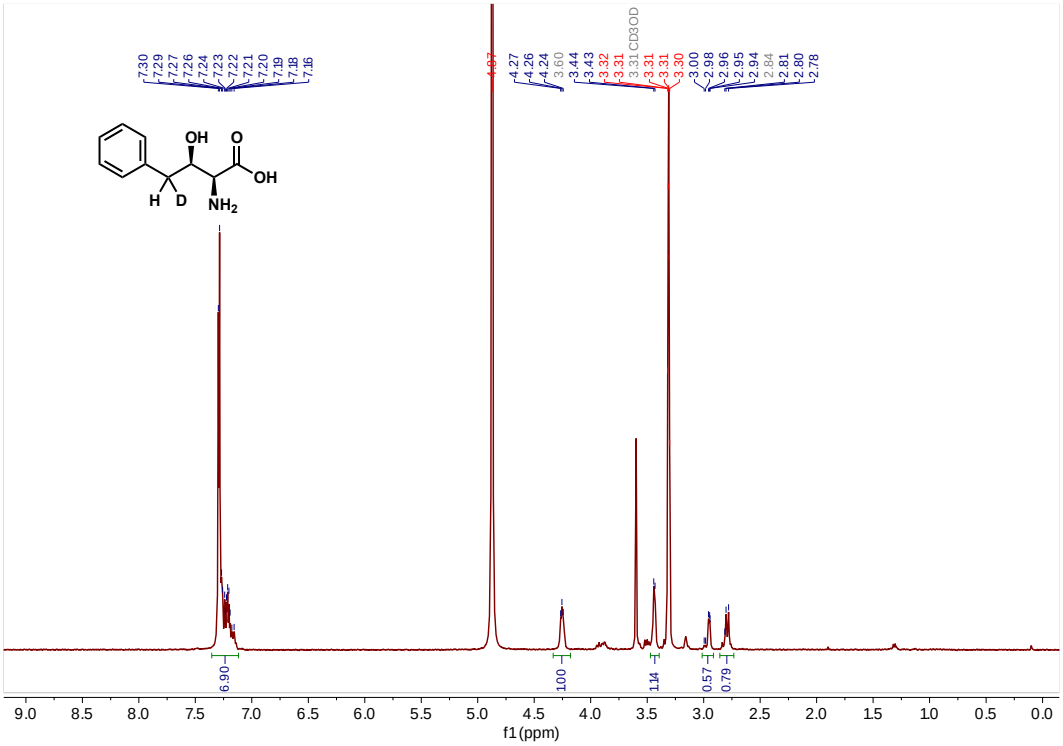

^{1}H NMR spectrum in CD_3OD at 500 MHz

(2*S*,3*R*)-2-Amino-3-hydroxy-4-phenylbutanoic-4,4-d_2 Acid (2b-4,4-d_2)

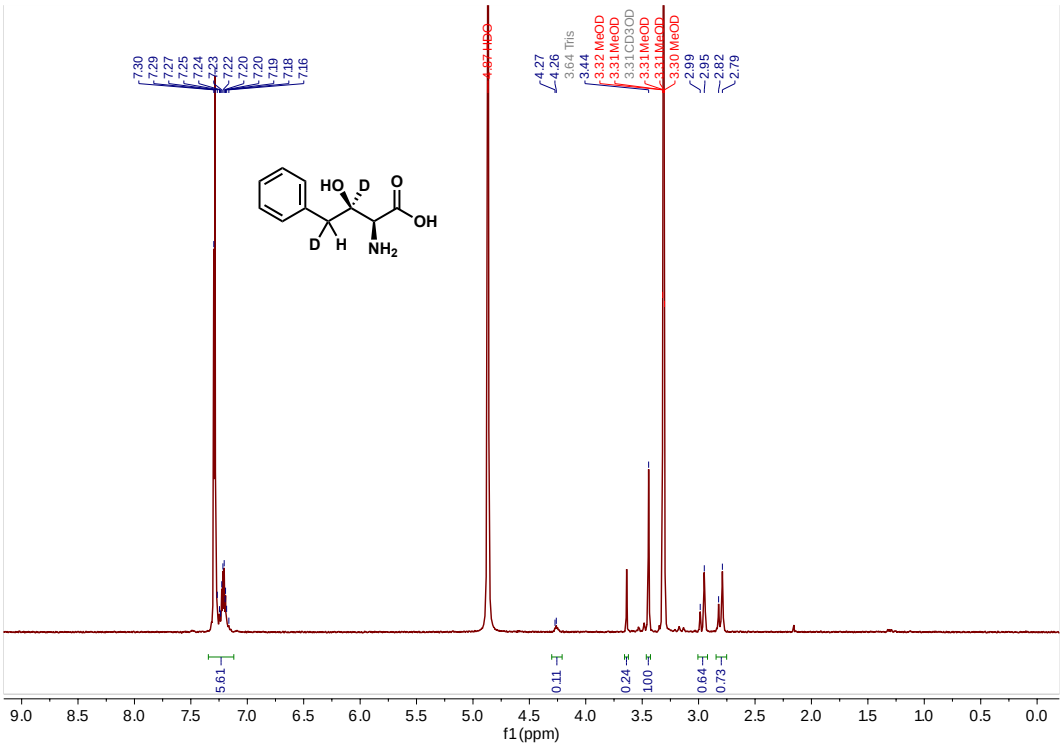

^{1}H NMR spectrum in CD_3OD at 500 MHz

(2*S*,3*R*)-2-Amino-3-hydroxy-4-phenylbutanoic-4,4-*d*$_2$ Acid (2b-4,4-*d*$_2$) via reaction in D_2O

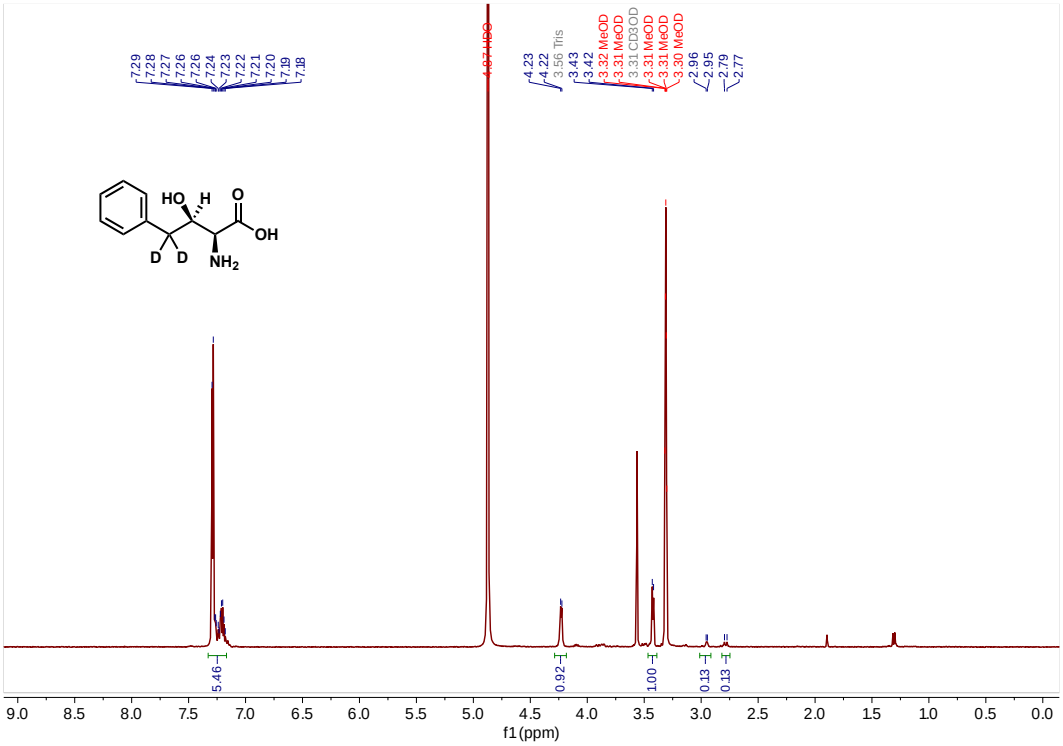

^{1}H NMR spectrum in CD_3OD at 500 MHz

(2*S*,3*R*)-2-Amino-3-hydroxy-4-phenylbutanoic-3-*d* Acid (2b-3-*d*$_1$) via **(±)-*cis*-2a-3-*d*$_1$**

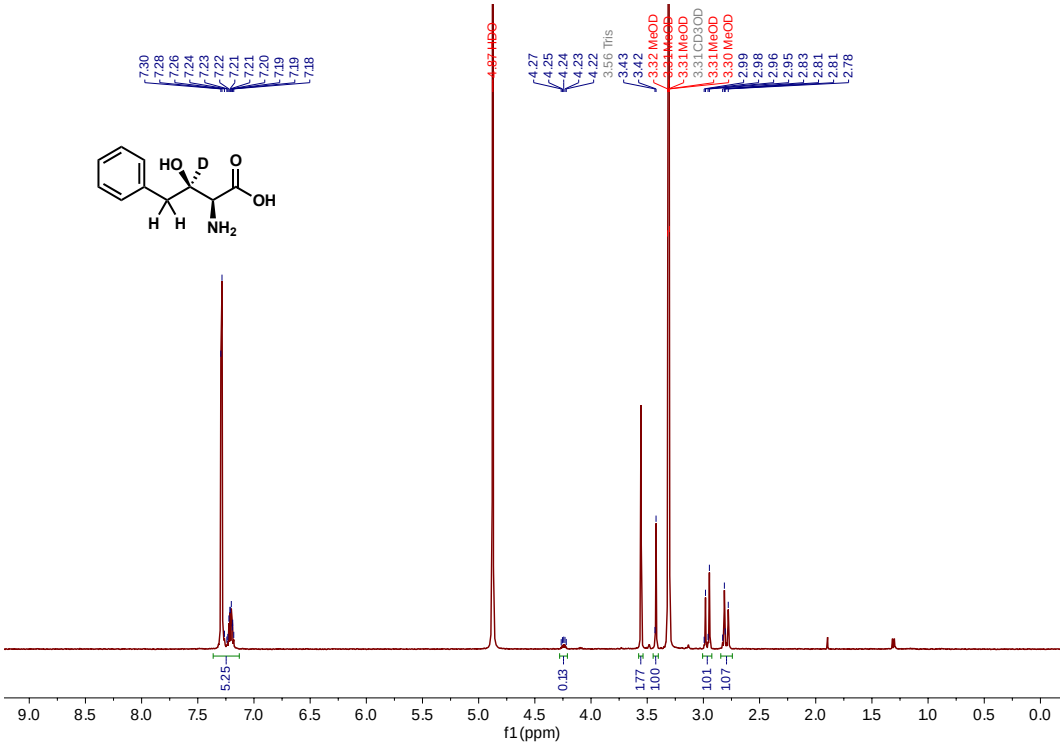

^{1}H NMR spectrum in CD_3OD at 500 MHz

(2*S*,3*R*)-2-Amino-3-hydroxy-4-phenylbutanoic-4-*d* Acid (2b-4-d_1) via **(±)-*trans*-2a-3-d_1**

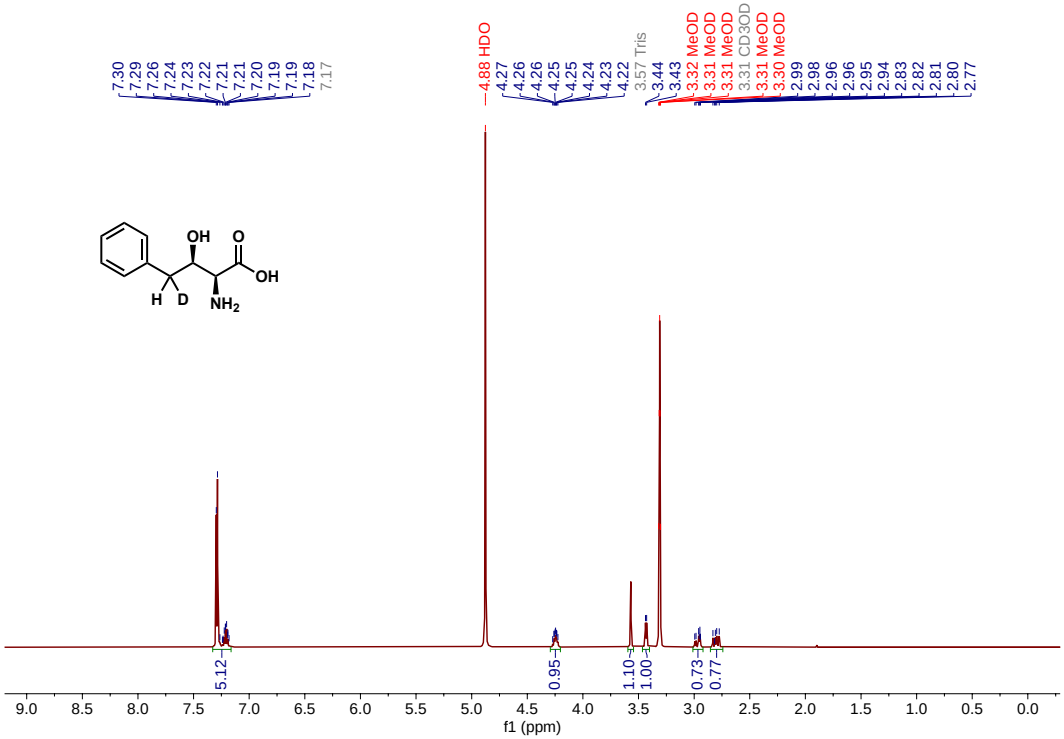

^{1}H NMR spectrum in CD_3OD at 500 MHz

(2*S*,3*R*)-2-Amino-3-hydroxy-4-phenylbutanoic-4-*d* Acid (2b-4-d_1) via **(±)-*trans*-2a-3-d_1** + ObiH

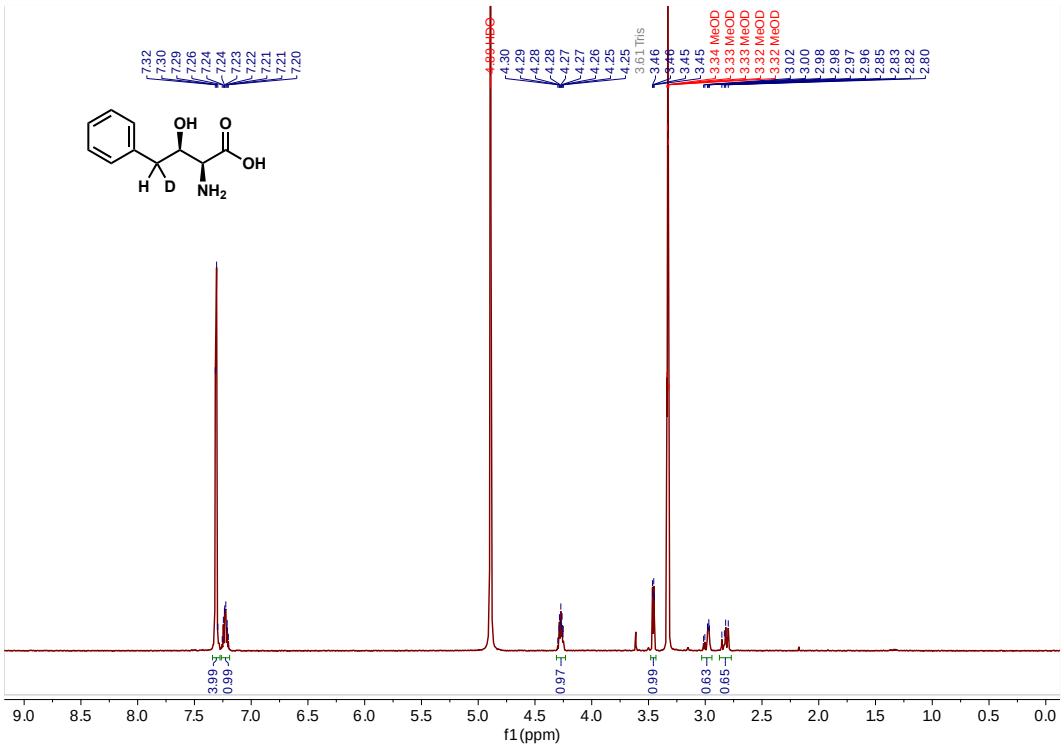

^{1}H NMR spectrum in CD_3OD at 500 MHz

(2*S*,4*R*)-2-Amino-4-hydroxy-5-phenylpentanoic Acid (24)

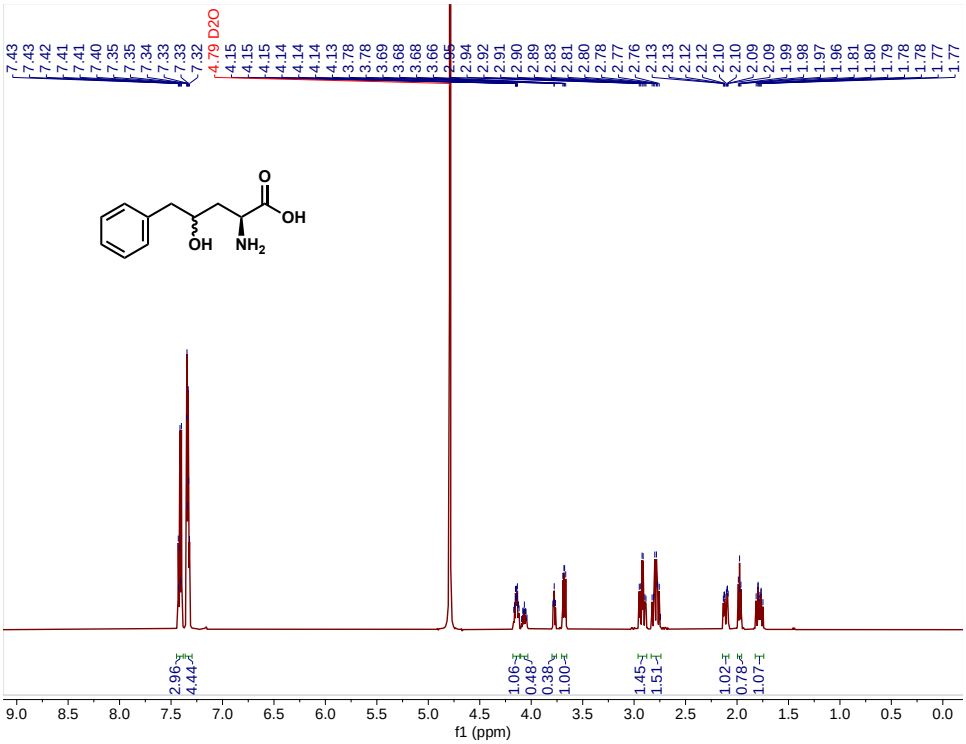

^{1}H NMR spectrum in D_2O at 500 MHz

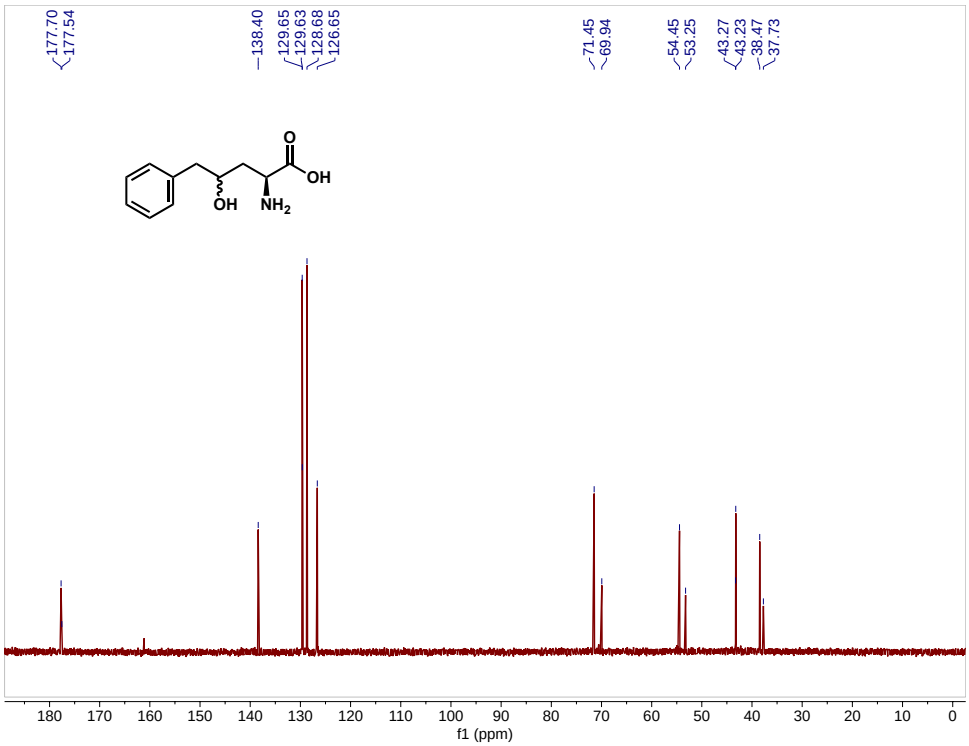

^{13}C NMR spectrum in D_2O at 126 MHz

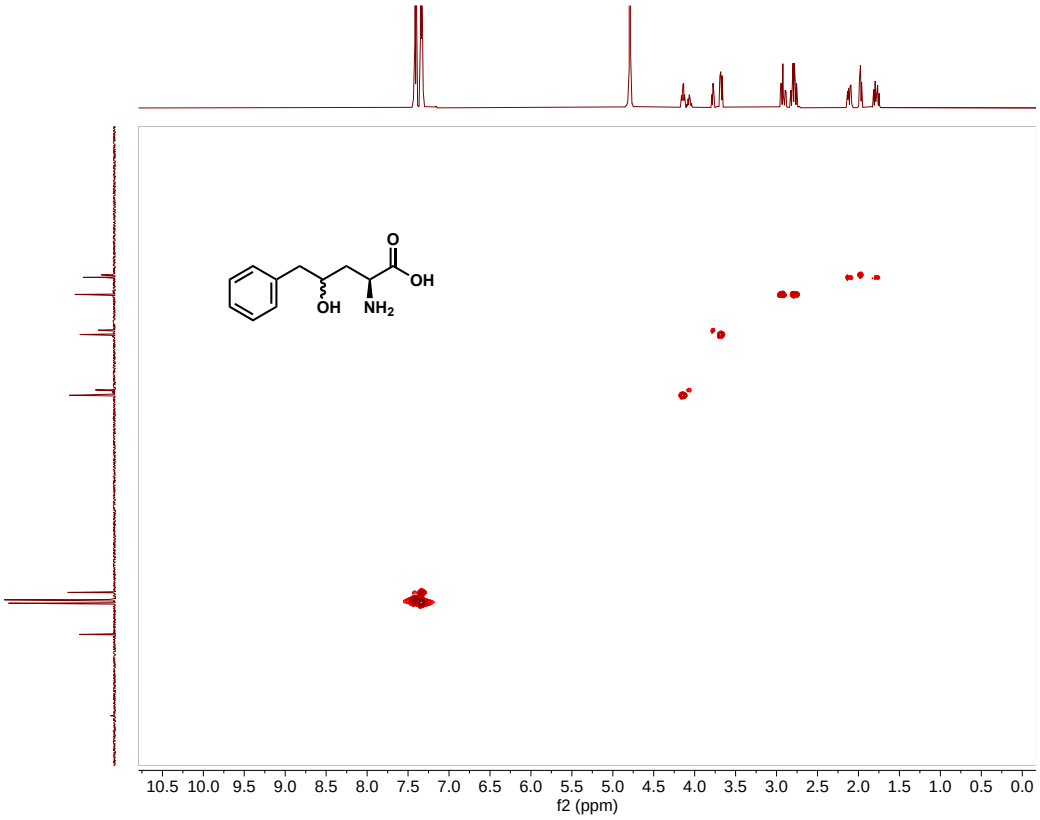

HSQC Spectrum in D_2O at 500 MHz and 126 MHz

(2*S*,4*R*)-2-Amino-4-hydroxy-5-phenylpentanoic-2,5,5-d_3 Acid (24-2,5,5-d_3)

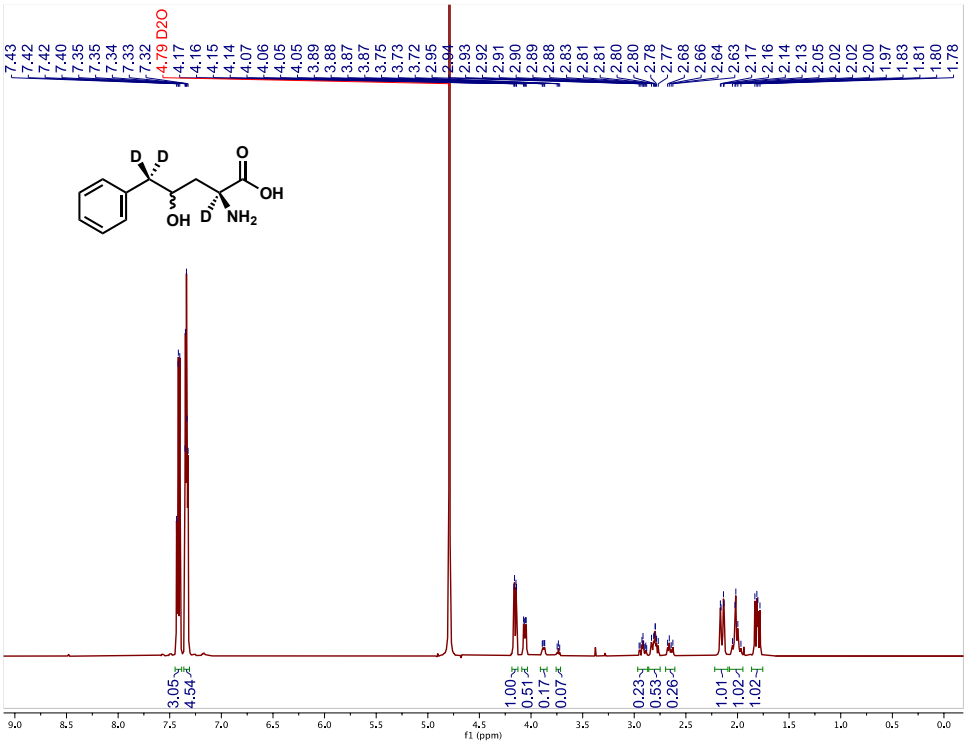

^1H Spectrum in D_2O at 500 MHz

(2*S*,4*R*)-2-Amino-5-(4-fluorophenyl)-4-hydroxypentanoic Acid (25)

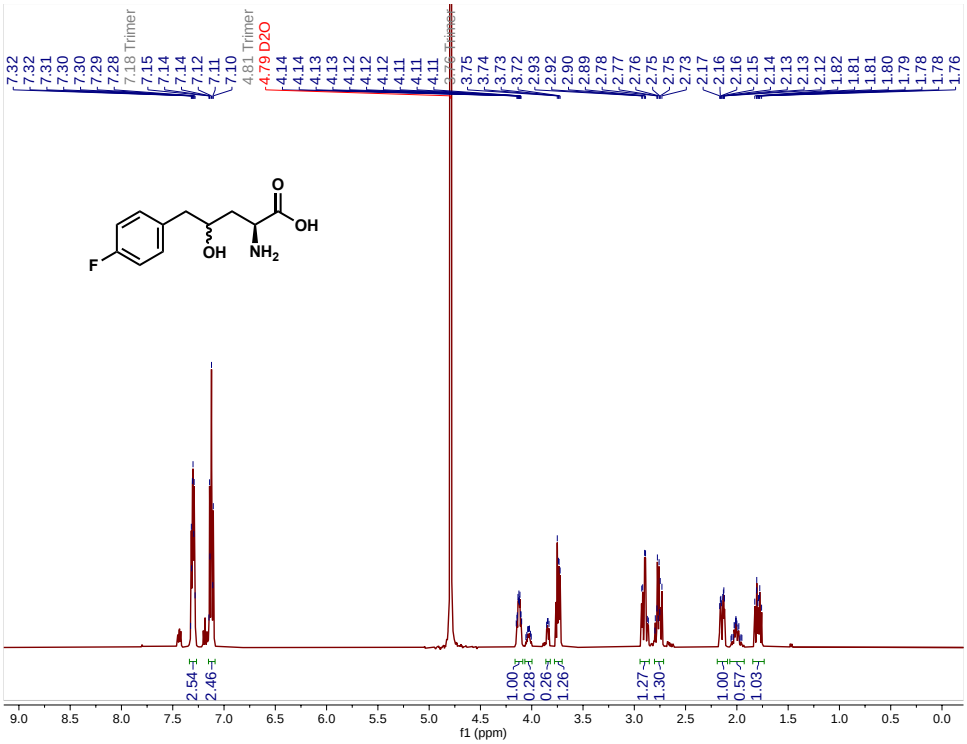

^{1}H NMR spectrum in D_2O at 500 MHz (Trimer = **26**, described below)

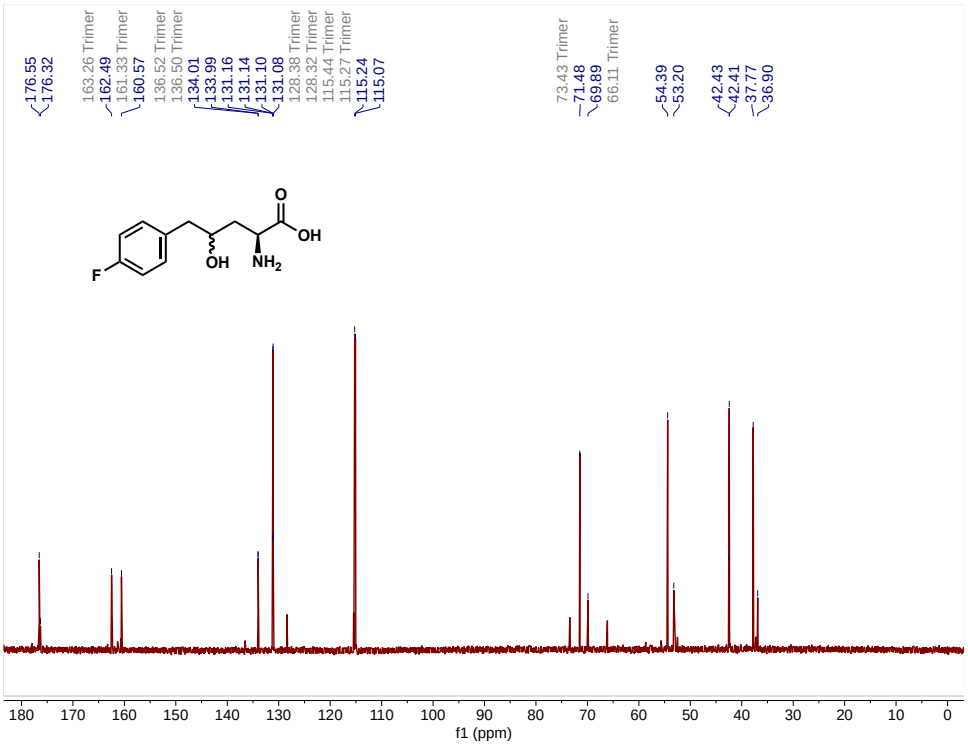

^{13}C NMR spectrum in D_2O at 126 MHz (Trimer = **26**, described below)

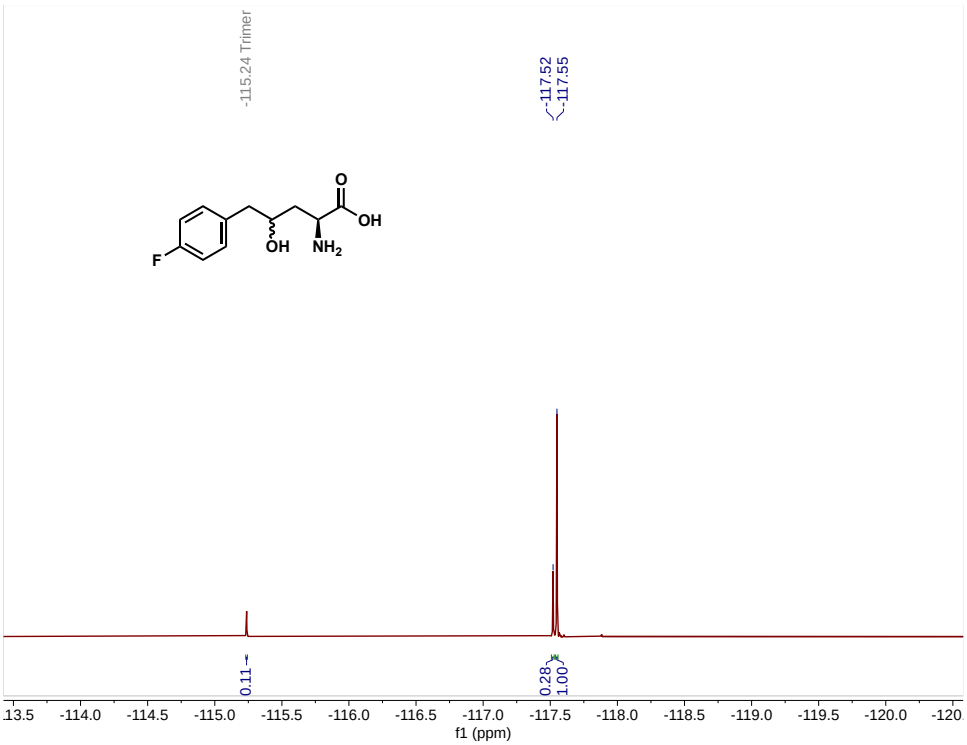

^{19}F NMR Spectrum in D_2O at 377 MHz (Trimer = **26**, described below)

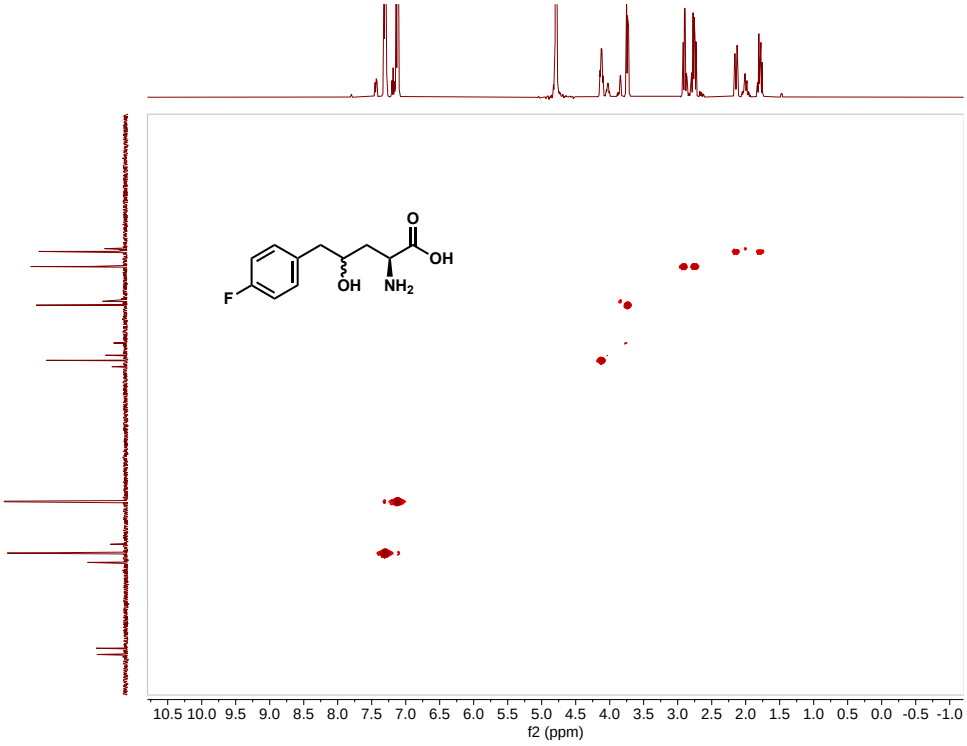

HSQC Spectrum in D_2O at 500 MHz and 126 MHz

(2*s*,4*s*,6*s*)-2,4,6-Tris(4-fluorobenzyl)-1,3,5-trioxane (26)

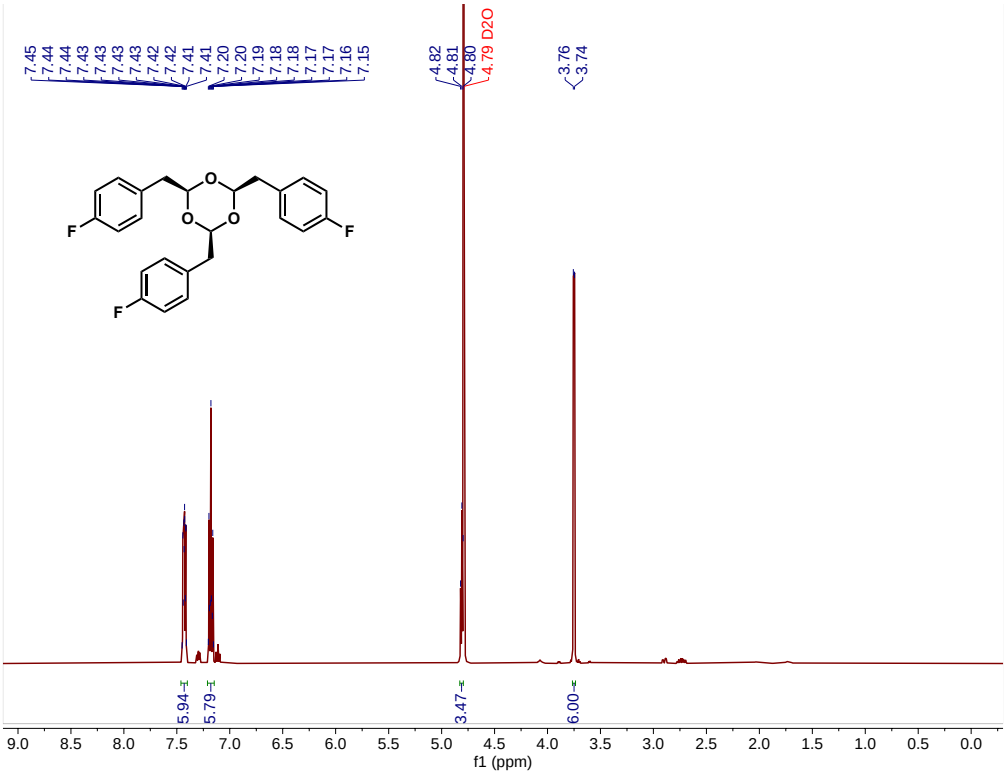

^{1}H NMR spectrum in D_2O at 500 MHz

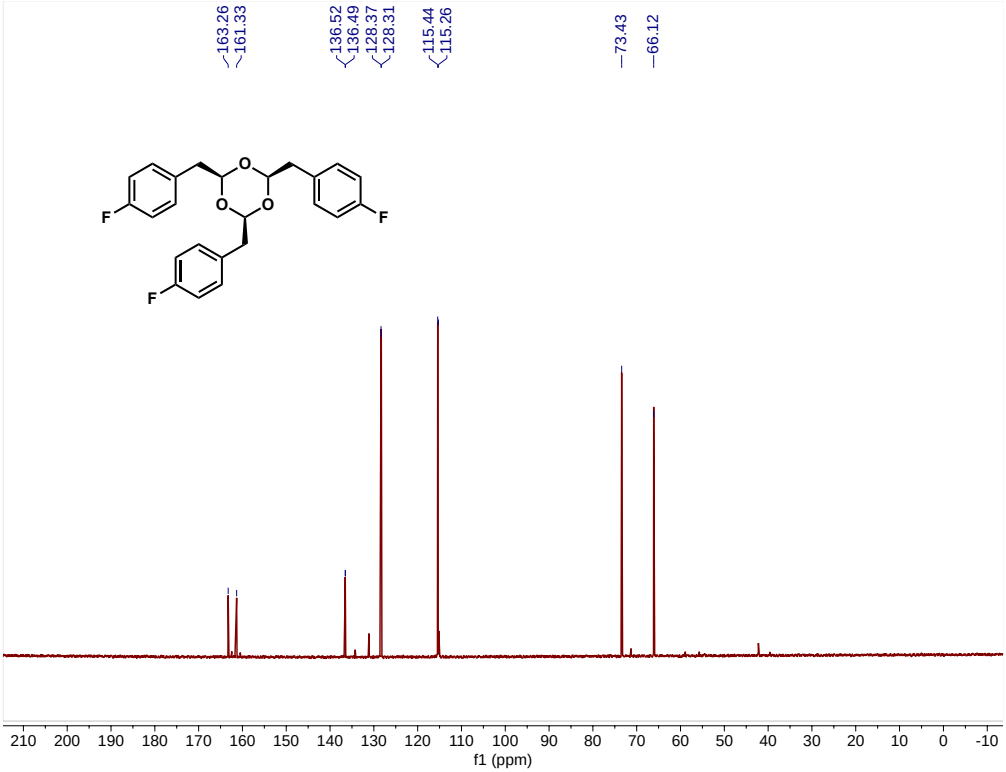

^{13}C NMR spectrum in D_2O at 126 MHz

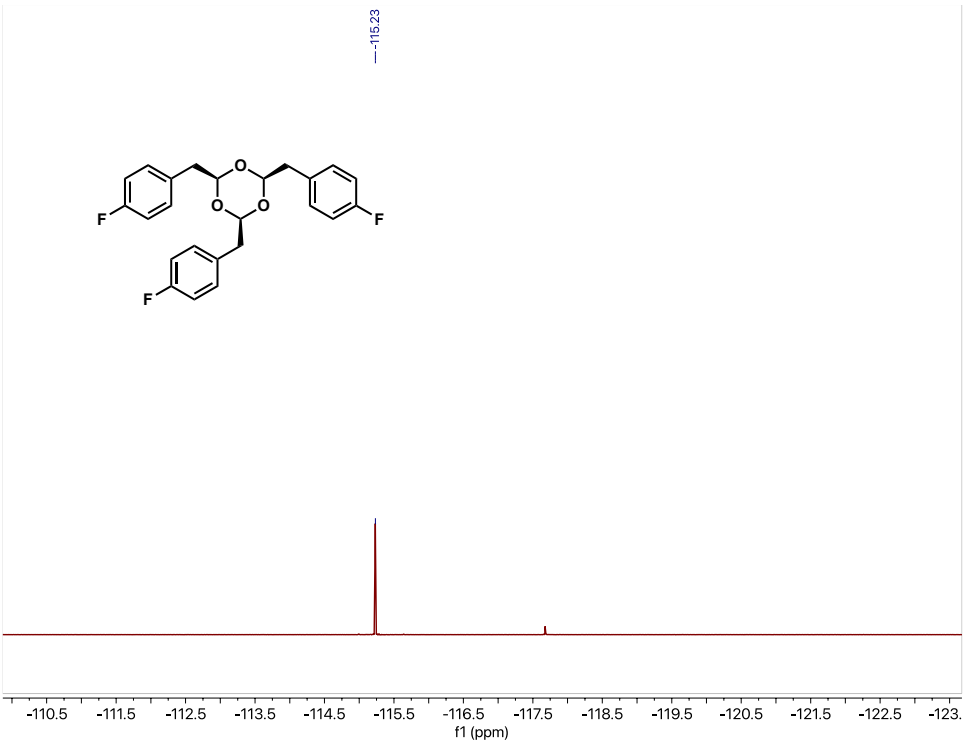

^{19}F NMR Spectrum in D_2O at 377 MHz

3. 6. References

(1) Schrittwieser, J. H.; Velikogne, S.; Hall, M.; Kroutil, W. Artificial Biocatalytic Linear Cascades for Preparation of Organic Molecules. *Chemical Reviews*. American Chemical Society January 2018, pp 270–348. https://doi.org/10.1021/acs.chemrev.7b00033.

(2) Muschiol, J.; Peters, C.; Oberleitner, N.; Mihovilovic, M. D.; Bornscheuer, U. T.; Rudroff, F. Cascade Catalysis-Strategies and Challenges En Route to Preparative Synthetic Biology. *Chemical Communications* **2015**, *51* (27), 5798–5811. https://doi.org/10.1039/c4cc08752f.

(3) Huffman, M. A.; Fryszkowska, A.; Alvizo, O.; Borra-Garske, M.; Campos, K. R.; Canada, K. A.; Devine, P. N.; Duan, D.; Forstater, J. H.; Grosser, S. T.; Halsey, H. M.; Hughes, G. J.; Jo, J.; Joyce, L. A.; Kolev, J. N.; Liang, J.; Maloney, K. M.; Mann, B. F.; Marshall, N. M.; Mclaughlin, M.; Moore, J. C.; Murphy, G. S.; Nawrat, C. C.; Nazor, J.; Novick, S.; Patel, N. R.; Rodriguez-Granillo, A.; Robaire, S. A.; Sherer, E. C.; Truppo, M. D.; Whittaker, A. M.; Verma, D.; Xiao, L.; Xu, Y.; Yang, H. Erratum: Design of an in Vitro Biocatalytic Cascade for the Manufacture of Islatravir. *Science*. 2020, pp 1255–1259. https://doi.org/10.1126/SCIENCE.ABC1954.

(4) Mcintosh, J. A.; Benkovics, T.; Silverman, S. M.; Hu, M. A.; Kong, J.; Maligres, P. E.; Itoh, T.; Yang, H.; Verma, D.; Pan, W.; Ho, H.; Vroom, J.; Knight, A. M.; Hurtak, J. A.; Klapars, A.; Fryszkowska, A.; Morris, W. J.; Strotman, N. A.; Murphy, G. S.; Maloney, K. M.; Fier, P. S. Engineered Ribosyl-1-Kinase Enables Concise Synthesis of Molnupiravir, an Antiviral for COVID-19. **2021**. https://doi.org/10.1021/acscentsci.1c00608.

(5) Chen, F. F.; Cosgrove, S. C.; Birmingham, W. R.; Mangas-Sanchez, J.; Citoler, J.; Thompson, M. P.; Zheng, G. W.; Xu, J. H.; Turner, N. J. Enantioselective Synthesis of Chiral Vicinal Amino Alcohols Using Amine Dehydrogenases. *ACS Catal* **2019**, *9* (12), 11813–11818. https://doi.org/10.1021/acscatal.9b03889.

(6) Mutti, F. G.; Knaus, T.; Scrutton, N. S.; Breuer, M.; Turner, N. J. Conversion of Alcohols to Enantiopure Amines through Dual-Enzyme Hydrogen-Borrowing Cascades. *Science (1979)* **2015**, *349* (6255), 1525–1529. https://doi.org/10.1126/science.aac9283.

(7) Nelson, D. L. ;; Cox, M. M. *Lehninger's Principles of Biochemistry*, 7th ed.; W.H. Freeman Company, 2017.

(8) Bednarski, M. D.; Waldmann, H. J.; Whitesides, G. M. Aldolase-Catalyzed Synthesis of Complex C8 and C9 Monosaccharides. *Tetrahedron Lett* **1986**, *27* (48), 5807–5810. https://doi.org/10.1016/S0040-4039(00)85332-0.

(9) Bednarski, M. D.; Simon, E. S.; Bischofberger, N.; Fessner, W. D.; Kim, M. J.; Lees, W.; Saito, T.; Waldmann, H.; Whitesides, G. M. Rabbit Muscle Aldolase as a Catalyst in Organic Synthesis. *J Am Chem Soc* **1989**, *111* (2), 627–635. https://doi.org/10.1021/ja00184a034.

(10) Marín-Valls, R.; Hernández, K.; Bolte, M.; Parella, T.; Joglar, J.; Bujons, J.; Clapés, P. Biocatalytic Construction of Quaternary Centers by Aldol Addition of 3,3-Disubstituted 2-Oxoacid Derivatives to Aldehydes. *J Am Chem Soc* **2020**, *142* (46), 19754–19762. https://doi.org/10.1021/jacs.0c09994.

(11) Fang, J.; Turner, L. E.; Chang, M. Biocatalytic Asymmetric Construction of Secondary and Tertiary Fluorides from B-Fluoro-α-ketoacids. *Angewandte Chemie International Edition* **2022**. https://doi.org/10.1002/anie.202201602.

(12) Moreno, C. J.; Hernández, K.; Charnok, S. J.; Gittings, S.; Bolte, M.; Joglar, J.; Bujons, J.; Parella, T.; Clapés, P. Synthesis of γ-Hydroxy-α-Amino Acid Derivatives by Enzymatic Tandem Aldol Addition–Transamination Reactions. *ACS Catal* **2021**, *11* (8), 4660–4669. https://doi.org/10.1021/acscatal.1c00210.

(13) Kumar, P.; Meza, A.; Ellis, J. M.; Carlson, G. A.; Bingman, C. A.; Buller, A. R. L -Threonine Transaldolase Activity Is Enabled by a Persistent Catalytic Intermediate. *ACS Chem Biol* **2021**, *16* (1), 86–95. https://doi.org/10.1021/acschembio.0c00753.

(14) Doyon, T. J.; Kumar, P.; Thein, S.; Kim, M.; Stitgen, A.; Grieger, A. M.; Madigan, C.; Willoughby, P. H.; Buller, A. R. Scalable and Selective β-Hydroxy-α-Amino Acid Synthesis Catalyzed by Promiscuous l-Threonine Transaldolase ObiH. *ChemBioChem* **2022**, *23* (2). https://doi.org/10.1002/cbic.202100577.

(15) Thompson, C. M.; McDonald, A. D.; Yang, H.; Cavagnero, S.; Buller, A. R. Modular Control of L-Tryptophan Isotopic Substitution via an Efficient Biosynthetic Cascade. *Org Biomol Chem* **2020**, *18* (22), 4189–4192. https://doi.org/10.1039/d0ob00868k.

(16) Sentheshannuganathan, S.; Elsden, S. R. The Mechanism of the Formation of Tyrosol by Saccharomyces Cerevisiae. *Biochem J* **1958**, *69* (2), 210–218. https://doi.org/10.1042/bj0690210.

(17) Hagel, J. M.; Facchini, P. J. Benzylisoquinoline Alkaloid Metabolism: A Century of Discovery and a Brave New World. *Plant Cell Physiol* **2013**, *54* (5), 647–672. https://doi.org/10.1093/pcp/pct020.

(18) Wang, Y.; Tappertzhofen, N.; Méndez-Sánchez, D.; Bawn, M.; Lyu, B.; Ward, J. M.; Hailes, H. C. Design and Use of de Novo Cascades for the Biosynthesis of New Benzylisoquinoline Alkaloids. *Angewandte Chemie - International Edition* **2019**, *58* (30), 10120–10125. https://doi.org/10.1002/anie.201902761.

(19) Ramsden, J. I.; Heath, R. S.; Derrington, S. R.; Montgomery, S. L.; Mangas-Sanchez, J.; Mulholland, K. R.; Turner, N. J. Biocatalytic N-Alkylation of Amines Using Either Primary Alcohols or Carboxylic Acids via Reductive Aminase Cascades. *J Am Chem Soc* **2019**, *141* (3), 1201–1206. https://doi.org/10.1021/jacs.8b11561.

(20) Hammer, S. C.; Kubik, G.; Watkins, E.; Huang, S.; Minges, H.; Arnold, F. H. Anti-Markovnikov Alkene Oxidation by Metal-Oxo–Mediated Enzyme Catalysis. *Science (1979)* **2017**, *358* (6360), 215–218. https://doi.org/10.1126/science.aao1482.

(21) Al-Smadi, D.; Enugala, T. R.; Norberg, T.; Kihlberg, J.; Widersten, M. Synthesis of Substrates for Aldolase-Catalysed Reactions: A Comparison of Methods for the Synthesis of Substituted Phenylacetaldehydes. *Synlett* **2018**, *29* (9), 1187–1190. https://doi.org/10.1055/s-0036-1591963.

(22) Wu, S.; Liu, J.; Li, Z. Biocatalytic Formal Anti-Markovnikov Hydroamination and Hydration of Aryl Alkenes. *ACS Catal* **2017**, *7* (8), 5225–5233. https://doi.org/10.1021/acscatal.7b01464.

(23) Wu, S.; Zhou, Y.; Seet, D.; Li, Z. Regio- and Stereoselective Oxidation of Styrene Derivatives to Arylalkanoic Acids via One-Pot Cascade Biotransformations. *Adv Synth Catal* **2017**, *359* (12), 2132–2141. https://doi.org/10.1002/adsc.201700416.

(24) Choo, J. P. S.; Li, Z. Styrene Oxide Isomerase Catalyzed Meinwald Rearrangement Reaction: Discovery and Application in Single-Step and One-Pot Cascade Reactions. *Org Process Res Dev* **2022**. https://doi.org/10.1021/acs.oprd.1c00473.

(25) Xin, R.; See, W. W. L.; Li, X.; Yun, H.; Li, Z. Enzyme-Catalyzed Meinwald Rearrangement with an Unusual Regioselective and Stereospecific 1,2-Methyl Shift. *Angewandte Chemie International Edition* **2022**. https://doi.org/10.1002/anie.202204889.

(26) Meinwald, J.; Labana, S.; Chanda, Mm. Peracid Reactions. III. The Oxidation of Bicyclo[2.2.1]Heptadiene. *J. Am. Chem. Soc* **1963**, *85* (5), 582–585.

(27) Lai, Y.; Chen, H.; Liu, L.; Fu, B.; Wu, P.; Li, W.; Hu, J.; Yuan, J. Engineering a Synthetic Pathway for Tyrosol Synthesis in Escherichia Coli . *ACS Synth Biol* **2022**. https://doi.org/10.1021/acssynbio.1c00517.

(28) Wu, S.; Zhou, Y.; Seet, D.; Li, Z. Regio- and Stereoselective Oxidation of Styrene Derivatives to Arylalkanoic Acids via One-Pot Cascade Biotransformations. *Adv Synth Catal* **2017**, *359* (12), 2132–2141. https://doi.org/10.1002/adsc.201700416.

(29) Choo, J. P. S.; Li, Z. Styrene Oxide Isomerase Catalyzed Meinwald Rearrangement Reaction: Discovery and Application in Single-Step and One-Pot Cascade Reactions. *Org Process Res Dev* **2022**. https://doi.org/10.1021/acs.oprd.1c00473.

(30) Ellis, J. M.; Campbell, M. E.; Kumar, P.; Geunes, E. P.; Bingman, C. A.; Buller, A. R. Biocatalytic Synthesis of Non-Standard Amino Acids by a Decarboxylative Aldol Reaction. *Nat Catal* **2022**, *5* (2), 136–143. https://doi.org/10.1038/s41929-022-00743-0.

(31) Ye, Y.; Minami, A.; Igarashi, Y.; Izumikawa, M.; Umemura, M.; Nagano, N.; Machida, M.; Kawahara, T.; Shin-ya, K.; Gomi, K.; Oikawa, H. Unveiling the Biosynthetic Pathway of the Ribosomally Synthesized and Post-Translationally Modified Peptide Ustiloxin B in Filamentous Fungi. *Angewandte Chemie - International Edition* **2016**, *55* (28), 8072–8075. https://doi.org/10.1002/anie.201602611.

(32) Kunjapur, A. M.; Tarasova, Y.; Prather, K. L. J. Synthesis and Accumulation of Aromatic Aldehydes in an Engineered Strain of Escherichia Coli. *J Am Chem Soc* **2014**, *136* (33), 11644–11654. https://doi.org/10.1021/ja506664a.

(33) Schaffer, J. E.; Reck, M. R.; Prasad, N. K.; Wencewicz, T. A. β-Lactone Formation during Product Release from a Nonribosomal Peptide Synthetase. *Nat Chem Biol* **2017**, *13* (7), 737–744. https://doi.org/10.1038/nchembio.2374.

(34) Scott, T. A.; Heine, D.; Qin, Z.; Wilkinson, B. An L-Threonine Transaldolase Is Required for L-Threo-β-Hydroxy-α-Amino Acid Assembly during Obafluorin Biosynthesis. *Nat Commun* **2017**, *8* (May), 1–11. https://doi.org/10.1038/ncomms15935.

(35) Marfey, P. Determination of D-Amino Acids. II. Use of a Bifunctional Reagent, 1,5-Difluoro-2,4-Dinitrobenzene. *Carlsberg Res Commun* **1984**, *49* (6), 591–596. https://doi.org/10.1007/BF02908688.

(36) Kimura, T.; P. Vassilev, V.; Shen, G.-J.; Wong, C.-H. Enzymatic Synthesis of β-Hydroxy-α-Amino Acids Based on Recombinant d- and l-Threonine Aldolases. *J Am Chem Soc* **1997**, *119* (49), 11734–11742. https://doi.org/10.1021/ja9720422.

(37) Harris, R. K.; Becker, E. D.; De Menezes, S. M. C.; Goodfellow, R.; Granger, P. NMR Nomenclature: Nuclear Spin Properties and Conventions for Chemical Shifts - IUPAC Recommendations 2001. *Solid State Nucl Magn Reson* **2002**, *22* (4), 458–483. https://doi.org/10.1006/snmr.2002.0063.

(38) Gibson, D. G. Enzymatic Assembly of Overlapping DNA Fragments; 2011; pp 349–361. https://doi.org/10.1016/B978-0-12-385120-8.00015-2.

(39) Fanning, K. N.; Jamieson, A. G.; Sutherland, A. Stereoselective β-Hydroxy-α-Amino Acid Synthesis via an Ether-Directed, Palladium-Catalysed Aza-Claisen Rearrangement. *Org Biomol Chem* **2005**, *3* (20), 3749–3756. https://doi.org/10.1039/b510808j.

(40) Fan, Y.; Tiffner, M.; Schörgenhumer, J.; Robiette, R.; Waser, M.; Kass, S. R. Synthesis of Cyclic Organic Carbonates Using Atmospheric Pressure CO2 and Charge-Containing Thiourea Catalysts. *Journal of Organic Chemistry* **2018**, *83* (17), 9991–10000. https://doi.org/10.1021/acs.joc.8b01374.

(41) Infante, R.; Nieto, J.; Andrés, C. Highly Homogeneous Stereocontrolled Construction of Quaternary Hydroxyesters by Addition of Dimethylzinc to α-Ketoesters Promoted by Chiral Perhydrobenzoxazines and B(OEt) 3. *Chemistry - A European Journal* **2012**, *18* (14), 4375–4379. https://doi.org/10.1002/chem.201102913.

(42) Romney, D. K.; Miller, S. J. A Peptide-Embedded Trifluoromethyl Ketone Catalyst for Enantioselective Epoxidation. *Org Lett* **2012**, *14* (4), 1138–1141. https://doi.org/10.1021/ol3000712.

(43) Ball, L. T.; Lloyd-Jones, G. C.; Russell, C. A. Gold-Catalysed Oxyarylation of Styrenes and Mono- and Gem-Disubstituted Olefins Facilitated by an Iodine(III) Oxidant. *Chemistry - A European Journal* **2012**, *18* (10), 2931–2937. https://doi.org/10.1002/chem.201103061.

(44) Bew, S. P.; Hiatt-Gipson, G. D.; Lovell, J. A.; Poullain, C. Mild Reaction Conditions for the Terminal Deuteration of Alkynes. *Org Lett* **2012**, *14* (2), 456–459. https://doi.org/10.1021/ol2029178.

(45) Hamman, S.; Beguin, C. G.; Charlon, C.; Luu-Duc, C. Synthese et Stereochimie de Formation d'amines Tertiaires β-Fluorees Par Fluoration d'aminoalcools Avec La Trifluro-1,1,2 Chloro-2 N,N-Diethyl Ethylamine (FAR) et Le Melange HF - Pyridine. *J Fluor Chem* **1987**, *37* (3), 343–356. https://doi.org/10.1016/S0022-1139(00)81971-5.

(46) Gao, F.; Hoveyda, A. H. α-Selective Ni-Catalyzed Hydroalumination of Aryl- and Alkyl-Substituted Terminal Alkynes: Practical Syntheses of Internal Vinyl Aluminums, Halides, or Boronates. *J Am Chem Soc* **2010**, *132* (32), 10961–10963. https://doi.org/10.1021/ja104896b.

(47) Fujisaka, T.; Miura, M.; Nojima, M.; Kusabayashi, S. *Synthesis and Reaction of I ,2,4-Trioxanes*; 1989.

Chapter 4

Exploring glycyl quinonoid reactivity with ketone electrophiles

Content in this chapter is part of a manuscript that is under preparation that has received significant contribution from Sam Bruffy and Tyler Doyon:

Bruffy, S. K.; **Meza, A.**; Doyon, T. J.; Huseth, K. G.; Buller, A.R. “Enzymatic aldol addition into un-activated ketones via a reactive carbon nucleophile” *Manuscript in preparation*

Chapter 4: Exploring glycyl quinonoid reactivity with ketone electrophiles

4. 1. Introduction

Enzymes are renowned for their excellent efficiency and selectivity and have been incorporated into synthetic strategies to produce fine chemicals and complex pharmaceuticals.[1] Functional group interconversions using transaminases, imine reductases, and lipases have been successfully applied in the process scale synthesis of numerous therapeutics. There are, however, relatively few examples of enzymes catalyzing asymmetric reactions between *C*-nucleophiles and *C*-electrophiles with the notable exceptions of hydroxynitrile lyases (HNL) and the recent process-scale biocatalytic synthesis of islatravir.[2,3] In a 9-enzyme cascade, A deoxyribose phosphate aldolase (DERA) was used to construct the ethynyl containing ribose sugar from acetaldehyde and a glyceraldehyde 3-phosphate analog as a mixture of isomers. Dynamic kinetic resolution of the reversible aldol reaction with downstream enzymes achieved high yields for the target compound. HNLs synthesize cyanohydrins from aldehydes or ketones with a cyanide source which can be added in excess and which can readily exist as an anion as the pKa of HCN is 9.2 in aqueous conditions.

The challenge of developing C-C bond forming biocatalytic systems is constrained by the properties of reactive carbon centers in aqueous reaction conditions and the routes from which enzymes access nucleophilic intermediates. Class I and class II aldolases generate carbon nucleophiles via deprotonation.[4] Specifically, class II aldolases generate enolate nucleophilic intermediates from alpha deprotonation of ketones or α-keto acids. The otherwise challenging generation of a carbanion is driven by thermodynamic stabilization of the conjugate base, as reflected in the lower pKa of the conjugate acid. Upon nucleophilic addition into a suitable C-electrophile, a new C-C bond is formed. However, all reactions are microscopically reversible and the same factors that enable formation of the C-nucleophile also make it a good leaving group, ie stabilization of the conjugate base. Consequently, for reactions to go to high yield, they require a

high-energy, potent electrophile, such as an aldehyde. Reactions with hindered or electronically deactivated electrophiles, such as ketones, pose significant thermodynamic and kinetic challenges.[5] The few examples of ketones as electrophiles for enzymes in the literature rely on activation via electron withdrawing substituents, spontaneous cyclization to drive unfavorable reactions forward, or thermodynamically favored hydrolysis of enzyme bound intermediates.[6–8] These fundamental challenges to reacting carbon nucleophiles with ketones can be bypassed using traditional synthetic strategies. High-energy *C*–nucleophilic intermediates (pKa of the conjugate acid is >15) can be readily generated by using strong metal bases that effect a highly thermodynamically-favorable C–H deprotonation.[9] However, such reactive modes are inaccessible in protic solutions due to the rapid protonation of highly basic carbanions.

In this chapter, we explore the ability of the PLP-dependent aldolase enzymes to catalyze a high-yielding aldol addition into ketone electrophiles. Natively, LTTAs catalyze the retro-aldol cleavage of Thr (**1**) to form a nucleophilic intermediate (E(Q^{Gly})), followed by an aldol-like addition into an aldehyde.[10] Our spectroscopic studies have showed that E(Q^{Gly}) is remarkably persistent in protic solvents, as protonation of this intermediate is kinetically disfavored (Figure 1b–c, Chapter 2).[11] We and others have exploited this unique reactivity to synthesize diverse β-hydroxy-α-amino acids (β-OH AAs) with aldehyde substrates.[12,13] We hypothesized that LTTA's may also react with ketone electrophiles, yielding tertiary β-OH AAs (Figure 1a). To probe the underlying kinetic basis for this reactivity, we directly compare to the mechanistically related Thr aldolases (LTAs), which access a chemically identical nucleophile through a kinetically facile proton transfer from glycine (**2**) (Figure 1d–e, Chapter 1). Here, we report the first example of PLP-dependent aldolases catalyzing addition into ketone substrates.

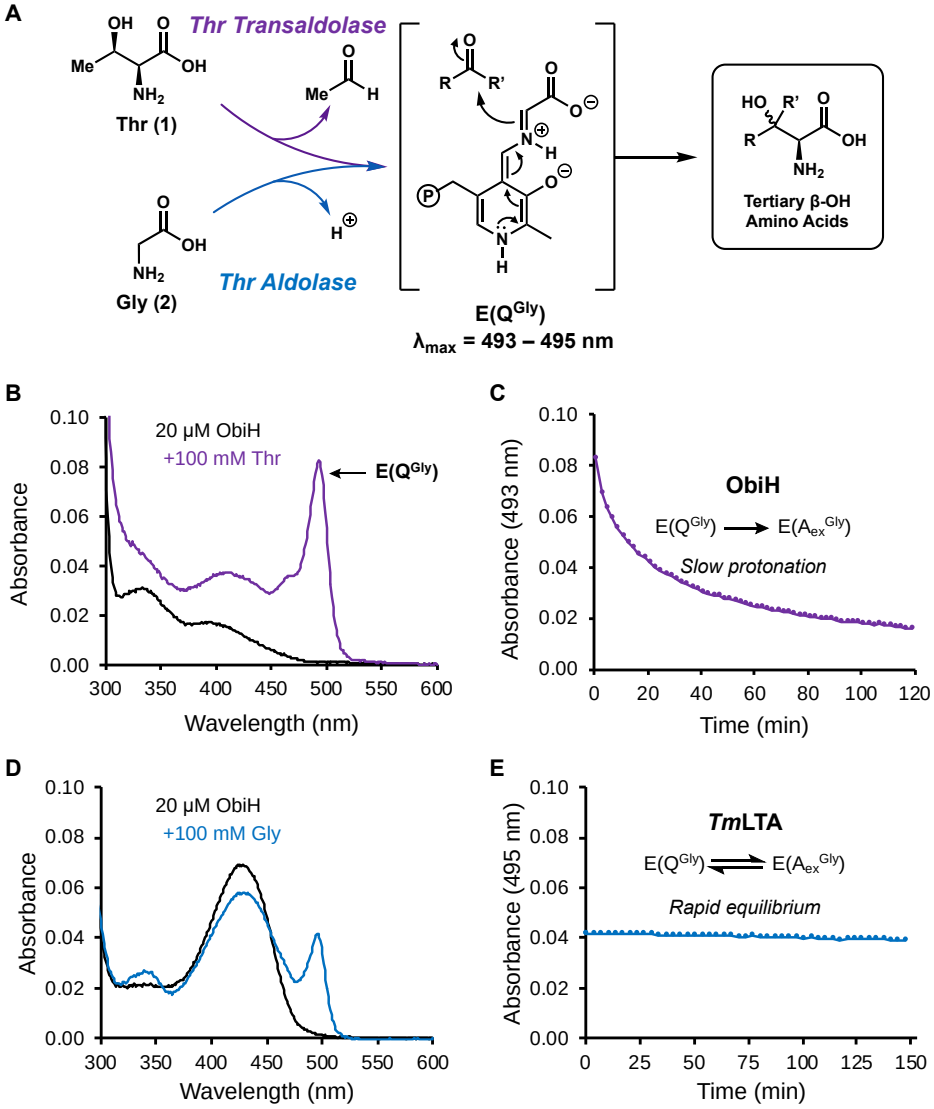

Figure 1. ObiH and *Tm*LTA form nucleophilic glycyl quinonoid intermediates. A) Threonine transaldolases form E(Q^{Gly}) through retro aldol cleavage of Thr while threonine aldolases can deprotonate glycine. Reactive E(Q^{Gly}) intermediates can be leveraged for nucleophilic attack into carbonyls to forms β-substituted amino acids. **B)** Absorbance spectra of phototreated ObiH (black) and ObiH after addition of Thr (purple) in 50 mM KP$_i$ pH 8.0. Addition of Thr results in large peak at 493 nm, E(Q^{Gly}). **C)** Plot of absorbance at 493 nm vs time after addition of Thr. 493 nm peak in maximum in the mixing time of the reaction (< 20s) and gradually decays over minutes. **D)** Absorbance spectra of *Tm*LTA (black) and *Tm*LTA after addition of Gly (Blue) in 50 mM KP$_i$ pH 8.0. Addition of Gly results in a peak at 495 nm, E(Q^{Gly}). **E)** Plot of absorbance at 495 nm vs time after addition of Gly. 495 nm peak in maximum in the mixing time of the reaction and is constant over time.

4. 2. Results and Discussion

4. 2. 1. ObiH and *Tm*LTA react with ketone substrates yielding tertiary β-hydroxy amino acids

We first investigated whether *Tm*LTA or ObiH could intercept ketone electrophiles. To maximize the chances of success, we began with an electronically activated ketone, 1,1,1-trifluoro-3-phenylacetone (**3a**) which is isosteric to α-aryl acetaldehyde substrates which have been shown to be efficient substrates with ObiH (Figure 2).[14–16] We observed product formation within minutes of reacting 10 µM *Tm*LTA via UPLC-MS with 10 mM **3a** and 100 mM of glycine (**2**) (Figure 2a). However, maximum product formation was achieved within the first hour of the reaction and the yield was very low (<1%). Under similar reaction conditions, ObiH was able to produce significantly more product than *Tm*LTA, reaching product titers of ~25% at 4h. Increasing the catalyst loading of ObiH 4-fold to 40 µM (0.40% mol. cat.) resulted in a modest increase the analytical yield of **3b** to ~45%. Increasing the concentration of *Tm*LTA did not increase the reaction yield, suggestive of a thermodynamic limitation to the reaction. We therefore repeated the reaction with 100 equivalents of Gly (1 M), which we hypothesized would increase yield of a reversible reaction through Le Chatlier's principle. This hypothesis was confirmed via the increased yield of **3b** to 4% using 10 µM TmLTA. Again, however, increasing the catalyst loading to 100 µM did not increase yields (Figure 2b). Both reactions yielded 4%, indicating that *Tm*LTA has reached the thermodynamic equilibrium of the reaction. The reactions with *Tm*LTA reaching equilibrium are also supported by the diastereomeric ratio of **3b** as the reaction progresses. In the first 2 minutes of the reaction, we measured an initial d.r. of > 50:1 and 40:1 with 10 µM and 100 µM *Tm*LTA respectively (Figure 2c). As the reactions progressed, the d.r. began to decrease as the product was able to reenter the active site and scramble the stereocenter at C_β, eroding to a d.r. of 5:1 and 1:1 at 4 h in reactions with 10 µM and 100 µM *Tm*LTA, respectively. Notably the total product concentration did not change. In contrast, reactions with 40 µM ObiH maintained high d.r. throughout the reaction with a d.r of 20:1 at 4 h while producing 10-fold more of **3b** than

*Tm*LTA. These features, combined with the improved yield with higher catalyst loading, indicated that the ObiH catalyzed reaction is subject to different thermodynamic constraints and that the catalyst itself appears to be subject to kinetic limitations under these reaction conditions.

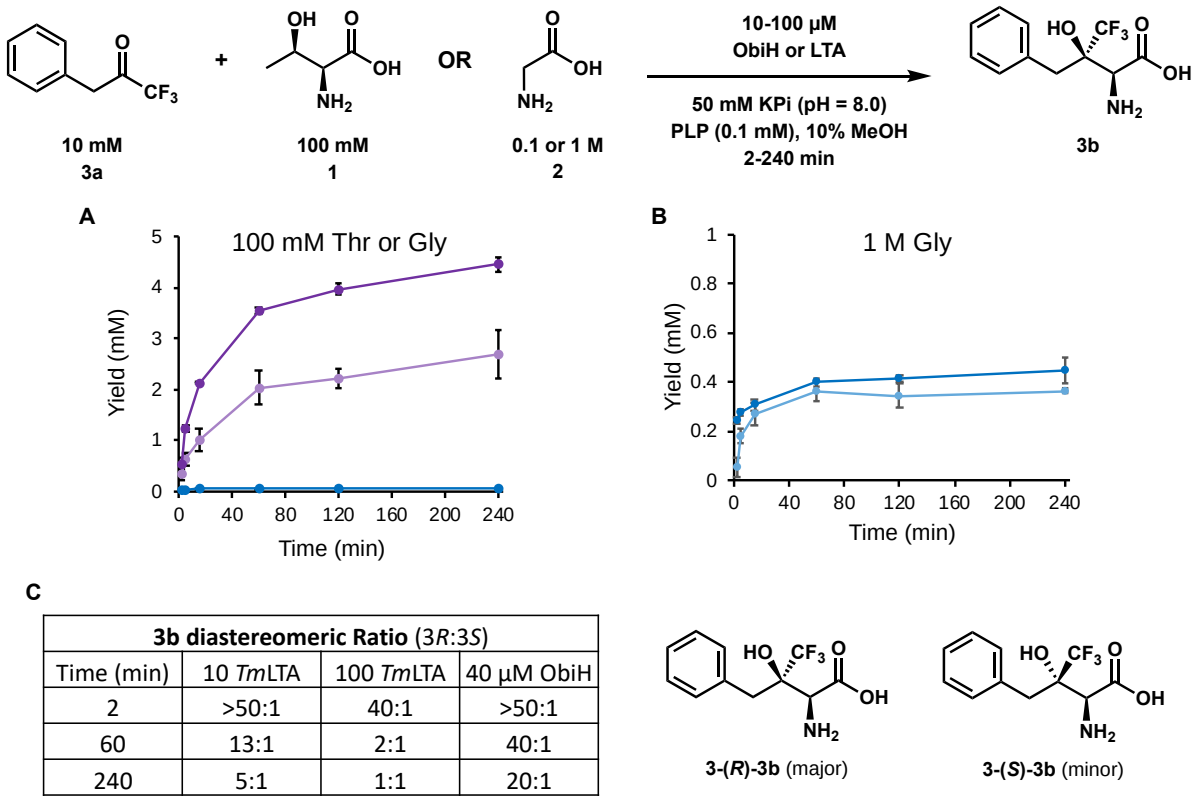

3b diastereomeric Ratio (3*R*:3*S*)			
Time (min)	10 *Tm*LTA	100 *Tm*LTA	40 µM ObiH
2	>50:1	40:1	>50:1
60	13:1	2:1	40:1
240	5:1	1:1	20:1

Figure 2. ObiH and *Tm*LTA react with an activated ketone substrate yielding a tertiary β-hydroxy amino acid. A) Reaction conditions for testing the activity of ObiH (Thr) and LTA (Gly) with an activated ketone substrate. **B)** Product formation over time for reactions with 40 µM ObiH (dark purple), 10 µM ObiH (light purple), or LTA (blue) with 100 mM Thr or 100 mM Gly. **C)** Product formation over time for reactions with 100 µM LTA (blue) or 10 µM LTA (light blue) with 1 M Gly. **D)** The two diastereomers of **3b** produced in reactions with ObiH and *Tm*LTA are readily separated via UPLC-MS. Product ratios were obtained from comparing the ion counts for **3-(*R*)-3b** and **3-(*S*)-3b**. Progress curves were a collaborative effort with Sam Bruffy.

We next assessed the ability of *Tm*LTA and ObiH to intercept non-activated ketone substrates. Under similar conditions with *p*-F phenylacetone (**4a**) as a substrate with 1 M Gly, reaction yields were measured to be ~0.1% and were constant at all timepoints (2–240 min). In contrast, when reactions were run with 100 µM ObiH and **4a** yielded significantly more **4b**, reaching yields of 6% in 2 min (Figure 3a). Unlike reactions with **3a,** product titers did not increase as the reaction progressed, rather, a small decrease in **4b** was observed. While the ability to overcome the thermodynamic limitations of LTA is intellectually stimulating, significant hurdles remain to achieve synthetic utility. We hypothesized that the reactive acetaldehyde product may play two distinct roles that limit the ability to achieve high yields. First, acetaldehyde is a good electrophile and, once formed, is a potent competitive inhibitor to reaction with alternative electrophiles. Second, the reaction appears to be thermodynamically unfavorable, as additional catalyst does not increase yields.

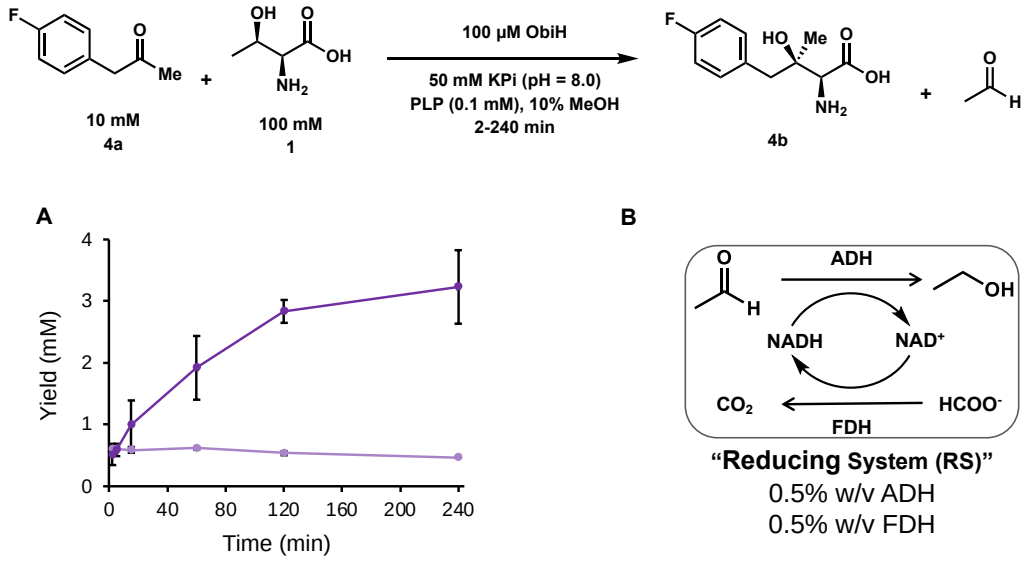

Figure 3. Removal of acetaldehyde increases reaction yields with ketone substrates. A) Product formation over time for reactions with 100 µM ObiH (Light purple) and 100 µM ObiH + reducing system (RS) (Dark purple). **B)** Acetaldehyde is reduced by *S. cerevisiae* alcohol dehydrogenase (ADH) into ethanol using NADH as a reductant. NAD^+ is regenerated from the oxidation of formate into CO_2 with *C. boidinii* formate dehydrogenase (FDH). Progress curves were a collaborative effort with Sam Bruffy.

We therefore sought to remove acetaldehyde from the reaction mixture and adopted a previously described system that has been used to removed acetaldehyde from transaldolase mediated reactions.[17] Xu et al. used an alcohol dehydrogenase (ADH) to convert acetaldehyde into ethanol using NADH as a reductant. The NAD^+ is then regenerated from the oxidation of formate into CO_2 with formate dehydrogenase (FDH). We expressed and prepared the two-enzyme system as clarified lysates and supplemented them to ObiH reactions as the "reducing system" (RS) (Figure 3b). The addition of 100 mM ammonium formate, 100 µM NAD^+, 0.5% w/v ADH lysate, and 0.5% w/v FDH lysate resulted in a 5-fold boost in **4b** to ~30% at 4h. We were excited to observe the increase in **4b** and began optimization for ObiH reactions with the RS. Although not discussed in this chapter, reaction optimization with 10 mM **4a** was led by Sam Bruffy and Dr. Tyler Doyon, who identified conditions that were increased the yield of **4b** to over 70%. Optimized conditions will subsequently be used for preparative synthesis of tertiary β-hydroxy amino acids (4. 2. 2.).

4. 2. 2. Removal of acetaldehyde enables preparative scale synthesis of tertiary β-hydroxy amino acids with ObiH

We next sought to apply optimized conditions of ObiH with the RS to a breadth of ketone substrates. In summary, the optimized conditions for the 3-enzyme system were determined to be pH 7.0 with 5-fold more *Sc*ADH lysate than in preliminary experiments with the RS. Discussed in this chapter is a select set of preparative scale reactions. When the RS was used with the activated ketone **3a**, we were successful at isolating **3b** at 81% yield with a d.r. >20:1 (Figure 4).

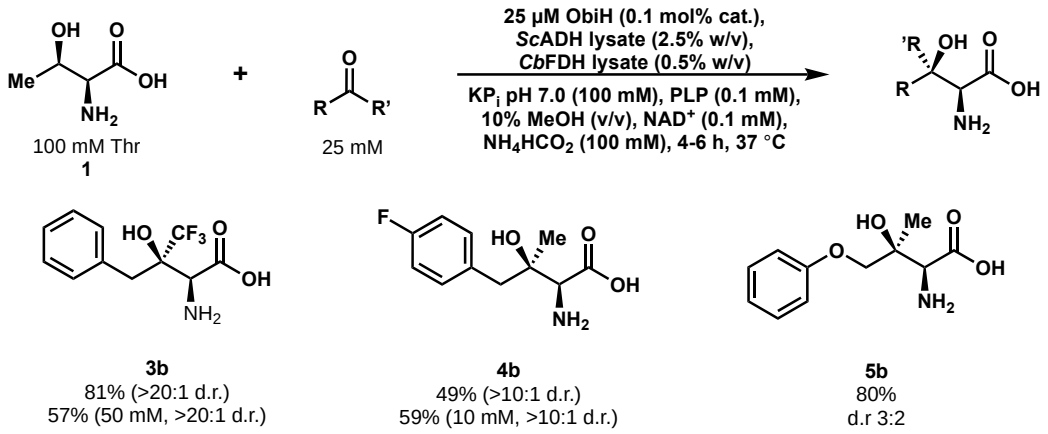

Figure 4. Preparative scale reactions with ObiH and reduction system. Reactions were conducted with 1 mmol ketone. Sam Bruffy prepared and isolated **3b**, **4b**, and **5b**.

Increases the substrate loading of **3a** to 50 mM was tolerated but resulted in a drop in yield to 57%. High substrate loading is often desired for process scale synthesis and 57% yield for **3b** at 50 mM was achieved without increasing the concentration of ObiH or the RS. Under standard preparative scale conditions, we isolated **4b** with a yield of 49%. When the concentration of 4a was reduced to 10 mM (matching the concentration used for optimization on analytical scale) yield of **4b** increased to 59%. Lastly, reactions with **5a** were efficient and we isolate **5b** with a yield of 80%, albeit with a low d.r of 3:2. We were surprised at the efficiency of **5a** with ObiH and rationalized the high activity was due to the phenol group on the carbon alpha to the carbonyl, providing small but significant electronic activation of the carbonyl.

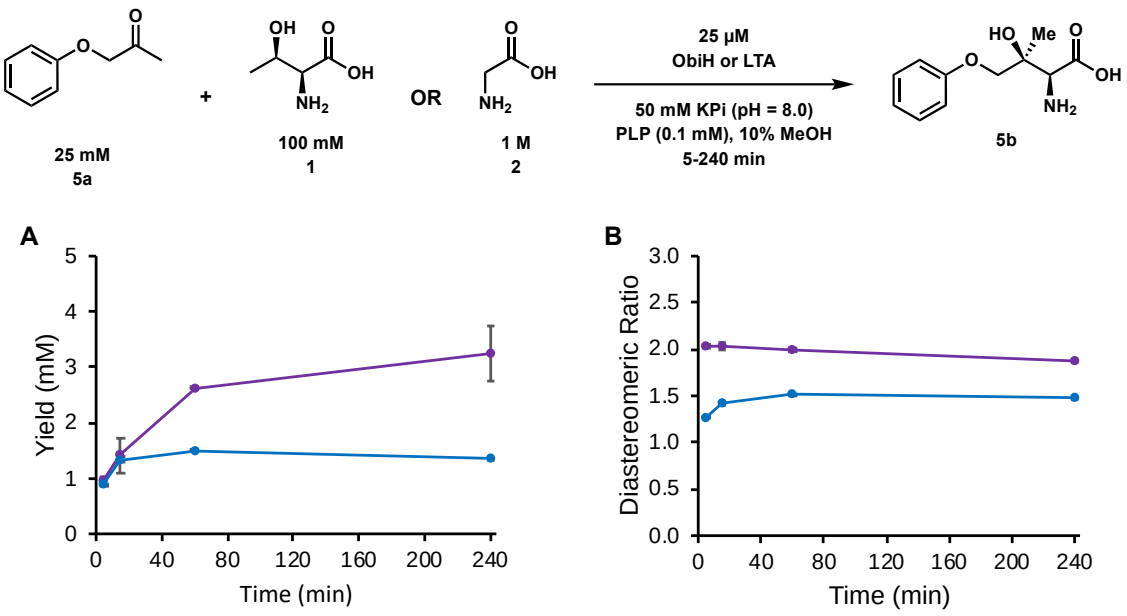

Figure 5. ObiH and TmLTA react with an activated ketone substrate yielding a tertiary β-hydroxy amino acid A) Product formation over time for reactions with 25 µM ObiH (purple) or 25 µM *Tm*LTA (Blue). Diastereomeric ratio of **5b** over time ObiH (purple) *Tm*LTA (blue).

To better understand the reactivity of 5a, we measured time courses the absence of the RS, as well as the corresponding reaction *Tm*LTA (Figure 5). Consistent with reactions with **3a** and **4a**, ObiH was able to produce more **5b** than *Tm*LTA. At pH 8.0 with 25 mM **5a**, ObiH produced 3 mM product which corresponds to a reaction yield of ~12% at 4 h while *Tm*LTA appears to be at equilibrium with a yield of 6%. Interestingly, the d.r. for both enzymes were largely unchanged during the course of the reaction. The initial d.r. in ObiH reactions was 2:1 and had only a minor decrease to 1.9:1 after 4 h. The observed d.r. in *Tm*LTA reactions was slightly different, beginning at 1.3:1 and slightly increasing to 1:5:1. The d.r. observations in these reactions indicate that the two enzymes are interacting with the respective substrates and products differently. The data with TmTLA suggest that the equilibrium ratio of diastereomers is 1.3:1 and that the modest 2:1 dr of the ObiH reaction is due to the effects within the enzyme active site.

4. 2. 3. Aryloxyacetone substrates are readily transformed by ObiH into tertiary β-hydroxy amino acids

We were pleased with the efficiency of the aryloxyacetone substrate (**5b**) in preparative scale reactions with ObiH and sought to expand the substrate scope with additional analogs. Other aryloxyacetone substrates were not commercially available, but we rationalized that reactions between phenol analogs and chloroacetone would be a viable synthetic strategy for their preparation (Figure 6). We identified reports of analogous transformations between thiophenol and chloroacetone and slightly modified the conditions.[18] Briefly, phenol was incubated with K_2CO_3 and KI in acetonitrile for 30 min. Chloroacetone was added slowly and the reaction was incubated overnight at 50 ºC. The reaction mixture was filtered and the flow through was concentrated. Compounds were isolated after normal phase purification on silica gel. We chose a select set of aryloxy containing substrates to synthesize ketones that could potentially be substrates for ObiH. Reactions with *p*-NO_2-phenol yielded ketone **6a** which is more electronically activated than **5a** due to the NO_2 substituent. **7a** was synthesized from 6-hydroxy coumarin, a small molecule with fluorescence properties. Lastly, we prepared **8a** from 8-hydroxy quinoline which is capable of binding divalent cations.

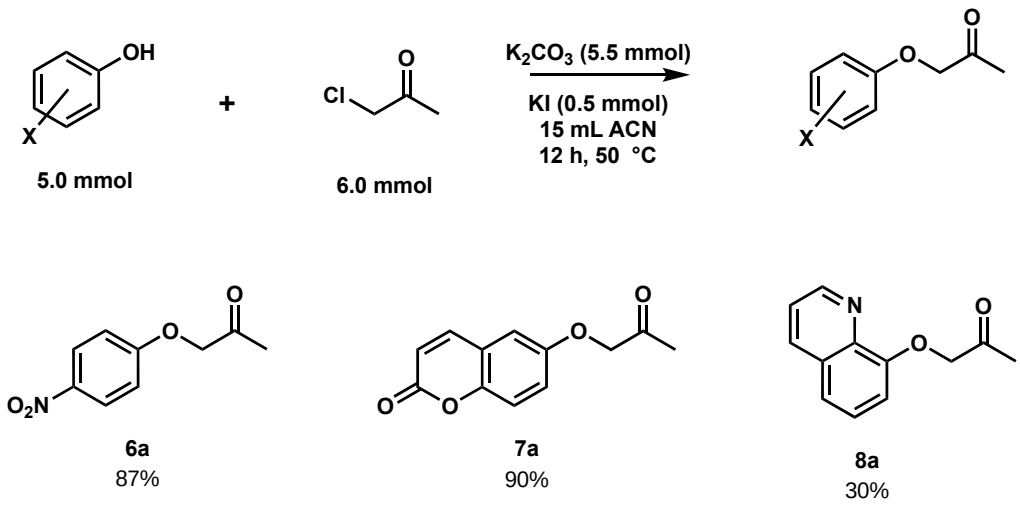

Figure 6. Synthesis of aryloxy acetone substrates.

We subjected the synthesized ketones to the optimized preparative conditions with ObiH and the RS (Figure 7). Reactions with **6a** were high yielding and we were able to isolate **6b** with a yield of 85% and a d.r. of 4:1. It is challenging to interpret the difference in yield between 6b (85%) and **5b** (80%), but reaction progress analysis with ObiH minus the RS and with *Tm*LTA could provide insights into the electronic activation of **6a** relative to **5a.** The coumarin derived ketone (**7a**) was less efficient with a yield of 50%. The hydroxy coumarin is more electronically deactivated than **5a** but may also impose additional steric challenges. Surprisingly, the quinoline containing ketone was successfully transformed into an amino acid product with an exceptional yield of 89% and a d.r. of 5:1.

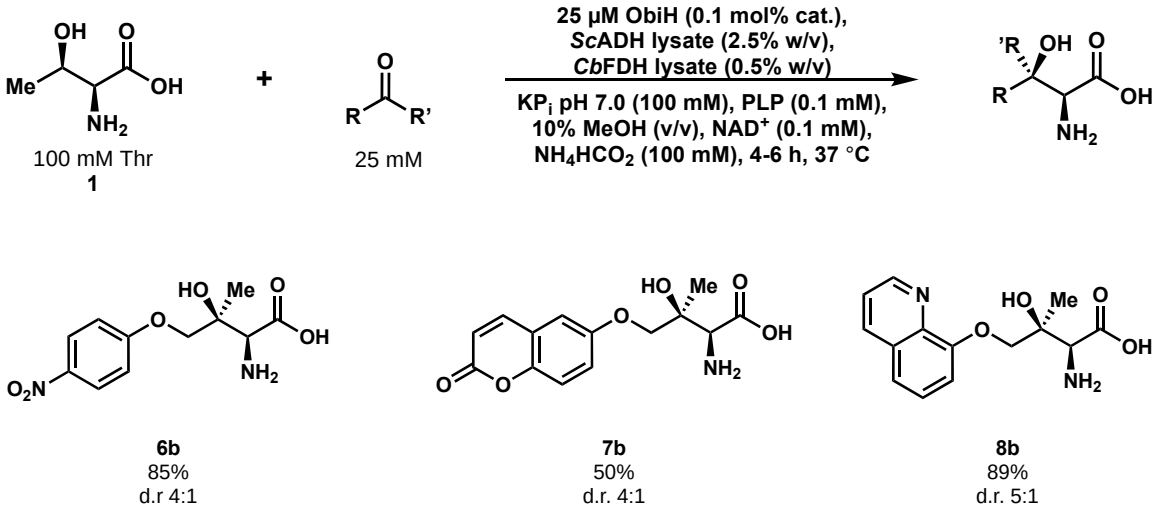

Figure 7. Preparative scale reactions with ObiH and reduction system. Reactions were conducted with 1 mmol ketone. Sam Bruffy prepared and isolated **8b**.

4. 3. Conclusions

Here we characterized the ability of the nucleophilic E(Q^{Gly}) intermediate in ObiH and *Tm*LTA to intercept ketone substrates. We demonstrate that ObiH and *Tm*LTA can react with ketone electrophiles, yielding tertiary β-OH AAs. However, although the E(Q^{Gly}) intermediate in both enzymes were able to react with ketones, reactions with ObiH were much more efficient than *Tm*LTA. While only trace activity (~0.1 %) was observed in reactions with the ketone **4a** and 100 equivalents of Gly, ObiH produced 60-fold more product (~6%) with only 10 equivalents of Thr.

We attribute this major difference in product formation between the two enzymes to the chemical equilibria of the reactions. Through spectroscopic studies, we show that *Tm*LTA is in rapid equilibrium with protonation of E(Q^{Gly}), while ObiH kinetically shields the analogous intermediate from protonation (Figure 1b-e). We identified acetaldehyde in ObiH mediated reactions as a potent limiting factor for high-yielding synthetic reactions with ketone substrates. We demonstrated that removal of acetaldehyde from the system effectively drives the formation E(Q^{Gly}) and increases yields of transaldolase mediated reactions with ketone substrates.

4. 4. Materials and Methods

General experimental procedures

Chemicals and reagents were purchased from commercial suppliers (Sigma-Aldrich, VWR, Chem-Impex International, Combi-blocks, Alfa Aesar, New England Biolabs, Zymo Research, Bio-Rad) and used without further purification unless otherwise noted. Pyridoxal 5'-phosphate (i.e., PLP) was purchased as the hydrate from Sigma-Aldrich. BL21 (DE3) *E. coli* cells were electroporated with a Bio-Rad MicroPulser electroporator at 2500 V. New Brunswick I26R, 120 V/60 Hz shaker incubators (eppendorf) were used for cell growth. Optical density was measured with an Amersham Biosciences Ultraspec 10 cell density meter. Cell distribution via sonication was performed with a Sonic Dismembrator 550 sonicator. UV-vis measurements were collected on a UV-2600 Shimadzu spectrophotometer (Shimadzu). UPLC-MS data were collected on an Acquity UHPLC with an Acquity Qda MS detector (Waters) using an Acquity UPLC CSH BEH C18 column (Waters) or an Intrada Amino Acid column (Imtakt). Preparative flash chromatographic separations were performed on an Isolera One Flash Purification system (Biotage). NMR spectra were recorded on a Bruker AVANCE III-500 MHz spectrometer equipped with a DCH cryoprobe. ^{1}H chemical shifts are reported in ppm (δ) relative to the solvent resonance D_2O (δ 4.79 ppm), DMSO-d_6 (δ 2.50 ppm), or CD_3OD (δ 3.31 ppm). ^{1}H NMR spectra acquired in

$CDCl_3$ were referenced to TMS (δ 0.00 ppm). ^{13}C NMR data were acquired with ^{1}H decoupling and chemical shifts are reported in ppm (δ) relative to the solvent resonance CD_3OD (δ 49.00 ppm), DMSO-d_6 (δ 39.52 ppm) or $CDCl_3$ (δ 77.16 ppm). All ^{19}F NMR and ^{13}C NMR acquired in D_2O without an internal standard were referenced to the absolute frequency of 0.00 ppm in the corresponding, internally referenced ^{1}H NMR spectrum (i.e., "Absolute Reference" or "Absolute Referencing").[19] Data are reported as follows: chemical shift (multiplicity [singlet (s), doublet (d), doublet of doublets (dd), multiplet (m)], coupling constants [Hz], integration). All NMR spectra were recorded at ambient temperature (20–25 °C). High resolution mass spectrometry data were collected with a Q Extraction Plus Orbitrap instrument (NIH 1S10OD020022-1) with samples ionized by electrospray ionization (ESI).

II-B. Cloning, Expression, and Purification of Proteins

Cloning and expression of ObiH and *Sc*ADH

A codon-optimized copy of each was inserted into a pET-28b(+) vector by the Gibson Assembly method.[20] BL21 (DE3) *E. coli* cells were subsequently transformed with the resulting cyclized DNA product via electroporation. After 45 min of recovery in Terrific Broth (TB) media at 37 °C, cells were plated onto Luria-Burtani (LB) plates with 50 µg/mL kanamycin (KAN) and incubated overnight. Single colonies were used to inoculate two 5 mL TB + 50 µg/mL KAN (TB-KAN), which were grown overnight at 37 °C, 200 rpm. Expression cultures, typically 1 L of TB-KAN, were inoculated from these starter cultures (1% inoculum) and shaken (200 rpm) at 37 °C. After 3.0 hours (OD_{600} = ~0.6), the expression cultures were chilled on ice. Expression is induced with 1.0 mM Isopropyl β-D-1-thiogalactopyranoside (IPTG), and the cultures were expressed for 16 hours at 20 °C with shaking at 200 rpm. Cells were then harvested by centrifugation at 4,300×g at 4 °C for 15 min. Cell pellets were frozen and stored at -20 °C until purification.

Cloning and expression of *Tm*LTA and *Cb*FDH

A codon-optimized copy of each was inserted into a pET-22b(+) vector by the Gibson Assembly method. BL21 (DE3) *E. coli* cells were subsequently transformed with the resulting cyclized DNA product via electroporation. After 45 min of recovery in TB media at 37 °C, cells were plated onto LB plates with 100 µg/mL ampicillin (Amp) and incubated overnight. Single colonies were used to inoculate two 5 mL TB + 100 µg/mL Amp (TB-Amp), which were grown overnight at 37 °C, 200 rpm. Expression cultures, typically 1 L of TB-Amp, were inoculated from these starter cultures (1% inoculum) and shaken (200 rpm) at 37 °C. After 3.0 hours (OD_{600} = ~0.6), the expression cultures were chilled on ice. Expression is induced with 1.0 mM IPTG, and the cultures were expressed for 16 hours at 20 °C with shaking at 200 rpm. Cells were then harvested by centrifugation at 4,300×g at 4 °C for 15 min. Cell pellets were frozen and stored at -20 °C until purification.

Purification and storage of ObiH and *Tm*LTA

To purify each protein, cell pellets were thawed on ice and then resuspended in lysis buffer (50 mM potassium phosphate (KP_i) buffer (pH = 8.0), 150 mM NaCl, 20 mM imidazole, 1 mg/mL Hen Egg White Lysozyme (GoldBio), 0.2 mg/mL DnaseI (GoldBio), 1 mM $MgCl_2$, and 400 µM pyridoxal 5′-phosphate (PLP)). A volume of 4 mL of lysis buffer per gram of wet cell pellet was used. After resuspension, the cell suspension was placed on ice in a metal container and subjected to lysis using a sonication device at 30% power for 2 s on and 2 s off for a total time of 10 min. The resulting lysate (pink for ObiH, yellow for *Tm*LTA) was then spun down at 50,000×*g* to pellet cell debris. Ni/NTA beads (GoldBio) were added to the supernatant and incubated on ice for 45 min prior to purification by Ni-affinity chromatography with a gravity column. The column was washed with 5 column volumes of 20 mM imidazole, 500 mM NaCl, 50 mM KP_i buffer (pH = 8.0). Washing with higher concentrations of imidazole resulted in slow protein elution. Each protein was eluted with 250 mM imidazole, 150 mM NaCl, 50 mM KP_i buffer, pH 8.0. Elution of the desired protein

product was monitored by the disappearance of its visible color (resulting from the release of the protein) from the column. The protein products were dialyzed to < 1 μM imidazole in 50-100 mM KP_i buffer (varying pH) with 150 mM NaCl. Purified enzyme was flash frozen in pellet form by pipetting enzyme dropwise into a crystallization dish filled with liquid nitrogen. The frozen enzyme was transferred to a plastic conical and stored at -80 °C until further use. Frozen pellets were thawed at room temperature and centrifuged before use. The concentration of protein was determined by Bradford assay using bovine serum albumin for a standard concentration curve. Generally, this procedure yielded 200 – 250 mg per L culture for ObiH and 500-600 mg per L culture for *Tm*LTA. Protein purity was analyzed by sodium dodecyl sulfate-polyacrylamide (SDS-PAGE) gel electrophoresis using 12% polyacrylamide gels.

Preparation and storage of *Sc*ADH and *Cb*FDH lysate

Cell pellets were thawed on ice and then resuspended in storage buffer (50-100 mM KP_i buffer (pH = 7.0) and 150 mM NaCl). A volume of 4 mL of storage buffer per gram of wet cell pellet was used, resulting in a 250 mg/mL lysate concentration. After resuspension, the cell suspension was placed on ice in a metal container and subjected to lysis using a sonication device at 30% power for 2 s on and 2 s off for a total time of 10 min. The resulting lysate was then spun down at 50,000×*g* to pellet cell debris and flash frozen in pellet form by pipetting lysate dropwise into a crystallization dish filled with liquid nitrogen. The frozen clarified lysate was transferred to a plastic conical and stored at -80 °C until further use. Frozen pellets were thawed at room temperature and centrifuged before use.

General procedure A: Preparative scale ObiH reactions with RS

Ketone (typically 1.0 mmol, 25 mM final concentration), MeOH (10% of total reaction volume), 100 mM KP_i, 100 mM ammonium formate pH 7.0 (delivered from a previously prepared 1 M KPi, 1 M ammonium formate, pH 7.0 [4.0 mL per 1.0 mmol of ketone]), Thr (4.0 mmol, 4 equiv., 100 mM final concentration), PLP (delivered from a previously prepared 20 mM aqueous stock

solution [200 µL per 1.0 mmol of ketone]), NAD^+ (0.1 mM final concentration [delivered from a previously prepared 10 mM aqueous stock [400 µL per 1.0 mmol of ketone]) were added to an Erlenmeyer flask. Reduction system components were then added: *Sc*ADH (delivered from 250 mg/mL clarified lysate stock [4.0 mL per 1.0 mmol of ketone, 2.5% w/v final concentration]), and *Cb*FDH (delivered from 250 mg/mL clarified lysate stock [800 µL per 1.0 mmol of ketone, 0.5% w/v final concentration]). Purified ObiH (0.1 mol% catalyst) was added directly to the reaction flask and ddH_2O was added to adjust the final reagent concentration to the appropriate amounts (40 mL final volume per 1.0 mmol of ketone). Reaction vessel was placed in the incubator at 37 °C, for 4-6 h. Product formation was monitored by UPLC-MS. After reaction completion, the reaction mixture was quenched with an equivalent volume of MeCN, heated at 70 °C for 15 mins and centrifuged (4,300×*g*, 15 min) to remove aggregated protein. The clarified supernatant was passaged over filter paper, and the filtrate was concentrated by rotary evaporation. The resulting material was loaded onto a reverse-phase C18 column pre-equilibrated with water. The resulting material was loaded onto a reversed-phase column (C18) and purified by automated flash purification with a water/methanol gradient. Fractions were analyzed by LC-MS to identify product containing fractions. Fractions containing pure product were pooled, concentrated by rotary evaporation, and dried via lyophilization.

Synthesis of aryloxyacetone substrates

Aryloxyacetone substrates were synthesized using a slightly modified protocol previously reported by Zhoa et. al.[18] K_2CO_3 (5.5 mmol) and KI (0.5 mmol) were added to a round bottom flask with 15 mL of acetonitrile at 40-50 ºC. The oxy containing substrate (5 mmol) was added to the flask followed by the slow addition of chloroacetone (6.0 mmol). The reactions were covered with a rubber septum with a needle to allow pressure to vent and were incubated at 40-50 ºC for 12-16 h. The resulting mixture was filtered and concentrated via rotary evaporation. The concentrated material was loaded onto silica gel with minimal dichloromethane (< 3 mL) and

purified via normal phase (Hexane/EtOAc: 19/1 –> 9/1 over ~20 column volumes). The product containing fractions were concentrated via rotary evaporation. Product purity was determined via ^{1}H NMR.

Preparation of phototreated ObiH

ObiH stock solutions (150 – 400 µM) or diluted samples in quartz cuvettes were placed on ice directly under an 8-Watt, green LED bulb for 10 min. The protein solutions were subsequently kept on ice or in the UV-spectrophotometer for 45 min, followed by a second round of green light treatment for 10 minutes which ensured complete abolishment of the 515 nm band.[11]

Kinetics and UV-Vis Spectroscopy

Data were collected between 600 and 250 nm on a UV-2600 Shimadzu spectrophotometer (Shimadzu) with a semi-micro quartz cuvette (Starna Cells) at 25 °C. ObiH and *Tm*LTA stock solutions were diluted to 20 µM in 50 mM KP_i buffer, at specified pH (typically 8.0) and phototreated. For quinonoid formation, Thr or Gly was added at 100 mM from a 500 mM stock prepared in 50 mM KPi pH 8.0. Spectra were collected every 120 seconds for 2 h.

Progress curves

Reactions were prepared in triplicate for ObiH and LTA at 10 µM, 40 µM or 100 µM. To ensure that pH was consistent between both enzyme as well as both concentrations, all enzymes were dialyzed into “reaction buffer” which was assembled and adjusted to pH 8.0. Amino acid stock solutions for Thr and Gly were prepared and adjusted to pH 8.0. For reactions with *Tm*LTA, reaction buffer was prepared to a final concentration of 56 mM KPi, 1.1 M Gly KPi, and 110 µM PLP. Reaction buffer and dialyzed enzyme (final volume of 450 µL) were combined with 50 µL of 100 mM ketone prepared in MeOH. 500 µL total reaction volume (50 mM KPi, 100 µM PLP, 1 M Gly, 10 mM ketone, 10% MeOH, *Tm*LTA [10 or 100 µM] at pH 8.0). 50 µL of reaction mixture was removed and quenched at 2, 5, 15, 60, 120, and 240 minutes with 50 µL of 3 M HCl in 1:1

H_2O:MeOH. Quenched reactions were centrifuged at 15,000 x g to remove precipitated biomolecules. Quantification was performed by UPLC-MS analysis on a BEH C18 column (Waters) and product concentration was determined with a standard curve.

For reactions with ObiH only, reaction buffer was prepared to a final concentration of 70 mM KPi and 140 µM PLP. Reaction buffer and dialyzed enzyme (final volume of 70 µL) were combined with 20 µL of 500 mM Thr and 10 µL of 100 mM ketone prepared in MeOH. 100 µL total reaction volume (50 mM KPi, 100 µM PLP, 100 mM Thr, 10 mM ketone, 10% MeOH, and ObiH [10, 25 or 40 µM] at pH 8.0). ObiH reactions were quenched at 2, 5, 15, 60, 120, and 240 minutes with 100 µL of acetonitrile. For reactions with ObiH + reduction system, reaction buffer was prepared to a final concentration of 70 mM KPi, 140 mM ammonium formate and 140 µM PLP. Reaction buffer and dialyzed enzyme (final volume of 325 µL) were combined with 10 µL of 250 mg/mL ADH lysate dialyzed in reaction buffer, 10 µL of 250 mg/mL FDH lysate dialyzed in reaction buffer, 5 µL of 10 mM NAD^+, 100 µL of 500 mM Thr and 50 µL of 100 mM ketone prepared in MeOH. 500 µL total reaction volume (50 mM KPi, 100 mM ammonium formate, 100 mM Thr, 10 mM ketone, 10% MeOH, 100 µM PLP, 100 µM NAD^+, 0.5% w/v ADH lysate, 0.5% w/v FDH lysate, and ObiH [10 or 100 µM] at pH 8.0). ObiH reactions were quenched at 2, 5, 15, 60, 120, and 240 minutes with 500 µL of acetonitrile. Quenched reactions were centrifuged at 15,000 x g to remove precipitated biomolecules. Quantification was performed by UPLC-MS analysis on a BEH C18 column (Waters) and product concentration was determined with a standard curve.

Details on the preparation and characterization of compounds discussed in chapter 4

(2*S*,3*R*)-2-amino-3-benzyl-4,4,4-trifluoro-3-hydroxybutanoic acid (3b)

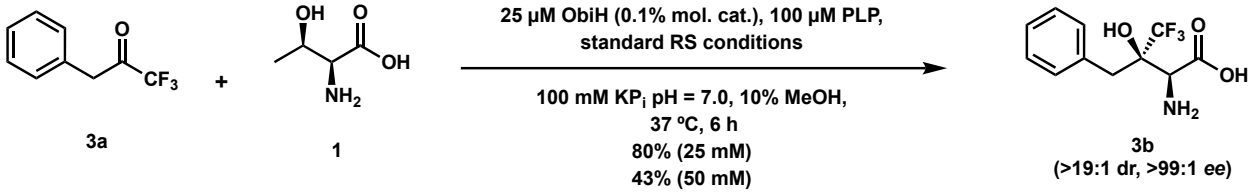

[0.1% mol. cat (25 mM)] Amino acid **3b** was prepared following General Procedure A with commercially available 1,1,1-trifluoro-3-phenylpropan-2-one (**3a,** 189 mg, 1.01 mmol), Thr (**1**, 475 mg, 4.0 mmol), PLP (200 µL via 20 mM solution in water, 0.004 mmol), NAD^+ (400 µL via 10 mM solution in water, 0.004 mmol), purified ObiH (1.00 mL via a 1.0 mM solution in 100 mM KP_i pH 8.0, final concentration 25 µM), *Sc*ADH lysate (4.00 mL via a 250 mg/mL solution in 100 mM KP_i pH 7.0, final concentration 25 mg/mL), *Cb*FDH lysate (0.80 mL via a 250 mg/mL solution in 100 mM KP_i pH 7.0, final concentration 5 mg/mL), buffer (4 mL via a 1 M KPi, NH_4HCOO solution pH 7.0, final concentration 100 mM KPi, 100 mM NH_4HCOO), 4 mL MeOH and 25.6 mL ddH_2O to a final volume of 40 mL. Purification by automated gradient flash chromatography (C18, MeOH:H_2O 1:99 to 1:0 over 30 column volumes) and subsequent lyophilization gave 213 mg of (**3b**) as a yellow solid (0.80 mmol, 80%). Subsequent isolations yielded a white solid. The yellow color was attributed to a trace PLP contaminant (<0.1%). ^{1}H NMR was used to assess stereochemical purity. Reaction, isolation, and characterization completed by Sam Bruffy.

[0.1% mol. cat (50 mM)] Using similar conditions as above, but with 50 mM ketone. 1,1,1-trifluoro-3-phenylpropan-2-one (**3a**, 192.4 mg, 1.02 mmol), Thr (**1**, 247 mg, 2.1 mmol), PLP (100 µL via 20 mM solution in water, 0.002 mmol), NAD^+ (200 µL via 10 mM solution in water, 0.002 mmol), purified ObiH (1.00 mL via a 1.0 mM solution in 100 mM KP_i pH 8.0, final concentration 50 µM), *Sc*ADH lysate (2.00 mL via a 250 mg/mL solution in 100 mM KP_i pH 7.0, final concentration 25

mg/mL), *Cb*FDH lysate (0.40 mL via a 250 mg/mL solution in 100 mM KP_i pH 7.0, final concentration 5 mg/mL), buffer (2 mL via a 1 M KPi, NH_4HCOO solution pH 7.0, final concentration 100 mM KPi, 100 mM NH_4HCOO), 2 mL MeOH and 12.3 mL ddH_2O to a final volume of 20 mL. Isolation gave 115 mg of **3b** as a yellow solid (0.43 mmol, 43%). ^{1}H NMR was used to assess stereochemical purity. Reaction, isolation, and characterization completed by Sam Bruffy.

^{1}H NMR (500 MHz, MeOD) δ 7.44 – 7.37 (m, 2H), 7.26 – 7.21 (m, 2H), 7.21 – 7.16 (m, 1H), 3.54 (s, 1H), 3.19 (d, *J* = 14.1 Hz, 1H), 3.14 (d, *J* = 14.0 Hz, 1H).

^{13}C{^{1}H} NMR (126 MHz, MeOD) δ 176.03, 136.59, 132.52, 128.68, 127.55, 126.36, 77.70, 77.50, 77.30, 77.10, 57.67, 37.70

19F{13C} NMR (377 MHz, CD_3OD): δ -77.60

HRMS (ESI^-): Calc. for $C_{11}H_{12}F_3NO_3^-$ $[M - H]^-$ requires 262.0696; found 262.0696.

(2*S*,3*R*)-2-amino-4-(4-fluorophenyl)-3-hydroxy-3-methylbutanoic acid (4b)

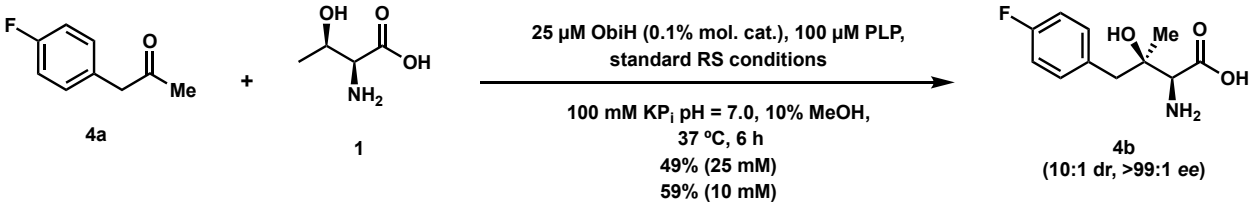

[0.1% mol. cat (25 mM)] Amino acid **4b** was prepared following General Procedure A with commercially available 1-(4-fluorophenyl)propan-2-one (**4a**, 152 mg, 1.00 mmol), Thr (**1**, 475 mg, 4.0 mmol), PLP (200 µL via 20 mM solution in water, 0.004 mmol), NAD^+ (400 µL via 10 mM solution in water, 0.004 mmol), purified ObiH (1.02 mL via a 980 µM solution in 100 mM KPi pH 8.0, final concentration 25 µM), *Sc*ADH lysate (4.00 mL via a 250 mg/mL solution in 100 mM KP_i pH 7.0, final concentration 25 mg/mL), *Cb*FDH lysate (0.80 mL via a 250 mg/mL solution in 100 mM KP_i pH 7.0, final concentration 5 mg/mL), buffer (4 mL via a 1 M KPi, NH_4HCOO solution pH 7.0, final concentration 100 mM KPi, 100 mM NH_4HCOO), 4 mL MeOH and 25.6 mL ddH_2O to a

final volume of 40 mL. Purification by automated gradient flash chromatography (C18, MeOH:H_2O 1:99 to 1:0 over 30 column volumes) and subsequent lyophilization gave 111 mg of **4b** as a white solid (0.49 mmol, 49%). Reaction and isolation completed by Sam Bruffy.

[0.1% mol. cat (10 mM)] Using similar conditions as above, but with 10 mM ketone. 1-(4-fluorophenyl)propan-2-one (**4a**, 77.2 mg, 0.51 mmol), Thr (**1**, 597 mg, 5.0 mmol), PLP (300 µL via 20 mM solution in water, 0.006 mmol), NAD^+ (500 µL via 10 mM solution in water, 0.005 mmol), purified ObiH (1.3 mL via a 400 µM solution in 100 mM KPi pH 8.0, final concentration 10 µM), *Sc*ADH lysate (5.00 mL via a 250 mg/mL solution in 100 mM KP_i pH 7.0, final concentration 25 mg/mL), *Cb*FDH lysate (1.0 mL via a 250 mg/mL solution in 100 mM KP_i pH 7.0, final concentration 5 mg/mL), buffer (5 mL via a 1 M KPi, NH_4HCOO solution pH 7.0, final concentration 100 mM KPi, 100 mM NH_4HCOO), 5 mL MeOH and 32 mL ddH_2O to a final volume of 50 mL. Isolation gave 115.3 mg of **4b** as a white solid (0.30 mmol, 59%). ^{1}H NMR was used to assess stereochemical purity.

^{1}H NMR (500 MHz, MeOD) δ 7.38 – 7.27 (m, 2H), 7.03 – 6.90 (m, 2H), 3.41 (s, 1H), 3.03 (d, J = 3.1 Hz, 2H), 1.10 (s, 3H).

^{13}C{^{1}H} NMR (126 MHz, MeOD) δ 173.15, 164.21, 162.28, 134.38, 134.36, 133.92, 133.86, 115.43, 115.26, 72.78, 63.11, 22.42.

19F{13C} NMR (377 MHz, CD3OD): δ -120.14.

HRMS (ESI^-): Calc. for $C_{11}H_{14}NO_3F^-$ $[M - H]^-$ requires 226.0885; found 226.0886.

(2*S*,3*S*)-2-amino-3-hydroxy-3-methyl-4-phenoxybutanoic acid (5b)

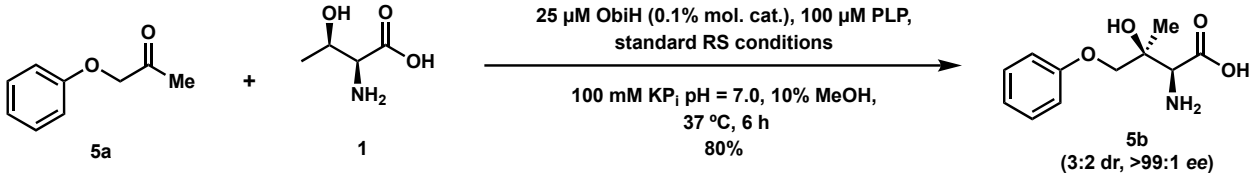

5a 1 5b (3:2 dr, >99:1 *ee*)

[0.1% mol. cat] Amino acid **5b** was prepared following General Procedure A with commercially available 1-phenoxypropan-2-one (**5a**, 152 mg, 1.01 mmol), Thr (**1**, 477 mg, 4.0 mmol), PLP (200 µL via 20 mM solution in water, 0.004 mmol), NAD^+ (400 µL via 10 mM solution in water, 0.004 mmol), purified ObiH (1.02 mL via a 980 µM solution in 100 mM KPi pH 8.0, final concentration 25 µM), *Sc*ADH lysate (4.00 mL via a 250 mg/mL solution in 100 mM KP_i pH 7.0, final concentration 25 mg/mL), *Cb*FDH lysate (0.80 mL via a 250 mg/mL solution in 100 mM KP_i pH 7.0, final concentration 5 mg/mL), buffer (4 mL via a 1 M KPi, NH_4HCOO solution pH 7.0, final concentration 100 mM KPi, 100 mM NH_4HCOO), 4 mL MeOH and 25.6 mL ddH_2O to a final volume of 40 mL. Purification by automated gradient flash chromatography (C18, MeOH:H_2O 1:99 to 1:0 over 30 column volumes) and subsequent lyophilization gave 182 mg of **5b** as a white solid (0.80 mmol, 80%). ^{1}H NMR was used to assess stereochemical purity. Reaction, isolation, and characterization completed by Sam Bruffy.

^{1}H NMR (500 MHz, MeOD, major diastereomer (*): minor diastereomer (^) = 3:2) δ 7.26 (*^, ddd, *J* = 8.8, 7.3, 1.4 Hz, 3H), 6.99 (*^, ddd, *J* = 8.8, 2.8, 1.0 Hz, 3H), 6.93 (*^, tq, *J* = 7.3, 1.2 Hz, 2H), 4.19 (*, d, *J* = 9.5 Hz, 1H), 4.10 (*, d, *J* = 9.4 Hz, 1H), 4.05 (^, zzd, *J* = 9.7 Hz, 0.55H), 3.94 (^, d, *J* = 9.7 Hz, 0.55H), 3.72 (*, s, 1H), 3.62 (^, s, 0.54H), 1.46 (^, s, 1.56H), 1.34 (*, s, 3H).

^{13}C{^{1}H} NMR (126 MHz, MeOD, major* minor^) δ 173.83*, 173.18^, 160.31*, 160.14^, 130.41*^, 122.18^, 122.05*, 115.87*^, 74.49*, 74.24^, 62.39^, 61.14*, 23.16^, 20.56*.

HRMS (ESI$^-$): Calc. for $C_{11}H_{15}NO_4^-$ $[M - H]^-$ requires 224.0928; found 224.0930.

1-(4-nitrophenoxy)propan-2-one (6a)

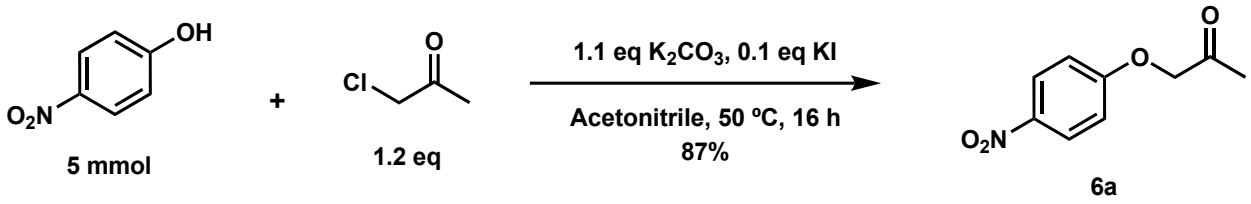

Ketone substrate **5a** was prepared with commercially available reagents. K_2CO_3 (770 mg, 5.57 mmol), KI (90 mg, 0.54 mmol), and 4-nitrophenol (682 µL, 696 mg, 5.00 mmol) were combined in a round bottom flask with 15 mL of acetonitrile at 50 ºC. Chloroacetone (499 µL 574 mg, 6.20 mmol) was added gradually over ~30 s. The reaction mixture was filtered and concentrated via rotary evaporation. Purification by automated gradient flash chromatography (silica gel, Hexane/EtOAc 19:1 to 9:1 over 20 column volumes) gave a crude product as a yellow solid (942 mg, 4.34 mmol, 90% pure). The crude material contained water and dichloromethane but was otherwise sufficiently pure for subsequent experiments. ^{1}H chemical shifts were consistent with previous reports.[21]

^{1}H NMR (400 MHz, $CDCl_3$) δ 8.28 – 8.16 (m, 2H), 7.01 – 6.91 (m, 2H), 4.67 (s, 2H), 2.31 (s, 3H)

(2*S*,3*S*)-2-amino-3-hydroxy-3-methyl-4-(4-nitrophenoxy)butanoic acid (6b)

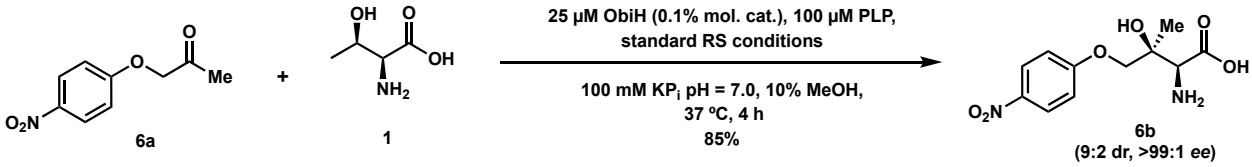

[0.1% mol. cat] Amino acid **6b** was prepared following General Procedure A with 1-(4-nitrophenoxy)propan-2-one (**6a**, 216 mg, 90% purity, 1.00 mmol), Thr (**1**, 478 mg, 4.0 mmol), PLP (200 µL via 20 mM solution in water, 0.004 mmol), NAD^+ (400 µL via 10 mM solution in water, 0.004 mmol), purified ObiH (2.5 mL via a 400 µM solution in 100 mM KPi pH 8.0, final concentration 25 µM), *Sc*ADH lysate (4.00 mL via a 250 mg/mL solution in 100 mM KP_i pH 7.0, final concentration 25 mg/mL), *Cb*FDH lysate (0.80 mL via a 250 mg/mL solution in 100 mM KP_i

pH 7.0, final concentration 5 mg/mL), buffer (4 mL via a 1 M KPi, NH_4HCOO solution pH 7.0, final concentration 100 mM KPi, 100 mM NH_4HCOO), 4 mL MeOH and 24.1 mL ddH_2O to a final volume of 40 mL. Purification by automated gradient flash chromatography (C18, MeOH:H_2O 1:99 to 1:0 over 30 column volumes) and subsequent lyophilization gave 239 mg of product as a yellow solid with 11 mg Thr contamination as determined by ^{1}H NMR, yielding 228 mg of **6b** (0.85 mmol, 85%). ^{1}H NMR was used to assess stereochemical purity. (i.e., 9:2 dr and >99% *ee*).

^{1}H NMR (500 MHz, MeOD, major diastereomer (*): minor diastereomer (^) = 9:2) δ 8.21 (*^, dd, J = 9.1, 1.9 Hz, 2.5H), 7.15 (*^, dd, 2.5H), 4.30 (*, d, J = 9.7 Hz, 1H), 4.22 (*, d, J = 9.6 Hz, 1H), 4.16 (^, d, J = 9.8 Hz, 0.24H), 4.06 (^, d, J = 9.8 Hz, 0.23H), 3.63 (*, s, 1H), 3.57 (^, s, 0.17H), 1.40 (^, s, 0.64H), 1.33 (*, s, 3H).

^{13}C{^{1}H} NMR (126 MHz, MeOD, major* minor^) δ 173.68*^, 165.56*^, 142.96*^, 126.73*, 126.70^, 116.08^, 116.06*, 75.09*, 74.70^, 72.62*^, 61.19*^, 22.36^, 20.43*.

HRMS (ESI$^-$): Calc. for $C_{11}H_{15}NO_4^-$ [M – H]$^-$ requires 269.0779; found 269.0780.

6-(2-oxopropoxy)-2*H*-chromen-2-one (7a)

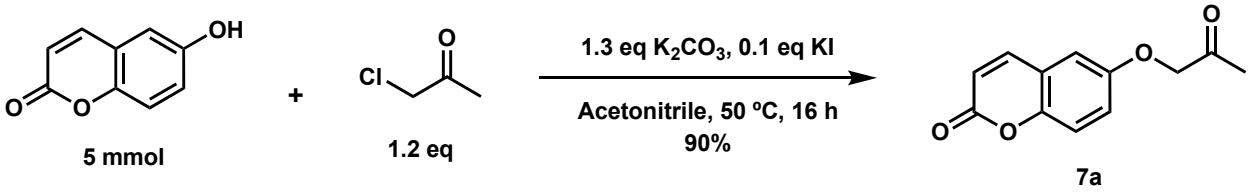

Ketone substrate **7a** was prepared with commercially available reagents. K_2CO_3 (923 mg, 6.68 mmol), KI (79 mg, 0.47 mmol), and 6-hydroxy-*2H*-chromen-2-one (836 mg, 5.15 mmol) were combined in a round bottom flask with 15 mL of acetonitrile at 50 ºC. Chloroacetone (483 µL 555 mg, 6.00 mmol) was added gradually over ~30 s. The reaction mixture was filtered and concentrated via rotary evaporation. Purification by automated gradient flash chromatography (silica gel, Hexane/EtOAc 19:1 to 9:1 over 20 column volumes) gave product as a white solid (1007 mg, 4.62 mmol, >95% pure). ^{1}H chemical shifts were consistent with previous reports.[22]

^{1}H NMR (400 MHz, $CDCl_3$) δ 7.66 (d, *J* = 9.6 Hz, 1H), 7.32 (d, *J* = 9.0 Hz, 1H), 7.16 (dt, *J* = 9.1, 1.9 Hz, 1H), 6.91 (d, *J* = 2.9 Hz, 1H), 6.47 (dd, *J* = 9.5, 1.1 Hz, 1H), 4.62 (d, *J* = 1.1 Hz, 2H), 2.32 (d, *J* = 1.2 Hz, 3H).

(2*S*,3*S*)-2-amino-3-hydroxy-3-methyl-4-((2-oxo-2H-chromen-6-yl)oxy)butanoic acid (7b)

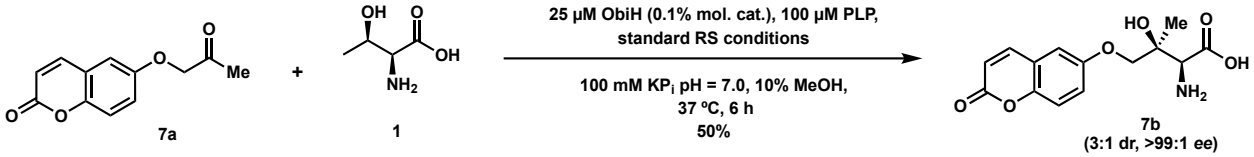

[0.1% mol. cat] Amino acid **7b** was prepared following General Procedure A with 6-(2-oxopropoxy)-2H-chromen-2-one (**7a**, 222 mg, >95% purity, 1.02 mmol), Thr (**1**, 479 mg, 4.0 mmol), PLP (200 µL via 20 mM solution in water, 0.004 mmol), NAD^+ (400 µL via 10 mM solution in water, 0.004 mmol), purified ObiH (1 mL via a 1.00 mM solution in 100 mM KPi pH 8.0, final concentration 25 µM), *Sc*ADH lysate (4.00 mL via a 250 mg/mL solution in 100 mM KP_i pH 7.0, final concentration 25 mg/mL), *Cb*FDH lysate (0.80 mL via a 250 mg/mL solution in 100 mM KP_i pH 7.0, final concentration 5 mg/mL), buffer (4 mL via a 1 M KPi, NH_4HCOO solution pH 7.0, final concentration 100 mM KPi, 100 mM NH_4HCOO), 4 mL MeOH and 25.6 mL ddH_2O to a final volume of 40 mL. Purification by automated gradient flash chromatography (C18, MeOH:H_2O 1:99 to 1:0 over 30 column volumes) and subsequent lyophilization gave 150 mg of **7b** as a white solid (0.51 mmol, 50%). ^{1}H NMR was used to assess stereochemical purity. (i.e., 3:1 dr and >99% *ee*).

^{1}H NMR (500 MHz, MeOD, major diastereomer (*): minor diastereomer (^) = 3:1) δ 7.94 (*^, dd, J = 9.6, 3.6 Hz, 1.37H), 7.31 (*^, d, J = 1.5 Hz, 2.66H), 7.25 (*^, s, 1.31H), 6.45 (*^, d, J = 9.5 Hz, 1.39H), 4.26 (*, d, J = 9.4 Hz, 1H), 4.17 (*, d, J = 9.4 Hz, 1H), 4.11 (^, d, J = 9.7 Hz, 0.44H), 4.01 (^, d, J = 9.7 Hz, 0.37H), 3.70 (*, s, 1H), 3.62 (^, s, 0.33H), 1.46 (^, s, 1H), 1.36 (*, s, 3H).

^{13}C{^{1}H} NMR (126 MHz, MeOD, major* minor^) δ 173.83*^, 163.12*, 163.10^, 157.09*, 156.95^, 149.91^, 149.85*, 145.60*, 145.57^, 121.74*^, 120.79*, 120.76^, 118.55*, 118.53^, 117.37*^, 112.74^, 112.63*, 75.24*, 75.00^, 72.62^, 72.54*, 62.12^, 61.21*, 22.82^, 20.50*.

HRMS (ESI$^-$): Calc. for $C_{11}H_{15}NO_4^-$ [M – H]$^-$ requires 292.0827; found 292.0830.

1-(quinolin-8-yloxy)propan-2-one (8a)

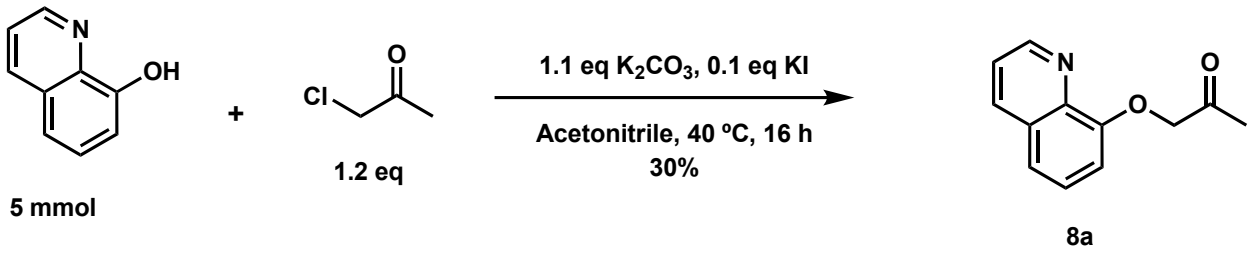

Ketone substrate **8a** was prepared with commercially available reagents. K_2CO_3 (758 mg, 5.48 mmol), KI (92 mg, 0.55 mmol), and quinolin-8-ol (724 mg, 4.99 mmol) were combined in a round bottom flask with 15 mL of acetonitrile at 50 ºC. Chloroacetone (483 µL 555 mg, 6.00 mmol) was added gradually over ~30 s. The reaction mixture was filtered and concentrated via rotary evaporation. Purification by automated gradient flash chromatography (silica gel, Hexane/EtOAc 19:1 to 9:1 over 20 column volumes) gave product as a brown solid (301 mg, 1.50 mmol, >95% pure). ^{1}H chemical shifts were consistent with previous reports.[23]

^{1}H NMR (500 MHz, $CDCl_3$) δ 8.95 (dd, *J* = 4.2, 1.7 Hz, 1H), 8.14 (dt, *J* = 8.3, 1.7 Hz, 1H), 7.47 – 7.38 (m, 3H), 6.89 (dt, *J* = 7.5, 1.5 Hz, 1H), 4.86 (s, 2H), 2.31 (s, 3H).

(2*S*,3*S*)-2-amino-3-hydroxy-3-methyl-4-(quinolin-8-yloxy)butanoic acid (8b)

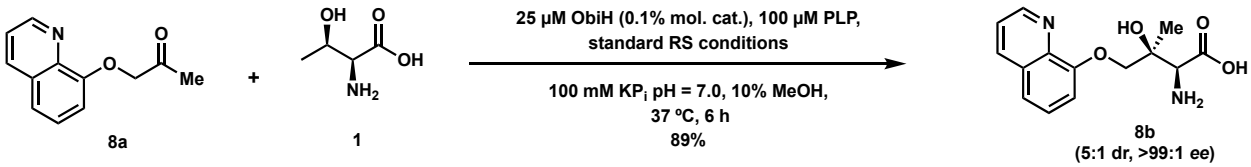

[0.1% mol. cat] Amino acid **8b** was prepared following General Procedure A with 1-(quinolin-8-yloxy)propan-2-one (**8a**, 206 mg, >95% purity, 1.02 mmol), Thr (**1**, 480 mg, 4.0 mmol), PLP (200 µL via 20 mM solution in water, 0.004 mmol), NAD$^+$ (400 µL via 10 mM solution in water, 0.004 mmol), purified ObiH (1 mL via a 1.00 mM solution in 100 mM KPi pH 8.0, final concentration 25 µM), *Sc*ADH lysate (4.00 mL via a 250 mg/mL solution in 100 mM KP$_i$ pH 7.0, final concentration

25 mg/mL), *Cb*FDH lysate (0.80 mL via a 250 mg/mL solution in 100 mM KP_i pH 7.0, final concentration 5 mg/mL), buffer (4 mL via a 1 M KPi, NH_4HCOO solution pH 7.0, final concentration 100 mM KPi, 100 mM NH_4HCOO), 4 mL MeOH and 25.6 mL ddH_2O to a final volume of 40 mL. Purification by automated gradient flash chromatography (C18, MeOH:H_2O 1:99 to 1:0 over 30 column volumes) and subsequent lyophilization gave 251 mg of **8b** as a white solid (0.90 mmol, 89%). ^{1}H NMR was used to assess stereochemical purity. (i.e., 5:1 dr and >99% *ee*).

^{1}H NMR (500 MHz, MeOD, major diastereomer (*): minor diastereomer (^) = 5:1) δ 8.86 (*, dd, *J* = 4.3, 1.7 Hz, 1H), 8.79 (^, dd, *J* = 3.8, 2.0 Hz, .13H), 8.36 (*, dd, *J* = 8.3, 1.7 Hz, 1H), 8.32 (^, dd, *J* = 8.3, 1.7 Hz, .19H), 7.62 – 7.55 (*^, m, 1.18H), 7.55 – 7.50 (*^m, 2.41H), 7.26 (*, dd, *J* = 6.5, 2.5 Hz, 1H), 7.24 – 7.21 (^,m, .18H), 4.51 (*, d, *J* = 9.2 Hz, 1H), 4.3 (^, d, *J* = 9.2 Hz, 0.2H), 4.28 (*, d, *J* = 9.2 Hz, 1H), 4.24 (^, d, *J* = 9.2 Hz, 0.21H), 3.87 (*, s, 1H), 3.72 (^, s, 0.19H), (^, 1.60 (s, 0.59H), 1.40 (*, s, 3H).

^{13}C{^{1}H} NMR (126 MHz, MeOD major* minor^) δ 172.95*^, 155.55^, 155.19*, 150.05^, 149.88*, 141.15^, 140.67*, 138.34*, 137.94^, 131.13*, 131.03^, 128.50*, 128.25^, 123.09*, 122.73^, 121.56^, 121.27*, 111.49^, 111.03*, 76.28^, 76.17*, 72.33*, 72.26^, 63.78^, 61.51*, 23.97^, 20.18*.

HRMS (ESI^-): Calc. for $C_{11}H_{15}NO_4^-$ $[M - H]^-$ requires 275.1037; found 275.1038.

NMR Spectra

(2*S*,3*R*)-2-amino-3-benzyl-4,4,4-trifluoro-3-hydroxybutanoic acid (3b)

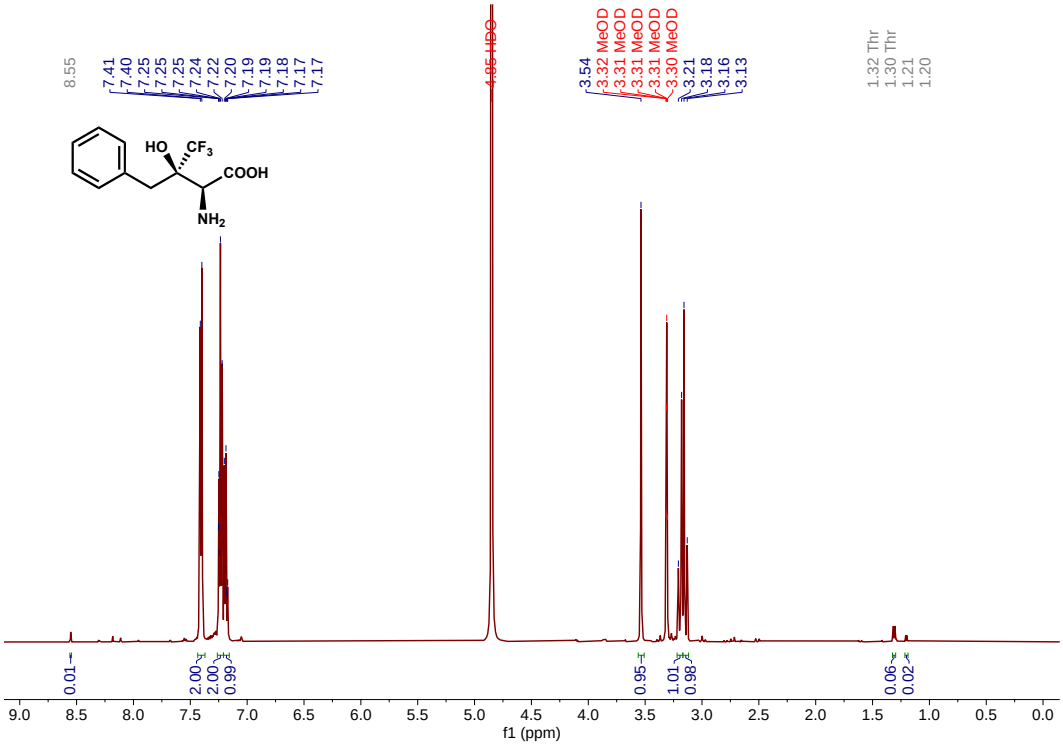

^{1}H NMR spectrum in CD_3OD at 500 MHz

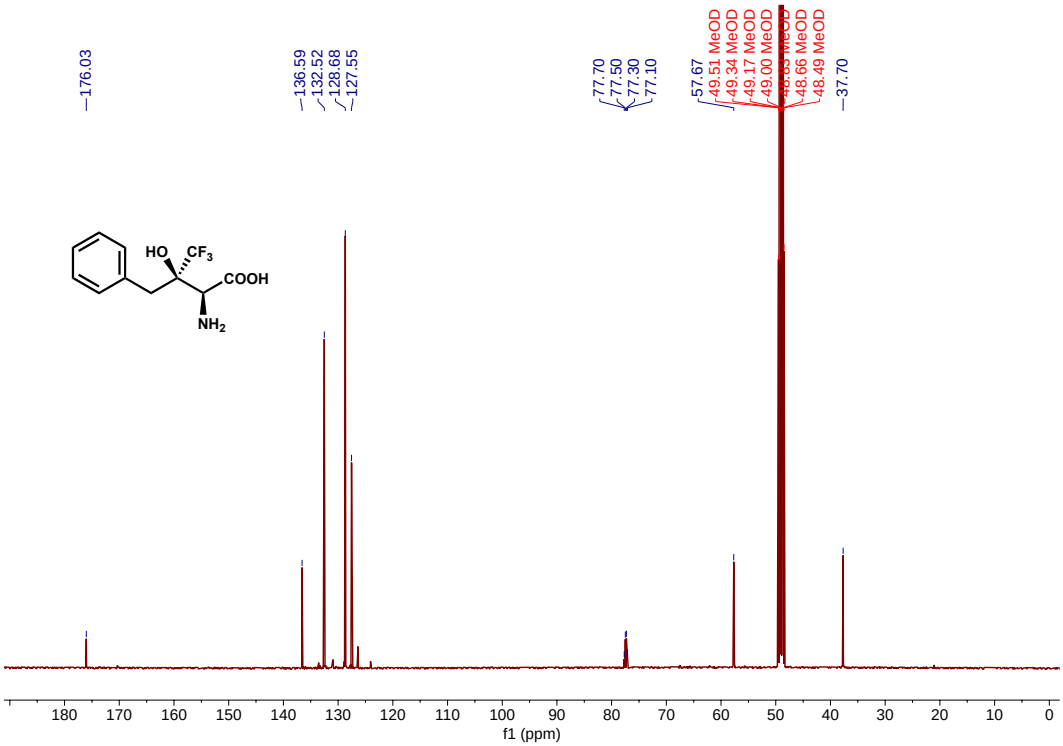

^{13}C NMR spectrum in CD_3OD at 126 MHz

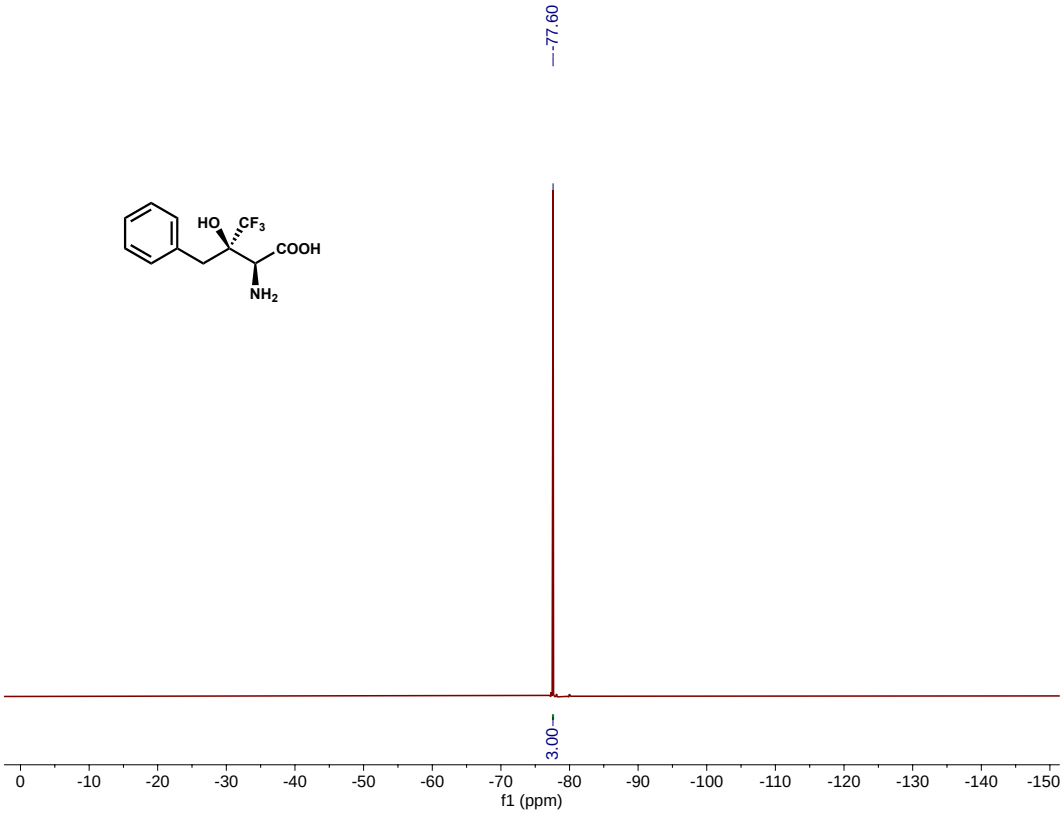

^{19}F NMR spectrum in CD_3OD at 377 MHz

(2*S*,3*R*)-2-amino-4-(4-fluorophenyl)-3-hydroxy-3-methylbutanoic acid (4b)

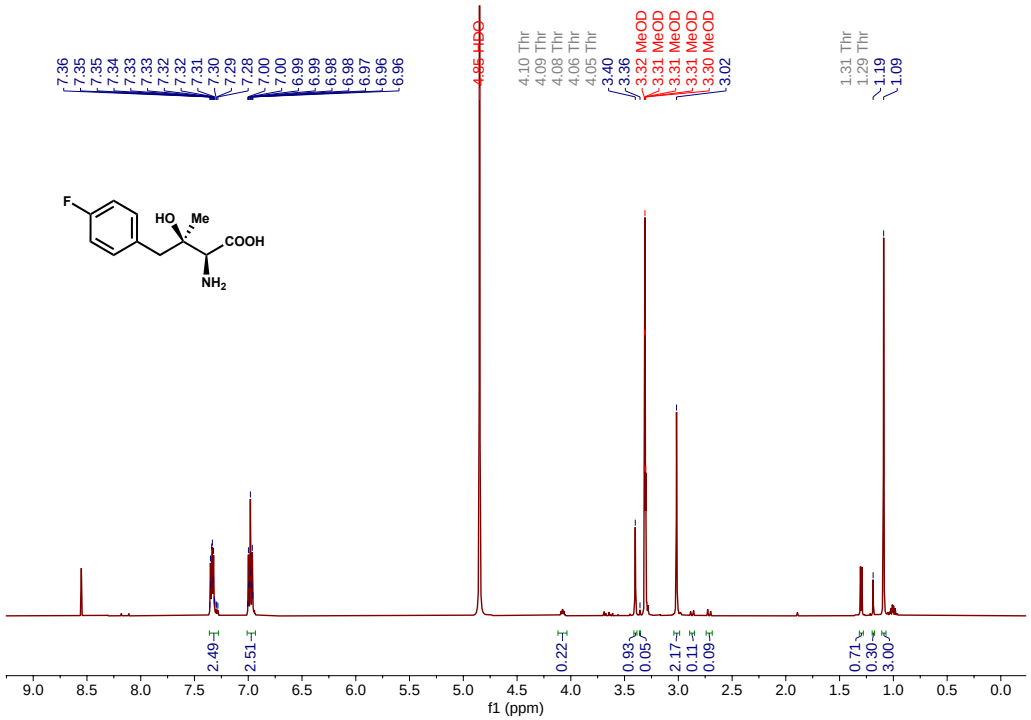

^{1}H NMR spectrum in CD_3OD at 500 MHz

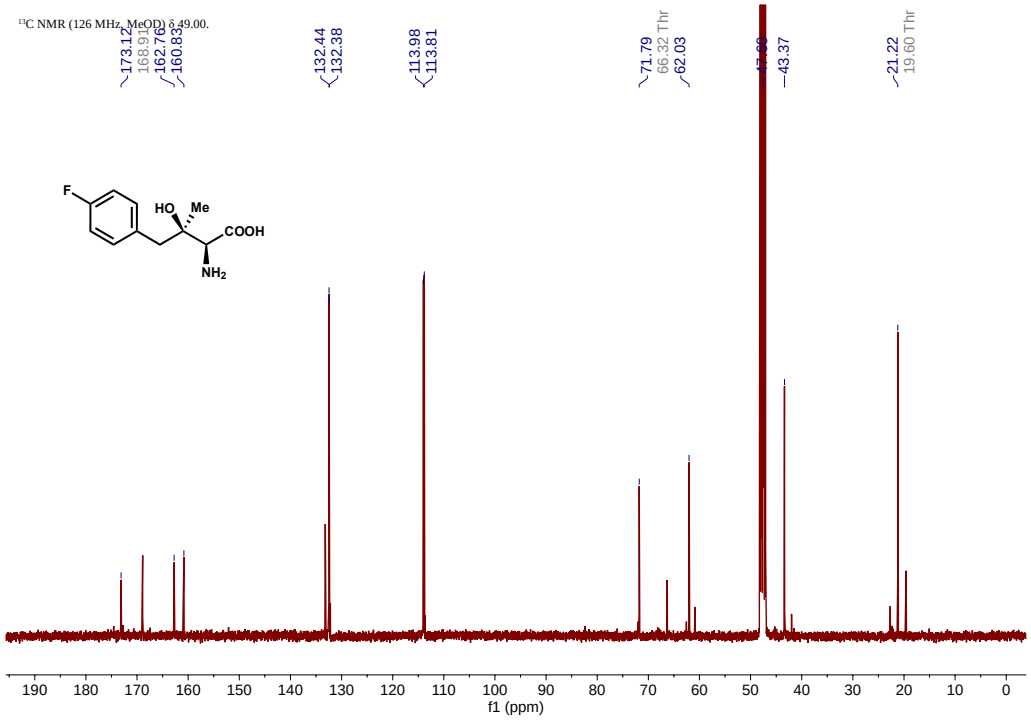

^{13}C NMR spectrum in CD_3OD at 126 MHz

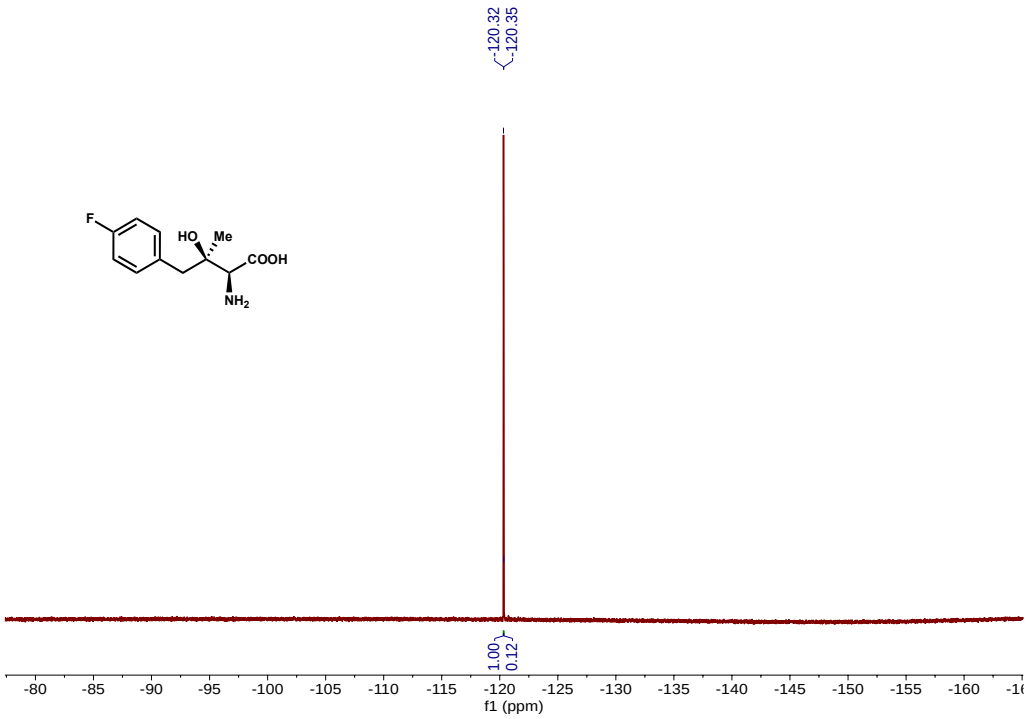

^{19}F NMR spectrum in CD_3OD at 377 MHz

(2*S*,3*S*)-2-amino-3-hydroxy-3-methyl-4-phenoxybutanoic acid (5b)

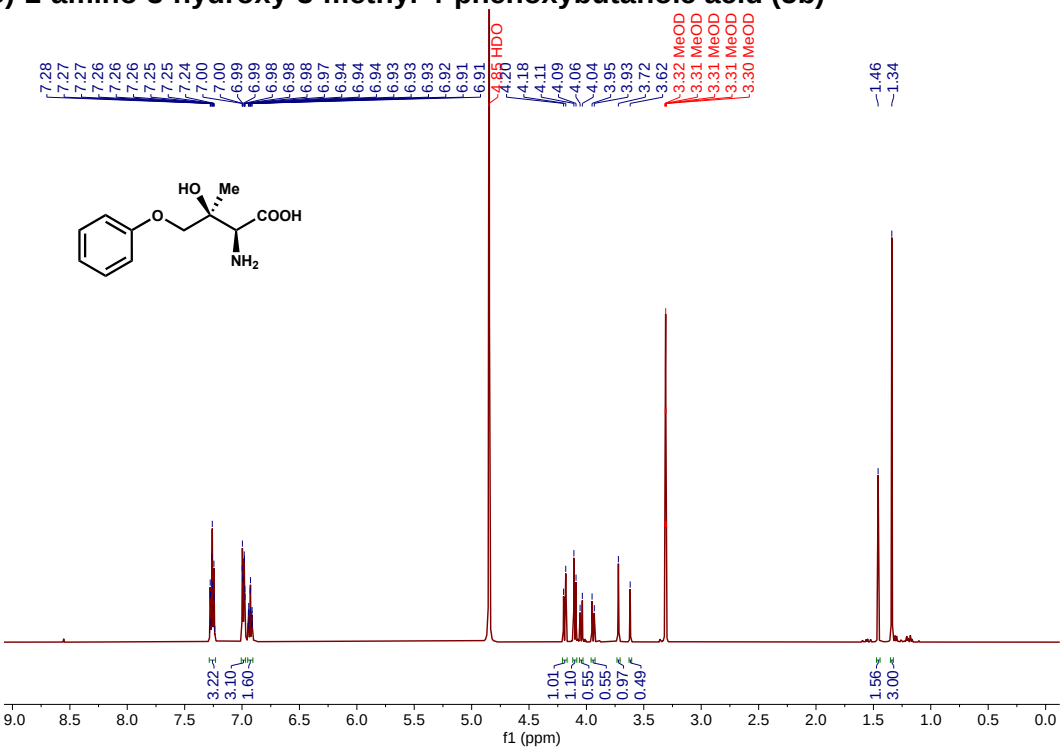

^{1}H NMR spectrum in CD_3OD at 500 MHz

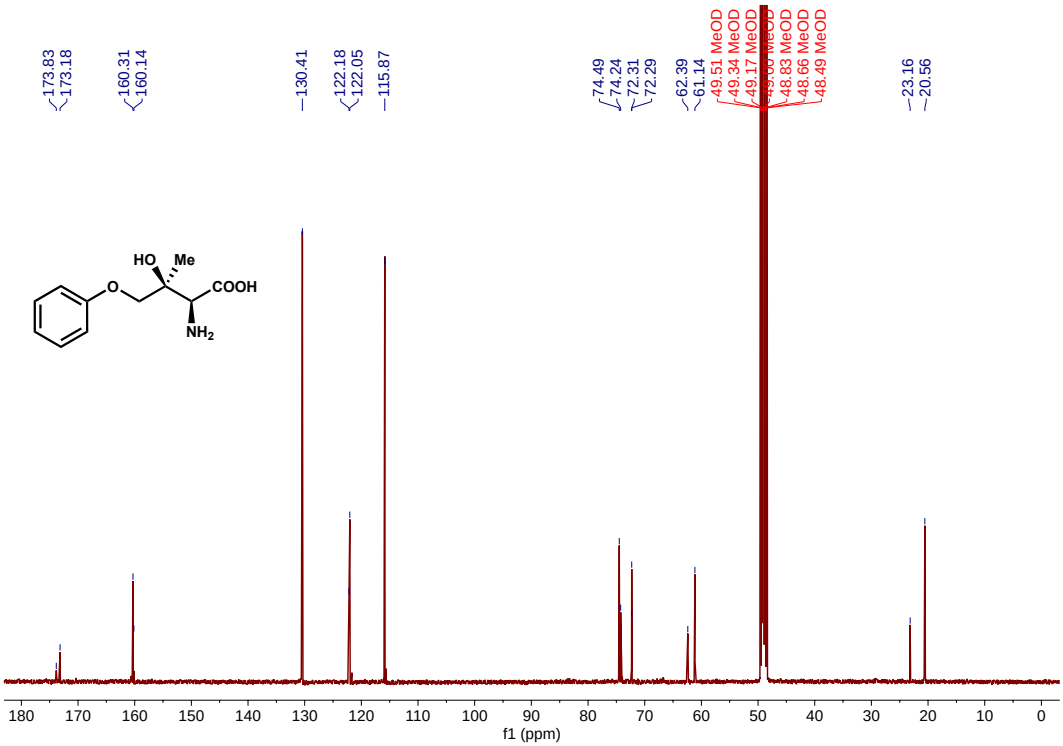

^{13}C NMR spectrum in CD_3OD at 126 MHz

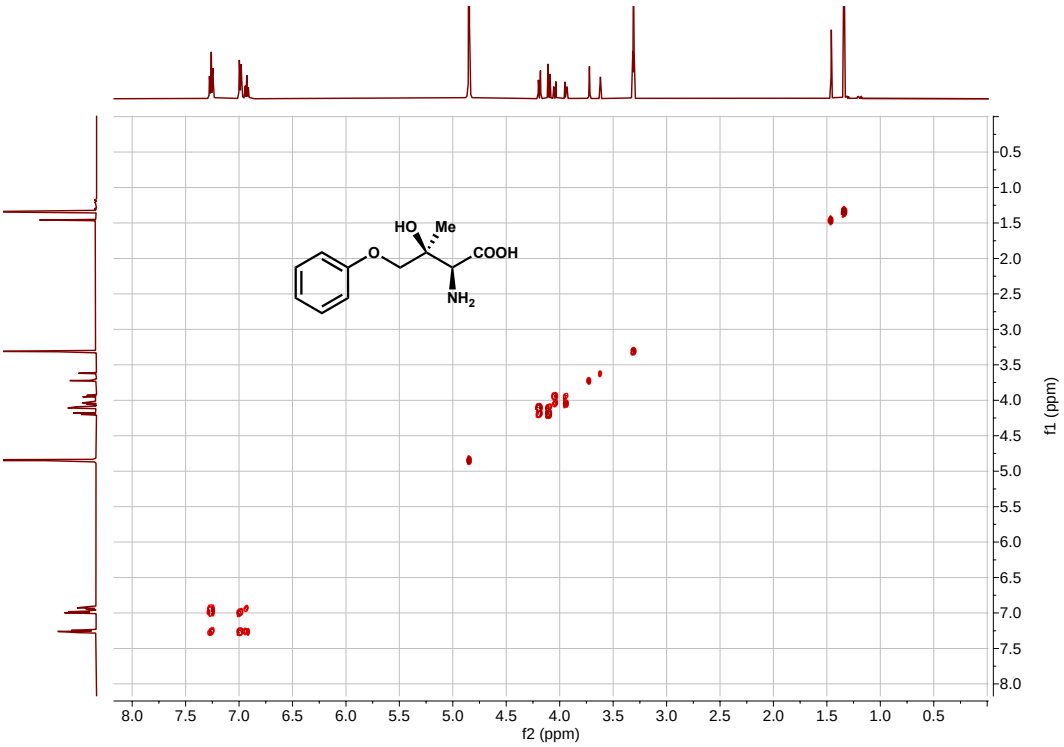

COSY Spectrum in CD_3OD at 500 MHz

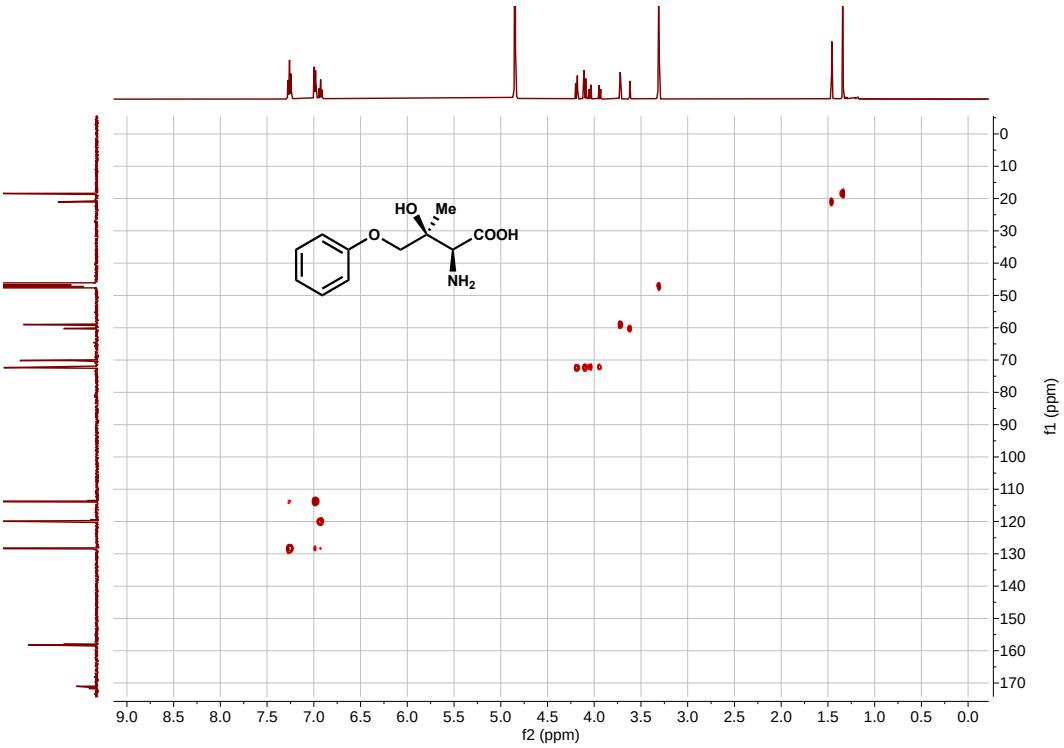

HSQC Spectrum in CD_3OD at 500 MHz and 126 MHz

1-(4-nitrophenoxy)propan-2-one (6a)

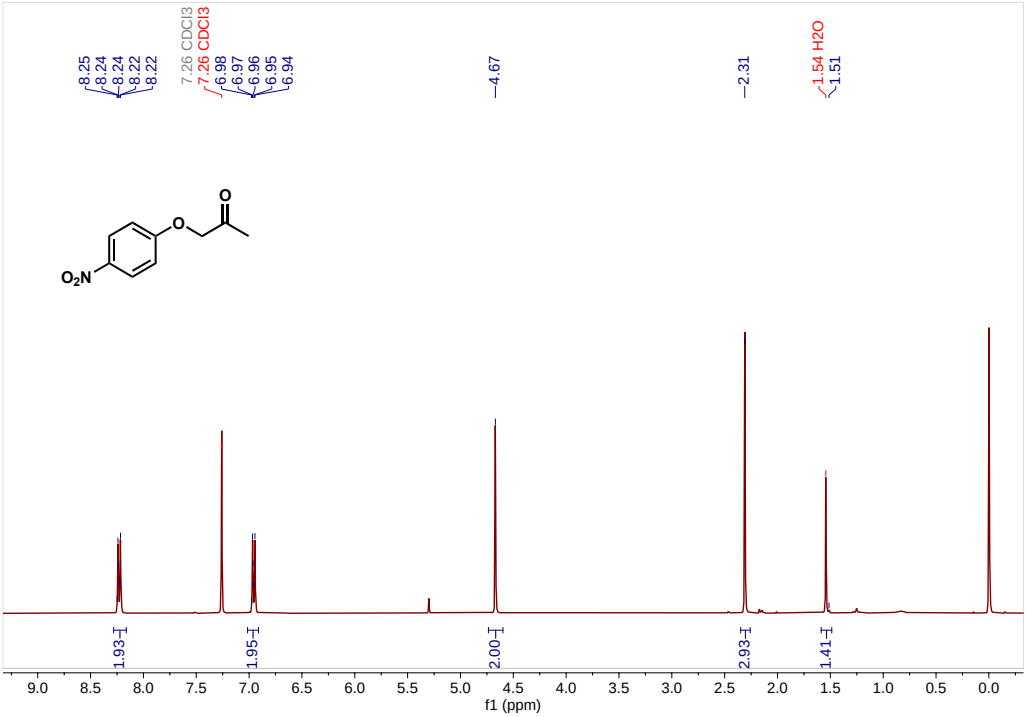

^{1}H NMR spectrum in $CDCl_3$ at 500 MHz

(2*S*,3*S*)-2-amino-3-hydroxy-3-methyl-4-(4-nitrophenoxy)butanoic acid (6b)

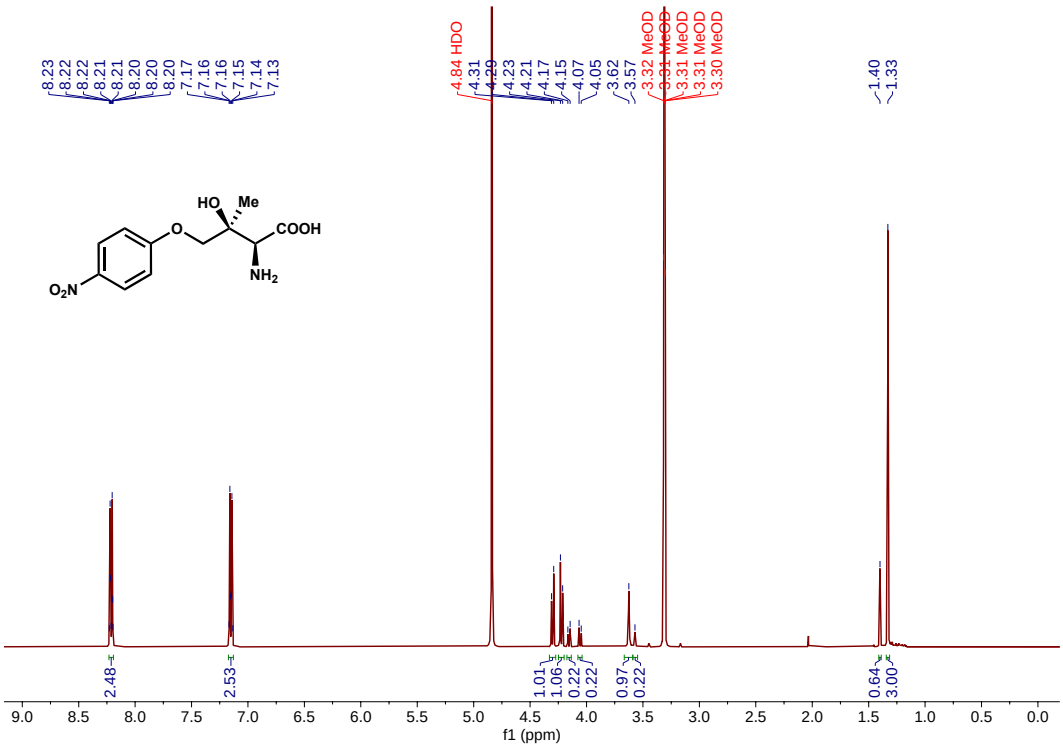

^{1}H NMR spectrum in CD_3OD at 500 MHz

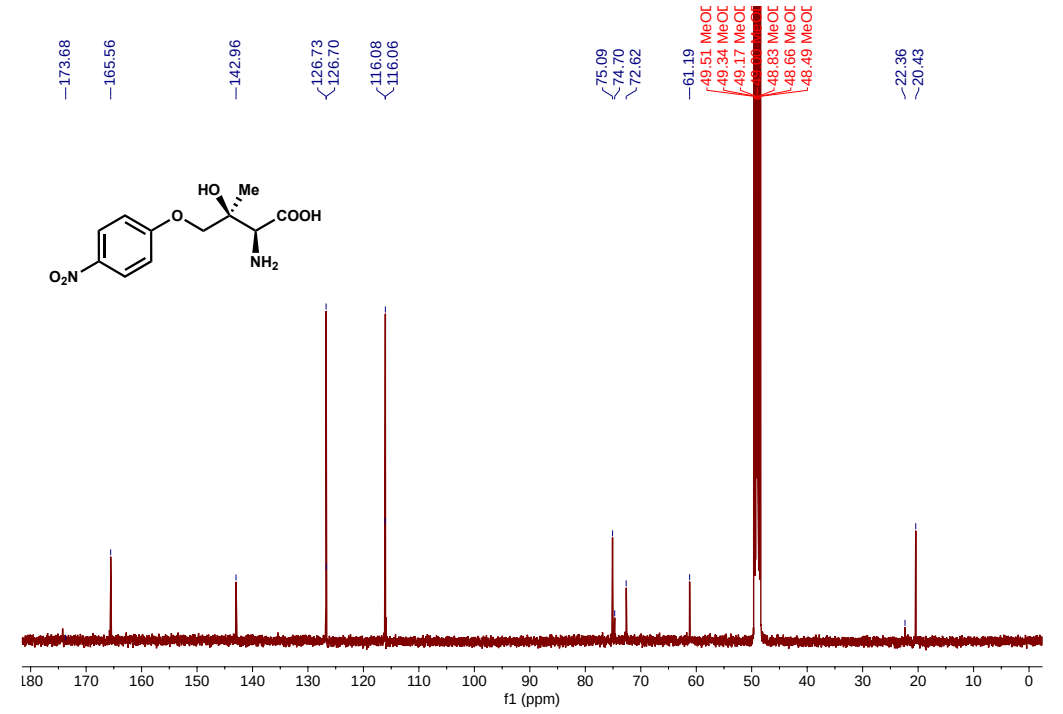

^{13}C NMR spectrum in CD_3OD at 126 MHz

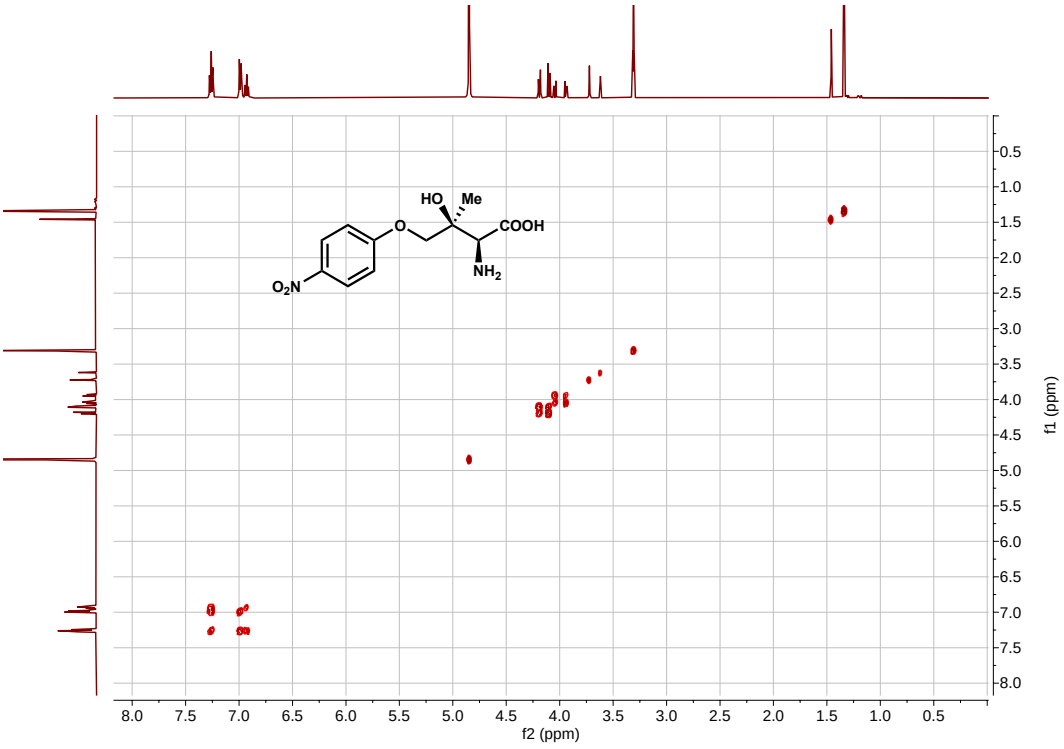

COSY Spectrum in CD_3OD at 500 MHz

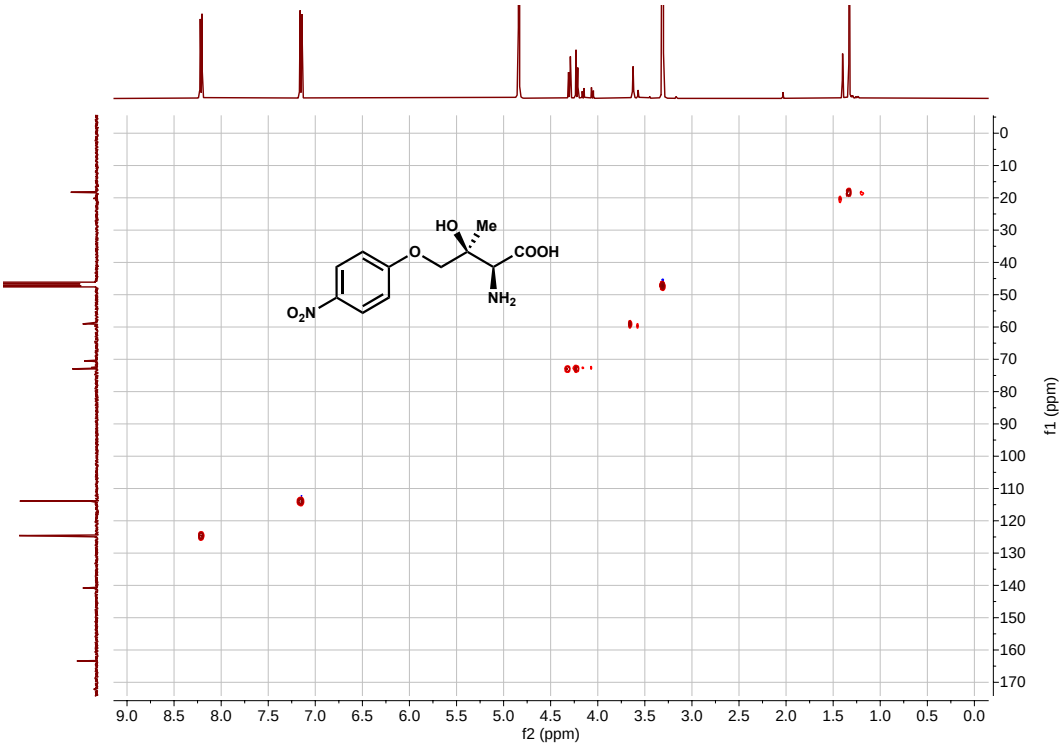

HSQC Spectrum in CD_3OD at 500 MHz and 126 MHz

6-(2-oxopropoxy)-2*H*-chromen-2-one (7a)

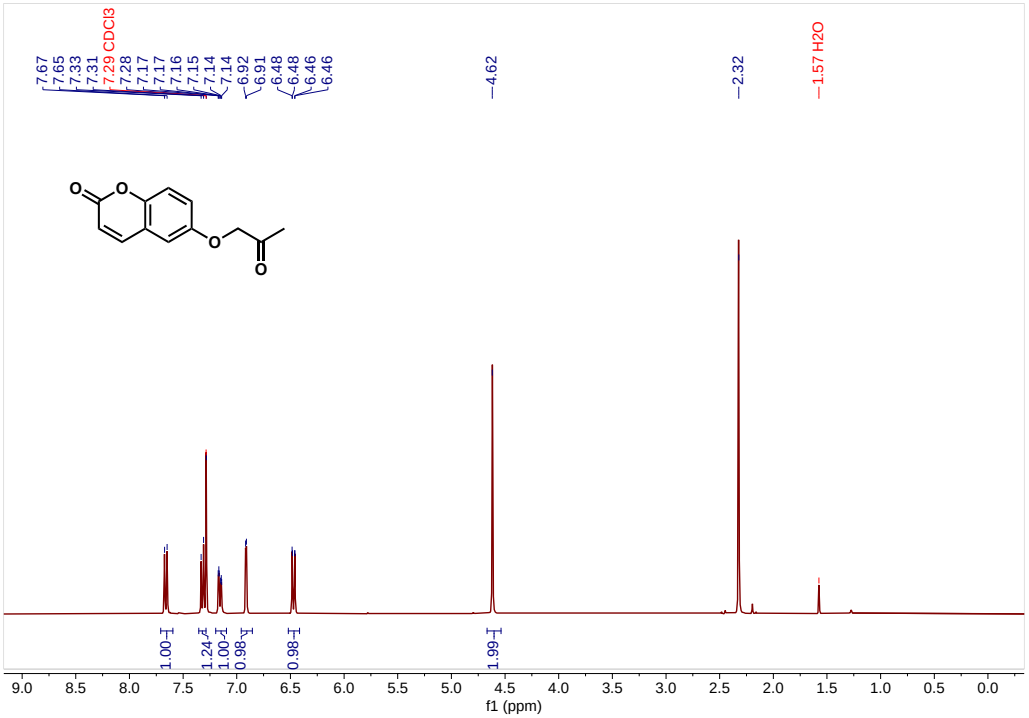

^{1}H NMR spectrum in $CDCl_3$ at 500 MHz

(2*S*,3*S*)-2-amino-3-hydroxy-3-methyl-4-((2-oxo-2H-chromen-6-yl)oxy)butanoic acid (7b)

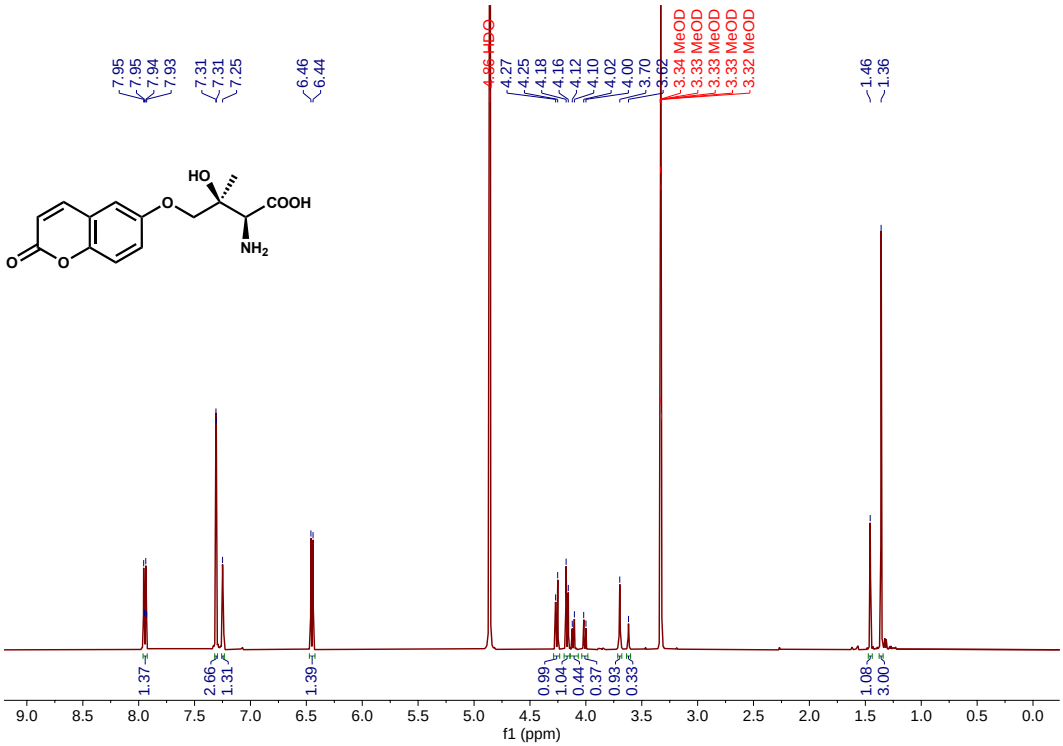

^{1}H NMR spectrum in CD_3OD at 500 MHz

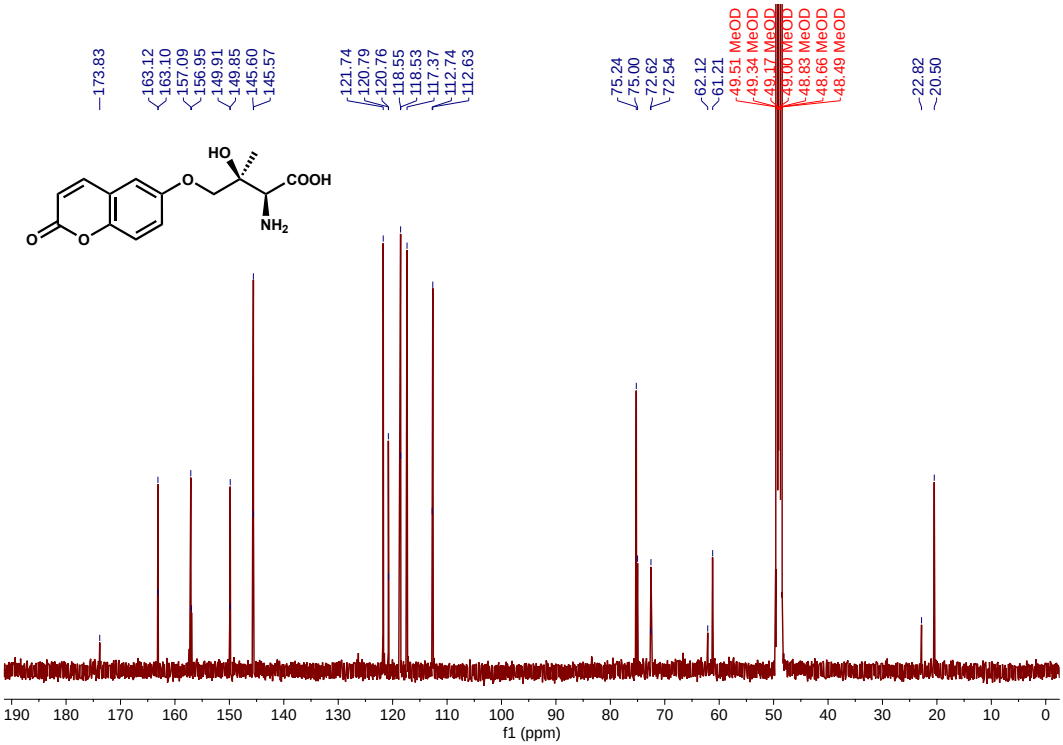

^{13}C NMR spectrum in CD_3OD at 126 MHz

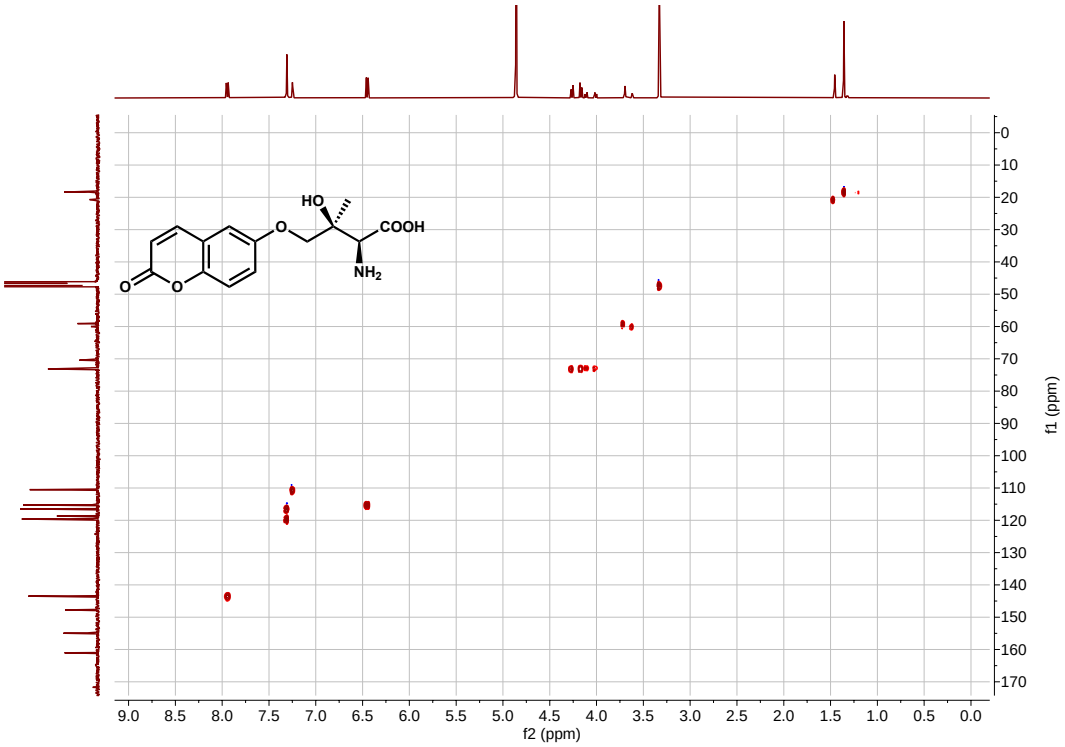

COSY Spectrum in CD_3OD at 500 MHz

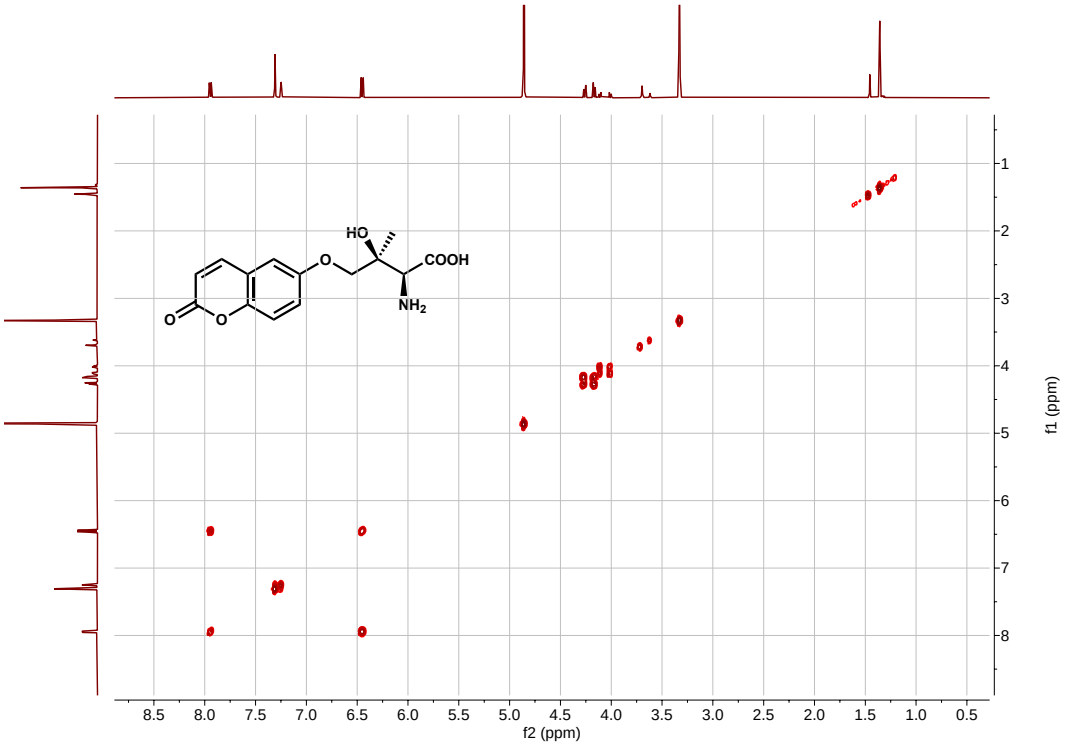

HSQC Spectrum in CD_3OD at 500 MHz and 126 MHz

1-(quinolin-8-yloxy)propan-2-one (8a)

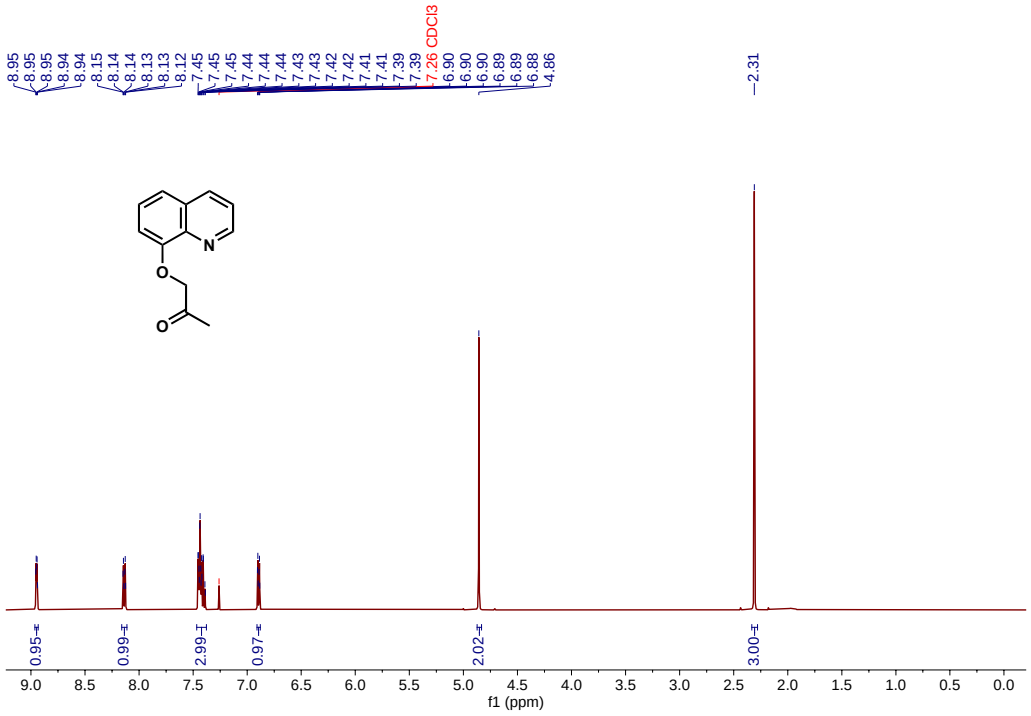

^{1}H NMR spectrum in $CDCl_3$ at 500 MHz

(2*S*,3*S*)-2-amino-3-hydroxy-3-methyl-4-(quinolin-8-yloxy)butanoic acid (8b)

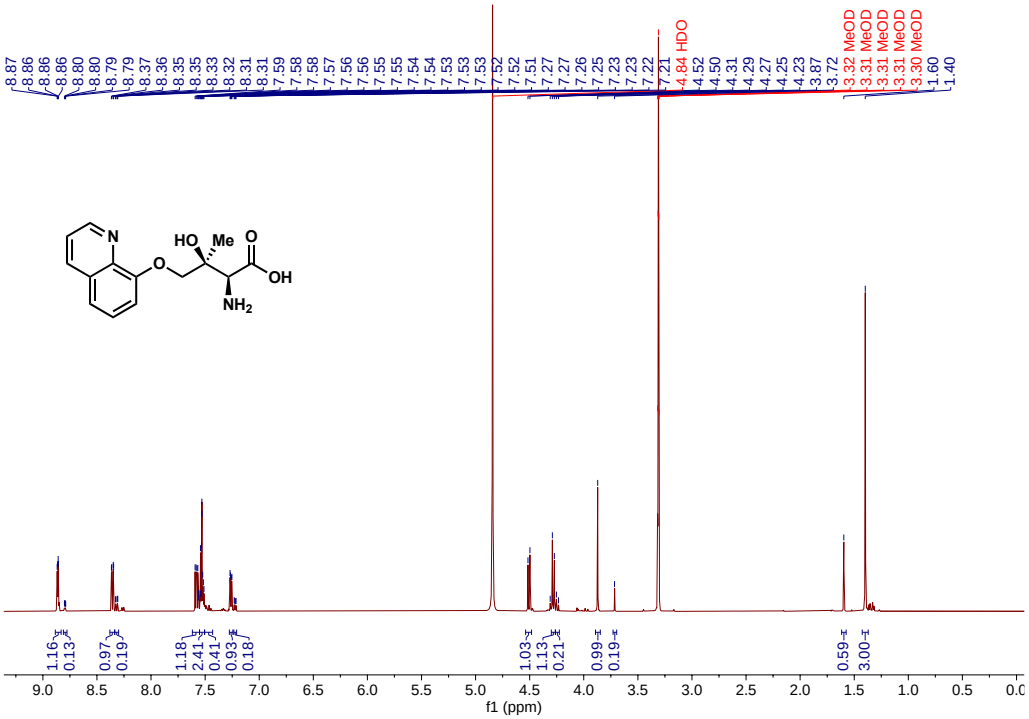

^{1}H NMR spectrum in CD_3OD at 500 MHz

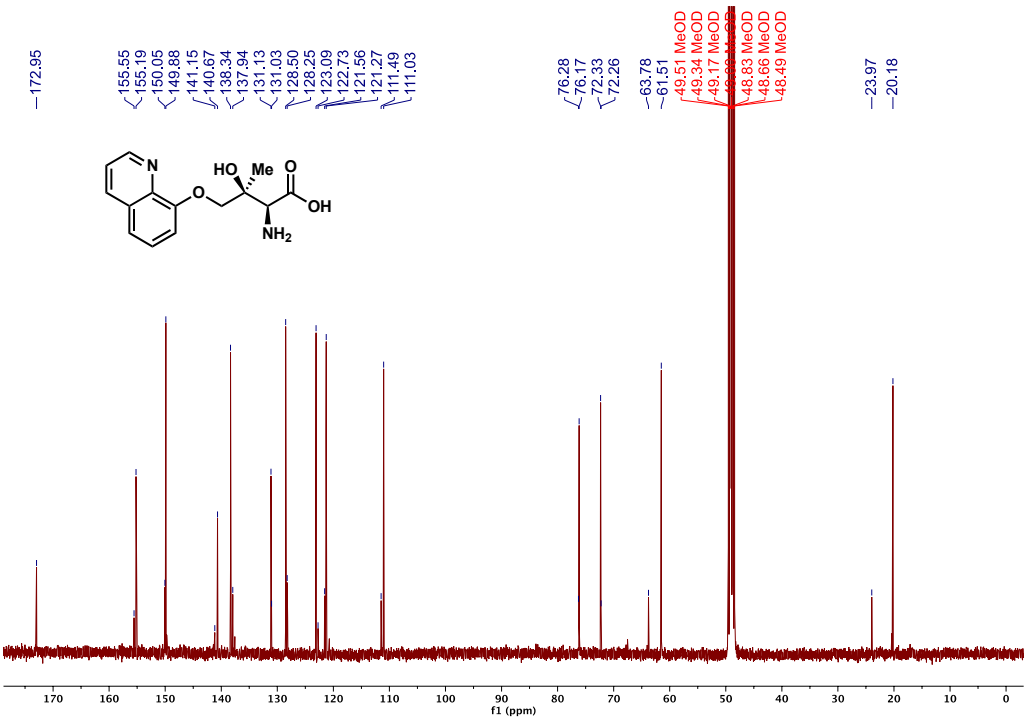

^{13}C NMR spectrum in CD_3OD at 126 MHz

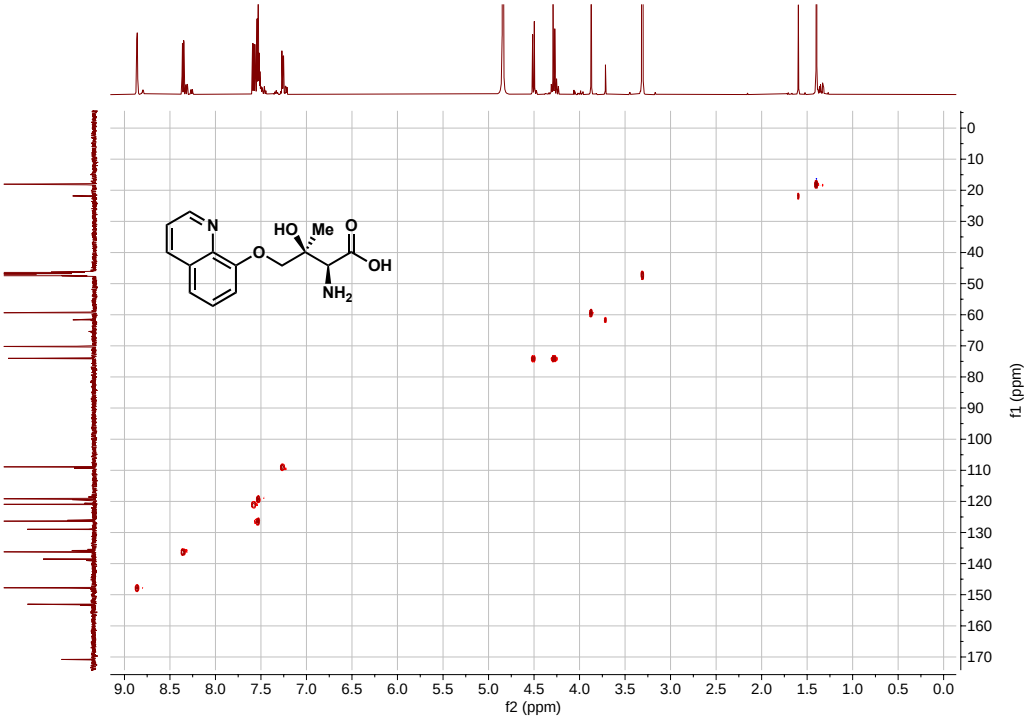

COSY Spectrum in CD_3OD at 500 MHz

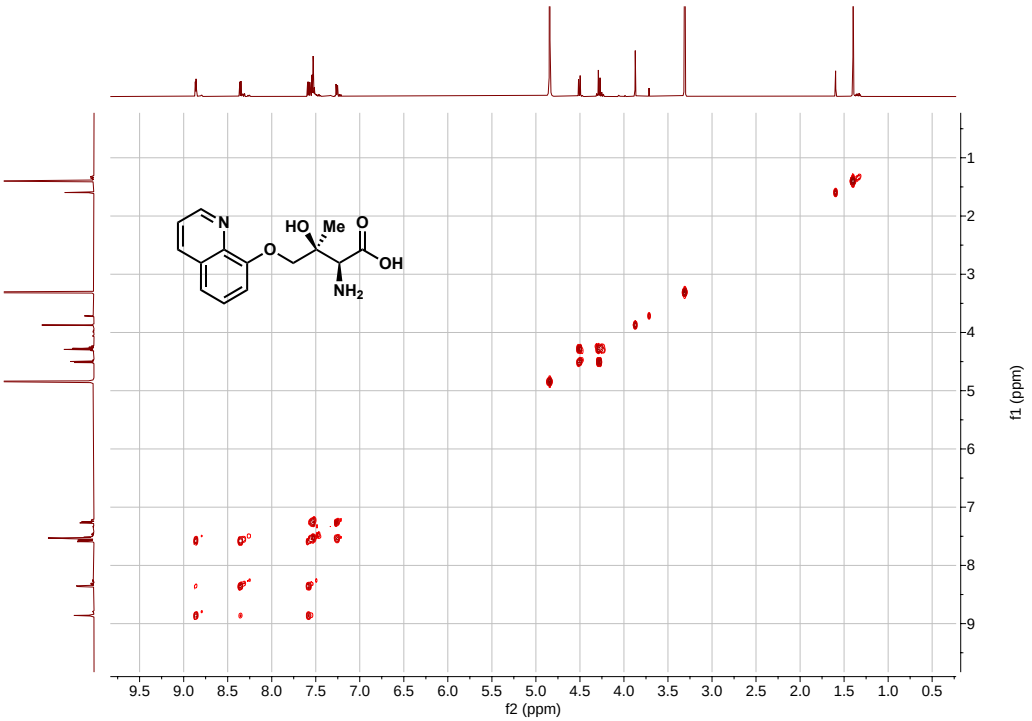

HSQC Spectrum in CD_3OD at 500 MHz and 126 MHz

4. 5. References

(1) France, S. P.; Lewis, R. D.; Martinez, C. A. The Evolving Nature of Biocatalysis in Pharmaceutical Research and Development. *JACS Au*. American Chemical Society March 27, 2022. https://doi.org/10.1021/jacsau.2c00712.

(2) Dadashipour, M.; Asano, Y. Hydroxynitrile Lyases: Insights into Biochemistry, Discovery, and Engineering. *ACS Catalysis*. September 2, 2011, pp 1121–1149. https://doi.org/10.1021/cs200325q.

(3) Huffman, M. A.; Fryszkowska, A.; Alvizo, O.; Borra-Garske, M.; Campos, K. R.; Canada, K. A.; Devine, P. N.; Duan, D.; Forstater, J. H.; Grosser, S. T.; Halsey, H. M.; Hughes, G. J.; Jo, J.; Joyce, L. A.; Kolev, J. N.; Liang, J.; Maloney, K. M.; Mann, B. F.; Marshall, N. M.; McLaughlin, M.; Moore, J. C.; Murphy, G. S.; Nawrat, C. C.; Nazor, J.; Novick, S.; Patel, N. R.; Rodriguez-Granillo, A.; Robaire, S. A.; Sherer, E. C.; Truppo, M. D.; Whittaker, A. M.; Verma, D.; Xiao, L.; Xu, Y.; Yang, H. Design of an in Vitro Biocatalytic Cascade for the Manufacture of Islatravir. *Science (1979)* **2019**, *366* (6470), 1255–1259. https://doi.org/10.1126/science.aay8484.

(4) Haridas, M.; Abdelraheem, E. M. M.; Hanefeld, U. 2-Deoxy-d-Ribose-5-Phosphate Aldolase (DERA): Applications and Modifications. *Applied Microbiology and Biotechnology*. Springer Verlag December 1, 2018, pp 9959–9971. https://doi.org/10.1007/s00253-018-9392-8.

(5) Li, Z.; Jangra, H.; Chen, Q.; Mayer, P.; Ofial, A. R.; Zipse, H.; Mayr, H. Kinetics and Mechanism of Oxirane Formation by Darzens Condensation of Ketones: Quantification of the Electrophilicities of Ketones. *J Am Chem Soc* **2018**, *140* (16), 5500–5515. https://doi.org/10.1021/jacs.8b01657.

(6) Laurent, V.; Gourbeyre, L.; Uzel, A.; Hélaine, V.; Nauton, L.; Traïkia, M.; De Berardinis, V.; Salanoubat, M.; Gefflaut, T.; Lemaire, M.; Guérard-Hélaine, C. Pyruvate Aldolases Catalyze Cross-Aldol Reactions between Ketones: Highly Selective Access to Multi-Functionalized Tertiary Alcohols. *ACS Catal* **2020**, *10* (4), 2538–2543. https://doi.org/10.1021/acscatal.9b05512.

(7) Laurent, V.; Darii, E.; Aujon, A.; Debacker, M.; Petit, J.-L.; Hélaine, V.; Liptaj, T.; Breza, M.; Mariage, A.; Nauton, L.; Traïkia, M.; Salanoubat, M.; Lemaire, M.; Guérard-Hélaine, C.; de Berardinis, V. Synthesis of Branched-Chain Sugars with a DHAP-Dependent Aldolase: Ketones Are Electrophile Substrates of Rhamnulose-1-Phosphate Aldolases. *Angewandte Chemie* **2018**, *130* (19), 5565–5569. https://doi.org/10.1002/ange.201712851.

(8) Theisen, M. J.; Misra, I.; Saadat, D.; Campobasso, N.; Miziorko, H. M.; Harrison, D. H. T. *3-Hydroxy-3-Methylglutaryl-CoA Synthase Intermediate Complex Observed in "'real-Time';"* 2004. www.povray.

(9) Seiple, I. B.; Mercer, J. A. M.; Sussman, R. J.; Zhang, Z.; Myers, A. G. Stereocontrolled Synthesis of Syn-β-Hydroxy-α-Amino Acids by Direct Aldolization of Pseudoephenamine Glycinamide. *Angewandte Chemie - International Edition* **2014**, *53* (18), 4642–4647. https://doi.org/10.1002/anie.201400928.

(10) Wang, S.; Deng, H. Peculiarities of Promiscuous L-Threonine Transaldolases for Enantioselective Synthesis of β-Hydroxy-α-Amino Acids. https://doi.org/10.1007/s00253-021-11288-w/Published.

(11) Kumar, P.; Meza, A.; Ellis, J. M.; Carlson, G. A.; Bingman, C. A.; Buller, A. R. L -Threonine Transaldolase Activity Is Enabled by a Persistent Catalytic Intermediate. *ACS Chem Biol* **2021**, *16* (1), 86–95. https://doi.org/10.1021/acschembio.0c00753.

(12) Xu, L.; Nie, D.; Su, B. M.; Xu, X. Q.; Lin, J. A Chemoenzymatic Strategy for the Efficient Synthesis of Amphenicol Antibiotic Chloramphenicol Mediated by an Engineered L-Threonine Transaldolase with High Activity and Stereoselectivity. *Catal Sci Technol* **2022**, *13* (3), 684–693. https://doi.org/10.1039/d2cy01670b.

(13) Doyon, T. J.; Kumar, P.; Thein, S.; Kim, M.; Stitgen, A.; Grieger, A. M.; Madigan, C.; Willoughby, P. H.; Buller, A. R. Scalable and Selective β-Hydroxy-α-Amino Acid Synthesis Catalyzed by Promiscuous l-Threonine Transaldolase ObiH. *ChemBioChem* **2022**, *23* (2). https://doi.org/10.1002/cbic.202100577.

(14) Scott, T. A.; Heine, D.; Qin, Z.; Wilkinson, B. An L-Threonine Transaldolase Is Required for L-Threo-β-Hydroxy-α-Amino Acid Assembly during Obafluorin Biosynthesis. *Nat Commun* **2017**, *8* (May), 1–11. https://doi.org/10.1038/ncomms15935.

(15) Schaffer, J. E.; Reck, M. R.; Prasad, N. K.; Wencewicz, T. A. β-Lactone Formation during Product Release from a Nonribosomal Peptide Synthetase. *Nat Chem Biol* **2017**, *13* (7), 737–744. https://doi.org/10.1038/nchembio.2374.

(16) Meza, A.; Campbell, M. E.; Zmich, A.; Thein, S. A.; Grieger, A. M.; McGill, M. J.; Willoughby, P. H.; Buller, A. R. Efficient Chemoenzymatic Synthesis of α-Aryl Aldehydes as Intermediates in C-C Bond Forming Biocatalytic Cascades. *ACS Catal* **2022**, *12* (17), 10700–10710. https://doi.org/10.1021/acscatal.2c02369.

(17) Xu, L.; Wang, L. C.; Su, B. M.; Xu, X. Q.; Lin, J. Multi-Enzyme Cascade for Improving β-Hydroxy-α-Amino Acids Production by Engineering L-Threonine Transaldolase and Combining Acetaldehyde Elimination System. *Bioresour Technol* **2020**, *310*, 123439. https://doi.org/10.1016/j.biortech.2020.123439.

(18) Zhao, F.; Lauder, K.; Liu, S.; Finnigan, J. D.; Charnock, S. B. R.; Charnock, S. J.; Castagnolo, D. Chemoenzymatic Cascades for the Enantioselective Synthesis of β-Hydroxysulfides Bearing a Stereocentre at the C−O or C−S Bond by Ketoreductases. *Angewandte Chemie - International Edition* **2022**, *61* (31). https://doi.org/10.1002/anie.202202363.

(19) Harris, R. K.; Becker, E. D.; De Menezes, S. M. C.; Goodfellow, R.; Granger, P. NMR Nomenclature: Nuclear Spin Properties and Conventions for Chemical Shifts - IUPAC Recommendations 2001. *Solid State Nucl Magn Reson* **2002**, *22* (4), 458–483. https://doi.org/10.1006/snmr.2002.0063.

(20) Gibson, D. G. Enzymatic Assembly of Overlapping DNA Fragments; 2011; pp 349–361. https://doi.org/10.1016/B978-0-12-385120-8.00015-2.

(21) El-Gamal, M. I.; Khan, M. A.; Tarazi, H.; Abdel-Maksoud, M. S.; Gamal El-Din, M. M.; Yoo, K. H.; Oh, C. H. Design and Synthesis of New RAF Kinase-Inhibiting

Antiproliferative Quinoline Derivatives. Part 2: Diarylurea Derivatives. *Eur J Med Chem* **2017**, *127*, 413–423. https://doi.org/10.1016/j.ejmech.2017.01.006.

(22) Chang, K. M.; Chen, H. H.; Wang, T. C.; Chen, I. L.; Chen, Y. T.; Yang, S. C.; Chen, Y. L.; Chang, H. H.; Huang, C. H.; Chang, J. Y.; Shih, C.; Kuo, C. C.; Tzeng, C. C. Novel Oxime-Bearing Coumarin Derivatives Act as Potent Nrf2/ARE Activators in Vitro and in Mouse Model. *Eur J Med Chem* **2015**, *106*, 60–74. https://doi.org/10.1016/j.ejmech.2015.10.029.

(23) Wang, T. C.; Chen, Y. L.; Tzeng, C. C.; Liou, S. S.; Chang, Y. L.; Teng, C. M. Antiplatelet α-Methylidene-γ-Butyrolactones: Synthesis and Evaluation of Quinoline, Flavone, and Xanthone Derivatives. *Helv Chim Acta* **1996**, *79* (6), 1620–1626. https://doi.org/10.1002/hlca.19960790612.